UC Berkeley
UC Berkeley Electronic Theses and Dissertations

**Title**

Pursuing Selectivity: Data-Science Driven Reaction Development and Catalysis

**Permalink**

https://escholarship.org/uc/item/4d13p7ct

**Author**

Rouget-Virbel, Caroline Alice

**Publication Date**

2022

Peer reviewed|Thesis/dissertation

eScholarship.org Powered by the California Digital Library
University of California

# Pursuing Selectivity:
# Data-Science Driven Reaction Development and Catalysis

by

Caroline Rouget-Virbel

A dissertation submitted in partial satisfaction of the

requirements for the degree of

Doctor of Philosophy

in

Chemistry

In the

Graduate Division

of the

University of California, Berkeley

Committee
Professor F. Dean Toste, Chair
Professor Richmond Sarpong
Professor Andreas Martin

Fall 2022

## Abstract

Pursuing Selectivity:
Data-Science Driven Reaction Development and Catalysis

By

Caroline Rouget-Virbel

Doctor of Philosophy in Chemistry

University of California, Berkeley

Professor F. Dean Toste, Chair

Throughout my doctoral studies, I have endeavored to address the questions and challenges stemming from structure-activity relationships in catalysis. Mechanistic understanding is of central importance in the reaction development and the design of novel catalyst classes to ensure control over reactivity and selectivity. Physical organic chemistry methods and statistical analysis, in particular, guide the rational and strategic construction of specific interactions between substrates and catalysts to achieve the desired transformations. The work presented in the following chapters encompasses collaborative efforts with the University of Utah, and Genentech, Inc., towards the efficient design of catalytic and synthetic platforms.

**Chapter 1**: The first chapter presented herein offers a brief overview of the historical development in organic synthesis and catalysis which have paved the way to the research work described thereafter. Some principles of selectivity in synthesis are explored, alongside with an introduction to physical organic tools such as linear-free energy relationships and statistical models. The principles delineated in this chapter are meant to provide a frame of reference for the discussion of rational catalyst design and reaction optimization outlined in the following chapters.

**Chapter 2:** The design of efficient catalysts for organic reactions often relies on understanding the subtle relationship between structure and reactivity. Historically, this process has laid the foundation for the development of catalysts heavily biased towards more rigid and sterically-incumbered structures. Indeed, venturing outside of these steric repulsion models often

complicates the generation of accurate predictions for a potential catalyst class to offer selectivity, due to the poorly understood nature of flexibility and its role in effecting attractive non-covalent interactions between catalysts and substrates. Herein, we disclose a novel class of flexible chiral phosphoric acid scaffold incorporating a single point of chirality. Data science techniques were first used to select a diverse training set of catalysts. Using a univariate classification algorithm and multivariate linear regression, key catalyst features necessary for high levels of selectivity were deconvoluted for the transfer hydrogenation of 8-aminoquinolines. The resulting model was found to accurately predict the selectivity of out-of-set catalysts. This workflow enabled extrapolation to a new catalyst providing higher selectivity than both peptide-type and BINOL-type catalysts (up to 95:5 er). These techniques were then successfully applied towards two additional transformations to illustrate the power of combining rational design with data science (*ab initio*) in the development of new catalysts.

**Chapter 3:** Even though substituted pyrazoles have been shown to possess beneficial biological activity in a variety of medicinal chemistry fields, the challenges facing their efficient synthesis have hindered their widespread application in hit-to-lead pharmaceutical pipelines. The practical and regioselective introduction of substitution into pyrazole motifs remains elusive, especially with regards to nitrogen substitution with electronically or sterically neutral moieties. The work presented herein describes the optimization process for the regioselective cyclization of N-methyl pyrazoles. Hoping to move away from substrate-driven selectivity, the small size of the hydrazine partner, lack of significant electronic induction from either starting materials, as well as the high variability of selectivity on multiple reaction parameters presented a challenge for traditional optimization methods. We describe the iterative use of Bayesian statistics to obtain catalyst-free yet selective reaction conditions for the synthesis of 3-(4-fluorophenyl)-1-methyl-1*H*-pyrazole, as well as the progress made towards the selective synthesis of isomer 5-(4-fluorophenyl)-1-methyl-1*H*-pyrazole

## Acknowledgments

I first need to thank my dissertation committee members: Prof. F. Dean Toste, Prof. Andreas Martin, and Prof. Richmond Sarpong, along with Prof. John Hartwig for participating in my Qualifying Examination committee. Mostly, thank you for allowing me to finish this degree. Dean, thanks for bearing with me through the wild ride that has been this PhD and keeping the lines of communication open and honest. Additionally, I must acknowledge the contributions made by the many collaborators that I worked with over the years. From the Toste group, Dr. René Rahimoff, Dr. Vlad Roytman, Abby Medlin, Emily Ruan – Thank you for sticking by my side even when science wasn't working and motivation was low (which was most of the time). Dr. Derek Dalton, Dr. Richard Walroth, Dr. Juno Siu, Dr. Francis Gosselin, and the rest of the process and high-throughput experimentation teams at Genentech, thank you for giving me the opportunity to experience research from the pharmaceutical perspective. Additionally, Prof. Matt Sigman and his group members have long collaborated with ours and deserve credit for some of the work detailed in this dissertation.

My teaching experiences were by far the highlights of my PhD and certainly the memories I will cherish the most after all is said and done and I walk away with my hood and my degree. Having the privilege to watch my former students grow and follow their progress through their own studies and lives has been a rare a precious gift. Prof. Bob Bergman played a particularly important role in my teaching experience. I am still, and will remain, in awe of the fact that I had the opportunity to teach alongside someone so passionate, experienced, and receptive of the needs of his students in his teaching philosophy. Vienna, Julie, Alex, Emily, Anna – and many more students that I have taught and tutored over the years - who not only allowed me to teach them chemistry, but adopted me as mentor and friend, and let me follow their progress (some for years now). Thank you. Some weeks you were my only reminders of why I loved chemistry in the first place, and the only reasons I sticked it out for so long. Thank you for keeping my passion alive with your curious minds and your love for learning.

To my fellow candidates from the cohort of 2018 (and years around us): Let's be kind and gentle on ourselves -- regardless of productivity, publications, and recognition -- for we did (mostly) manage to keep standing on our feet through two and a half years of a world-wide pandemic. We showed up to lab and kept moving when the world came to abrupt stand-still that none of us could have predicted would last half of our PhDs. For that, let's be proud.

I could probably write a dissertation's worth of thank you's to the many people who have, in small and big ways, helped me get to where I am in life. Unfortunately, I should restrict myself to a non-exhaustive list that fits in a few of pages, which hardly gives credit to the many who have shaped me into the woman I have become. Of course, I must acknowledge all members of the Toste group, past and present. A particular piece of my heart is reserved for the original crew of Latimer 629: Lilly, Spencer, and Megan, who welcomed me in my first year and made that room a safe space in the chaotic midst that is the first year of graduate school. Another piece of my heart goes to the members of 629 who have since filled the spaces of those who left: Wendy, Jennifer, Abby, Marcus, Andrew. Thank you for the laughs and shared experiences. I hope that board above our door starts growing numbers in the double digits again at some point. Anna, Alec, Mari, and all the senior grad students and postdocs who were there when I started, thank you for letting first year (and 4.5$^{th}$ year) me pester you with questions pretty much all the time, and for any proofreading and/or guidance you have provided.

At the very top of the list of people that I need to thank for their influence on my PhD and my life is Dr. Lily Hale. The universe decided that we would start in the lab the same week at adjacent benches, and I am so very thankful for that. People say that representation matters and my friendship with Lily is the first time that I really felt it so strongly. Witnessing you go through the ups and downs of life in and out of the lab has been a true gift and example for me to follow. There are so many things I wish I could say to describe how thankful I am, but none of the words that come to mind could ever do the job. I'll just say thank you and I can't wait to see where our next trip is going to be.

Abby, Annika: Thank you for being rocks for me these past couple of years. Your ability to relate to the daily struggles even in the smallest way made me feel at home. You are both like little sisters to me, and watching you grow has made me happy. Annika, you always bring such gentleness and peace to our lab, which sorely needs it. Abby – please keep being yourself, completely and unapologetically. Science needs more women like you two. I hope you keep your heads up, keep building confidence, and not letting the environment of chemistry make you forget your values and how beautiful your souls are. I wish you could see the growth you both have accomplished and how amazing you are doing from the outside.

Vlad – Thanks for becoming my wise uncle (*or much, much older old brother?)* and always being willing to hear me vent and let steam out, as much as discussing wild chemistry ideas. In hindsight you were exactly the kind of collaborator that I needed, someone to balance out my energy and provide unending optimism and a deep love for science when the grind of the PhD had taken all of that away from me. I am in awe of your ability to remain mellow and kind and to keep perspective in the face of frustration. You've become my go-to person when I need to ask silly questions, and somehow you even managed to find the patience to try and teach me how to use computers. Trying to teach me how to Excel can't have been easy, but you did it. Someone should give you a medal for that. Most of all, I am grateful for the amazing banter. I don't know how, but you without fail have managed to get a laugh out of me on days when I honestly could not remember what joy felt like and my neurons were fighting for the 0.001 ppm of serotonin left in my brain (eg the past two month). You've been one of the most steady, reliable, and supportive people in my life this year and I really, really needed that.

Kay Xia – It meant the world to me when you reached out to asked me if I was ok and to talk about the climate in the lab. Kay has not stopped to amaze me since with the amazing DEI meetings that she has organized and her thoughtfulness. It takes great courage and composure to take the lead on articulating these issues and tensions and maintaining these conversations in an environment like this one. There needs to be more credit and recognition given to those who give time, effort and thought to starting and maintaining these conversations in an environment such as ours and she certainly has been one of those people to us.

Emilia, Michael, Misha, Jacob: friendships I didn't expect, but each came at just the right time. Life sure doesn't take the time to stop just because you're trying to get a PhD. The ups and downs keep coming, and you have seen quite a few of mine over the years. I am so very grateful for always finding friends in you, a laugh, a kind word, a (sometimes) long-distance-mental embrace to make me feel better. I'm also absurdly thankful for the care packages, coffee, chocolate, and funny postcards that always seemed to land at my door just the days I needed them the most.

I feel very lucky to have found a community outside of UC Berkeley over the years I spent in the Bay Area. I am indebted to Amanda, Mark, and the staff of Sweet Adeline for their (literal) sweetness and the unreasonable amount of coffee they made for me. Also, for letting me be blessed by Cara's presence on my lap once in a while. The world needs more Cara's. To the East Bay SPCA, and to Oakland Animal Services, thank you for providing me with much needed happiness and stress relief in the forms of baby animals. What more could a girl ever ask for than cakes and kittens, really? The past few months of single-puppy motherhood would have also been much harder without the welcoming faces of the Bus Lab. You all welcomed me in a way I did not expect and reminded me that sharing a beer with some friends at 5:30pm is really, after all, an important goal to have in life.

There is a long list of people from my past I need to acknowledge, to name just a few: Mme Goulard, RPL, Marty Semmelhack, Paul Reider, David MacMillan, Megan Shaw, Jack Twilton, Jeff Lipszults, Yufan Liang, Gabby Lovett, Russell Smith, Thom Brewer, Jens *(and many more)*. Perhaps someday I will be able to articulate the extent of my gratitude. Some of you have no idea what kind of impact you've had on me. No gesture was too small when it paved the way to a future like the one you've helped me build. There are no words that could repay you for the advice, support, and mentorship I received from you.

In mentions of the past, one deserves a highlight: Katia Kiston. Thank you for knowing a part of me so few in this country do, and for relating deeply to the conflict of wanting one life and missing another. Your understanding of the challenges brought by changing so much in so little time made a world of difference this year. Life made it so our paths would cross again after years of growth, and it did not disappoint. Maybe it was fate, maybe good karma, maybe true friendship. Maybe a little bit of all of that. All I know is that you've refilled my cup with a taste of home, and you've refilled my lungs with a breath of non-chemically contaminated fresh air that I so desperately needed the past couple years.

To my family and especially my parents - I've never been agile at expressing how thankful I have been all these years. You've had so much faith and trust in me to follow my heart and to know what was best for myself, no matter the sacrifices that you had to make so I could chase after the life I wanted. People always tell me it must have taken courage for an 18-year-old from a small French town to leave everything behind and build a new life here. Truth is, I can't possibly fathom how much courage and sacrifice it must have taken to watch your child go, and to remain supportive at every step of the way, regardless of how far and unavailable it made her. I promise to do my best to make up for all this time, some way, somehow.

Finally – to my 5-year-old, 10-year-old, 15-year-old selves – you did it, kind of. No, you didn't cure cancer, or win a Nobel. You didn't even publish a single good paper, for that matter. Turns out science isn't quite that easy. You sure lost a lot in the process: time away from those who love you most, mental energy fighting against systems much bigger than you, many nights of decent sleep. But you did build a new life, you set the bar high, you worked hard for your degrees, got them, and you gained a lot in the process too. Resilience, self-worth, a much thicker skin, priceless life lessons. And many, many irreplaceable, beautiful friendships. Who would have ever thought you'd make it this far? I certainly didn't. And now I can't wait to see what my 50-year-old self wishes she could say to my 25-year-old self.

# Table of Contents

*Table of Contents* *iv*

*Table of Figures* *vi*

*List of Tables* *viii*

*List of Abbreviations* *ix*

**Chapter 1** **1**

**Introduction to Catalysis and Selectivity** **1**

*I. A Brief History of Synthetic Organic Chemistry* *2*
1.1. Synthetic Organic Chemistry: an overview 2
1.2. The progress of Synthetic Methodology 2

*II. Catalysis* *5*
2.1. The Place of Catalysis in Synthetic Chemistry 5
2.2. The Challenge of Selectivity in Synthesis and Catalysis 7
2.3. Tools and Recent Innovations in Catalysis and Selectivity 13

*III. Conclusions* *17*

*IV. References* *18*

**Chapter 2** **25**

**Data-Science Driven Development of Flexible, Point-Chiral Phosphoric Acid Catalysts** **25**

*I. Introduction* *26*
1.1. A Primer on Asymmetric Catalysis 26
1.2. Chiral Phosphoric Acids: Privileged Structures for Asymmetric Catalysis 27
1.3. Harnessing Non-Covalent Interactions and Conformational Flexibility 33
1.4. Data-driven tools to understand the role of NCIs in asymmetric catalysis 34

*II. Project Design* *36*
2.1. A Hybrid Catalyst Class 36
2.2. Training Set Design and Computational Workflow 37

*III. Results and Discussion* *39*
3.1. Synthesis of the Catalyst LIbrary 39
3.2. Reaction Screening and data collection 40
3.3. Statistical Modeling and Structure-Activity Relationship Analysis 42
3.4. Transferability of the model to other reaction types 49

*IV. Analysis of the Low Performing Catalysts* *52*

*V. Conclusions and outlook* *54*

*VI. References* *55*

*VII. Supplemental Information* *61*
7.1. General Information 61
7.2. Catalyst Synthesis and Characterization 63
7.2.1. General Procedures 63
7.2.2. Catalyst Purification Procedures and Notes 74
7.2.3. Fragments used for diversification 75

7.2.2. Synthesis and Characterization of Non-Commercially Available fragments 80
7.2.3. Synthesis and Characterization of Intermediates 8a-w 95
7.2.4. Synthesis and Characterization of Intermediates 9a-w 138
7.2.7. Synthesis and Characterization of Intermediates 9a-w 188
7.2.8. Enantiopurity Considerations 245
7.3. Reaction Screening 253
7.3.3. Transfer Hydrogenation of 8-Aminoquinoline 1 253
i.3.2. Atroposelective Cyclodehydration 256
7.3.3. Oxetane Desymmetrization 260
7.4. Computational Details 263
7.4.1. General Computational Methods 263
7.4.2. Computational Training Set Design Workflow 263
7.4.3. Catalyst Parameters 265
7.4.4. Model Development 266
7.4.5. Model Validation: Transfer Hydrogenation of 8-aminoquinoline 1 267
7.4.6. Model Validation: Global Three-Reaction Statistical Model 267
7.5. Supplemental Figures 268
8. References 270

**Chapter 3** **274**

**Aiming for regioselectivity in the synthesis of N-Methyl Pyrazoles** **274**

*I. Introduction* *275*
1.1. The importance of N-containing heterocycles 275
1.2. Pyrazoles: an important yet synthetically challenging motif 276

*II. Project Design* *278*

*III. Results and Discussion* *279*
3.1. Initial Screening of Brønsted Acid Catalysts 279
3.2. Bayesian Optimization and Regioselectivity Results 284

*IV. Conclusions and Outlook* *289*

*V. Supplemental Information* *290*

*VI. References* *293*

## Table of Figures

**Chapter 1**

Figure 1 : A) Wöhler's synthesis of urea (1828). B) Strecker amino acid synthesis (1850). C) Aldol reaction. D) Examples of complex natural product syntheses. ..... 3
Figure 2 : General classes of objectives driving new synthetic methodologies ..... 4
Figure 3 : Representative energy diagrams of catalytic processes ..... 5
Figure 4 : A) Curtin-Hammett principle. B) Representation of thermodynamic and kinetic control. ..... 8
Figure 5 : A) Discovery of chirality by Paster in 1848. B) *(R)*- and *(S)*-thalidomide. ..... 9
Figure 6 : Reaction coordinate for an unselective reaction yielding racemic product. B) Reaction coordinate for an enantioselective reaction ..... 10
Figure 7 : A) Initial proof of concept by Knowles. B) Monsanto synthesis of L-DOPA. C) Sharpless epoxidation of allylic alcohols. D) Noyori's asymmetric hydrogenation of $\beta$-ketoesters. ..... 11
Figure 8 : Examples of privileged catalysts and ligands used in asymmetric catalysis. B) Common selectivity models for chiral induction ..... 12
Figure 9 : A) Hammett Relationship for the ionization of benzoic acid. B) Some examples of commonly used molecular descriptors ..... 15
Figure 10 : Overview of the research projects covered in the following chapters. ..... 17

**Chapter 2**

Figure 1: A) Early reports of asymmetric organocatalysis by Marckwald (1904). B) Bredig and Fiske (1912). C) Hajos-Parrish-Sauer-Wiechert reaction. ..... 26
Figure 2: A) Jacobsen's enantioselective Strecker reaction (1998). B) Asymmetric Aldol reaction (List, 2000). C) Enantioselective Diels-Alder reaction (MacMillan, 2000). ..... 27
Figure 3: Common structures of Brønsted acids ..... 28
Figure 4: Synthesis of BINOL phosphoric acid (Fouquey, 1971) ..... 28
Figure 5: Cornforth's design of phosphinic acid catalysts (1978) ..... 29
Figure 6: A) Akiyama's enantioselective Mannich-type reaction (2004). B) Terada's CPA-catalyzed Mannich-type reaction (2004). ..... 30
Figure 7: Privileged axially chiral backbones for phosphoric acid catalysis. ..... 31
Figure 8: Key features of BINOL-based chiral phosphoric acid catalysts. ..... 31
Figure 9: A) Significant non-covalent interactions. B) Triazole-bearing CPA (Toste, 2013). ..... 32
Figure 10: A) Inoue, conjugate addition of thiols to enones. B) Juliá-Colonna, epoxidation of chalcones. C) Kinetic resolution and acylation catalyzed by small peptides (Miller, 1998). D) pTh-catalyzed transfer hydrogenation of 8-aminoquinolines (Miller, 2015). ..... 33
Figure 11: non-exhaustive examples of data-science methods used for the deconvolution of structure-activity relationships in selectivity trends. ..... 35
Figure 12: Envisioned structure of hybrid flexible phosphoric acid catalysts. ..... 36
Figure 13: Training set design ..... 37
Figure 14 : Training set library and analytical workflow. ..... 38
Figure 15 : Synthetic route for the catalyst library ..... 39
Figure 16 : Transformations selected to test the training set of hybrid catalysts. ..... 40
Figure 17 : Catalyst nomenclature used in this section ..... 42
Figure 18 : General representation of the classification method development by the Doyle and Sigman groups. ..... 44

Figure 19 : A) Univariate classification for the selectivity cliff observed in the transfer hydrogenation of 8-aminoquinolines. B) Partial charge visualization for the classification terms. C) MLR model for the transfer hydrogenation reaction. ..... 45
Figure 20 : A) Prediction and experimental data for the external validation catalysts. B) Univariate correlations for the two classes of catalysts. ..... 47
Figure 21 : Data modeling and parameters for the three-reaction system. ..... 50
Figure 22 : Proposed racemization pathway and enantiopurity of the catalysts ..... 52
Figure 23: Opportunities for future studies ..... 54

**Chapter 3**

Figure 1: A) Types of N-containing heterocycles. B) Examples of pyrazole-based drug compounds. ..... 275
Figure 2: A) Knorr synthesis of pyrazole (1883). B) Proposed Knorr-type mechanism. C) Nomenclature of pyrazole substitution. ..... 276
Figure 3: Examples of recent synthetic methods for substituted pyrazoles. ..... 277
Figure 4: Initial objectives for the project ..... 278
Figure 5: Initial set of Brønsted acid catalysts. ..... 279
Figure 15: Some representative screening data from extensive experimentation for the cyclization of the phthalimide-protected model substrate. ..... 280
Figure 7: Representative screening results for the *N*-Boc protected model substrate. ..... 281
Figure 8: Representative screening results for the simplified model substrate. ..... 281
Figure 9: Challenges encountered in reaction optimization. ..... 282
Figure 10: Additional exploration into solvent effects, additives, and phase transfer catalysis. 283
Figure 11: Reaction optimization methods and tools ..... 284
Figure 12: Graphical summary of Bayesian Optimization methods. ..... 285
Figure 13: Initial Bayesian Optimization Training Set ..... 286
Figure 14: Three consecutive iterations of Bayesian Optimization were performed. ..... 287
Figure 15: Final iteration and combined results ..... 288
Figure 16: Opportunities for future work ..... 289

Figure S 1 : Full synthetic route for the catalysts ..... 63
Figure S 2 : Trends for classification of selective vs non-selective catalysts ..... 268
Figure S 3 : Title Hydrogen bonding network observed in sulfonamide catalysts P13, P19, and V2. ..... 268
Figure S 4 : Title of Univariate N—H bond length vs selectivity for amide catalysts ..... 269
Figure S 5 : Univariate NBO O(P3) vs dihedral angle of the chiral pocket ..... 269

## List of Tables

Table 1: Transfer hydrogenation results ..... 41
Table 2: Summary of the molecular descriptors discussed in the modeling of the catalysts..... 43
Table 3: Atroposelective Cyclodehydration[a] ..... 51
Table 4: Oxetane Desymmetrization[a] ..... 51

Table S1: Carboxylic acids and sulfonyl chlorides used for the diversification of secondary amide $R_1$..... 75
Table S2: Amine fragments used in the diversification of tertiary amide $R_2$. ..... 78
Table S 3: Full Training Set Screening Data for Transfer Hydrogenation. ..... 254
Table S 4: Selectivity Data for Atroposelective Cyclodehydration. ..... 258
Table S 5: Selectivity Data for Oxetane Desymmetrization. ..... 261

## List of Abbreviations

| | |
|---|---|
| δ | chemical shift |
| $\Delta\Delta G^{\ddagger}$ | difference in transition state energies |
| ν | IR frequency |
| 2D | two-dimensional |
| Ac | acyl |
| Ad | adamantyl |
| Ar | aryl |
| Aq | aqueous |
| B | base |
| BINAP | (2,2′-bis(diphenylphosphino)-1,1′-binaphthyl) |
| BINOL | 1,1′-Bi-2-naphthol |
| BDE | bond dissociation energy |
| Bn | benzyl |
| Boc | *tert*-butoxycarbonyl |
| bs | broad singlet |
| Bu | butyl |
| Cat. | catalyst |
| Cbz | carboxybenzyl |
| $CDCl_3$ | deuterated chloroform |
| ChelpG | charges from electrostatic potentials using a grid based method |
| CPA | chiral phosphoric acid |
| Cy | cyclohexyl |
| d | doublet |
| D | deuterium |
| DCM | dichloromethane |
| DCE | dichloroethane |
| dd | doublet of doublets |
| DFT | density functional theory |
| DMF | dimethylformamide |
| dppm | diphenylphosphonomethane |
| DOE | design of experiment |
| DMSO | dimethylsulfoxide |
| dr | diastereomeric ratio |
| equiv. | equivalents |
| er | enantiomeric ratio |
| ESP | electrostatic potential |
| ESI-TOF | electrospray ionization-time of flight |
| Et | ethyl |

| | |
|---|---|
| $Et_2O$ | diethyl ether |
| $Et_3N$ | triethylamine |
| EtOAc | ethyl acetate |
| EtOH | ethanol |
| Fmoc | fluorenylmethoxycarbonyl |
| FTIR | Fourier transform infrared spectroscopy |
| g | gram |
| GC | gas chromatography |
| h | hour |
| HOMO | highest occupied molecular orbital |
| HPLC | high pressure liquid chromatography |
| HRMS | high resolution mass spectrometry |
| HTE | high-throughput experimentation |
| Hz | hertz |
| IPA | isopropyl alcohol |
| iPr | isopropyl |
| IR | infrared (spectrum) |
| LFER | linear free energy relationship |
| LUMO | lowest unoccupied molecular orbital |
| m | multiplet |
| *m* | meta |
| M | molar |
| MAE | margin of absolute error |
| Me | methyl |
| MeCN | acetonitrile |
| MeOH | methanol |
| Mes | mesityl, 1,3,5-trimethylphenyl |
| mg | milligram |
| min | minute |
| mL | milliliter |
| mmol | millimole |
| mol | mole |
| MS | mass spectrometry |
| ML | machine learning |
| MLR | multivariate linear regression |
| NBS | N-bromosuccinimide |
| NCI | non-covalent interaction |
| NMR | nuclear magnetic resonance |
| NSAID | non-steroidal anti-inflammatory drug |
| Nu | nucleophile |

| | |
|---|---|
| *o* | ortho |
| OH | hydroxy |
| OMe | methoxy |
| OTf | trifluoromethanesulfonate |
| *p* | para |
| P450 | pigment 450 |
| Ph | phenyl |
| Phth | phthaloyl |
| pThr | phosphothreonine |
| QSAR | quantitative structure activity relationship |
| q | quartet |
| R | generic subsituent |
| $R^2$ | correlation factor |
| r.t. | room temperature |
| s | singlet |
| SFC | supercritical fluid chromatography |
| t | triplet |
| TBAF | Tetrabutylammonium fluoride |
| tBu | *tert*-butyl |
| Tf | trifluoromethylsulfonyl |
| THF | tetrahydrofuran |
| tht | tetrahydrothiophene |
| TLC | thin layer chromatography |
| TMS | trimethylsilyl |
| tol | toluyl |
| Ts | tosyl, 4-toluenesulfonyl |
| TS | transition state |
| TST | transition state theory |
| UV | ultraviolet |
| $\%V_{bur}$ | percent buried volume |

# Chapter 1

# Introduction to Catalysis and Selectivity

# I. A Brief History of Synthetic Organic Chemistry

## 1.1. Synthetic Organic Chemistry: an overview

Amongst the many subfields of molecular sciences, synthetic organic chemistry has come to fill a particularly critical space in our society. From the agrochemical, food, and pharmaceutical industries to novel materials or environmental safety and preservation, the synthetic chemistry research of today aims to tackle a wide array of contemporary challenges. The discovery of novel reactions and methods for the construction of new and complex molecular structures has been central to health-related industries in the past two decades, and organic synthetic methods are increasingly finding applications in material sciences, polymer chemistry, energy-related field, and petroleum industries.

Organic chemistry, defined as the study of the structure and reactivity of carbon-based molecules, became a prolific area of research in the 20th century as breakthroughs in the discovery, structural elucidation, and syntheses of complex natural products became unbound. Since the first reported synthesis of urea in 1828 by Wöhler marked one of the field's initial landmarks (Figure 1, A),[1] synthetic organic chemistry has witnessed an ever-growing community of minds and diversity of molecular targets. Even prior to Kekulé's proposal of the tetravalent bonding structure of carbon in 1857,[2] chemists were making way in the discovery and development of synthetic methods. The 1850 Strecker amino acid synthesis from aldehydes, ammonia, and potassium cyanide remains a landmark for organic chemistry (Figure 1, B).[3,4] The same could be said regarding the aldol reaction, first observed by Kane as the self-condensation of acetone in 1838 and further developed independently by Borodin and Wurtz in the 1870s (Figure 1, C).[5,6] The goal of achieving the synthesis of terpenes,[7,8] carbohydrates,[9] hormones,[10] and other biologically relevant molecular scaffolds provided a plethora of synthetic challenges and a wide platform for the development of synthetic methodologies (Figure 1, D).[11,12] The pioneering studies and achievements of Woodward, Eschenmoser, Corey, Kishi, and many others have drastically expanded the realm of synthetic possibilities and accessible complexity for target organic molecules.[13-19]

## 1.2. The progress of Synthetic Methodology

Synthetic chemistry has come a long way from its early successes. With the increasing structural complexity of molecular targets came an increased demand for new strategic synthetic methods. A particularly notable shift in the field occurred in the 20th century when chemists began to not only consider the synthesis of whole natural products to instead focus on "single-bond" construction. This new focus on single steps marked the branching out of two distinct but intertwined subfields of organic chemistry: total synthesis and methodology. With the impressive advances of total synthesis by the end of the 20th century, the question evolved from *"can we make it?"* to *"how efficiently can we make it?"*. This different frame of thinking about chemical synthesis set the stage for extensive work on the discovery and improvements of single bond-forming reactions sometimes challenging or unknown in nature.[13]

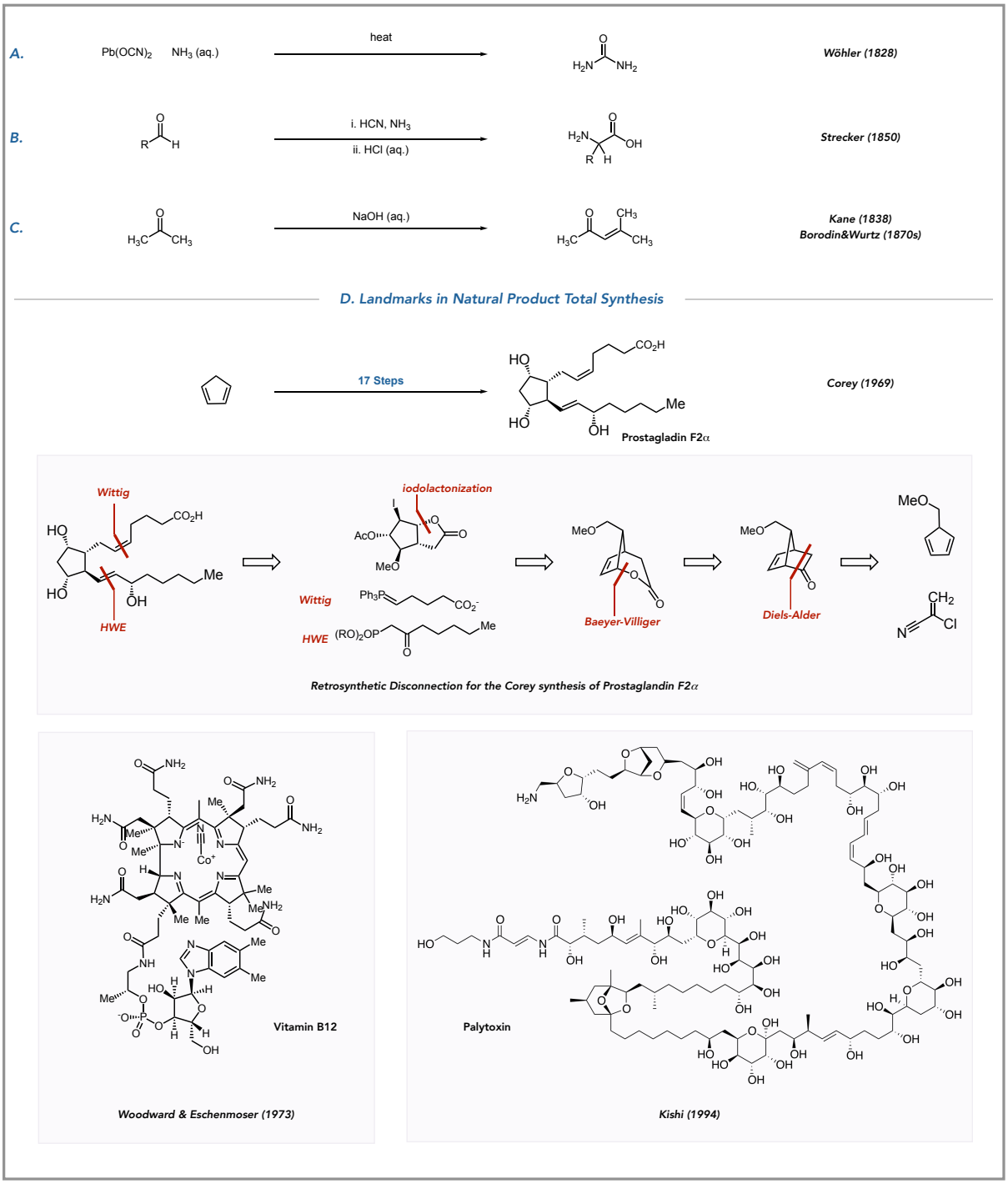



Figure 1 : A) Wöhler's synthesis of urea (1828). B) Strecker amino acid synthesis (1850). C) Aldol reaction. D) Examples of complex natural product syntheses.

This shift in paradigm from target-oriented synthesis towards methodology development placed new concepts such as atom economy and diversity-oriented synthesis front and center in the chemical research space. A prime example of this shift in paradigm is EJ Corey's development of retrosynthetic logic, describing the fundamental ideas of multistep synthesis for complex

molecular structures (Figure 1, D).[20] Complex structures were now broken down to singular, stepwise challenges which could independently be optimized in both efficiency and selectivity. The unprecedented level of efficiency, selectivity, and diversity of possible disconnections strategies that can be achieved today offers a vast chemical space to meet the needs of the industries relying on chemical synthesis, from the production of small molecule libraries of thousands of compounds for drug candidate testing, to the building of large molecular scaffolds from cheap and readily available building blocks.[21,22]

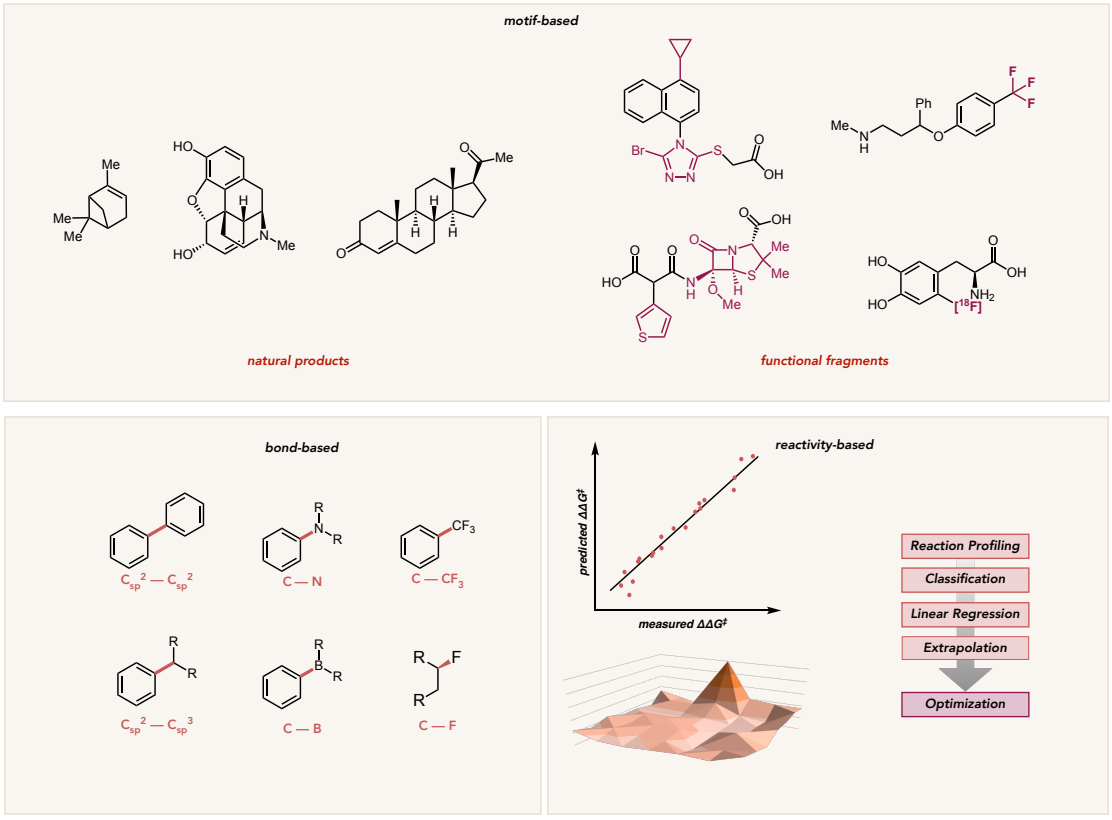



Figure 2 : General classes of objectives driving new synthetic methodologies

Synthetic methodology research can now be generally assigned to three main categories (Figure 2): (a) motif-motivated, (b) bond-motivated, or (c) reactivity-motivated. Motif- and bond-based research are relatively similar in that the objective of the reaction development is a specific bond or functional group to be obtained in order to make known processes more efficient or to attain bonds or substructures currently not achievable.[23] The main objective remains to expand the toolbox of chemists thinking about possible disconnections in the synthesis of complex, often pharmaceutically relevant compounds. On the other hand, reactivity-based methodology is focused on understanding the reactivity trends and features of a specific system to build the foundations upon which to guide its use in synthetic applications. Reactivity-based endeavors have been at the source of many prolific mechanistic investigations and the birth of physical organic chemistry – a field without which chemists' ability to reason, rationalize, and propose novel reactivity would be drastically stifled.

## II. Catalysis

### 2.1. The Place of Catalysis in Synthetic Chemistry

Chemistry pioneers of the eighteenth century paved the way to the development of chemical concepts by revolutionizing the framework in which chemical experimentation was performed. Observations by Cavendish, Scheele, Lavoisier, and others laid the foundations for modern chemistry.[24] A particularly significant advance in synthetic organic chemistry was the development of catalysis. Many chemists and philosophers attempted to understand and define early experimental observations of catalytic processes, from the ancient process of sugar fermentation to produce alcohols, or the first catalytic uses of Brønsted acids towards the production of ethylene from ethanol and ethers,[25] to the experimental observations of transition-metal catalysis by Humphry Davy in the early nineteenth century.[26] The term catalysis was coined by Berzelius in 1835 to mean "the property of exerting on other bodies an action which is very different from chemical affinity. By means of this action, they produce decomposition in bodies, and form new compounds into the composition of which they do not enter".[27,28] Although this description comes relatively close to the current explanation of chemical catalysis, the first modern definition of the concept is, however, more often attributed to Wilhelm Ostwald.

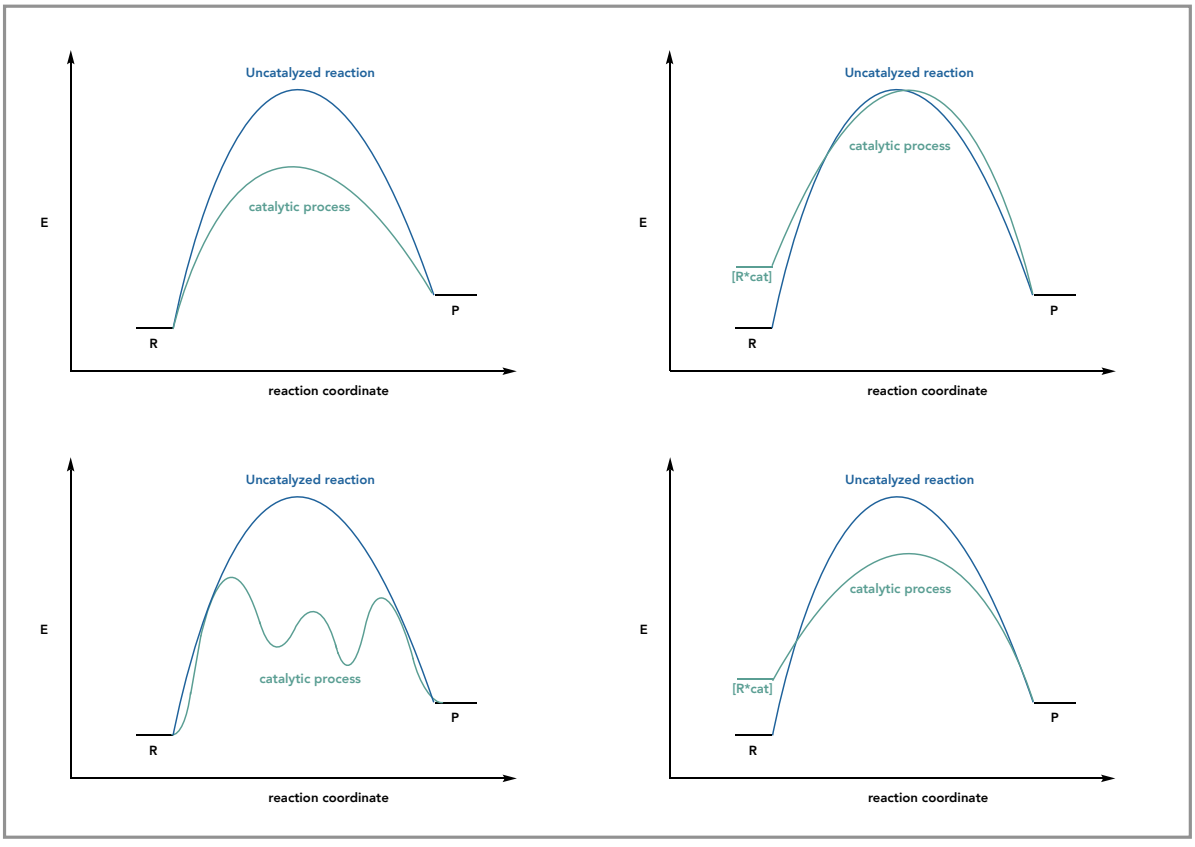



Figure 3 : Representative energy diagrams of catalytic processes

Ostwald defined "catalysis" in the late 1880s based upon the understanding of chemical kinetics of the time, leading to a Nobel prize for his work as one of the founders of the field of

physical chemistry in 1909.[29-31] Today, a chemical catalyst is understood to be a substance which accelerates the rate a reaction while itself being unchanged by the reaction.[32] Amongst the plethora of important new concepts that evolved from the recognition of catalytic processes by the scientific community, chemical kinetics - and physical organic chemistry - emerged as new sciences that led the way to a much deeper understanding of the fundamental principles of chemical reactivity, equilibria and rates, and the endless synthetic possibilities offered by the idea that sub-stoichiometric additives could alter the rate and/or products formed in chemical reactions. In today's landscape of chemical synthesis, catalysis has become a crucial platform for the development of new bond-forming methodologies, enabling the elaboration of complex molecular architectures in a more time- and energy-efficient manner, often having profound impacts on the growth and development of our society.[31,33,34] It is estimated that over 80% industrial chemical processes involved catalysis at the dawn of the 21st century, a number which promises to only increase in the future as sustainable practices and atom economy become vital to synthetic reaction design.[35-37]

The presence of a catalyst does not change the thermodynamics of a reaction. Catalysts can instead affect the product distributions of chemical reactions by providing alternative mechanistic pathways for the reactants with lower energies leading to the transition states relative to uncatalyzed systems. The ways in which a catalyst can lead to faster reaction rates are manifold, and some general representations of these processes are provided in Figure 3, but all rely on the principle that the rate-determining step of the transformation must have a lower activation energy ($\Delta G^{\ddagger}$) than that of the uncatalyzed process. Broadly speaking, this is usually achieved by a change in mechanism, or by the stabilization of the transition state, destabilization of the reactant's ground state, or both.

Although catalysis has tremendously branched out from its early years, within organic chemistry, it is usually divided between heterogeneous catalysis, homogeneous catalysis, and biocatalysis. Each class of catalysis as witnessed incredible intellectual and industrial success and recognition for their impact on synthetic chemistry. In 1912, Sabatier's work on the catalysis of hydrogenation by finely ground metals (nickel and ruthenium) was recognized with the Nobel Prize in Chemistry.[38] The Haber-Bosch process, one of the first industrial-scale heterogeneous catalytic processes to generate ammonia, received the Nobel only a few years later in 1918, and is generally credited with sparking a global population boom previously unseen.[39-41] The following years witnessed a rapid emergence of new industrial catalytic processes. Organometallic polymerization was awarded yet another Nobel Prize for the work of Ziegler and Natta in 1963,[42,43] followed a short ten years later by the discoveries of Wilkinson and Fischer on organometallic complexes and their catalytic activities.[44-47] Discoveries in the fields of catalysis have not slowed down since then, and have become increasingly central to the efficient and safe production of necessary pharmaceutical and agrochemical compounds in large scale processes. Asymmetric homogeneous organometallic catalysis and asymmetric organocatalysis using small molecule catalysts marked a particularly significant turn in the way chemists reason through selectivity challenges in synthesis.[48-51] As environmental concerns grow and the scarcity of material resources such as costly and rare transition metals intensifies, chemists have endeavors to use nature's own enzymes to address synthetic challenges of the 21st century.[52-55] Creative multi-catalytic platforms have been developed to harness reactive intermediates once thought to be too elusive for synthetic methods.[56-61] All of this work and progress has converged towards one goal: "*how can we provide efficient, safe, and environmentally conscious methods to synthesize the challenging molecular structures needed to address the health, materials, and environmental challenges of our days?*"

## 2.2. The Challenge of Selectivity in Synthesis and Catalysis

Synthetic methodology established in its framework a form of single-step reductionism which enabled chemists to focus not only on the efficiency of a given reaction of interest, but also, and importantly, on its ***selectivity***. The applications of regio- and stereoselectivity were once limited to a small fraction of synthetic transformations (Figure 4). The successes of homogeneous catalysis had profound impacts on chemists' ability to ***selectively*** synthesize small molecule targets.[62-65]

Under uncatalyzed reaction conditions, the same starting material can generate multiple different products, and will often yield mixtures of regioisomers difficult to sway without significant steric influence from substituents or the use of directing auxiliaries. The classical example of the Markovnikov rule for alkene additions is typically the first exposure to regioselectivity covered in undergraduate organic chemistry courses.[66] Although often simplified depictions of the complex interactions at play in organic reactions, these rules and mnemonic are commonly taught and used to rationalize or predict the general selectivity of transformations. The Baldwin rules for ring closure,[67-69] the Burgi-Bunitz trajectory[70] along with the Falkin-Anh[71,72] model for the addition of nucleophile to carbonyl compounds, or the Zimmerman-Traxler transition state model for aldol condensations[73], to name a few, should sound familiar to seasoned chemists, and provide generally reliable qualitative estimations for simple systems.

The Curtin-Hammett principle is a particularly helpful rationalization of selectivity in transformations in which two or more competing pathways (Figure 4, A).[32,74] The concept at the center of the Curtin-Hammett principle is that reactions will progress through the lowest energy surface available, independently of ground state thermodynamics of intermediates or products. In the generic reaction depicted in Figure 4, the energy barrier for the interconversion of intermediates $I^1$ and $I^2$ is lower than either energy barriers leading to products $P^1$ and $P^2$ ($\Delta G^{\ddagger}_{iso} < \Delta G^{\ddagger}_{P1}$ ; ($\Delta G^{\ddagger}_{iso} < \Delta G^{\ddagger}_{P2}$). It is the difference between the energies of transition states $TS_1$ and $TS_2$ that determine the product distribution ($\Delta\Delta G^{\ddagger}$). Here, $\Delta G^{\ddagger}_{P1} < \Delta G^{\ddagger}_{P2}$. As such, $I^1$ will be consumed towards the formation of $P^1$. As this transformation is occurring, the rapid interconversion between $I^1$ and $I^2$ ensures that they remain in equilibrium by forcing the interconversion to the right towards $I^1$. The Curtin-Hammett principle can be mathematically summarized by relating the product ratio to the equilibrium constant Keq between $I^1$ and $I^2$, as well as the respective rate constants of product formations (**eq. 1**).

$$\frac{[P_1]}{[P_2]} = K_{eq}\left(\frac{k_1}{k_2}\right) \qquad \textbf{(eq. 1)}$$

It is important to note that the Curtin-Hammett postulate is not applicable to all stereo-divergent reactions, as some lack the prerequisite of the presence of rapidly interconverting intermediates, each leading to one product. Other forms of kinetic or thermodynamic controls can be in effect when reactions are not under Curtin-Hammett conditions (Figure 4, B).[32] Generally, the statement that the lower energy pathway will be preferred remains true. As such, in **example 1**, the thermodynamic and kinetic products are the same. In **example 2,** however, kinetic preference would bias the product distribution towards product **P2**, despite being thermodynamically less favorable than product **P1**.[32]

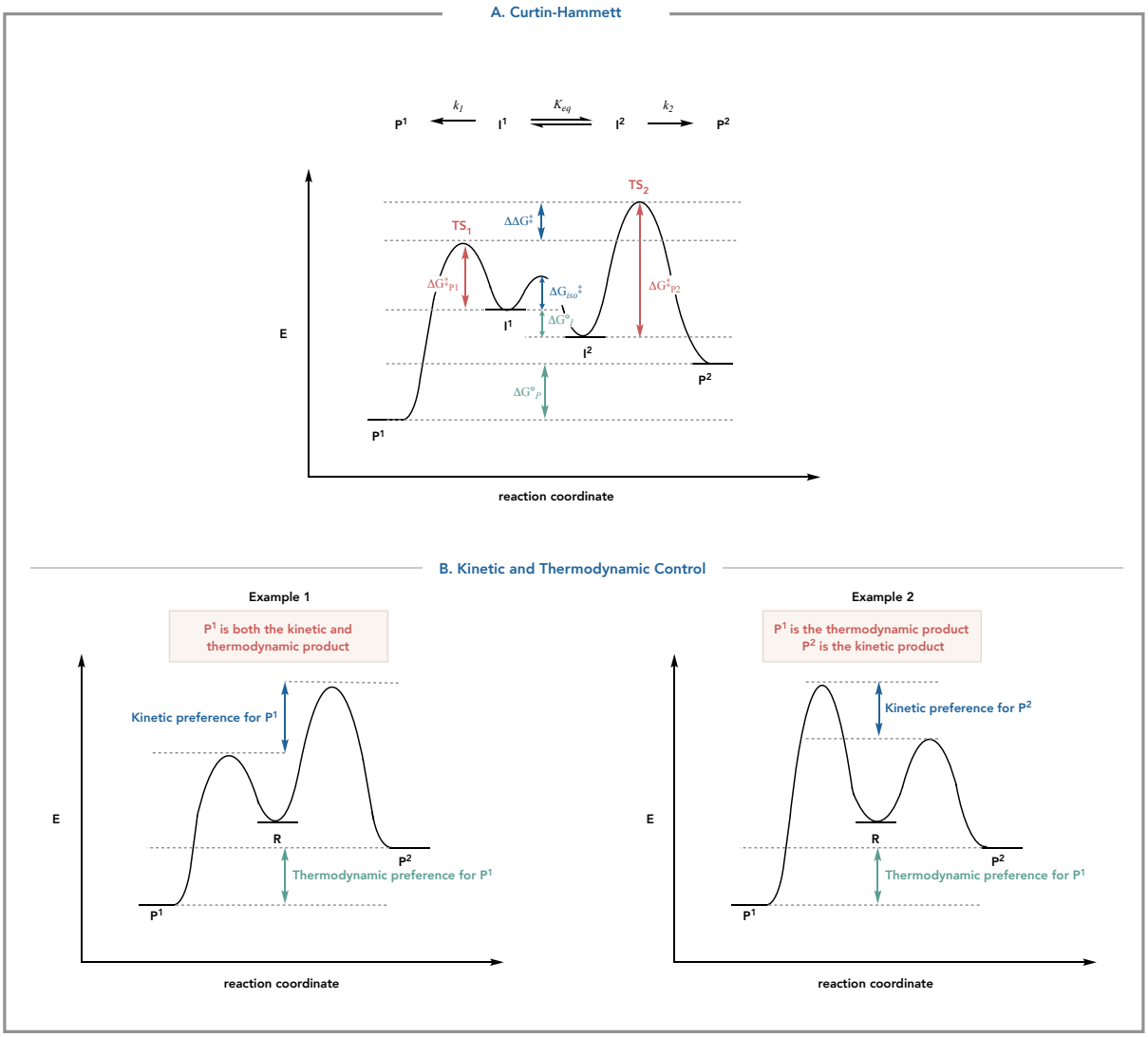



Figure 4 : A) Curtin-Hammett principle. B) Representation of thermodynamic and kinetic control.

The importance of selectivity in synthesis is not solely centered on sustainable practices and atom economy. It has been long known that exact 3D structure of molecular scaffolds has profound effects on their biological activities. The discovery of molecular chirality was made in 1848 by Louis Pasteur, with the observation that sodium ammonium para-tartrate crystallized in arrays that mirrored each other and rotated light in equal amount but opposite directions.[75-77] The discovery of chirality not only impacted the way chemists thought about molecular structure and synthesis. The understanding of handedness in biological systems – from small molecule compounds showing biological activity to cellular machinery such as proteins and DNA, and the resulting interactions – has deep implications in the way chemical synthesis and health sciences intertwine.

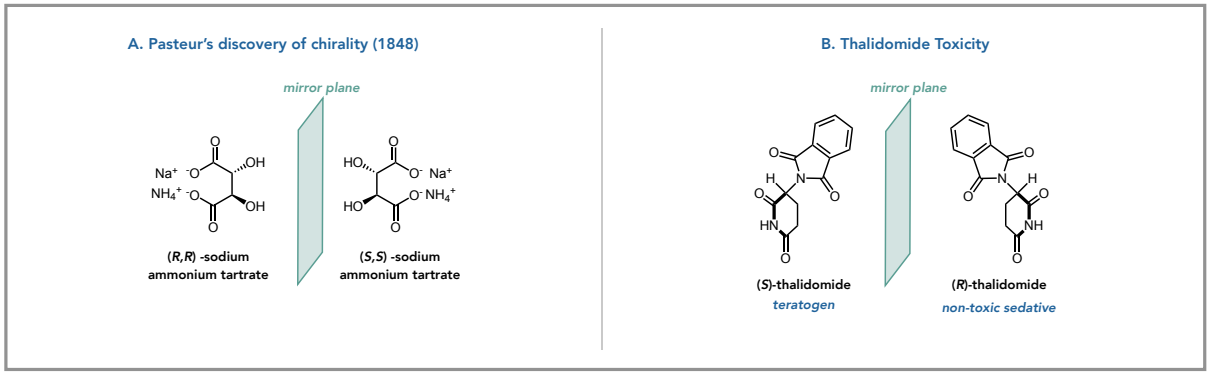



Figure 5 : A) Discovery of chirality by Paster in 1848. B) *(R)*- and *(S)*-thalidomide.

The notorious case of Thalidomide in the 1950s remains an unfortunate reminder and classroom example of the importance of stereochemistry in biologically active compounds.[78,79] First marketed over-the-counter in Germany as a racemic mixture indicated for the management of pregnancy symptoms such as morning sickness and insomnia, it's use led to an estimated 10,000 affected infants, of which 40% did not survive, leaving the others with significant birth defects.[80,81] The teratogenicity of racemic Thalidomide was shown to not be limited to its use during pregnancy, and could affect both male and female reproductive health.[82] Thousands of studies aiming to understand the biological basis for the toxicity Thalidomide were published by the 2000s.[83] Although a conclusion has not yet been reached on the exact biological mechanism of action, it was demonstrated early on that only one of the enantiomers, (S)-Thalidomide, is teratogenic, while (R)-Thalidomide acts as a sedative without strong indications of adverse effects on reproductive health.[84]

The tragedy of Thalidomide, despite its unfortunate consequences, has one silver lining. It led to the development of much stricter regulatory policies in many countries to ensure the safety and efficacy of drug candidates through extensive preclinical and clinical trials from the early stages of candidate compound discovery to synthetic route development and purity assessments.[85,86] The ability to selectively setting stereocenters in small molecules has become particularly important for the pharmaceutical, agrochemical and fragrance industries, all of which heavily rely on exact interactions and "fit" between compounds and biological targets such as receptors, enzymes, and proteins *in vivo*. Asymmetric catalysis encompasses current methods to do so and an ever more widening body of research targeting the development of new techniques and the deepening of our understanding of the chemical principles and interactions governing enantioselective reactions.

Although the initial formation of chiral molecules is still a mystery and source of debate in the scientific community,[87] the dependance of life on these chiral centers point to the first, original enantioselective catalysts: enzymes. While biocatalysis is a relatively young field within synthetic organic chemistry, the structure and reactivity of enzymes has been a rich source of inspiration to chemists hoping to induce selectivity in chemical reactions. The ability of enzymes to catalyze chemical transformations in a highly selective and efficient manner can be assigned to a multitude of factors, notably the fit of the binding pockets around their active sites and the multiple

stabilizing interactions between amino acids in those active sites and the transition states. These features allow enzymes to be incredibly specific with regards to the substrates that they bind, the orientation in which they bind those substrates, the selectivity of the transformation they perform, and the rapid rates at which they perform.[88] Conceptually, the principles governing the selectivity of enzymatic reactions is the same as those governing the designs of selective small-molecule catalysts: lowering the energetic costs of a desired pathways, and raising that of undesired pathways.

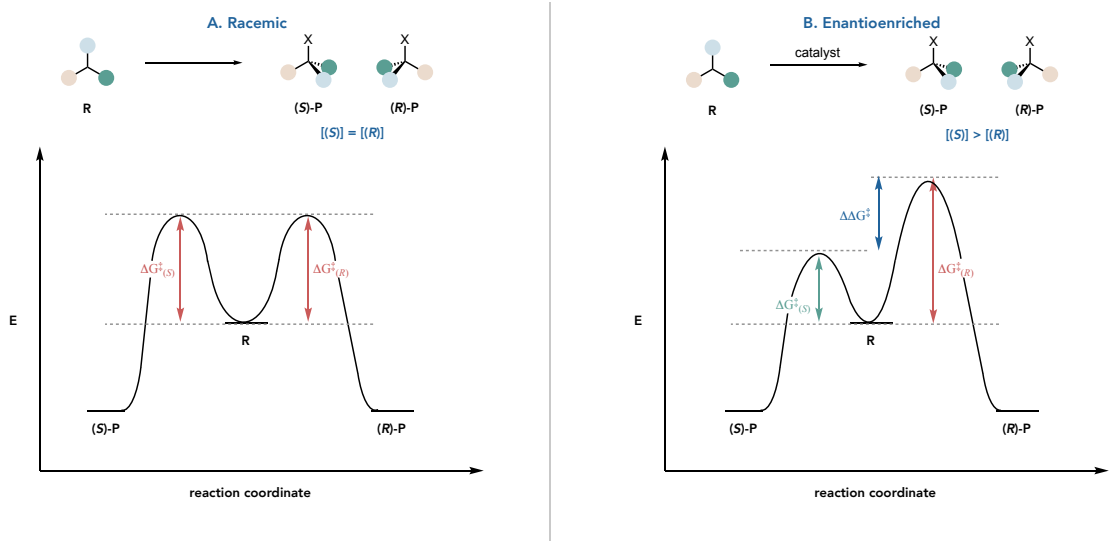



Figure 6 : Reaction coordinate for an unselective reaction yielding racemic product. B) Reaction coordinate for an enantioselective reaction.

Enantioselectivity, similarly to regioselectivity, can be understood from physical organic chemistry as a competition between reaction rates.[89] Under uncatalyzed and unselective reaction conditions, enantiomeric products have equal thermodynamic properties, and the activation energies leading to the transition states of either product are equal. As such, no preference is shown for one of the enantiomers and the product mixture would be a racemic, 50:50 ratio of both. Asymmetric catalysis aims to bias this ratio towards a desired enantiomer. While the thermodynamics of the enantiomeric products remains the same regardless of the reaction conditions, inclusion of a catalyst can induce a change in the reaction rates of one or both pathways leading to products: by lowering the $\Delta G^{\ddagger}$ of one, raising the other, or a combination of the two. This introduces asymmetry in the reaction's potential energy surface and biases the product ratio towards one enantiomer over the other correlated to the difference in activation energy between the two pathways ($\Delta\Delta G^{\ddagger}$) (Figure 6)[32]

The first successful application of these principles in homogeneous catalysis are owed to Knowles's groundbreaking study of hydrogenation reactions catalyzed by transition-metals using Mislow's chiral phosphine ligands in combination with Wilkinson's rhodium catalyst in 1968 (Figure 7, A).[90,91] Although the enantioselectivity demonstrated in this initial report was modest (57.5:42.5 er), it was a proof of concept which led to the launch of an entire area of chemical

research. The landmark synthesis of L-DOPA by Monsanto in 1977 demonstrated the applicability of this discovery and its importance in all branches of chemical research (Figure 7, B).[92,93]

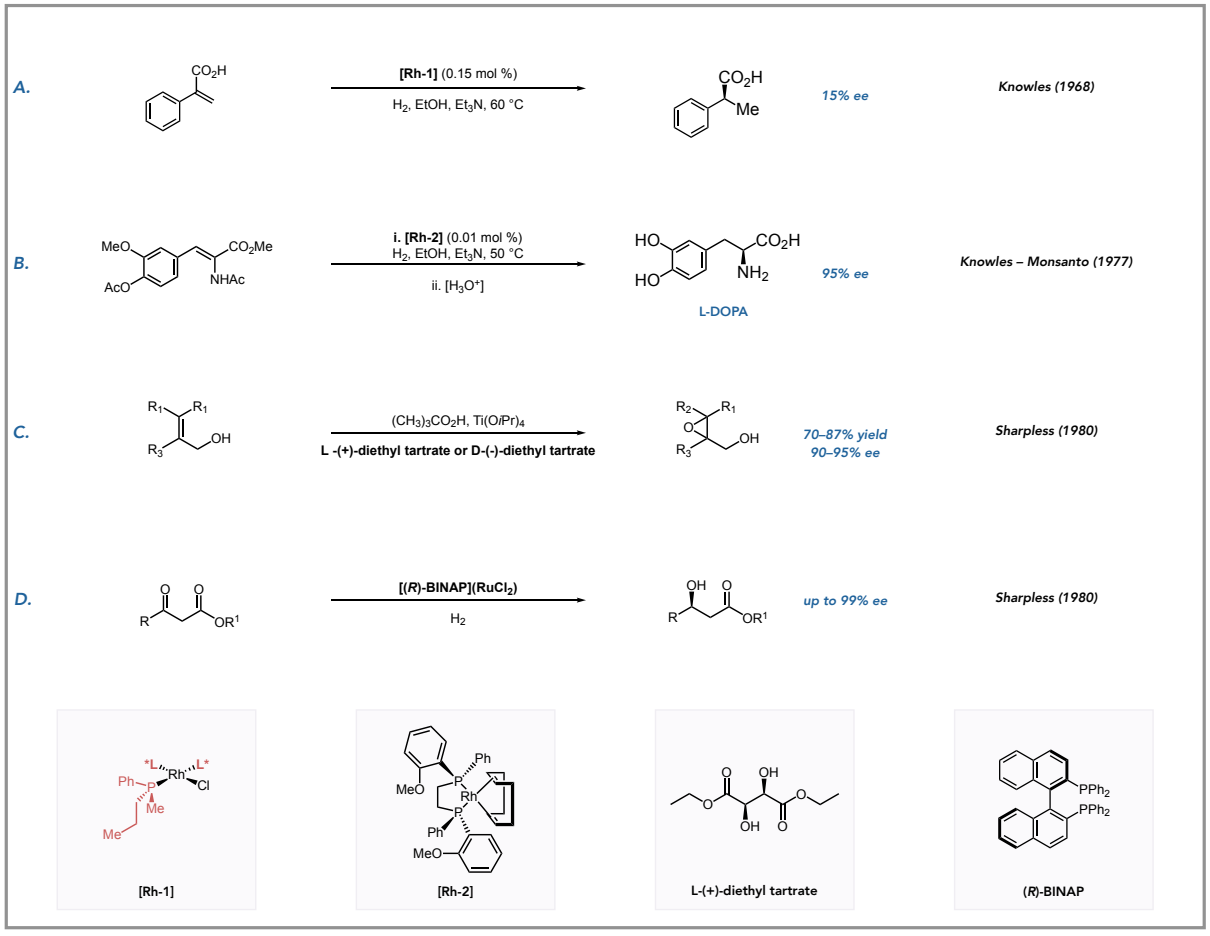



Figure 7 : A) Initial proof of concept by Knowles. B) Monsanto synthesis of L-DOPA. C) Sharpless epoxidation of allylic alcohols. D) Noyori's asymmetric hydrogenation of $\beta$-ketoesters.

These initial developments of asymmetric catalysis were followed by an explosion of innovation and mechanistic studies in the field. In 1980, Sharpless and co-workers disclosed a method for asymmetric epoxidation of allylic alcohols using $Ti(OiPr)_4$ and deriving chiral information from the (R,R)-diethyl tartrate and (S,S)-diethyl tartrate (Figure 7, C).[94] This was followed shortly thereafter by Noyori's syntheses of bidentate phosphine ligands such as BINAP enabled the demonstration of asymmetric hydrogenations on β-ketoesters to yield chiral alcohols in 1987 (Figure 7, D).[95] These landmark studies were awarded the Nobel Prize in Chemistry in 2001 for Knowles's, Noyori's, and Sharpless's development of and contributions to asymmetric catalysis.

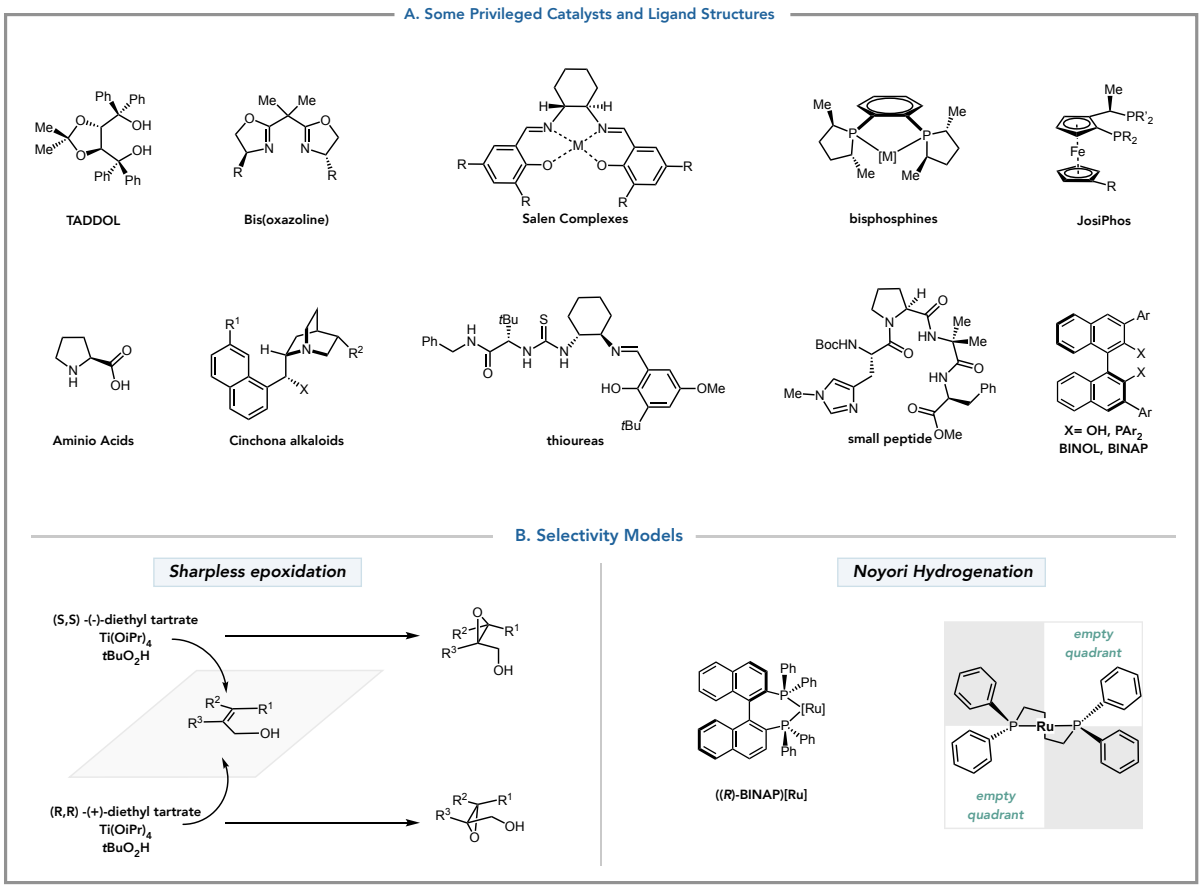



Figure 8 : Examples of privileged catalysts and ligands used in asymmetric catalysis. B) Common selectivity models for chiral induction.

Since the 1970s, chemists have endeavored to develop chiral ligands and catalysts for a wide range of reactions. Large libraries of chiral phosphine ligands are now readily available for efficient screening of chiral transition metal catalysts. Some ligands and catalysts have even proved themselves to be competent in diverse reactions independent of modes of activations or mechanism. These structures have been deemed "privileged" and are often the starting point of catalyst optimization studies (Figure 8).[96,97] Of those privileged structures, many were originally made or inspired by nature. Cinchona alkaloids, for examples, are naturally-occurring small molecule organocatalysts which have shown great selectivity in a surprising number of nantioselective transformations.[98] Bis(oxazoline) and Salen-type ligands were designed to imitate structural features from the active sites of vitamin $B_{12}$ and heme porphyrins of P-450 enzymes.[99] TADDOL was synthesized from tartrate, one of the most readily available and affordable chiral starting material.[96] Even single amino acids such as proline and its derivatives have been reported to efficiently induce enantioselectivity in a range of transformations.[100-102] In recent years, urea, thiourea, and small peptides have also been exploited for their extensive hydrogen bonding abilities enabling efficient chirality transfer.[103-105] Privileged BINOL and BINAP-based ligands and catalysts, along with diphosphine (JosiPhos-type) ligands[106,107] are perhaps the exception in the fact that they were entirely man-made and designed. However, their axial chirality – due to the hindered

rotation about the aryl bond – has made those structures staples in asymmetric catalysis, leading to the wide diversification of their structures by elaboration on the standard backbones.

Both qualitative and quantitative models have been generated to enable the rationalization, and sometimes prediction, of enantioselectivity based on both chemical intuition and an understanding of the underlying interactions driving the selectivity.[108,109] For the most part, these models rely on an understanding of steric and electronic features of the catalyst's structures and possible non-covalent interactions it can have with substrates to orient the transition state geometry to favor one enantiomer over the other. In the case of the asymmetric hydrogenations developed by Noyori, for example, selectivity was proposed to arise from an increase in steric repulsion between the catalyst ligand and the substrate in the transition state leading to the minor enantiomer. This rationalization can be visualized as the axial chirality of the catalyst generating quadrants around the metal center, forcing the substrate to position itself in the open (sterically unhindered) quadrants (Figure 8, B).[110,111] This yields degenerate, diastereomeric transition states for the two enantiomers, and therefore an kinetic preference for one over the other.

The arc of synthetic organic chemistry has thus far enabled the elaboration of more and more complex structures, multi-component synthetic methods, and highly tailored catalyst structures to address the ever-changing needs of the industries relying on more efficient, selective methods. As the needs for efficiency and specificity increases, principles of physical organic chemistry and a more detailed mechanistic understanding of interactions and mechanisms have become increasingly necessary to guide chemists' creativity for the development of novel transformations. The drastic technological advancements of the 20th and 21st century – accompanied by a multitude of new quantitative tools for chemistry – have supported these endeavors in situations where reliance on qualitative chemical intuition alone is not sufficient to rationalize or predict selectivity.

## 2.3. Tools and Recent Innovations in Catalysis and Selectivity

Transition state analysis is nowadays one of the more popular ways to analyze potentially significant interactions throughout reaction coordinates. Originating from seminal work by Eyring,[112,113] Transition State Theory (TST) aims to provide a straightforward method to formulate reaction rates and provide mechanistic insights based on thermodynamic, kinetic, and statistical mechanical concepts.[114] In Eyring's Transition State Theory, the rate of a simple reaction can be predicted from the energy barrier leading to the transition state, Gibbs Free Energy of Activation ($\Delta G^{\ddagger}$).

$$k = \kappa \frac{k_B T}{h} e^{-\frac{\Delta G^{\ddagger}}{RT}} \qquad \textbf{(eq. 2)}$$

$\boldsymbol{k}$: rate constant; $\kappa$: transmission coefficient; $\boldsymbol{k_B}$: Boltzmann constant; $\boldsymbol{h}$: Planck constant

$\boldsymbol{R}$: Gas constant; $\boldsymbol{T}$: Temperature; $\boldsymbol{\Delta G^{\ddagger}}$: Gibbs Free Energy of Activation

While the multidimensional potential energy surface describing chemical reactions can be quite complex, TST enables the extrapolation of ground state characteristics such as electronic, steric, and electrostatic features of a given chemical system to qualitatively assess the nature of transition states along the reaction's path by relying on key assumptions and statistical distributions such as the Boltzmann distribution. Multiple theories building on and refining the concepts of TST

have emerged since Eyring's original reports, thereby expanding the field of modern quantum chemistry, including but not limited to work from Marcus and Rice,[115,116] Magee,[117] and many others**.**

Data-driven methods have emerged out of the field of physical organic chemistry as important tools to understand and predict structure-reactivity relationships.[32,118-120] The seminal publication in 1935 by Hammett describing linear free energy relationships (LFERs) could be named as the starting point for the development of modeling tools in organic chemistry.[121] The concept of LFERs was first used to describe, using simple mathematical equations, the relationship between the structure of substituted benzoic acids and their ionization in water, with the introduction of the first molecular descriptor, *σ,* denoting the structural characteristic of the aryl substituent (Figure 9, A)(**eq 3**). More specifically for the Hammett parameter, *σ* represents the electronic contribution of these substituents, with *σ* values less than zero corresponding to substituents that are more electron donating than a hydrogen while substituents with *σ* values greater than zero are more electron withdrawing.[9]

$$\log\left(\frac{K_X}{K_H}\right) = \rho\sigma_X \qquad \textbf{(eq. 3)}$$

One particularly significant aspect of the Hammett study is that it allowed the line between thermodynamics and kinetics to be blurred. Intuitively falling out of the Hammond postulate[122] is the idea that a reaction that is more exothermic (thermodynamically favorable) *"should"* proceed faster (with a higher rate constant) due to the resemblance of the transition state to the intermediate it is closest to energetically. The Hammett parametrization of benzoic acid ionization of water provided backing for this intuition by mathematically relating the rate constants to the thermodynamic parameter *σ* with ϱ being the sensitivity factor for each reaction (Figure 9).

These two terms taken together provide meaningful mechanistic insight into the reaction at hand. For negative ϱ values, the rate of the reaction increases with the electron donating ability of the substituent. This suggests that positive charge is building up in the transition state. On the other hand, positive ϱ values indicate that the transition state is stabilized in the presence of electron withdrawing substituents, suggesting a build-up of negative charge. Breaks in mechanisms or changes in the rate determining steps of the reaction are typically observed as breaks or changes in the slope of the corresponding Hammett plot.

Numerous follow up studies over the course of the 20th century since the first report of the Hammett study of benzoic acid dissociation have shown the relationship between known, established reaction parameters and the rates of reactions in new chemical systems.[32,123-129] In an effort to describe both steric and electronic contributions from substituents, Taft and co-workers released a series of reports describing new linear free energy relationships for steric parameters based on the rate of hydrolysis of methyl esters.[123,125] Linear free-energy relationships for factors such as solvent effects (Grunwald-Winstein),[130] nucleophilicity (Swain-Scott, Mayr),[131,132] and basicity (Brønsted),[133] amongst others, were developed thereafter, demonstrating the power of LFER to provide mechanistic insights based on the thermodynamic features of the chemical system at hand. As more complex chemical reactions became of interest in parametrization, simple, single parameter (*univariate*) models became inadequate to accurately capture the interactions at play, which led to the emergence of multiparameter modeling approaches to the study of structure-activity relationships.[134]

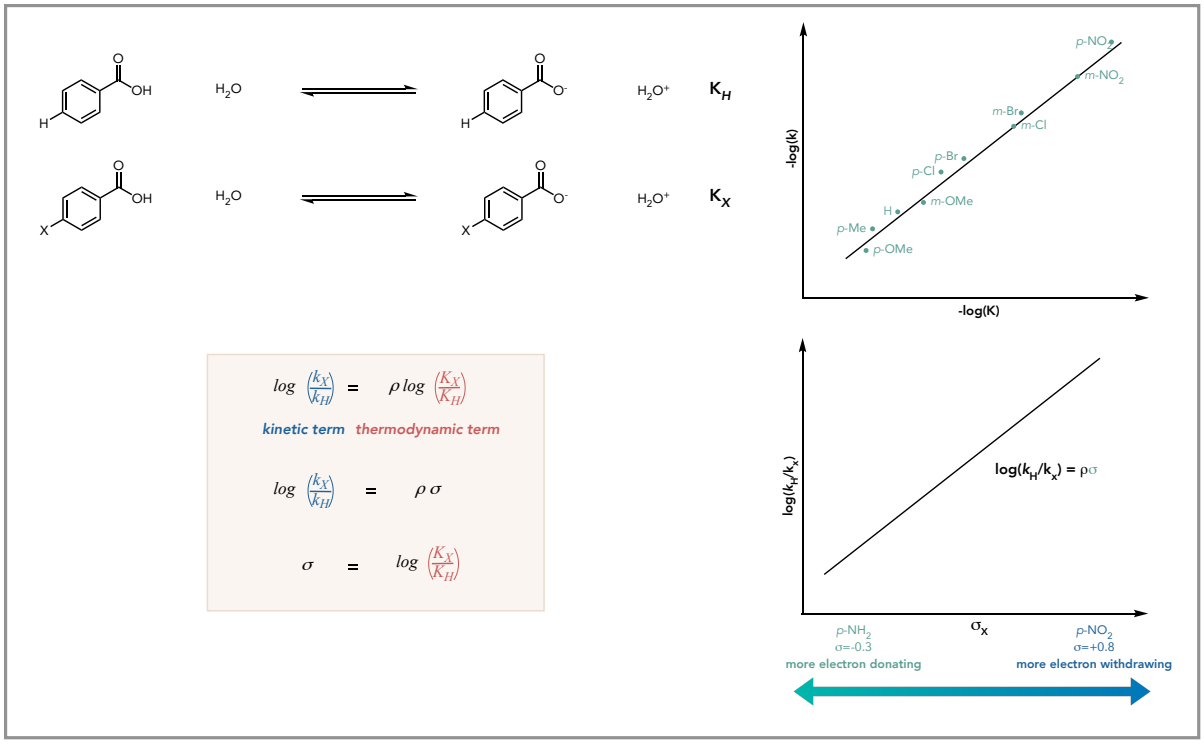



**Figure 9** : A) Hammett Relationship for the ionization of benzoic acid. B) Some examples of commonly used molecular descriptors.

For most reactions applicable to the current academic and industrial research landscape, it can be challenging to deconvolute the contributions of various elements that can control catalytic efficiency and simplify an equation to a single representative parameter. Swain and Lupon began to address this limitation of univariate regression by decoupling two electronic parameters, induction (F), and resonance (F) (**eq. 4**).[135] This led them to propose a linear combination of terms to describe electronic substituent effects on reaction rates. This approach was quickly adopted in various mechanistic studies, combining established parameters for steric and electronic features, but also describing new, updated parameters such as the use of carbonyl vibrational frequencies,[136] or C–H bond dissociation energies[137-139] to provide in-depth mechanistic insight into established and novel reactions.

$$\log\left(\frac{k_{\mathrm{X}}}{k_{\mathrm{H}}}\right) = f\mathrm{F} + r\mathrm{R} \qquad \textbf{(eq. 4)}$$

Technological advances have aided the application of these methods to larger data sets and increasingly more complex chemical systems. Supercomputing made its way into chemical research in the 1980s, allowing the parallelization of computational tasks to rapidly obtain computational results sometimes faster than experimental data.[140,141] The constant technological advances of the past century have tremendously expanded the ability of chemists to understand, predict, and customize catalyst structures and reactivity to their specific needs. In particular, non-covalent interactions have been shown to significantly influence the transition state geometries and energies and therefore catalytic efficacy.[142] These interactions are challenging to predict due

to their dependence on multiple factors such as solvents, temperature, additives in the reaction mixtures etc.[143] Poor understanding of these subtle effects can be prohibitive for efficient reaction and catalyst optimization, in which the traditional "single variable modification" experimental methods can often overlook important cooperative effects.[144-146]

Although modern quantum chemistry, boosted by the impressive technological advances of the past century, has witnessed widespread success in organic synthesis and catalysis, its applications have in majority been limited to rationalizing – posteriori – the efficiency and/or selectivity of a given reaction, leaving the optimization of conditions and catalyst structure to be addressed experimentally.[147] The main limiting factor for the application of transition state analysis for predictive analysis and reaction optimization stems from the prohibitively high cost and effort necessary to perform high level calculations on the large data sets required for these applications. Indeed, these calculations are often complicated by the multitude of possible transition state conformations for each mechanistic possibility for any given elementary step. In the context of stereochemical selectivity, the process to obtain reliable stereochemical predictions would involves extensive minimization of transition state geometries for each different combination of substrate and catalyst. For systems containing more than a handful of catalysts or substrates, this process quickly becomes time consuming and computationally costly. Aiming to address these limitations, methods and softwares such as AFIR (artificial force induced reaction),[148-151] AARON (An Automated Reaction Optimizer for New catalysts),[147] and automated high-throughput transition state searching tools (AutoTST),[152,153] have been designed to facilitate the determination of approximated transition state structures.[154-156] While these methods are showing much promise in the continued adoption of transition state analysis and quantum chemistry to computationally guided optimization of reaction conditions and catalyst structure optimization, they still often remain more costly and work intensive than established experimental methods routinely used in industrial settings such as High Through-Put Experimentation (HTE) or Design of Experiment (DOE).The adoption of high-throughput experimentation came relatively late in the field of synthetic chemistry compared to other disciplines such as biology.[157] It has however been broadly adopted today, especially in industry where it has proved itself an indispensable asset to both medicinal and process chemistry.[158,159] In the context of data-science driven approaches to solving chemical challenges, larger data sets and HTE enabled the solidification of both qualitative and quantitative analytical methods and learning algorithms facilitating the understanding of structural and mechanistic features in a wide variety of chemical research endeavors.[157,160-165]

Data science-driven workflows allow the interrogation of multiple reaction components simultaneously to provide a more holistic understanding of the mechanistic and structural features driving the efficiency of catalysis, especially subtle non-covalent interactions which might not present themselves as noticeably to human cognitive recognition abilities.[145] From the first reported application of artificial intelligence and machine learning algorithms to chemical challenges in the late 1960s by Lederberg, Jurs, and Kowalski, subdisciplines such have chemometrics and cheminformatics have emerged to specialize in the refinement of computational resources for chemical research.[166-172] Since then, tools such as multidimensional linear regressions (MLR) and classifications (threshold analysis) and logistics regressions have been popularized in chemistry research over the last few decades to address the high costs of performing either fully experimentally guided or transition state analysis guided reaction optimizations by replacing them with ground state calculations combined with smaller experimental data sets.[118,160]

## III. Conclusions

The prognostics made by Seebach in 1990 on the future of synthetic chemistry have so far been spot on.[13] As new challenges present themselves to address the needs for more diverse drug candidates, safer agrochemicals, and more efficient process designs, chemists have had to constantly innovate on the fundamental principles of chemistry. Enlisting tools from neighboring disciplines to answer the questions at hand and uncover the next ones, the chemical sciences are now more interdisciplinary than ever, benefitting from expertise and creativity from mathematics, data-science, biology, or physics to move the field up and forward every day.

The research work described herein aims to utilize the foundations of physical organic chemistry and computational tools to address contemporary challenges in synthetic methodology. Chapter 2 will focus on the development of a new class of phosphoric acid catalysts and the application of statistical modeling to understanding the effects of flexibility and non-covalent interactions on reaction efficiency and selectivity. Chapter 3 will present the use of machine learning to solve complex challenges in the regioselective synthesis of N-methyl-pyrazoles. Lastly, the fourth chapter will interrogate the implications of ligand and metal identity in homogeneous bimetallic catalysis.

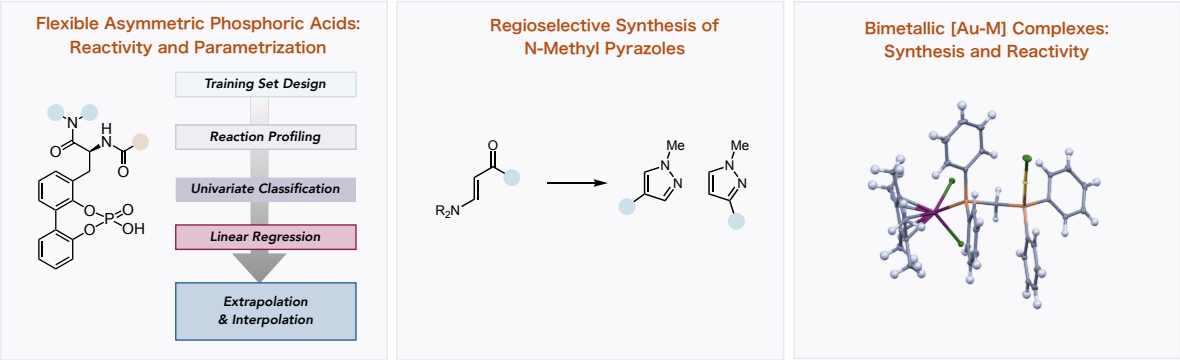



Figure 10 : Overview of the research projects covered in the following chapters.

## IV. References


1. Wöhler, F. (1828). Ueber künstliche Bildung des Harnstoffs. Annalen der Physik *88*, 253–256.
2. Kekulé, A. (1857). Ueber die s. g. gepaarten Verbindungen und die Theorie der mehratomigen Radicale. Annalen der Chemie und Pharmacie *104*, 129–150.
3. Strecker, A. (1850). Ueber die künstliche Bildung der Milchsäure und einen neuen, dem Glycocoll homologen Körper. Justus Liebigs Ann. Chem. *75*.
4. V. von Richter. aus St. Petersburg am 17. October 1869. (1869). Ber. Dtsch. Chem. Ges. *2*, 552–554.
5. Kane, R. (1838). Ueber den Essiggeist und einige davon abgeleitete Verbindungen. J. Prakt. Chem *15*, 129–155.
6. Wurtz, C.A. (1872). Sur un aldéhyde-alcool. Bull. Soc. Chim. Fr. *17*, 436–442.
7. Wallach, O. (1910). Alicyclic Compounds Nobel Lecture.
8. Wieland, H. (1927). The Chemistry of Bile Acid. Nobel Lecture.
9. Fischer, E. (1902). Syntheses of Purine and Sugar Group. Nobel Lecture.
10. Ruzicka, L. (1939). Multimembered Rings, Higher Terpene Compounds and Male Sex Hormones. Nobel Lecture.
11. Windaus, A. (1928). Constitution of Sterols and Their Connection with Other Substances Occurring in Nature. Nobel Lecture.
12. Haworth, N., and Karrer, P. (1937). Carotenoids, Flavins and Vitamin A and B2. Nobel Lecture.
13. Seebach, D. (1990). Organic Synthesis – Where Now? Angew Chem Int Ed Engl *29*, 1320–1367.
14. Whitesides, G.M. (2018). Complex Organic Synthesis: Structure, Properties, and/or Function? Isr. J. Chem. *58*, 142–150.
15. Nicolaou, K.C., and Sorensen, E.J. (1996). Classics in Total Synthesis: Targets, Strategies, Methods (Wiley).
16. Woodward, R.B. (1965). Recent Advances in the Chemistry of Natural Products. Nobel Lecture.
17. Corey, E.J. (1991). The Logic of Chemical Synthesis: Multistep Synthesis of Complex Carbogenic Molecules (Nobel Lecture). Angew Chem Int Ed Engl *30*, 455–465.
18. Nicolaou, K.C., Vourloumis, D., Winssinger, N., and Baran, P.S. (2000). The Art and Science of Total Synthesis at the Dawn of the Twenty-First Century. Angew Chem Int Ed Engl *39*, 44–122.
19. Suh, E.M., and Kishi, Y. (1994). Synthesis of Palytoxin from Palytoxin Carboxylic Acid. J. Am. Chem. Soc. *116*, 11205–11206.
20. Corey, E.J., and Cheng, X.-M. (1989). The logic of chemical synthesis (Wiley).
21. Yan, B., Zhang, B., and Czarnik, A.W. (2009). Analytical Methods in Combinatorial Chemistry, 2 Edition (Taylor & Francis Group).
22. Bohacek, R.S., McMartin, C., and Guida, W.C. (1996). The Art and Practice of Structure-Based Drug Design: A Molecular Modeling Perspective. Med. Res. Rev. *16*, 3–50.
23. Shapiro, N.D., and Toste, F.D. (2010). A Reactivity-Driven Approach to the Discovery and Development of Gold-Catalyzed Organic Reactions. Synlett *5*, 675–691.
24. Ihde, A.J. (1984). The Development of Modern Chemistry (Dover Publications, Inc.).

25. Fourcroy, A.F. (1797). Sur Trois Espèces Différentes de Gaz Hydrogène, Retirées de l'Éther et de l'Alcool par Différents Procédés, Envoyés à l'Institut par la Société des Chimistes Hollandais. Ann. Chim. *21*, 48–71.
26. Davy, H. (1806). The Bakerian Lecture on Some Chemical Agencies of Electricity Phil. Trans. *97*, 1–56.
27. Wisniak, J. (2010). The History of Catalysis. From the Beginning to Nobel Prizes. Educ. Quím. *21*, 60–69.
28. Berzelius, J.J. (1836). Quelques Idées sur une Nouvelle Force Agissant Dans les Combinaisons des Corps Organiques. Ann. Chim. *61*, 146–151.
29. Mejía, E. (2020). Introduction: Catalysis, Oxygen and Sustainability … Quo vadis? In Catalytic Aerobic Oxidations, E. Mejía, ed. (Royal Society of Chemistry). 10.1039/9781839160332.
30. Ostwald, W. (1920). Das große Elixier. Die Wissenschaftslehre (Dürr & Weber G.m.b.H.).
31. Ostwald, W. (1909). On Catalysis. Nobel Lecture.
32. Anslyn, E.V., and Dougherty, D.A. (2006). Modern Physical Organic Chemistry (University Science Books).
33. Catlow, C.R., Davidson, M., Hardacre, C., and Hutchings, G.J. (2016). Catalysis making the world a better place. Phil. Trans. R. Soc. A *374*, 20150089.
34. Sheldon, R.A. (2000). Atom efficiency and catalysis in organic synthesis. Pure Appl. Chem. *72*, 1233–1246.
35. Baerns, M. (2010). Basic Principles in Applied Catalysis (Springer Berlin Heidelberg).
36. Ertl, G. (2008). Reactions at Surfaces: From Atoms to Complexity (Nobel Lecture). Angew. Chem. Int. Ed. Engl. *47*, 3524–3535.
37. Wender, P., Poliakoff, M., Kiessling, L., Alvisatos, P., Wooley, K., Meijer, E.W.B., King, D., Aizenberg, J., and Fleming, G. (2011). What lies ahead. Nature *469*, 23–25.
38. Sabatier, P. (1912). The Method of Direct Hydrogenation by Catalysis. Nobel Lecture.
39. Bosch, C. (1908) Process of producing ammonia.
40. Haber, F. (1905). Thermodynamik technischer Gasreaktionen, 1st ed. Edition (Salzwasser Verlag).
41. Haber, F. (1920). The Synthesis of Ammonia from Its Elements. Nobel Lecture.
42. Ziegler, K. (1963). Consequences and Development of an Invention. Nobel Lecture.
43. Natta, G. (1963). From the Stereospecific Polymerization to the Asymmetric Autocatalytic Synthesis of Macromolecules. Nobel Lecture.
44. Osborn, J.A., Jardine, F.H., Young, J.F., and Wilkinson, G. (1966). The preparation and properties of tris(triphenylphosphine)halogenorhodium(I) and some reactions thereof including catalytic homogeneous hydrogenation of olefins and acetylenes and their derivatives. J. Chem. Soc. A, 1711–1732
45. Fischer, E.O. (1955). Metallverbindungen des Cyclopentadiens und des Indens. Angew. Chem. *67*, 210–214.
46. Fischer, E.O. (1973). On the Road to Carbene and Carbyne Complexes. Nobel Lecture.
47. Wilkinson, G. (1973). The Long Search for Stable Transition Metal Alkyls. Nobel Lecture.
48. Hartwig, J.F. (2009). Organotransition Metal Chemistry: From Bonding to Catalysis (University Science Book).

49. MacMillan, D.W.C. (2008). The advent and development of organocatalysis. Nature *455*, 304–308.
50. Jacobsen, E.N., and MacMillan, D.W.C. (2010). Organocatalysis. PNAS *107*, 20618–20619.
51. Kampen, D., Reisinger, C.M., and List, B. (2010). Chiral Brønsted acids for asymmetric organocatalysis. Top. Curr. Chem. *291*, 395–456.
52. Pyser, J.B., Chakrabarty, S., Romero, E.O., and Narayan, A.R.H. (2021). State-of-the-Art Biocatalysis. ACS Cent. Sci. *7*, 1105–1116.
53. Hughes, G., and Lewis, J.C. (2018). Introduction: Biocatalysis in Industry. Chem. Rev. *118*, 1–3.
54. Arnold, F.H. (2018). Directed Evolution: Bringing New Chemistry to Life. Angew. Chem. Int. Ed. Engl. *57*, 4143–4148.
55. Sheldon, R.A., and Woodley, J.M. (2018). Role of Biocatalysis in Sustainable Chemistry. Chem. Rev. *118*, 801–838.
56. Dehovitz, J.S., Loh, Y.Y., Kautzky, J.A., Meichan, A.J., Yamauchi, M., MacMillan, D.W.C., and Hyster, T.K. (2020). Static to inducibly dynamic stereocontrol: The convergent use of racemic β-substituted ketones. Science *369*, 1113–1118.
57. Shaw, M.H., Twilton, J., and MacMillan, D.W.C. (2016). Photoredox Catalysis in Organic Chemistry. J. Org. Chem. *81*, 6898–6926.
58. Chan, A.Y., Perry, I.B., Bissonette, N.B., Buksh, B.F., Edwards, G.A., Frye, L.I., Garry, O.L., Lavagnino, M.N., Li, B.X., Liang, Y., et al. (2022). Metallaphotoredox: The Merger of Photoredox and Transition Metal Catalysis. Chem. Rev. *122*, 1485–1542.
59. Murray, P.R.D., Cox, J.H., Chiappini, N.D., Roos, C.B., McLoughlin, E.A., Hejna, B.G., Nguyen, S.T., Ripberger, H.H., Ganley, J.M., Tsui, E., et al. (2022). Photochemical and Electrochemical Applications of Proton-Coupled Electron Transfer in Organic Synthesis. Chem. Rev. *122*, 2017–2291.
60. Kang, K., Loud, N.L., DiBenedetto, T.A., and Weix, D.J. (2021). A General, Multimetallic Cross-Ullmann Biheteroaryl Synthesis from Heteroaryl Halides and Heteroaryl Triflates. J. Am. Chem. Soc. *143*, 21484–21491.
61. Palkowitz, M.D., Laudadio, G., Kolb, S., Choi, J., Oderinde, M.S., Ewing, T.E.-H., Bolduc, P., Chen, T., Zhang, H., Cheng, P.T.W., et al. (2022). Overcoming Limitations in Decarboxylative Arylation via Ag-Ni Electrocatalysis. ChemRxiv *Preprint 2022*.
62. Trost, B.M. (1985). Sculpting Horizons in Organic Chemistry. Science *227*, 908–916.
63. Trost, B.M. (1991). The Atom Economy — A Search for Synthetic Efficiency. Science *254*, 1471–1477.
64. Wender, P.A., and Miller, B.L. (2009). Synthesis at the Molecular Frontier. Nature *460*, 197–201.
65. Gaich, T., and Baran, P.S. (2010). Aiming for the Ideal Synthesis. J. Org. Chem. *75*, 4657–4673.
66. Markovnikov, W. (1870). Ueber die Abhängigkeit der verschiedenen Vertretbarkeit des Radical wasserstoffs in den isomeren Buttersäuren. Annalen der Pharmacie *153*, 228–259.
67. Baldwin, J.E. (1976). Rules for ring closure. Chem. Commun. *18*, 734–736.
68. Baldwin, J.E. (19976). Approach vector analysis: a stereocheical approach to reactivity. Chem. Commun. *18*, 738–741.

69. Baldwin, J.E., Cutting, J., Dupont, W., Kruse, L., Silberman, L., and Thomas, R.C. (1976). 5-Endo-trigonal reactions: a disfavoured ring closure. Chem. Commun. *18*, 736–738.
70. Bürgi, H.B., Dunitz, J.D., Lehn, J.M., and Wipff, G. (1974). Stereochemistry of reaction paths at carbonyl centres. Tetrahedron *30*, 1563-1572.
71. Chérest, M., Felkin, H., and Prudent, N. (1969). orsional strain involving partial bonds. The stereochemistry of the lithium aluminium hydride reduction of some simple open-chain ketones Tetrahedron *9*, 2199–2204.
72. Anh, N.T., and Eisenstein, O. (1977). Theoretical interpretation of 1-2 asymmetric induction. The importance of antiperiplanarity. Nouv. J. Chim. *1*, 61–70.
73. Zimmerman, H.E., and Traxler, M.D. (1957). The Stereochemistry of the Ivanov and Reformatsky Reactions. I. J. Am. Chem. Soc. *79*, 1920–1923.
74. Seeman, J.I. (1983). Effect of Conformational Change on Reactivity in Organic Chemistry. Evaluations, Applications, and Extensions of Curtin-Hammett/Winstein-Holness Kinetics. . Chem. Rev. *83*, 83–134.
75. Pasteur, L. (1848). Ann. Chim. Phys. Sér. 3 *24*, 442–459.
76. Pasteur, L. (1848). Mémoire sur la relation qui peut exister entre la forme cristal- line et la composition chimique, et sur la cause de la polarisation rotatoire. Comptes rendus hebdomadaires des séances de l'Académie des Sciences *26*, 535–538.
77. Gal, J. (2017). Pasteur and the art of chirality. Nature Chem. *9*, 604–605.
78. Tokunaga, E., Yamamoto, T., Ito, E., and Shibata, N. (2018). Understanding the Thalidomide Chirality in Biological Processes by the Self-disproportionation of Enantiomers. Sci. Rep. *8*, 17131.
79. Diggle, G.E. (2001). Thalidomide: 40 years on. Int. J. Clin. Pract. *55*, 627–631.
80. Miller, M.T. (1991). Thalidomide embryopathy: a model for the study of congenital incomitant horizontal strabismus. Trans. Am. Ophthalmol. Soc. *89*, 623–674.
81. Kim, J.H., and Scialli, A.R. (2011). Thalidomide: the tragedy of birth defects and the effective treatment of disease. Toxicol. Sci. *122*, 1–6.
82. Smith, S.W. (2009). Chiral toxicology: it's the same thing… only different. Toxicol. Sci. *110*, 4–30.
83. Stephens, T.D., Bunde, C.J., and Fillmore, B.J. (2000). Mechanism of action in thalidomide teratogenesis. Biochem. Pharmacol. *59*, 1489–1499.
84. Vargesson, N. (2015). Thalidomide-induced teratogenesis: history and mechanisms. Birth Defects Res. *105* (*Part C, Embryo Today*), 140–156.
85. Eichler, H.-G., Abadie, E., Baker, M., and Rasi, G. (2012). Fifty years after thalidomide; what role for drug regulators? Br. J. Clin. Pharmacol. *74*, 731–733.
86. Glauberman, S.P., and Hutt, P.B. (1997). The Real Thalidomide Baby: The Evolution Of The FDA In The Shadow of Thalidomide, 1960–1997. Food and Drug Law *Winter* (*Harvard Library. Office for Scholarly Communication.*).
87. Guijarro, A., and Yus, M. (2008). The Origin of Chirality in the Molecules of Life: A Revision from Awareness to the Current Theories and Perspectives of this Unsolved Problem (Royal Society of Chemistry).
88. Sheldon, R.A., Brady, D., and Bode, M.L.T. (2020). he hitchhiker's guide to biocatalysis: recent advances in the use of enzymes in organic synthesis. Chem. Sci. *11*, 2587–2605.
89. Clayden, J., Greeves, N., Warren, S., and Wothers, P. (2001). Organic Chemistry, 1st ed Edition (Oxford University Press).

90. Knowles, W.S., and Sabacky, M. (1968). Catalytic asymmetric hydrogenation employing a soluble, optically active, rhodium complex. J. Chem. Commun., 1445–1446.
91. Korpium, O., Lewis, R.A., Chickos, J., and Mislow, K. (1968). J. Am. Chem. Soc. *90*, 4842–4846.
92. Vineyard, B.D., Knowles, W.S., Sabacky, M.J., Bachman, G.L., and Weinkauff, D.J. (1977). J. Am. Chem. Soc. *99*, 5946–5952.
93. Knowles, W.S. (1986). Application of organometallic catalysis to the commercial production of L-DOPA. J. Chem. Educ. *63*, 222–225.
94. Katsuki, T., and Sharpless, K.B. (1980). The first practical method for asymmetric epoxidation. J. Am. Chem. Soc. *102* (*18*), 5974–5976.
95. Noyori, R., Ohkuma, T., Kitamura, M., Takaya, H., Sayo, N., Kumobayashi, H., and Akutagawa, S. (1987). Asymmetric hydrogenation of beta-keto carboxylic esters. A practical, purely chemical access to beta-hydroxy esters in high enantiomeric purity. J. Am. Chem. Soc. *109*, 5856–5858.
96. Yoon, T.P., and Jacobsen, E.N. (2003). Privileged Chiral Catalysts. Science *299*, 1691-1693.
97. Knowles, W.S. (2002). Asymmetric Hydrogenations (Nobel Lecture). Angew. Chem. Int. Ed. Engl. *41*, 1998-2007.
98. Kacprzak, K., and Gawroński, J. (2001). Cinchona Alkaloids and Their Derivatives: Versatile Catalysts and Ligands in Asymmetric Synthesis. Synthesis *7*, 961–998.
99. Katsuki, T. (2003). Some Recent Advances in Metallosalen Chemistry. Synlett *3*, 281–297.
100. List, B. (2002). Proline-catalyzed asymmetric reactions. Tetrahedron *58*, 5573–5590.
101. Eder, U., Sauer, G., and Wiechert, R. (1971). New type of asymmetric cyclization to optically active steroid CD partial stuctures. Angew. Chem. Int. Ed. Engl. *10*, 496–497.
102. Hajos, Z.G., and Parrish, D.R. (1974). Asymmetric synthesis of bicyclic intermediates of natural product chemistry. J. Org. Chem. *39*, 1615–1621.
103. Steppeler, F., Iwan, D., Wokaczyńska, E., and Wonjaczyński, J. (2020). Chiral Thioureas—Preparation and Significance in Asymmetric Synthesis and Medicinal Chemistry. Molecules *25*, 401.
104. Metrano, A.J., Chinn, A.J., Shugrue, C.R., Stone, E.A., Kim, B., and Miller, S.J. (2020). Asymmetric Catalysis Mediated by Synthetic Peptides, Version 2.0: Expansion of Scope and Mechanisms. Chem. Rev. *120*, 11479–11615.
105. Doyle, A.G., and Jacobsen, E.N. (2007). Small-Molecule H-Bond Donors in Asymmetric Catalysis. Chem. Rev. *107*, 5713−5743.
106. Ito, Y., Sawamura, M., and Hayashi, T. (1986). Catalytic asymmetric aldol reaction: reaction of aldehydes with isocyanoacetate catalyzed by a chiral ferrocenylphosphine-gold(I) complex. J. Am. Chem. Soc. *108*, 6405–6406.
107. Togni, A., Breutel, C., Schnyder, A., Spindler, F., Landert, H., and Tijani, A. (1994). A Novel Easily Accessible Chiral Ferrocenyldiphosphine for Highly Enantioselective Hydrogenation, Allylic Alkylation, and Hydroboration Reactions. J. Am. Chem. Soc. *116*, 4062–4066.
108. Alleman, C., Gordillo, R., Clemente, F.R., Cheong, P.H.-Y., and Houk, K.N. (2004). Theory of asymmetric organocatalysis of aldol and related reactions: rationalizations and predictions. Acc. Chem. Res. *37*, 558–569.

109. Bahmanyar, S., and Houk, K.N. (2001). The origin of stereoselectivity in proline-catalyzed intramolecular aldol reactions. J. Am. Chem. Soc. *123*, 12911–12912.
110. Ohta, T., Takaya, H., and Noyori, R. (1988). Bis(diarylphosphino)-1,1 binaphthyl (BINAP)-ruthenium(II) dicarboxylate complexes: new, highly efficient catalysts for asymmetric hydrogenations. Inorg. Chem. *27*, 566–569.
111. Noyori, R., Tokunaga, M., and Kitamura, M. (1995). Stereoselective Organic Synthesis via Dynamic Kinetic Resolution. Bull. Chem. Soc. Jpn. *68*, 36–55.
112. Rosentock, H.M., Wallenstein, M.B., Wahrhaftig, A.L., and Eyring, H. (1952). Absolute Rate Theory for Isolated Systems and the Mass Spectra of Polyatomic Molecules. PNAS *38*, 667–378. 10.1073/pnas.38.8.667.
113. Giddings, J.C., and Eyring, H. (1954). Equilibrium theory of unimolecular reactions. J. Chem. Phys. *22*, 538–542. 10.1063/1.1740102.
114. Laidler, K.J., and King, M.C. (1983). Development of transition-state theory. J. Phys. Chem. *87*, 2657−2664.
115. Marcus, R.A., and Rice, O.K. (1951). The Kinetics of the Recombination of Methyl Radicals and Iodine Atoms. J. Phys. Colloid Chem. *55*, 894–908.
116. Marcus, R.A. (1952). Unimolecular Dissociations and Free Radical Recombination Reactions. J. Chem. Phys. *20*, 359–364. 10.1063/1.1700424.
117. Magee, J.L. (1952). Theory of the Chemical Reaction Rate Constant. PNAS *38*, 764–770. 10.1073/pnas.38.9.764.
118. Varnek, A., and Baskin, I. (2011). Chemoinformatics as a Theoretical Chemistry Discipline. Mol. Inf. *30*, 20−32. 10.1002/minf.201000100.
119. de Almeida, A.F., Moreira, R., and Rodrigues, T. (2019). Synthetic Organic Chemistry Driven by Artificial Intelligence. Nat. Rev. Chem. *3*, 589−604.
120. Haywood, A.L., Redshaw, J., Gaertner, T., Taylor, A., Mason, A.M., and Hirst, J.D. (2020). Machine Learning in Chemistry: The Impact of Artificial Intelligence. In Machine Learning for Chemical Synthesis, (The Royal Society of Chemistry), pp. 169−194. 10.1039/ 9781839160233-00169.
121. Hammett, L.P. (1937). The Effect of Structure upon the Reactions of Organic Compounds. Benzene Derivatives. . J. Am. Chem. Soc. *59*, 96–103.
122. Hammond, G.S. (1955). A Correlation of Reaction Rates. J. Am. Chem. Soc. *77*, 334–338.
123. Taft, R.W. (1952). Polar and Steric Substituent Constants for Aliphatic and O-Benzoate Groups from Rates of Esterification and Hydrolysis of Esters. J. Am. Chem. Soc. *74*, 3120−3128.
124. Taft, R.W. (1952). Linear Free Energy Relationships from Rates of Esterification and Hydrolysis of Aliphatic and Ortho-Substituted Benzoate Esters. J. Am. Chem. Soc. *74*, 2729−2732.
125. Taft, R.W. (1953). Linear Steric Energy Relationships. J. Am. Chem. Soc. *75*, 4538−4539.
126. Taft, R.W., and Topsom, R.D. (2007). The Nature and Analysis of Substitutent Electronic Effects. Prog. Phys. Org. Chem. *16*, 1–83.
127. Hansch, C., Maloney, P.P., Fujita, T., and Muir, R.M. (1962). Correlation of Biological Activity of Phenoxyacetic Acids with Hammett Substituent Constants and Partition Coefficients. Nature *194*, 178−180.

128. Palucki, M., Finney, N.S., Pospisil, P.J., Güler, M.L., Ishida, T., and Jacobsen, E.N. (1998). The Mechanistic Basis for Electronic Effects on Enantioselectivity in the (Salen)Mn(III)-Catalyzed Epoxidation Reaction. J. Am. Chem. Soc. *120*, 948–954.
129. Hansch, C., Leo, A., and Taft, R.W. (1991). A Survey of Hammett Substituent constants and Resonance and Field Parameters. Chem. Rev. *91*, 165−195.
130. Grunwald, E., and Winstein, S. (1947). The Correlation of Solvolysis Rates. J. Am. Chem. Soc. *70*, 846–854.
131. Swain, C.G., and Scott, C.B. (1953). Quantitative Correlation of Relative Rates. Comparison of Hydroxide Ion with Other Nucleophilic Reagents toward Alkyl Halides, Esters, Epoxides and Acyl Halides. J. Am. Chem. Soc. *75*, 141–147.
132. Mayr, H., and Patz, M. (1994). Scales of Nucleophilicity and Electrophilicity: A System for Ordering Polar Organic and Organometallic Reactions. Angew. Chem. Int. Ed. Engl. *33*, 938–957.
133. Brønsted, J.N., and Pedersen, K.J. (1924). Zeitschrift für Phys. Chemie, Stöchiometrie und Verwandtschaftslehre *108*, 185–235.
134. Zahrt, A.F., Athavale, S.V., and Denmark, S.E. (2020). Quantitative Structure−Selectivity Relationships in Enantioselective Catalysis: Past, Present, and Future. Chem. Rev. *120*, 1620–1689.
135. Swain, C.G., and Lupton, E.C. (1968). Field and Resonance Components of Substituent Effects. J. Am. Chem. Soc. *90*, 4328–4337.
136. Milo, A., Bess, E.N., and Sigman, M.S. (2014). Interrogating Selectivity in Catalysis Using Molecular Vibrations. Nature *507*, 210–214.
137. Tedder, J.M. (1982). Which Factors Determine the Reactivity and Regioselectivity of Free Radical Substitution and Addition Reactions? Angew. Chem. Int. Ed. Engl. *21*, 401–410.
138. Chen, M.S., and White, M.C. (2010). Combined Effects on Selectivity in Fe-Catalyzed Methylene Oxidation. Science *327*, 566–571.
139. Liu, F., Yang, Z., Yu, Y., Mei, Y., and Houk, K.N. (2017). Bimodal Evans−Polanyi Relationships in Dioxirane Oxidations of sp3 C−H: Non-perfect Synchronization in Generation of Delocalized Radical Intermediates. J. Am. Chem. Soc. *139*, 16650−16656.
140. Jensen, K.F., and Truhlar, D.G. (1987). An Introduction. In Supercomputer Research in Chemistry and Chemical Engineering, (American Chemical Society), pp. 1–14. 10.1021/bk-1987-0353.
141. Senkan, S.M. (1992). Detailed Chemical Kinetic Modeling: Chemical Reaction Engineering of the Future. Adv. Chem. Eng. *18*, 95–196.
142. Davis, H.J., and Phipps, R.J. (2017). Harnessing non-covalent interactions to exert control over regioselectivity and site-selectivity in catalytic reactions. Chem. Sci. *8*, 864–877.
143. Knowles, R.R., and Jacobsen, E.N. (2010). Attractive noncovalent interactions in asymmetric catalysis: Links between enzymes and small molecule catalysts. PNAS *107*, 20678–20685.
144. Robbins, D.W., and Hartwig, J.F. (2011). A simple, multidimensional approach to high-throughput discovery of catalytic reactions. Science *333*, 1423–1427. 10.1126/science.1207922.
145. Reid, J.P., and Sigman, M.S. (2019). Holistic prediction of enantioselectivity in asymmetric catalysis. Nature *571*, 343–348. 10.1038/s41586-019-1384-z.

146. McNally, A., Prier, C.K., and MacMillan, D.W.C. (2011). Discovery of an α-amino C-H arylation reaction using the strategy of accelerated serendipity. Science *334*, 1114–1117. 10.1126/science.1213920.
147. Guan, Y., Ingman, V.M., Rooks, B.J., and Wheeler, S.E. (2018). AARON: An Automated Reaction Optimizer for New Catalysts. J. Chem. Theory Comput. *14*, 5249–5261.
148. Sameera, W.M.C., Maeda, S., and Morokuma, K. (2016). Computational Catalysis Using the Artificial Force Induced Reaction Method. Acc. Chem. Res. *49*, 763–773.
149. Maeda, S., and Morokuma, K. (2010). Communications: A Systematic Method for Locating Transition Structures of a+B→X Type Reactions. J. Chem. Phys. *132*, 241102.
150. Maeda, S., and Morokuma, K. (2011). Finding Reaction Pathways of Type A + B → X: Toward Systematic Prediction of Reaction Mechanisms. J. Chem. Theory Comput. *7*, 2335−2345.
151. Maeda, S., Ohno, K., and Morokuma, K. (2013). Systematic Exploration of the Mechanism of Chemical Reactions: The Global Reaction Route Mapping (Grrm) Strategy Using the Addf and Afir Methods. Phys. Chem. Chem. Phys. *15*, 3683−3701.
152. Bhoorasingh, P.L., Slakman, B.L., Seyedzadeh Khanshan, F., Cain, J.Y., and West, R.H. (2017). Automated Transition State Theory Calculations for High-Throughput Kinetics. J. Phys. Chem. A *121*, 6896−6904.
153. Bhoorasingh, P.L., and West, R.H. (2015). Transition State Geometry Prediction Using Molecular Group Contributions. Phys. Chem. Chem. Phys. *17*, 32173−32182.
154. Jacobson, L.D., Bochevarov, A.D., Watson, M.A., Hughes, T.F., Rinaldo, D., Ehrlich, S., Steinbrecher, T.B., Vaitheeswaran, S., Philipp, D.M., Halls, M.D., and Friesner, R.A. (2017). Automated Transition State Search and Its Application to Diverse Types of Organic Reactions. J. Chem. Theory Comput. *13*, 5780−5797.
155. Dewyer, A.L., Argüelles, A.J., and Zimmerman, P.M. (2018). Methods for Exploring Reaction Space in Molecular Systems. WIREs Comput. Mol. Sci. *8*, e1354.
156. Bochevarov, A.D., Harder, E., Hughes, T.F., Greenwood, J.R., Braden, D.A., Philipp, D.M., Rinaldo, D., Halls, M.D., Zhang, J., and Friesner, R.A. (2013). Jaguar: A High-Performance Quantum Chemistry Software Program with Strengths in Life and Materials Sciences. Int. J. Quantum Chem. *113*, 2110−2142.
157. Reymond, J.L., and Awale, M. (2012). Exploring chemical space for drug discovery using the chemical universe database. ACS Chem. Neurosci. *3*, 649–657. 10.1021/cn3000422.
158. Lusher, S.J., McGuire, R., Schaik, R.C., van Nicholson, C.D., and Vlieg, J. (2014). Data-Driven Medicinal Chemistry in the Era of Big Data. Drug Discovery Today *19*, 859–868.
159. Shevlin, M. (2017). Practical High-Throughput Experimentation for Chemists. ACS Med. Chem. Lett. *8*, 601–607.
160. Williams, W.L., Zeng, L., Gensch, T., Sigman, M.S., Doyle, A.G., and Anslyn, E.V. (2021). The Evolution of Data-Driven Modeling in Organic Chemistry. ACS Cent Sci *7*, 1622-1637. 10.1021/acscentsci.1c00535.
161. Corey, E.J., and Wipke, W.T. (1969). Computer-Assisted Design of Complex Organic Syntheses. Science *166*, 19–38.
162. Chen, H., Engkvist, O., Wang, Y., Olivecrona, M., and Blaschke, T. (2018). The Rise of Deep Learning in Drug Discovery. Drug Discovery Today *23*, 1241–1250.

163. Bersohn, M., and Esack, A. (1976). Computers and Organic Synthesis. Chem. Rev. *76*, 269–282.
164. Sternberg, M.J.E., Lewis, R.A., King, R.D., and Muggleton, S. (1992). Modelling the Structure and Function of Enzymes by Machine Learning. Faraday Discuss. *93*, 269−280.
165. Kowalski, B.R., and Bender, C.F. Pattern Recognition. Powerful Approach to Interpreting Chemical Data. J. Am. Chem. Soc. *94*, 5632−5639.
166. Kubinyi, H. (1988). Free Wilson Analysis. Theory, Applications and Its Relationship to Hansch Analysis. Quant. Struct.-Act. Relat. *7*, 121–133.
167. Bereton, R.G. (2015). Pattern Recognition in Chemometrics. Chemom. Intell. Lab. Syst. *149*, 90–96.
168. Free, S.M., and Wilson, J.W. (1964). A Mathematical Contribution to Structure-Activity Studies. J. Med. Chem. *7*, 395–399.
169. Jurs, P.C., Kowalski, B.R., and Isenhour, T.L. (1969). Computerized Learning Machines Applied to Chemical Problems. Molecular Formula Determination from Low Resolution Mass Spectrometry. Anal. Chem. *41*, 21–27.
170. Kowalski, B.R., Jurs, P.C., Isenhour, T.L., and Reilley, C. (1969). Computerized Learning Machines Applied to Chemical Problems. Multicategory Pattern Classification by Least Squares. Anal. Chem. *41*, 695–700.
171. Jurs, P.C., Kowalski, B.R., Isenhour, T.L., and Reilley, C. (1969). Investigation of Combined Patterns from Diverse Analytical Data Using Computerized Learning Machines. Anal. Chem. *41*, 1949–1953.
172. Lederberg, J., Sutherland, G.L., Buchanan, B.G., Feigenbaum, E.A., Robertson, A.V., Duffield, A.M., and Djerassi, C. (1969). Applications of Artificial Intelligence for Chemical Inference. I. Number of Possible Organic Compounds. Acyclic Structures Containing Carbon, Hydro- gen, Oxygen, and Nitrogen. J. Am. Chem. Soc. *91*, 2973–2976.

# Chapter 2

## Data-Science Driven Development of Flexible, Point-Chiral Phosphoric Acid Catalysts

The work presented hereafter was performed collaboratively between the Toste group at UC Berkeley and the Sigman Group at the University of Utah.

**UC Berkeley** – René Rahimoff, Abby Medlin, Vladislav A. Roytman, F. Dean Toste.

**University of Utah** – Jordan P. Liles, Julie Hofstra-Wahlman, Veronica O'Connor, Jennifer M. Crawford, Matthew S. Sigman.

*Sections of this chapter were co-authored with Jordan P. Liles*

# I. Introduction

## 1.1. A Primer on Asymmetric Catalysis

Despite the rapid development of catalysis since the early years of the 20th century, small organic molecules in that context received only little attention until recently.[1] Early examples by German chemists Marckwald, Bredig, and Fiske provided the first proofs of concept that small molecules could be used to transfer chirality in asymmetric syntheses.[2,3] In 1904, Marckwald reported the synthesis of enantioentiched ethylmethylacetoc acid by thermal decarboxylation of ethylmethylmalonic acid (Figure 1, A). In this example, the starting material was complexed by a sub-stoichiometric amount of monobrucine. While the enantio-enrichment of the product was modest (about 10%), this marked one of the very early and first examples of asymmetric organocatalysis.[4] In 1912, Bredig and Fiske described the first use of cinchona alkaloids in the synthesis of enantioenriched cyanohydrin, also obtaining a modest 10% enrichment (Figure 1, B).[3] Despite their great conceptual significance, these reports did not lead to more than a handful follow up reports of organic catalysts for asymmetric syntheses over the following fifty years.[5-8] The 1971 saw a brief revival of asymmetric organocatalysis with the discovery that L-Proline could efficiently catalyzed asymmetric aldol cyclodehydrations. This reaction was coined the Hajos-Parrish-Eder-Sauer-Wiechert reaction and has become a landmark for the field of organocatalysis.[9,10]

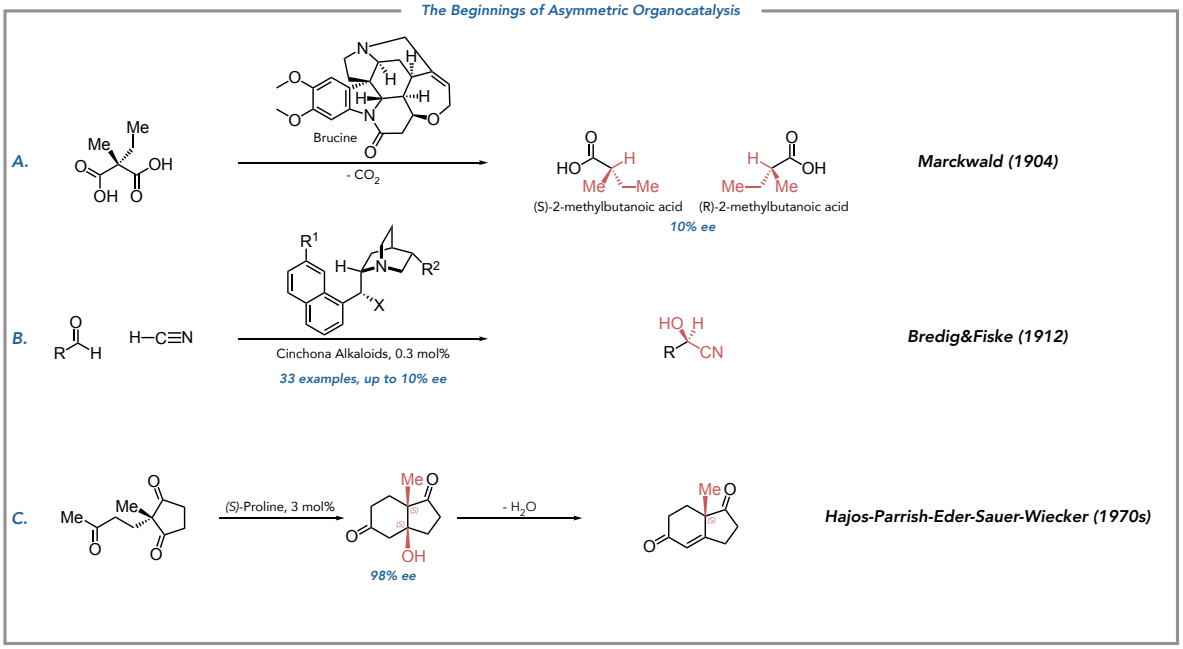



**Figure 1:** A) Early reports of asymmetric organocatalysis by Marckwald (1904). B) Bredig and Fiske (1912). C) Hajos-Parrish-Sauer-Wiechert reaction.

At the dawn of the 21st century, the time of glory of organocatalysis had come. In 1998, Sigman and Jacobsen demonstrated that the hydrogen bonding capacity of chiral Schiff bases could lead to high levels of enantioselectivity in the Strecker reaction.[11] In 2000, pioneering work by the

List and MacMillan groups fueled a new, and this time long-lasting, interest in small organic molecules' capacity to catalyze enantioselective reactions (Figure 2).[12,13] List's publication of proline-catalyzed asymmetric aldol reactions, followed only a few months later by MacMillan's enantioselective Diels-Alder, marked the beginning of extensive research efforts in the discovery and development of highly selective organocatalysts. These efforts were well rewarded. In 2021, the Nobel Prize in Chemistry was awarded to David MacMillan and Ben List for their development of and contribution to the field of asymmetric organocatalysis.

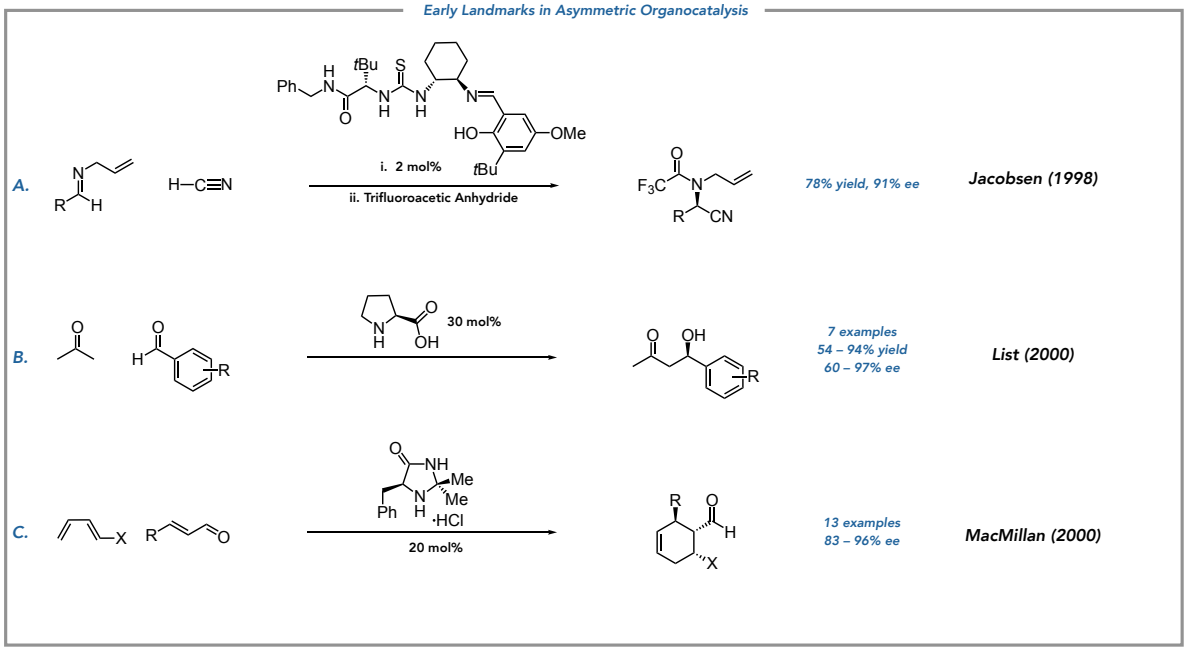



Figure 2: A) Jacobsen's enantioselective Strecker reaction (1998). B) Asymmetric Aldol reaction (List, 2000). C) Enantioselective Diels-Alder reaction (MacMillan, 2000).

## 1.2. Chiral Phosphoric Acids: Privileged Structures for Asymmetric Catalysis

Although Brønsted acids have been extensively studied for their structure and reactivity since the independent reports by Brønsted and Lowry on the nature of acid-base equilibria in 1923, their use in asymmetric organocatalysis is relatively recent.[14,15] Classical Brønsted acids used in asymmetric catalysis generally contain moieties such as a phosphoric acid, a carboxylic acid, or s sulfonamide, although recent research endeavors have led to the inclusion of a variety of Brønsted-acidic functional groups (Figure 3). Since the early 2000s, they have become a central pillar of organocatalysis and continue to receive significant attention for their robustness in a multitude of synthetic transformations.[16]

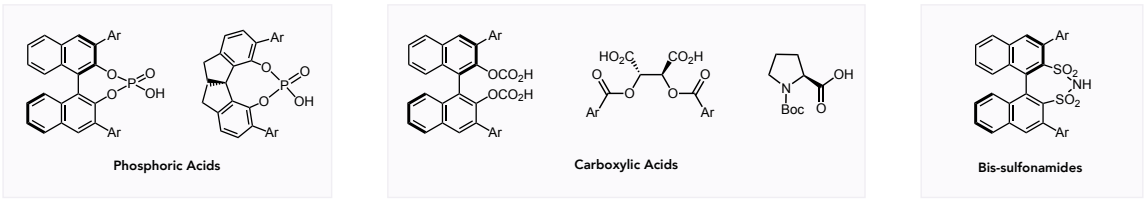



Figure 3: Common structures of Brønsted acids.

BINOL-derived phosphoric acids witnessed a rather slow adoption into the field. The first reported synthesis of BINOL phosphoric acid by Marschalk in 1928 was generally overlooked by the scientific community until the 1970s when chiral phosphoric acid began to be used for the chiral resolution of amines, as demonstrated by Jacques and Fouquey in 1971 (Figure 4).[17,18] A series of publications of a handful of new and improved methods for the synthesis of BINOL-phosphoric acid ensued in the following years.[19] It is worth noting that the current state of the art for chiral phosphoric acids does not differ greatly from the conditions reported in 1989. Changes in solvents aside, the phosphorylation of BINOL is generally performed in pyridine using phosphoryl chloride at refluxing temperatures, yielding the phosphoric acid chloride. The latter can be reacted either with aqueous HCl or the addition of water under basic conditions. The final acid is then purified by recrystallization. At the time of publication of these synthetic procedures, the synthesis was usually performed on racemic BINOL. The enantioenriched phosphoric acid products could be obtained by chiral resolution using cinchonine,[20-22] strychnine,[23] and other naturally occurring chiral small molecules to form diastereomeric salts. With the development of more accessible synthetic routes, chiral phosphoric acids became a popular auxiliary for the chiral resolutions of pharmaceutically-relevant compounds, including Cephalosporin antibiotics in 1980,[24] benzodiazepine derivatives in 1981, and barbituric derivatives in 1987.[25]

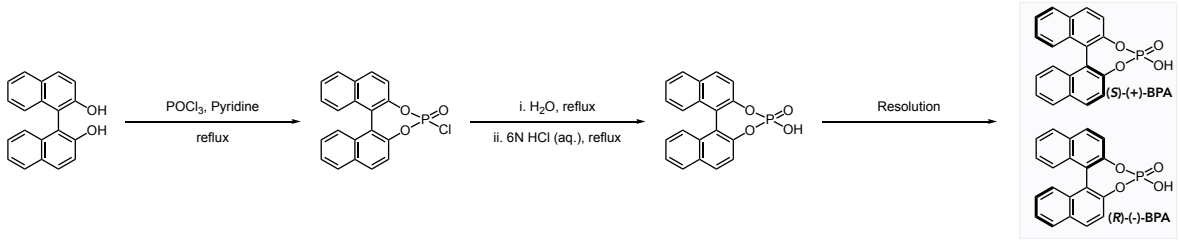



Figure 4: Synthesis of BINOL phosphoric acid (Fouquey, 1971)

Concurrently, a 1978 publication from Cornforth planted the conceptual seed for chiral phosphoric acids used as catalysts in organic transformations.[26] Hoping to imitate the steric confinement and stabilizing non-covalent interactions observed in enzyme-catalyzed mechanisms to obtain stereoselectivity in the hydration of olefins, he began pioneering studies on the synthesis and reactivity of phosphinic acids over the next decades of his career (Figure 5).26,27 The guiding principles of Cornforth's design of phosphinic acids greatly resembles the key features of chiral phosphoric acid catalysts used in asymmetric catalysis today. Indeed, Cornforth envisioned that a rigid backbone flanked by sterically and electronically tunable substituents on either side of the

acid moiety would provide the steric confinement necessary to effect stereospecificity. A series of phosphinic acids provided efficient catalysis in the hydration of alkenes, but enantioselectivity results were unfortunately never published.[27-31] Nevertheless, the conceptual design of these phosphinic acids provided a solid foundation for the design of modern chiral phosphoric acids.[32]

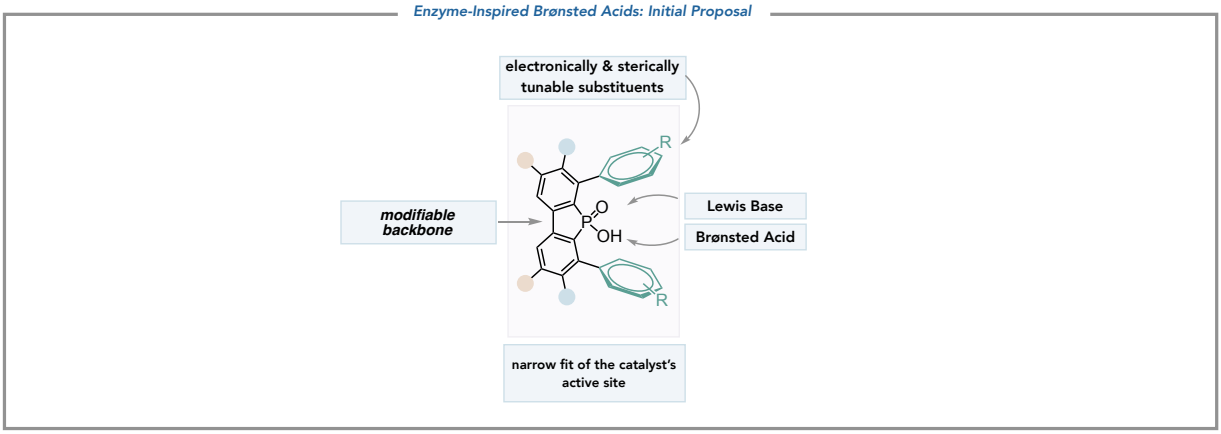



Figure 5: Cornforth's design of phosphinic acid catalysts (1978)

In 2004, a seminal report by Akiyama[33] and coworkers of an enantioselective Mannich reaction of ketene silyl radicals and aldimines provided the first modern example of chiral Brønsted acid catalysis (Figure 6, A). Therein, they described the synthesis and reactivity of 3,3'-substituted *(R)*-BINOL-derived phosphoric acids, yielding the desired β-aminoester products in great yields and up to 96% ee. A short month later, Terada and coworkers revealed another Mannich-type reaction to enantioselectively synthesize β-aminoketones using similarly substituted BINOL-based phosphoric acids as catalysts (Figure 6, B).[34] Importantly, mechanistic studies highlighted the importance of large substituents at the 3,3'-positions of the BINOL backbone for both reactivity and selectivity. Since these independent reports in 2004, BINOL-derived, axially chiral phosphoric acids have become a staple in asymmetric organocatalysis. A large variety of 3,3'-subsitution patterns have become synthetically accessible, and a significant number of these scaffolds are even widely commercially available. Their reliable catalytic performances in an ever-growing compendium of transformations including reductive aminations,[35-37] allylations,[38] Friedel-Crafts alkylations,[39-41] and asymmetric radical additions,[42] has earned them the title of "privileged" structures in asymmetric organocatalysis.[32]

A handful of common privileged backbones are used as foundation for the development chiral phosphoric acid (Figure 7), in particular BINOL, SPINOL, and octahydro-(H8)-BINOL scaffolds have gained tremendous popularity for their axial chirality stemming from hindered rotation. Elaboration of the backbone with substitution at the 6,6' or 7,7' is also possible to generate further steric induction around the catalyst. Decoration of the 3,3' positions not only allows access to higher enantioselectivities due to steric confinement and preorganization of the transition, but electronic tuning of the catalysts has been possible by the incorporation of more imaginative fragments such as triazoles or simple electron-withdrawing substitutions around a 3,3' phenyl ring.[43] Similarly, substitution around the backbone, as well as partial hydrogenation of the BINOL backbone has also received some attention in the tuning of catalytic properties of these scaffolds.[44,45] The possible diversifications of the backbone along with the possibility to vary from

phosphoric acids to other Brønsted acidic moieties (phosphoramides, thiophosphoramides) have made the general BINOL backbone a particularly prolific starting point for the development of highly tailored organocatalysts.[46-51]

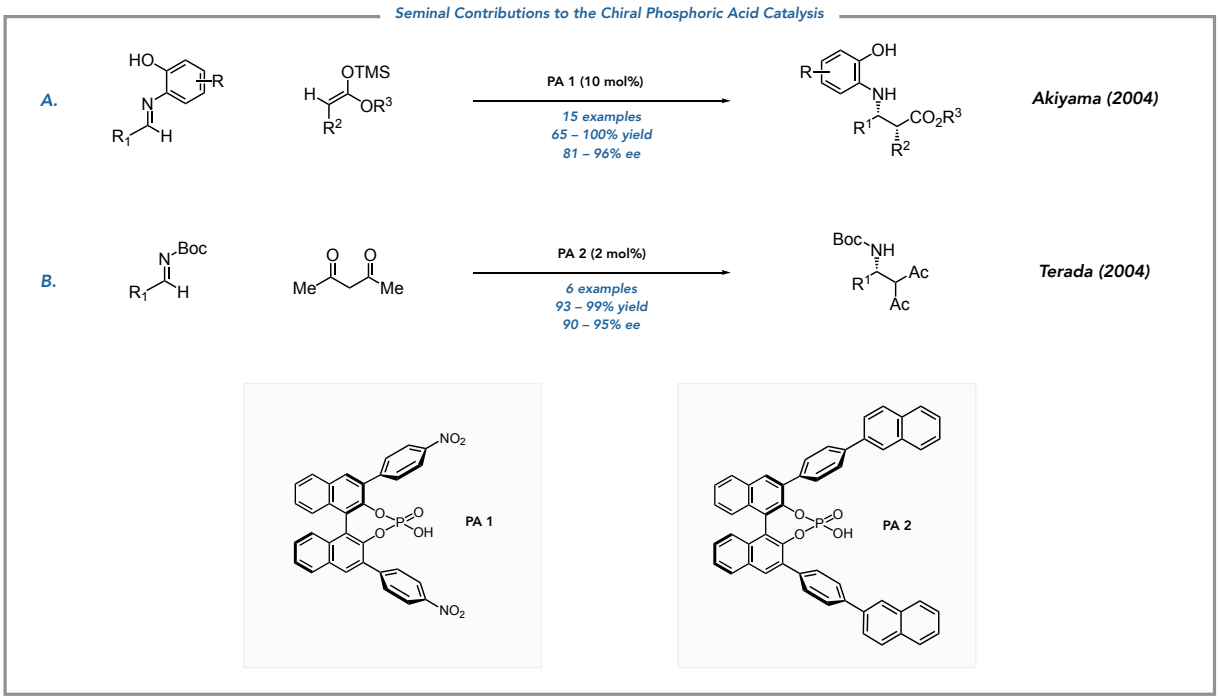



Figure 6: A) Akiyama's enantioselective Mannich-type reaction (2004). B) Terada's CPA-catalyzed Mannich-type reaction (2004).

Much like the diversity in possible catalyst structures, the modes of activation of phosphoric acid are manifold. Early reports on chiral phosphoric acid catalysis proposed mechanisms going through the mono-activation of substrates via protonation followed by ion pairing, or via single-point hydrogen bonding between the phosphoric acid moiety and the Lewis basic site on the substrate (usually an imine nitrogen) (Figure 8). The phosphoric acid would in that context provide LUMO-lowering catalysis, activating the imine (or iminium) substrate for nucleophilic addition. Rueping and coworkers have dedicated significant research effort towards deconvoluting the mechanisms and key interactions in phosphoric acid-catalyzed transformations, and have demonstrated that these mechanisms are often more complex than simple the mono-activations initially proposed.[52] Three main classes of activations have emerged depending on the reaction: mono-activation (including a spectrum of ion-paining and single-point hydrogen bonding, dual activation (multi-point hydrogen bonding network), and bifunctional activation (in which both reaction partners are independently getting activated at the phosphate) (Figure 8). Bifunctional activation has become the more commonly invoked mechanism of activation for chiral phosphoric acid catalyzed reactions.[53,54]

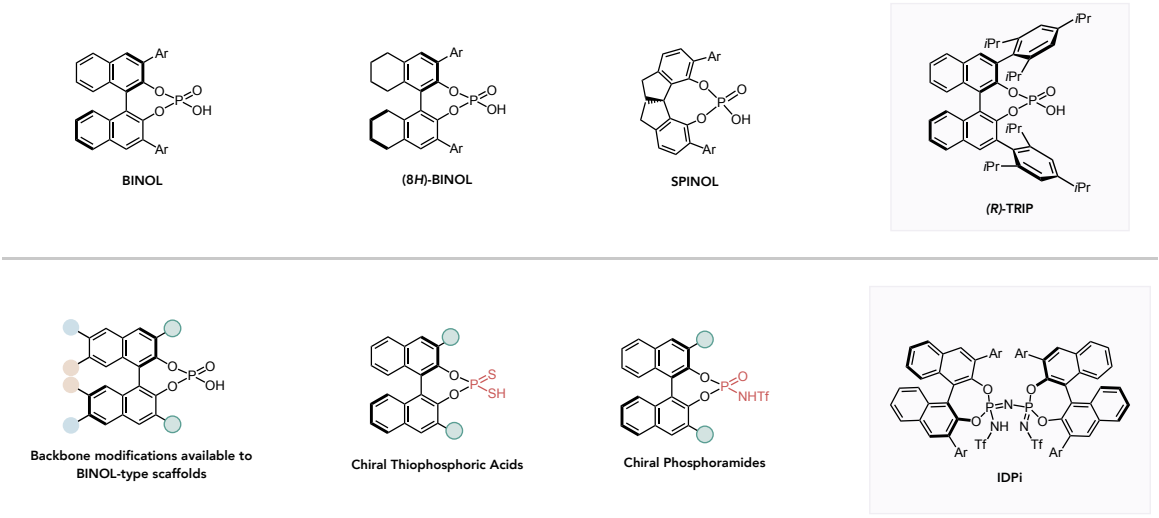



Figure 7: Privileged axially chiral backbones for phosphoric acid catalysis.

Independently of the mode of activation at play during catalysis, a significant emphasis has generally been placed on the impact of large 3,3'-substituents on catalytic activity.[53] By far one of the most commonly used chiral phosphoric acid catalysts, (*R*)-TRIP and (*S*)-TRIP (Figure 7), was developed by List and co-workers in 2010, features 2,4,6-triisopropylphenyl at the 3,3' substitution.[55] Models to rationalize and predict the selectivity of CPAs based on computational investigations of various transformations have been developed. Projection of the general catalyst structure allows the visualization of filled and empty quadrants. For transformations in which bifunctional is invoked, hydrogen bonding to the electrophile and the nucleophile is proposed to pre-organize the reacting species within the two empty quadrants, leading to an efficient transfer of chiral information from catalyst to product (Figure 8).

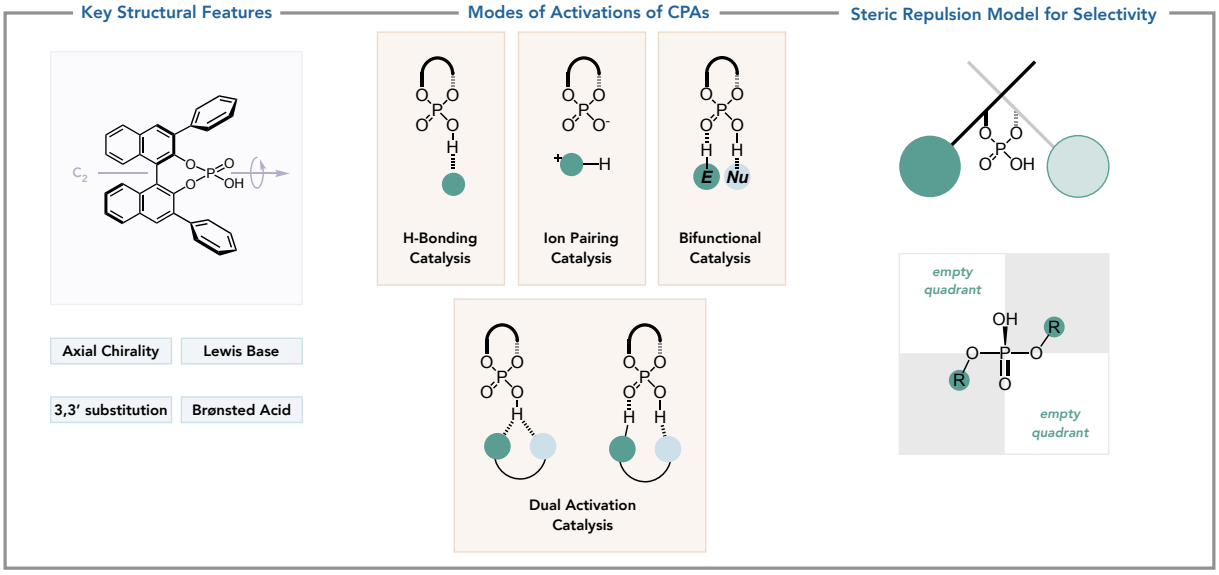



Figure 8: Key features of BINOL-based chiral phosphoric acid catalysts.

It is important to note that these simplified models generally rely heavily on steric repulsion arguments from the 3,3'-substitution to rationalize chirality transfer. As a result, catalyst development and optimization efforts over the past few years have also heavily relied on the introduction of increasingly large and rigid groups to provide further steric confinement around the catalytic active site.[56,57] More recently, new classes of catalysts have emerged presenting multiple axes of chirality. IDPi catalysts, developed by List and coworkers, have served as the foundation for the growth of novel "superacids", often boasting very low pKa's and high molecular weights (Figure 7).[49,51,58,59]

Nevertheless, the efficiency of enzymes in asymmetric catalysis reminds us that non-steric, non-covalent interactions are still quite essential in the rational design of new catalysts. Although the energetic contributions of electrostatic, π–π, π–cation, or π–anion interactions are relatively low (0.5–3 kcal.mol$^{-1}$), studies have shown that rationally designing 3,3'substituents to promote multiple of these interactions in the transition state can be advantageous.[60-64] Deviating from the rather hydrophobic nature of traditional substituents, the Toste group reported novel triazole-bearing BINOL-phosphates competent in the catalysis of a previously inaccessible enantioselective C–N bond formation for the synthesis of 1,2,3,4-tetrahydroisoquinoline derivatives with good selectivities (Figure 9).[43] The authors noted that classical phosphoric acids failed to provide adequate selectivity, and proposed a tight ion-paired transition state for the triazole-bearing catalysts in which the Lewis basic sites on the 3,3'-substituents provide anchoring for the coordination of the substrate, thereby improving the selectivity of the reaction.

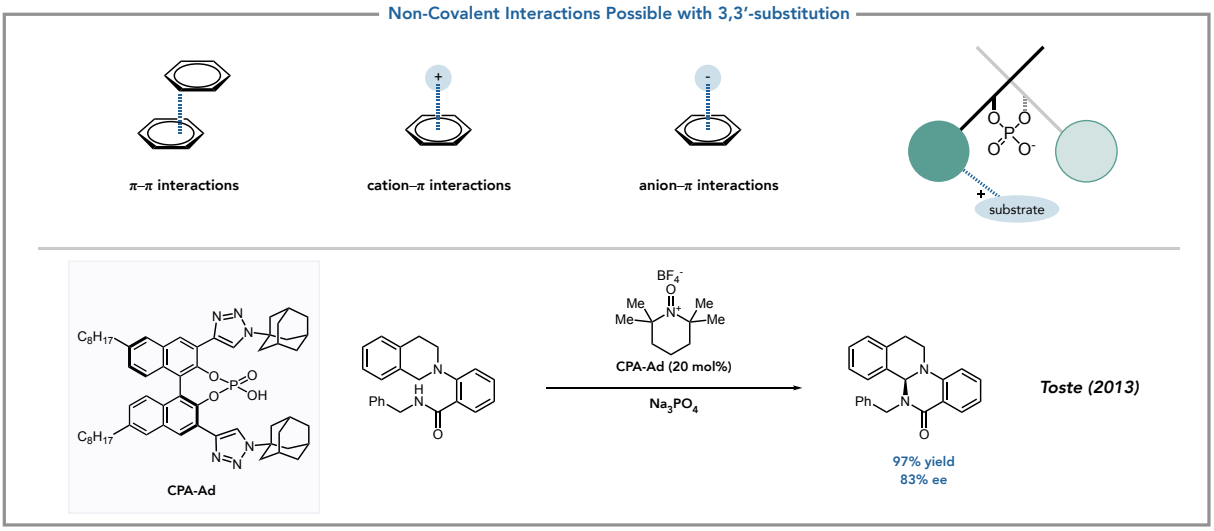



Figure 9: A) Significant non-covalent interactions. B) Triazole-bearing CPA (Toste, 2013).

## 1.3. Harnessing Non-Covalent Interactions and Conformational Flexibility

Although phosphoric acid catalysis has been following a trend towards increasingly rigid and bulky scaffolds, hydrogen-bonding-based organocatalytic platforms have witnessed an opposite trajectory in which conformational flexibility is an advantage.[65,66] Small peptides, usually containing more than one rotatable bond, can adopt multiple secondary structures in solution. Yet, they have been demonstrated to yield exquisite selectivity in a wide range of transformations.[67]

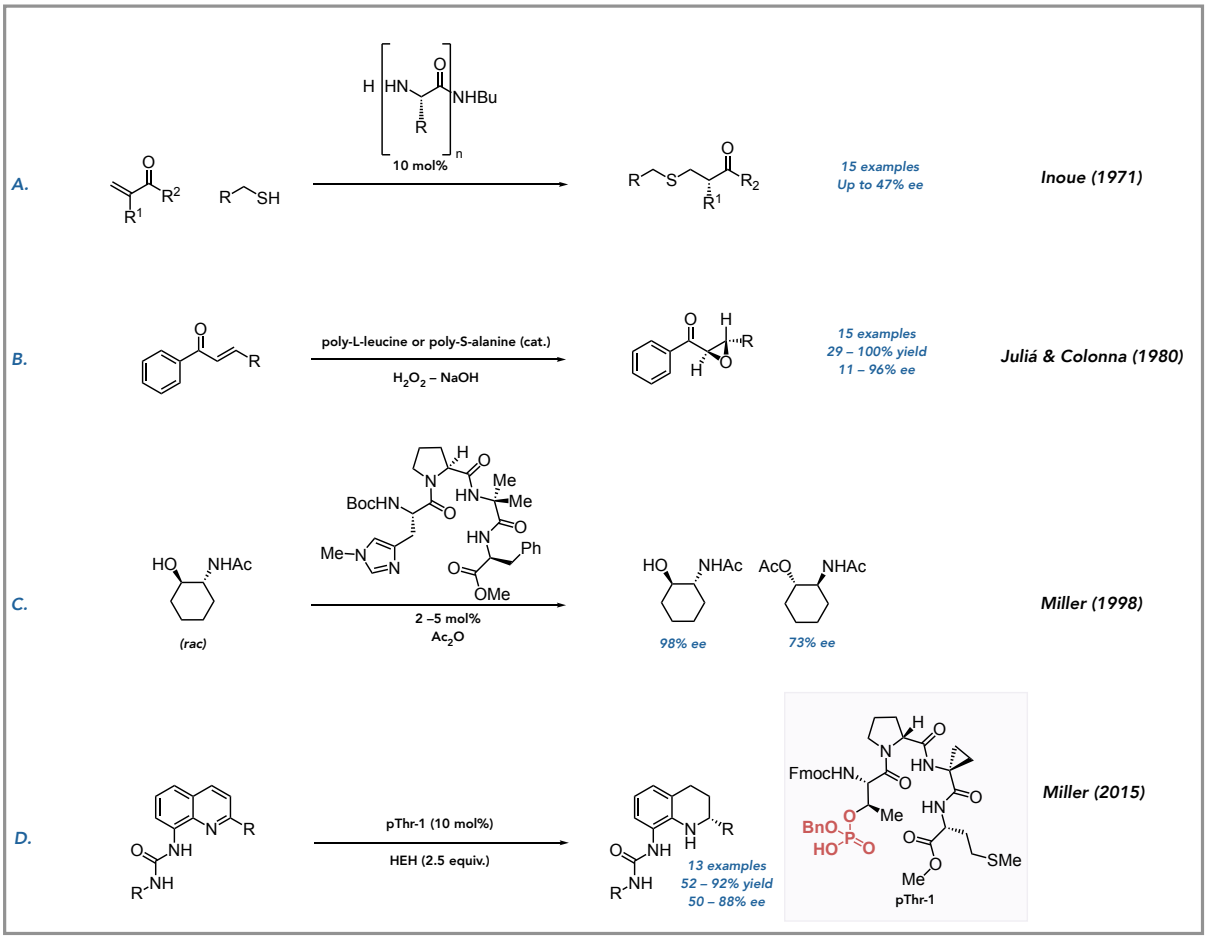



Figure 10: A) Inoue, conjugate addition of thiols to enones. B) Juliá-Colonna, epoxidation of chalcones. C) Kinetic resolution and acylation catalyzed by small peptides (Miller, 1998). D) pTh-catalyzed transfer hydrogenation of 8-aminoquinolines (Miller, 2015).

Some of the first examples of poly(amino acid) chains used as catalysts came from Inoue and coworkers throughout the 1970s in a series of asymmetric addition reactions using small, peptide-like amine polymers inspired by enzymatic catalysis (Figure 10, A).68-73 These reports were followed shortly thereafter by the publication of the Juliá-Colonna epoxidation of chalcones by poly-*(S)*-alanine and poly-*(S)*-leucine in 1980 (Figure 10, B).[74,75] Now at the forefront of this catalytic platform, the Miller group reported a small peptide catalyzed enantioselective acyl

transfer reaction in 1998 (Figure 10, C).[76] Despite their flexibility, some of the peptide catalysts studied could provide the desired trans-2-amidocyclohexyl acetate product via kinetic resolution and selective acylation of trans-2-acetamidocyclohexanol in up to 99% ee.

Observing the ubiquity of phosphorylated proteins in biological systems, the Miller group envisioned to merge the flexibility of peptides with the catalytic activity of Brønsted acids.[77,78] In 2015, a phosphothreonine-based (pThr) tetrapeptide catalyst was reported to selectively catalyze the transfer hydrogenation of 8-aminoquinolines (Figure 10, D).[79] This publication highlighted design elements strikingly different from the classical framework of chiral phosphoric acid optimization. Namely, the lack of rigidity and $C_2$ axial chirality did not, in fact, hinder the ability of the peptide catalysts to provide selectivity comparable to traditional TRIP phosphoric acid in the transformation at hand. Additionally, the modular aspect of peptide synthesis opened an immense and diverse chemical space for the design of similar catalysts for applications in different reactions.[80] This modularity, in conjunction with the ease of synthesis of these catalysts (often via well-established solid-phase peptide synthesis), and the high selectivities observed, have fueled the development of this platform for the catalysis of a plethora of transformations including aldol reactions, epoxidations, or halogenations, quite often bringing complementarity to more traditional classes of organocatalysts.[60,67,81]

## 1.4. Data-driven tools to understand the role of NCIs in asymmetric catalysis

Chemists have historically been driven to understand forces at play in reactivity and selectivity in order to improve upon the known systems and developing better, or more situation-tailored catalytic platforms. The case of peptide catalysis developed by the Miller group presents an interesting conceptual challenge: understanding the interactions driving their selectivity in catalysis. A broader overview of computational tools was presented in Chapter 1. Data-science and computational methods have recently gained popularity to complement traditional physical organic mechanistic studies in gaining a more holistic understanding of selectivity trends in catalytic systems in which multiple subtle but cooperative interactions can convolute the mechanism.[80] Mechanistic studies aiming to uncover and gauge the importance of NCIs in asymmetric organocatalysis have been performed on a wide range of reaction and catalyst types. Iminium catalysts developed by MacMillan and coworkers, for example, were found by Gilmour and coworker to form highly preorganized intermediates due to non-obvious π–π and cation–π interactions. Importantly, some flexibility in the catalyst seems important to allow the folding of the activated complex conformation leading to selectivity.[82]

Despite some challenges in deconvoluting selectivity-determining interactions, successful models have developed various molecular descriptors to address the physical features of these catalysts. Studies integrating NMR techniques, transitions state analysis, molecular dynamics, and multivariate linear regressions, along with more classical physical organic chemistry tools such as kinetic/Eyring studies, have come a long way in providing accurate rationalizations and predictions of selectivity in various catalytic systems.[83-88] Importantly, these methods taken together have supported the rational design of catalysts so central to obtaining highly optimized, selective conditions with lower experimental costs.[89-95] Multivariate Linear Regression (MLR) and Machine Learning (ML)-based algorithms developed to predict optimized structures for specific reactions

have been demonstrated on chiral phosphoric acids by Denmark and coworkers.[96] In their study of enantioselective addition of thiols to N-acylimines, they developed a workflow starting with the in silico design of a catalyst library, followed by a selection of a representative sample of those catalysts to be screened against the reaction of choice. The results obtained from the training set, along with a list of molecular descriptors extracted from the structures in the library, allowed the visualization of catalyst performance in the "chemical space" represented by the library, and thereby the prediction of highly optimized catalyst structures within that space. Importantly, the chemical space here is defined by the molecular descriptors extracted computationally from the catalysts' structures. The latter can be sorted through Principal Component Analysis to reduce the variables to three main axes which can be plotted to visualize the chemical space covered by the library.[97] These type of workflow has worked well in diverse areas of catalysis, including the design of transition metal catalysts.[98,99]

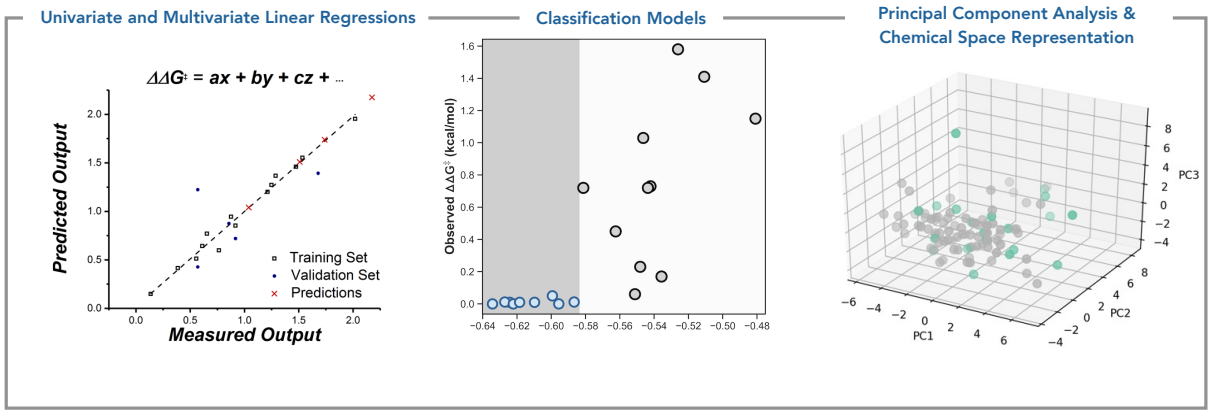



Figure 11: non-exhaustive examples of data-science methods used for the deconvolution of structure-activity relationships in selectivity trends.

One caveat to be noted in the use of ML tools, however, is the relatively large number of experimental data points (in the case of the Denmark's study, over 2,000) necessary to confidently assess the performance of the training set and validate the model generated. While the advent of high-throughput experimentation has enabled easier and more reliable access to large data sets, this scale of experimentation might still represent a challenge for a lot of academic groups working on their own catalyst optimization projects. On the other hand, MLR methods usually rely on a rather small selection of known molecular descriptors which can overlook complex interactions in novel and less understood catalyst classes. Indeed, these computationally assisted optimization workflows have thus far been generally limited to catalysts classes in which the structure-activity and significant interactions are well known and understood.

## II. Project Design

### 2.1. A Hybrid Catalyst Class

The foundations of the project described herein were born of long-standing collaborations between the Toste group at UC Berkeley, the Miller group at Yale University, and the Sigman group at the University of Utah. The trend towards rigidity in classical phosphoric catalysis, the exquisite selectivities achievable in flexible, small peptide catalysis, and the overall need for smaller scale, yet accurate, modeling and prediction methods on novel catalyst structures all led to the questions asked at the dawn of this project:

- Can the privileged featured of phosphoric acid catalysts be minimized away from the trend of increasing molecular weights and still retain selectivity in asymmetric transformations?

- Can elements of flexibility be integrated in a new catalyst scaffold to provide positive non-covalent interactions in lieu of steric repulsion used in classical phosphoric acid catalysis?

- Can the design of these novel, highly selective catalyst structures be guided by computational and data-science tools without reliance on large scale high-throughput experimentation?

To address these questions, a hybrid catalyst class integrating fragments for both phosphoric acid and peptide catalysis was envisioned (Figure 12). Truncating the backbone from a traditional 1,1'-bi-2-naphtol and limiting the substitution from 3,3' to the 3 position only, were intended to boost the conformational flexibility of the catalysts. Taking inspiration from the Miller group's success using amino acid building blocks in asymmetric catalysis, we hoped that substituting the 3-position of the backbone with a single amino acid fragment would offer flexibility around the rotatable bonds of the fragment, a natural point of chirality, as well as two points of diversification. Indeed, we envisioned that both the α-amine and the carboxylic acid moieties could be diversely substituted, thereby offering modularity in the catalyst structures necessary for the development of a library and the expansion of the chemical space covered by these hybrid catalysts.

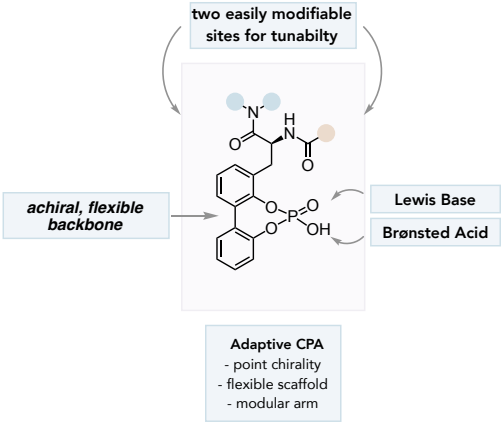



Figure 12: Envisioned structure of hybrid flexible phosphoric acid catalysts.

## 2.2. Training Set Design and Computational Workflow

The design of the training set began with the idea that more structural diversity in the catalyst library would provide a more diverse set of results for the selected transformation, and therefore better data for statistical modeling purposes. As such, a search for commercially available fragments which could be used to diversify the amine and carboxylic acid moieties of the backbone was performed. The latter resulted in over 300,000 possible fragment combinations, including a variety of carboxylic acids, acyl chlorides, sulfonyl chlorides, and secondary amines. The process of training set design and curation was iterative (Figure 13). First, the fragments were screened for synthetic compatibility, and each fragment was analyzed a lower level of theory to obtain 2D and 3D molecular descriptors using Quantitative Structure Activity Relationship (QSAR).[100] This allowed a rapid and cost-efficient first clustering of the fragments to be performed by k-means with a cluster number of 30, upon which the fragment selection was reduced to 10% of its original sample size. The 55,000 remaining possible combinations were analyzed further to select a random sample containing 2%, or 1,100 combinations.

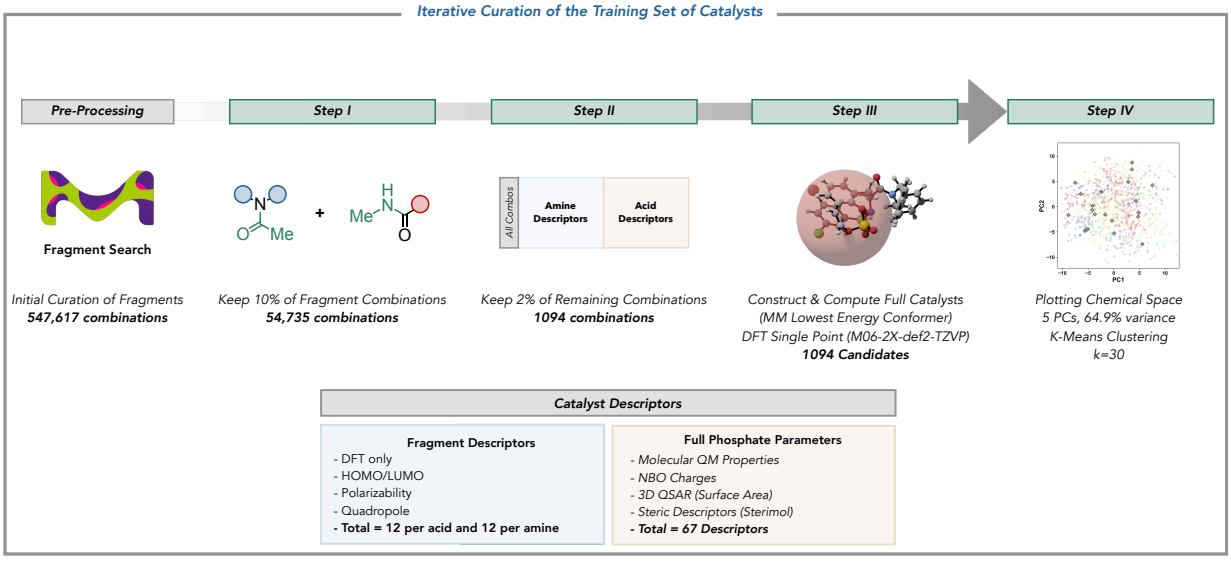



Figure 13: Training set design

The 1,100 combinations of fragments were then constructed as full catalyst structures to build the final candidate library in silico. Optimization of the catalysts using molecular mechanics and computational analysis at the DFT level (M06-2X/def2-TZVP) provided a new set of molecular descriptors for each final catalyst structures.[101] The descriptors obtained were combined for principal component analysis (PCA). PCA is a data reduction technique aiming to determine which of the hundreds of parameters extracted from the structures might have the most impact on the variance (which of the parameters differ the most across the catalyst library). Doing so, the most significant parameters can be grouped as Principal Components. In this case, reduction to the top five principal components was estimated to contribute to 65% of the variance of the library, which was deemed suitable for the purpose of training set design. The PCA enabled the representation of the library within chemical space (here represented as a 2D map).[102,103] Further k-means clustering provided 30 areas of chemical space, and an arbitrary candidate was chosen

from each cluster of chemical space, ensuring as little bias as possible would be introduced into the training set (Figure 14).

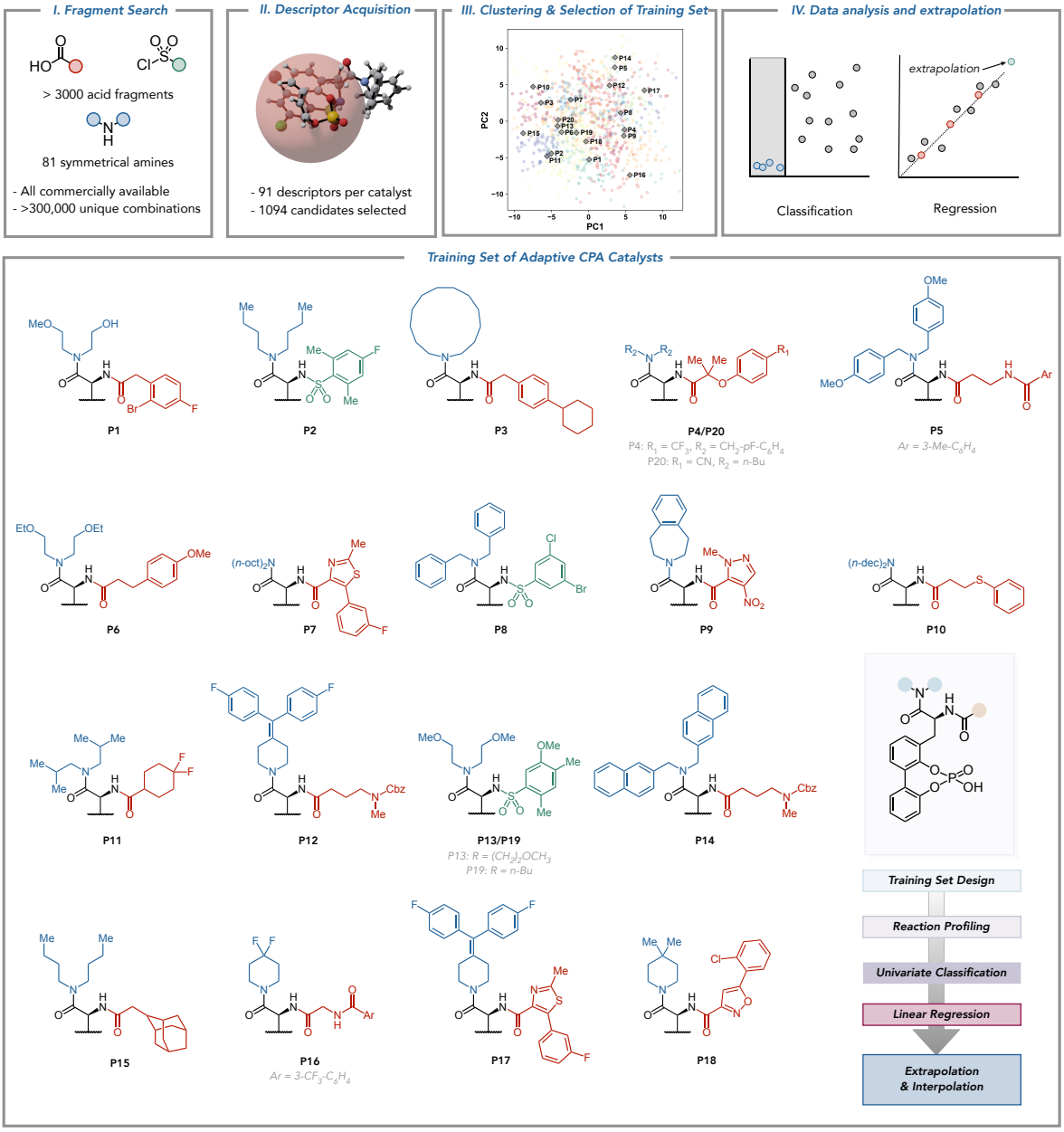



Figure 14 : Training set library and analytical workflow.

We hoped to gain insight into the performance of this new hybrid catalyst class and into any potential selectivity-determining structural features, especially the effect flexibility and non-covalent interactions might have on catalysis. A logical first step to do so was the benchmarking of the catalysts' performance in known organic transformations, which would provide a solid foundation for a holistic mechanistic and structural understanding. Analysis of the reactivity data by statistical modeling and multivariate linear regressions would hopefully enable the rationalization of selectivity trends, and the extrapolation of the latter towards the rational design of highly optimized catalyst structures for the desired transformations.

## III. Results and Discussion

*Portions of this section were co-authored with Jordan P. Liles at the University of Utah.*

### 3.1. Synthesis of the Catalyst LIbrary

The synthesis of the catalyst library was optimized to nine steps (Figure 15) and began similarly to the synthesis of transitional phosphoric acids. Protection of 2,2'-biphenol (**3**) with chloromethyl ethyl ether with sodium hydride proceeds nearly quantitatively (97%) on large scale. The protected biphenol (**4**) is submitted to lithiation and iodination. This step provides a mixture of mono- and bis-iodinated products, although conversion to the desired mono-iodinated product (**5**) can still be obtained in 80 % yield. Separation of the two iodinated products was not deemed necessary to proceed to the Negishi coupling of the mixture with a commercially available boc-(*S*)-iodoalanine methyl ester partner (**6**).[104] Catalyst precursor (**7**) can therefore be obtained in 56% yield on large scale across the first three steps of the synthesis. Deprotection of the boc group with *tert*-butyldimethylsilyl trifluoromethanesulfonate and under basic conditions using 2,6-lutidine followed by tetrabutylammonium fluoride provided the free amine backbone. The free amine precursor could be stored for several months at -20 °C without decomposition or observable racemization, although storage at room temperature did lead to partial racemization of the α-stereocenter. Initial control experiments suggested that no racemization occurred during the cross-coupling or the functionalization of the backbone (see supplementary information).

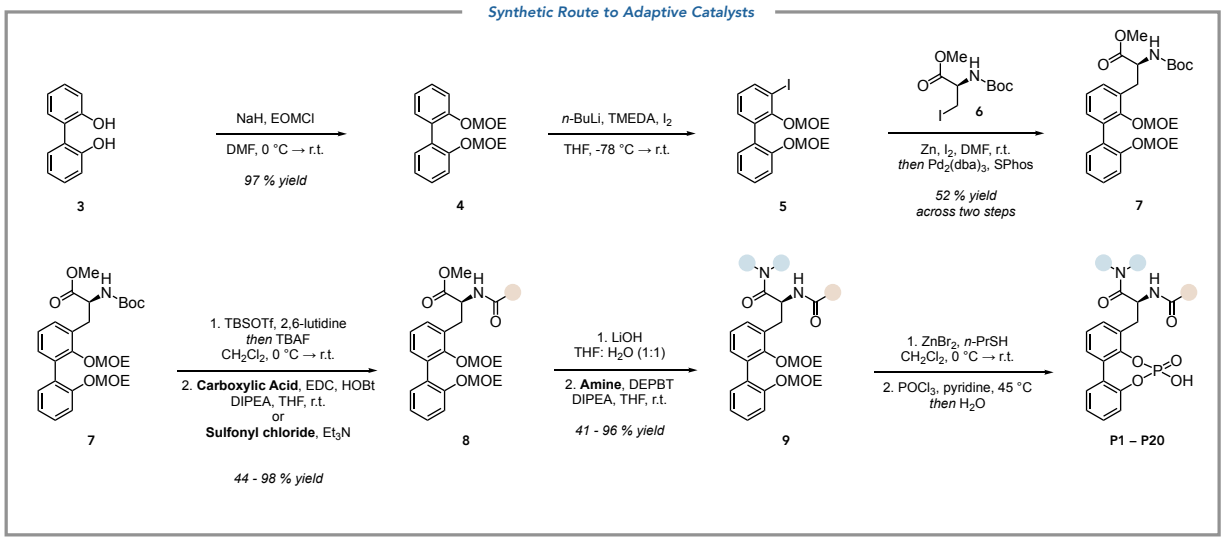



Figure 15 : Synthetic route for the catalyst library

Diversification of the catalyst backbone was first done at the amine moiety with the installation of either (a) carboxylic acid fragments or (b) sulfonyl chloride fragments. The carboxylic fragments were installed via an amide coupling using 1-Ethyl-3-(3-dimethylaminopropyl)carbodiimide (EDC) and hydroxybenzotriazole as coupling agents under basic conditions, providing the amide intermediates (**8**) in 44–98% yield. The sulfonyl chlorides were installed directly under basic conditions to yield the corresponding intermediates in 57–97% yield. Saponification of the methyl ester under basic aqueous conditions was followed by a second amide coupling to install a symmetrical secondary amine at the second point of diversification

using 3-(diethoxyphosphoryloxy)-1,2,3-benzotriazin-4(3H)-one (DEPBT) as coupling agent. The MOE-protected, fully diversified precursors (**9**) to the catalysts were obtained upon purification in 41–96% yield.[105] The MOE protecting group could be cleaved using HCl in dioxane (4 M), or $ZnBr_2$ with *n*-PrSH when acid-sensitive functional groups were present.[36] Phosphorylation with $POCl_3$ in anhydrous pyridine was performed as reported in the phosphoric acid literature, followed by hydrolysis of the phosphoryl chloride intermediate with water under basic conditions.

## 3.2. Reaction Screening and data collection

In order to obtain meaningful and representative performance data for the training set, we envisioned that known and well-studied organic transformations would be a good starting point for data collection. A survey of the literature for chiral phosphoric acids provided an initial list of a dozen transformations that we hoped would be viable systems to test the catalyst library. Of those, initial screening on a small subset of catalyst allowed the filtering of those reactions which did not provide high enough yields to gather reliable data, yielding three main transformations to test our system (Figure 16): (i) The transfer hydrogenation of 8-aminoquinoline 1;[79] (ii) The atroposelective cyclodehydration of **10**;[106] and (iii) A selective oxetane desymmetrization of **12**.[107]

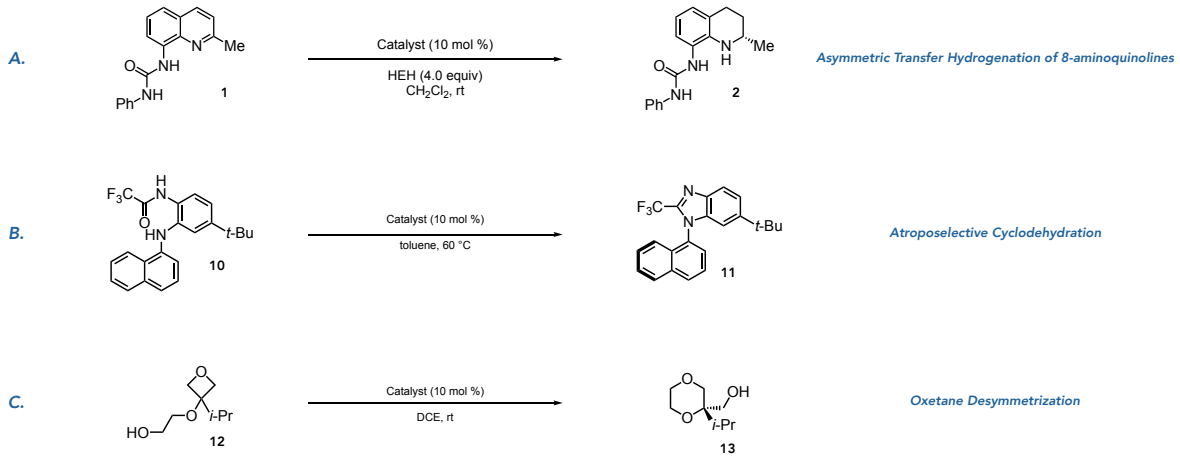
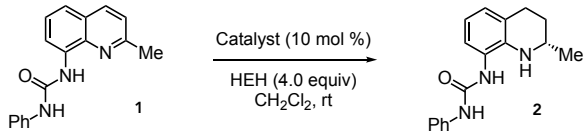



Figure 16 : Transformations selected to test the training set of hybrid catalysts.

With the fully synthesized catalyst training set in hands, we began our investigation of their reactivity and selectivity on the transfer hydrogenation of aminoquinoline **1**, for which literature precedents provide modest to good levels of enantioselectivity (up to 86:14 er).[79] We were pleased to observe a good range of selectivity across the training catalyst library, ranging from racemic to 93.5:6.5 e.r., which was consistent with the selection of a training set of catalyst covering diverse areas of chemical space. Interestingly, the catalysts bearing sulfonamide moieties all seemed to perform well relative to the amide-bearing candidates, providing selectivities greater or equal to 85:15 e.r. (Table 1). It was also observed that nine of amide-bearing catalysts did not provide any

selectivity in the transformation. This apparent "selectivity cliff" is a motif that data-science tools could provide insight into.

**Table 1:** Transfer hydrogenation results




| Catalyst | % yield[b] | e.r.[b] |
|---|---|---|
| **P1** | 39 | 50.5 : 49.5 |
| **P2** | 71 | 91.5 : 8.5 |
| **P3** | 73 | 50.5 : 49.5 |
| **P4** | 89 | 77.5 : 22.5 |
| **P5** | 76 | 49.5 : 50.5 |
| **P6** | 74 | 57 : 43 |
| **P7** | 81 | 87.5 : 12.5 |
| **P8** | 71 | 77 : 23 |
| **P9** | 48 | 50 : 50 |
| **P10** | 71 | 50 : 50 |
| **P11** | 71 | 52 : 48 |
| **P12** | 58 | 85 : 15 |
| **P13** | 69 | 50 : 50 |
| **P14** | 63 | 50 : 50 |
| **P15** | 77 | 49.5 : 50.5 |
| **P16** | 77 | 59.5 : 40.5 |
| **P17** | 65 | 77 : 23 |
| **P18** | 54 | 52.5 : 47.5 |
| **P19** | 83 | 93.5 : 47.5 |
| **P20** | 75 | 68 : 32 |

[a]Conditions: **1** (0.025 mmol), Hantzsch Ester Hydride (HEH, 0.1 mmol), catalyst (10 mol%), $CH_2Cl_2$ (0.25 mL) for 18 h in a sealed half dram vial. Representative selection of catalysts from training set. [b]Yields determined using NMR. Selectivity analyzed using chiral SFC.

### 3.3. Statistical Modeling and Structure-Activity Relationship Analysis

Aiming to gain an in-depth understanding of how the structural features of the catalysts affected the selectivity trends observed in the transfer hydrogenation reaction, a more comprehensive computational analysis was performed. Molecular mechanics search in Macromodel allowed the acquisition of conformational ensembles for each of the catalysts, with the optimal number of clusters determined using the minimum Kelley Penalty score (see supplemental information for details).[37] Each conformer was optimized at the DFT level (PW6B95D3/6-31G+(d,p)) with single-point energy corrections (PW6B95D3/cc-PVTZ) and a library of over 500 descriptors per catalyst was compiled. A nomenclature of the catalysts' atomic labelling is included in Figure 17 for clarity, and a summary of all values for the molecular descriptors discussed in the following sections is provided in Table 2.

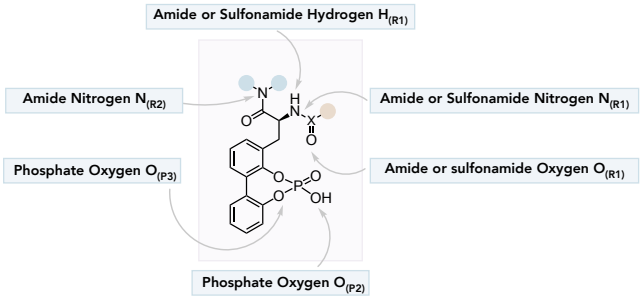



Figure 17 : Catalyst nomenclature used in this section

The analysis of catalyst performance began with classifying the library into a set of selective catalysts and a set of unselective catalysts. Upon removal of data points with yields of or under 10%, the transfer hydrogenation selectivities were processed using a classification algorithm recently disclosed by the Doyle and Sigman groups.[108] The basic principle of this classification algorithm stems from the observation that some reaction profiles show non-linear dependence on molecular descriptors, wherein a threshold value must be met to obtain selectivity. Graphically, this corresponds to a binary response, with unselective catalysts aggregating under both the selectivity threshold and the required value for the selected molecular descriptor. The aforementioned algorithm uses a single node decision tree to classify catalysts into selective and non-selective categories for each molecular descriptor. Accurate classification is obtained from the parameter(s) providing the least number of catalysts assigned in the false negative or false positive regions of the graph (Figure 18).

Table 2: Summary of the molecular descriptors discussed in the modeling of the catalysts

| | Catalyst | ChelpG $O_{(R1)}$ | Hirsch $N_{(R1)}$ | ChelpG $O_{(P2)}$ | Hirsch $H_{(R1)}$ | NBO $O(P_3)$ | NMR $N_{(R2)}$ | Vbur $R_1$ | θ Backbone |
|---|---|---|---|---|---|---|---|---|---|
| Unselective Amides | P1 | - 0.62 | - 0.09 | - 0.79 | 0.11 | - 0.77 | 132.83 | 53.35 | 14.77 |
| | P3 | - 0.59 | - 0.08 | - 0.73 | 0.09 | - 0.77 | 127.51 | 47.13 | 19.41 |
| | P5 | - 0.61 | - 0.09 | - 0.76 | 0.11 | - 0.77 | 129.65 | 60.33 | 15.68 |
| | P6 | - 0.63 | - 0.09 | - 0.77 | 0.11 | - 0.78 | 127.26 | 51.33 | 23.15 |
| | P10 | - 0.63 | - 0.08 | - 0.80 | 0.09 | - 0.78 | 129.74 | 59.50 | 25.19 |
| | P11 | - 0.60 | - 0.09 | - 0.75 | 0.09 | - 0.77 | 127.99 | 51.86 | 16.49 |
| | P12 | - 0.60 | - 0.09 | - 0.71 | 0.12 | - 0.79 | 118.02 | 52.94 | 28.83 |
| | P14 | - 0.62 | - 0.08 | - 0.68 | 0.10 | - 0.80 | 117.20 | 47.75 | 38.83 |
| | P15 | - 0.62 | - 0.09 | - 0.75 | 0.11 | - 0.78 | 125.51 | 59.72 | 23.01 |
| Selective Amides | P4 | - 0.55 | - 0.08 | - 0.72 | 0.09 | - 0.77 | 113.72 | 46.98 | 18.93 |
| | P7 | - 0.54 | - 0.08 | - 0.74 | 0.09 | - 0.80 | 131.69 | 68.26 | 31.27 |
| | P9 | - 0.57 | - 0.08 | - 0.70 | 0.09 | - 0.77 | 111.73 | 48.11 | 16.84 |
| | P16 | - 0.55 | - 0.09 | - 0.78 | 0.09 | - 0.77 | 131.65 | 41.81 | 19.28 |
| | P17 | - 0.54 | - 0.08 | - 0.74 | 0.09 | - 0.80 | 135.40 | 44.08 | 31.79 |
| | P18 | - 0.55 | - 0.08 | - 0.73 | 0.10 | - 0.77 | 136.75 | 33.61 | 20.92 |
| | P20 | - 0.56 | - 0.08 | - 0.76 | 0.09 | - 0.78 | 128.22 | 44.70 | 23.78 |
| Selective Sulfonamides | P2 | - 0.51 | - 0.13 | - 0.73 | 0.11 | - 0.80 | 124.09 | 50.11 | 37.77 |
| | P8 | - 0.48 | - 0.13 | - 0.77 | 0.09 | - 0.80 | 120.89 | 53.19 | 36.52 |
| | P13 | - 0.55 | - 0.13 | - 0.77 | 0.11 | - 0.81 | 127.73 | 51.97 | 35.12 |
| | P19 | - 0.53 | - 0.14 | - 0.72 | 0.10 | - 0.80 | 124.42 | 52.61 | 35.60 |
| Validation Sulfonamides | V1 | - 0.54 | - 0.14 | 0.69 | 0.11 | - 0.81 | 138.92 | 48.32 | 38.78 |
| | V2 | - 0.50 | - 0.13 | 0.67 | 0.09 | - 0.81 | 142.87 | 48.92 | 41.84 |
| | V3 | - 0.51 | - 0.14 | 0.70 | 0.11 | - 0.81 | 133.84 | 43.19 | 38.87 |

In the treatment of the transfer hydrogenation results, the selectivity threshold was set to 0.06 kcal/mol, corresponding to a selectivity of 5% ee or above, for which the best classification was found to rely on the partial charge on the oxygen of the secondary amide substituent using the parameter ChelpG $O_{(R1)}$. ChelpG charges (Charges from Electrostatic Potentials using a Grid-based method) are a quantification method of atomic charges based on molecular electrostatic potential maps calculated for the Boltzmann-weighted average of the conformational ensemble.[109] Gratifyingly, this partial charge term could classify the full catalyst training set without any falsely assigned data points (Figure 19) for a threshold cutoff of ChelpG $O_{(R1)}$ of -0.58.

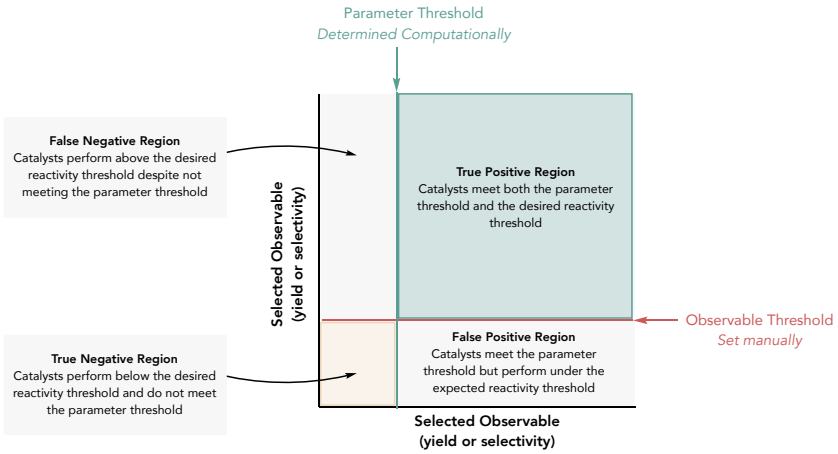



Figure 18 : General representation of the classification method development by the Doyle and Sigman groups.

The identification of the ChelpG $O_{(R1)}$ parameter revealed that all catalysts classifying as non-selective were amides with significant electron density build up at the secondary amide oxygen. Alkyl substituent on the $R_1$ amide resulted in larger negative charges at $O_{(R1)}$ and complete lack of selectivity in the transformation. In contrast, amides bearing aromatic substituents on the secondary amide provided modest to good selectivity (**P9**, **P17**). Despite the diversity of tertiary amides across the training set, the nature of the $R_2$ substituents do not seem to significantly influence selectivity cliff or the partial charge estimated for $O_{(R1)}$. For example, **P15** bears a partial charge of -0.64, where **P19** with the same tertiary amide results in a partial charge of -0.48, each falling on opposite sides of the classification threshold (-0.58).

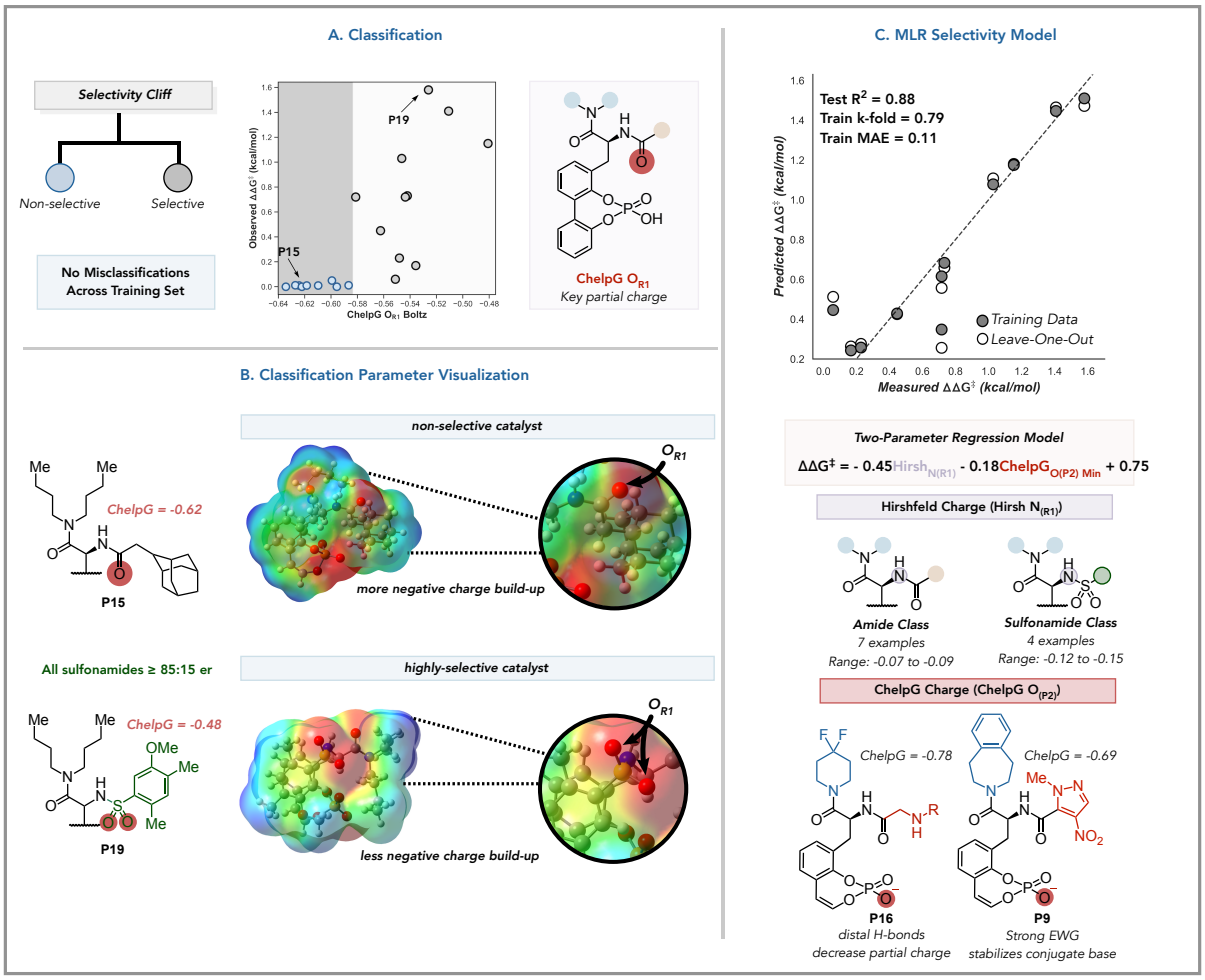



Figure 19 : A) Univariate classification for the selectivity cliff observed in the transfer hydrogenation of 8-aminoquinolines. B) Partial charge visualization for the classification terms. C) MLR model for the transfer hydrogenation reaction.

Of particular interest in the initial design of these hybrid catalysts was the possibility of intramolecular and intermolecular hydrogen bonding and their effect on catalytic efficiency. It is worthy to note that the presence of distal hydrogen bond donors or acceptors on either arm led to non-selective catalysts which were accurately classified out based on ChelpG $O_{(R1)}$ charges. This suggests that the $O_{(R1)}$ electron density is responsive to the presence of these hydrogen bonds. Multiple possible ways to rationalize this response could be speculated. It is possible that an increased electron density on the secondary amide oxygen might encourage intramolecular hydrogen bonding within the catalyst structure (see supplemental Figure S1). These intramolecular hydrogen bonds between $O_{(R1)}$ might fold the catalysts in catalytically inactive conformations (for example, unable to complex the starting material). Alternatively, the intramolecular hydrogen bonds between $O_{(R1)}$ and either side chains might compete with and prevent the hydrogen bonding of $O_{(R1)}$ with the phosphate hydrogen and/or substrate throughout the reaction.

Turning our attention to the eleven catalysts providing some selectivity, we hoped to gain further insight into the structure-activity relationships driving the selectivity trends observed in the

transfer hydrogenation. Data analysis was performed using forward-stepwise linear regression. This process begins with a null model (no selected parameters) and a manual input for the number of parameters desired in the final modeling. The algorithm then works through variables one at a time to determine the parameter with the best linear correlation to the data (has the smallest p-value or leads to the highest increase in line fit $R^2$). The latter is assigned the highest coefficient in the final model equation. The process is repeated, adding terms, one at a time, until the initially set number of terms is reached.[110] Due to relatively small data set (11 data points) and to ensure a minimal inclusion of background variations, the maximum number of parameters was set to two. A two-parameter linear regression model was generated, presenting good statistical fidelity with R2= 0.88 (Figure 19, C). The two parameters identified as critical for selectivity by this model were two partial charges terms: the Hirshfeld charge of the secondary amide/sulfonamide nitrogen $N_{R1}$ (of the lowest energy conformer) with a larger coefficient, and the minimum ChelpG charge on the negatively charged phosphate oxygen $O_{(P2)}$ across all conformers, with a lower coefficient. Hirshfeld charges analysis is a method to obtain an estimation of charge densities of atoms in a molecule based on the charge density deformation relative to the free atoms.[111] These two terms together largely describe the electron density distribution of the $R_1$ substituent of the chiral arm.

A negative correlation was observed between the $N_{(R1)}$ nitrogen Hirshfeld coefficient and reaction selectivity, suggesting an increase in selectivity with increasing electron density at that position in the catalyst structure. The amide catalysts were estimated to have partial charges ranging from -0.07 to -0.09, while the sulfonamide catalysts span partial charges from -0.12 to -0.15, suggesting that this term acts as a linear classifier between the sulfonamides and amides at the secondary position with a cutoff of about -0.10. While negative charge build-up at the $N_1$ position is inherently correlated to the identity of the functional group of the attached fragment, additional analysis revealed multiple intramolecular hydrogen-bonding networks were responsible for the observed differences in partial charge within each subclass of catalysts (**Figure S2).**

The opposite trend was observed for the ChelpG charge on phosphate oxygen $O_{(P2)}$, for which a higher negative charge was inversely correlated with selectivity. The presence of distal hydrogen-bond donor sites on the secondary position was strongly associated with the lowest values of ChelpG (**P16**), corroborating our earlier observation that distal H-bonding sites lead to non-selective catalysts.

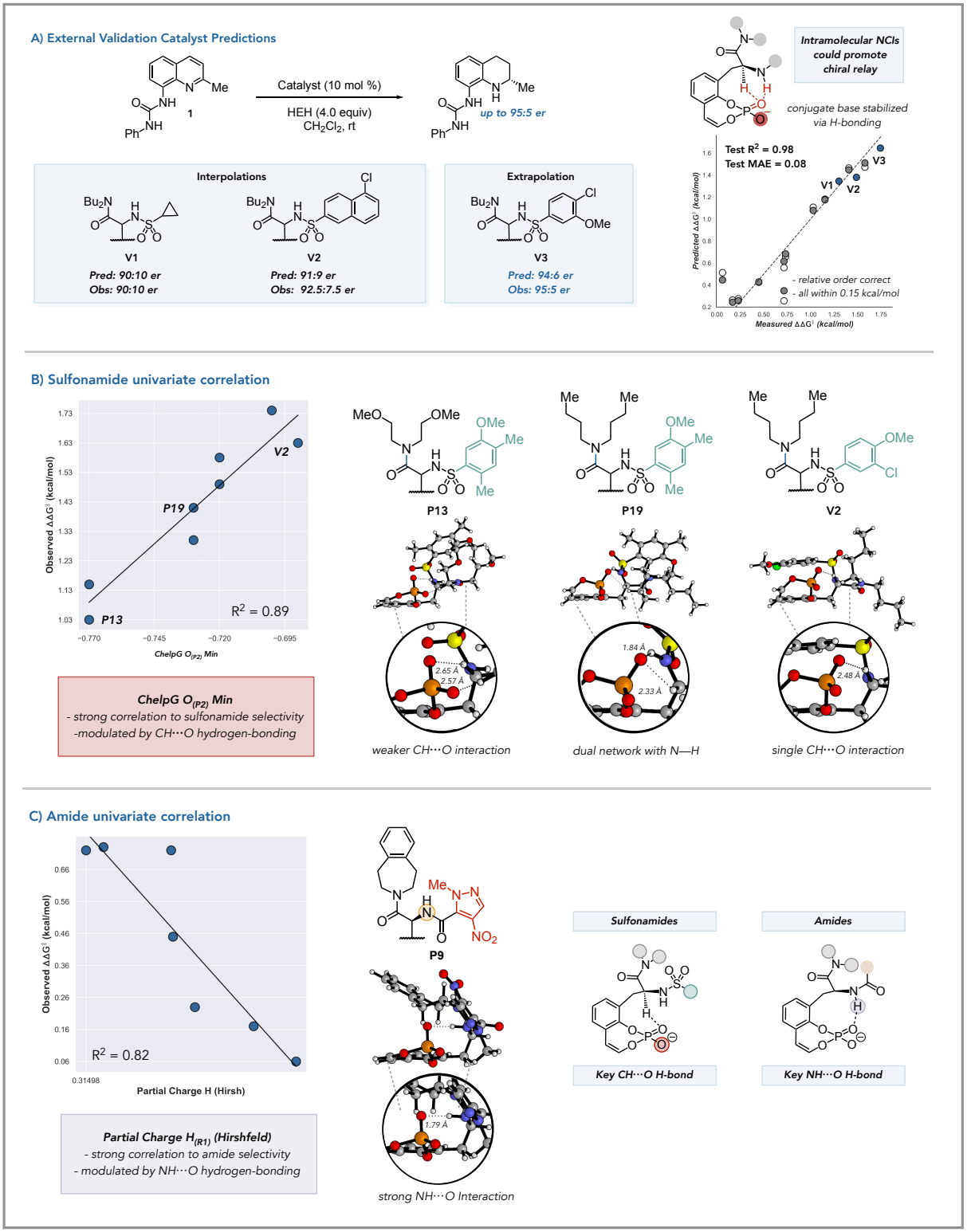



**Figure 20 :** A) Prediction and experimental data for the external validation catalysts. B) Univariate correlations for the two classes of catalysts.

An important objective of library generation and data-science based modeling is the ability to use the structure-activity trends extracted from training set results to predict the selectivity of other catalysts within the chemical space. Noting that the sulfonamide-bearing catalysts tended to provide high selectivities in the transfer hydrogenation reaction, the initial chemical space was re-inspected to select a set of validation candidates (Figure 20). The absence of parameters representing the tertiary amide $R_2$ suggested that this position could be kept constant while modulating the substitution on the secondary amide $R_1$. Predictions for the chosen catalysts interpolated V1 and V2 to 90:10 e.r. and 91:9 e.r., respectively, while V3 was extrapolated to provide the best selectivity of the full catalyst set (94:6 e.r.). We were pleased to find that the experimental selectivities by these catalysts fit the model quite accurately within 0.15 kcal/mol of the predicted values. Although the selectivity provided by catalyst **V1** was diminished, the substitution of aryl substituents for a small alkyl (cyclopropyl) side chain did not inhibit selectivity. Extending the steric bulk and π-stacking opportunities in catalyst **V2** did not provide an increase in selectivity, consistent with the absence of any steric terms in the model. To our delight, extrapolation to sulfonamide **V3** was found to be accurate, providing a new best-in-class catalyst for the transfer hydrogenation of **1** (95:5 er), outperforming previously reported BINOL-type and phosphothreonine-type catalysts for this transformation.[112] Revisiting the model with our validation catalysts, excellent statistics were noted, with a Test $R^2$ of 0.98 and MAE (mean absolute error) of 0.08 kcal/mol (Figure 20).

Observing that each of the sulfonamide catalysts outperformed any of the amides, we hoped to understand the structural features responsible for these disparities in catalyst performance. Based on the statistical model, it was hypothesized that the minimum partial charge ChelpG at $O_{(P2)}$ would correlate with differences in selectivity among each catalyst subclass. Indeed, plotting ChelpG $O_{(P2)}$ against the experimental sulfonamide selectivities provided a strong univariate correlation ($R^2$ = 0.89, Figure 20, B). We postulated this partial charge could relate to the stabilization of the conjugate base through electron delocalization via intramolecular hydrogen-bonding networks, which could enhance the acidity of the phosphoric acid moiety. To probe this, we turned to DFT calculations to analyze the potential stabilizing interactions across the sulfonamides.

Inspection of the sulfonamide catalyst structures revealed that all sulfonamide catalysts share a common CH···O hydrogen-bonding interaction between the methine C—H and the upper P=O bond.[113] The shortened bond length of these interactions (2.33 – 2.65 Å) suggests a strong hydrogen-bond.[114] More electron withdrawing groups in the vicinity would increase the propensity of this proton to act as a hydrogen-bond donor. Accordingly, the least selective sulfonamide **P13** demonstrates the longest observed H-bond length, at 2.65 Å. However, DFT analysis also revealed that the methine C—H can adopt an extended hydrogen-bonding network with the neighboring N—H, resulting in a notably reduced CH···O bond length (2.33 Å, Figure S3). Notably, best in class catalyst **V3** demonstrates a single CH···O bond with pronounced π-stacking between the aryl sulfonamide and backbone, potentially reinforcing this interaction.

Despite the accuracy of the correlation between sulfonamide selectivity and the ChelpG $O_{(P2)}$ partial charge, the subset of selective amide catalysts did not provide significant correlation to the same term in a univariate regression model. Instead, a strong univariate correlation between partial charge on the secondary amide hydrogen ($H_1$) and selectivity was observed ($R^2$ = 0.82,

Figure 21, C). The importance of this term implied that amides may preferentially adopt conformations possessing the N—H hydrogen bond over the CH···O interaction found for sulfonamides. Indeed, DFT calculations on the selective amide catalysts displayed a globally conserved N—H hydrogen-bonding network for which the length of the H-bond correlated to the partial charge of the hydrogen with an $R^2$ of 0.77 (Figure S5). This is supportive of the earlier observation that the Hirshfeld partial charge at $N_{(R1)}$ was central to the amide selectivity trends.

### 3.4. Transferability of the model to other reaction types

Finally, we sought to assess whether the performance trends of the catalyst training set observed in the transfer hydrogenation were transferable to other reaction types. To do so, we examined the catalysts' performance in the next two chosen reactions: an atroposelective cyclodehydration and oxetane desymmetrization. Although the ranges in selectivities obtained were more modest than in the transfer hydrogenation, similar trends could be observed. Importantly, the same non-selective catalysts from the transfer hydrogenation once again provided completely racemic product in both the atroposelective cyclodehydration and the oxetane desymmetrization. Similarly, the sulfonamide-bearing catalysts seemed to provide superior selectivities than the amide-bearing catalysts overall (Table 3, Table 4)

Observing the similarities in selectivity trends, we reasoned that the classification term ChelpG $O_{(R1)}$ might once again be a meaningful predictive tool to determine if a catalyst would be selective or not regardless of the reaction at hand. Satisfactorily, classification of all three reaction data sets with this single partial charge provided high levels of accuracy (0.92, Figure 21).

Further statistical modeling revealed that the stereochemical outcome of all three transformations could be rationalized with the same three catalyst parameters (Figure 21): a Boltzmann-weighted NBO $O_{(P3)}$ charge, the predicted NMR shift at the $N_{(R2)}$ position (tertiary amide) and the maximum buried volume at the $R_1$ (secondary amide) position (Figure 21, B). The inclusion of the predicted NMR $N_{(R2)}$ shift in the modeling terms departs from the single-reaction model derived for the transfer hydrogeneration, which did not show dependence on the nature of the tertiary amide substituents, suggesting that reactions with different activation modes might be more significantly affected by the whole catalyst structure rather than an emphasis on the $R_1$ arm.

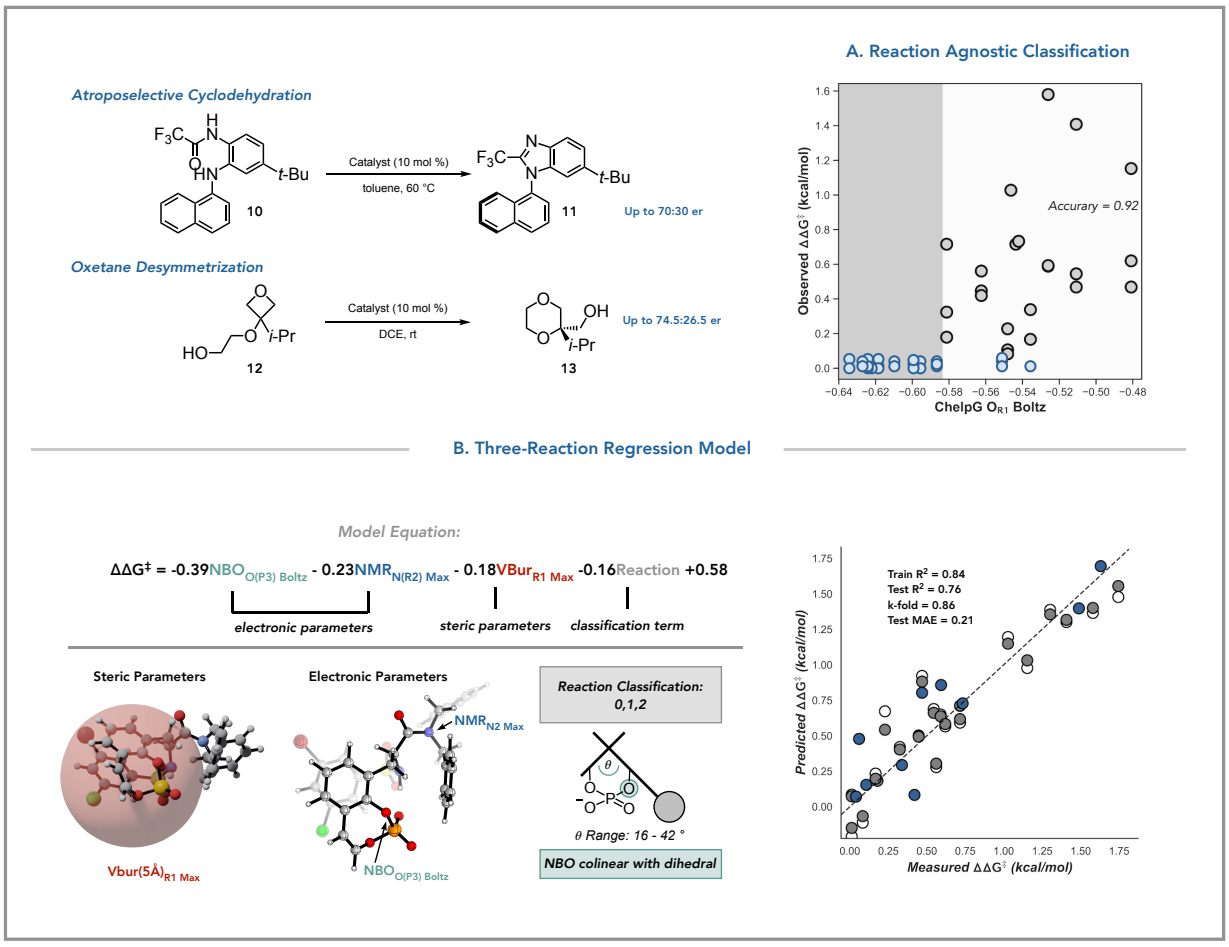
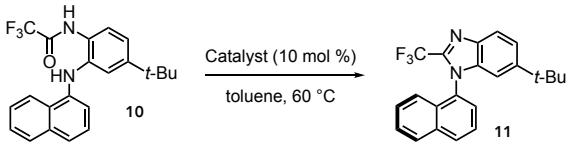



Figure 21 : Data modeling and parameters for the three-reaction system.

Although the model fit to the transfer hydrogenation model did not contain steric terms, the appearance of a steric parameter in the reaction-agnostic model suggests that the cyclodehydration and oxetane desymmetrization both benefit from smaller substituents at the $R_1$ position. Interestingly, the highest weighted term, NBO $O_3$, was found to be co-linear with the dihedral angle of the catalyst backbone (Figure S6). An increase in the dihedral angle – and as such, a wider active site near the phosphoric acid moiety – was correlated to the increase in electron density at the backbone phosphate oxygen $O_{(P3)}$, and to higher selectivities. In traditional BINOL phosphoric acid scaffolds, the dihedral angle is generally enforced by the 3,3' substitution. Despite intentionally moving away from this steric-heavy di-substitution pattern in the design of these hybrid catalysts, the terms extracted by the model still seem to suggest a dependence of the chirality transfer on the steric features of the of scaffold.

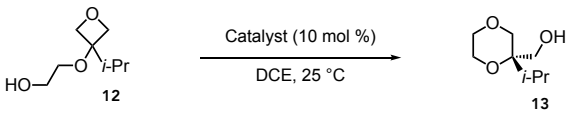
**Table 3:** Atroposelective Cyclodehydration[a]




| Catalyst | % yield[b] | e.r.[b] |
|---|---|---|
| **P1** | 78 | 48 : 52 |
| **P2** | 83 | 67 : 33 |
| **P3** | 35 | 48.5 : 51.5 |
| **P4** | 51 | 87.5 : 12.5[d] |
| **P5** | 30 | 48.5 : 51.5 |
| **P6** | 65 | 48.5 : 51.5 |
| **P7** | 95 | 62.5 : 37.5 |
| **P8** | 79 | 67 : 33 |
| **P9** | 83 | 62 : 38 |
| **P10** | 80 | 48 : 52 |
| **P11** | 80 | 48.5 : 51.5 |
| **P12** | 66 | 50 : 50 |
| **P13** | 5 | 57 : 43 |
| **P14** | 8 | 50 : 50 |
| **P15** | 50 | 48 : 52 |
| **P16** | 27 | 54 : 46 |
| **P17** | 6 | 64 : 36 |
| **P18** | 77 | 51.5 : 48.5 |
| **P19** | 82 | 71 : 29 |
| **P20** | 95 | 70 : 30 |

[a]Conditions: substrate (0.025 mmol), catalyst (10 mol%), in toluene at 60 °C for 14 h in a sealed 4 mL vial. [b]Yields determined by $^{19}$F NMR. Selectivity analyzed using chiral HPLC. [c]Selectivities for catalysts with < 5% yield not obtained. [d]Removed from modeling.

**Table 4:** Oxetane Desymmetrization[a]




| Catalyst | % yield[b] | e.r.[b] |
|---|---|---|
| **P1** | 98 | 50 : 50 |
| **P2** | 96 | 71 : 28 |
| **P3** | 20 | 51 : 49 |
| **P4** | 4[c] | - |
| **P5** | 24 | 50.5 : 49.5 |
| **P6** | 27 | 50.5 : 49.5 |
| **P7** | 23 | 49.5 : 50.5 |
| **P8** | 100 | 49.5 : 50.5 |
| **P9** | 100 | 74 : 26 |
| **P10** | 80 | 57.5 : 42.5 |
| **P11** | 86 | 50 : 50 |
| **P12** | 69 | 50 : 50 |
| **P13** | 0[c] | 51 : 49 |
| **P14** | 0[c] | - |
| **P15** | 12 | - |
| **P16** | 18 | 50 : 50 |
| **P17** | 0[c] | - |
| **P18** | 33 | 50.5 : 49.5 |
| **P19** | 100 | 73 : 27 |
| **P20** | 34 | 67 : 33 |

[a]Conditions: substrate (0.025 mmol), catalyst (10 mol%), DCE (0.25 mL) for 18 h in a sealed 4 mL vial. [b]Yields determined using $^{1}$H NMR. Selectivity analyzed using chiral SFC. [c]Selectivities for catalysts with < 5% yield not obtained.

## IV. Analysis of the Low Performing Catalysts

Upon identifying important parameters influencing the performance of the catalysts, we turned our attention back to the lower performing catalysts hoping to gain a better understanding of their lack of selectivity. Although initial control experiments on the synthetic route suggested that no racemization would occur during the synthesis, the building of larger libraries of catalysts creates an analytical challenge when it comes to checking the enantiopurity of each catalyst within the library. As such, the enantiopurity of the 9 lower performing catalysts which were classified out was analyzed, revealing partial erosion of the chiral center (down to 68% ee). We were pleased to find that the sulfonamide catalysts did not suffer any enantio-erosion, along with amide catalysts bearing substituents which might hinder the rotation of the secondary amide arm. Attempting to probe which of the synthetic steps lead to racemization of the stereocenter, HPLC analysis of all intermediates along the route narrowed down the possibilities to the saponification of methyl ester intermediate **8**, or to the second amide coupling using DEBPT as coupling agent to **9**. While these steps had been assessed by HPLC prior to the generation of the catalyst library, we found that some amide catalysts were more prone to undergoing erosion of the α-amino stereocenter via the pathway proposed in Figure 22.

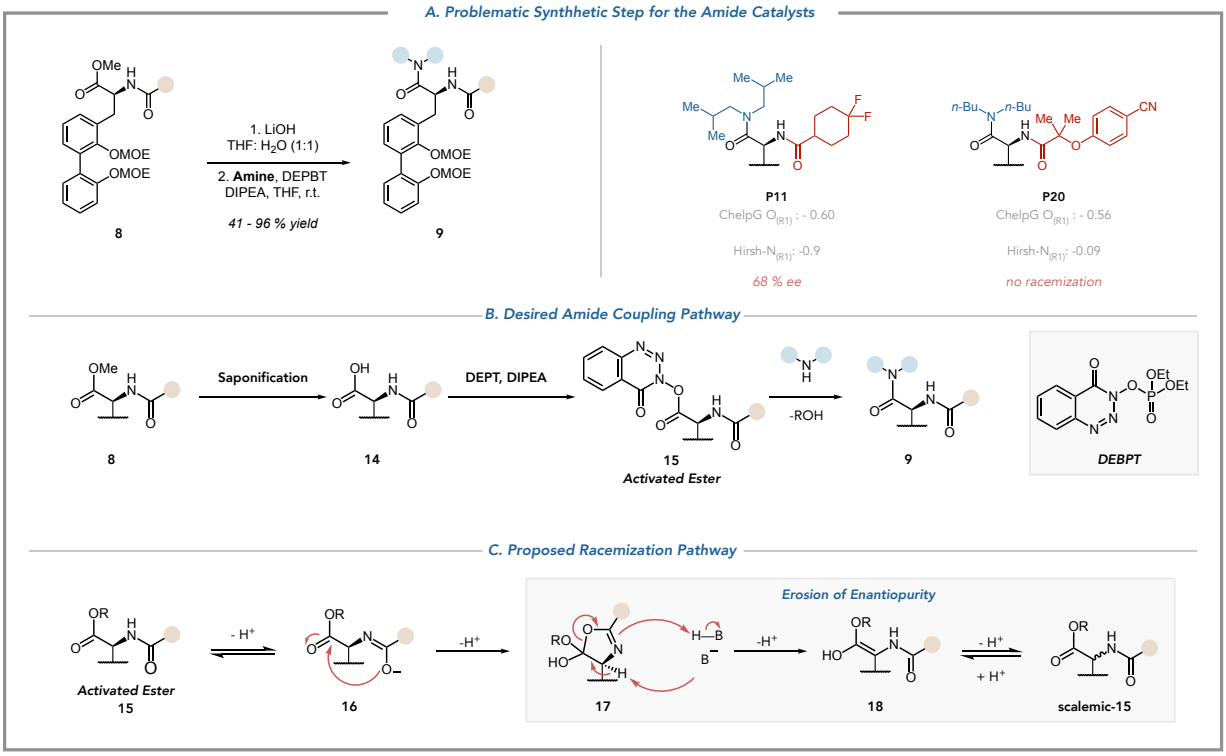



Figure 22 : Proposed racemization pathway and enantiopurity of the catalysts

Through this pathway, we envision that amide fragments with highly electron rich oxygen $O_{(R1)}$ could compete with the secondary amine coupling partner for the displacement of the activated ester **15**. In cases for which the amine is a poor nucleophile, or $O_{(R1)}$ bears a large enough negative charge as observed by the ChelpG $O_{(R1)}$ data, the rate of intramolecular ring formation would

outcompete the intermolecular nucleophilic addition of the amine partner. The resulting oxazole **17** can undergo deprotonation at the chiral stereocenter to planar intermediate **18**. Unselective tautomerization of the later to regenerates the activated ester **15** as a scalemic mixture. Given this proposed pathway, the nucleophilicity of the $O_{(R1)}$ oxygen would provide a basis for the propensity of the intermediate to cyclize. As noted in the discussion of the ChelpG $O_{(R1)}$ trends, the electron-density on the sulfonamide oxygens appears to be lower than that of any of the amides. This can be rationalized by the resonance delocalization of the negative charge of the conjugate base upon deprotonation of the N–H proton, expected to make either of those oxygens poor nucleophiles to outcompete the amine coupling partners.

Interestingly, **P11** and **P20** experienced drastically different extents of racemization, with **P11** dropping to 68% ee, while no erosion of enantiopurity was observed for **P20**. Considering the very similar ChelpG $O_{(R1)}$ and Hirshfeld charge on the secondary amide nitrogen $N_{(R1)}$, this difference in the racemization could be rationalized by a combination of factors. Firstly, the amine partner used in the synthesis of **P11** bears more steric bulk directly around the nucleophilic nitrogen from the isobutyl substituent than the linear alkyl chains of the **P20** amine partner. This increase in steric congestion could decrease the rate of nucleophilic addition of the di-isobutyl amine relative to the di-*n*-butylamine, offering more opportunities for cyclization. Additionally, the presence of the gem-dimethyl groups alpha to the amide could hinder the deprotonation of the activated ester **15**, as planarization to **16** would generate a significant amount of allylic-1,3 strain. As a result, this deprotonation might be kinetically sluggish, thereby lowering the nucleophilicity of $O_{(R1)}$ in **P20**. Finally, it is likely that, even in the event of this deprotonation occurring, the steric congestion provided by the gem-dimethyl substituent would make the cyclization to oxazole **17** unfavorable.

In the context of diversity-oriented synthesis and the generation of catalyst libraries encompassing extended areas of chemical space, it can rapidly become impractical and costly to obtain enantiopurity data for each catalyst candidate within the space once the synthetic route has been validated on one or a handful of examples. A reliable classification model should – hopefully – separate catalysts lacking selectivity, provide some insight into the features leading to their poor performance, as well as highlighting any significant flaws or oversight in the library design. Gratifyingly, the classification provided herein achieved all these goals.

## V. Conclusions and outlook

Seeking to understand the effect of non-covalent interactions and flexibility could play in chiral phosphoric acid catalysis, we developed a new class of adaptative hybrid catalysts a minimalist and conformationally flexible backbone bearing a single point of chirality. A reactivity-based investigation of the selectivity profile of these catalysts was performed by incorporating data-science tools, beginning with the design of a structurally diverse catalyst library training set. A combination of classification and multivariate linear regression tools provided insight into the key features for the selectivity trends observed in the enantioselective transfer hydrogenation of 8-aminoquinolines, enabled the rapid identification of a new class of sulfonamide-bearing phosphoric acid catalysts providing higher levels of selectivity (up to 95:5 er) than the current state-of-the art for this reaction. Further structural analysis suggests that intramolecular hydrogen-bonding networks are responsible for reinforcing the chiral environments present in each catalyst subclass, providing additional evidence that elements of conformational flexibility should not be ignored in favor of steric repulsion when developing chiral catalysts. Importantly, the application of this workflow to an atroposelective cyclodehydration and an oxetane desymmetrization reaction revealed that the selectivity-driving features were conserved across transformations, thereby demonstrating the applicability of classification workflows as predictive tools in novel catalyst design and optimization.

It is important to note that the modeling presented herein relates ground state structural features of the catalysts to their selectivity. However, they do not provide direct evidence into the nature of the transition states for the transformations or the interactions between catalyst and substrate. As such, although important characteristics such as the presence of internal hydrogen bonding networks were shown to be necessary to observe selectivity, it is not guaranteed that these networks are conserved during catalysis, or how exactly they might affect the nature of the activated complex or the transition state. Additional kinetic studies and transition state analysis would be necessary to decipher these outstanding questions. These studies would be particularly important in the development of novel transformations with unknown mechanisms in which catalyst-substrate interactions might be complex or be susceptible to non-linear effects.

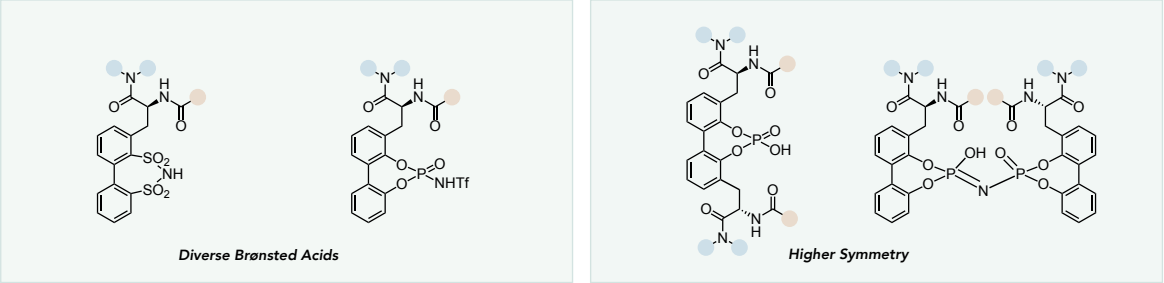



Figure 23: Opportunities for future studies

## VI. References


1. Ardevines, S., Marqués-López, E., and Herrera, R.P. (2022). Horizons in Asymmetric Organocatalysis: En Route to the Sustainability and New Applications. Catalysts *12*. 10.3390/catal12010101.
2. Marckwald, W. (1904). Ueber asymmetrische Synthese. Ber. Dtsch. Chem. Ges. *37*, 349–354.
3. Bredig, G., and Fiske, P.S. (1912). Biochem. Z. *46*, 7.
4. Kenyon, J., and Ross, W.A. (1952). A New Reaction Mechanism for the Marckwald Asymmetric Synthesis. J. Chem. Soc., 2307–2310.
5. Fischer, F.G., and Marschall, A. (1931). Über die Beschleunigung von Aldol-Kondensationen durch Amino-säuren. Ber. Dtsch. Chem. Ges. *64*, 2825–2827.
6. Kuhn, R., Badstubner, W., and C., G. (1936). Über Aldehyd-Kondensationen mit sekundären Aminen (Knoevenagel-Reaktion). Ber. Dtsch. Chem. Ges. *69*, 98–107.
7. Pracejus, H. (1960). Organische Katalysatoren, LXI. Asymmetrische Synthesen mit Ketenen, I. Alkaloid-katalysierte asymmetrische Synthesen von α-Phenyl-propionsäureestern. Liebigs Ann. Chem. *634*, 9–22.
8. Pracejus, H. (1960). Asymmetrische Synthesen mit Ketenen, II. Stereospezifische Addition von α-Phenyl-äthylamin an Phenyl-methyl-keten. Liebigs Ann. Chem. *634*, 23–29.
9. Eder, U., Sauer, G., and Wiechert, R. (1971). New type of asymmetric cyclization to optically active steroid CD partial stuctures. Angew. Chem. Int. Ed. Engl. *10*, 496–497.
10. Hajos, Z.G., and Parrish, D.R. (1974). Asymmetric synthesis of bicyclic intermediates of natural product chemistry. J. Org. Chem. *39*, 1615–1621.
11. Sigman, M.S., and Jacobsen, E.N. (1998). Schiff Base Catalysts for the Asymmetric Strecker Reaction Identified and Optimized from Parallel Synthetic Libraries. J. Am. Chem. Soc. *120*, 4901–4902.
12. List, B., Lerner, R.A., and Barbas, C.F. (2000). Proline-Catalyzed Direct Asymmetric Aldol Reactions. J. Am. Chem. Soc. *122*, 2395–2396.
13. Ahrendt, K.A., Borths, C.J., and MacMillan, D.W.C. (2000). New Strategies for Organic Catalysis: The First Highly Enantioselective Organocatalytic Diels−Alder Reaction. J. Am. Chem. Soc. *122*, 4243–4244.
14. Brønsted, J.N. (1923). Einige Bemerkungen über den Begriff der Säuren und Basen. Recueil des Travaux Chimiques des Pays-Bas *42*, 718–728.
15. Lowry, T.M. (1923). The uniquness of hydrogen. J. Soc. Chem. Ind. *42*, 43–47.
16. Rueping, M., Parmar, D., and Sugiono, E. (2016). Asymmetric Brønsted Acid Catalysis (Wiley-VCH Verlag GmbH & Co. KGaA).
17. Marschalk, C. (1928). Bull. Soc. Chim. Fr. *43*, 1388.
18. Jacques, J., Fouquey, C., and Viterbo, R. (1971). Enantiomeric cyclic binaphthyl phosphoric acids as resolving agents. Tetrahedron Lett. *12*, 4617–4620.
19. Jacques, J., and Fouquey, C. (1989). Enantiomeric (S)-(+)- and (R)-(−)-1,1'-Binaphthyl-2,2’-diyl Hydrogen Phosphate. Org. Synth. *67*, 1.
20. Viterbo, R., and Jacques, J. (1974) Optical isomers of binaphthyl-phosphoric acids. patent application US00233793A.

21. Kyba, E.P., Gokel, G.W., de Jong, F., Koga, K., Sousa, L.R., Siegel, M.G., Kaplan, L., Sogah, G.D.Y., and Cram, D.J. (1977). Host-guest complexation. 7. The binaphthyl structural unit in host compounds. J. Org. Chem. *42*, 4173–4184.
22. Miyano, S., Tobita, M., and Hashimoto, H. (1981). Asymmetric Synthesis of Axially Dissymmetric 1,1'-Binaphthyls via an Intramolecular Ullmann Coupling Reaction of (R)- and (2)-2,2'-Bis(1-bromo-2-naphthylcarbonyloxy)-1,1'-binaphthyl. Bull. Chem. Soc. Jpn. *54*, 3522–3526.
23. Hoyano, Y.Y., and Pincock, R.E. (1980). Carbon catalyzed organic reactions: carbon promoted solvolysis of a phosphate ester derived from 1,1'-bi-2-naphthol. Can. J. Chem. *58*, 134–137.
24. Edwards, M.L. (1989) 7-[[Amino(1,3-dihydrobenzo[c]thienyl)acetyl]amino]cephalosporin derivatives. patent application 883409.
25. Werner, W., Jungstand, W., Gutsche, W., and Wohlrabe, K. (1981) Verfahren zur herstellung von chiralen 6,6A,7,8,13A-hexahydro-eckige klammer auf 1 eckige klammer zu-benopyrano-eckige klammer auf 4,3-B eckige klammer zu-1,5-benzodiazepinen. Ger. (East) Patent.
26. Cornforth, J. (1978). Review lecture - The imitation of enzymic catalysis. Proc. R. Soc. London, Ser. B *203*, 101. 10.1098/rspb.1978.0095.
27. Cornforth, J. (1996). Synthesis of substituted dibenzophospholes. Part 9. Preparation of two water-soluble phosphinic–polyphosphonic acids. J. Chem. Soc., Perkin Trans. *1*, 2889–2893.
28. Cornforth, J., Cornforth, R.H., and Gray, R.T.J. (1982). Synthesis of substituted dibenzophospholes. Part 1. J. Chem. Soc., Perkin Trans. *1*, 2289-2297
29. Cornforth, J., Sierakowski, A.F., and Wallace, W.T. (1982). Synthesis of substituted dibenzophospholes. Part 2. Syntheses of intermediate biphenyls and quaterphenyls. J. Chem. Soc., Perkin Trans. *1*, 2299–2315.
30. Cornforth, J., Ridley, D.D., Sierakowski, A.F., Uguen, D., and Wallace, W.T. (1982). Synthesis of substituted dibenzophospholes. Part 3. Synthesis of 4,6-diaryldibenzophospholes from m-quaterphenyls. J. Chem. Soc., Perkin Trans., 2317–2331.
31. Cornforth, J., Ridley, D.D., Sierakowski, A.F., Uguen, D., and Wallace, W.T. (1982). Synthesis of substituted dibenzophospholes. Part 4. Chemical transformations of 4,6-diaryl-3,7-dialkoxydibenzophosphole 5-oxides. J. Chem. Soc., Perkin Trans., 2333–2339.
32. Parmar, D., Sugiono, E., Raja, S., and Rueping, M. (2014). Complete field guide to asymmetric BINOL-phosphate derived Bronsted acid and metal catalysis: history and classification by mode of activation; Bronsted acidity, hydrogen bonding, ion pairing, and metal phosphates. Chem. Rev. *114*, 9047–9153. 10.1021/cr5001496.
33. Akiyama, T., Itoh, J., Yokota, K., and Fuchibe, K. (2004). Enantioselective Mannich-type reaction catalyzed by a chiral Brønsted acid. Angew Chem Int Ed Engl *43*, 1566–1568. 10.1002/anie.200353240.
34. Uraguchi, D., and Terada, M. (2004). Chiral Brønsted Acid-Catalyzed Direct Mannich Reactions via Electrophilic Activation. J. Am. Chem. Soc. *126*, 5356–5357. 10.1021/ja0491533.

35. Storer, R.I., Carrera, D.E., Ni, Y., and C., M.D.W. (2006). Enantioselective Organocatalytic Reductive Amination. J. Am. Chem. Soc. *128*, 84–86. 10.1021/ja057222n.
36. Rueping, M., Sugiono, E., Azap, C., Theissmann, T., and Bolte, M. (2005). Enantioselective Brønsted acid catalyzed transfer hydrogenation: organocatalytic reduction of imines. Org. Lett. *7*, 3781–3783. 10.1021/ol0515964.
37. Hoffman, S., Seayad, A.M., and List, B. (2005). A powerful Brønsted acid catalyst for the organocatalytic asymmetric transfer hydrogenation of imines. Angew. Chem. Int. Ed. Engl. *44*, 7424–7427. 10.1002/anie.200503062.
38. Jain, P., and Antilla, J.C. (2010). Chiral Brønsted Acid-Catalyzed Allylboration of Aldehydes. J. Am. Chem. Soc. *132*, 11884–11886.
39. Terada, M., and Sorimachi, K. (2007). Enantioselective Friedel-Crafts Reaction of Electron-Rich Alkenes Catalyzed by Chiral Brønsted Acid. J. Am. Chem. Soc. *129*, 292–293. 10.1021/ja0678166.
40. Itoh, J., Fuchibe, K., and Akiyama, T. (2008). Chiral Phosphoric Acid Catalyzed Enantioselective Friedel-Crafts Alkylation of Indoles with Nitroalkenes: Cooperative Effect of 3Å Molecular Sieves. Angew. Chem. Int. Ed. Engl. *47*, 4016–4018. 10.1002/anie.200800770.
41. He, Y., Lin, M., Li, Z., Liang, X., Li, G., and Antilla, J.C. (2011). Direct Synthesis of Chiral 1,2,3,4-Tetrahydropyrrolo[1,2-a]pyrazines via a Catalytic Asymmetric Intramolecular Aza-Friedel-Crafts Reaction. Org. Lett. *13*, 4490–4493.
42. Lee, S., and Kim, S. (2009). Enantioselective radical addition reactions to imines using binaphthol-derived chiral N-triflyl phosphoramides. Tetrahedron *50*, 3345–3348.
43. Neel, A.J., Hehn, J.P., Tripet, P.F., and Toste, F.D. (2013). Asymmetric Cross-Dehydrogenative Coupling Enabled by the Design and Application of Chiral Triazole-Containing Phosphoric Acids. J. Am. Chem. Soc. *135*.
44. Wang, J., Zheng, S., Rajkumar, S., Xie, J., Yu, N., Peng, Q., and Yang, X. (2020). Chiral phosphoric acid-catalyzed stereodivergent synthesis of trisubstituted allenes and computational mechanistic studies. Nat. Commun. *11*, 5527.
45. Tay, J.-H., Argüelles, A.J., and Nagorny, P. (2015). Direct Interconversion of BINOL and H8-BINOL-Based Chiral Brønsted Acids Using Single-Step Red/Ox Manipulations. Org. Lett. *17*, 3774−3777.
46. Yepes, D., Neese, F., List, B., and Bistoni, G. (2020). Unveiling the delicate Balance of Steric and Dispersion Interactions in Organocatalysis using High-Level Computational Methods. J. Am. Chem. Soc. *142*, 3613–3625.
47. Fan, Y.-S., Jiang, Y.-J., An, D., Sha, D., Antilla, J.C., and Zhang, S. (2014). H8-BINOL Chiral Imidodiphosphoric Acids Catalyzed Enantioselective Synthesis of Dihydroindolo-/-pyrrolo[1,2-a]quinoxalines. Org. Lett. *16*, 6112−6115.
48. Momiyama, N., Konno, T., Furiya, Y., Iwamoto, T., and Terada, M. (2011). Design of Chiral Bis-phosphoric Acid Catalyst Derived from (R)-3,30-Di(2-hydroxy-3-arylphenyl)binaphthol: Catalytic Enantioselective DielsAlder Reaction of α,β-Unsaturated Aldehydes with Amidodienes. J. Am. Chem. Soc. *133*, 19294–19297.
49. Schreyer, L., Properzi, R., and List, B. (2019). IDPi Catalysis. Angew. Chem. Int. Ed. Engl. *58*, 12761–12777. 10.1002/anie.201900932.

50. Honjo, T., Phipps, R.J., Rauniyar, V., and Toste, F.D. (2012). A Doubly Axially Chiral Phosphoric Acid Catalyst for the Asymmetric Tandem Oxyfluorination of Enamides. Angew. Chem. Int. Ed. Engl. *51*, 1–6.
51. Guo, Q.S., Du, D.M., and Xu, J. (2008). The development of double axially chiral phosphoric acids and their catalytic transfer hydrogenation of quinolines. Angew. Chem. Int. Ed. Engl. *47*, 759–762. 10.1002/anie.200703925.
52. Fleischmann, M., Drettwan, D., Sugiono, E., Rueping, M., and Gschwind, R.M. (2011). Brønsted acid catalysis: hydrogen bonding versus ion pairing in imine activation. Angew. Chem. Int. Ed. Engl. *50*, 6364–6369.
53. Reid, J.P., Simon, L., and Goodman, J.M. (2016). A Practical Guide for Predicting the Stereochemistry of Bifunctional Phosphoric Acid Catalyzed Reactions of Imines. Acc. Chem. Res. *49*, 1029–1041. 10.1021/acs.accounts.6b00052.
54. Reid, J.P., and Sigman, M.S. (2019). Holistic prediction of enantioselectivity in asymmetric catalysis. Nature *571*, 343–348. 10.1038/s41586-019-1384-z.
55. Klussmann, M., Ratjen, L., Hoffmann, S., Wakchaure, V., Goddard, R., and List, B. (2010). Synthesis of TRIP and Analysis of Phosphate Salt Impurities. Synlett *14*, 2189−2192.
56. Melikian, M., Gramuller, J., Hioe, J., Greindl, J., and Gschwind, R.M. (2019). Bronsted acid catalysis - the effect of 3,3'-substituents on the structural space and the stabilization of imine/phosphoric acid complexes. Chem. Sci. *10*, 5226–5234. 10.1039/c9sc01044k.
57. Reid, J.P., and Goodman, J.M. (2016). Goldilocks Catalysts: Computational Insights into the Role of the 3,3' Substituents on the Selectivity of BINOL-Derived Phosphoric Acid Catalysts. J. Am. Chem. Soc. *138*, 7910–7917. 10.1021/jacs.6b02825.
58. Coric, I., and List, B. (2012). Asymmetric spiroacetalization catalysed by confined Bronsted acids. Nature *483*, 315–319. 10.1038/nature10932.
59. Xu, F., Huang, D., Han, C., Shen, W., Lin, X., and Wang, Y. (2010). SPINOL-derived phosphoric acids: synthesis and application in enantioselective Friedel-Crafts reaction of indoles with imines. J. Org. Chem. *75*, 8677–8680. 10.1021/jo101640z.
60. Knowles, R.R., and Jacobsen, E.N. (2010). Attractive noncovalent interactions in asymmetric catalysis: Links between enzymes and small molecule catalysts. PNAS *107*, 20678–20685.
61. Neel, A.J., Hilton, M.J., Sigman, M.S., and Toste, F.D. (2017). Exploiting non-covalent pi interactions for catalyst design. Nature *543*, 637–646. 10.1038/nature21701.
62. Davis, H.J., and Phipps, R.J. (2017). Harnessing non-covalent interactions to exert control over regioselectivity and site-selectivity in catalytic reactions. Chem. Sci. *8*, 864–877.
63. Milo, A., Neel, A.J., Toste, F.D., and Sigman, M.S. (2015). Organic chemistry. A data-intensive approach to mechanistic elucidation applied to chiral anion catalysis. Science *347*, 737–743.
64. Toste, F.D., Sigman, M.S., and Miller, S.J. (2017). Pursuit of Noncovalent Interactions for Strategic Site-Selective Catalysis. Acc. Chem. Res. *50*, 609–615.
65. Doyle, A.G., and Jacobsen, E.N. (2007). Small-Molecule H-Bond Donors in Asymmetric Catalysis. Chem. Rev. *107*, 5713−5743.
66. Crawford, J.M., and Sigman, M.S. (2019). Conformational Dynamics in Asymmetric Catalysis: Is Catalyst Flexibility a Design Element? Synthesis *51*, 1021–1026.

67. Colby Davie, E.A., Mennen, S.M., Xu, Y., and Miller, S.J. (2007). Asymmetric Catalysis Mediated by Synthetic Peptides. Chem. Rev. *107*, 5759−5812.
68. Inoue, S., Ohashi, S., Tabata, A., and Tsuruta, T. (1971). Asymmetric Addition Catalyzed By Optically Active Polymers II. Makromol. Chem. *150*.
69. Oku, J.-i., Ito, N., and Inoue, S. (1979). Asymmetric Cyanohydrin Synthesis Catalyzed by Synthetic Dipeptides, 1. Makromol. Chem. *180*, 1089–1091.
70. Ohashi, S., and Inoue, S. (1972). Asymmetric Addition Catalyzed by Optically Active Polymers. 3. Makromol. Chem. *160*, 69–81.
71. Inoue, S., Unno, U., and Ohashi, S. (1972). Asymmetric Addition Catalyzed By Optically Active Polymers. 4. Addition of Lauryl Mercaptan to Dimetryl Maleate and Dimethyl Fumarate. Polym. J. *3*, 611–616.
72. Fukushima, H., and Inoue, S. (1975). Asymmetric synthesis catalyzed by poly(4-benzyl L-asapartate). Makromol. Chem. *176*, 3609–3611.
73. Ueyanagi, K., and Inoue, S. (1977). Asymmetric synthesis catalyzed by (S)-alanine-N-propylamide as a terminal model of poly[(S)-alanine]. Makromol. Chem. *178*, 375–381.
74. Juliá, S., Guixer, J., Masana, J., Rocas, J., Colonna, S., Annuziata, R., and Molinari, H. (1982). Synthetic enzymes. Part 2. Catalytic asymmetric epoxidation by means of polyamino-acids in a triphase system. J. Chem. Soc. Perkin Trans., 1317–1324.
75. Juliá, S., Masana, J., and Vega, J.C. (1980). "Synthetic Enzymes". Highly Stereoselective Epoxidation of Chalcone in a Triphasic Toluene-Water-Poly[(S)-alanine] System. Angew. Chem. Int. Ed. Engl. *19*, 929–931.
76. Copeland, G.T., Jarvo, E.R., and Miller, S.J. (1998). Minimal Acylase-Like Peptides. Conformational Control of Absolute Stereospecificity. J. Org. Chem. *63*, 6784–6785.
77. Barford, D., Das, A.K., and Egloff, M.-P. (1998). The Structure and Mechanism of Protein Phosphatases: Insights into Catalysis and Regulation. Annu. Rev. Biophys. Biomol. Struct. *27*, 133−164.
78. Mahajan, A., Yuan, C., Lee, H., Chen, E.S.-W., Wu, P.-Y., and Tsai, M.-D. (2008). Structure and Function of the Phosphothreonine-Specific FHA Domain. Sci. Signaling *1*, re12.
79. Shugrue, C.R., and Miller, S.J. (2015). Phosphothreonine as a Catalytic Residue in Peptide-Mediated Asymmetric Transfer Hydrogenations of 8-Aminoquinolines. Angew Chem Int Ed Engl *54*, 11173–11176. 10.1002/anie.201505898.
80. Reid, J.P. (2021). Open questions on the transfer of chirality. Communications Chemistry *4*. 10.1038/s42004-021-00614-y.
81. Miller, S.J. (2004). In Search of Peptide-Based Catalysts for Asymmetric Organic Synthesis. Acc. Chem. Res. *37*, 601–610. 10.1021/ar030061c.
82. Holland, M.C., Paul, S., Schweizer, W.B., Bergander, K., Mück-Lichtenfeld, C., Lakhdar, S., Mayr, H., and Gilmour, R. (2013). Noncovalent Interactions in Organocatalysis: Modulating Conformational Diversity and Reactivity in the MacMillan Catalyst. Angew. Chem. Int. Ed. Engl. *52*, 7967–7971.
83. Santiago, C.B., Guo, J.Y., and Sigman, M.S. (2018). Predictive and mechanistic multivariate linear regression models for reaction development. Chem. Sci. *9*, 2398–2412. 10.1039/c7sc04679k.
84. Orlandi, M., Coelho, J.A.S., Hilton, M.J., Toste, F.D., and Sigman, M.S. (2017). Parametrization of Non-covalent Interactions for Transition State Interrogation Applied to Asymmetric Catalysis. J. Am. Chem. Soc. *139*, 6803–6806.

85. Prochazkova, E., Kolmer, A., Ilgen, J., Schwab, M., Kaltschnee, L., Fredersdorf, M., Schmidts, V., Wende, R.C., Schreiner, P.R., and Thiele, C.M. (2016). Uncovering Key Structural Features of an Enantioselective Peptide-Catalyzed Acylation Utilizing Advanced NMR Techniques. Angew. Chem. Int. Ed. Engl. *55*, 15754–15759.
86. Krenske, E.H., and Houk, K.N. (2013). Aromatic Interactions as Control Elements in Stereoselective Organic Reactions. Acc. Chem. Res. *46*, 979–989.
87. Yan, X.C., Metrano, A.J., Robertson, M.J., Abascal, N.C., Tirado-Rives, J., Miller, S.J., and Jorgensen, W.L. (2018). Molecular Dynamics Simulations of a Conformationally Mobile Peptide-Based Catalyst for Atroposelective Bromination. ACS Catal. *8*, 9968–9979.
88. Sigman, M.S., Harper, K.C., Bess, E.N., and Milo, A. (2016). The Development of Multidimensional Analysis Tools for Asymmetric Catalysis and Beyond. Acc. Chem. Res. *49*, 1292–1301.
89. Poree, C., and Schoenebeck, F. (2017). A Holy Grail in Chemistry: Computational Catalyst Design: Feasible or Fiction? Acc. Chem. Res. *50*, 605–608.
90. Foscato, M., and Jensen, V.R. (2020). Automated in Silico Design of Homogeneous Catalysts. ACS Catal. *10*, 2354–2377.
91. Houk, K.N., and Cheong, P.H.-Y. (2008). Computational prediction of small-molecule catalysts. Nature *455*, 309–313.
92. Ahn, S., Hong, M.H., Sundararajan, M., Ess, D.H., and Baik, M.-H. (2019). Design and Optimization of Catalysts Based on Mechanistic Insights Derived from Quantum Chemical Reaction Modeling. Chem. Rev. *119*, 6509–6560.
93. Christensen, M., Yunker, L., Adedeji, F., Häse, F., Roch, L., Gensch, T., dos Passos Gomes, G., Zepel, T., Sigman, M.S., Aspuru-Guzik, A., and Hein, J. (2021). Data-science driven autonomous process optimization. Commun. Chem. *4*, 112.
94. Zahrt, A.F., Athavale, S.V., and Denmark, S.E. (2020). Quantitative Structure−Selectivity Relationships in Enantioselective Catalysis: Past, Present, and Future. Chem. Rev. *120*, 1620–1689.
95. Wheeler, S.E., Seguin, T.J., Guan, Y., and Doney, A.C. (2016). Noncovalent Interactions in Organocatalysis and the Prospect of Computational Catalyst Design. Acc. Chem. Res. *149*, 1061–1069.
96. Zahrt, A.F., Henle, J.J., Rose, B.T., Wang, Y., Darrow, W.T., and Denmark, S.E. (2019). Prediction of higher-selectivity catalysts by computer-driven workflow and machine learning. Science *363*, 247.
97. Bro, R., and Smilde, A.K. (2014). Principal component analysis. Anal. Methods *6*, 2812–2831.
98. See, X.Y., X., W., Wheeler, T.A., Klein, C.K., Goodpaster, J.D., Reiner, B.R., and Tonks, I.A. (2020). Iterative Supervised Principal Component Analysis Driven Ligand Design for Regioselective Ti-Catalyzed Pyrrole Synthesis. ACS Catal. *10*, 13504–13517.
99. Ahneman, D.T., Estrada, J.G., Lin, S., Dreher, S.D., and Doyle, A.G. (2018). Predicting reaction performance in C-N cross-coupling using machine learning. Science *360*, 186–190.
100. Moriwaki, H., Tian, Y.S., Kawashita, N., and Takagi, T. (2018). Mordred: a molecular descriptor calculator. J. Cheminform *10*, 4. 10.1186/s13321-018-0258-y.

101. Frisch, M.J., Trucks, G.W., Schlegel, H.B., Scuseria, G.E., Robb, M.A., Cheeseman, J.R., Scalmani, G., Barone, V., Petersson, G.A., Nakatsuji, H., et al. (2016). Gaussian 16. Revision C.01 (Gaussian, Inc.).
102. Jolliffe, I.T., and Cadima, J. (2016). Principal component analysis: a review and recent developments. Philos. Trans. A. Math. Phys. Eng. Sci. *374*. 10.1098/rsta.2015.0202.
103. Likas, A., Vlassis, N., and Verbeek, J. (2003). The global k-means clustering algorithm. Pattern Recognition *36*, 451–461. 10.1016/S0031-3203(02)00060-2.
104. Brittain, W.D.G., and Cobb, S.L. (2017). Negishi cross-couplings in the synthesis of amino acids. Org. Biomol. Chem. *16*, 10–20. 10.1039/c7ob02682j.
105. Ye, Y.H., Li, H., and Jiang, X. (2005). DEPBT as an efficient coupling reagent for amide bond formation with remarkable resistance to racemization. Biopolymers *80*, 172–178. 10.1002/bip.20201.
106. Kwon, A., Chinn, A.J., Byoungmoo, K., and Miller, S.J. (2018). Divergent Control of Point and Axial Stereogenicity: Catalytic Enantioselective C−N Bond-Forming Cross-Coupling and Catalyst-Controlled Atroposelective Cyclodehydration. Angew Chem Int Ed Engl *57*, 6251–6255. 10.1002/anie.201802963.
107. Yang, W., and Sun, J. (2016). Organocatalytic Enantioselective Synthesis of 1,4-Dioxanes and Other Oxa-Heterocycles by Oxetane Desymmetrization. Angew Chem Int Ed Engl *55*, 1868-1871. 10.1002/anie.201509888.
108. Newman-Stonebraker, S.H., Smith, S.R., Borowski, J.E., Peters, E., Gensch, T., Johnson, H.C., Sigman, M.S., and Doyle, A.G. (2021). Univariate classification of phoshine ligation state and reactivity in cross-coupling catalysis. Science *374*, 301–308.
109. Breneman, C.M., and Wiberg, K.B. (1990). Determining atom-centered monopoles from molecular electrostatic potentials. The need for high sampling density in formamide conformational analysis. J. Comp. Chem. *11*, 361–373.
110. Hocking, R.R. (1976). The Analysis and Selection of Variables in Linear Regression. Biometrics *32*, 1–49.
111. Hirshfeld, F.L. (1977). Bonded-Atom Fragments for Describing Molecular Charge Densities. Theoret. Chim. Acta *44*, 129–138.
112. Shugrue, C.R., and Miller, S.J. (2015). Phosphothreonine as a catalytic residue in peptide-mediated asymmetric transfer hydrogenations of 8-aminoquinolines. Angew Chem Int Ed Engl *54*, 11173-11176. 10.1002/anie.201505898.
113. Gu, Y., Kar, T., and Schiener, S. (1999). Fundamental Properties of the CH—O Interaction: Is It a True Hydrogen Bond? J. Am. Chem. Soc. *121*, 9411–9422.
114. Grabowski, S.J. (2020). Hydrogen Bond – Definitions, Criteria of Existence and Various Types. In Understanding Hydrogen Bonds: Theoretical and Experimental Views, (The Royal Society of Chemistry), pp. 1–40. 10.1039/9781839160400-00001

## VII. Supplemental Information

### 7.1. General Information

Unless otherwise noted, all reactions were carried out under an ambient atmosphere using oven-dried or flame-dried glassware equipped with a magnetic stir bar. Commercial reagents were purified prior to use according to the procedures outlined by Perrin and Armarego unless otherwise indicated.[1] Dry organic solvents (Tetrahydrofuran, Toluene, Acetonitrile, Dichloromethane, Diethyl Ether, *N*,*N*-Dimethyl Formamide, Benzene, and Pentanes) were purified according to the method of Grubbs et al. and used directly after withdrawal from dry Argon solvent stills after passing through activated alumina.[2] Pyridine was dried over KOH followed by fractional distillation and stored over 5Å molecular sieves prior to use. Solutions in organic solvents were concentrated *in vacuo* using a Büchi rotary evaporator equipped with a temperature-controlled water bath and an isopropyl alcohol-dry ice bath to trap volatile compounds, and further dried on Schlenk high-vacuum lines.

Chromatographic purification of products was accomplished using flash chromatography on silica gel (Sigma-Aldrich, 60 Å pore size, 230–400 mesh particle size, 40–63 μm particle size) according to the method of Still,[3] or by reverse-phased flash chromatography using a CombiFlash-*Rf* ® (Teledyne ISCO) and Teledyne-ISCO RediSep-*Rf* $C_{18}$ Silica Columns (60 Å pore size, 230–400 mesh particle size, 40–63 μm particle size), or a Biotage Selekt equipped with a 12 g or 60 g Sfär C18 HC D. Preparative TLC was conducted using glass backed Silicycle Silica Gel 60 F254 plates (250 μm thickness). Analytical thin-layer chromatography (TLC) was performed on TLC plates from Silicycle Siliaplate™ glass-backed TLC plates (250 μm thickness, 60 Å porosity, F-254 indicator). Visualization of the developed plates was accomplished by fluorescence quenching under a 254 nm UV lamp or staining with $KMnO_4$ or Cerium Ammonium Molybdate (CAM) solutions.

$^{1}H$ NMR, $^{13}C$ NMR, $^{19}F$ NMR, and $^{31}P$ NMR spectra were taken with Bruker spectrometers operating at 300, 400, 500, or 600 MHz at the UC Berkeley NMR Facility in the College of Chemistry,* or a Bruker Ascend 500 MHz equipped with a $N_2$ CryoProbe Prodigy at the University of Utah.** The $^{1}H$ and $^{13}C$ NMR spectra were internally referenced to the residual protic $CHCl_3$ (7.26 ppm ($^{1}H$), 77.16 ppm ($^{13}C$), Cambridge Isotope Laboratories Inc.) signal, $(CH_3)_2SO$ (2.50 ppm ($^{1}H$), 39.52 ppm ($^{13}C$), Cambridge Isotope Laboratories Inc.) signal, or $CH_3CN$ (1.94 ppm ($^{1}H$), 118.26 ppm ($^{13}C$), Cambridge Isotope Laboratories Inc.) unless otherwise indicated. $^{1}H$ NMR data reported in this work follow the format: chemical shift (δ ppm), multiplicity (s = singlet, d = doublet, t = triplet, q = quartet, m = multiplet, dd = doublet of doublets, dt = doublet of triplets, br = broad), coupling constant (Hz), integration.

Chiral separations and enantiomeric ratio (er) data were obtained using HPLC at UC Berkeley on a Shimatzu VP Series Chiral HPLC and columns (chiral supports, 5 μm particle size, 4.6 x 250 nm) from Daicel Chemical Industries, or by supercritical fluid chromatography (SFC) on a Waters Acquity UPC$^2$ using Waters Trefoil CEL 1/CEL 2 columns at the University of Utah. Optical rotations were recorded on a Perkin-Elmer Polarimeter 241 at the sodium D line (589 nm) using a Type 40T TempTrolTM cell of 1.0 dm path length at UC Berkeley, or a Perkin-Elmer Polarimeter

341 at the sodium D line (1.0 dm path length) at the University of Utah. Data is reported as follows: $[\alpha]\lambda^{temp}$, concentration (*c*, in g/100 mL), and solvent.

IR spectra were recorded on a Bruker Vertex 80 FTIR spectrometer at the UC Berkeley Catalysis Center and are reported in wavenumbers ($cm^{-1}$). High-Resolution Mass Spectra were obtained from the UC Berkeley QB3/Chemistry Mass Spectrometry Facility on a Waters Fourier Transform Ion Cyclotron Resonance Mass Spectrometer with ESI/TOF, or a Waters LCP Premier XE instrument by ESI/TOF at the University of Utah.

*** We thank Dr. Hasan Celik and UC Berkeley's NMR facility in the College of Chemistry (CoC-NMR) for spectroscopic assistance. The instruments used in this work are supported by the National Science Foundation under Grant No. 2019784.**

**** Construction of the D.M. Grant NMR facility was funded by the University of Utah and NIH Awards 1C06RR017539-01A1 and 3R01GM063540-17W1. NMR instruments were purchased with support of NIH Award 1S10OD25241-01and the University of Utah.**

## 7.2. Catalyst Synthesis and Characterization

### 7.2.1. General Procedures

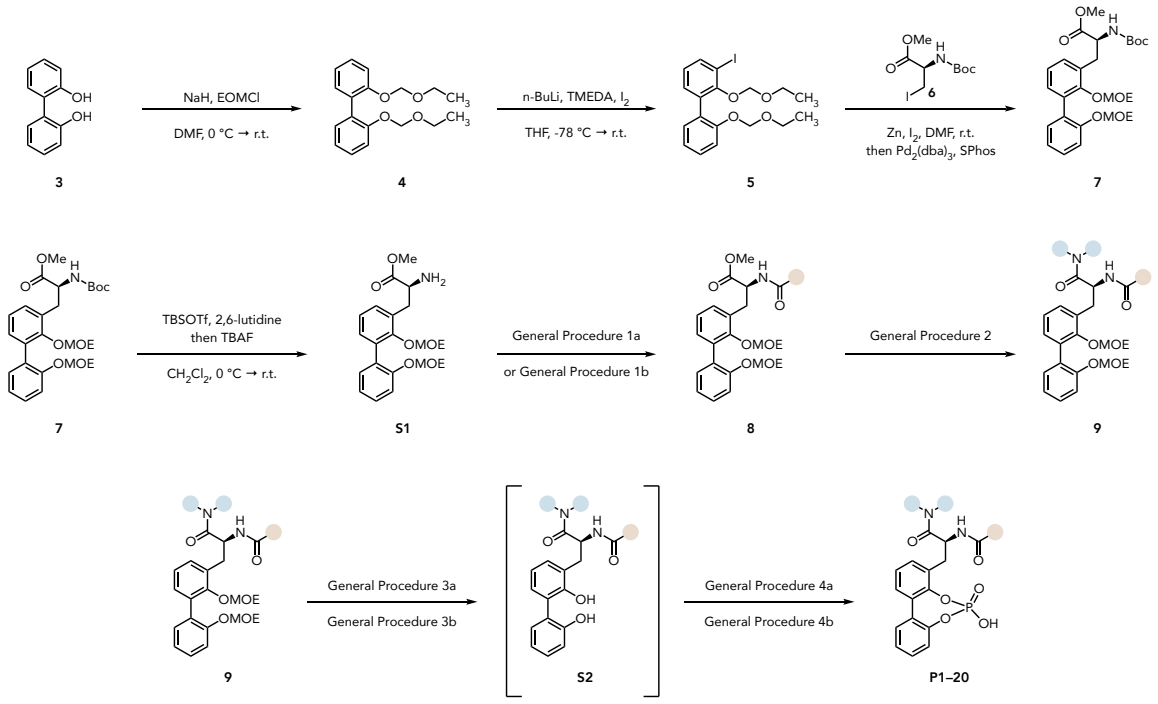
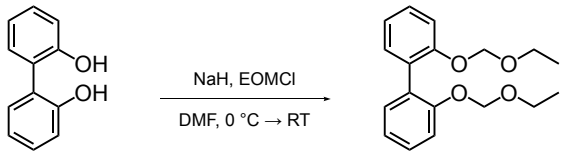



Figure S 1 : Full synthetic route for the catalysts

**A) <u>Backbone Synthesis</u>**




**2,2'-bis(ethoxymethoxy)-1,1'-biphenyl (4).**

NaH (60% in mineral oil, 36.1 g, 902 mmol, 2.4 equiv.) was added to a 3-necked, 2 L round bottom flask under an atmosphere of $N_2$ and sequentially washed with hexanes (200 mL x 2) to remove the mineral oil. Anhydrous DMF (500 mL) was added, and the flask was cooled to 0 °C before the slow addition of 2,2'-biphenol **(3)**, 70.0 g, 376 mmol, 1.0 equiv.) through a powder funnel. *<u>Caution: $H_2$ gas is evolved in the process, **3** added slowly in batches.</u>* The reaction was allowed to stir for 30 minutes, then chloromethyl ethyl ether (90.7 mL, 977 mmol, 2.6 equiv.) was added dropwise via an addition funnel. *<u>Caution: HCl gas evolution occurs</u>*. The reaction was then warmed to room temperature and stirred for 30 minutes, then sat. aq. $NH_4Cl$ (600 mL) was added and vigorously stirred for 15 minutes to ensure quenching of excess EOMCl. The solution was then poured into a 2 L separatory funnel and extracted with $Et_2O$ (800 mL x 3). The combined organic layers were washed with brine and purified by column chromatography with a gradient of

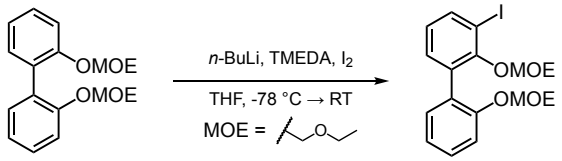
0-7% EtOAc/Hx to yield 110 g of the title compound (97% yield) as a white solid. Characterization data matches reported literature.[4]

**$^1$H NMR (400 MHz, CDCl3)** δ 7.31 (m, 2H), 7.26 – 7.20 (m, 4H), 7.06 (td, *J* = 7.3, 1.5 Hz, 2H), 5.11 (s, 4H), 3.58 (q, *J* = 7.1 Hz, 4H), 1.15 (t, *J* = 7.1 Hz, 6H).

**$^{13}$C NMR (101 MHz, CDCl3)** δ 155.2, 131.6, 129.3, 128.8, 121.8, 115.8, 94.1, 64.1, 15.2.

**HRMS (ESI+/TOF, *m/z*):** Exact mass calculated for $[C_{18}H_{22}O_4+Na]^+$ calc. 325.1416; found 325.1386.

***Safety Note:*** *Precaution must be taken when handling sodium hydride in DMF to prevent thermal decomposition.[4]*




**4** **5**

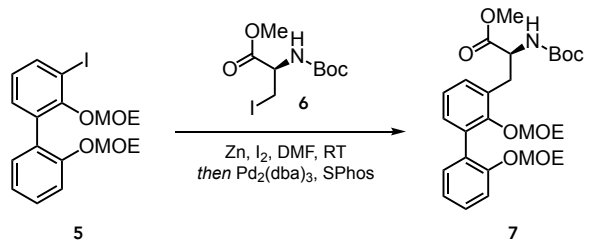
**2,2'-bis(ethoxymethoxy)-3-iodo-1,1'-biphenyl (5).**

A 2 L round bottom flask was charged with **4** (68.6 g, 227 mmol, 1.0 equiv), then evacuated and backfilled with $N_2$. TMEDA (37.5 mL, 250 mmol, 1.1 equiv) and anhydrous THF (650 mL) were added. The flask was cooled to 0 °C and *n*-butyllithium (100 mL, 2.5 M in hexanes, 250 mmol, 1.1 equiv) was cannulated into the reaction dropwise. The reaction continued to stir for 90 minutes before being cooled to –78 °C. Iodine (63.5 g, 250 mmol, 1.1 equiv) was added neat, then the reaction was warmed to room temperature and allowed to stir overnight. The reaction was quenched with sat. aq. $Na_2SO_3$ (300 mL), then extracted with EtOAc (300 mL x 3). The combined organic layers concentrated to provide the crude oil which was used in the next step without further purification. The crude reaction mixture was analyzed via $^1$H NMR to obtain reaction conversion (80%). A sample was also purified by column chromatography to provide analytically pure product for characterization.

**$^1$H NMR (400 MHz, $CDCl_3$):** δ 7.79 (dd, *J* = 7.9, 1.6 Hz, 1H), 7.36 – 7.19 (m, 4H), 7.05 (td, *J* = 7.4, 1.2 Hz, 1H), 6.89 (t, *J* = 7.7 Hz, 1H), 5.16 (s, 2H), 4.74 (s, 2H), 3.62 (q, *J* =7.1Hz,2H),3.31 (q, *J* =7.0Hz,2H), 1.17 (t, *J* =7.1Hz, 3H), 0.99 (t, *J* =7.1Hz, 3H).

**$^{13}$C NMR (101 MHz,$CDCl_3$):** δ 154.8, 154.8, 138.9, 133.6, 132.4, 131.6, 129.3, 128.5, 125.7, 121.8, 115.4, 98.0, 93.7, 93.0, 65.6, 64.4, 15.2, 15.0.

**HRMS (ESI+) m/z:** Exact mass calculated for $[C_{18}H_{21}O_4I+Na]^+$ requires 451.0382; found 451.0402.



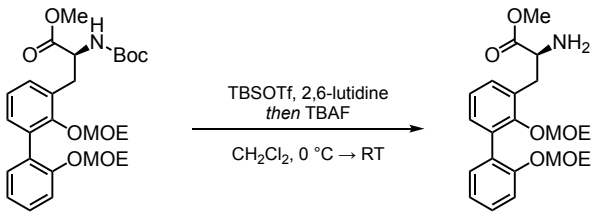

**Methyl (*S*)-3-(2,2'-bis(ethoxymethoxy)-[1,1'-biphenyl]-3-yl)-2-((*tert*-butoxycarbonyl)amino)propanoate (7).**

A 1 L round bottom flask was charged with a stir bar and zinc dust (37 g, 568 mmol, 2.5 equiv). The flask was flame-dried under vacuum and then backfilled with $N_2$. Upon complete cooling, 50 mL of DMF was added and the flask was placed in a RT water bath. Then, iodine (8.7 g, 34 mmol, ß0.15 equiv) was added to the flask and the mixture was stirred until the color dissipated. The alkyl iodide **6** (78.5 g, 242 mmol, 1.05 equiv) was dissolved in 100 mL of DMF and slowly added dropwise via cannula to the zinc. Following the complete addition of **6**, additional iodine (8.7 g, 34 mmol, 0.15 equiv) was added and the mixture was stirred at room temperature for 1 hour. After 1 hour, full consumption of alkyl iodide was confirmed by TLC. The $Pd_2dba_3$ (6.2 g, 6.8 mmol, 0.03 equiv) and SPhos (5.6 g, 6.8 mmol, 0.06 equiv) were then added, followed by aryl iodide **5** dissolved in 80 mL of DMF. The reaction continued to stir under an $N_2$ atmosphere for 16 hours and was then purified by column chromatography (silica, 10 to 30% EtOAc/hexanes) to yield 60 g of **7** (52% yield over 2 steps) as a brown oil**.**

**$^1$H NMR (500 MHz, $CDCl_3$)** δ 7.33 – 7.26 (m, 2H), 7.26 – 7.23 (m, 1H), 7.18 (ddd, *J* = 9.5, 7.5, 1.9 Hz, 2H), 7.13 – 7.08 (m, 1H), 7.05 (td, *J* = 7.4, 1.3 Hz, 1H), 5.64 (d, *J* = 7.8 Hz, 1H), 5.16 (s, 2H), 4.60 – 4.51 (m, 3H), 3.74 (s, 3H), 3.64 – 3.56 (m, 2H), 3.55 – 3.41 (m, 2H), 3.22 – 3.11 (m, 2H), 1.39 (s, 9H), 1.16 (t, *J* = 7.1 Hz, 3H), 1.10 (t, *J* = 7.1 Hz, 3H).

**$^{13}$C NMR (126 MHz, $CDCl_3$)** δ 173.1, 155.7, 154.9, 154.5, 132.2, 131.7, 131.2, 130.1, 130.0, 129.1, 128.9, 124.1, 121.9, 115.7, 98.1, 93.8, 79.7, 65.5, 64.2, 54.9, 52.3, 32.7, 28.4, 15.2, 15.1.

**HRMS (ESI+/TOF, *m/z*):** Exact mass calculated for $[C_{27}H_{37}NO_8+Na]^+$ calc. 526.2417; found 526.2417.




7 S1

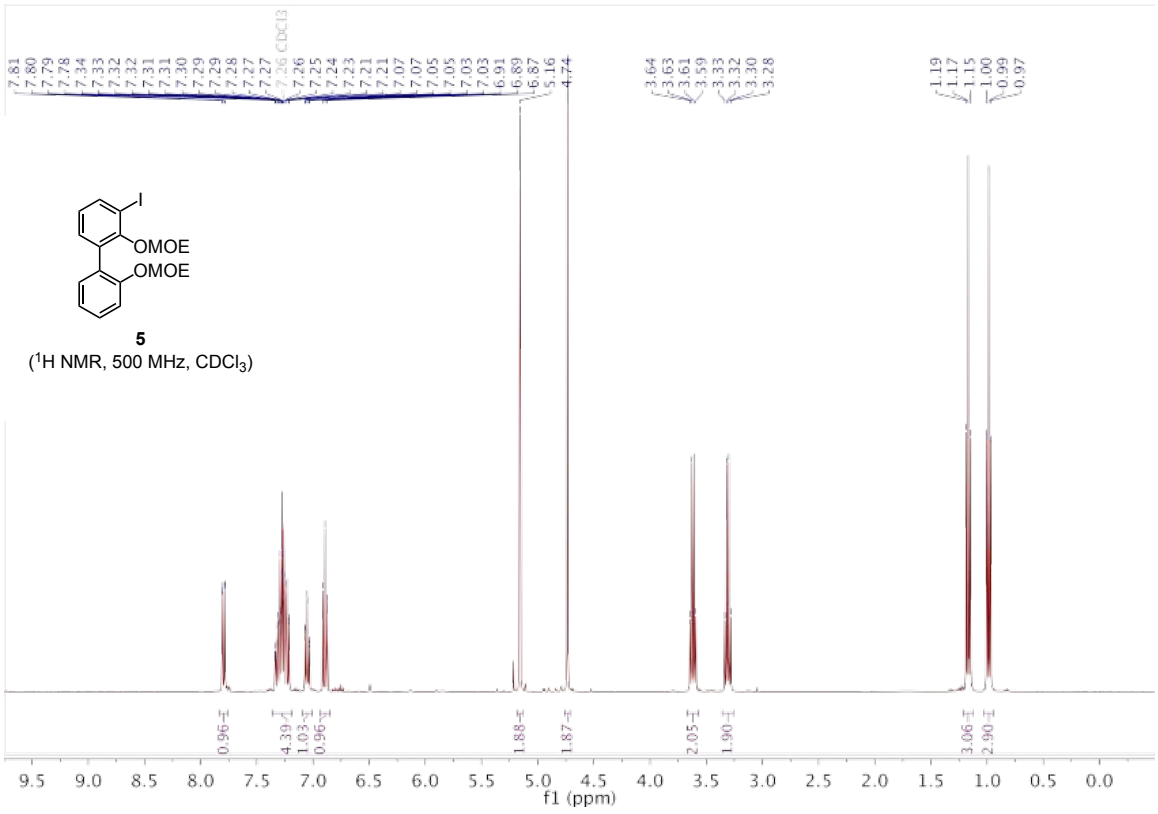
**Methyl (*S*)-2-amino-3-(2,2'-bis(ethoxymethoxy)-[1,1'-biphenyl]-3-yl)propanoate** (**S1**).

To a 2 L round bottom flask containing **7** (102 mmol, 0.84 equiv.) was added $CH_2Cl_2$ (240 mL). The flask was put under an atmosphere of $N_2$ and cooled to 0 °C and 2,6-lutidine (28 mL, 242 mmol, 2.0 equiv.) was added. The TBSOTf (42 mL, 182 mmol, 1.5 equiv.) was added to an addition funnel and added dropwise over the course of 30 minutes. Upon complete addition, the reaction was warmed to room temperature and stirred for 3 hours. The flask was then cooled to 0 °C and TBAF (135 mL, 1 M in THF, 135 mmol, 1.1 equiv.) was added slowly with the use of an addition funnel. Upon complete addition, the reaction was warmed to room temperature and stirred for 1 hour, then was quenched with MeOH (250 mL). The reaction flask was connected directly to the rotary evaporator to remove majority of the solvent and was then transferred to a high vacuum setup and concentrated until a thick sludge was obtained. The crude mixture was dissolved in $CH_2Cl_2$ and stored at -20 °C to prevent racemization. The crude product was characterized with Q-NMR and used as a solution in the next step without further purification. A sample was purified by normal phase chromatography (EtOAc/Hexanes) for analytical characterization.

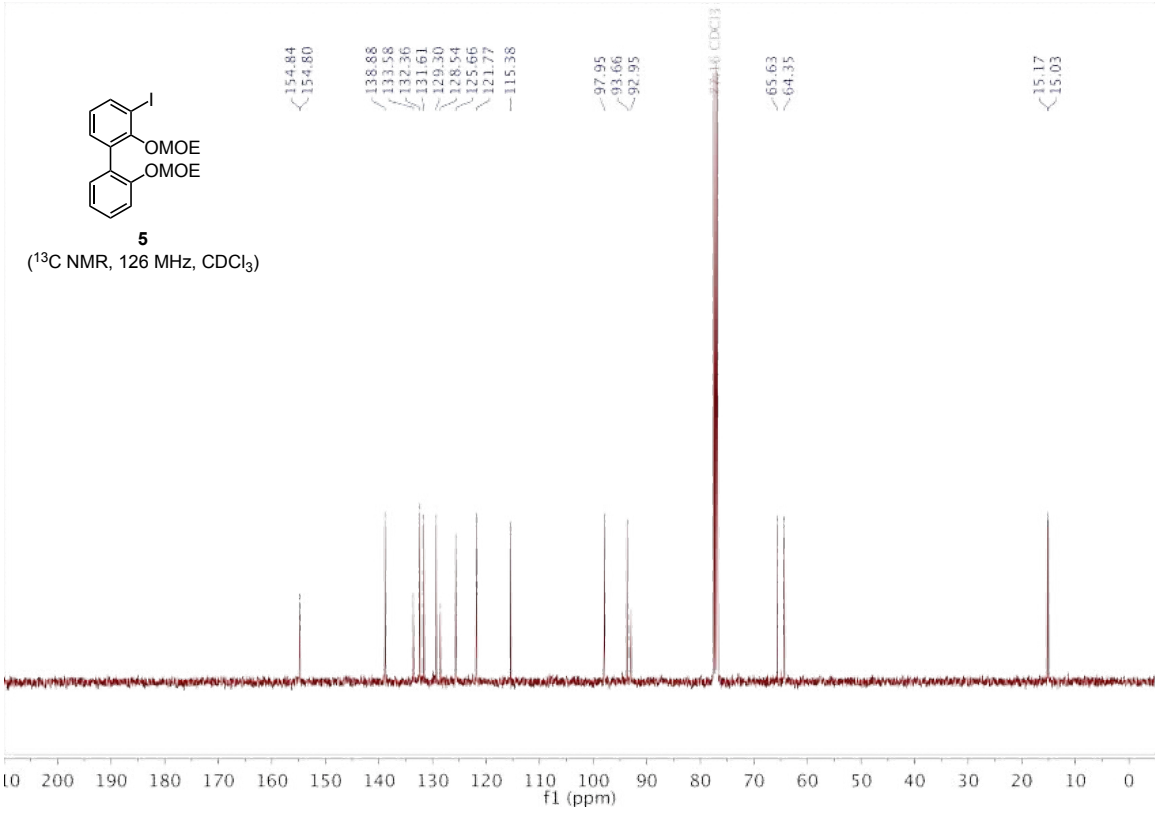
**$^1$H NMR (500 MHz, $CDCl_3$)** δ: 7.33 – 7.26 (m, 2H), 7.24 – 7.13 (m, 3H), 7.12 – 7.00 (m, 2H), 5.72 (d, *J* = 7.6 Hz, 1H), 5.14 (q, *J* = 6.9 Hz, 2H), 4.65 (td, *J* = 8.1, 5.1 Hz, 1H), 4.55 (dd, 2H), 3.71 (s, 3H), 3.66 – 3.51 (m, 3H), 3.48 – 3.40 (m, 1H), 3.21 (dd, *J* = 13.8, 8.6 Hz, 1H), 3.08 (dd, *J* = 13.7, 5.1 Hz, 1H), 1.15 (t, *J* = 7.1 Hz, 3H), 1.06 (t, *J* = 7.1 Hz, 3H). *Note: single amine N—H observed.*

**$^{13}$C NMR (126 MHz, $CDCl_3$)** δ 173.5, 157.0, 154.8, 154.7, 131.9, 131.7, 131.0, 130.3, 129.9, 129.1, 129.0, 123.9, 121.8, 115.6, 98.1, 93.7, 65.6, 64.3, 54.3, 52.1, 32.7, 15.1, 15.0. *Note: O-Ar rotamer present.*

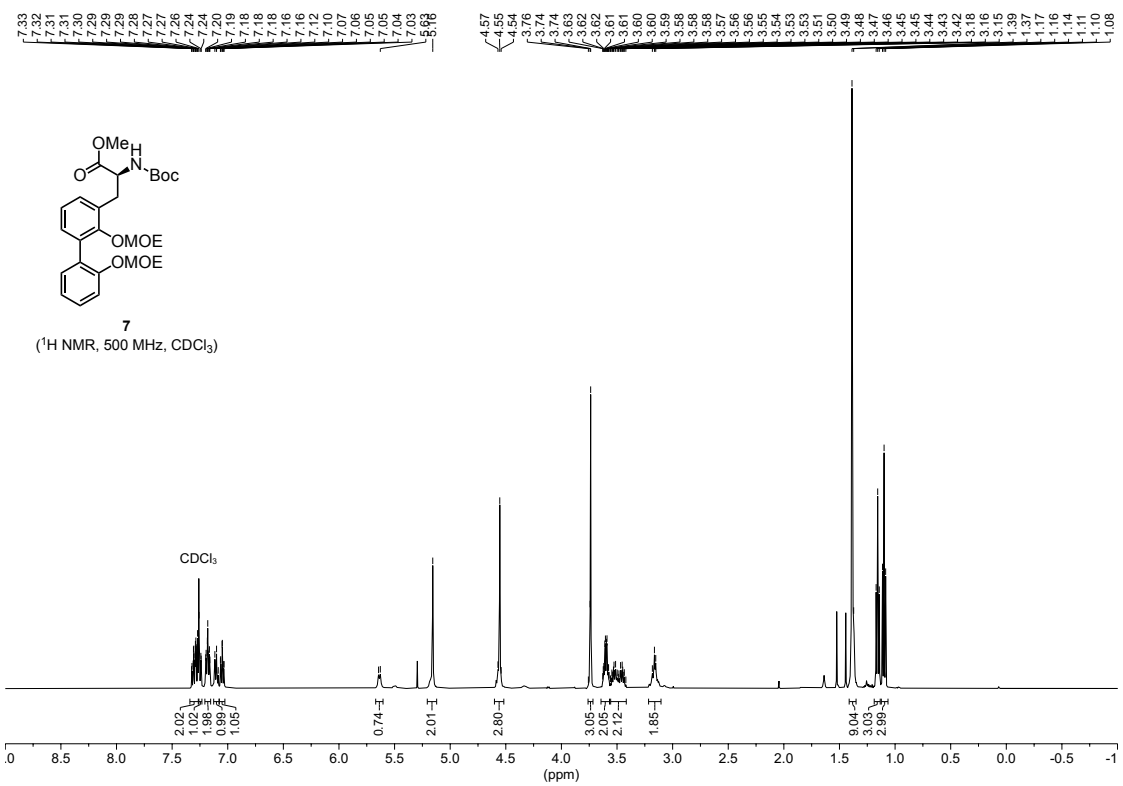
**HRMS (ESI+/TOF, *m/z*):** Exact mass calculated for $[C_{22}H_{29}NO_6+H]^+$ calc. 404.2073; found 404.2079.



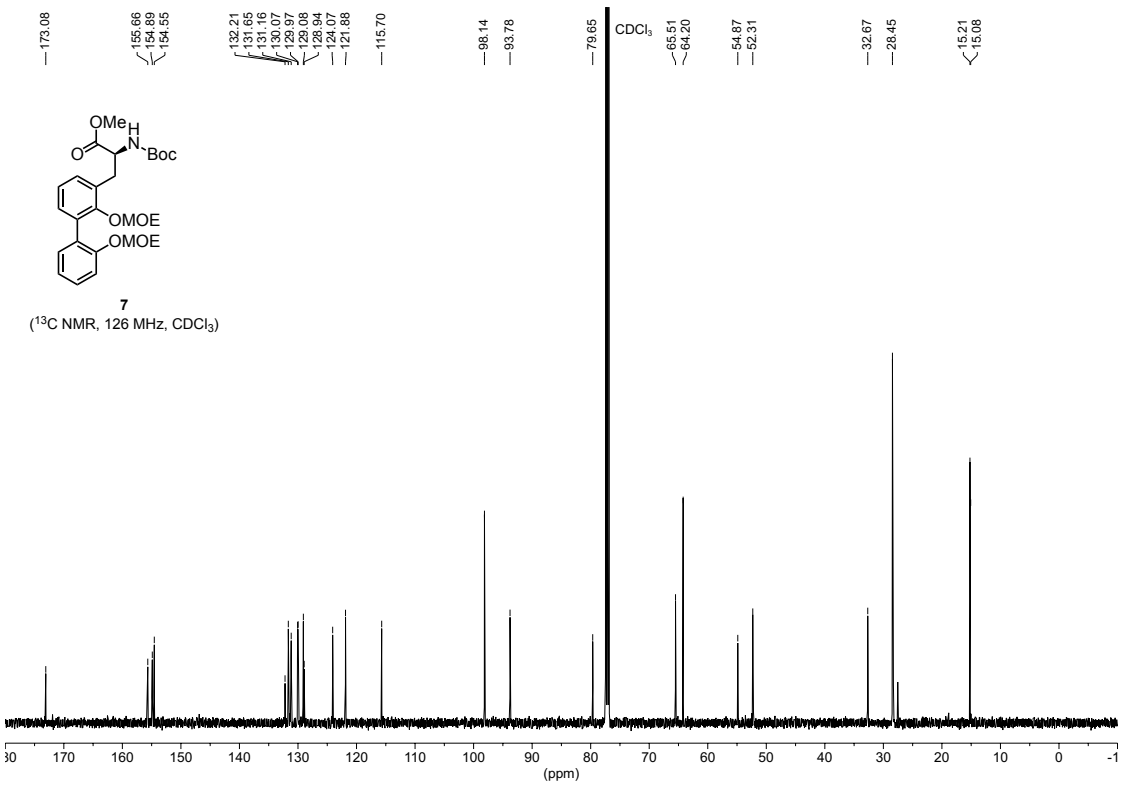

**5**
($^1$H NMR, 500 MHz, $CDCl_3$)



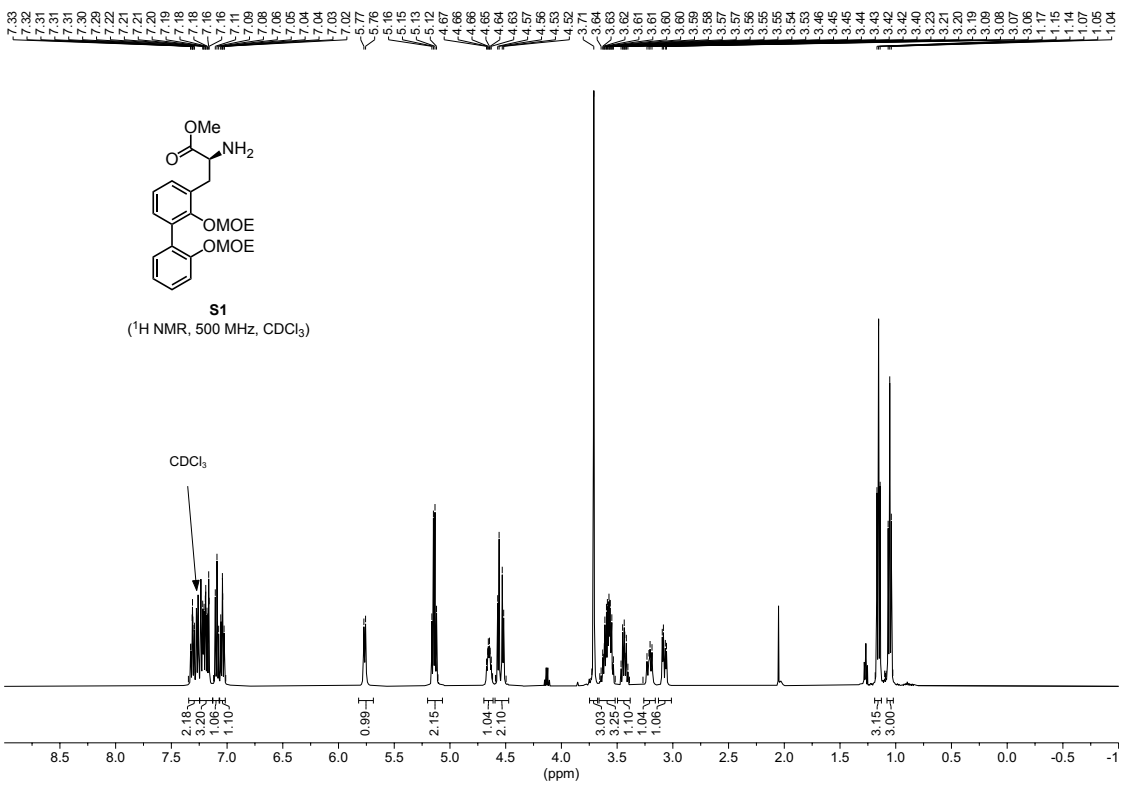

**5**
($^{13}$C NMR, 126 MHz, $CDCl_3$)



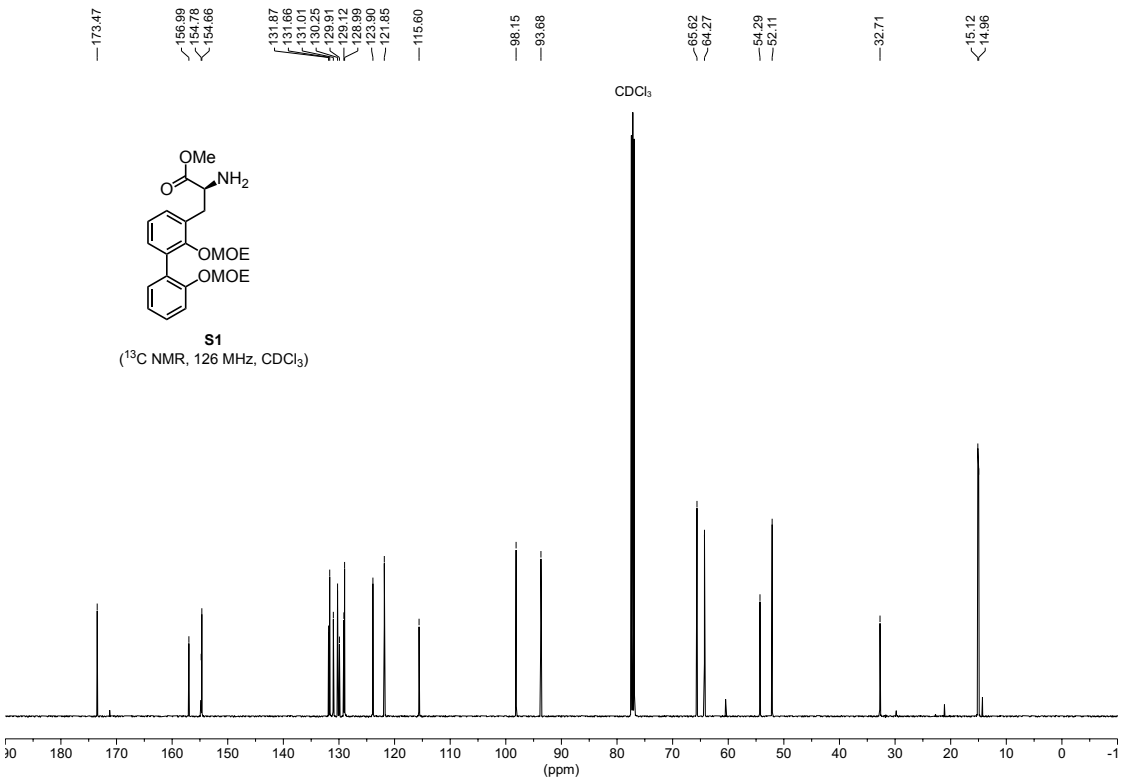

**7**
($^1$H NMR, 500 MHz, $CDCl_3$)




**7**
($^{13}$C NMR, 126 MHz, $CDCl_3$)

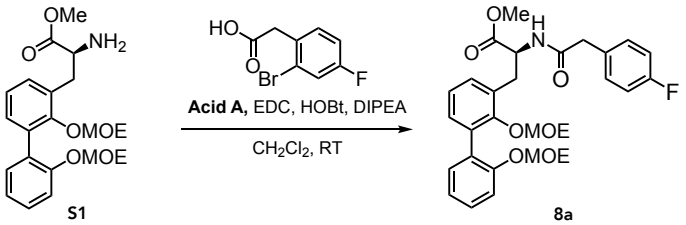



**S1**
($^1$H NMR, 500 MHz, $CDCl_3$)



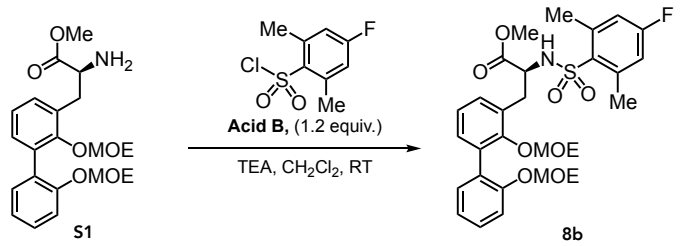

**S1**
($^{13}$C NMR, 126 MHz, $CDCl_3$)

## B) General Procedures for Catalyst Diversification



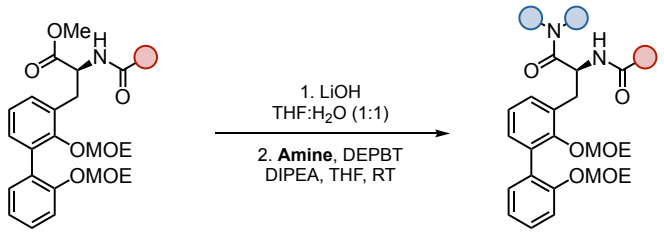

**General Procedure 1A: Representative First Amide Coupling (*Carboxylic Acids*)**

To a 100 mL round bottom flask containing a solution of S1 (5 or 10 mmol, 1.0 equiv.) in $CH_2Cl_2$ (0.2 M), was added Acid A (1.2 equiv.), $HOBt \cdot H_2O$ (0.6 equiv.), and DIPEA (3.0 equiv.), followed by the addition of EDC·HCl (1.2 equiv.). The reaction was stirred overnight at room temperature, and then quenched with 100 mL of $H_2O$. The mixture was then diluted with 100 mL $CH_2Cl_2$ and transferred to a separatory funnel. The layers were separated, and the organic layer was washed sequentially with 1M HCl (100 mL), water (100 mL), and aq. sat. $NaHCO_3$ (100 mL). The organics were dried with $Na_2SO_4$, filtered, and concentrated. The crude residue was purified by column chromatography (silica, EtOAc/Hexanes) to afford the desired product.




**General Procedure 1B: Representative First Fragment Coupling (*Sulfonyl Chlorides*)**

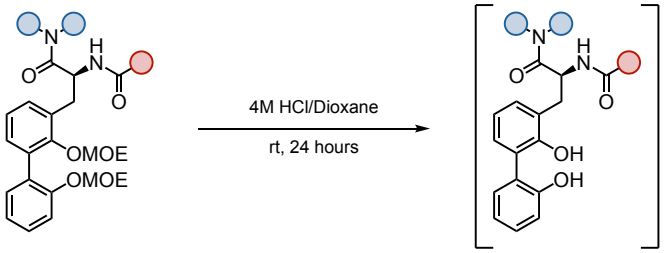
To a 100 mL round bottom flask containing a solution of 7 (5 or 10 mmol, 1.0 equiv.) in $CH_2Cl_2$ (0.2 M), was added the sulfonyl chloride (1.1 equiv.) followed by $NEt_3$ (3.0 equiv.). The reaction was stirred overnight at room temperature, and then quenched with 100 mL of $H_2O$. The mixture was then diluted with 100 mL $CH_2Cl_2$ and transferred to a separatory funnel. The layers were separated, and the organic layer was washed sequentially with 1M HCl (100 mL), aq. sat. $NaHCO_3$ (100 mL), and brine (100 mL). The organics ere dried with $MgSO_4$, filtered, and concentrated. The crude residue was purified by column chromatography (silica, EtOAc/Hexanes) to afford the desired product.




8 9

**General Procedure 2: Saponification of Methyl Esters 8 and Second Amidation using DEPBT.**

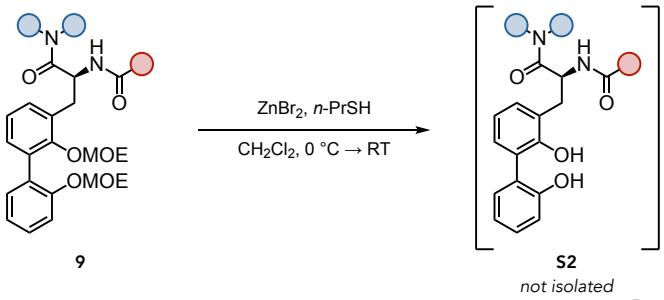
To a 100 mL round bottom flask containing 8 (1.0 equiv.) was added THF (25 mL), $H_2O$ (25 mL), and LiOH (3.0 equiv.), sequentially. The reaction was stirred at overnight at room temperature and monitored via TLC. Upon completion, the reaction was quenched with 1M HCl until the pH = 1. The aqueous layer was extracted with EtOAc (3 x 50 mL), and the combined organic layers were dried with $Na_2SO_4$, filtered, and concentrated to provide the crude acid. The crude acid was taken up in dry THF (0.2 M) in a 100 mL round bottom flask equipped with a magnetic stir bar. Amine was added, followed by DIPEA (3.0 equiv.) and DEPBT (2.0 equiv.) and the reaction mixture was allowed to stir at room temperature overnight. The reaction was diluted with 100 mL EtOAc and quenched with the addition of 100 mL $H_2O$. The mixture was transferred to a separatory funnel, the layers were separated, and the organic layer was washed sequentially with 1M HCl (100 mL), $H_2O$ (100 mL) aq. sat. $NaHCO_3$ (100 mL), and brine (100 mL). The organics were dried with $Na_2SO_4$, filtered, and concentrated. The crude residue was purified by column chromatography (silica, EtOAc/Hexanes) to afford the desired product.




9 S2
*not isolated*

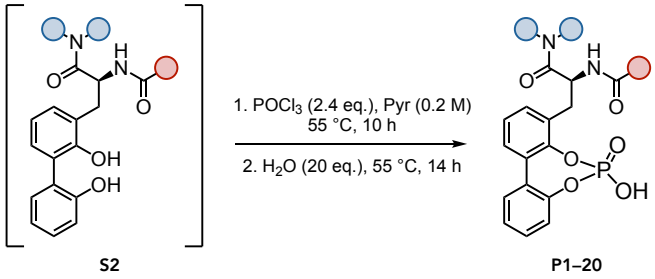
**General Procedure 3A: MOE Deprotection with 4 M HCl in Dioxane**

A 20 mL scintillation vial equipped with a magnetic stir bar was charged with catalyst precursor 9a–w (0.3 mmol, 1.0 equiv.). A solution of HCl in dioxane (4 M) was cooled down to 0 °C, of which 1.5 mL was added to the reaction vial (6.0 mmol, 20 equiv.) for a final concentration of 0.2 M. The reaction mixture was warmed to room temperature and monitored by TLC (20% EtOAc/Hexanes or 5% MeOH/$CH_2Cl_2$). Upon full consumption of the starting material, the crude mixture was concentrated in vacuo. The residue was re-dissolved in $CH_2Cl_2$ and concentrated once more to provide a white or yellow foam which was carried over to the phosphorylation step (procedure 4a or 4b) without further purification.



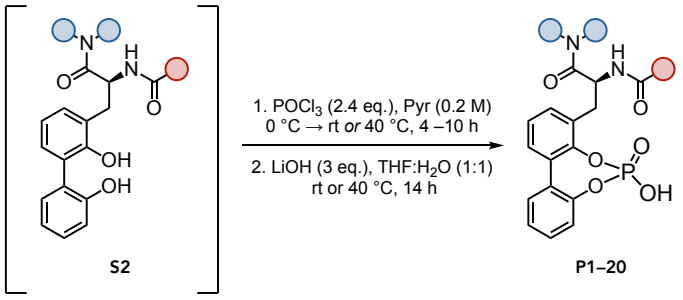

**General Procedure 3B: MOE Deprotection with $ZnBr_2$ and *n*-PrSH[5]**

A 20 mL scintillation vial equipped with a magnetic stir bar was charged with catalyst precursor 9 (0.3 mmol, 1.0 equiv.) and anhydrous $CH_2Cl_2$ (1.5 mL, 0.2 M). The reaction mixture was cooled to 0 °C before $ZnBr_2$ (268 mg, 1.2 mmol, 4.0 equiv.) was added, followed by *n*-PrSH (90.7 mg, 108 µL, 1.2 mmol, 4.0 equiv.). The reaction mixture was warmed to room temperature and monitored by TLC. Upon full consumption of the starting material, saturated $NaHCO_3$ (*aq.*) was added to quench the reaction. The biphasic solution was passed through a plug of celite and rinsed with $CH_2Cl_2$. The organic layer of the resulting filtrate was separated and dried over sodium sulfate. Removal of solvent under reduced pressure resulted in a crude oil or foam which was carried over to the phosphorylation step (General Procedure 4A or 4B) without further purification.




**General Procedure 4A: Phosphorylation and Hydrolysis**

A 20 mL scintillation vial equipped with a magnetic stir bar was charged with deprotected catalyst precursor S2 (0.3 mmol, 1.0 equiv.) and anhydrous pyridine (1.5 mL). The reaction mixture was cooled to 0 °C before $POCl_3$ (110 mg, 67 µL, 715 µmol, 2.4 equiv.) was added. The reaction mixture was then heated to 55 °C for 4 hours, then cooled to 0 °C again. With vigorous stirring, water (100 µL, 6.0 µmol, 20 equiv.) was added dropwise. The reaction mixture was heated to 55 °C once more and stirred overnight. After cooling to room temperature, the reaction mixture was concentrated under reduced pressure to remove pyridine. The crude residue was then dissolved in a 10% isopropanol/$CH_2Cl_2$ solution and extracted with sat. aq. $NH_4Cl$. The aqueous layer was extracted three more times with 10% isopropanol/$CH_2Cl_2$, and the organic layers were combined, dried over sodium sulfate, and concentrated to yield a crude oil. The latter was purified by column chromatography (see purification methods).




**General Procedure 4b: Phosphorylation and Hydrolysis**

A 20 mL scintillation vial equipped with a magnetic stir bar was charged with freshly deprotected catalyst precursor S2 (0.3 mmol, 1.0 equiv.) and anhydrous pyridine (1.5 mL). The reaction mixture was cooled to 0 °C before $POCl_3$ (110 mg, 67 µL, 715 µmol, 2.4 equiv.) was added. It was then warmed to room temperature or 40 °C and stirred overnight. After 10 – 14 hours, the crude reaction mixture was concentrated to half of its original volume. $CH_2Cl_2$ was added and the suspension was filtered through a plug of cotton and sand to remove any solids and salts. The filtrate was further concentrated, and the resulting residue was dissolved in anhydrous toluene and concentrated again. This process was repeated 3 – 5 times to remove as much pyridine and its salts as possible.

The resulting phosphoryl chloride intermediate was then dissolved in THF (0.25 M). With stirring, a 1 M aqueous solution of LiOH (3.0 equiv.) was added. The resulting reaction mixture was left to stir at room temperature or heated to 40 °C until TLC monitoring showed the full consumption of the intermediate (TLC solvents used: 10–15% MeOH/$CH_2Cl_2$ on normal phase, or 15 % MeCN/$H_2O$ for reverse phase). Upon completion, the THF was removed under reduced pressure. The remaining solution was acidified to pH= 2 with 1 M HCl (aq.). The resulting suspension was then extracted 3 – 5 times with $CH_2Cl_2$, 10% IPA/ $CH_2Cl_2$ or EtOAc. This step often resulted in thick emulsions challenging to separate. In those cases, addition of a small amount of sat. aq. $NH_4Cl$ could usually break up the emulsion and simplify the separation. The combined organic layers were dried over sodium sulfate and concentrated to yield a crude oil or thick foam. The latter was purified by column chromatography (see purification method section).

### 7.2.2. Catalyst Purification Procedures and Notes

The purification of the final catalysts required various methods depending on structure and general procedures are individually noted by catalyst. We encourage the thoughtful selection of purification technique when attempting to access similar structures and offer several potentially useful insights.

i. Recrystallization from water by addition of HCl was generally found to be inefficient.
ii. Certain catalysts (procedures noted) were tolerant of normal phase silica in high MeOH/$CH_2Cl_2$ gradient (above 10%) with a high flow rate to avoid long interactions of the substrates with the silica gel
iii. C18 reverse phase silica was found to be effective using acetonitrile/water as solvent system. The addition of 0.1 - 1.0% formic acid was sometimes helpful to provide cleaner product elution.
iv. Below is a representative list of mobile phase systems used in the separations. We recommend using these conditions as a starting point for the purification of structurally similar compounds.
    - 10–40% MeOH in $CH_2Cl_2$ (normal phase silica)
    - 10–40% MeOH in $CH_2Cl_2$, 1% formic acid (normal phase silica)
    - 10–60% Acetonitrile in Water (C18)
    - 10–50% Acetonitrile in Water, 0.1–1% formic acid (C18)

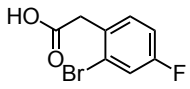
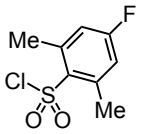
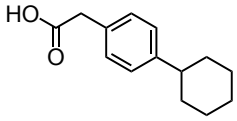
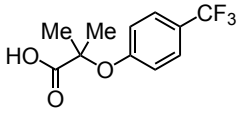
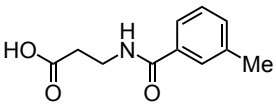
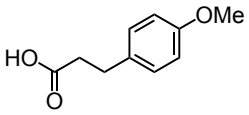
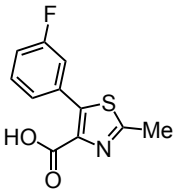
*Note: it was sometimes necessary to perform an acid wash (with 4 M HCl aq.) to obtain the free acid rather than a salt of the conjugate base after the column.*

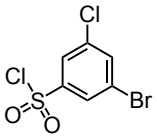
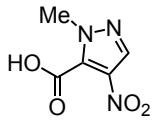
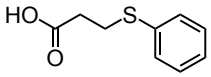
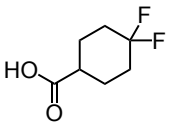
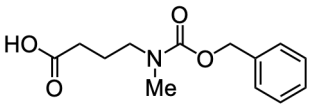
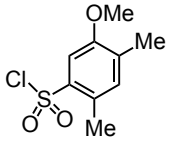
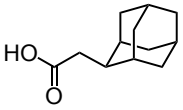
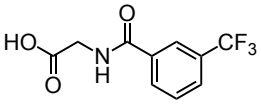
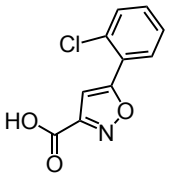
v. For normal phase purifications, the relevant fractions were concentrated to dryness. The residue was re-dissolved in 10% isopropanol/$CH_2Cl_2$. Aq. HCl (4 M) was added, and the layers were separated. The aqueous phase was extracted three more times with 10% isopropanol/$CH_2Cl_2$. *Note: addition of a small amount of sat. aq. $NH_4Cl$ was helpful in separating the phases when emulsions were formed*. The organic layers were collected, dried over $Na_2SO_4$, and concentrated in vacuo to afford the pure phosphoric acid.

vi. For reverse phase columns, the relevant fractions were concentrated to a minimal volume (residual water present). The remaining solution was transferred to a separatory funnel, aq. HCl (4 M) was added. 10% isopropanol/$CH_2Cl_2$ was subsequently added, and the aqueous layer was extracted 3–5 times. The organic layers were collected, dried over $Na_2SO_4$, and concentrated in vacuo to afford the pure phosphoric acid.

### 7.2.3. Fragments used for diversification

**Table S1:** Carboxylic acids and sulfonyl chlorides used for the diversification of secondary amide $R_1$.

| Structure | Name and Label | Purchased from/Synthetic Details |
|---|---|---|
|  | 2-(2-bromo-4-fluorophenyl)acetic acid **Acid A** | Purchased from AK Scientific |
|  | 4-fluoro-2,6-dimethylbenzenesulfonyl chloride **Acid B** | Prepared according to reported procedure (*see next section)*[6] |
|  | 2-(4-cyclohexylphenyl)acetic acid **Acid C** | Synthesis and characterization reported below. |
|  | 2-methyl-2-(4-(trifluoromethyl)phenoxy)propanoic acid **Acid D** | Prepared according to reported procedure (*see next section)*.[7] |
|  | 3-(3-methylbenzamido)propanoic acid **Acid E** | Synthesis was adapted from a reported procedure (*see next section)*.[8] Full characterization provided below. |
|  | 3-(4-methoxyphenyl)propanoic acid **Acid F** | Purchased from Synthonix |
|  | 5-(3-fluorophenyl)-2-methylthiazole-4-carboxylic acid **Acid G** | Prepared according to reported procedure (see next section).[9] |

| | | |
|---|---|---|
|  | 3-bromo-5-chlorobenzenesulfonyl chloride<br>**Acid H** | Purchased from Oakwood Chemical |
|  | 1-methyl-4-nitro-1*H*-pyrazole-5-carboxylic acid<br>**Acid I** | Purchased from Combi Blocks |
|  | 3-(phenylthio)propanoic acid<br>**Acid J** | Purchased from Oakwood Chemical |
|  | 4,4-difluorocyclohexane-1-carboxylic acid<br>**Acid K** | Purchased from Combi Blocks |
|  | 4-<br>(((benzyloxy)carbonyl)(methyl)amino)butanoic acid<br>**Acid L** | Prepared according to reported procedure (see next section).[10] |
|  | 5-methoxy-2,4-dimethylbenzenesulfonyl chloride<br>**Acid M** | Synthesis and characterization reported below. |
|  | 2-(adamantan-2-yl)acetic acid<br>**Acid O** | Prepared according to reported procedure (see next section).[11] |
|  | 3-(trifluoromethyl)benzoyl)glycine<br>**Acid P** | Prepared according to reported procedure (see next section).[12] |
|  | 5-(2-chlorophenyl)isoxazole-3-carboxylic acid<br>**Acid R** | Prepared according to reported procedure (see next section).[13] |

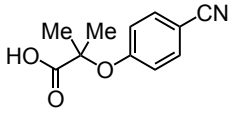
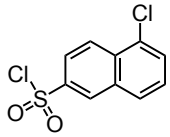
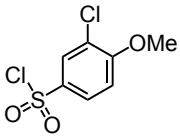
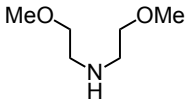
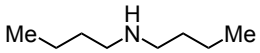
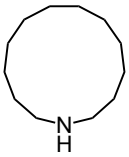
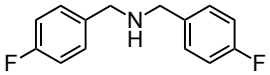
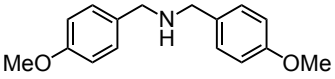
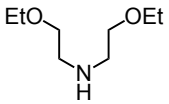
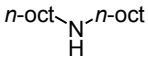
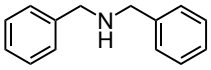
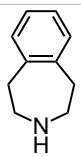
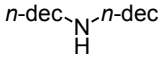
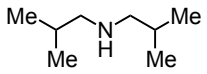
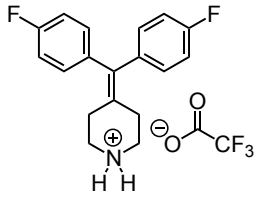
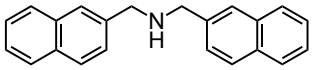
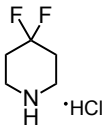
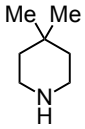
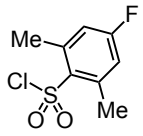
| | | |
|---|---|---|
|  | 2-(4-cyanophenoxy)-2-methylpropanoic acid<br>**Acid T** | Purchased from Combi Blocks |
|  | cyclopropanesulfonyl chloride<br>**Acid U** | Purchased from Combi Blocks |
|  | 5-chloronaphtalene-2-sulfonyl chloride<br>**Acid V** | Purchased from Combi Blocks |
|  | 3-chloro-4-methoxybenzensulfonyl chloride<br>**Acid W** | Purchased from Combi Blocks |

Table S2: Amine fragments used in the diversification of tertiary amide $R_2$.

| Structure | Name and Label | Purchased from/Synthetic Details |
|---|---|---|
|  | bis-(2-methoxyethyl)amine<br>**Amine A** | Purchased from Oakwood Chemical |
|  | dibutylamine<br>**Amine B** | Purchased from Oakwood Chemical |
|  | azacyclotridecane<br>**Amine C** | Purchased from AA Blocks |
|  | bis(4-fluorobenzyl)amine<br>**Amine D** | Prepared according to reported procedure (*see next section*).[14] |
|  | bis(4-methoxybenzyl)amine<br>**Amine E** | Purchased from Combi Blocks |
|  | bis(2-ethoxyethyl)amine<br>**Amine F** | Purchased from Combi Blocks |
|  | dioctylamine<br>**Amine G** | Purchased from TCI America |
|  | dibenzylamine<br>**Amine H** | Purchased from Millipore Sigma |
|  | 2,3,4,5-tetrahydro-1*H*-benzo[*d*]azepine<br>**Amine I** | Purchased from Matrix Scientific |
|  | didecylamine<br>**Amine J** | Purchased from TCI America |

| | | |
|---|---|---|
|  | diisobutylamine<br>**Amine K** | Purchased from Millipore Sigma |
|  | 4,4-(bis(4-fluorophenyl)methylene)piperidin-1-ium trifluoroacetate<br>**Amine L** | Prepared according to reported procedure (*see next section*).[15] |
|  | bis(naphthalen-2-ylmethyl)amine<br>**Amine N** | Prepared according to reported procedure (*see next section*).[16] |
|  | 4,4-Difluoropiperidine hydrochloride<br>**Amine P** | Purchased from Oakwood Chemical |
|  | 4,4-dimethylpiperidine<br>**Amine R** | Purchased from Enamine |

### 7.2.2. Synthesis and Characterization of Non-Commercially Available fragments

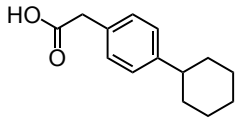



**4-fluoro-2,6-dimethylbenzenesulfonyl chloride (Acid B)**
The synthesis of Acid B was adapted from patent US2008/153843, 2008, A1, column 63 (Gruenenthal Pharma GmbH &Co).[6] An oven-dried 50 mL round-bottom flask equipped with a magnetic stir bar was charged with 1-fluoro-3,5-dimethylbenzene (0.2 g, 1 equiv., 2 mmol) and $CH_2Cl_2$ (20 mL, 0.2 M) and was cooled to 0 °C. Chlorosulfonic acid (0.8 g, 0.4 mL, 4 equiv., 6 mmol) was then added dropwise with vigorous stirring. The reaction mixture was allowed to warm to room temperature and stirred for 3 hours. Upon full consumption of the starting material as monitored by TLC (20% EtOAc/Hexanes), the reaction mixture was poured onto ice. The aqueous layer was extracted with CH2Cl2 three times, and the combined organic layers were combined, dried over sodium sulfate, and concentrated in vacuo. Further purification by column chromatography using 0–10% EtOAc/Hexanes as eluent provided 100 mg of the desired product (30 % yield) as a white solid.

**$^1$H NMR (500 MHz, $CDCl_3$)** δ 6.93 (d, *J* = 8.9 Hz, 2H), 2.76 (d, *J* = 2.7 Hz, 6H).

**$^{13}$C NMR (126 MHz, $CDCl_3$)** δ 164.8 (d, *J* = 258.6 Hz), 143.8 (d, *J* = 9.9 Hz), 138.8 (d, *J* = 3.0 Hz), 118.5 (d, *J* = 21.9 Hz), 23.5.

**$^{19}$F NMR (471 MHz, $CDCl_3$)** δ -103.12 (t, *J* = 8.7 Hz, 1F). **GC-MS (EI, *m/z*)**: Exact mass calculated for [$C_8H_8ClFO_2S$] requires 221.2; found 221.2. *Note: unable to ionize using ESI.*

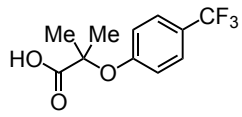



**2-(4-cyclohexylphenyl)acetic acid (Acid C)** was prepared in two steps from iodocyclohexane and ethyl 2-(4-bromophenyl)acetate. To a flame-dried round bottom flask was added pyridine (10 mol%, 4 mmol, 0.34 mL), Mn (4.4 equiv., 100 mmol, 5.5 g), and 4,4'-Di-*tert*-butyl-2,2'-dipyridyl (11 mol%, 4.3 mmol, 1.29 g). The flask was purged under vacuum and backfilled with nitrogen three times. N-Methyl-2-Pyrrolidone (NMP) was added via cannula (0.25 M, 160 mL) followed by iodocyclohexane (1.1 equiv., 44 mmol, 5.69 mL). The reaction was stirred for 5 minutes followed by the addition of ethyl 2-(4-bromophenyl)acetate (1 equiv., 40 mmol, 6.3 mL). The reaction mixture was heated to 80 °C and reacted overnight under a nitrogen atmosphere (16 hours). The mixture was cooled to room temperature, quenched with 100 mL aqueous $NaHSO_4$ (1M), and diluted with 150 mL $Et_2O$. The biphasic mixture was filtered through celite, and the organic layer was separated and dried over $Na_2SO_4$. The resulting crude product was passed through a silica plug using 20% EtOAc/Hexanes and concentrated under reduced pressure to afford crude ethyl 2-(4-cyclohexylphenyl)acetate (25% yield, 9.90 mmol, 2.3 g). The product was dissolved in 20 mL of THF and 20 mL of $H_2O$ was added followed LiOH (3 equiv., 30 mmol, 0.72 g). The reaction was stirred at room temperature for 24 hours until full conversion of the ester judged by TLC. The reaction was quenched by the slow addition of 1 M HCl to achieve a pH of 1-2 and extracted with EtOAc. The organics were separated, dried over $MgSO_4$, and concentrated under reduced pressure to obtain pure 2-(4-cyclohexylphenyl)acetic acid as a waxy white solid (69% yield, 6.87 mmol, 1.5 g).

**$^1$H NMR (500 MHz, $CDCl_3$)** δ 7.19 (q, *J* = 8.2 Hz, 4H), 3.62 (s, 2H), 2.49 (brm, 1H), 1.86 (brt, *J* = 12.2, 4.0 Hz, 4H), 1.75 (brd, 1H), 1.47 – 1.33 (m, 4H), 1.32 – 1.20 (m, 1H).

**$^{13}$C NMR (126 MHz, $CDCl_3$)** δ 178.2, 147.3, 130.7, 129.4 (s, 2C), 127.3 (s, 2C), 44.3, 40.8, 34.6 (s, 2C), 27.0 (s, 2C), 26.3.

**HRMS (ESI-/TOF, *m/z*):** Exact mass calculated for $[C_{14}H_{17}O_2]^-$ requires 217.1229; found 217.1232.



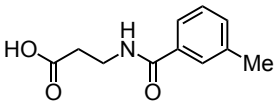

**2-methyl-2-(4-(trifluoromethyl)phenoxy)propanoic acid (Acid D)** was prepared on 20 mmol scale according to reported procedure[7] yielding a white solid (69% yield, 14 mmol, 3.44 g). Characterization data matches reported literature.[7]

**$^1$H NMR (500 MHz, $CDCl_3$)** δ 7.53 (d, *J* = 8.6 Hz, 2H), 6.97 (d, *J* = 8.5 Hz, 2H), 1.68 (s, 6H).

**$^{13}$C NMR (126 MHz, $CDCl_3$)** δ 180.0, 157.9, 126.8 (q, *J* = 3.5 Hz, 2C), 124.7 (q, *J* = 33.3 Hz, 1C), 124.4 (q, *J* = 271.0 Hz, 1C), 119.1 (s, 2C), 79.4, 25.4 (s, 2C).

**$^{19}$F NMR (471 MHz, $CDCl_3$)** δ -61.82 (s, 3F).

**HRMS (ESI-) m/z:** Exact mass calculated for $[C_{11}H_{10}F_3O_3]^-$ requires 247.0582; found 247.0584.

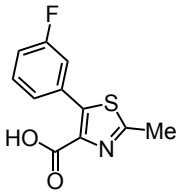



**3-(3-methylbenzamido)propanoic acid (Acid E)** was prepared on 20 mmol scale with a modified reported procedure[8] using β-alanine and *m*-toluoyl chloride, yielding a white solid (73% yield, 14.6 mmol, 3.03 g). Full characterization provided.

**$^1$H NMR (500 MHz, $CDCl_3$)** δ 10.28 (s, 1H), 7.49 (s, 1H), 7.43 (dq, *J* = 6.1, 4.0, 3.1 Hz, 1H), 7.23 – 7.15 (m, 2H), 6.97 (t, *J* = 6.1 Hz, 1H), 3.63 (q, *J* = 6.0 Hz, 2H), 2.61 (t, *J* = 5.9 Hz, 2H), 2.27 (s, 3H).

**$^{13}$C NMR (126 MHz, $CDCl_3$)** δ 176.8, 168.5, 138.6, 134.0, 132.6, 128.6, 127.9, 124.1, 35.5, 33.9, 21.4.

**HRMS (ESI-/TOF, *m/z*):** Exact mass calculated for $[C_{11}H_{12}NO_3]^-$ requires 206.0817; found 206.0818.



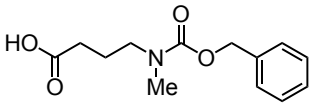

**5-(3-fluorophenyl)-2-methylthiazole-4-carboxylic acid (Acid G)** was prepared on 25 mmol scale in three steps according to literature,[9,17] yielding a white solid (52% across three steps, 13 mmol, 3.08 g). Full characterization provided; characterization data matches available reported literature.[17]

**$^{1}$H NMR (500 MHz, Acetone) δ** 7.51 – 7.43 (m, 1H), 7.45 – 7.34 (m, 2H), 7.25 – 7.17 (m, 1H), 2.71 (s, 3H).

**$^{13}$C NMR (126 MHz, Acetone) δ** 165.7, 163.5 (d, *J* = 244.8 Hz, 1C), 163.1, 145.1 (d, *J* = 2.3 Hz, 1C), 141.9, 134.3 (d, *J* = 8.9 Hz, 1C), 131.5 (d, *J* = 8.4 Hz, 1C), 127.4 (d, *J* = 3.0 Hz, 1C), 117.8 (d, *J* = 144.6 Hz, 1C) 117.6 (d, *J* = 143. Hz, 1C), 19.5.

**$^{19}$F NMR (471 MHz, Acetone) δ** -111.53 – -117.88 (m, 1F).

**HRMS (ESI-/TOF, *m/z*):** Exact mass calculated for $[C_{11}H_7FNO_2S]^-$ requires 236.0182; found 236.0181.

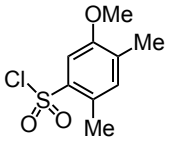



**4-(((benzyloxy)carbonyl)(methyl)amino)butanoic acid (Acid L)** was prepared on 16.2 mmol scale according to literature,[10] yielding a thick, yellowish oil (85% yield, 13.8 mmol, 3.46 g). Characterization data matches reported literature.[10]

**$^{1}$H NMR (500 MHz, $CDCl_3$) δ** 9.51 (s, 1H), 7.38 – 7.27 (m, 5H), 5.13 (s, 2H), 3.35 (q, *J* = 6.9 Hz, 2H), 2.93 (s, 3H), 2.35 (dt, *J* = 20.9, 7.2 Hz, 2H), 1.93 – 1.81 (m, 2H).

**$^{13}$C NMR (126 MHz, $CDCl_3$) δ** 178.2, 156.7, 156.5, 136.8, 128.5, 128.0, 127.9, 67.3, 48.3, 47.9, 34.7, 34.1, 31.2, 31.0, 23.0, 22.7. *Note: rotameric mixture*.

**HRMS (ESI-/TOF, *m/z*):** Exact mass calculated for $[C_{13}H_{16}NO_4]^-$ requires 250.1079; found 250.1080.

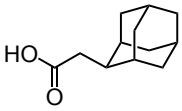



**5-methoxy-2,4-dimethylbenzenesulfonyl chloride (Acid M)**. An oven-dried 100 mL round-bottom flask equipped with a magnetic stir bar was charged with 1-methoxy-2,4-dimethylbenzene (20 mmol, 1 equiv, 2.72 g) and $CH_2Cl_2$ (100 mL, 0.2 M) and was cooled to 0 °C. Chlorosulfonic acid (4 equiv, 100 mmol) was then added dropwise. The reaction mixture was allowed to warm to room temperature and stirred for an addition 2 hours. The reaction was quenched by pouring onto ice. The organic layer was separated and washed 1x with $H_2O$ and brine. The organic layer was separated, dried over sodium sulfate, and concentrated in vacuo. Further purification by column chromatography using 0–15% EtOAc/Hexanes as eluent provided 100 mg of the desired product (57% yield, 11.4 mmol, 2.67 g) as a pink solid.

**$^1$H NMR (500 MHz, $CDCl_3$) δ** 7.44 (s, 1H), 7.15 (s, 1H), 3.89 (s, 3H), 2.66 (s, 3H), 2.27 (s, 3H).

**$^{13}$C NMR (126 MHz, $CDCl_3$) δ** 155.8, 140.6, 135.5, 135.2, 129.7, 109.4, 55.8, 19.3, 16.4.

**GC-MS (EI, *m/z*)**: Exact mass calculated for [$C_9H_{11}ClFO_3S$] requires 234.0; found 234.0. *Note: unable to ionize using ESI*.

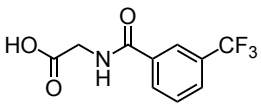


**2-(adamantan-2-yl)acetic acid (Acid O)** was prepared in three steps on 20 mmol scale according to reported procedure (60% yield across three steps, 12 mmol, 2.33 g).[11] Characterization data matches reported literature.[18]

**$^1$H NMR (500 MHz, DMSO)** δ 12.09 (s, 1H), 2.33 (d, *J* = 7.5 Hz, 2H), 2.12 – 2.05 (m, 1H), 1.88 – 1.61 (m, 12H), 1.48 (d, *J* = 12.6 Hz, 2H).

**$^{13}$C NMR (126 MHz, DMSO)** δ 174.2, 40.5, 38.4, 37.7, 37.6, 31.2, 31.0, 27.3, 27.3.

**HRMS (ESI-/TOF, *m/z*):** Exact mass calculated for $[C_{12}H_{18}O_2]^-$ requires 193.1229; found 193.1228.



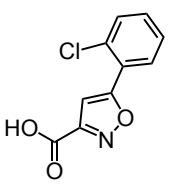
**(3-(trifluoromethyl)benzoyl)glycine (Acid P)** was prepared on 15 mmol scale according to reported procedure,[12] yielding a white solid (90% yield, 13.5 mmol, 3.34 g). Characterization data matches reported literature.[12]

**$^1$H NMR (500 MHz, DMSO)** δ 12.67 (s, 1H), 9.14 (t, *J* = 5.9 Hz, 1H), 8.21 (s, 1H), 8.18 (d, *J* = 7.7 Hz, 1H), 7.93 (d, *J* = 7.8 Hz, 1H), 7.75 (t, *J* = 7.9 Hz, 1H), 3.96 (d, *J* = 5.8 Hz, 2H).

**$^{13}$C NMR (126 MHz, DMSO)** δ 171.1, 165.0, 134.6, 131.4, 129.8, 129.2 (q, *J* = 32.0 Hz, 1C), 128.0 (q, *J* = 3.5 Hz, 1C), 124.0 (q, *J* = 272.1 Hz, 1C), 123.8 (q, *J* = 3.8 Hz, 1C), 41.2.

**$^{19}$F NMR (471 MHz, DMSO)** δ -61.20 (s, 3F).

**HRMS (ESI-/TOF, *m/z*):** Exact mass calculated for $[C_{10}H_7F_3NO_3]^-$ requires 246.0378; found 246.0379.

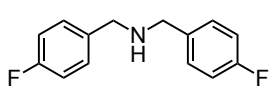


**5-(2-chlorophenyl)isoxazole-3-carboxylic acid (Acid R)** was prepared on 25 mmol scale in three steps according to reported procedure,[13,19] yielding a white solid (54% yield across three steps, 13.4 mmol, 3.0 g). Characterization data matches reported literature.[13]

**$^1$H NMR (500 MHz, DMSO)** δ 7.96 (d, *J* = 7.6, 2.0 Hz, 1H), 7.73 – 7.68 (m, 1H), 7.62 – 7.52 (m, 2H), 7.33 (s, 1H).

**$^{13}$C NMR (126 MHz, DMSO**) δ 167.7, 160.7, 157.6, 132.4, 131.0, 131.0, 130.0, 128.1, 124.9, 104.9.

**HRMS (ESI-/TOF, *m/z*):** Exact mass calculated for $[C_{10}H_6ClNO_3+Na]^-$ requires 245.9934; found 245.9936.



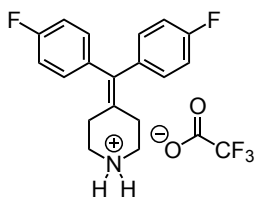
**bis(4-fluorobenzyl)amine (Amine D)** was prepared on 20 mmol scale in two steps according to reported procedure,[14] yielding bis(4-fluorobenzyl)amine as a yellowish oil (60% across two steps, 12 mmol, 2.8 g). Characterization data matches reported literature.[14]

**$^1$H NMR (500 MHz, $CDCl_3$)** δ 7.30 (dd, *J* = 8.4, 5.5 Hz, 4H), 7.01 (t, *J* = 8.7 Hz, 4H), 3.76 (s, 4H), 1.58 (s, 1H).

**$^{13}$C NMR (126 MHz, $CDCl_3$)** δ 162.1 (d, J = 243.6 Hz, 2C), 136.0 (d, J = 3.0 Hz, 2C), 129.7 (d, J = 8.1 Hz, 4C), 115.3 (d, J = 21.0 Hz, 4C), 52.5 (2C).

**$^{19}$F NMR (471 MHz, $CDCl_3$)** δ -115.94 – -116.04 (m, 2F).

**HRMS (ESI-/TOF, *m/z*):** Exact mass calculated for $[C_{14}H_{14}F_2N]^-$ requires 234.1094; found 234.1098.



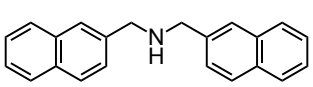
**4-(bis(4-fluorophenyl)methylene)piperidin-1-ium trifluoroacetate (Amine L)**. Prepared in two steps on 20 mmol scale according to reported procedure,[15] yielding a white solid (60% across two steps, 12 mmol, 4.79 g). Full characterization provided.

**$^1$H NMR (500 MHz, DMSO) δ** 8.87 (s, 1H), 7.18 (d, *J* = 7.3 Hz, 4H), 3.37 (s, 2H), 3.15 (t, *J* = 5.9 Hz, 2H), 2.42 (t, *J* = 5.9 Hz, 2H).

**$^{13}$C NMR (126 MHz, DMSO) δ** 161.1 (d, *J* = 244.5 Hz, 2C), 158.2 (q, J =30.8 Hz, 1C), 137.4 (d, J =3.4 Hz, 2C), 135.7, 131.2 (d, J = 8.3 Hz, 4C), 130.7, 117.3 (q, J = 299.5 Hz, 1C), 115.2 (d, J = 21.3 Hz, 4C), 44.2 (s, 2C), 27.8 (s, 2C).

**$^{19}$F NMR (471 MHz, DMSO)** δ -73.60 (s, 2F), -115.32 (p, *J* = 7.4 Hz, 2F).

**HRMS (ESI-/TOF, *m/z*):** Exact mass calculated for $[C_{18}H_{18}F_2N]^-$ requires 286.1407; found 286.1411.

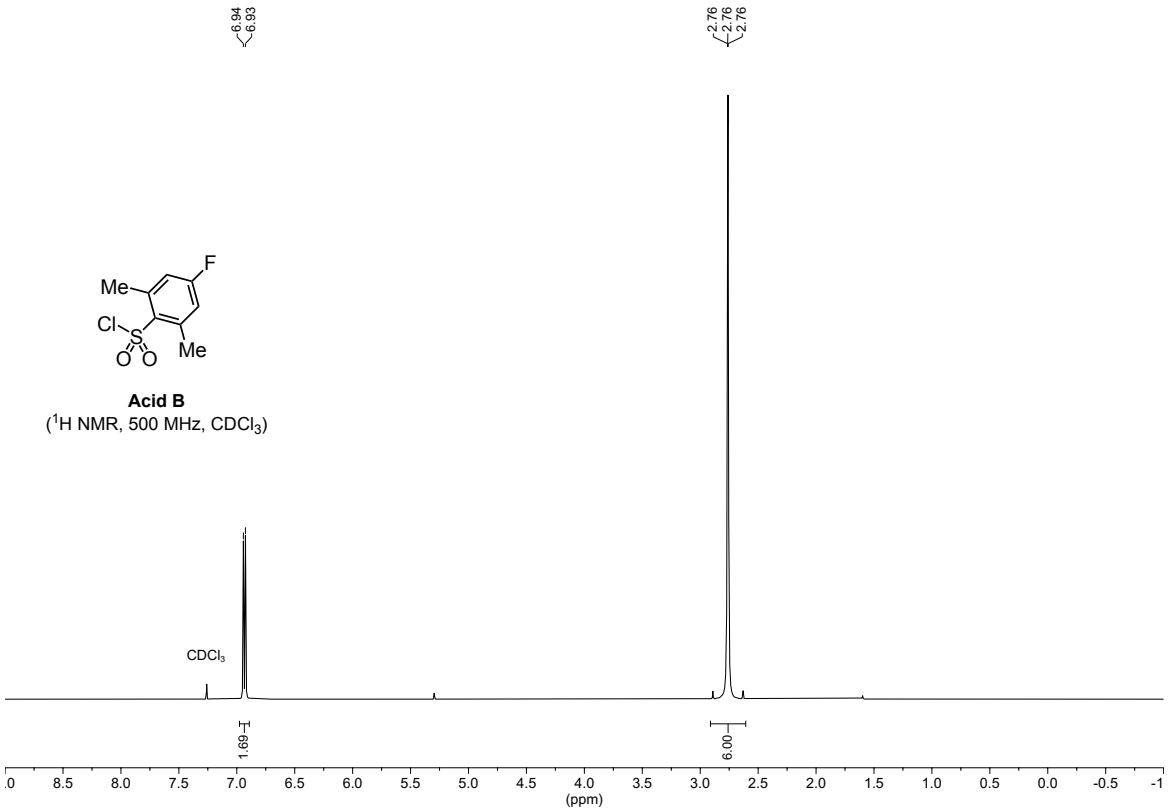


**bis(naphthalen-2-ylmethyl)amine (Amine N)** was prepared on 20 mmol scale according to reported procedure,[16] yielding a white solid (53% yield, 10.6 mmol, 3.15 g). Characterization data matches reported literature.[16]

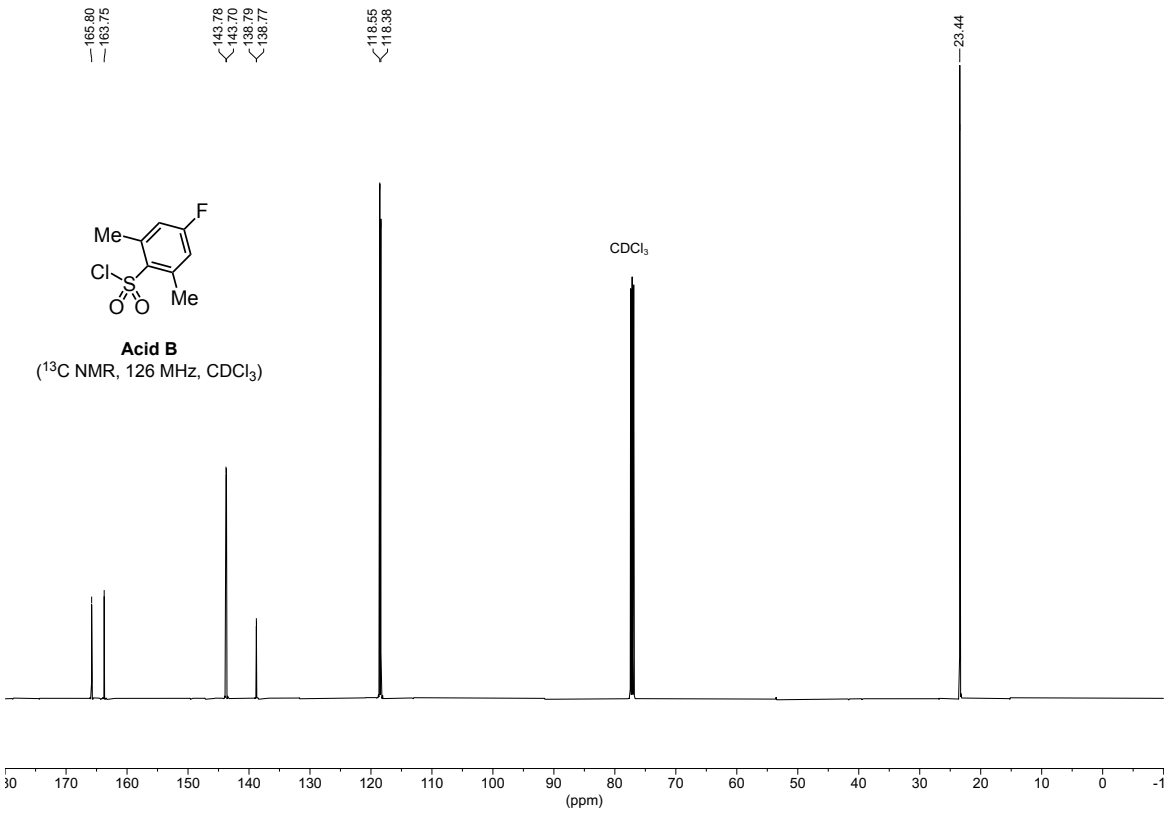
**$^1$H NMR (500 MHz, $CDCl_3$)** δ 7.88 – 7.77 (m, 8H), 7.55 – 7.41 (m, 6H), 4.02 (s, 4H).

**$^{13}$C NMR (126 MHz, $CDCl_3$) δ** 137.9, 133.6, 132.8, 128.3, 127.8, 127.8, 126.8, 126.7, 126.2, 125.7, 53.4.

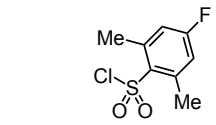
**HRMS (ESI-/TOF, *m/z*):** Exact mass calculated for $[C_{22}H_{20}N]^-$ requires 298.1596; found 298.1602.




**Acid B**
($^1$H NMR, 500 MHz, $CDCl_3$)

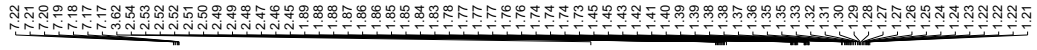


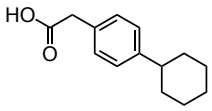

**Acid B**
($^{13}$C NMR, 126 MHz, $CDCl_3$)



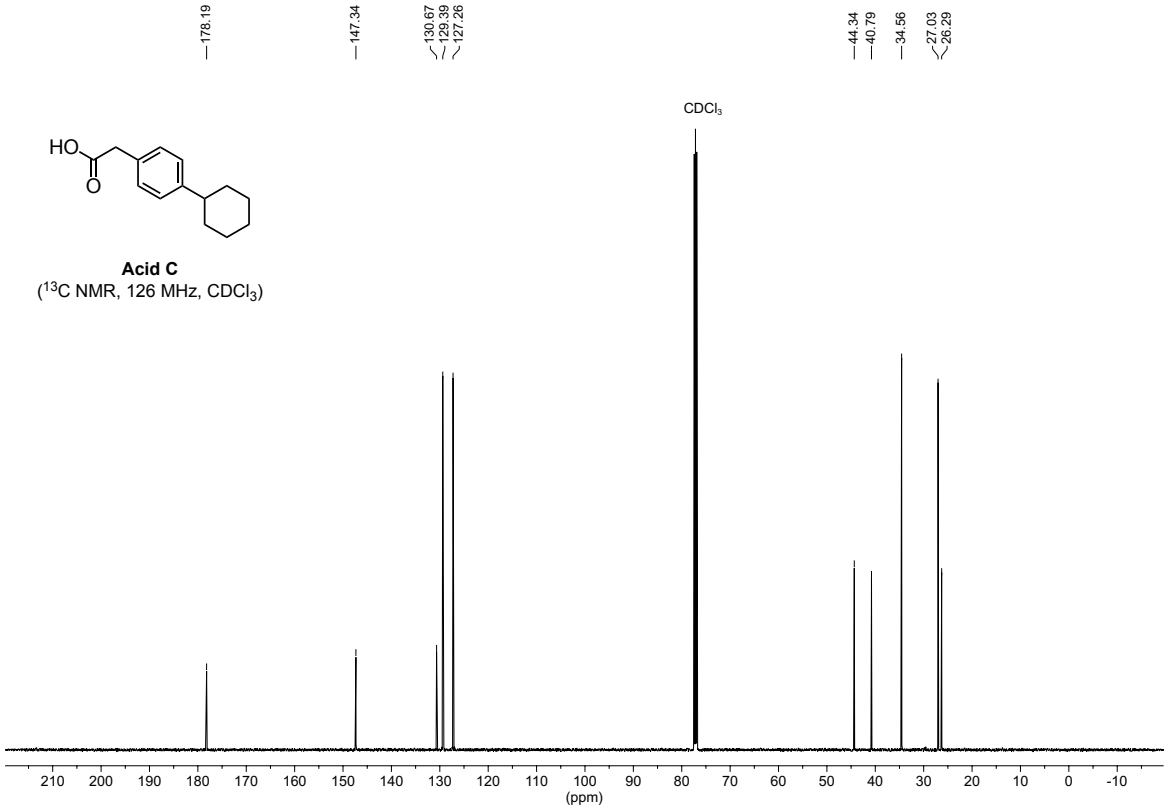

**Acid B**
($^{19}$F NMR, 471 MHz, $CDCl_3$)



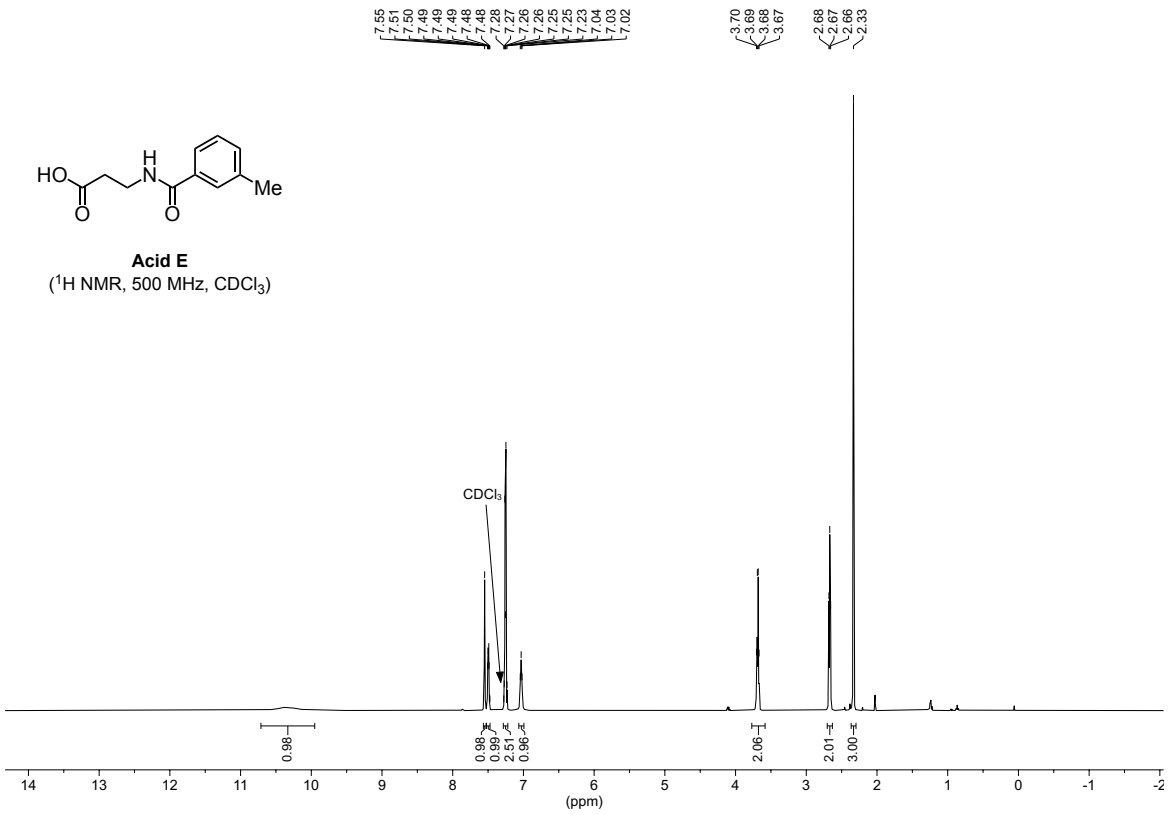





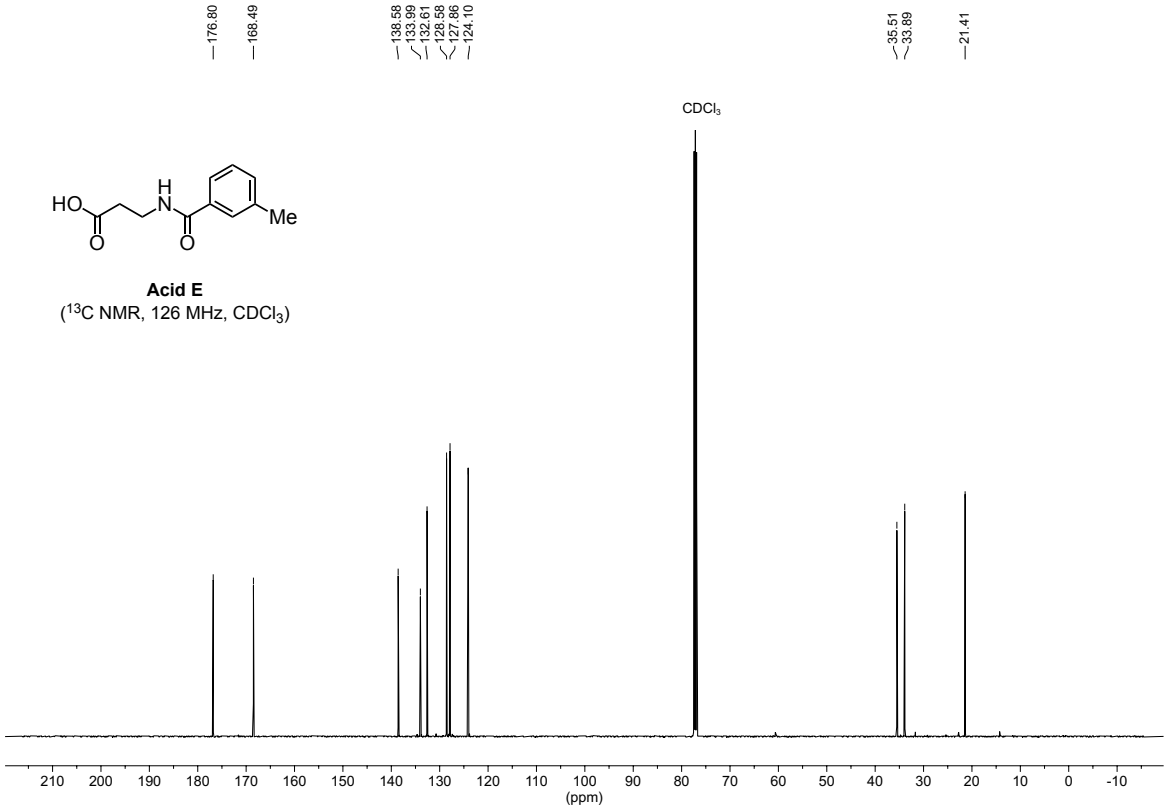

**Acid C**
($^{1}$H NMR, 500 MHz, $CDCl_3$)



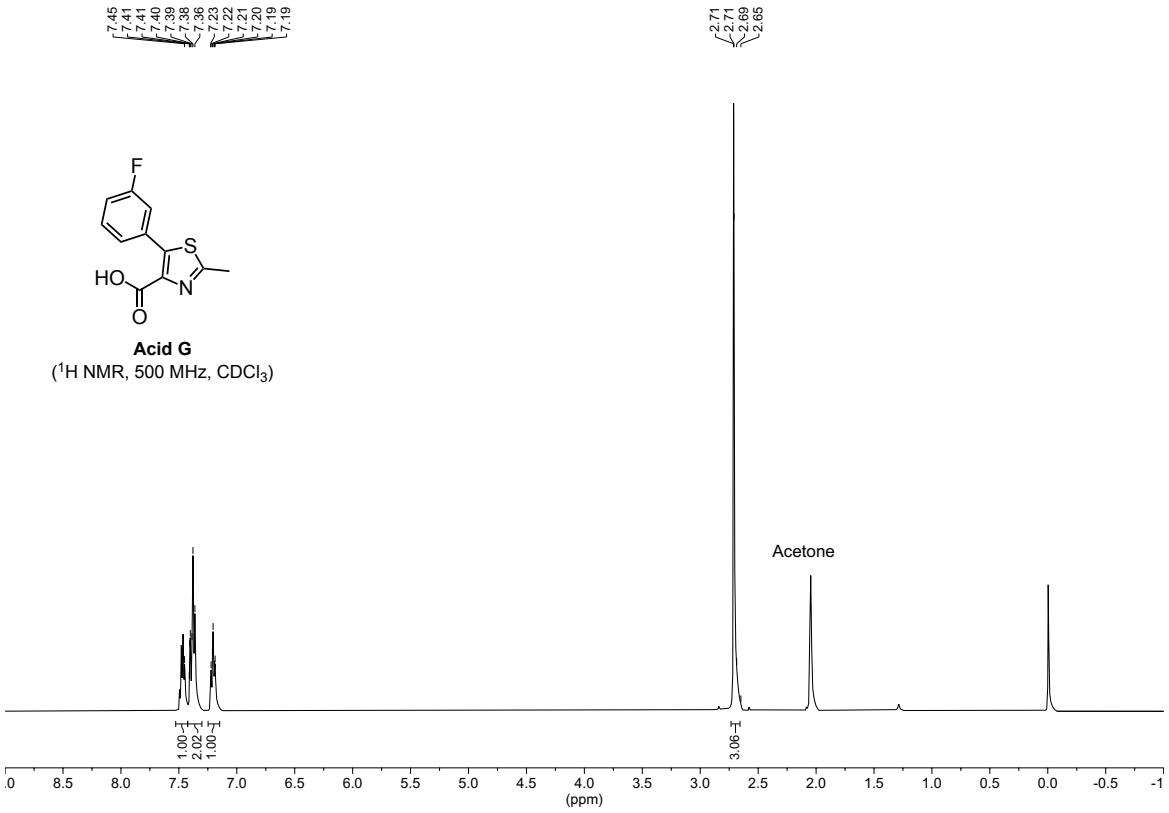

**Acid C**
($^{13}$C NMR, 126 MHz, $CDCl_3$)



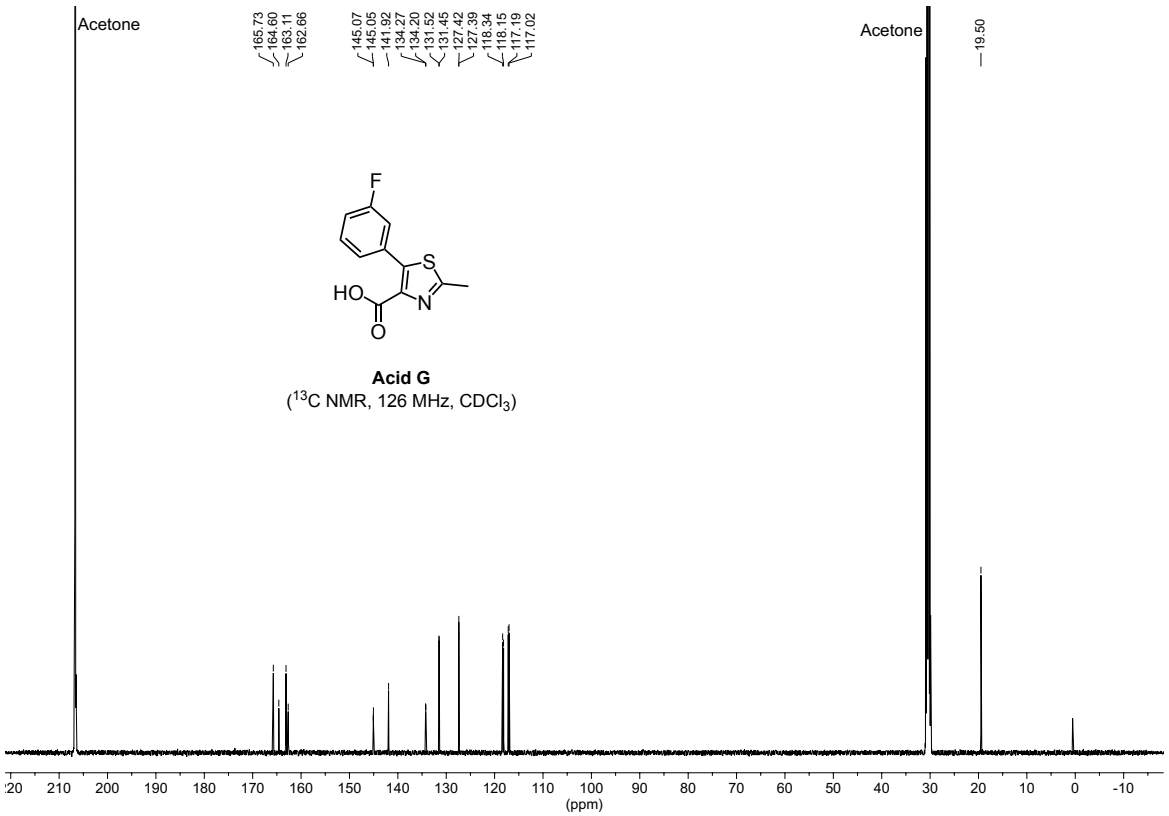

**Acid E**
($^{1}$H NMR, 500 MHz, $CDCl_3$)



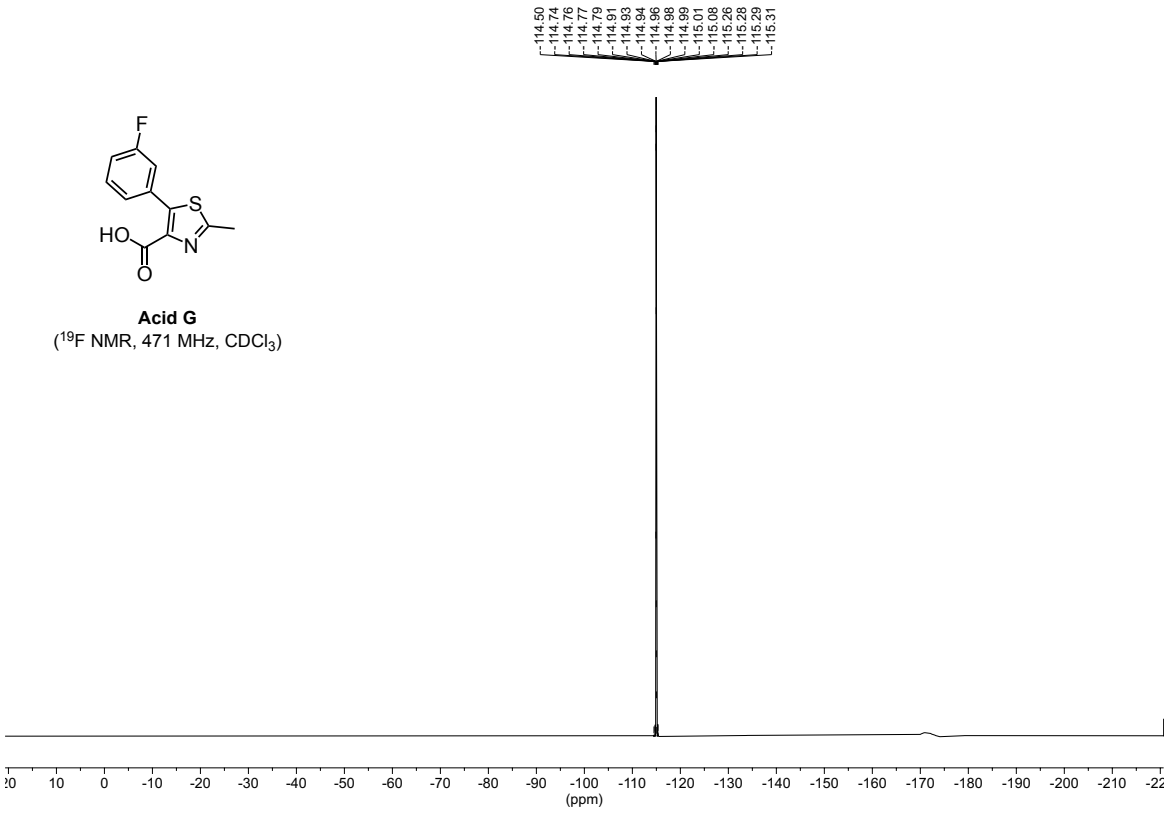

**Acid E**
($^{13}$C NMR, 126 MHz, $CDCl_3$)



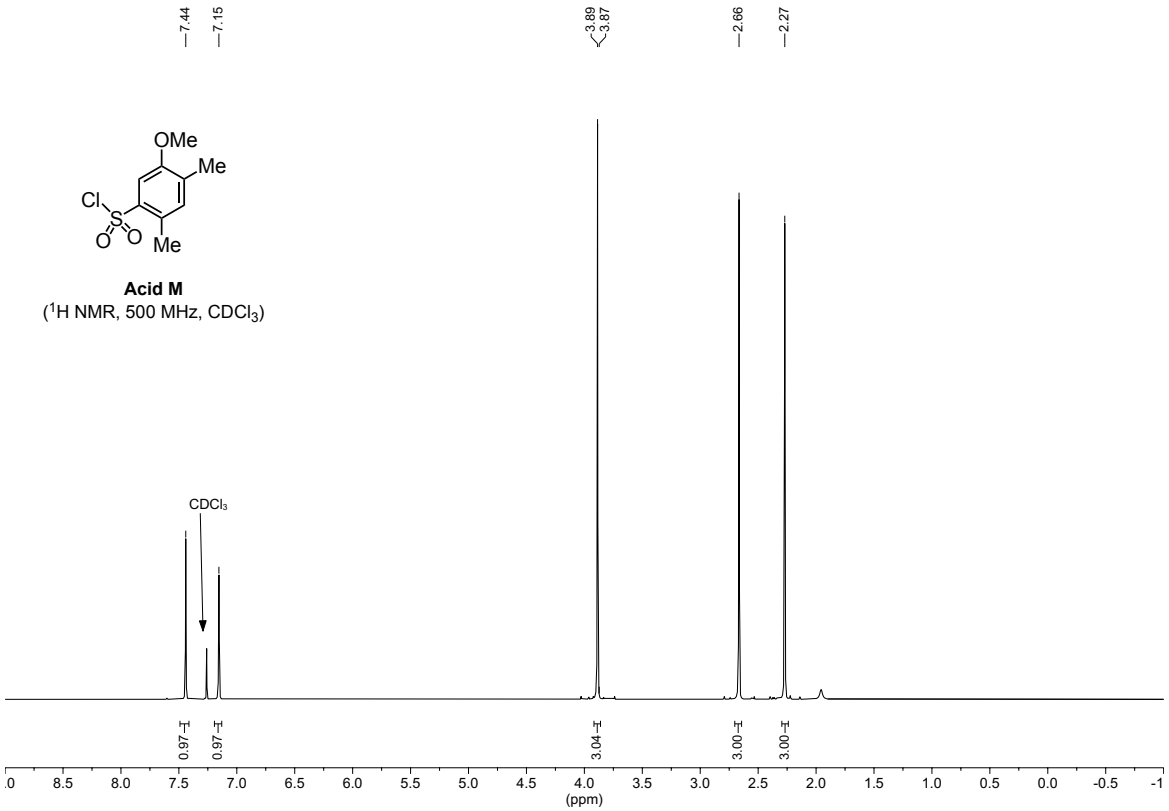

**Acid G**
($^{1}$H NMR, 500 MHz, $CDCl_3$)



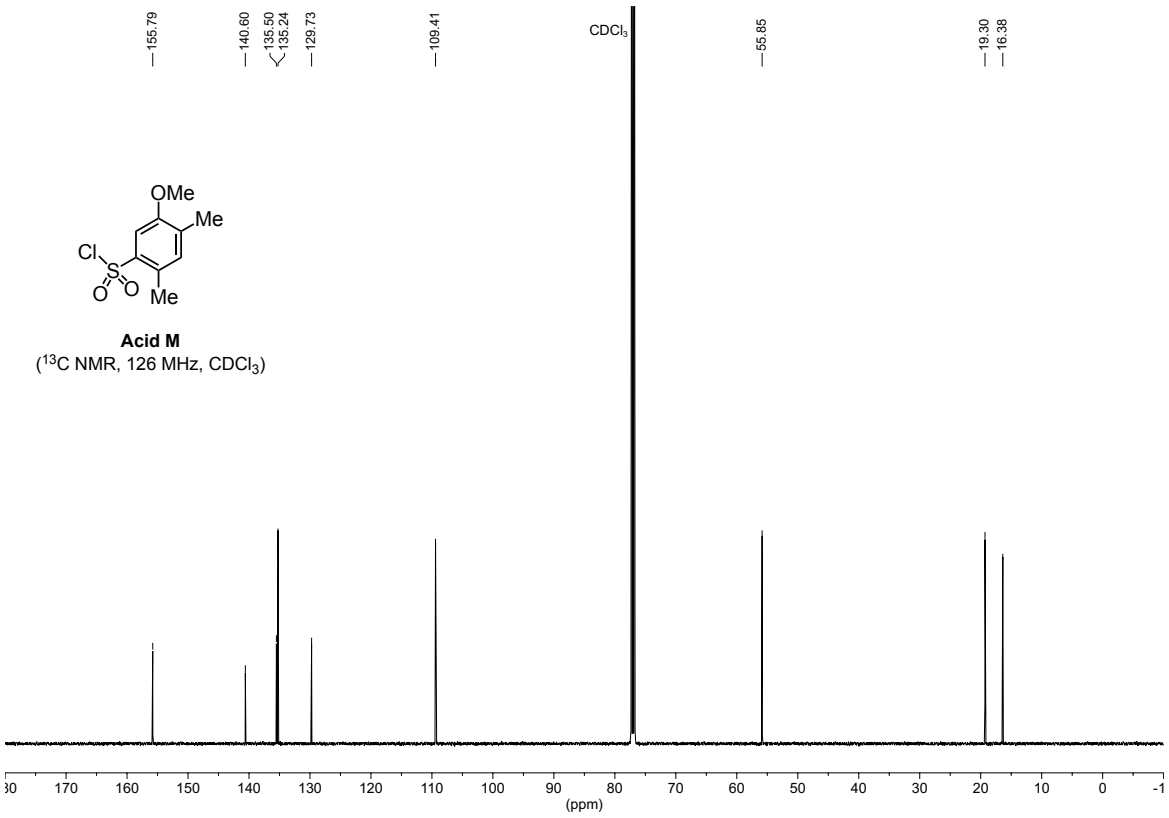

**Acid G**
($^{13}$C NMR, 126 MHz, $CDCl_3$)



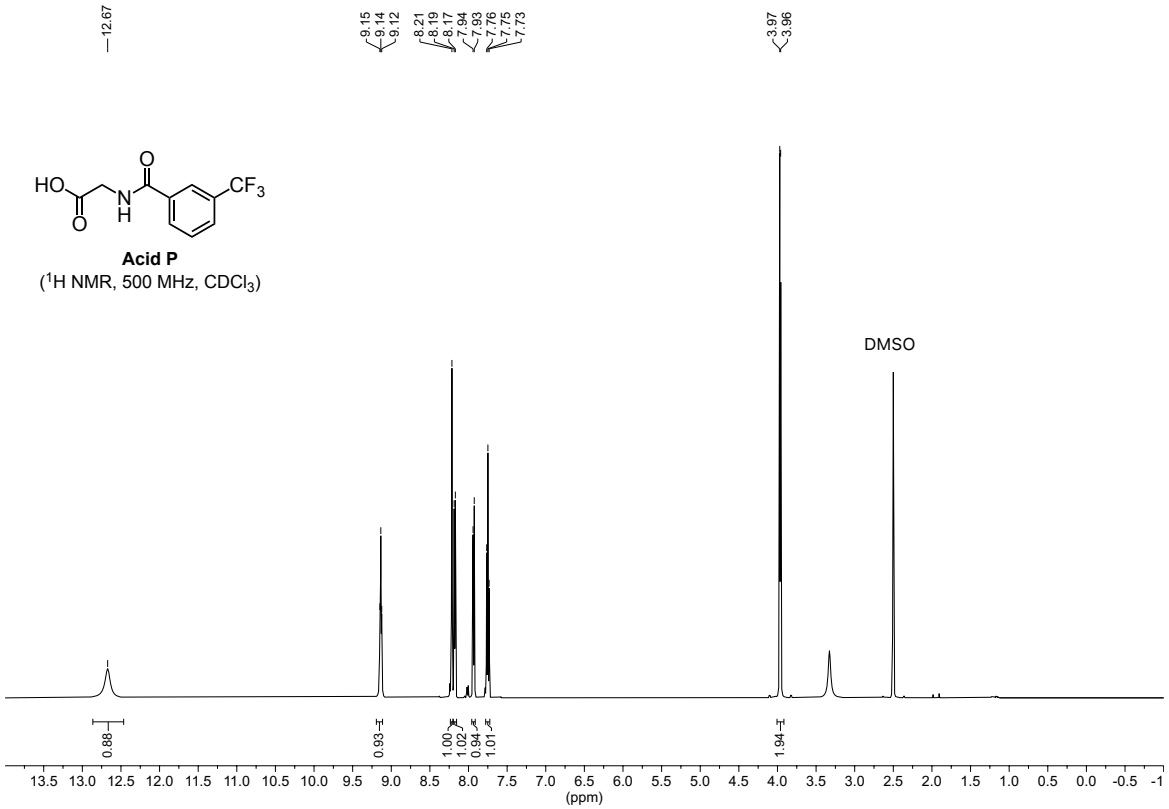

**Acid G**
($^{19}$F NMR, 471 MHz, $CDCl_3$)



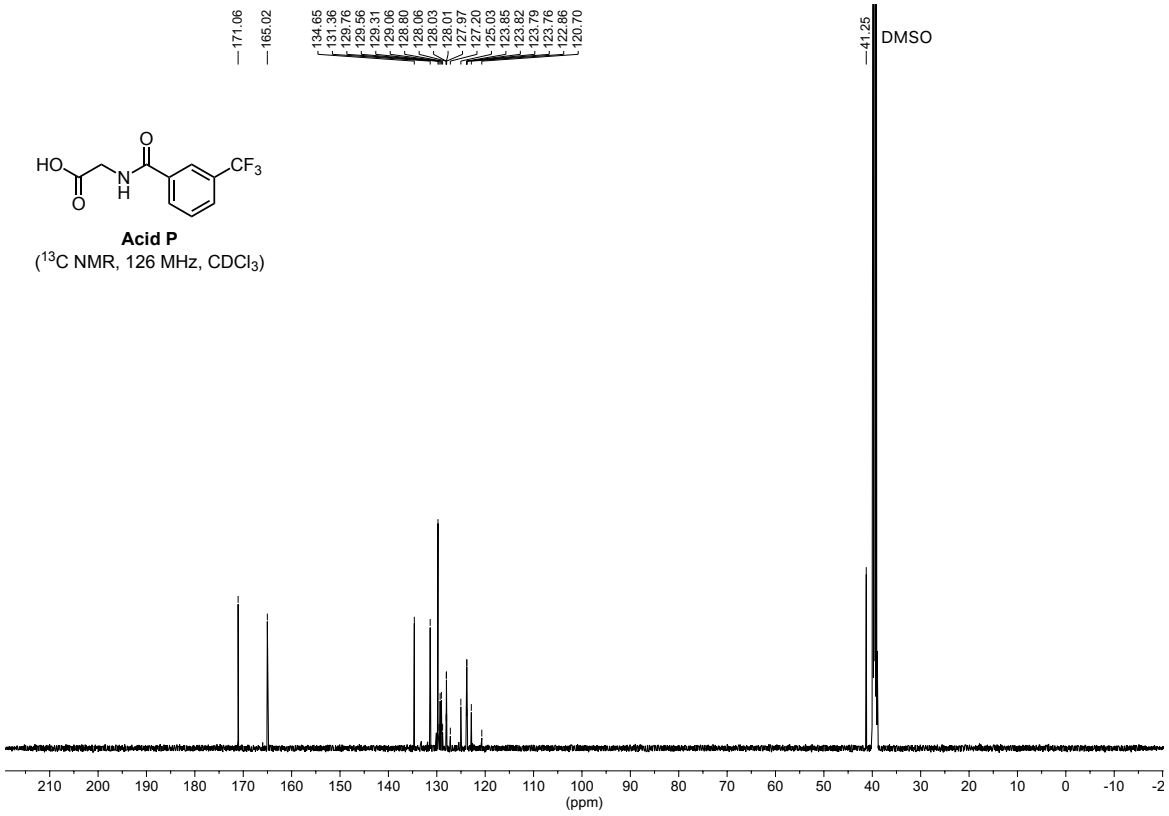

**Acid M**
($^1$H NMR, 500 MHz, $CDCl_3$)



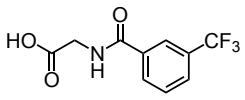

**Acid M**
($^{13}$C NMR, 126 MHz, $CDCl_3$)




**Acid P**
($^1$H NMR, 500 MHz, $CDCl_3$)

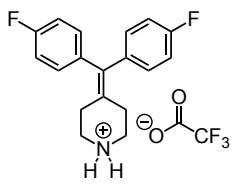



**Acid P**
($^{13}$C NMR, 126 MHz, $CDCl_3$)

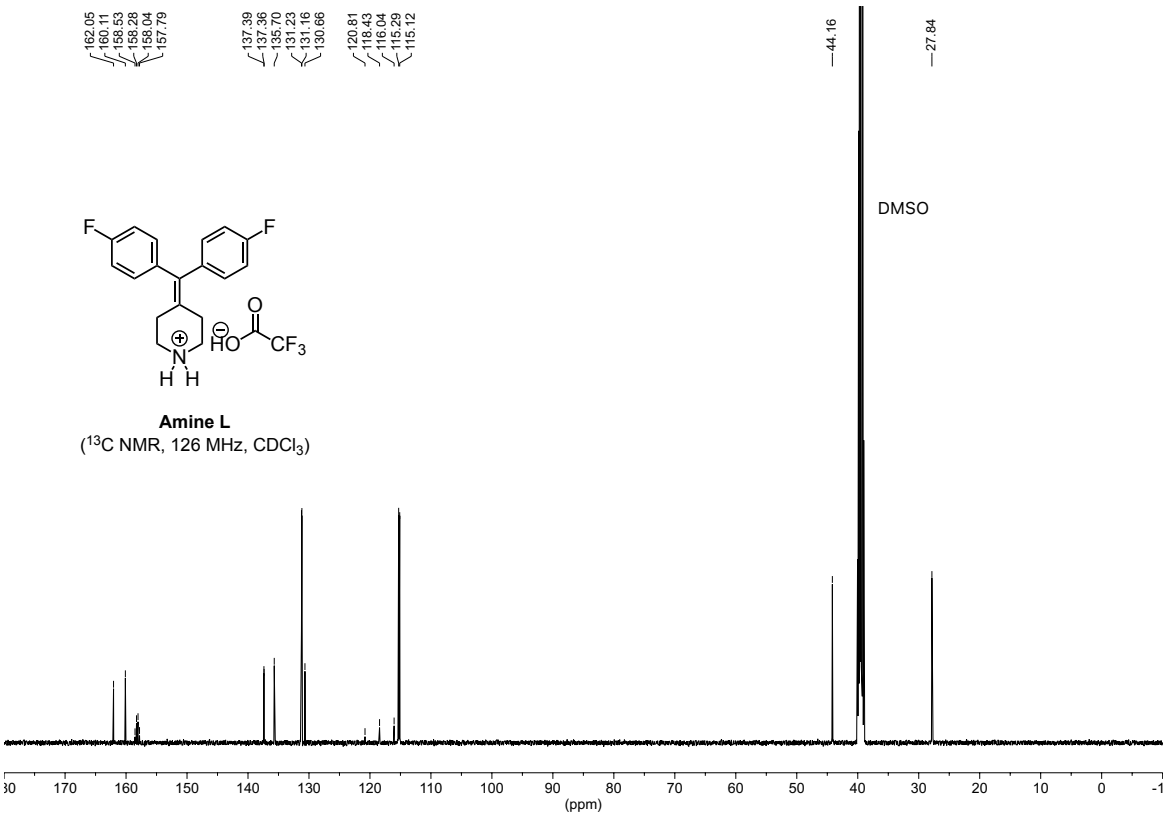


**Acid P**
($^{19}$F NMR, 471 MHz, $CDCl_3$)

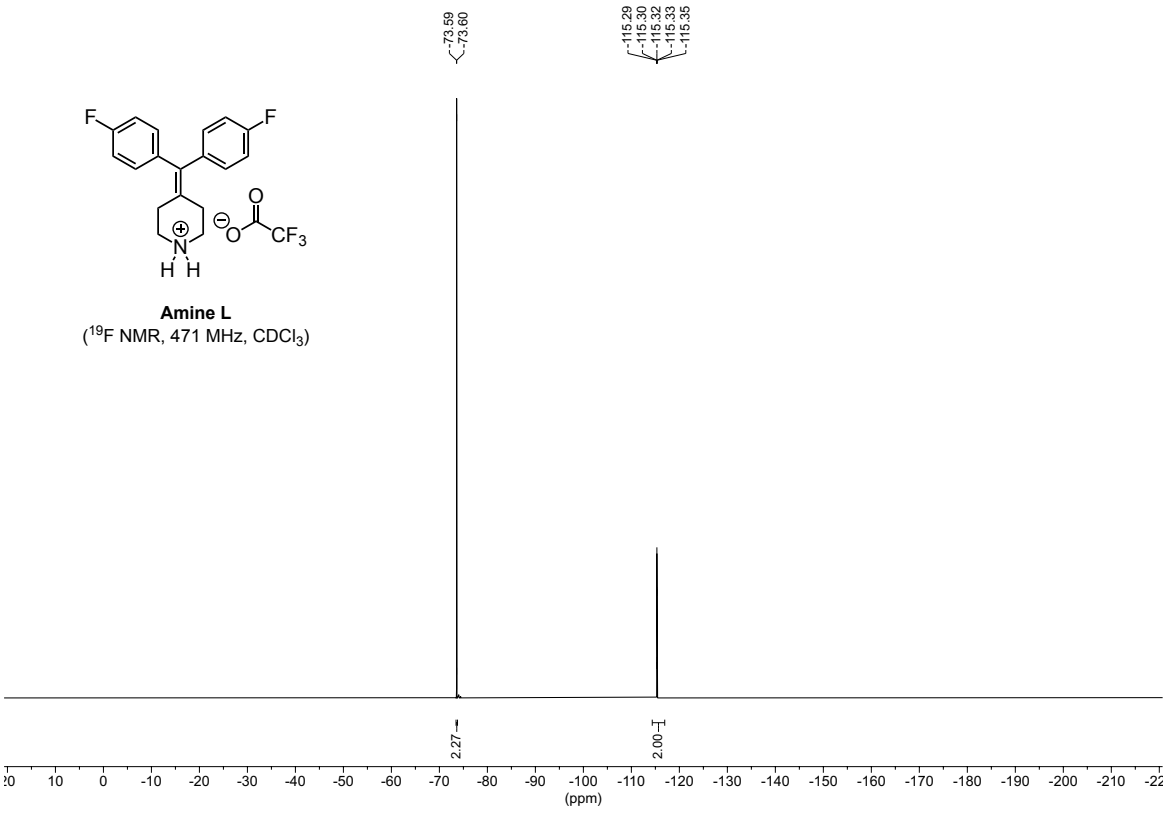


**Amine L**
($^1$H NMR, 500 MHz, $CDCl_3$)

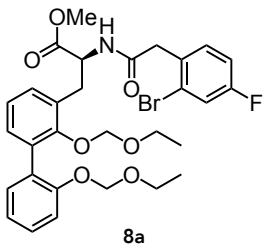



**Amine L**
($^{13}$C NMR, 126 MHz, $CDCl_3$)




**Amine L**
($^{19}$F NMR, 471 MHz, $CDCl_3$)

### 7.2.3. Synthesis and Characterization of Intermediates 8a-w




**8a**

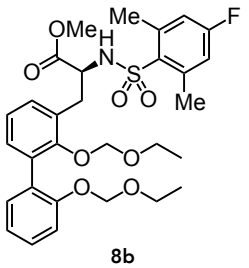
**methyl (*S*)-3-(2,2'-bis(ethoxymethoxy)-[1,1'-biphenyl]-3-yl)-2-(2-(2-bromo-4-fluorophenyl)acetamido)propanoate (8a)** was synthesized following General Procedure 1A from **7** using **Acid A**. Crude material purified by normal-phase column chromatography using EtOAc/Hx (0-30%) to give **8a** as a yellowish oil (68% yield).

**$^{1}$H NMR (500 MHz, $CDCl_3$)** δ 7.35 – 7.29 (m, 1H), 7.26 – 7.13 (m, 6H), 7.12 – 7.04 (m, 2H), 7.02 (d, *J* = 7.3 Hz, 1H), 6.93 (td, *J* = 8.3, 2.7 Hz, 1H), 5.12 (s, 2H), 4.82 (ddd, *J* = 10.2, 7.3, 4.6 Hz, 1H), 4.50 (s, 2H), 3.75 (s, 3H), 3.69 – 3.62 (m, 1H), 3.62 – 3.53 (m, 4H), 3.44 (dq, *J* = 9.6, 7.1 Hz, 1H), 3.30 – 3.22 (m, 1H), 3.13 (dd, *J* = 13.9, 4.7 Hz, 1H), 1.14 (dt, *J* = 9.9, 7.1 Hz, 6H).

**$^{13}$C NMR (126 MHz, $CDCl_3$)** δ 172.4, 169.7, 161.6 (d, *J* = 250.4 Hz, 1C), 154.9, 154.8, 132.4 (d, *J* = 8.8 Hz, 1C), 132.2, 131.7, 131.3, 131.0 (d, *J* = 3.5 Hz, 1C), 129.83, 129.80, 129.2, 128.7, 125.0 (d, *J* = 9.1 Hz, 1C), 124.3, 121.9, 120.0 (d *J* = 24.6 Hz, 1C), 115.7, 114.9 (d *J* = 21.3 Hz, 1C), 98.5, 93.7, 65.8, 64.3, 54.0, 52.4, 42.6, 31.6, 15.2, 15.0.

**$^{19}$F NMR (471 MHz, $CDCl_3$)** δ -113.46 (q, *J* = 7.8 Hz, 1F**).**

**HRMS (ESI+/TOF, *m/z*):** Exact mass calculated for $[C_{30}H_{33}BrFNO_7+H]^+$: 618.1503; found: 618.1509.




**8b**

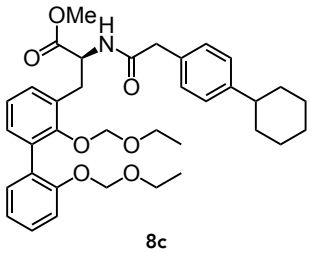
**methyl (*S*)-3-(2,2'-bis(ethoxymethoxy)-[1,1'-biphenyl]-3-yl)-2-((4-fluoro-2,6-dimethylphenyl)sulfonamido)propanoate (8b)** was synthesized following General Procedure 1B from **7** using **Acid B**. Crude material purified by normal-phase column chromatography using EtOAc/Hx (10-30%) to give **8b** as a yellow oil (87% yield).

**$^1$H NMR (500 MHz, $CDCl_3$)** δ 7.34 – 7.29 (m, 1H), 7.25 (d, *J* = 10.4 Hz, 1H), 7.20 (d, *J* = 7.4 Hz, 1H), 7.17 (dd, *J* = 7.3, 2.0 Hz, 1H), 7.05 (t, *J* = 7.4 Hz, 1H), 7.00 – 6.92 (m, 2H), 6.75 (d, *J* = 9.0 Hz, 2H), 6.24 (d, *J* = 9.1 Hz, 1H), 5.16 (s, 2H), 4.56 (d, *J* = 6.5 Hz, 1H), 4.51 (d, *J* = 6.5 Hz, 1H), 4.10 (td, *J* = 9.7, 4.9 Hz, 1H), 3.74 – 3.65 (m, 1H), 3.65 – 3.60 (m, 2H), 3.60 (s, 3H), 3.52 (dt, *J* = 9.7, 7.1 Hz, 1H), 3.27 (dd, *J* = 13.6, 10.1 Hz, 1H), 2.96 (dd, *J* = 13.8, 4.9 Hz, 1H), 2.50 (s, 6H), 1.18 (td, *J* = 7.1, 4.7 Hz, 6H).

**$^{13}$C NMR (126 MHz, $CDCl_3$)** δ 172.3, 163.4 (d, *J* = 253.4, 1C), 154.9, 154.8, 143.31 (d, *J* = 9.2 Hz, 2C), 132.62 (d, *J* = 3.0 Hz, 1C), 132.3, 131.6, 131.4, 129.3, 129.2, 129.1, 128.5, 124.2, 121.8, 117.5 (d, *J* = 21.2 Hz, 2C), 115.4, 98.3, 93.6, 65.8, 64.3, 56.7, 52.4, 32.7, 23.2 (s, 2C), 15.2, 15.0.

**$^{19}$F NMR (471 MHz, $CDCl_3$)** δ -109.0 (t, *J* = 9.1 Hz, 1F).

**HRMS (ESI/TOF, *m/z*):** Exact mass calculated for $[C_{30}H_{36}FNO_8S+Na]^+$ requires 612.2043; found: 612.2047.



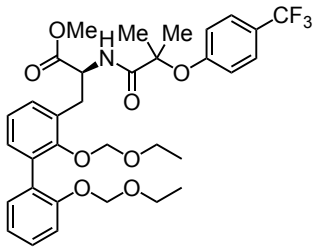
8c

**methyl (*S*)-3-(2,2'-bis(ethoxymethoxy)-[1,1'-biphenyl]-3-yl)-2-(2-(4-cyclohexylphenyl)acetamido)propanoate (8c)** was synthesized following General Procedure 1A from **7** using **Acid C**. Crude material purified by normal-phase column chromatography using EtOAc/Hx (0-30%) to give **8c** as a yellowish oil (64% yield).

**$^1$H NMR (500 MHz, $CDCl_3$)** δ 7.33 (ddd, *J* = 8.9, 7.3, 1.8 Hz, 1H), 7.25 – 7.20 (m, 2H), 7.20 – 7.16 (m, 1H), 7.13 – 7.03 (m, 7H), 6.80 (d, *J* = 7.4 Hz, 1H), 5.11 (s, 2H), 4.81 (ddd, *J* = 9.2, 7.4, 4.9 Hz, 1H), 4.49 – 4.42 (m, 2H), 3.72 (s, 3H), 3.61 – 3.47 (m, 3H), 3.47 (s, 2H), 3.38 (dq, *J* = 9.6, 7.1 Hz, 1H), 3.19 (dd, *J* = 13.8, 9.4 Hz, 1H), 3.12 (dd, *J* = 13.8, 4.9 Hz, 1H), 2.44 (dd, *J* = 7.5, 4.5 Hz, 1H), 1.82 (d, *J* = 7.2 Hz, 4H), 1.77 – 1.71 (m, 1H), 1.44 – 1.31 (m, 4H), 1.29 – 1.20 (m, 1H), 1.14 (t, *J* = 7.1 Hz, 3H), 1.08 (t, *J* = 7.1 Hz, 3H).

**$^{13}$C NMR (126 MHz, $CDCl_3$)** δ 172.4, 171.3, 154.8, 154.6, 146.8, 132.2, 132.2, 131.7, 131.3, 130.0, 129.9, 129.3 (s, 2C), 129.1, 128.9, 127.3 (s, 2C), 124.1, 121.9, 115.8, 98.2, 93.8, 65.6, 64.3, 53.8, 52.3, 44.3, 43.0, 34.6 (s, 2C), 32.1, 27.0 (s, 2C), 26.2, 15.2, 15.0.

**HRMS (ESI/TOF, *m/z*):** Exact mass calculated for $[C_{36}H_{45}NO_7+H]^+$ requires 604.3274; found: 604.3276.



8d

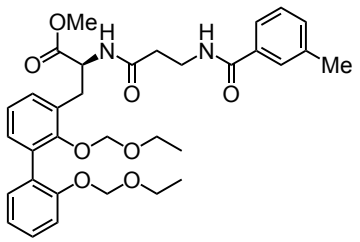
**Methyl (*S*)-3-(2,2'-bis(ethoxymethoxy)-[1,1'-biphenyl]-3-yl)-2-(2-methyl-2-(4-(trifluoromethyl)phenoxy)propanamido)propanoate (8d)** was synthesized following General Procedure 1A from **7** using **Acid D**. Crude material purified by normal-phase column chromatography using EtOAc/Hx (10-40%) to give **8d** as a yellow oil (80% yield).

**$^1$H NMR (500 MHz, $CDCl_3$)** δ 7.71 (d, *J* = 7.3 Hz, 1H), 7.46 (d, *J* = 8.5 Hz, 2H), 7.29 (td, *J* = 8.0, 7.3, 1.8 Hz, 1H), 7.22 (d, *J* = 8.2 Hz, 1H), 7.18 – 7.10 (m, 2H), 7.09 (dd, *J* = 7.5, 1.8 Hz, 1H), 7.04 (t, *J* = 7.6 Hz, 1H), 6.97 (t, *J* = 7.4 Hz, 1H), 6.93 (d, *J* = 8.4 Hz, 2H), 5.11 (s, 2H), 4.89 – 4.80 (m, 1H), 4.47 (d, *J* = 6.4 Hz, 1H), 4.42 (brs, 1H), 3.75 (s, 3H), 3.56 (qd, *J* = 7.1, 2.2 Hz, 2H), 3.47 – 3.37 (m, 1H), 3.36 – 3.25 (m, 1H), 3.23 (brd, *J* = 9.5 Hz, 2H), 1.51 (s, 3H), 1.38 (s, 3H), 1.14 (t, *J* = 7.0 Hz, 3H), 0.97 (t, *J* = 7.1 Hz, 3H).

**$^{13}$C NMR (126 MHz, $CDCl_3$)** δ 174.6, 172.2, 157.7, 154.8, 154.5, 132.4, 131.6, 131.5, 129.9, 129.7, 129.1, 128.5, 126.62 (q, *J* = 3.8 Hz, 2C), 124.4 (q, *J* = 271.8 Hz, 1C), 124.7 (q, *J* = 33.0 Hz, 1C), 124.2, 121.7, 120.4 (s, 2C), 115.6, 98.3, 93.7, 81.6, 65.5, 64.3, 53.8, 52.4, 31.9, 25.8, 24.5, 15.2, 14.9.

**$^{19}$F NMR (471 MHz, $CDCl_3$)** δ -61.8 (s, 3F).

**HRMS (ESI/TOF, *m/z*):** Exact mass calculated for $[C_{33}H_{38}F_3NO_8+H]^+$ requires 634.2628; found 634.2634.



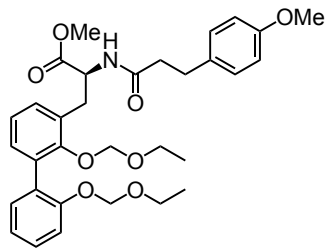
8e

**Methyl (*S*)-3-(2,2'-bis(ethoxymethoxy)-[1,1'-biphenyl]-3-yl)-2-(3-(3-methylbenzamido)propanamido)propanoate (8e)** was synthesized following General Procedure 1A from **7** using **Acid E**. Crude material purified by normal-phase column chromatography using EtOAc/Hx (50-80%) to give **8e** as a white foam (79% yield).

**$^1$H NMR (500 MHz, $CDCl_3$)** δ 7.60 (s, 1H), 7.56 – 7.50 (m, 1H), 7.32 (ddd, *J* = 8.8, 7.4, 1.8 Hz, 1H), 7.25 (s, 2H), 7.25 – 7.19 (m, 2H), 7.18 (td, *J* = 7.1, 1.8 Hz, 2H), 7.15 – 7.08 (m, 2H), 7.10 – 7.02 (m, 2H), 5.14 – 5.07 (m, 2H), 4.81 – 4.72 (m, 1H), 4.58 – 4.48 (m, 2H), 3.80 – 3.69 (m, 4H), 3.68 – 3.48 (m, 4H), 3.45 (dq, *J* = 9.6, 7.0 Hz, 1H), 3.25 (dd, *J* = 13.8, 10.3 Hz, 1H), 3.14 (dd, *J* = 13.9, 4.4 Hz, 1H), 2.50 – 2.37 (m, 2H), 2.36 (s, 3H), 1.11 (dt, *J* = 12.6, 7.1 Hz, 6H).

**$^{13}$C NMR (126 MHz, $CDCl_3$)** δ 172.5, 172.5, 167.5, 154.7, 154.7, 138.3, 134.6, 132.3, 132.2, 131.6, 131.4, 129.8, 129.7, 129.3, 128.7, 128.4, 127.9, 124.3, 124.2, 122.1, 115.8, 98.4, 93.8, 65.9, 64.3, 54.4, 52.5, 35.9, 35.2, 31.6, 21.4, 15.2, 15.0.

**HRMS (ESI/TOF, *m/z*):** Exact mass calculated for $[C_{33}H_{40}N_2O_8+H]^+$ requires 593.2863; found 593.2864.



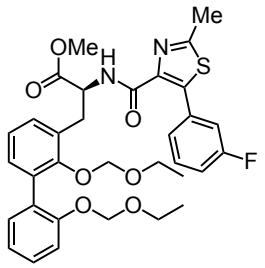

**8f**

**Methyl (*S*)-3-(2,2'-bis(ethoxymethoxy)-[1,1'-biphenyl]-3-yl)-2-(3-(4-methoxyphenyl)propanamido)propanoate (8f)** was synthesized following General Procedure 1A from **7** using **Acid F**. Crude material purified by normal-phase column chromatography using EtOAc/Hx (20-40%) to give **8f** as a colorless oil (72% yield).

**$^1$H NMR (500 MHz, $CDCl_3$)** δ 7.12 – 7.08 (m, 1H), 7.00 (brd, 2H), 6.97 (dd, *J* = 7.3, 2.0 Hz, 1H), 6.95 – 6.87 (m, 2H), 6.86 – 6.79 (m, 3H), 6.72 (d, *J* = 7.4 Hz, 1H), 6.60 – 6.56 (m, 2H), 4.90 – 4.84 (m, 2H), 4.57 (ddd, *J* = 9.6, 7.3, 4.6 Hz, 1H), 4.38 – 4.31 (m, 2H), 3.56 (s, 3H), 3.54 (s, 3H), 3.48 – 3.38 (m, 1H), 3.37 – 3.21 (m, 3H), 3.06 (dd, *J* = 13.8, 9.7 Hz, 1H), 2.89 (dd, *J* = 13.8, 4.6 Hz, 1H), 2.61 (ddd, *J* = 8.8, 7.2, 2.1 Hz, 2H), 2.25 – 2.12 (m, 2H), 0.96 – 0.87 (m, 6H).

**$^{13}$C NMR (126 MHz, $CDCl_3$)** δ 172.6, 172.4, 158.1, 154.8, 154.6, 133.2, 132.2, 131.6, 131.3, 123.0, 129.9, 129.3 (s, 2C), 129.2, 128.8, 124.3, 121.9, 115.8, 114.0 (s, 2C), 98.4, 93.7, 65.8, 64.3, 55.4, 54.0, 52.4, 38.3, 31.8, 30.7, 15.2, 15.1.

**HRMS (ESI/TOF, *m/z*):** Exact mass calculated for $[C_{32}H_{39}NO_8+H]^+$ requires 566.2754; found 566.2764.




**8g**

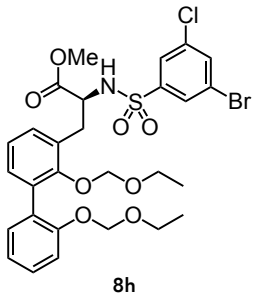
**Methyl (*S*)-3-(2,2'-bis(ethoxymethoxy)-[1,1'-biphenyl]-3-yl)-2-(5-(3-fluorophenyl)-2-methylthiazole-4-carboxamido)propanoate (8g)** was synthesized following General Procedure 1A from **7** using **Acid G**. Crude material purified by normal-phase column chromatography using EtOAc/Hx (40-60%) to give **8g** as an off-white foam (51% yield).

**$^{1}$H NMR (500 MHz, $CDCl_3$)** δ 8.27 (d, *J* = 7.8 Hz, 1H), 7.36 – 7.20 (m, 6H), 7.20 (dt, *J* = 7.7, 2.4 Hz, 2H), 7.08 (t, *J* = 7.6 Hz, 1H), 7.07 – 6.98 (m, 2H), 5.09 (q, *J* = 7.0 Hz, 2H), 4.96 (q, *J* = 7.3 Hz, 1H), 4.63 – 4.56 (m, 2H), 3.72 (s, 3H), 3.55 (q, *J* = 7.0 Hz, 2H), 3.49 (q, *J* = 7.0 Hz, 2H), 3.30 (d, *J* = 6.9 Hz, 2H), 2.69 (s, 3H), 1.13 (t, *J* = 7.1 Hz, 3H), 1.07 (t, *J* = 7.1 Hz, 3H).

**$^{13}$C NMR (126 MHz, $CDCl_3$)** δ 172.4, 163.4, 163.23 (d, *J* = 246.4 Hz, 1C), 161.3, 154.9, 154.4, 141.8 (d, *J* = 2.4 Hz, 1C), 141.6, 132.55 (d, *J* = 8.8 Hz, 1C), 132.0, 131.9, 131.4, 130.1, 129.5 (d, *J* = 8.4 Hz, 1C), 129.0, 129.0, 126.2, 126.2, 123.9, 121.7, 117.5 (d, *J* = 23.1 Hz, 1C), 115.78 (d, *J* = 21.0 Hz, 1C), 115.77, 97.9, 93.8, 65.4, 64.3, 53.4, 52.4, 33.1, 19.1, 15.2, 15.1**.**

**$^{19}$F NMR (471 MHz, $CDCl_3$)** δ -113.27 – -113.38 (m, 1F).

**HRMS (ESI/TOF, *m/z*):** Exact mass calculated for $[C_{33}H_{35}FN_2O_7S+H]^+$ requires 623.2227; found 623.2236.



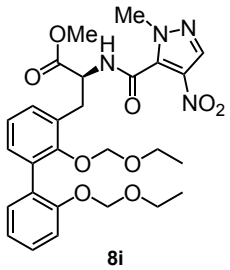

**8h**

**Methyl (*S*)-3-(2,2'-bis(ethoxymethoxy)-[1,1'-biphenyl]-3-yl)-2-((3-bromo-5-chlorophenyl)sulfonamido)propanoate (8h)** was synthesized following General Procedure 1B from **7** using **Acid H**. Crude material purified by normal-phase column chromatography using EtOAc/Hx (0-25%) to give **8h** as a yellow oil (69% yield).

**$^1$H NMR (500 MHz, $CDCl_3$)** δ 7.65 (s, 1H), 7.58 (s, 1H), 7.52 (s, 1H), 7.37 – 7.27 (m, 2H), 7.24 – 7.17 (m, 2H), 7.07 (t, *J* = 7.7 Hz, 1H), 7.03 – 6.96 (m, 2H), 6.44 (s, 1H), 5.28 – 5.11 (m, 2H), 4.59 – 4.49 (m, 2H), 4.14 (s, 1H), 3.72 (s, 3H), 3.69 – 3.48 (m, 4H), 3.25 (dd, *J* = 13.7, 10.9 Hz, 1H), 2.99 (dd, *J* = 13.7, 4.6 Hz, 1H), 1.16 (t, *J* = 7.1 Hz, 6H).

**$^{13}$C NMR (126 MHz, $CDCl_3$)** δ 171.9, 155.0, 154.7, 135.9, 135.2, 132.5, 131.9, 131.6 (s, 2C), 129.4 (s, 2C), 128.5, 128.4, 128.2, 125.8, 124.4, 123.2, 121.9, 115.4, 98.4, 93.7, 65.9, 64.3, 57.6, 52.7, 32.6, 15.2, 15.0.

**HRMS (ESI/TOF, *m/z*):** Exact mass calculated for $[C_{28}H_{31}BrClNO_8S+Na]^+$ requires 678.0540; found 678.0541.



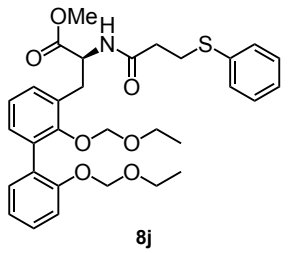

**8i**

**Methyl (*S*)-3-(2,2'-bis(ethoxymethoxy)-[1,1'-biphenyl]-3-yl)-2-(1-methyl-4-nitro-1*H*-pyrazole-5-carboxamido)propanoate (8i)** was synthesized following General Procedure 1A from **7** using **Acid I**. Crude material purified by normal-phase column chromatography using EtOAc/Hx (20-50%) to give **8i** as an off-white foam (44% yield).

**$^1$H NMR (500 MHz, $CDCl_3$)** δ 8.53 (d, *J* = 7.3 Hz, 1H), 7.98 (s, 1H), 7.33 – 7.24 (m, 2H), 7.21 (dd, *J* = 7.5, 1.8 Hz, 3H), 7.14 (t, *J* = 7.5 Hz, 1H), 7.04 (t, 1H), 5.09 (s, 2H), 5.08 – 5.00 (m, 1H), 4.47 – 4.41 (m, 2H), 3.83 (s, 6H), 3.71 – 3.62 (m, 1H), 3.58 (dt, *J* = 21.8, 7.8 Hz, 2H), 3.39 – 3.26 (m, 3H), 1.15 (t, *J* = 7.1 Hz, 3H), 1.00 (t, *J* = 7.1 Hz, 3H).

**$^{13}$C NMR (126 MHz, $CDCl_3$)** δ 171.5, 157.7, 155.0, 154.7, 135.5, 134.0, 133.0, 132.3, 131.7 (s, 2C), 131.6, 129.7, 129.2 (s, 2C), 124.3, 122.0, 115.6, 98.6, 93.7, 65.9, 64.3, 54.6, 52.7, 39.7, 31.6, 15.2, 14.7.

**HRMS (ESI/TOF, *m/z*):** Exact mass calculated for $[C_{27}H_{32}N_4O_9+Na]^+$ requires 579.2067; found 579.2072.



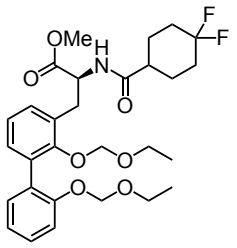
**8j**

**Methyl (*S*)-3-(2,2'-bis(ethoxymethoxy)-[1,1'-biphenyl]-3-yl)-2-(3-(phenylthio)propanamido)propanoate (8j)** was synthesized following General Procedure 1A from **7** using **Acid *J***. Crude material purified by normal-phase column chromatography using EtOAc/Hx (0-30%) to give **8j** as a colorless oil (98% yield).

**$^1$H NMR (500 MHz, $CDCl_3$)** δ 7.35 – 7.27 (m, 3H), 7.28 – 7.13 (m, 7H), 7.10 (t, *J* = 7.5 Hz, 1H), 7.04 (td, *J* = 7.5, 1.1 Hz, 1H), 7.00 (d, *J* = 7.4 Hz, 1H), 5.13 – 5.06 (m, 2H), 4.82 – 4.74 (m, 1H), 4.54 (q, *J* = 6.5 Hz, 2H), 3.75 (s, 3H), 3.68 – 3.46 (m, 3H), 3.44 (dt, *J* = 9.5, 7.1 Hz, 1H), 3.31 – 3.23 (m, 1H), 3.18 – 3.04 (m, 3H), 2.52 – 2.35 (m, 2H), 1.12 (q, *J* = 7.0 Hz, 6H).

**$^{13}$C NMR (126 MHz, $CDCl_3$)** δ 172.5, 171.1, 154.8, 154.7, 135.8, 132.3, 131.6, 131.3, 130.0, 129.8, 129.6 (s, 2C), 129.2, 129.1 (s, 2C), 128.9, 126.4, 124.3, 122.0, 115.8, 98.4, 93.8, 65.8, 64.3, 54.0, 52.4, 36.0, 31.8, 29.3, 15.2, 15.0.

**HRMS (ESI/TOF, *m/z*):** Exact mass calculated for $[C_{31}H_{37}NO_7S+Na]^+$ requires 590.2188; found 590.2198.



**8k**

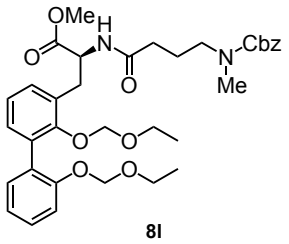
**Methyl (*S*)-3-(2,2'-bis(ethoxymethoxy)-[1,1'-biphenyl]-3-yl)-2-(4,4-difluorocyclohexane-1-carboxamido)propanoate (8k)** was synthesized following General Procedure 1A from **7** using **Acid K**. Crude material purified by normal-phase column chromatography using EtOAc/Hx (0-20%) to give **8k** as a yellow oil (95% yield).

**$^1$H NMR (500 MHz, $CDCl_3$)** δ 7.36 – 7.29 (m, 1H), 7.25 – 7.15 (m, 4H), 7.14 – 7.02 (m, 2H), 6.96 (d, *J* = 7.2 Hz, 1H), 5.12 (s, 2H), 4.83 – 4.75 (m, 1H), 4.57 (s, 2H), 3.75 (s, 3H), 3.67 – 3.51 (m, 3H), 3.51 – 3.42 (m, 1H), 3.27 (dd, *J* = 13.8, 9.8 Hz, 1H), 3.15 (dd, *J* = 13.9, 4.6 Hz, 1H), 2.17 – 1.98 (m, 3H), 1.93 – 1.84 (m, 1H), 1.82 – 1.58 (m, 5H), 1.14 (q, *J* = 7.0 Hz, 6H).

**$^{13}$C NMR (126 MHz, $CDCl_3$)** δ 174.3, 172.5, 154.8, 154.3, 132.3, 131.6, 131.4, 130.0, 129.3, 128.7, 124.4, 122.8 (t, *J* = 240.6 Hz, 1C), 122.0, 120.3, 115.9, 98.3, 93.8, 65.8, 64.4, 53.8, 52.4, 42.1, 32.8 (t, *J* = 24.6 Hz, 2C), 31.8, 25.6 (t, *J* = 10.8 Hz, 2C), 15.2, 15.0.

**$^{19}$F NMR (471 MHz, $CDCl_3$)** δ -93.66 (d, *J* = 235.2 Hz, 1F), -99.81 (d, *J* = 238.2 Hz, 1F).

**HRMS (ESI/TOF, *m/z*):** Exact mass calculated for $[C_{29}H_{37}F_2NO_7+H]^+$ requires 550.2616; found 550.2617.



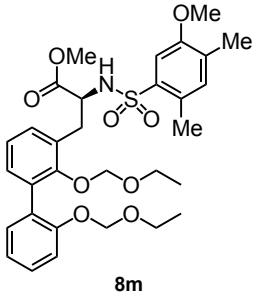
**8l**

**Methyl (*S*)-2-(4-(((benzyloxy)carbonyl)(methyl)amino)butanamido)-3-(2,2'-bis(ethoxymethoxy)-[1,1'-biphenyl]-3-yl)propanoate (7l)** was synthesized following General Procedure 1A from **7** using **Acid L**. Crude material purified by normal-phase column chromatography using EtOAc/Hx (50-80%) to give **7l** as an off-white foam (64% yield).

**$^1$H NMR (500 MHz, $CDCl_3$)** δ 7.37 – 7.28 (m, 6H), 7.25 – 7.20 (m, 2H), 7.18 (dd, *J* = 7.6, 1.6 Hz, 2H), 7.13 – 7.02 (m, 2H), 6.87 (s, 1H), 5.15 – 5.07 (m, 4H), 4.79 (brs, 1H), 4.60 – 4.53 (m, 2H), 3.74 (s, 3H), 3.69 – 3.42 (m, 4H), 3.30 – 3.09 (m, 4H), 2.87 (s, 3H), 2.18 – 2.02 (m, 2H), 1.85 – 1.73 (m, 2H), 1.14 (td, *J* = 7.1, 4.6 Hz, 6H).

**$^{13}$C NMR (126 MHz, $CDCl_3$)** *rotameric mixture*: δ 172.6, 172.3, 156.5, 156.3, 154.7, 154.6, 137.0, 132.2, 131.6, 131.2, 129.9, 129.8, 129.1, 128.8, 128.5, 128.0, 127.9, 124.2, 124.1, 121.9, 115.7, 98.3, 93.7, 67.1, 65.7, 65.7, 64.2, 53.8, 52.3, 48.3, 48.1, 34.8, 34.1, 33.0, 32.9, 32.0, 31.7, 23.7, 23.5, 15.1, 15.0.

**HRMS (ESI/TOF, *m/z*):** Exact mass calculated for $[C_{35}H_{44}N_2O_9+H]^+$ requires 637.3125; found 637.3121.



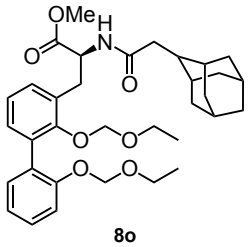

**8m**

**Methyl (*S*)-3-(2,2'-bis(ethoxymethoxy)-[1,1'-biphenyl]-3-yl)-2-((5-methoxy-2,4-dimethylphenyl)sulfonamido)propanoate (8m)** was synthesized following General Procedure 1B from **7** using **Acid M**. Crude material purified by normal-phase column chromatography using EtOAc/Hx (0-30%) to give **8m** as a yellowish oil (91% yield).

**$^1$H NMR (500 MHz, $CDCl_3$)** δ 7.36 – 7.29 (m, 2H), 7.29 – 7.22 (m, 1H), 7.19 (ddd, *J* = 13.4, 6.6, 2.7 Hz, 2H), 7.09 – 7.02 (m, 1H), 7.01 (q, *J* = 3.1, 2.2 Hz, 2H), 6.93 (s, 1H), 6.06 (d, *J* = 9.0 Hz, 1H), 5.16 (s, 2H), 4.57 (d, *J* = 6.4 Hz, 1H), 4.52 (d, *J* = 6.4 Hz, 1H), 4.18 (td, *J* = 9.4, 5.1 Hz, 1H), 3.83 (s, 3H), 3.69 – 3.55 (m, 6H), 3.57 – 3.48 (m, 1H), 3.31 – 3.21 (m, 1H), 2.99 (dd, *J* = 13.8, 5.1 Hz, 1H), 2.29 (s, 3H), 2.21 (s, 3H), 1.17 (t, *J* = 7.0 Hz, 6H).

**$^{13}$C NMR (126 MHz, $CDCl_3$)** δ 172.3, 155.4, 154.9, 154.8, 135.4, 134.7, 132.3, 131.8, 131.6, 131.3, 129.6, 129.2, 129.1, 129.1, 128.7, 124.1, 121.8, 115.5, 111.0, 98.3, 93.6, 65.7, 64.3, 56.8, 55.8, 52.4, 33.1, 18.9, 16.1, 15.2, 15.0.

**HRMS (ESI/TOF, *m/z*):** Exact mass calculated for $[C_{31}H_{39}NO_9S+Na]^+$ requires 624.2243; found 624.2250.



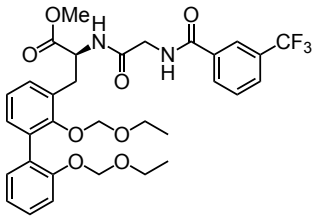
**8o**

**Methyl (*S*)-2-(2-(adamantan-2-yl)acetamido)-3-(2,2'-bis(ethoxymethoxy)-[1,1'-biphenyl]-3-yl)propanoate (8o)** was synthesized following General Procedure 1A from **7** using **Acid O**. Crude material purified by normal-phase column chromatography using EtOAc/Hx (0-20%) to give **8o** as a colorless oil (51% yield).

**$^1$H NMR (500 MHz, $CDCl_3$)** δ 7.33 (td, *J* = 7.9, 7.4, 1.8 Hz, 1H), 7.29 – 7.23 (m, 2H), 7.20 (d, *J* = 7.5 Hz, 2H), 7.12 (t, *J* = 7.6 Hz, 1H), 7.07 (t, *J* = 7.4 Hz, 1H), 6.86 (d, *J* = 7.4 Hz, 1H), 5.18 – 5.11 (m, 2H), 4.83 (ddd, *J* = 9.9, 7.4, 4.7 Hz, 1H), 4.59 (s, 2H), 3.76 (s, 3H), 3.69 (dq, *J* = 9.7, 7.1 Hz, 1H), 3.66 – 3.55 (m, 2H), 3.51 (dq, *J* = 9.6, 7.1 Hz, 1H), 3.33 – 3.24 (m, 1H), 3.14 (dd, *J* = 13.8, 4.7 Hz, 1H), 2.33 – 2.21 (m, 2H), 2.17 (brt, *J* = 7.3 Hz, 1H), 1.90 – 1.66 (m, 12H), 1.53 (s, 1H), 1.47 (d, *J* = 12.9 Hz, 1H), 1.17 (t, *J* = 7.0 Hz, 6H).

**$^{13}$C NMR (126 MHz, $CDCl_3$)** δ 173.0, 172.7, 154.8, 154.6, 132.2, 131.6, 131.2, 130.0, 129.8, 129.1, 128.9, 124.2, 121.9, 115.8, 98.4, 93.8, 65.7, 64.3, 53.7, 52.3, 41.6, 40.0, 39.0, 38.4, 31.9, 31.9, 31.8, 31.8, 31.7, 31.7, 28.1, 28.0, 15.2, 15.0.

**HRMS (ESI/TOF, *m/z*):** Exact mass calculated for $[C_{34}H_{45}NO_7+H]^+$ requires 580.3274; found 580.3272.



**8p**

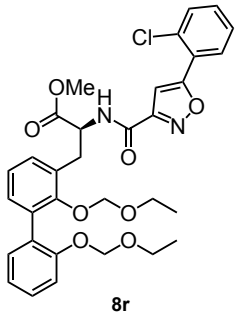
**Methyl (*S*)-3-(2,2'-bis(ethoxymethoxy)-[1,1'-biphenyl]-3-yl)-2-(2-(3-(trifluoromethyl)benzamido)acetamido)propanoate (8p)** was synthesized following General Procedure 1A from **7** using **Acid P**. Crude material purified by normal-phase column chromatography using EtOAc/Hx (40-70%) to give **8p** as a colorless oil (51% yield).

**$^1$H NMR (500 MHz, $CDCl_3$):** δ 8.09 (s, 1H), 7.96 (d, *J* = 7.8 Hz, 1H), 7.73 (d, *J* = 7.8 Hz, 1H), 7.53 (d, *J* = 7.2 Hz, 1H), 7.49 (t, *J* = 7.8 Hz, 1H), 7.35 (ddd, *J* = 8.7, 7.5, 1.8 Hz, 1H), 7.26 – 7.15 (m, 5H), 7.14 – 7.05 (m, 2H), 5.09 (s, 2H), 4.76 (ddd, *J* = 10.7, 7.0, 4.2 Hz, 1H), 4.50 (s, 2H), 4.11 (t, *J* = 7.0 Hz, 2H), 3.77 (s, 3H), 3.64 – 3.41 (m, 4H), 3.30 (dd, *J* = 13.8, 10.1 Hz, 1H), 3.17 (dd, *J* = 13.8, 4.2 Hz, 1H), 1.13 (td, *J* = 7.1, 4.6 Hz, 6H).

**$^{13}$C NMR (126 MHz, $CDCl_3$):** δ 171.8, 168.7, 165.7, 154.6, 154.5, 134.6, 132.3, 131.4, 131.3, 131.2 (q, *J* = 32.8 Hz, 1C), 130.2, 129.9, 129.5, 129.2, 129.1, 129.0, 128.2 (q, *J* = 3.6 Hz, 1C), 124.5, 124.4 (q, *J* = 3.8 Hz, 1C), 123.9 (q, *J* = 272.3 Hz, 1C), 122.3, 116.2, 98.4, 94.2, 65.8, 64.3, 54.6, 52.4, 42.9, 31.6, 15.0, 14.9.

**$^{19}$F NMR** (471 MHz, $CDCl_3$) δ -62.77 (s, 3F).

**HRMS (ESI/TOF, *m/z*):** Exact mass calculated for $[C_{32}H_{35}F_3N_2O_8+H]^+$ requires 633.2424; found 633.2429.



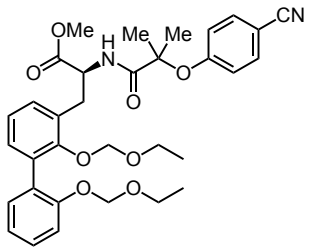

**8r**

**methyl (*S*)-3-(2,2'-bis(ethoxymethoxy)-[1,1'-biphenyl]-3-yl)-2-(5-(2-chlorophenyl)isoazole-3-carboxamido)propanoate (8r)** was synthesized following General Procedure 1A from **7** using **Acid R**. Crude material purified by normal-phase column chromatography using EtOAc/Hx (20-50%) to give **8r** as a white foam (66% yield).

**$^1$H NMR (500 MHz, $CDCl_3$)** δ 8.03 (brs, 1H), 7.96 – 7.88 (m, 1H), 7.56 – 7.49 (m, 1H), 7.44 – 7.37 (m, 2H), 7.33 – 7.27 (m, 3H), 7.25 – 7.18 (m, 3H), 7.10 (t, *J* = 7.5 Hz, 1H), 7.04 (brt, *J* = 7.4, 1.2 Hz, 1H), 5.14 – 5.06 (m, 2H), 5.02 (q, *J* = 7.5 Hz, 1H), 4.66 – 4.60 (m, 2H), 3.77 (s, 3H), 3.62 – 3.49 (m, 4H), 3.42 – 3.29 (m, 2H), 1.11 (td, *J* = 7.1, 2.1 Hz, 6H).

**$^{13}$C NMR (126 MHz, $CDCl_3$)** δ 171.7, 167.9, 159.1, 158.8, 154.9, 154.4, 132.4, 132.2, 131.8, 131.6, 131.4, 131.1, 130.1, 129.7, 129.5, 129.1, 128.8, 127.4, 125.9, 124.2, 121.9, 115.6, 104.1, 98.1, 93.8, 65.6, 64.2, 54.1, 52.6, 32.7, 15.2, 15.1.

**HRMS (ESI/TOF, *m/z*):** Exact mass calculated for $[C_{32}H_{33}ClN_2O_8+H]^+$ requires 609.2004; found 609.2013.



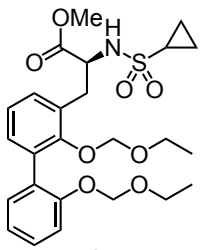

**8t**

**Methyl (*S*)-3-(2,2'-bis(ethoxymethoxy)-[1,1'-biphenyl]-3-yl)-2-(2-(4-cyanophenoxy)-2-methylpropanamido)propanoate (8t)** was synthesized following General Procedure 1A from **7** using **Acid T**. Crude material purified by normal-phase column chromatography using EtOAc/Hx (0-30%) to give **8t** as a yellowish oil (91% yield).

**$^1$H NMR (500 MHz, $CDCl_3$)** δ 7.60 (d, *J* = 7.4 Hz, 1H), 7.48 (d, *J* = 8.8 Hz, 2H), 7.31 (ddd, *J* = 8.8, 7.3, 1.8 Hz, 1H), 7.25 – 7.21 (m, 1H), 7.16 (dd, *J* = 7.5, 1.8 Hz, 1H), 7.14 – 7.07 (m, 2H), 7.07 – 6.97 (m, 2H), 6.89 (d, *J* = 8.4 Hz, 2H), 5.15 – 5.08 (m, 2H), 4.86 (q, *J* = 7.5 Hz, 1H), 4.47 (d, *J* = 6.4 Hz, 1H), 4.40 (brs, 1H), 3.75 (s, 3H), 3.57 (qd, *J* = 7.1, 3.5 Hz, 2H), 3.49 – 3.41 (m, 1H), 3.33 (dq, *J* = 9.4, 7.0 Hz, 1H), 3.22 (d, *J* = 9.2 Hz, 2H), 1.52 (s, 3H), 1.38 (s, 3H), 1.15 (t, *J* = 7.1 Hz, 3H), 0.98 (t, *J* = 7.1 Hz, 3H.

**$^{13}$C NMR (126 MHz, $CDCl_3$)** δ 174.1, 172.1, 158.7, 154.8, 154.5, 133.6, 132.4, 131.5, 131.5, 129.8, 129.6, 129.2, 128.4, 124.3, 121.8, 120.5, 119.0, 115.6, 105.8, 98.3, 93.7, 81.9, 65.5, 64.3, 53.7, 52.4, 31.8, 25.8, 24.5, 15.2, 14.9.

**HRMS (ESI/TOF, *m/z*):** Exact mass calculated for $[C_{33}H_{38}N_2O_8+H]^+$ requires 591.2706; found 591.2720.



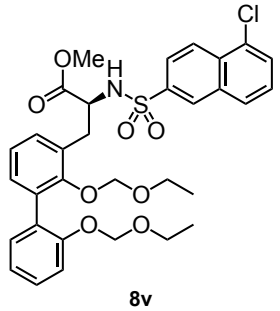
**8u**

**Methyl (*S*)-3-(2,2'-bis(ethoxymethoxy)-[1,1'-biphenyl]-3-yl)-2-(cyclopropanesulfonamido)propanoate (8u)** was synthesized following General Procedure 2a from **7** using **Acid U**. Crude material purified by normal-phase column chromatography using EtOAc/Hx(0-20%) to give **8u** as a colorless oil (57% yield).

**$^1$H NMR (500 MHz, $CDCl_3$)** δ 7.32 (td, *J* = 7.8, 7.2, 1.7 Hz, 1H), 7.28 – 7.22 (m, 3H), 7.20 (dd, *J* = 7.6, 1.8 Hz, 1H), 7.12 (t, *J* = 7.5 Hz, 1H), 7.05 (td, *J* = 7.4, 1.2 Hz, 1H), 5.67 (brs, 1H), 5.18 (s, 2H), 4.61 – 4.53 (m, 2H), 4.45 – 4.34 (m, 1H), 3.78 (s, 3H), 3.66 – 3.56 (m, 3H), 3.53 – 3.47 (m, 1H), 3.23 – 3.12 (m, 2H), 2.05 (tt, *J* = 8.0, 4.8 Hz, 1H), 1.15 (dt, *J* = 17.4, 7.0 Hz, 6H), 1.06 – 0.98 (m, 1H), 0.97 – 0.89 (m, 1H), 0.77 – 0.62 (m, 2H).

**$^{13}$C NMR (126 MHz, $CDCl_3$)** δ 172.6, 154.8, 154.7, 132.3, 131.32, 131.29, 130.3, 129.6, 129.1, 128.4, 124.0, 121.7, 115.2, 98.0, 93.4, 65.4, 64.1, 57.2, 52.5, 33.8, 30.5, 15.1, 14.9, 5.4, 5.0.

**HRMS (ESI/TOF, *m/z*):** calc'd for $[C_{25}H_{33}NO_8S+Na]^+$ requires 530.1825; found 530.1827.



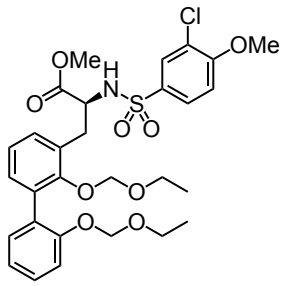

**8v**

**Methyl(*S*)-3-(2,2'-bis(ethoxymethoxy)-[1,1'-biphenyl]-3-yl)-2-((5-chloronaphthalene)-2-sulfonamido)propanoate (8v)** was synthesized following General Procedure 1b from **7** using **Acid V**. Crude material purified by normal-phase column chromatography using EtOAc/Hx(0-20%) to give **8v** as a yellowish oil (66% yield).

**$^1$H NMR (500 MHz, $CDCl_3$)** δ 8.23 (s, 1H), 8.11 (d, *J* = 9.0 Hz, 1H), 7.73 (d, *J* = 8.3 Hz, 1H), 7.63 (m, 2H), 7.41 (t, *J* = 7.9 Hz, 1H), 7.33 – 7.23 (m, 2H), 7.09 (m, 2H), 7.01 (m, 1H), 6.84 (brs, 1H), 6.71 (t, *J* = 7.5 Hz, 1H), 6.55 (d, *J* = 8.4 Hz, 1H), 5.20 (s, 2H), 4.60 – 4.48 (m, 2H), 4.21 (brs, 1H), 3.64 – 3.51 (m, 7H), 3.22 (dd, *J* = 13.7, 10.7 Hz, 1H), 3.00 (dd, *J* = 13.9, 4.7 Hz, 1H), 1.14 (q, *J* = 7.5 Hz, 6H).

**$^{13}$C NMR (126 MHz, $CDCl_3$)** δ 172.0, 154.7, 154.5, 137.8, 133.0, 132.0, 131.72, 131.70, 131.2, 131.1, 129.4, 129.0, 128.7, 128.6, 128.3, 128.1 (brs, 2C), 127.1, 125.7, 124.0, 123.1, 121.5, 115.0, 98.0, 93.3, 65.5, 64.0, 57.1, 52.3, 32.7, 15.0, 14.8.

**HRMS (ESI/TOF, *m/z*):** Exact mass calculated for $[C_{32}H_{34}ClNO_8+Na]^+$ requires 650.1591; found 650.1597.



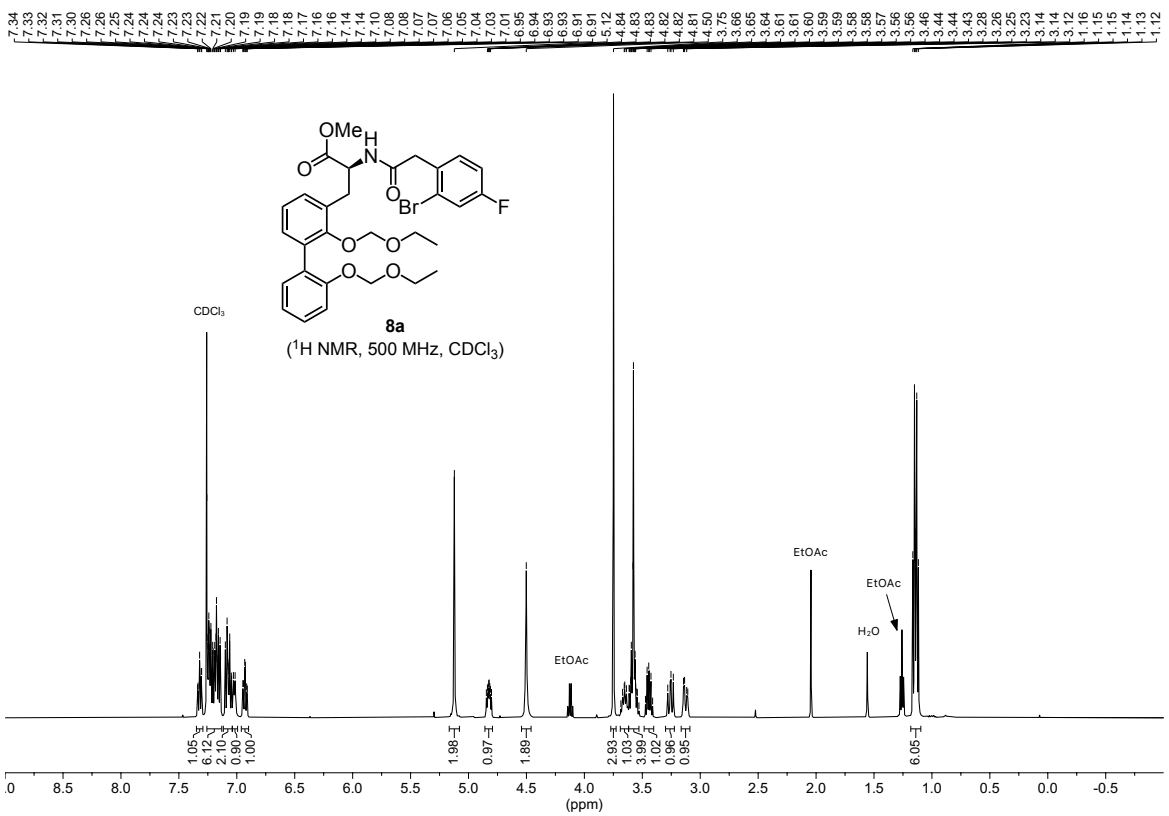

**8w**

**Methyl (*S*)-3-(2,2'-bis(ethoxymethoxy)-[1,1'-biphenyl]-3-yl)-2-((3-chloro-4-methoxyphenyl)sulfonamido)propanoate (8w)** was synthesized following General Procedure 1b from **7** using **Acid W**. Crude material purified by normal-phase column chromatography using EtOAc/Hx(0-20%) to give **8w** as a yellowish oil (97% yield).

**$^1$H NMR (500 MHz, $CDCl_3$)** δ 7.60 (d, *J* = 2.3 Hz, 1H), 7.49 (brd, *J* = 8.7 Hz, 1H), 7.35 – 7.25 (m, 2H), 7.21 – 7.15 (m, 2H), 7.04 (td, *J* = 7.3, 1.4 Hz, 1H), 6.97 (m, 2H), 6.79 (brd, *J* = 8.7 Hz, 1H), 6.15 (d, *J* = 8.5 Hz, 1H), 5.19 (brs, 2H), 4.58 – 4.47 (m, 2H), 4.14 – 4.06 (m, 1H), 3.88 (s, 3H), 3.71 – 3.47 (m, 7H), 3.20 (dd, *J* = 13.6, 10.5 Hz, 1H), 2.97 (dd, *J* = 13.7, 4.8 Hz, 1H), 1.14 (dt, *J* = 9.8, 7.0 Hz, 6H).

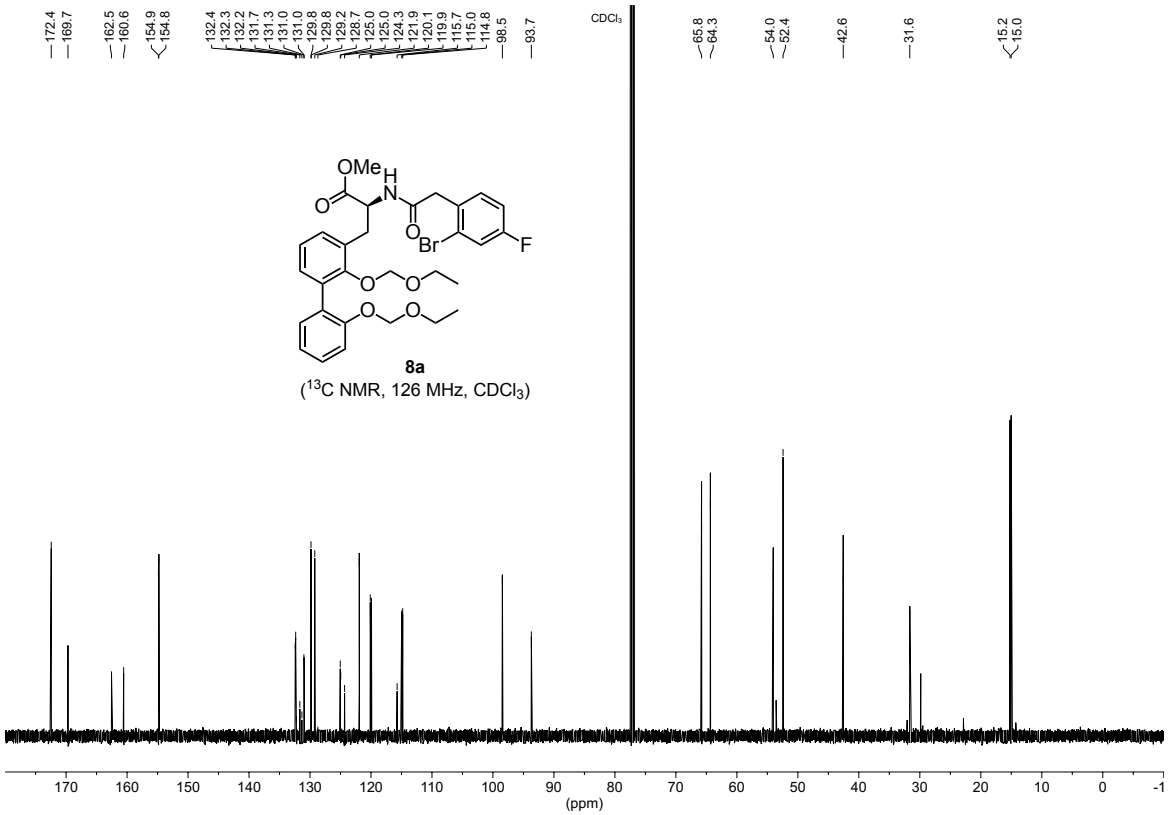
**$^{13}$C NMR (126 MHz, $CDCl_3$)** δ 172.1, 158.0, 154.9, 154.6, 132.3 (brs, 2C), 131.4 (brs, 2C), 129.6, 129.2, 129.0, 128.8, 128.4, 127.4, 124.1, 122.9, 121.7, 115.3, 111.4, 98.2, 93.5, 65.6, 64.2, 57.1, 56.5, 52.5, 32.9, 15.1, 14.9.

**HRMS (ESI/TOF, *m/z*):** Exact mass calculated for $[C_{29}H_{34}ClNO_9S+Na]^+$ requires 630.1540; found 630.1551.



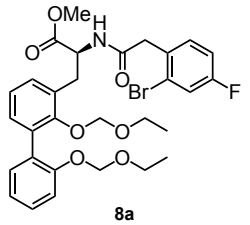

**8a**

($^1$H NMR, 500 MHz, $CDCl_3$)




**8a**

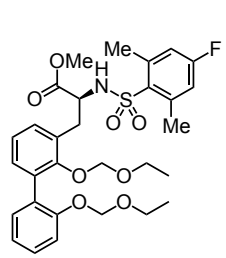
($^{13}$C NMR, 126 MHz, $CDCl_3$)



**8a**

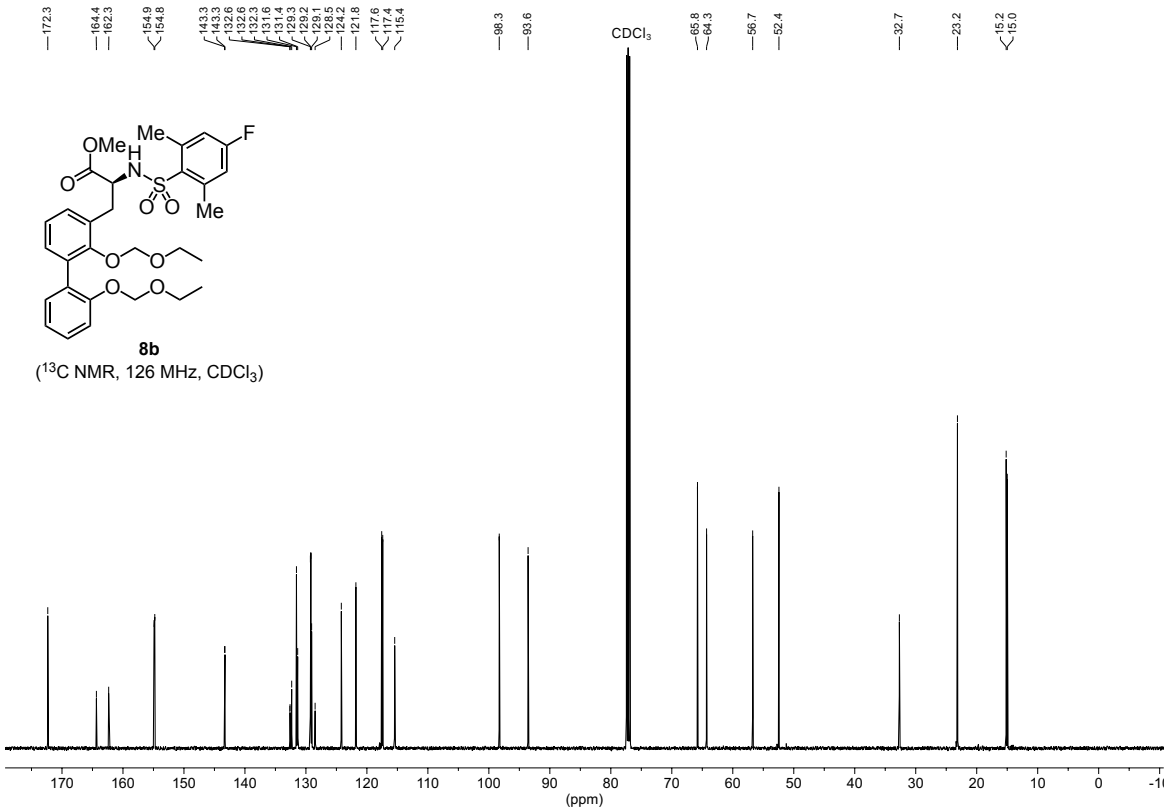
($^{19}$F NMR, 471 MHz, $CDCl_3$)



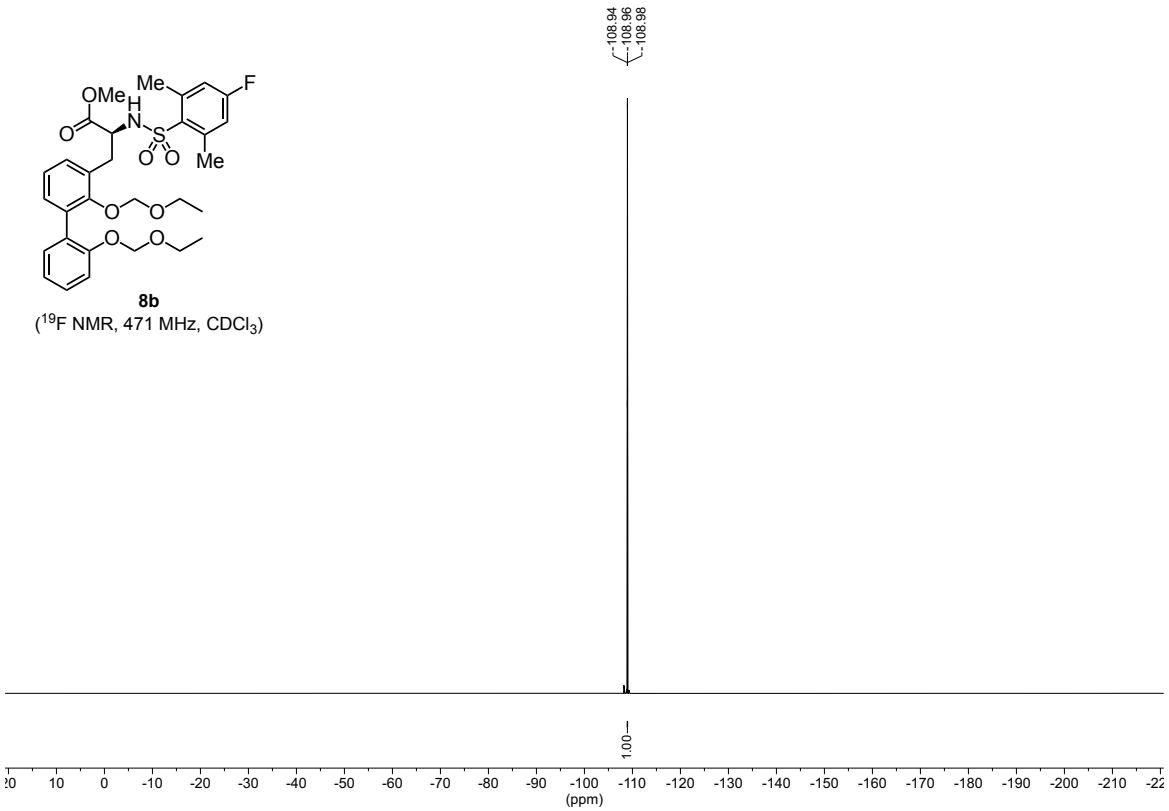
**8b**

($^{1}$H NMR, 500 MHz, $CDCl_3$)



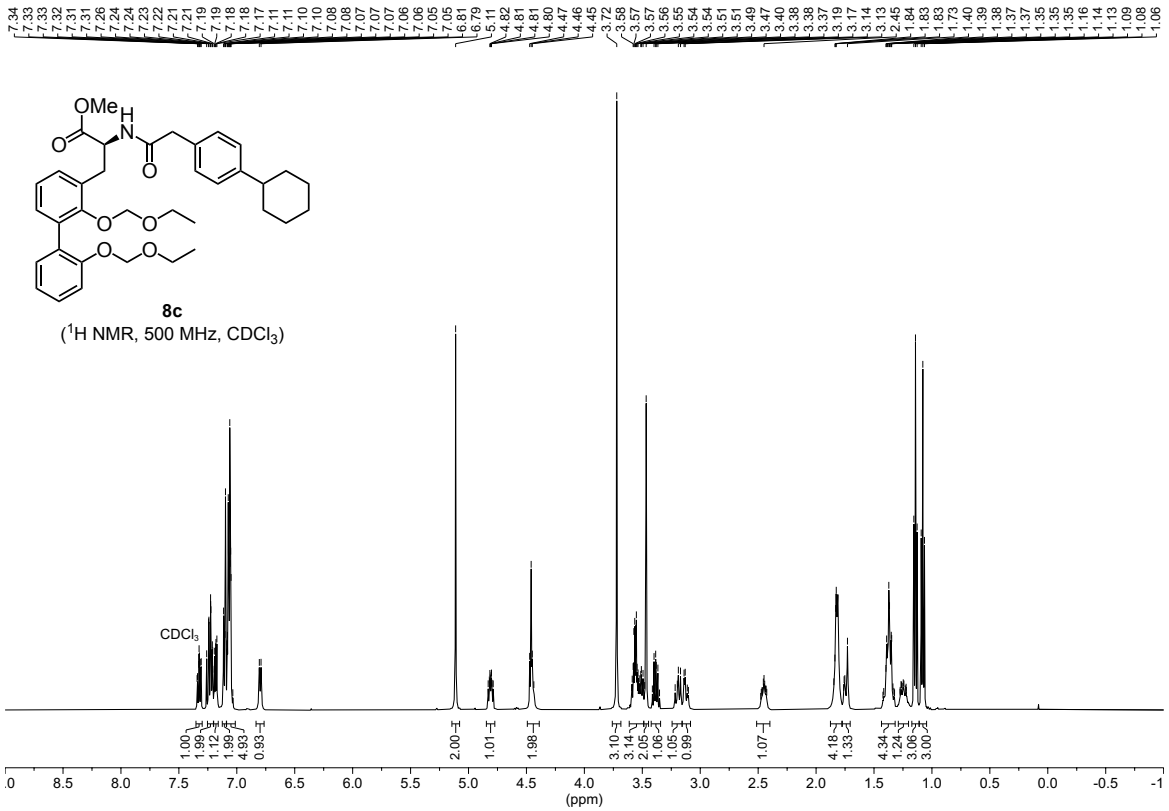

**8b**

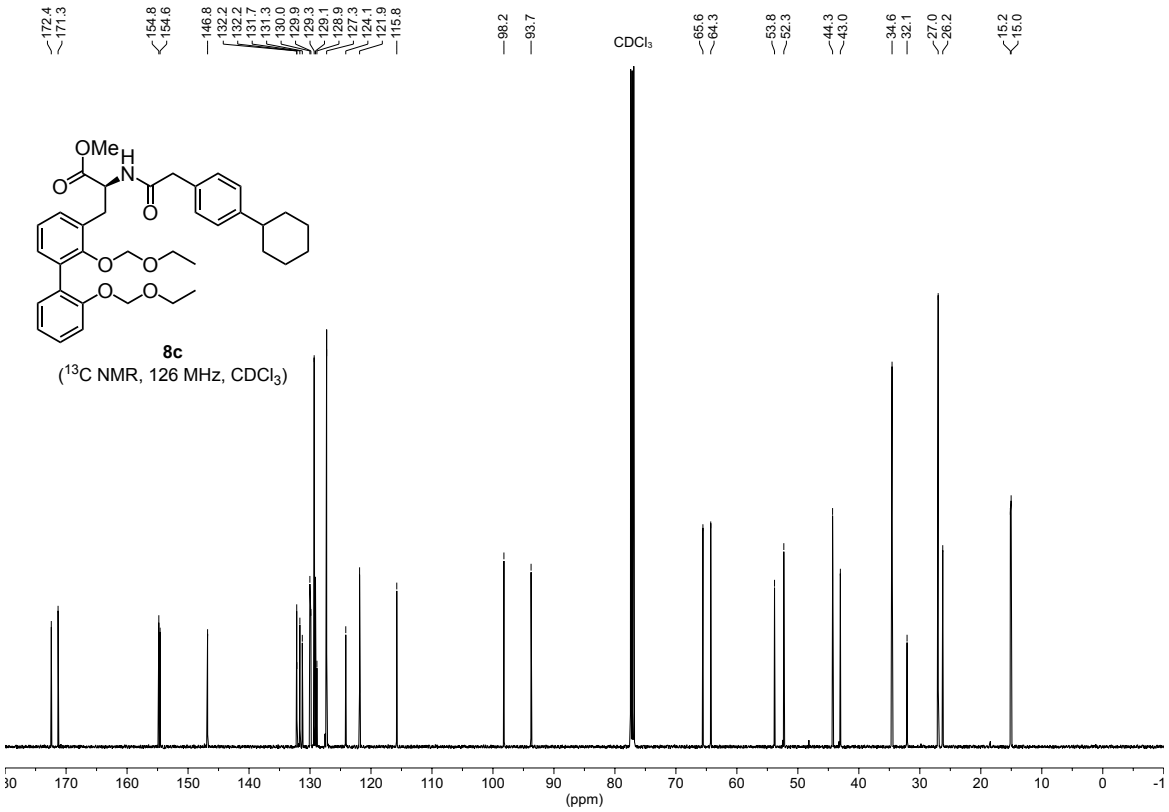
($^{13}$C NMR, 126 MHz, $CDCl_3$)

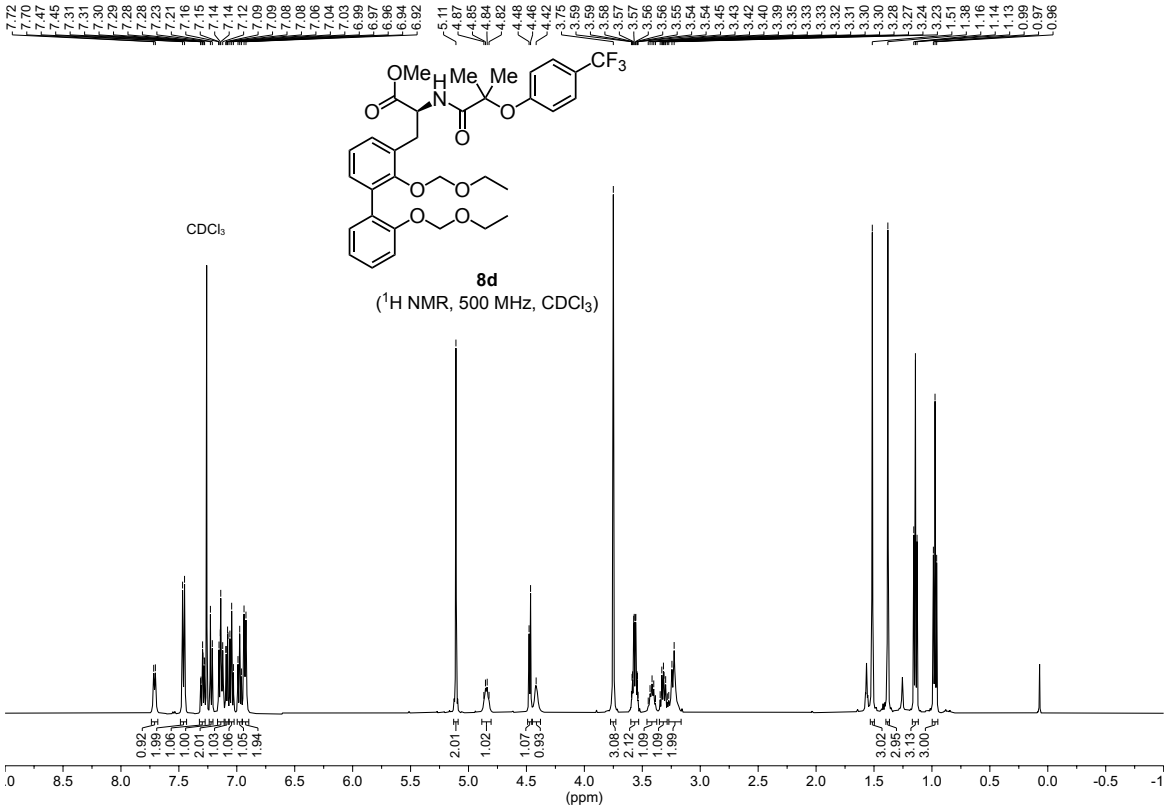



**8b**

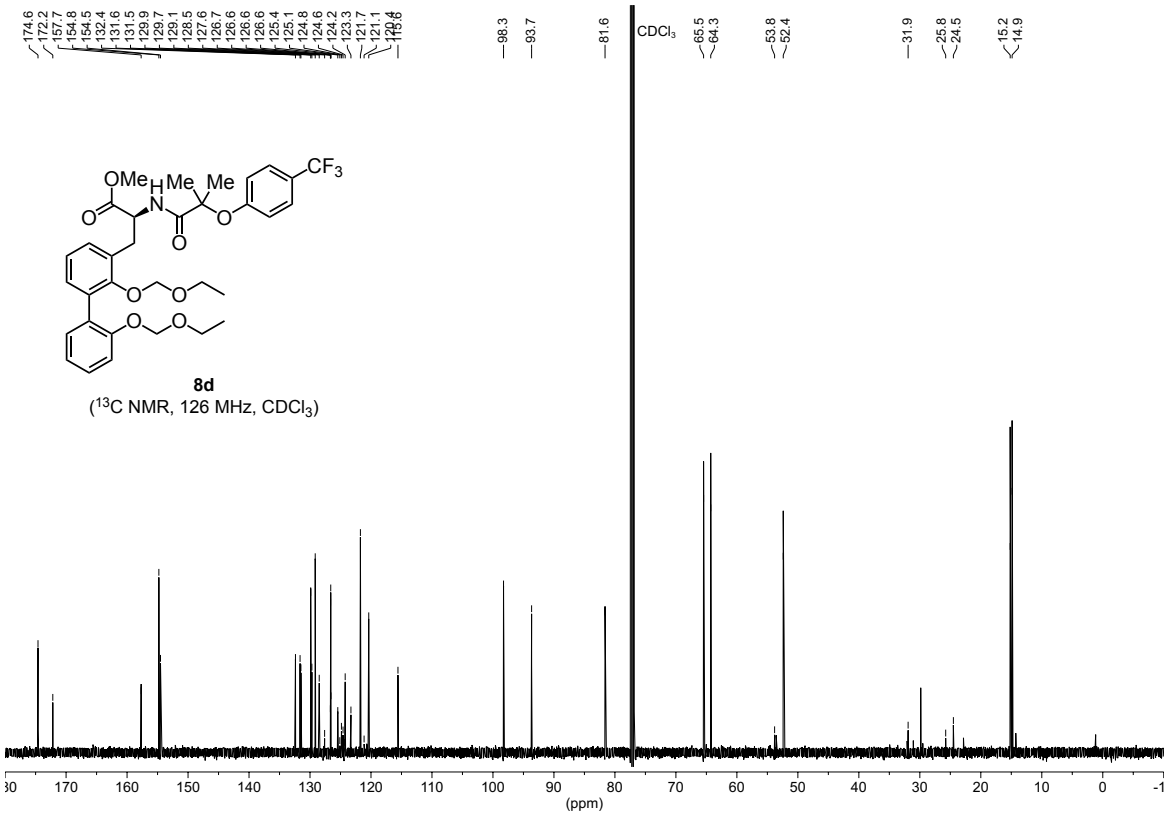
($^{19}$F NMR, 471 MHz, $CDCl_3$)


OMe
H
N
O
O
O
O
O
O
8c
(1H NMR, 500 MHz, CDCl3)
CDCl3
(ppm)

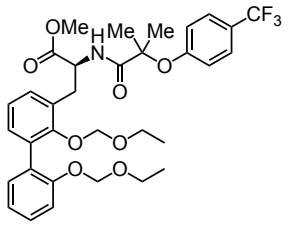

OMe
H
N
O
O
O
O
O
O
8c
(13C NMR, 126 MHz, CDCl3)
CDCl3
(ppm)




**8d**
($^1$H NMR, 500 MHz, $CDCl_3$)

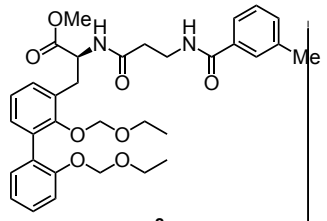



**8d**
($^{13}$C NMR, 126 MHz, $CDCl_3$)

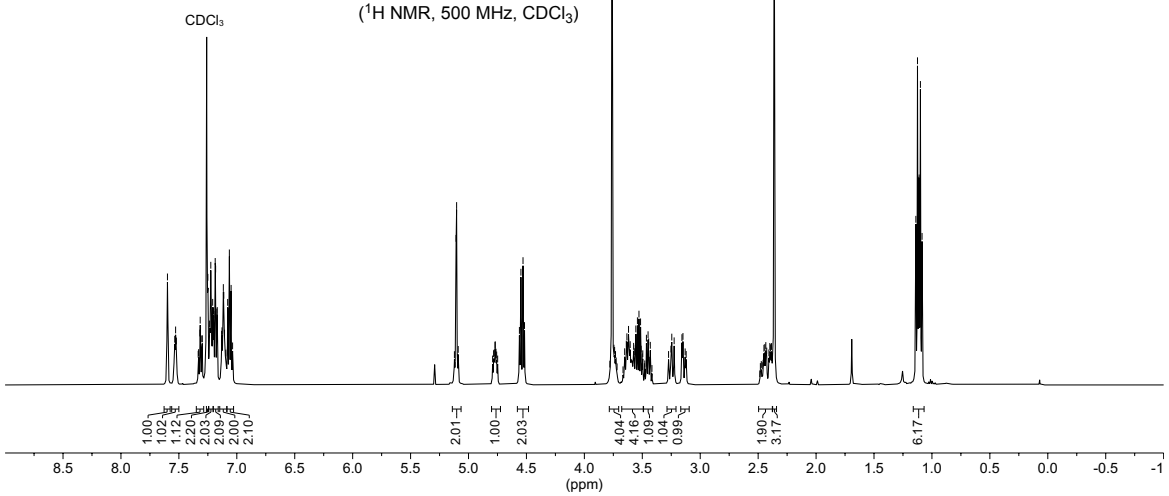


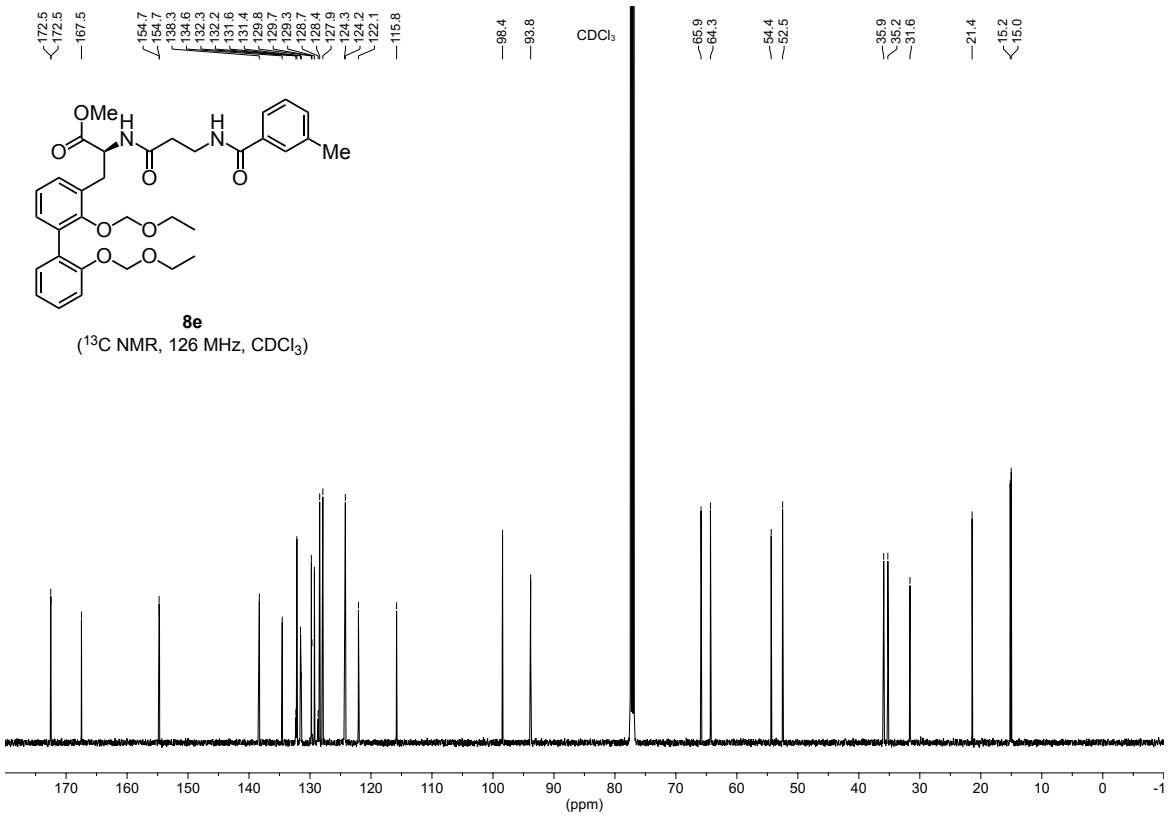
**8d**
($^{19}$F NMR, 471 MHz, $CDCl_3$)



**8e**
($^1$H NMR, 500 MHz, $CDCl_3$)

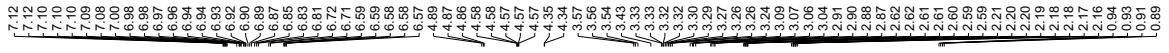


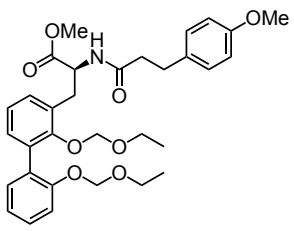



**8e**

($^{13}$C NMR, 126 MHz, $CDCl_3$)

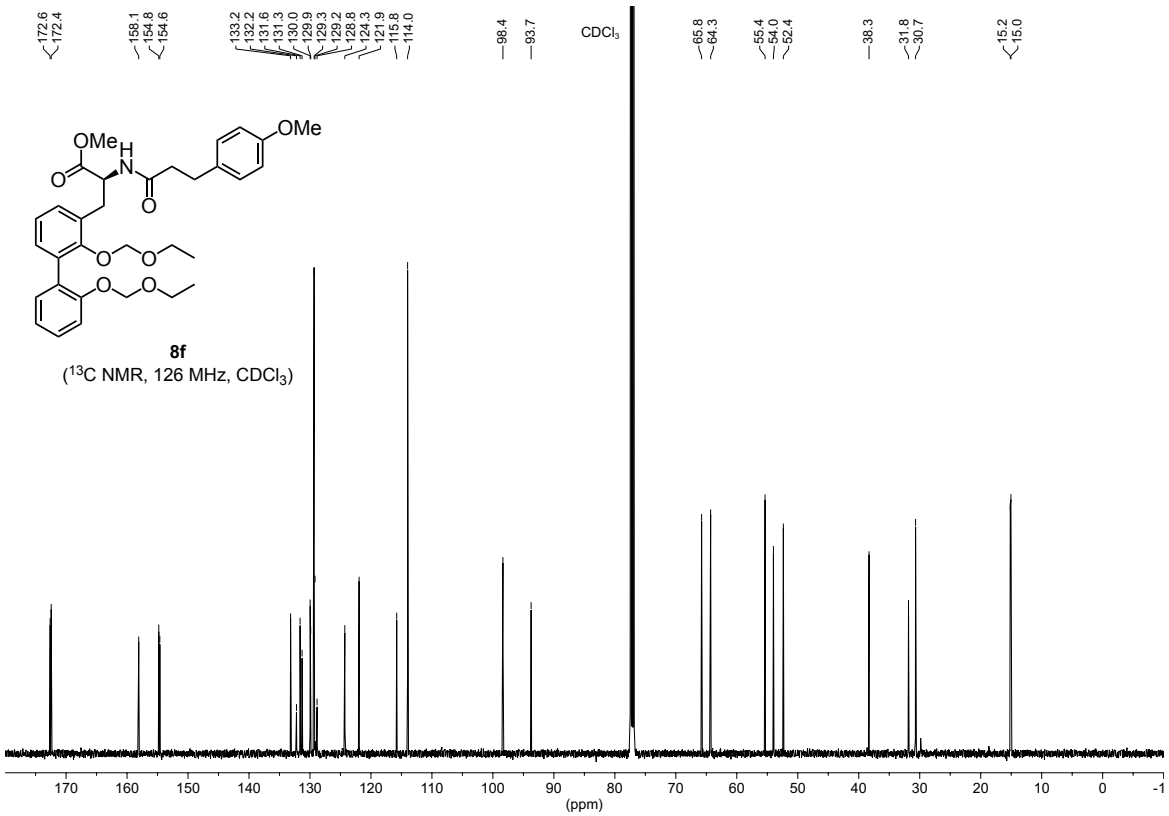


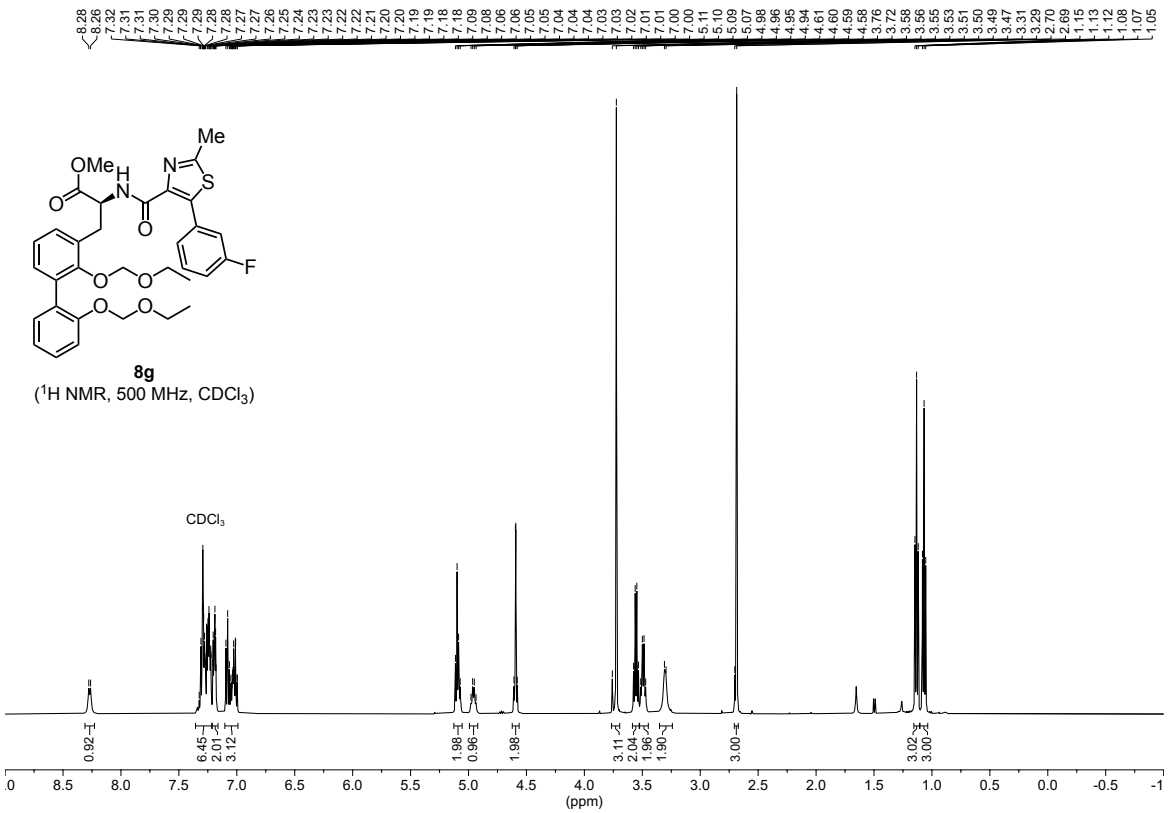



**8f**

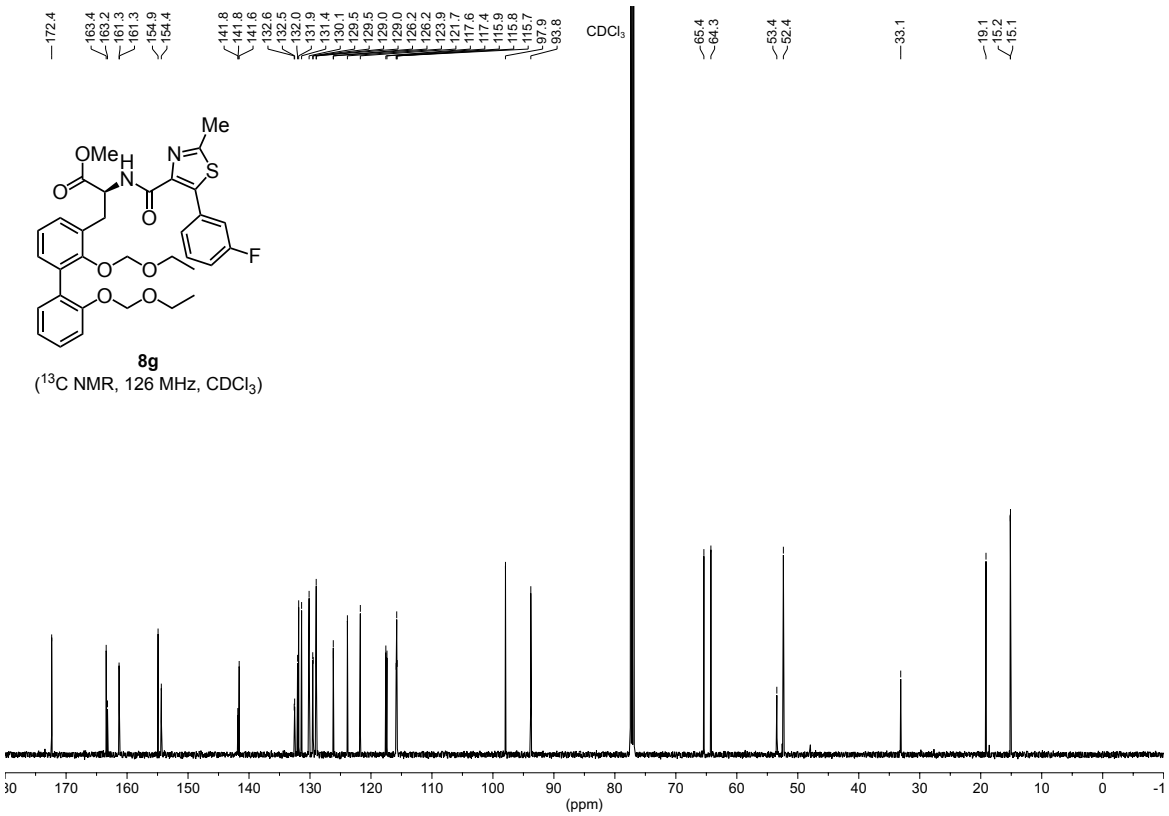
($^{1}$H NMR, 500 MHz, $CDCl_3$)




**8f**
($^{13}$C NMR, 126 MHz, $CDCl_3$)

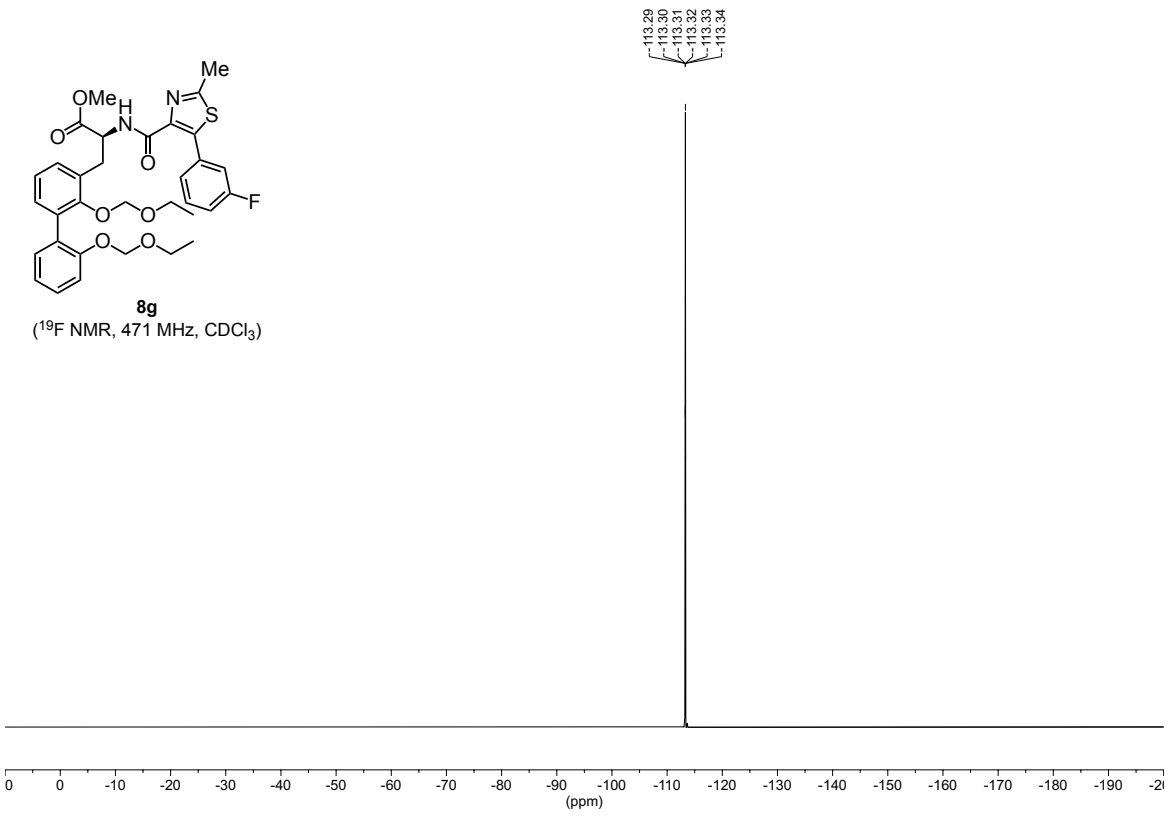



**8g**
($^{1}$H NMR, 500 MHz, $CDCl_3$)



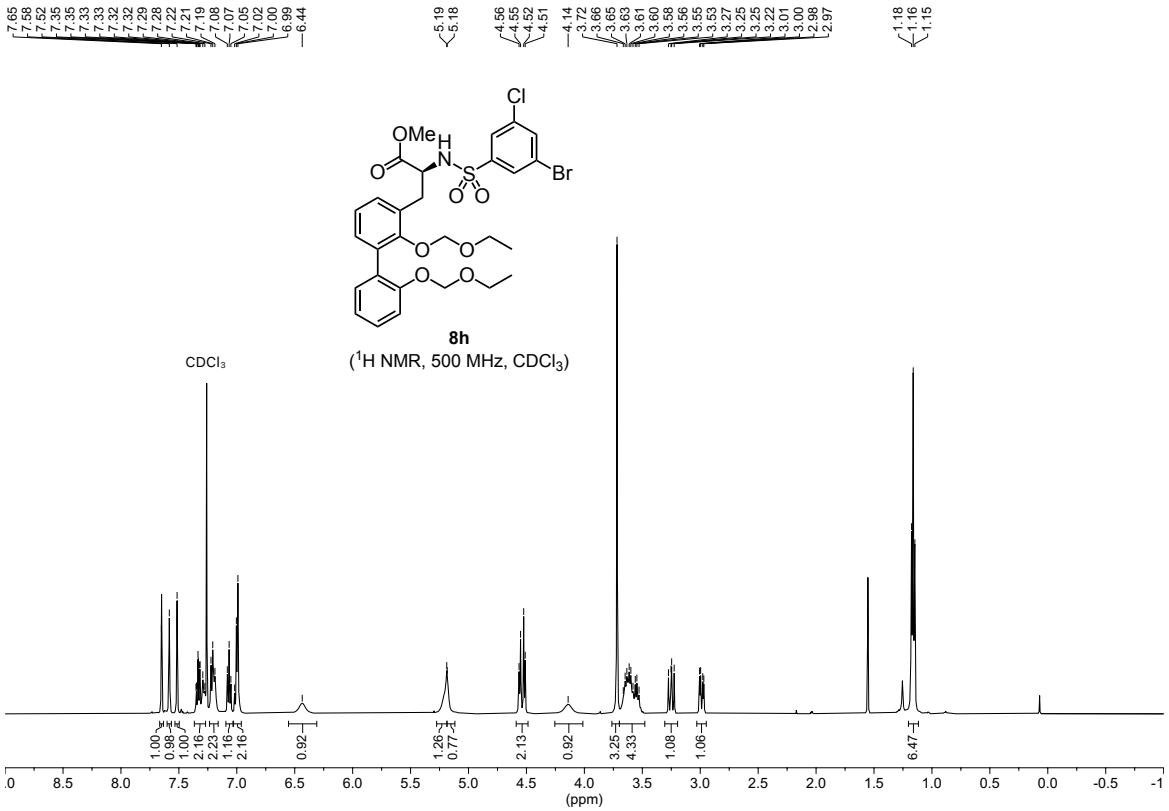

**8g**

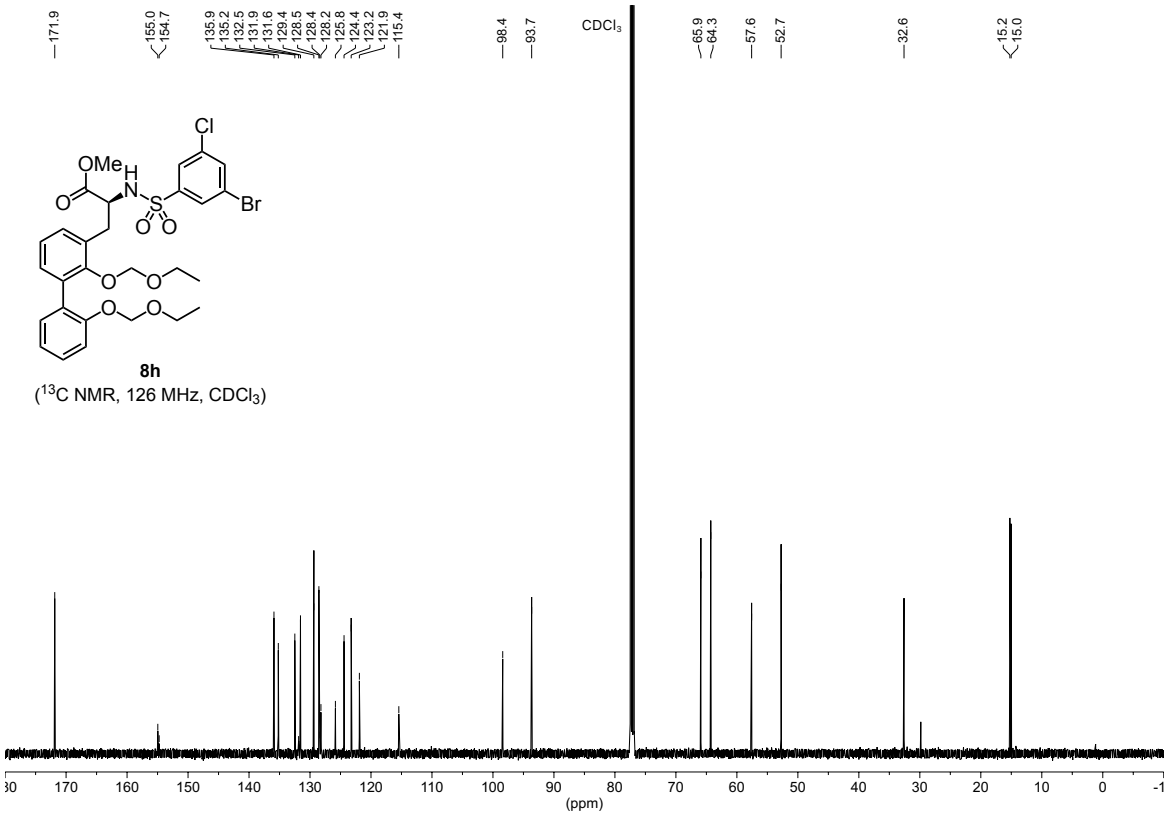
($^{13}$C NMR, 126 MHz, $CDCl_3$)

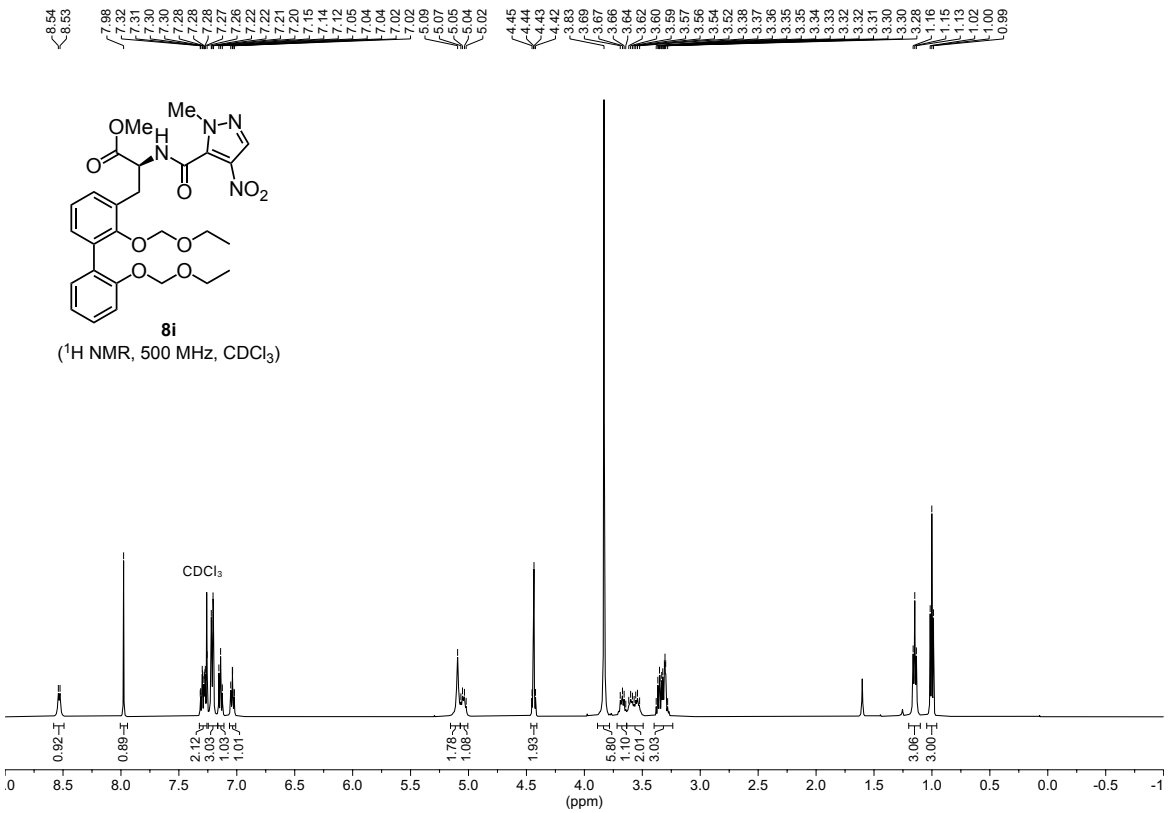


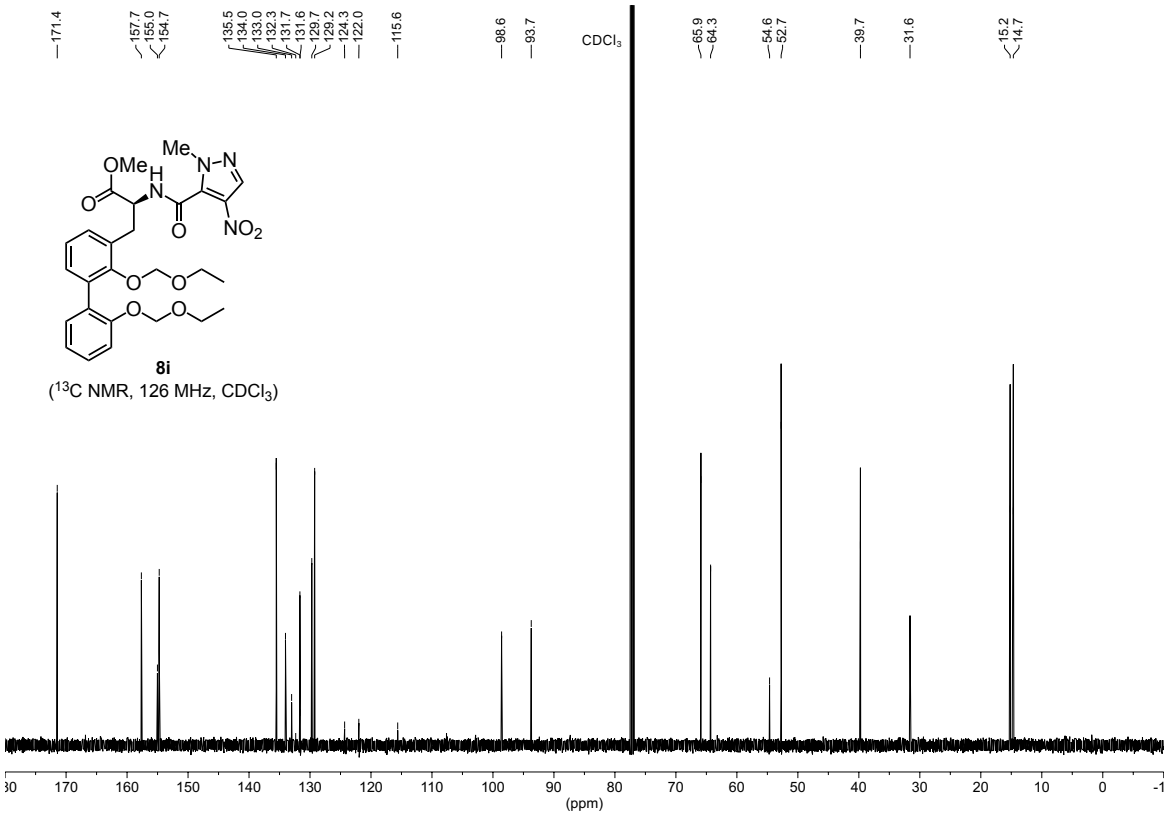

**8g**

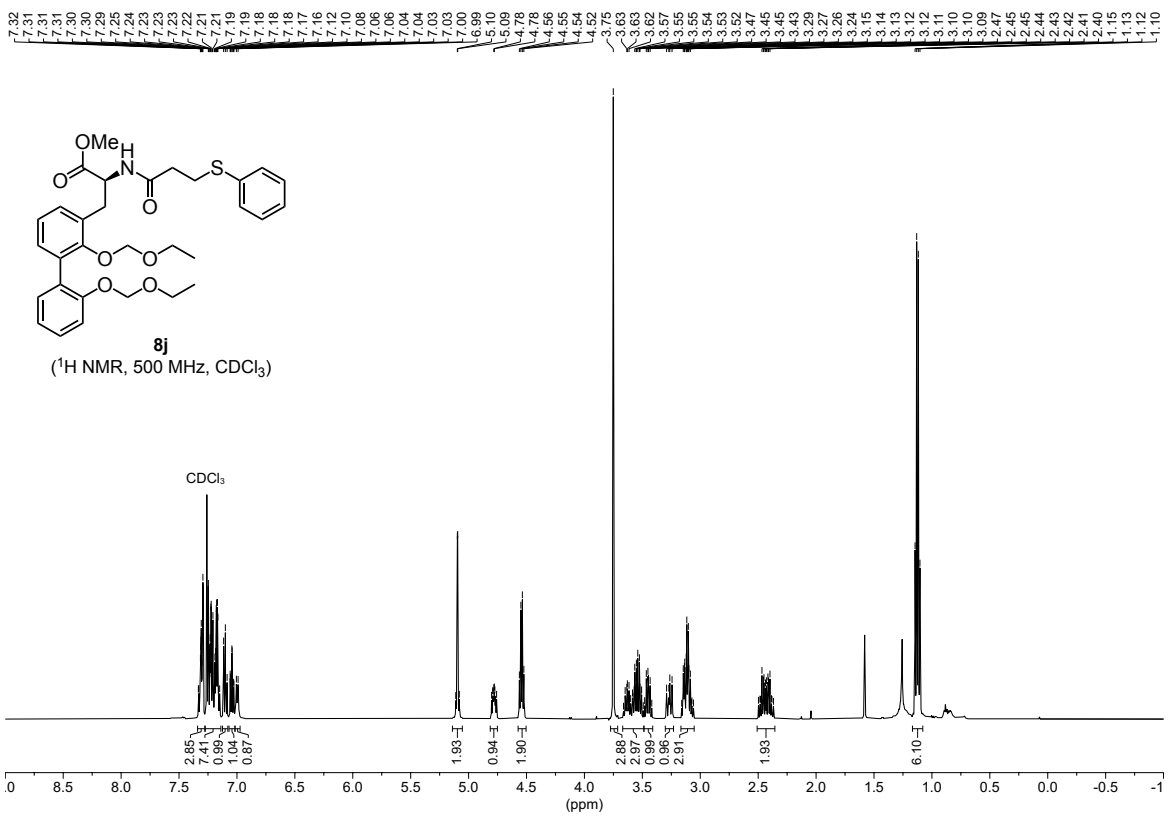
($^{19}$F NMR, 471 MHz, $CDCl_3$)


7.65
7.58
7.52
7.35
7.35
7.33
7.33
7.32
7.32
7.29
7.28
7.22
7.21
7.19
7.08
7.07
7.05
7.02
7.00
6.99
6.44
5.19
5.18
4.56
4.55
4.52
4.51
4.14
3.72
3.66
3.65
3.63
3.61
3.60
3.58
3.56
3.55
3.53
3.27
3.25
3.22
3.01
3.00
2.98
2.97
1.18
1.16
1.15
Cl
OMe
H
N
O
S
O
O
Br
O
O
O
O
8h
($^1$H NMR, 500 MHz, $CDCl_3$)
$CDCl_3$
1.00
0.98
1.00
2.16
2.23
1.16
2.16
0.92
1.26
0.77
2.13
0.92
3.25
4.33
1.08
1.06
6.47
(ppm)

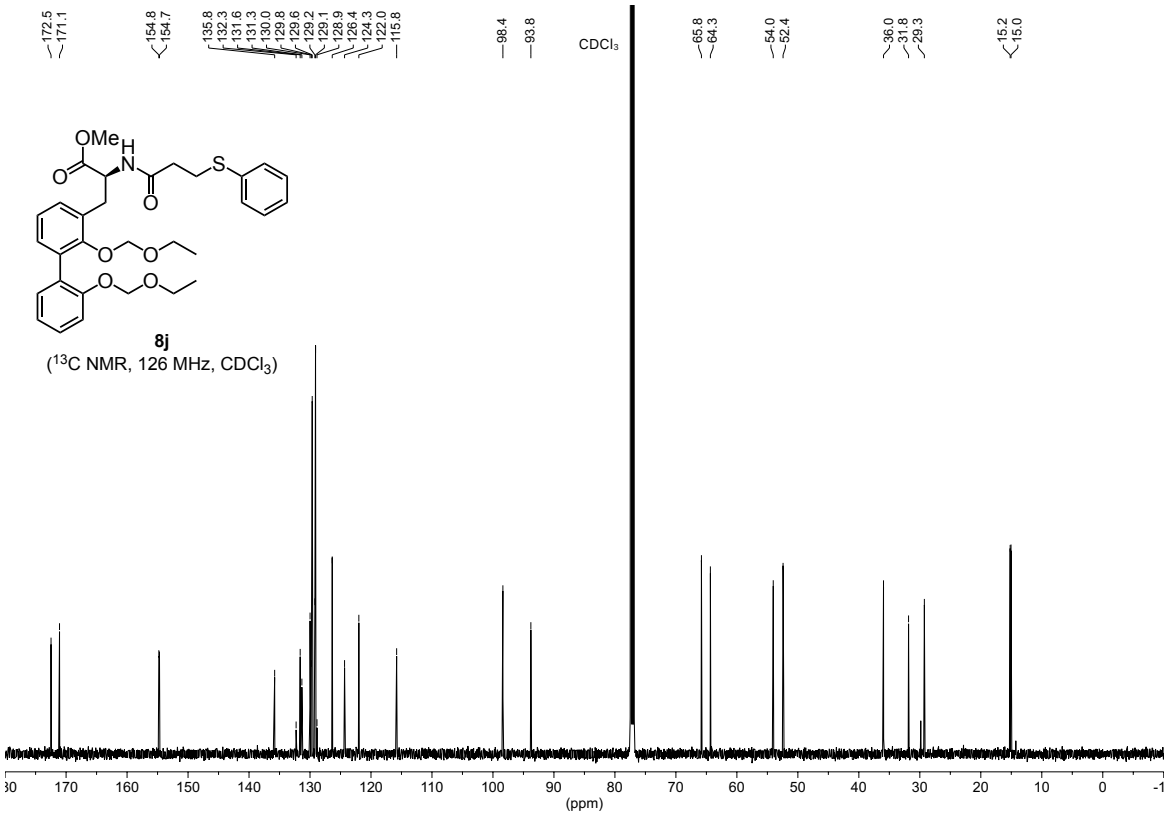

171.9
155.0
154.7
135.9
135.2
132.5
131.9
131.6
129.4
128.5
128.4
128.2
125.8
124.4
123.2
121.9
115.4
98.4
93.7
$CDCl_3$
65.9
64.3
57.6
52.7
32.6
15.2
15.0
Cl
OMe
H
N
O
S
O
O
Br
O
O
O
O
8h
($^{13}$C NMR, 126 MHz, $CDCl_3$)
(ppm)


8.54
8.53
7.98
7.32
7.31
7.30
7.30
7.28
7.28
7.28
7.27
7.26
7.22
7.22
7.21
7.20
7.15
7.14
7.12
7.05
7.04
7.04
7.02
7.02
5.09
5.07
5.05
5.04
5.02
4.45
4.44
4.43
4.42
3.83
3.69
3.67
3.66
3.64
3.62
3.60
3.59
3.57
3.56
3.54
3.52
3.38
3.37
3.36
3.35
3.35
3.34
3.33
3.32
3.32
3.31
3.30
3.30
3.28
1.16
1.15
1.13
1.02
1.00
0.99
Me
N-N
OMe
H
N
O
O
O
NO2
O
O
O
O
8i
(1H NMR, 500 MHz, CDCl3)
CDCl3
0.92
0.89
2.12
3.03
1.03
1.01
1.78
1.08
1.93
5.80
1.10
2.01
3.03
3.06
3.00
(ppm)

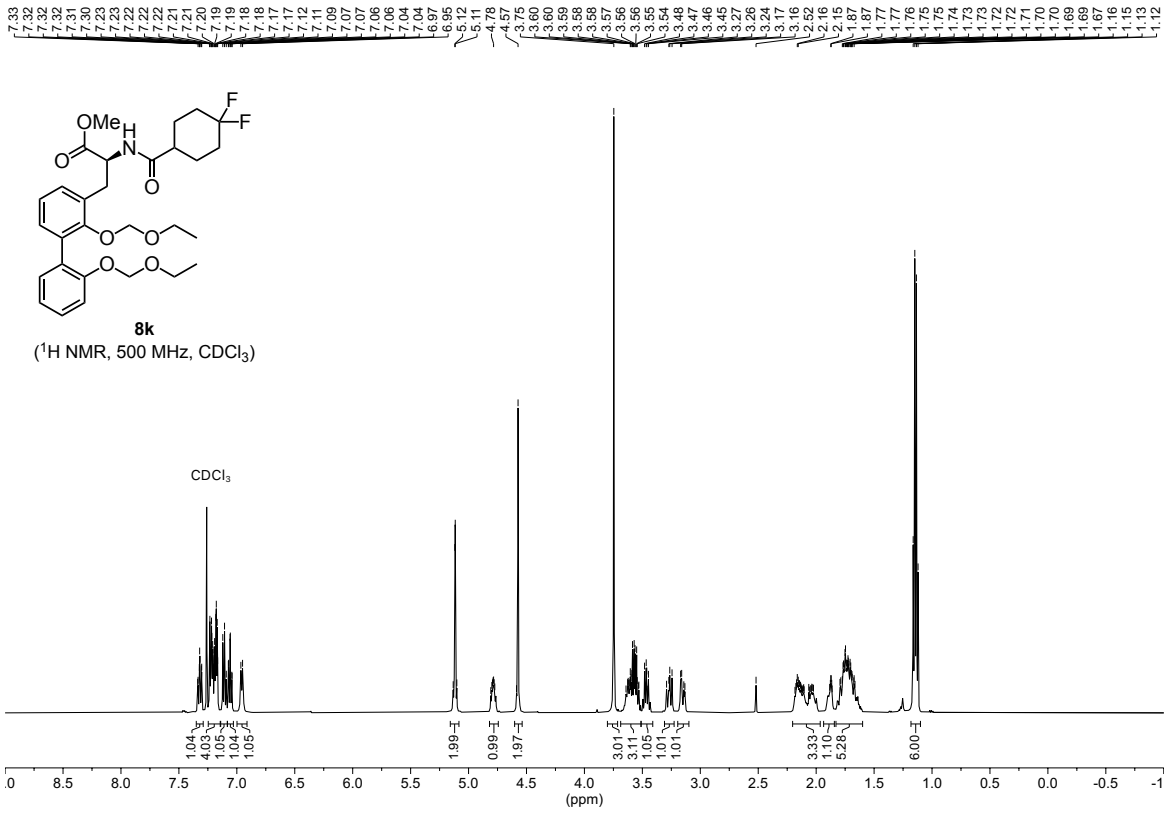

171.4
157.7
155.0
154.7
135.5
134.0
133.0
132.3
131.7
131.6
129.7
129.2
124.3
122.0
115.6
98.6
93.7
CDCl3
65.9
64.3
54.6
52.7
39.7
31.6
15.2
14.7
Me
N-N
OMe
H
N
O
O
O
NO2
O
O
O
O
8i
(13C NMR, 126 MHz, CDCl3)
(ppm)



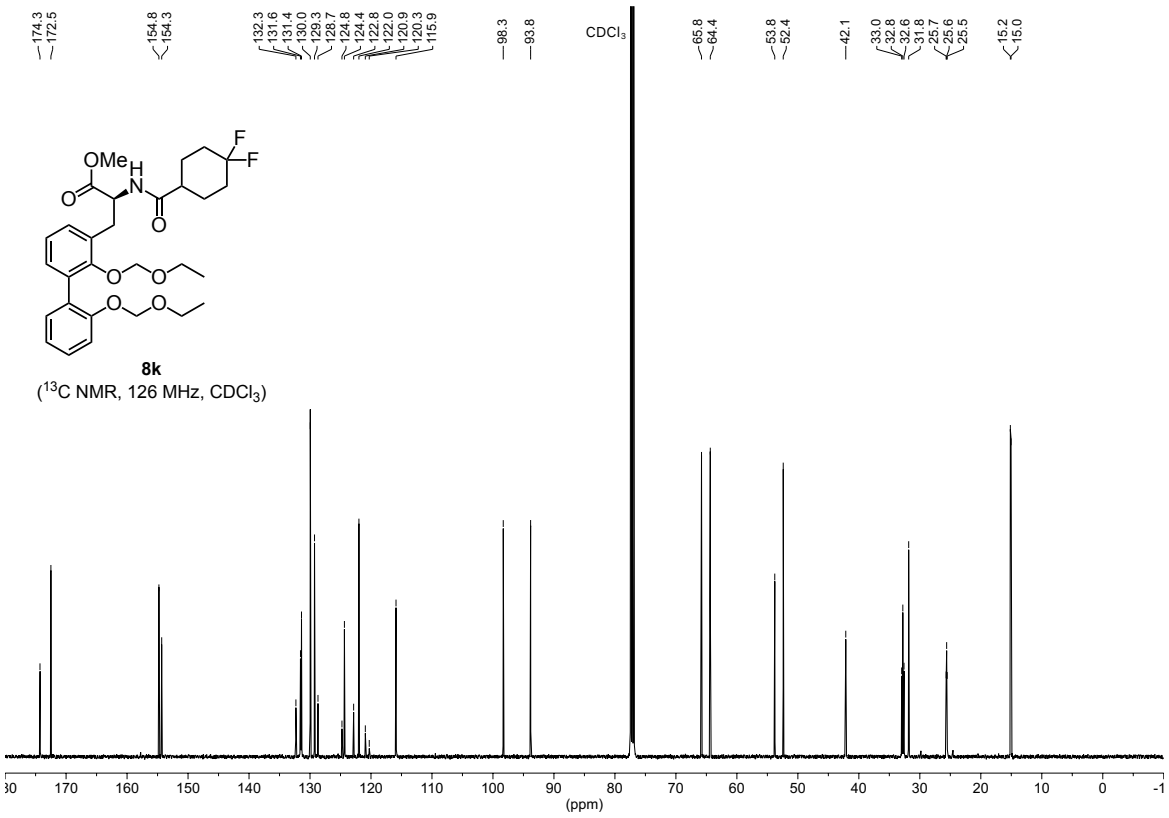

**8j**
($^1$H NMR, 500 MHz, $CDCl_3$)



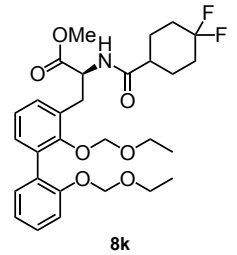

**8j**
($^{13}$C NMR, 126 MHz, $CDCl_3$)




**8k**
($^1$H NMR, 500 MHz, $CDCl_3$)



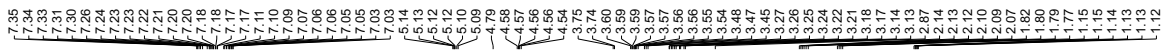

**8k**
($^{13}$C NMR, 126 MHz, $CDCl_3$)

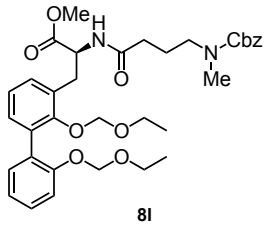


**8k**

($^{19}$F NMR, 471 MHz, $CDCl_3$)

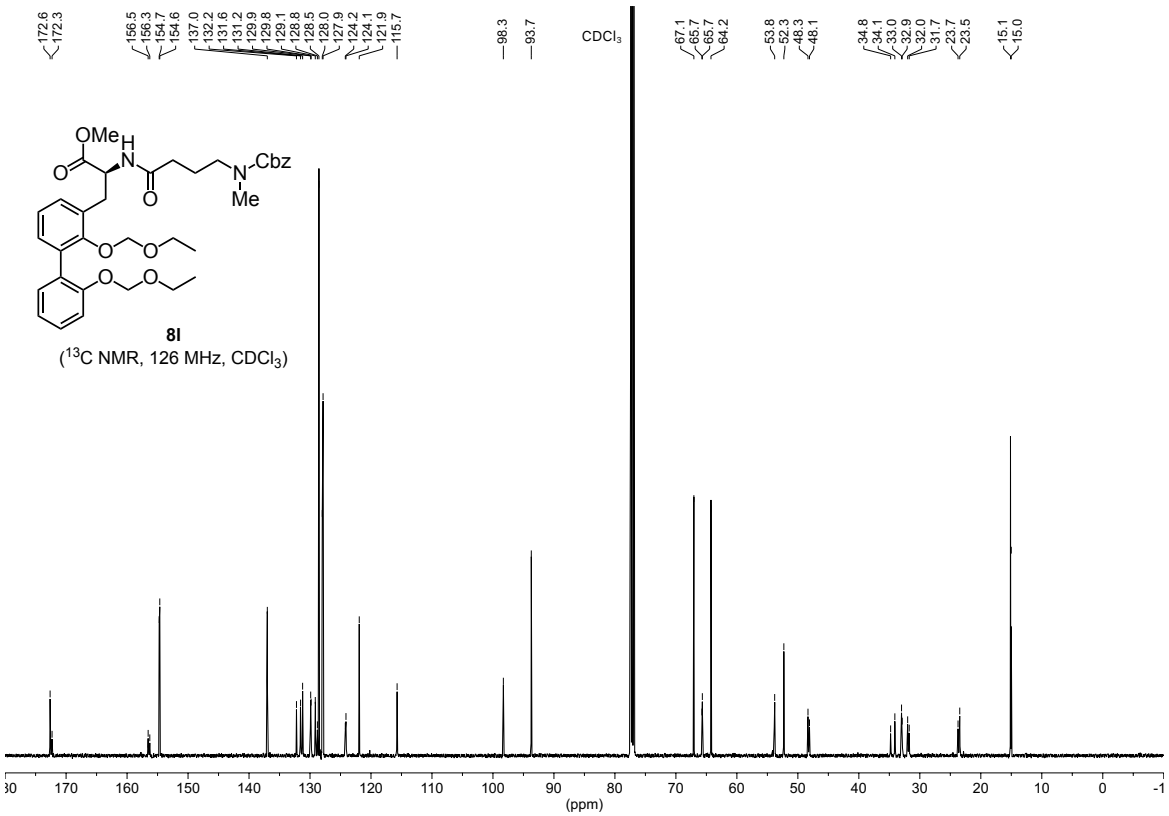


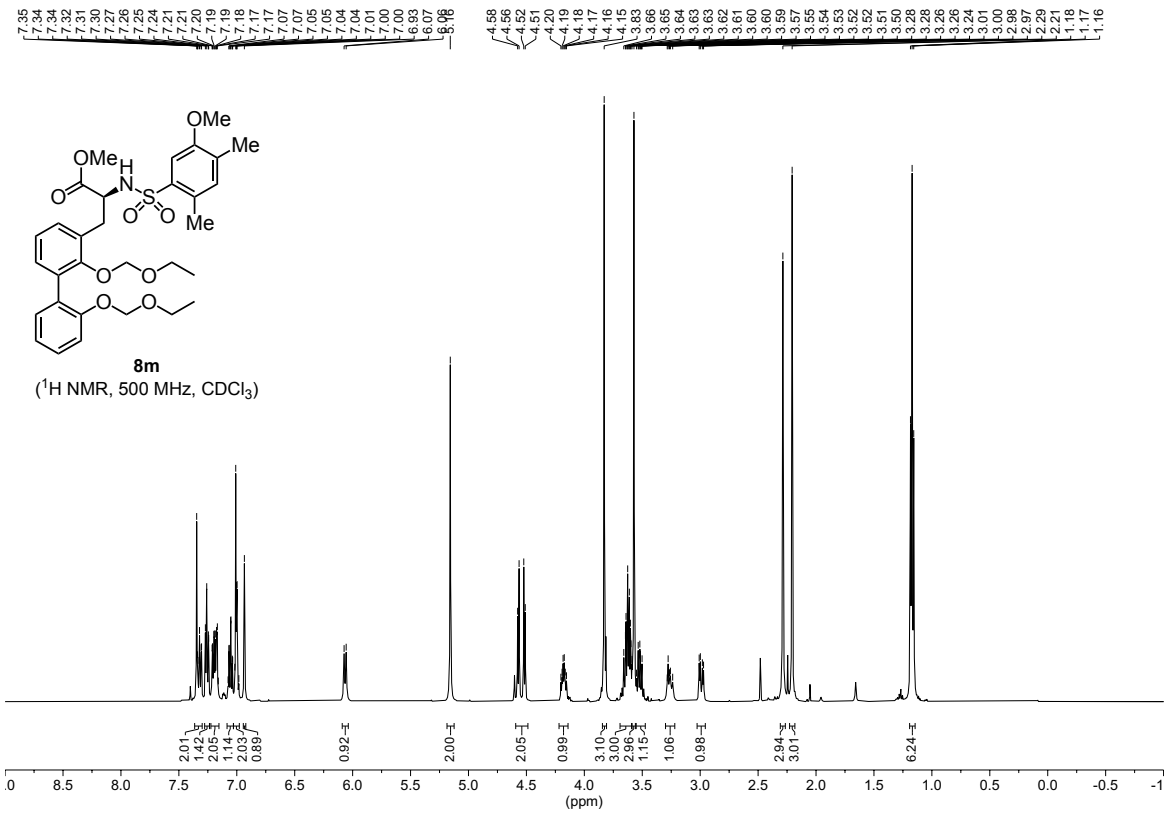



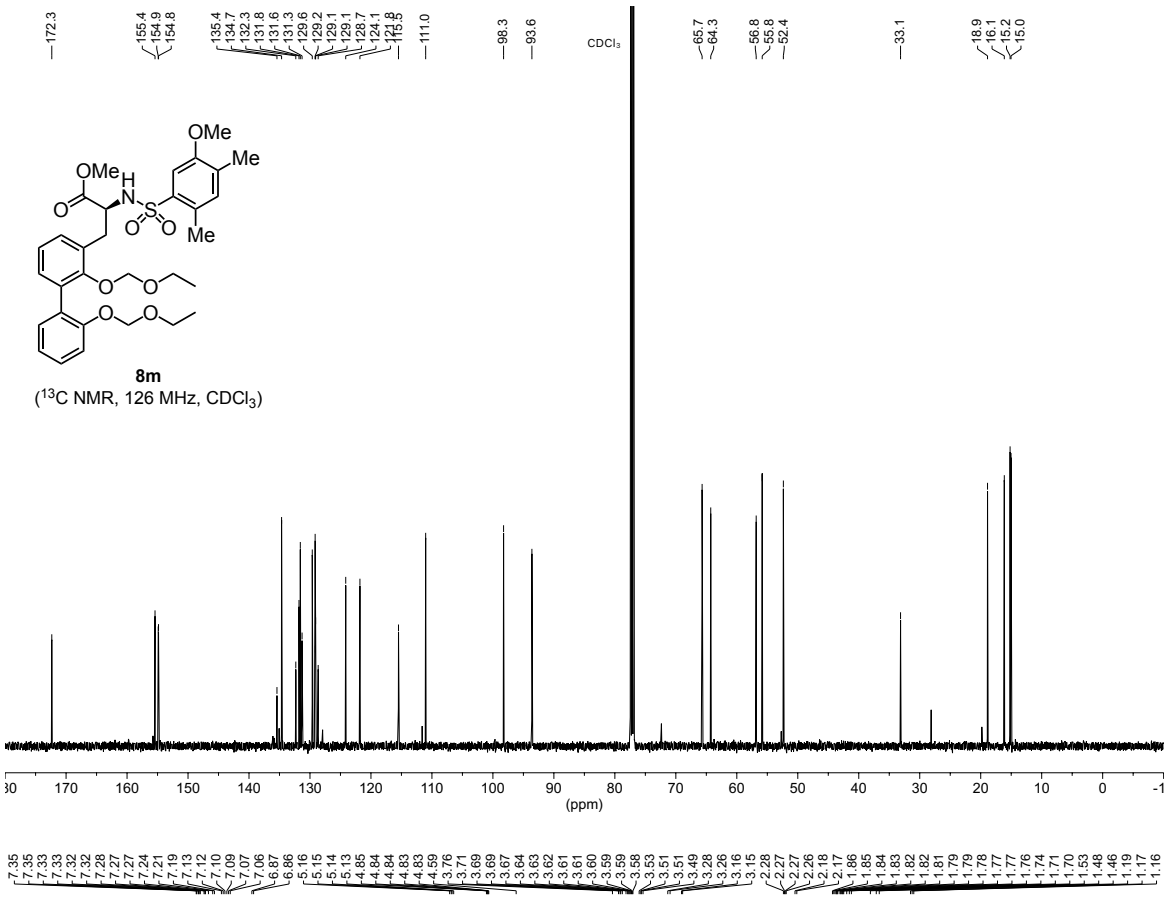


**8l**

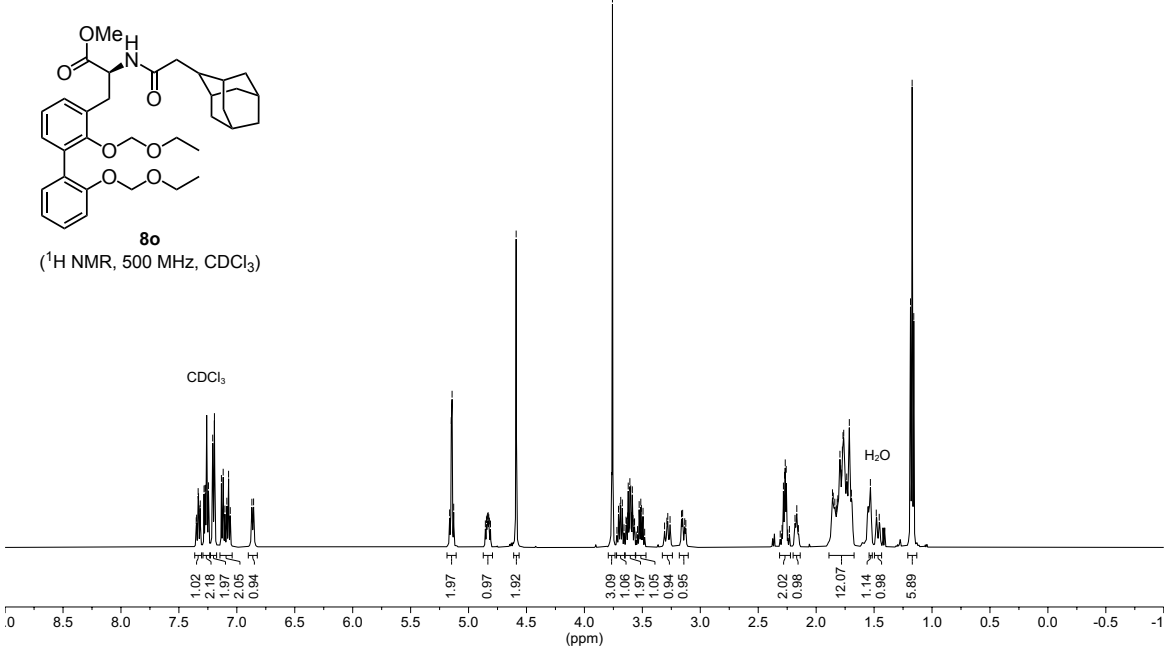
($^{1}$H NMR, 500 MHz, $CDCl_3$)


172.6
172.3
156.5
156.3
154.7
154.6
137.0
132.2
131.6
131.2
129.9
129.8
129.1
128.8
128.5
128.0
127.9
124.2
124.1
121.9
115.7
98.3
93.7
CDCl3
67.1
65.7
65.7
64.2
53.8
52.3
48.3
48.1
34.8
34.1
33.0
32.9
32.0
31.7
23.7
23.5
15.1
15.0
OMe
H
N
O
O
N
Cbz
Me
O
O
O
O
O
O
8l
(13C NMR, 126 MHz, CDCl3)
170
160
150
140
130
120
110
100
90
80
70
60
50
40
30
20
10
0
(ppm)

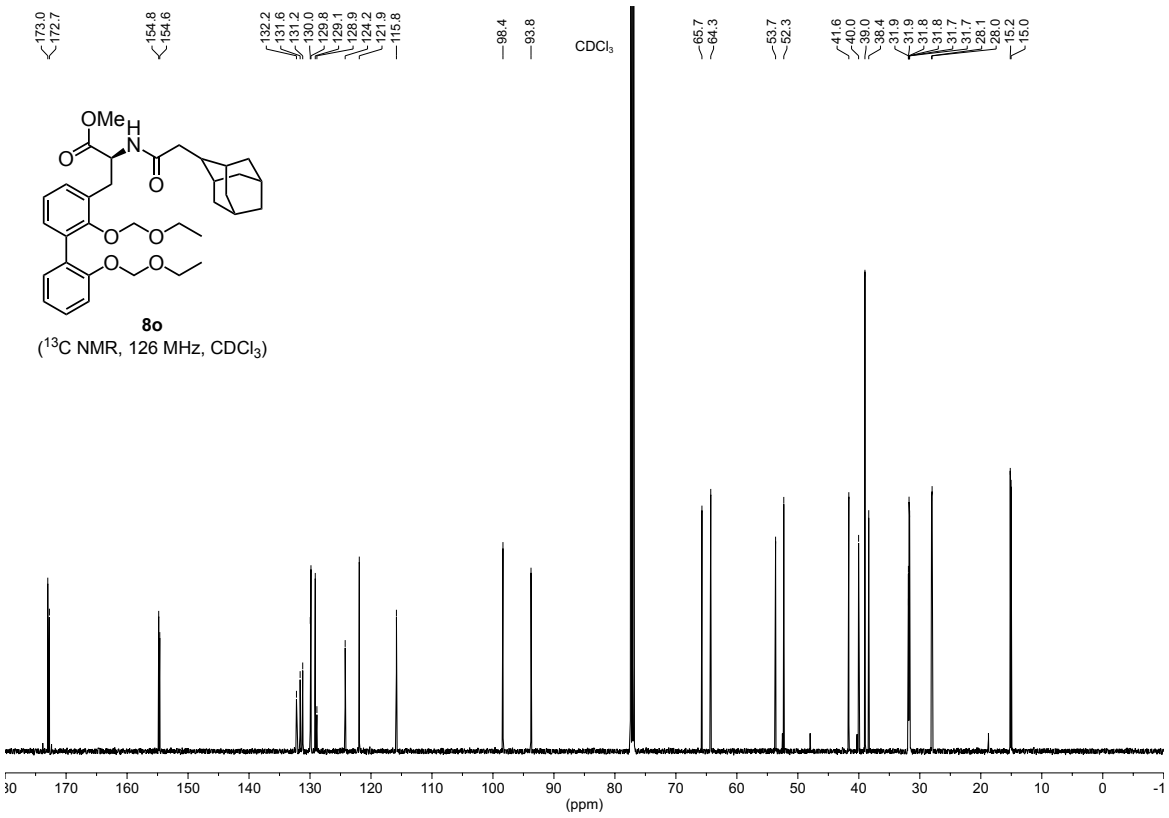

7.35
7.34
7.34
7.32
7.31
7.30
7.27
7.26
7.25
7.24
7.21
7.21
7.20
7.19
7.19
7.18
7.17
7.17
7.07
7.07
7.05
7.05
7.04
7.04
7.01
7.00
7.00
6.93
6.07
4.58
4.56
4.52
4.51
4.20
4.19
4.18
4.17
4.16
4.15
3.83
3.66
3.65
3.64
3.63
3.63
3.62
3.61
3.60
3.60
3.59
3.57
3.55
3.54
3.53
3.52
3.52
3.51
3.50
3.28
3.28
3.26
3.26
3.24
3.01
3.00
2.98
2.97
2.29
2.21
1.18
1.17
1.16
OMe
Me
OMe
H
N
S
O
O
O
Me
O
O
O
O
8m
(1H NMR, 500 MHz, CDCl3)
2.01
1.42
2.05
1.14
2.03
0.89
0.92
2.00
2.05
0.99
3.10
3.00
2.96
1.15
1.06
0.98
2.94
3.01
6.24
8.5
8.0
7.5
7.0
6.5
6.0
5.5
5.0
4.5
4.0
3.5
3.0
2.5
2.0
1.5
1.0
0.5
0.0
-0.5
(ppm)




**8m**
($^{13}$C NMR, 126 MHz, $CDCl_3$)



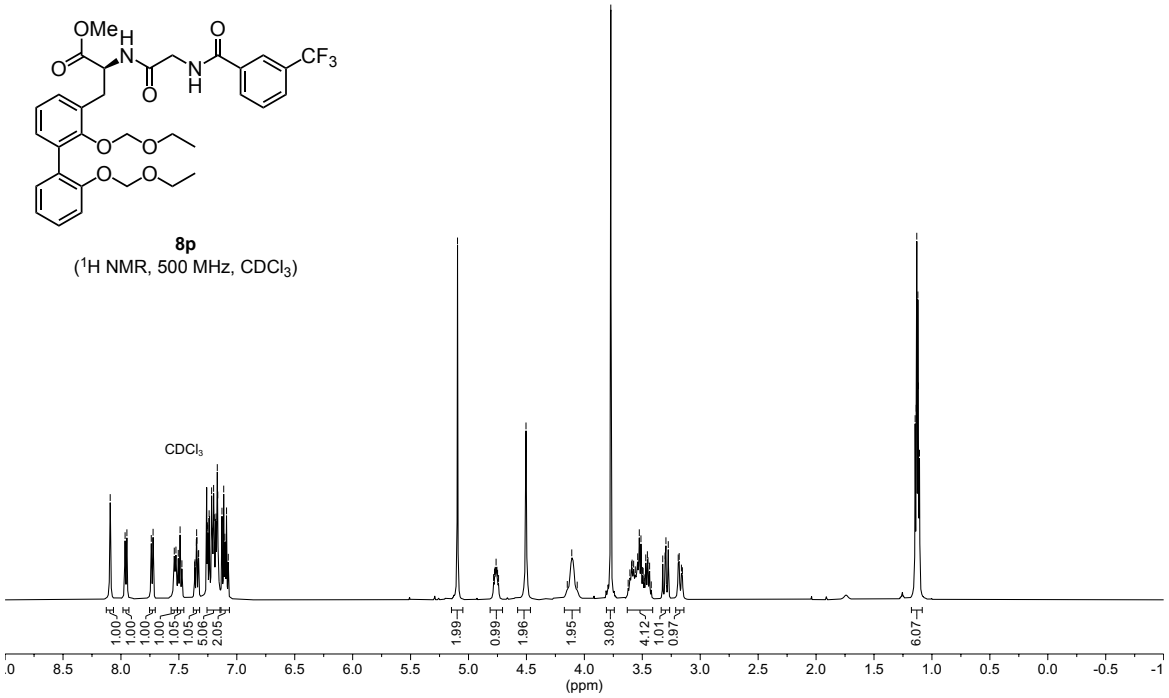

**8o**
($^{1}$H NMR, 500 MHz, $CDCl_3$)




**8o**

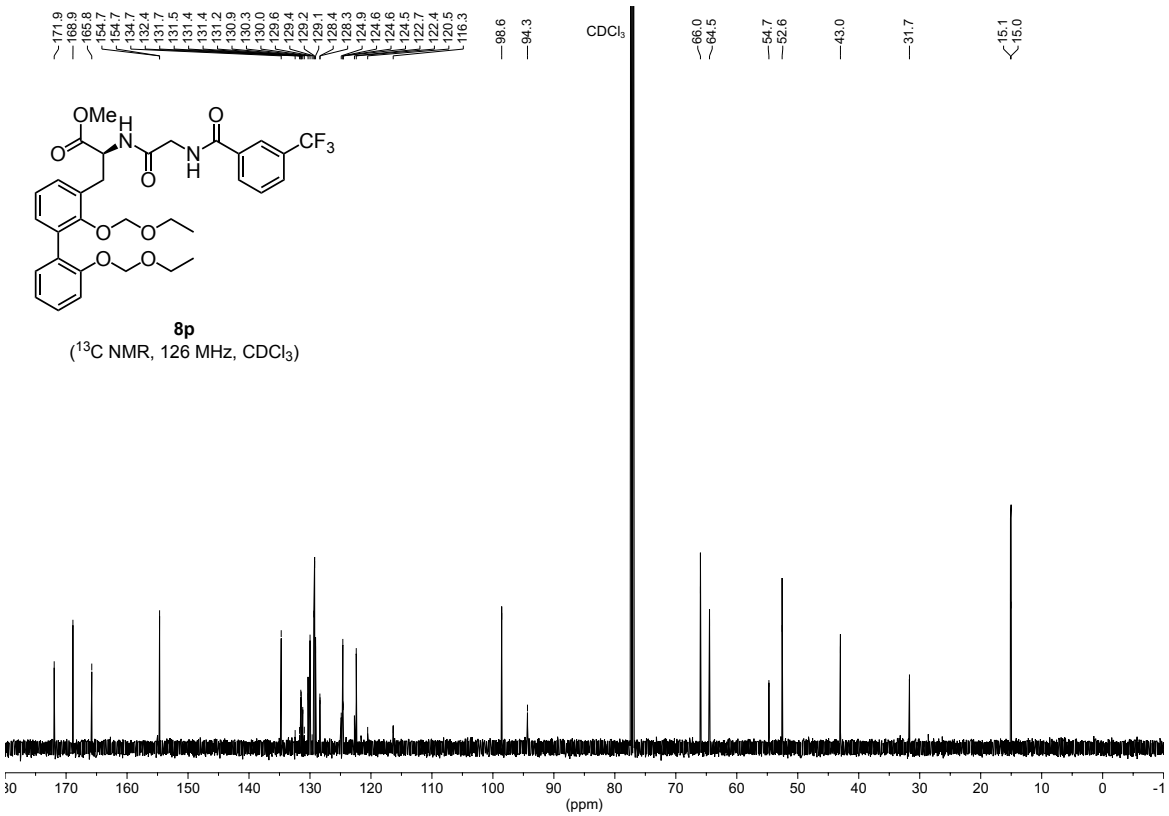
($^{13}$C NMR, 126 MHz, $CDCl_3$)



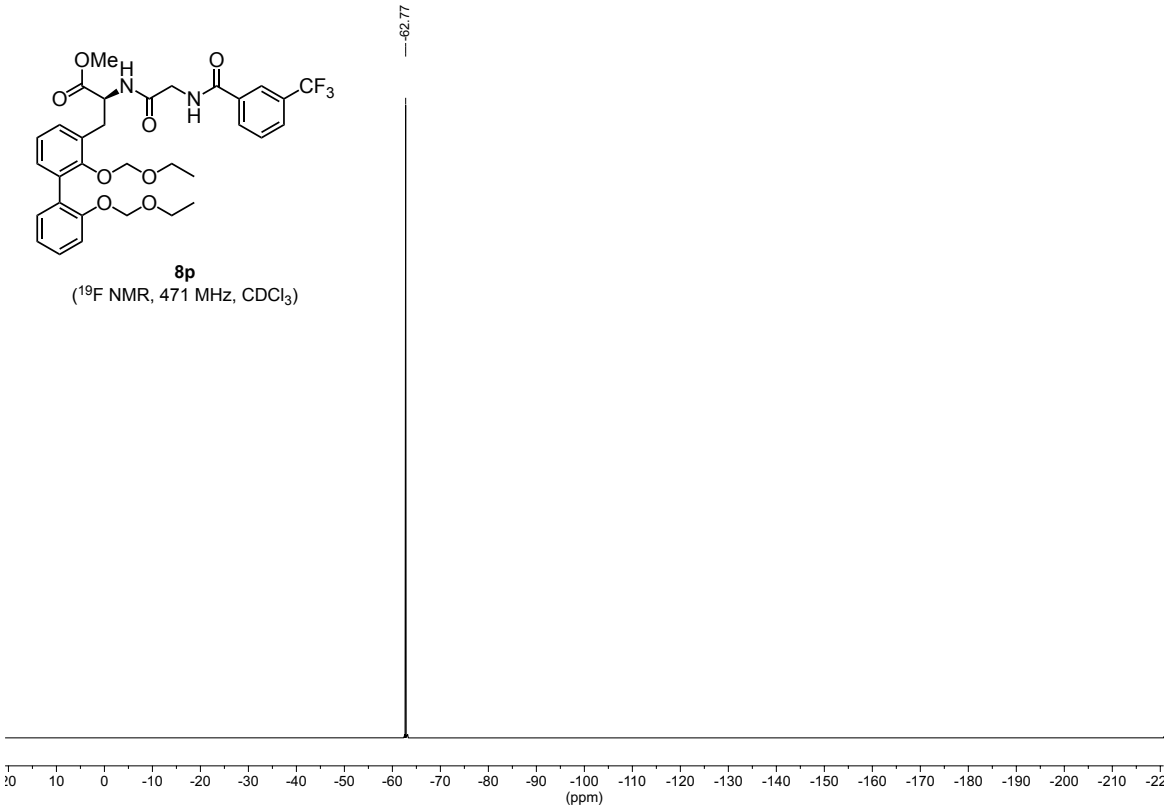



**8p**

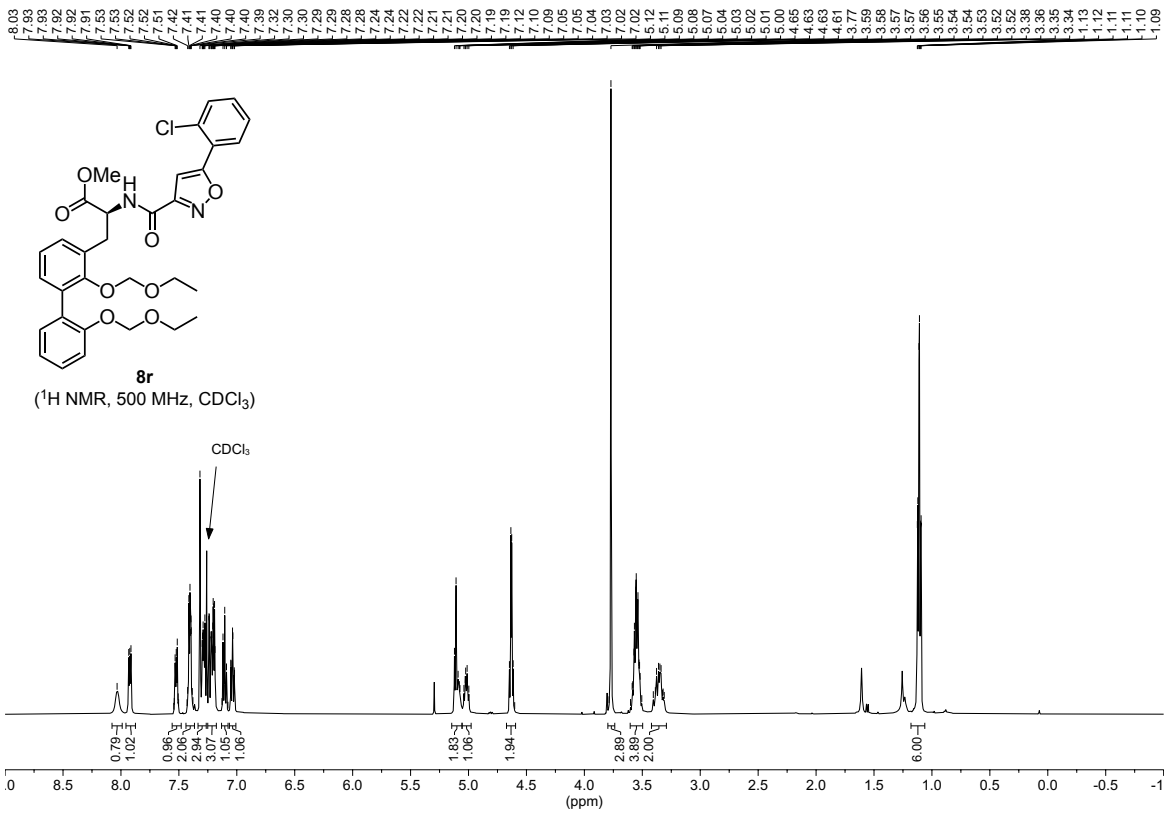
($^{1}$H NMR, 500 MHz, $CDCl_3$)



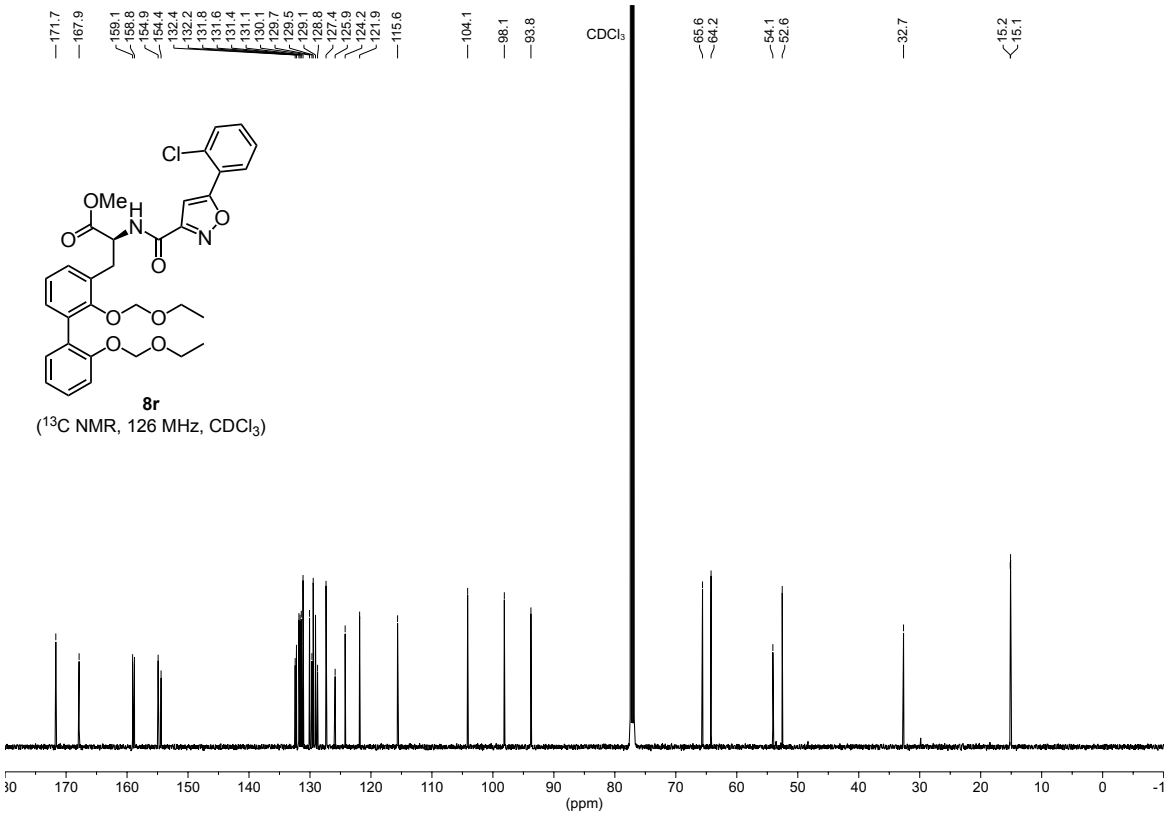

**8p**
($^{13}$C NMR, 126 MHz, $CDCl_3$)



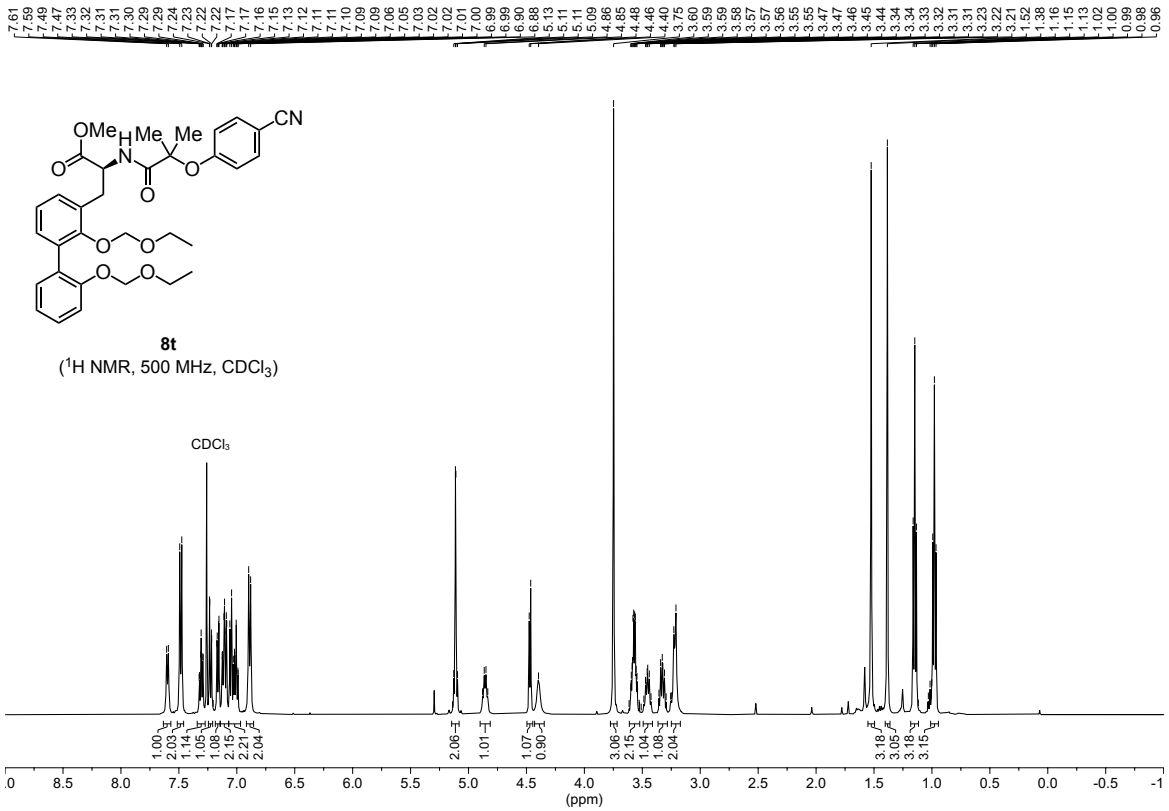

**8p**
($^{19}$F NMR, 471 MHz, $CDCl_3$)



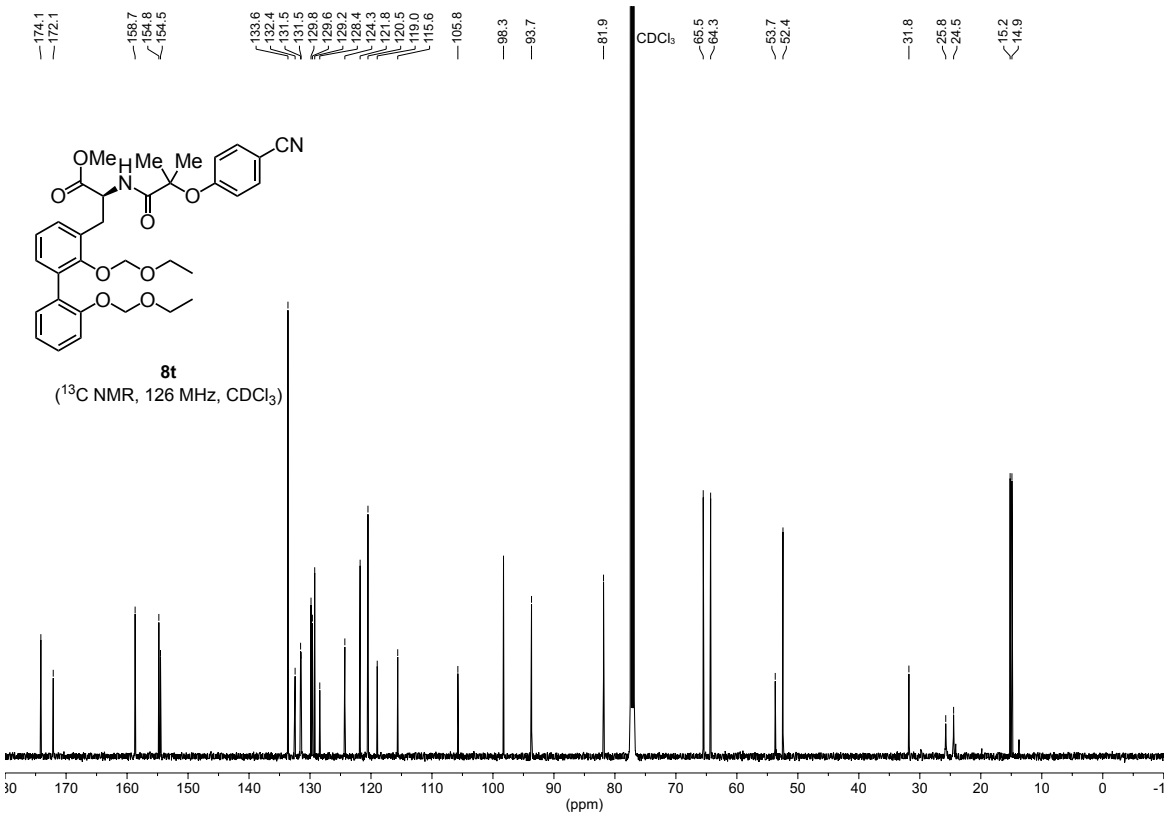

**8r**
($^1$H NMR, 500 MHz, $CDCl_3$)



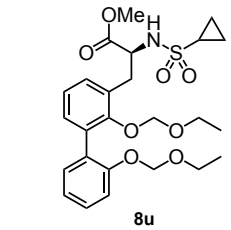

**8r**
($^{13}$C NMR, 126 MHz, $CDCl_3$)




**8t**
($^1$H NMR, 500 MHz, $CDCl_3$)

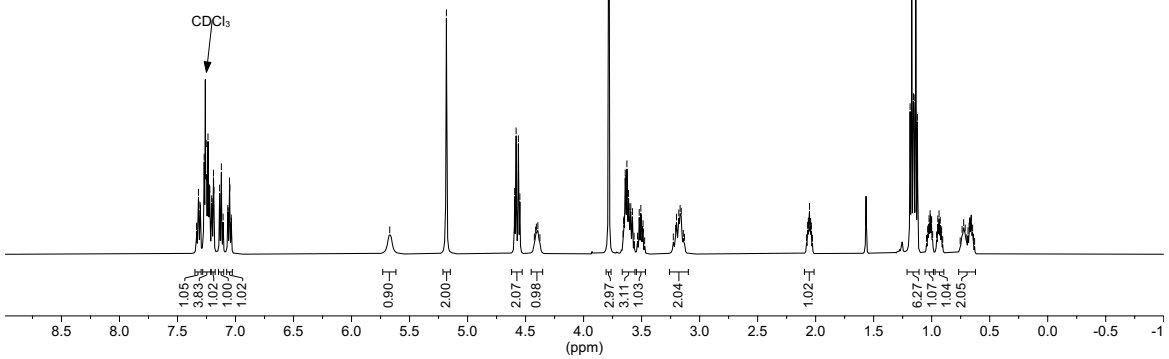


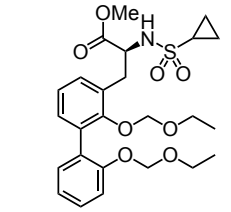

**8t**
($^{13}$C NMR, 126 MHz, $CDCl_3$)



**8u**

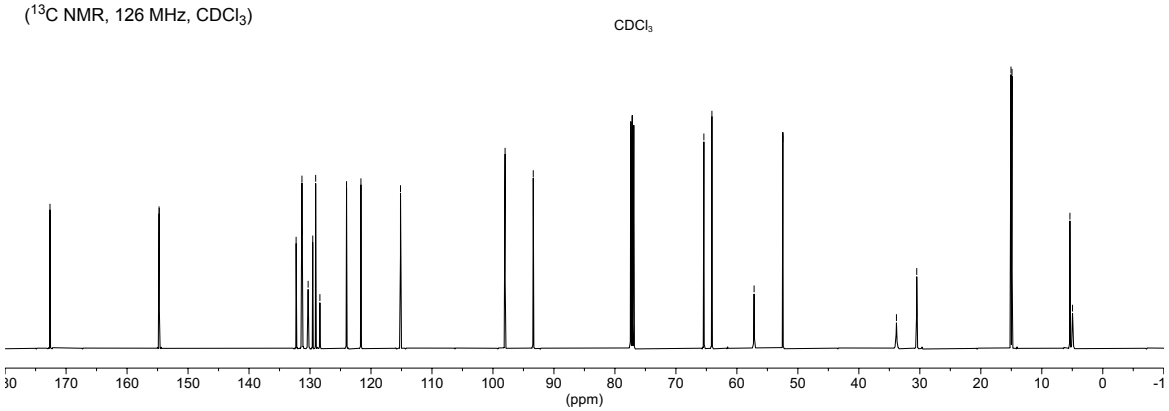
($^1$H NMR, 500 MHz, $CDCl_3$)

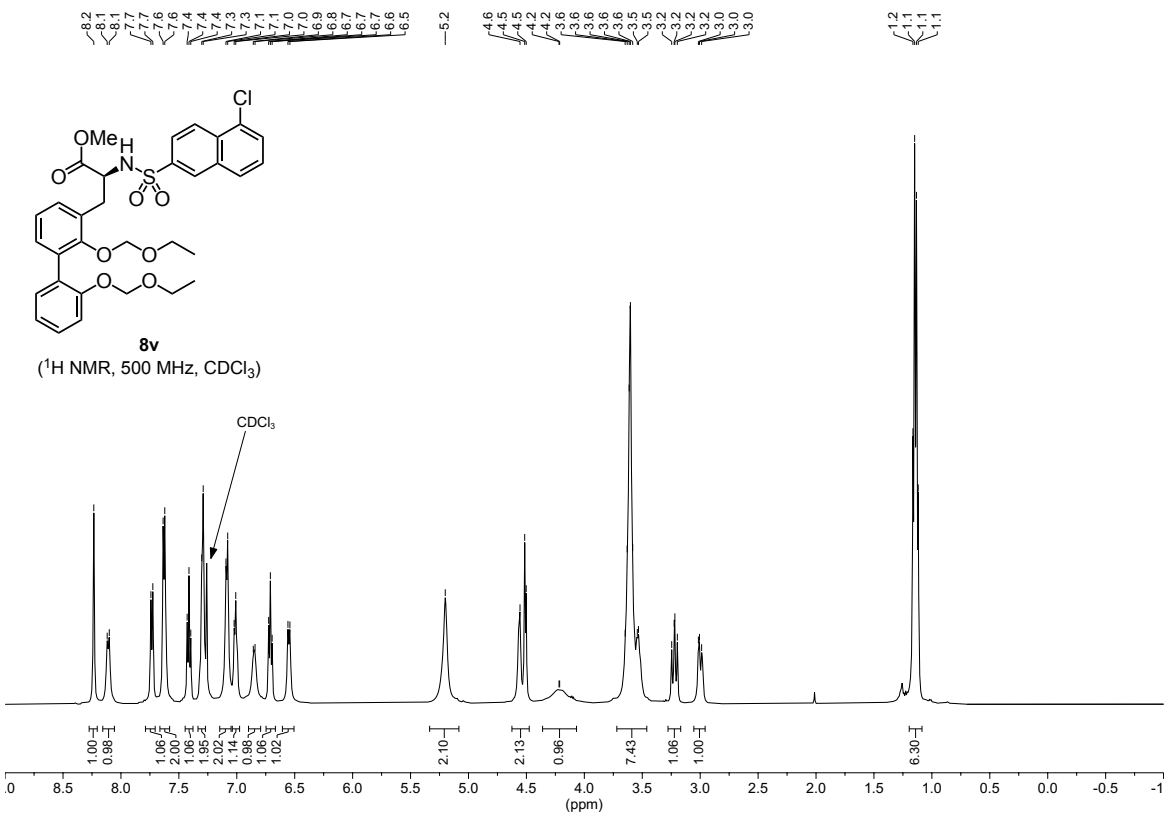


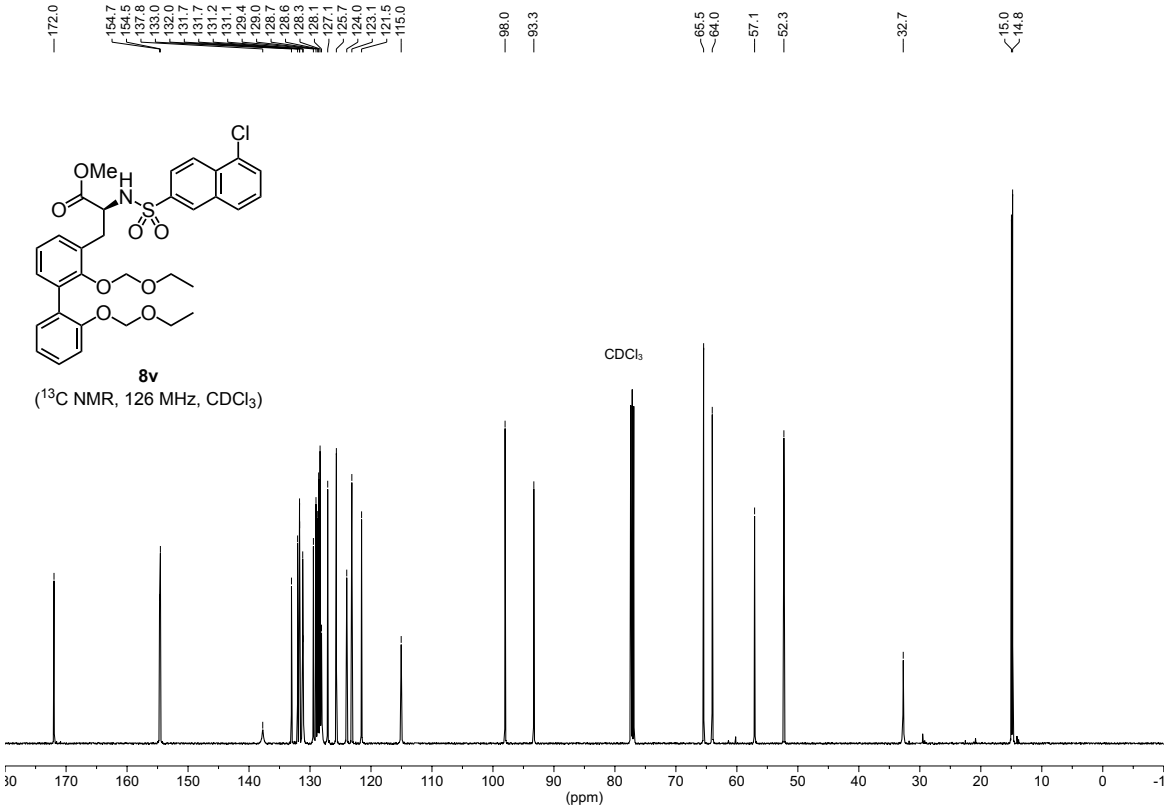



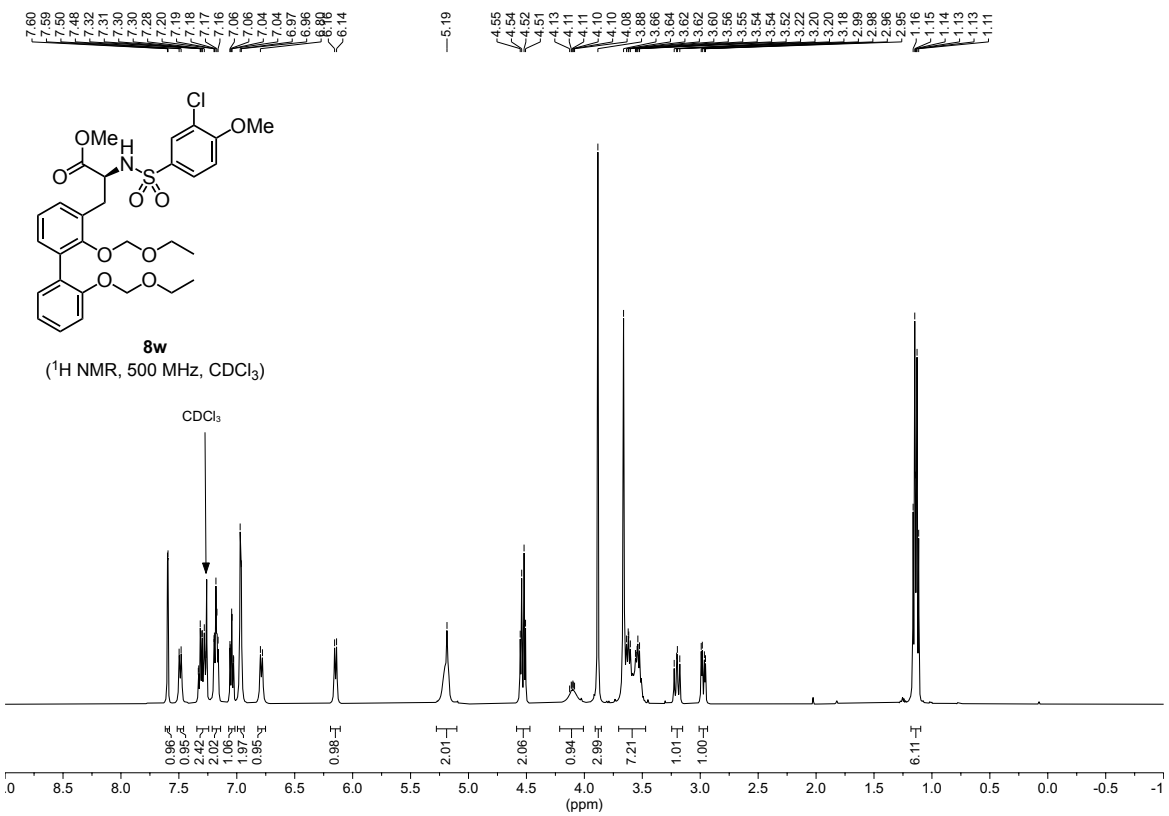
**8u**

($^{13}$C NMR, 126 MHz, $CDCl_3$)

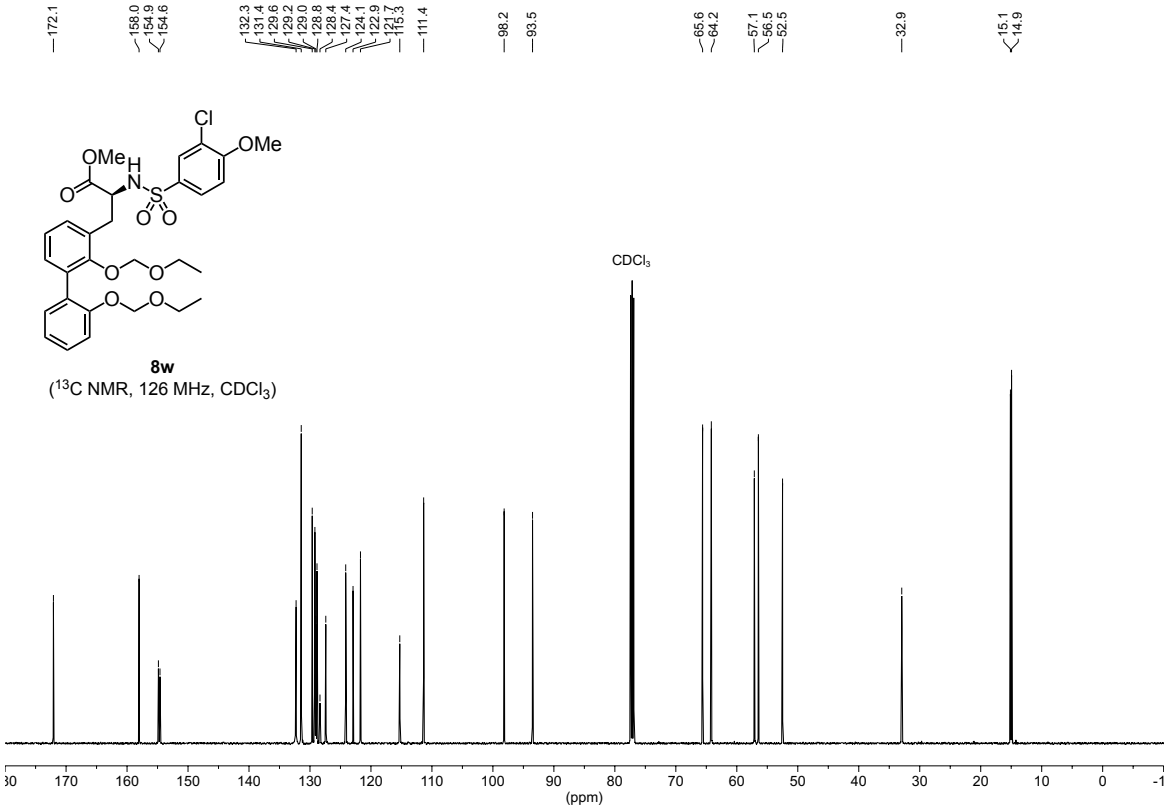



Cl
OMe
H
N
S
O
O
O
O
O
O
O
O
8v
(1H NMR, 500 MHz, CDCl3)
CDCl3
(ppm)


Cl
OMe
H
N
S
O
O
O
O
O
O
O
O
8v
(13C NMR, 126 MHz, CDCl3)
CDCl3
(ppm)

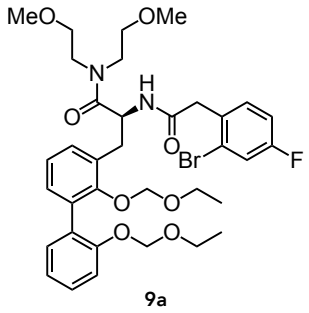


**8w**
($^1$H NMR, 500 MHz, $CDCl_3$)



**8w**
($^{13}$C NMR, 126 MHz, $CDCl_3$)

### 7.2.4. Synthesis and Characterization of Intermediates 9a-w




**9a**

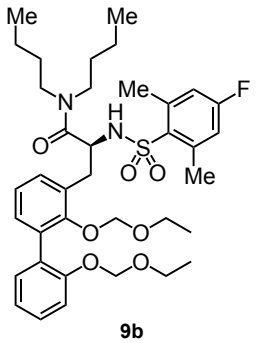
**(*S*)-3-(2,2'-bis(ethoxymethoxy)-[1,1'-biphenyl]-3-yl)-2-(2-(2-bromo-4-fluorophenyl)acetamido)-*N*,*N*-bis(2-methoxyethyl)propenamide (9a)** was synthesized following General Procedure 2 from **8a** using **Amine A**. Crude material purified by normal-phase column chromatography using EtOAc/Hx (10-40%) to give **9a** as a yellowish oil (96% yield).

**$^1$H NMR (500 MHz, $CDCl_3$)** δ 7.31 (ddd, *J* = 8.8, 7.3, 1.7 Hz, 1H), 7.25 – 7.19 (m, 4H), 7.19 – 7.13 (m, 2H), 7.11 – 6.99 (m, 3H), 6.91 (td, *J* = 8.3, 2.7 Hz, 1H), 5.27 (ddd, *J* = 10.1, 8.1, 5.0 Hz, 1H), 5.17 – 5.10 (m, 2H), 4.56 (s, 2H), 4.08 (dq, *J* = 16.5, 8.3, 7.0 Hz, 1H), 3.84 – 3.74 (m, 1H), 3.67 – 3.45 (m, 12H), 3.36 (s, 3H), 3.35 – 3.31 (m, 1H), 3.30 (s, 3H), 2.90 (dd, *J* = 13.7, 4.9 Hz, 1H), 1.15 (td, *J* = 7.0, 5.0 Hz, 6H).

**$^{13}$C NMR (126 MHz, $CDCl_3$)** δ 172.7, 169.2, 161.6 (d, *J* = 250.0 Hz, 1C), 155.2, 154.8, 132.3 (d, *J* = 8.9 Hz, 1C), 132.1, 131.7, 131.3 (d, *J* = 3.6 Hz, 1C), 131.0, 130.7, 130.0, 129.1, 128.8, 125.0 (d, *J* = 9.7 Hz, 1C), 124.1, 121.8, 120.0 (d, *J* = 24.4 Hz, 1C), 115.4, 114.8 (d, *J* =21.1 Hz, 1C), 98.3, 93.4, 71.1, 71.0, 65.8, 64.3, 59.1, 59.0, 50.7, 49.0, 47.2, 42.6, 32.7, 15.2, 15.1.

**$^{19}$F NMR (471 MHz, $CDCl_3$)** δ -113.73 (q, *J* = 7.5 Hz, 1F).

**HRMS (ESI+/TOF, *m*/*z*):** Exact mass calculated for $[C_{35}H_{44}BrFN_2O_8+H]^+$ requires 719.2343; found 719.2349.




**9b**

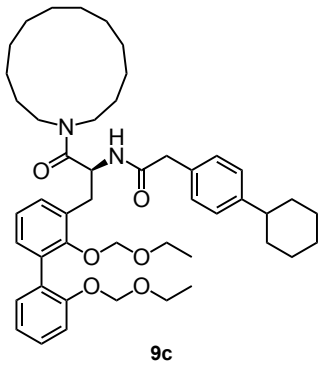
**(*S*)-3-(2,2'-bis(ethoxymethoxy)-[1,1'-biphenyl]-3-yl)-*N*,*N*-dibutyl-2-((4-fluoro-2,6-dimethylphenyl)sulfonamido)propenamide (9b)** was synthesized following General Procedure 2 from **8b** using **Amine B**. Crude material purified by normal-phase column chromatography using EtOAc/Hx (10-40%) to give **9b** as a yellow oil (77% yield).

**$^{1}$H NMR (500 MHz, $CDCl_3$)** δ 7.31 (td, *J* = 7.8, 7.2, 1.7 Hz, 1H), 7.25 (dd, *J* = 9.8, 2.0 Hz, 1H), 7.22 (dd, *J* = 7.5, 1.7 Hz, 1H), 7.16 (dd, *J* = 7.6, 1.8 Hz, 1H), 7.09 – 6.99 (m, 2H), 6.98 (t, *J* = 7.5 Hz, 1H), 6.75 (d, *J* = 9.0 Hz, 2H), 6.06 (d, *J* = 9.0 Hz, 1H), 5.16 (s, 2H), 4.57 (s, 2H), 4.48 (q, *J* = 8.0 Hz, 1H), 3.62 (q, *J* = 7.1 Hz, 2H), 3.44 – 3.32 (m, 2H), 3.32 – 3.21 (m, 2H), 3.02 (dt, *J* = 14.0, 7.5 Hz, 2H), 2.96 (brs, 1H), 2.85 (brs, 1H), 2.64 (s, 6H), 1.39 – 1.24 (m, 3H), 1.24 – 1.18 (m, 4H), 1.17 (t, *J* = 7.1 Hz, 4H), 1.03 (t, *J* = 7.0 Hz, 3H), 0.90 (dt, *J* = 9.0, 7.0 Hz, 6H). [1]

**$^{3}$C NMR (126 MHz, $CDCl_3$)** δ 170.7, 163.4 (d, *J* = 253.6 Hz, 1C), 154.8, 154.1, 142.75 (d, *J* = 8.9 Hz, 2C), 133.9 (d, *J* = 3.2 Hz, 1C), 131.75, 131.72, 131.5, 130.7, 129.9, 129.0, 128.6, 123.7, 121.6, 117.6 (d, *J* = 21.3 Hz, 2C), 115.5, 97.7, 93.5, 65.6, 64.3, 53.1, 47.3, 46.3, 36.4, 31.0, 29.7, 23.3 (s, 2C), 20.3, 20.2, 15.2, 15.1, 13.9, 13.8.

**$^{19}$F NMR (471 MHz, $CDCl_3$)** δ -109.34 (t, *J* = 9.2 Hz, 1F).

**HRMS (ESI+/TOF, *m/z*):** Exact mass calculated for $[C_{37}H_{51}FN_2O_7S+Na]^+$ requires 709.3299; found 709.3301.



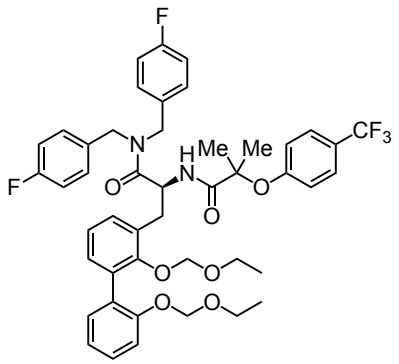
**9c**

**(*S*)-*N*-(3-(2,2'-bis(ethoxymethoxy)-[1,1'-biphenyl]-3-yl)-1-(azacyclotridecan-1-yl)-1-oxopropan-2-yl)-2-(4-cyclohexylphenyl)acetamide (9c)** was synthesized following General Procedure 2 from **8c** using **Amine C**. Crude material purified by normal-phase column chromatography using EtOAc/Hx (0-20%) to give **9c** as a yellow oil (59% yield).

**$^1$H NMR (500 MHz, $CDCl_3$)** δ 7.30 (ddd, *J* = 8.7, 7.2, 1.8 Hz, 1H), 7.26 – 7.21 (m, 2H), 7.17 (dd, *J* = 7.2, 2.1 Hz, 1H), 7.11 (d, *J* = 8.1 Hz, 2H), 7.07 – 6.96 (m, 5H), 6.72 (brd, *J* = 8.4 Hz, 1H), 5.20 (td, *J* = 8.5, 6.2 Hz, 1H), 5.12 (s, 2H), 4.55 (q, *J* = 6.3 Hz, 2H), 3.59 (q, *J* = 7.1 Hz, 2H), 3.54 – 3.46 (m, 1H), 3.42 (s, 4H), 3.38 – 3.23 (m, 3H), 3.16 (t, *J* = 11.3 Hz, 1H), 2.91 (dd, *J* = 13.7, 6.1 Hz, 1H), 2.46 (tq, *J* = 11.3, 3.2 Hz, 1H), 1.89 – 1.50 (m, 10H), 1.44 – 1.19 (m, 20H), 1.15 (t, *J* = 7.1 Hz, 3H), 1.05 (t, *J* = 7.1 Hz, 3H).

**$^{13}$C NMR (126 MHz, $CDCl_3$) δ** 171.8, 170.6, 154.8, 154.6, 146.7, 132.4, 132.0, 131.8, 131.1, 130.4, 130.3, 129.2, 129.0, 128.9, 127.3, 123.7, 121.7, 115.5, 98.0, 93.6, 65.5, 64.3, 50.1, 49.0, 47.7, 44.3, 43.1, 34.6, 34.6, 34.2, 27.1, 27.0, 26.3, 25.7, 25.6, 25.4, 25.2, 25.2, 24.8, 24.5, 15.2, 15.1.

**HRMS (ESI+/TOF, *m/z*):** Exact mass calculated for $[C_{47}H_{66}N_2O_6+H]^+$ requires 755.4999; found 755.5004.



**9d**

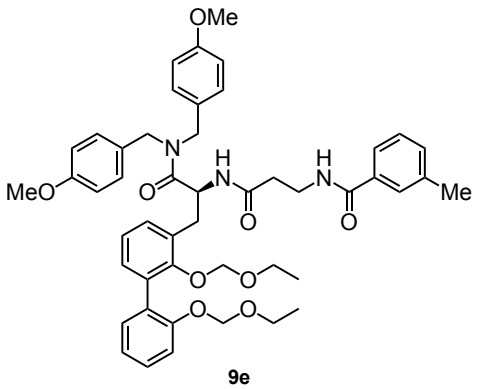
**(*S*)-3-(2,2'-bis(ethoxymethoxy)-[1,1'-biphenyl]-3-yl)-*N*,*N*-bis(4-fluorobenzyl)-2-(2-methyl-2-(4-(trifluoromethyl)phenoxy)propanamido)propenamide (9d)** was synthesized following General Procedure 2 from **8d** using **Amine D**. Crude material purified by normal-phase column chromatography using EtOAc/Hx (0-30%) to give **9d** as a white foam (80% yield).

**$^{1}$H NMR (500 MHz, $CDCl_3$)** δ 7.62 (s, 1H), 7.45 (d, *J* = 8.5 Hz, 2H), 7.35 – 7.26 (m, 1H), 7.25 – 7.19 (m, 3H), 7.18 – 7.03 (m, 6H), 7.01 – 6.89 (m, 6H), 6.85 (d, *J* = 7.6 Hz, 1H), 5.35 (brs, 1H), 5.04 (s, 2H), 4.76 – 4.67 (m, 2H), 4.59 – 4.16 (m, 4H), 3.52 (q, *J* = 7.2 Hz, 2H), 3.43 – 3.29 (m, 2H), 3.25 (dd, *J* = 13.5, 9.6 Hz, 1H), 2.96 (brdd, 1H), 1.54 (s, 3H), 1.43 (s, 3H), 1.11 (t, *J* = 7.1 Hz, 3H), 0.96 (t, *J* = 7.1 Hz, 3H).

**$^{13}$C NMR (126 MHz, $CDCl_3$)** δ 174.2, 172.4, 162.5 (d, *J* = 246.2 Hz, 1C), 162.3 (d, *J* = 246.2 Hz, 1C), 157.5, 154.8, 154.4, 132.6 (d, *J* = 3.2 Hz, 1C), 132.3, 132.3, 131.5, 131.5, 130.1, 130.0 (d, *J* = 8.0 Hz, 2C), 129.9 (d, *J* = 8.0 Hz, 2C, *note: overlapping with doublet at 130 ppm*), 129.2, 129.1, 128.3, 126.7 (q, *J* = 3.8 Hz, 2C), 124.9 (q, *J* = 33.0 Hz, 1C), 124.4 (q, *J* = 271.6 Hz, 1C), 124.0, 121.7, 120.6 (s, 2C), 116.0 (d, *J* = 21.5 Hz, 2C), 115.0 (d, *J* = 21.5 Hz, 2C), 115.3, 98.0, 93.5, 81.7, 65.5, 64.2, 50.5, 49.4, 47.7, 34.1, 25.3, 25.0, 15.1, 15.0.

**$^{19}$F NMR (471 MHz, $CDCl_3$)** δ -61.78 (s, 3F), -114.31 (s, 1F), -115.01 (s, 1F).

**HRMS (ESI+/TOF, *m/z*):** Exact mass calculated for $[C_{46}H_{47}F_5N_2O_7+H]^+$ requires 835.3382; found 835.3371.



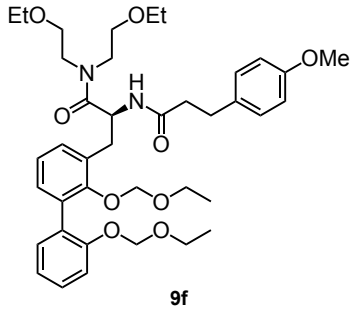

**9e**

**(*S*)-*N*-(3-((1-(bis(4-methoxybenzyl)amino)-3-(2,2'-bis(ethoxymethoxy)-[1,1'-biphenyl]-3-yl)-1-oxopropan-2-yl)amino)-3-oxopropyl)-3-methylbenzamide (9e)** was synthesized following General Procedure 2 from **8e** using **Amine E**. Crude material purified by normal-phase column chromatography using EtOAc/Hx (50-80%) to give **9e** as a white foam (62% yield).

**$^1$H NMR (500 MHz, $CDCl_3$)** δ 7.65 (d, *J* = 1.9 Hz, 1H), 7.55 (dt, *J* = 7.6, 1.7 Hz, 1H), 7.29 (ddd, *J* = 8.9, 7.3, 1.8 Hz, 2H), 7.24 – 7.08 (m, 9H), 7.06 – 6.98 (m, 2H), 6.90 (dd, *J* = 8.1, 6.0 Hz, 3H), 6.82 (dq, *J* = 9.5, 3.0, 2.5 Hz, 3H), 5.32 – 5.23 (m, 1H), 5.04 (s, 2H), 4.82 (d, *J* = 14.6 Hz, 1H), 4.70 (d, *J* = 16.3 Hz, 1H), 4.51 (d, *J* = 1.1 Hz, 2H), 4.37 (d, *J* = 16.0 Hz, 1H), 4.22 (brd, *J* = 14.7 Hz, 1H), 3.79 (s, 4H), 3.77 (s, 3H), 3.59 (td, *J* = 8.3, 3.8 Hz, 1H), 3.54 – 3.44 (m, 3H), 3.44 – 3.34 (m, 1H), 3.22 (dd, *J* = 13.5, 10.2 Hz, 1H), 2.88 (dd, *J* = 13.7, 4.8 Hz, 1H), 2.48 – 2.35 (m, 2H), 2.32 (s, 3H), 1.09 (t, *J* = 7.1 Hz, 3H), 0.99 (t, *J* = 7.1 Hz, 3H).

**$^{13}$C NMR (126 MHz, $CDCl_3$)** δ 172.5, 172.2, 167.5, 159.4, 159.1, 154.7, 154.6, 138.2, 134.5, 132.1, 132.1, 131.6, 131.3, 130.0, 129.9, 129.7, 129.2, 129.0, 128.7, 128.6, 128.4, 128.3, 128.1, 124.3, 124.0, 121.9, 115.5, 114.5, 114.1, 98.1, 93.5, 65.7, 64.2, 55.5, 55.4, 51.4, 49.3, 47.7, 36.3, 35.7, 33.5, 21.4, 15.1, 15.0.

**HRMS (ESI+/TOF, *m/z*):** Exact mass calculated for $[C_{48}H_{55}N_3O_9+H]^+$ requires 818.4017; found 818.4001.



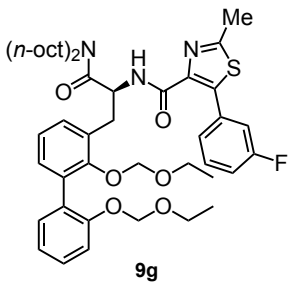

**9f**

**(*S*)-3-(2,2'-bis(ethoxymethoxy)-[1,1'-biphenyl]-3-yl)-*N*,*N*-bis(2-ethoxyethyl)-2-(3-(4-methoxyphenyl)propanamido)propanamide (9f)** was synthesized following General Procedure 2 from **8f** using **Amine F**. Crude material purified by normal-phase column chromatography using EtOAc/Hx (10-40%) to give **9f** as an off-white foam (83% yield).

**$^1$H NMR (500 MHz, $CDCl_3$)** δ 7.30 (ddd, *J* = 8.8, 7.3, 1.8 Hz, 1H), 7.25 – 7.13 (m, 4H), 7.10 – 6.98 (m, 4H), 6.84 (d, *J* = 8.2 Hz, 1H), 6.81 – 6.74 (m, 2H), 5.31 – 5.21 (m, 1H), 5.09 (q, *J* = 7.1 Hz, 2H), 4.60 (t, *J* = 5.1 Hz, 2H), 3.88 (s, 1H), 3.76 (s, 3H), 3.72 – 3.39 (m, 15H), 3.30 (brt, *J* = 13.6, 9.3 Hz, 1H), 2.90 (dd, *J* = 13.6, 5.5 Hz, 1H), 2.75 (ddd, *J* = 9.0, 7.1, 2.4 Hz, 2H), 2.34 (ddd, *J* = 10.3, 8.8, 7.0 Hz, 2H), 1.22 – 1.09 (m, 12H).

**$^{13}$C NMR (126 MHz, $CDCl_3$)** δ 172.7, 171.7, 158.0, 154.9, 154.8, 133.2, 132.0, 131.8, 131.0, 130.5, 130.2, 129.3, 129.0, 128.9, 123.9, 121.8, 115.5, 114.0, 98.2, 93.5, 68.8, 68.6, 66.8, 66.5, 65.7, 64.2, 55.3, 50.1, 48.9, 47.3, 38.4, 33.3, 30.8, 15.3, 15.2, 15.1.

**HRMS (ESI+/TOF, *m/z*):** Exact mass calculated for $[C_{39}H_{54}N_2O_9+H]^+$ requires 695.3908; found 695.3908.




**9g**

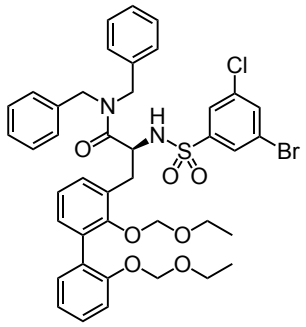
**(*S*)-*N*-(3-(2,2'-bis(ethoxymethoxy)-[1,1'-biphenyl]-3-yl)-1-(dioctylamino)-1-oxopropan-2-yl)-5-(3-fluorophenyl)-2-methylthiazole-4-carboxamide (9g)** was synthesized following General Procedure 2 from **8g** using **Amine G**. Crude material purified by normal-phase column chromatography using EtOAc/Hexanes (10-35%) to give **9g** as a yellowish foam (41% yield).

**$^{1}$H NMR (500 MHz, $CDCl_3$)** δ 8.18 (d, *J* = 9.1 Hz, 1H), 7.30 – 7.26 (m, 1H), 7.24 – 7.16 (m, 7H), 7.04 – 6.96 (m, 3H), 5.40 (dt, *J* = 9.3, 7.3 Hz, 1H), 5.10 (s, 2H), 4.60 (q, *J* = 6.0 Hz, 2H), 3.58 (q, *J* = 7.1 Hz, 3H), 3.49 (d, *J* = 10.9 Hz, 1H), 3.44 – 3.34 (m, 2H), 3.24 – 3.09 (m, 2H), 3.09 – 2.95 (m, 2H), 2.68 (s, 3H), 1.57 – 1.37 (m, 4H), 1.31 – 1.19 (m, 20H), 1.14 (t, *J* = 7.1 Hz, 3H), 1.00 (t, *J* = 7.1 Hz, 3H), 0.86 (dt, *J* = 10.1, 6.8 Hz, 6H).

**$^{13}$C NMR (126 MHz, $CDCl_3$)** δ 171.3, 163.5, 162.3 (d, *J* = 246.3 Hz, 1C), 160.3, 154.8, 154.5, 142.0, 141.1 (d, *J* = 2.2 Hz, 1C), 132.7 (d, *J* = 8.9 Hz, 1C), 132.0, 131.7, 131.2, 130.7, 130.6, 129.4 (d, *J* = 8.4 Hz, 1C), 128.9, 128.8, 126.05 (d, *J* = 3.0 Hz, 1C), 123.4, 121.6, 117.4 (d, *J* = 22.8 Hz, 1C), 115.50 (d, *J* = 23.64 Hz, 1C), 115.45, 97.8, 93.6, 65.3, 64.2, 49.0, 47.7, 46.4, 35.6, 31.9, 31.9, 29.5, 29.4, 29.4 (s, 2C), 29.3, 27.6, 27.2, 27.0, 22.8, 22.7, 19.1, 15.2, 15.1, 14.2, 14.2.

**$^{19}$F NMR (471 MHz, $CDCl_3$)** δ -113.44 – -113.54 (m, 1F).

**HRMS (ESI+/TOF, *m/z*):** Exact mass calculated for $[C_{48}H_{66}FN_3O_6S+H]^+$ requires 832.4735; found 832.4722.



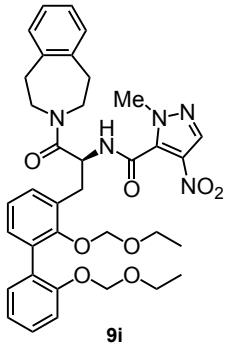

**9h**

**(*S*)-*N*,*N*-dibenzyl-3-(2,2'-bis(ethoxymethoxy)-[1,1'-biphenyl]-3-yl)-2-((3-bromo-5-chlorophenyl)sulfonamido)propenamide (9h)** was synthesized following General Procedure 2 from **8h** using **Amine H**. Crude material purified by normal-phase column chromatography using EtOAc/Hx (0-30%) to give **9h** as a white foam (67% yield).

**$^1$H NMR (500 MHz, $CDCl_3$)** δ 7.65 (s, 1H), 7.54 (t, *J* = 1.9 Hz, 1H), 7.51 (s, 1H), 7.44 – 7.38 (m, 2H), 7.36 – 7.29 (m, 5H), 7.27 – 7.09 (m, 7H), 7.04 (t, *J* = 7.3 Hz, 1H), 6.79 (t, *J* = 7.6 Hz, 1H), 6.58 (d, *J* = 7.6, 1.8 Hz, 1H), 6.49 (brs, 1H), 5.13 – 5.03 (m, 2H), 4.94 (d, *J* = 14.8 Hz, 1H), 4.86 – 4.54 (m, 2H), 4.50 (s, 2H), 4.32 (d, *J* = 14.9 Hz, 2H), 3.56 (q, *J* = 7.1 Hz, 2H), 3.46 – 3.30 (m, 2H), 3.11 (dd, *J* = 13.5, 10.3 Hz, 1H), 2.91 – 2.84 (m, 1H), 1.16 – 1.08 (m, 3H), 1.01 (t, *J* = 7.1 Hz, 3H).

**$^{13}$C NMR (126 MHz, $CDCl_3$)** δ 172.1, 155.0, 154.2, 136.6, 136.3, 135.8, 135.1, 132.1, 131.7 (brs, 2C), 131.5, 130.1, 129.22 (s, 2C), 129.21, 129.1, 128.8 (s, 2C), 128.4 (s, 2C), 128.2, 128.1, 127.7, 127.2 (s, 2C), 125.7, 123.9, 123.2 (s, 2C), 121.7, 115.2, 97.8, 93.5, 65.8, 64.1, 54.7, 49.9, 48.9, 35.1, 15.2, 15.0.

**HRMS (ESI+/TOF, *m/z*):** Exact mass calculated for $[C_{41}H_{42}BrClN_2O_7S+H]^+$ requires 821.1663; found 821.1665.



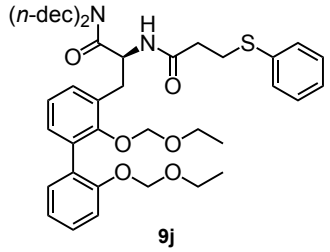

**9i**

**(*S*)-*N*-(3-(2,2'-bis(ethoxymethoxy)-[1,1'-biphenyl]-3-yl)-1-oxo-1-(1,2,4,5-tetrahydro-3*H*-benzo[*d*]azepin-3-yl)propan-2-yl)-1-methyl-4-nitro-1*H*-pyrazole-5-carboxamide (9i)** was synthesized following General Procedure 2 from **8i** using **Amine I**. Crude material purified by normal-phase column chromatography using EtOAc/Hx (10-30%) to give **9i** as a white foam (42% yield).

**$^1$H NMR (500 MHz, $CDCl_3$)** δ 8.49 (d, *J* = 8.1 Hz, 1H), 7.99 (s, 1H), 7.32 (ddd, *J* = 8.8, 7.3, 1.7 Hz, 1H), 7.27 – 7.17 (m, 4H), 7.17 – 7.03 (m, 6H), 5.64 (td, *J* = 9.0, 5.8 Hz, 1H), 5.18 – 5.14 (m, 2H), 4.54 (dd, *J* = 32.1, 6.1 Hz, 2H), 4.04 – 3.95 (m, 2H), 3.76 (s, 3H), 3.71 – 3.56 (m, 4H), 3.53 – 3.44 (m, 1H), 3.44 – 3.34 (m, 1H), 3.34 – 3.26 (m, 1H), 3.18 – 3.10 (m, 2H), 3.04 – 2.95 (m, 1H), 2.93 – 2.80 (m, 2H), 1.18 (t, *J* = 7.1 Hz, 3H), 1.05 (t, *J* = 7.1 Hz, 3H).

**$^{13}$C NMR (126 MHz, $CDCl_3$)** δ 169.8, 156.9, 154.9, 154.7, 141.0, 140.1, 135.6, 134.1, 133.0, 132.2, 131.7, 131.6, 130.4, 129.9, 129.8, 129.8, 129.2, 128.4, 126.9, 126.7, 123.8, 121.8, 115.3, 98.2, 93.5, 65.9, 64.3, 50.6, 48.5, 45.8, 39.8, 38.1, 37.2, 34.0, 15.2, 14.9.

**HRMS (ESI+/TOF, *m/z*):** Exact mass calculated for $[C_{36}H_{41}N_5O_8+Na]^+$ requires 694.2853; found 694.2858.



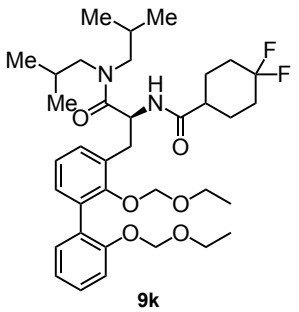

**9j**

**(*S*)-3-(2,2'-bis(ethoxymethoxy)-[1,1'-biphenyl]-3-yl)-*N*,*N*-didecyl-2-(3-(phenylthio)propanamido)propenamide (9j)** was synthesized following General Procedure 2 from **8j** using **Amine J**. Crude material purified by normal-phase column chromatography using EtOAc/Hx (0-25%) to give **9j** as a yellow oil (77% yield).

**$^1$H NMR (500 MHz, $CDCl_3$)** δ 7.33 – 7.29 (m, 3H), 7.29 – 7.21 (m, 4H), 7.21 – 7.13 (m, 3H), 7.09 – 7.00 (m, 2H), 6.79 (d, *J* = 8.2 Hz, 1H), 5.19 (td, *J* = 8.7, 5.9 Hz, 1H), 5.17 – 5.10 (m, 2H), 4.64 – 4.56 (m, 2H), 3.66 – 3.53 (m, 3H), 3.54 – 3.31 (m, 3H), 3.30 – 3.21 (m, 2H), 3.16 – 3.01 (m, 3H), 2.90 (brd, *J* = 14.0, 5.9 Hz, 1H), 2.49 – 2.32 (m, 2H), 1.71 – 1.62 (m, 1H), 1.56 (dq, *J* = 15.3, 5.5 Hz, 1H), 1.51 – 1.43 (m, 2H), 1.35 – 1.23 (m, 28H), 1.16 (t, *J* = 7.1 Hz, 3H), 1.10 (t, *J* = 7.0 Hz, 3H), 0.94 – 0.85 (m, 6H).

**$^{13}$C NMR (126 MHz, $CDCl_3$)** δ 171.5, 170.2, 154.8, 154.8, 135.8, 132.0, 131.8, 131.2, 130.3, 130.2, 129.7, 129.1, 129.0, 128.8, 126.4, 123.8, 121.8, 115.5, 98.1, 93.6, 65.7, 64.3, 50.0, 48.0, 46.7, 36.1, 34.2, 32.0, 29.8, 29.7, 29.7, 29.7, 29.6, 29.5, 29.5, 29.5, 29.4, 27.8, 27.2, 27.1, 22.8, 15.2, 15.1, 14.2. (*Note: didecylamine carbon peaks overlap from 294.4 – 290.0*).

**HRMS (ESI+/TOF, *m/z*):** Exact mass calculated for $[C_{50}H_{76}N_2O_6S+H]^+$ requires 855.5322; found 855.5304.




**9k**

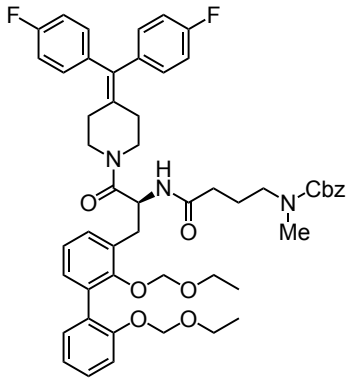
**(*S*)-*N*-(3-(2,2'-bis(ethoxymethoxy)-[1,1'-biphenyl]-3-yl)-1-(diisobutylamino)-1-oxopropan-2-yl)-4,4-difluorocyclohexane-1-carboxamide (9k)** was synthesized following General Procedure 2 from **8k** using **Amine K**. Crude material purified by normal-phase column chromatography using EtOAc/Hx (0-30%) to give **9k** as a yellow oil (65% yield).

**$^{1}$H NMR (500 MHz, $CDCl_3$)** δ 7.33 – 7.27 (m, 1H), 7.26 – 7.20 (m, 2H), 7.18 – 7.11 (m, 2H), 7.08 – 7.01 (m, 2H), 6.73 – 6.66 (m, 1H), 5.29 (td, *J* = 9.2, 5.3 Hz, 1H), 5.14 (q, *J* = 7.0 Hz, 2H), 4.65 – 4.55 (m, 2H), 3.59 (ddt, *J* = 9.6, 7.1, 3.3 Hz, 3H), 3.53 – 3.44 (m, 1H), 3.44 – 3.31 (m, 2H), 3.31 – 3.23 (m, 1H), 3.17 (d, *J* = 11.7 Hz, 1H), 3.02 – 2.88 (m, 2H), 2.16 – 2.05 (m, 2H), 2.04 – 1.92 (m, 3H), 1.81 – 1.56 (m, 6H), 1.16 (t, *J* = 7.0 Hz, 3H), 1.08 (t, *J* = 7.1 Hz, 3H), 0.96 (dd, *J* = 16.7, 6.6 Hz, 6H), 0.83 (dd, *J* = 15.8, 6.6 Hz, 6H).

**$^{13}$C NMR (126 MHz, $CDCl_3$)** δ 173.4, 172.6, 154.8, 154.6, 132.0, 131.7, 131.3, 130.4, 130.1, 129.1, 128.7, 123.8, 122.8 (t, *J* = 241.6 Hz, 1C), 121.8, 115.6, 98.1, 93.6, 65.7, 64.3, 55.6, 54.2, 49.7, 42.4, 34.2, 32.8 (t, *J* = 24.6 Hz, 2C), 28.6, 26.7, 25.7 (t, *J* = 9.6 Hz, 2C), 20.5, 20.3, 20.2, 20.0, 15.2, 15.1.

**$^{19}$F NMR (471 MHz, $CDCl_3$)** δ -93.40 (d, *J* = 236.2 Hz, 1F), -100.04 (d, *J* = 236.4 Hz, 1F).

**HRMS (ESI+/TOF, *m/z*):** Exact mass calculated for $[C_{36}H_{52}F_2N_2O_6+H]^+$ requires 647.3872; found 647.3873.



**9l**

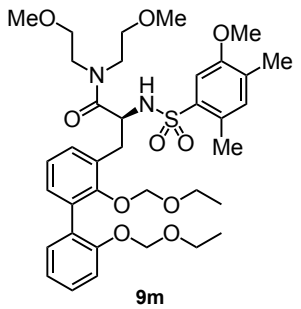
**Benzyl (*S*)-(4-((1-(4-(bis(4-fluorophenyl)methylene)piperidin-1-yl)-3-(2,2'-bis(ethoxymethoxy)-[1,1'-biphenyl]-3-yl)-1-oxopropan-2-yl)amino)-4-oxobutyl)(methyl)carbamate (9l)** was synthesized following General Procedure 2 from **8l** using **Amine L**. Crude material purified by normal-phase column chromatography using EtOAc/Hx (50-80%) to give **9l** as an off-white foam (62% yield).

**$^1$H NMR (500 MHz, $CDCl_3$)** δ 7.39 – 7.28 (m, 6H), 7.26 – 7.08 (m, 5H), 7.08 – 6.79 (m, 10H), 5.34 (q, *J* = 7.7 Hz, 1H), 5.17 – 5.02 (m, 4H), 4.62 – 4.52 (m, 2H), 3.62 (t, *J* = 6.3 Hz, 2H), 3.55 (q, *J* = 6.9 Hz, 3H), 3.49 – 3.32 (m, 3H), 3.32 – 3.10 (m, 3H), 2.94 (s, 1H), 2.87 (s, 3H), 2.32 (ddq, *J* = 14.1, 7.5, 3.9 Hz, 2H), 2.25 (d, *J* = 6.5 Hz, 1H), 2.20 – 2.05 (m, 2H), 1.99 (dq, *J* = 11.5, 3.7 Hz, 1H), 1.79 (d, *J* = 7.4 Hz, 2H), 1.14 (t, *J* = 7.1 Hz, 3H), 1.02 (t, *J* = 7.0 Hz, 3H).

**$^{13}$C NMR (126 MHz, $CDCl_3$)** *rotameric mixture*: δ 171.9, 171.6, 170.7, 170.6, 161.8 (d, *J* = 246.7 Hz, 1C), 161.7 (d, *J* = 246.2 Hz, 1C), 156.6, 156.3, 154.8, 154.5, 137.7, 137.6, 137.0, 135.8, 135.7, 134.3, 134.1, 132.2, 131.6, 131.3 (d, *J* = 7.8 Hz, 4C), 130.6, 130.5, 130.2, 130.1, 129.1, 128.6, 128.0, 127.9, 123.8, 121.8, 115.4, 115.3 (d, *J* = 21.5 Hz, 2C), 115.2 (d, *J* = 21.2 Hz. 2C), 97.9, 93.6, 67.1, 65.5, 64.2, 49.1, 49.1, 48.4, 48.2, 46.6, 43.5, 34.7, 34.1, 33.3, 31.9, 31.1, 23.8, 23.6, 15.1, 15.1.

**$^{19}$F NMR (471 MHz, $CDCl_3$)** δ -115.42 (brd, *J* = 33.8 Hz, 2F).

**HRMS (ESI+/TOF, *m/z*):** Exact mass calculated for $[C_{52}H_{57}F_2N_3O_8+H]^+$ requires 890.4192; found 890.4180.



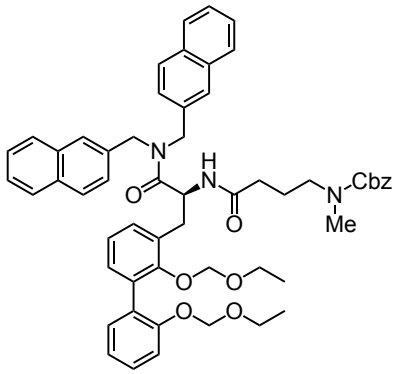

**9m**

**(*S*)-3-(2,2'-bis(ethoxymethoxy)-[1,1'-biphenyl]-3-yl)-2-((5-methoxy-2,4-dimethylphenyl)sulfonamido)-*N*,*N*-bis(2-methoxyethyl)propenamide (9m)** was synthesized following General Procedure 2 from **8m** using **Amine M**. Crude material purified by normal-phase column chromatography using EtOAc/Hx (10-40%) to give **9m** as a white foam (72% yield).

**$^1$H NMR (500 MHz, $CDCl_3$)** δ 7.34 – 7.28 (m, 2H), 7.27 – 7.18 (m, 2H), 7.15 (dd, *J* = 7.5, 1.8 Hz, 1H), 7.10 – 6.92 (m, 4H), 6.04 (d, *J* = 9.2 Hz, 1H), 5.20 – 5.11 (m, 2H), 4.62 – 4.51 (m, 3H), 3.81 (s, 3H), 3.62 (q, *J* = 7.0 Hz, 2H), 3.56 – 3.36 (m, 6H), 3.30 (p, *J* = 5.9, 5.2 Hz, 3H), 3.25 (s, 3H), 3.25 – 3.21 (m, 4H), 3.19 – 3.08 (m, 1H), 2.92 (dd, *J* = 13.8, 5.5 Hz, 1H), 2.39 (s, 3H), 2.18 (s, 3H), 1.17 (t, *J* = 7.1 Hz, 3H), 1.09 (t, *J* = 7.0 Hz, 3H).

**$^{13}$C NMR (126 MHz, $CDCl_3$)** δ 172.1, 155.4, 154.9 (s, 2C), 136.5, 134.8, 132.1, 131.8, 131.6, 131.2, 130.3, 130.1, 129.3, 129.0, 128.9, 123.9, 121.7, 115.4, 110.5, 97.9, 93.6, 70.8, 70.7, 65.6, 64.3, 58.9, 58.9, 55.7, 53.3, 48.4, 46.9, 35.1, 19.0, 16.1, 15.2, 15.2.

**HRMS (ESI+/TOF, *m/z*):** Exact mass calculated for $[C_{36}H_{50}N_2O_{10}S+H]^+$ requires 703.3264; found 703.3264.



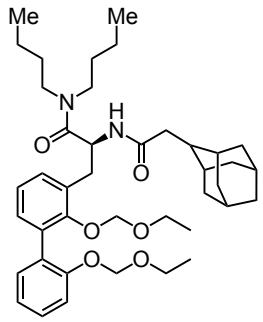
**9n**

**Benzyl (*S*)-(4-((3-(2,2'-bis(ethoxymethoxy)-[1,1'-biphenyl]-3-yl)-1-(bis(naphthalen-2-ylmethyl)amino)-1-oxopropan-2-yl)amino)-4-oxobutyl)(methyl)carbamate (9n)** was synthesized following General Procedure 2 from **8l** using **Amine N**. Crude material purified by normal-phase column chromatography using EtOAc/Hx (50-80%) to give **9n** as an off-white foam (91% yield).

**$^1$H NMR (500 MHz, $CDCl_3$)** δ 7.89 – 7.74 (m, 6H), 7.69 (d, *J* = 1.8 Hz, 1H), 7.63 (s, 1H), 7.55 – 7.43 (m, 4H), 7.43 – 7.27 (m, 7H), 7.25 (s, 1H), 7.21 – 6.90 (m, 5H), 6.84 – 6.58 (m, 2H), 5.38 (s, 1H), 5.13 (d, *J* = 12.6 Hz, 2H), 4.97 (d, *J* = 23.6 Hz, 3H), 4.90 – 4.61 (m, 3H), 4.56 – 4.47 (m, 2H), 3.63 – 3.51 (m, 1H), 3.50 – 3.40 (m, 3H), 3.40 – 3.32 (m, 1H), 3.28 – 3.11 (m, 2H), 2.85 (s, 4H), 2.23 – 2.04 (m, 2H), 1.85 – 1.76 (m, 2H), 1.09 – 1.00 (m, 6H).

**$^{13}$C NMR (126 MHz, $CDCl_3$)** *rotameric mixture*: δ 173.3, 172.3, 172.0, 156.6, 156.3, 154.8, 137.1, 135.4, 134.4, 133.5, 133.5, 133.1, 132.9, 132.8, 132.1, 131.6, 131.1, 130.1, 130.0, 129.1, 129.1, 128.7, 128.6, 128.0, 128.0, 127.9, 127.9, 127.8, 127.2, 126.6, 126.3, 126.0, 125.3, 123.9, 121.8, 115.4, 98.1, 93.5, 67.1, 65.7, 64.1, 50.8, 50.4, 48.9, 48.5, 48.2, 34.8, 34.2, 33.2, 24.0, 23.7, 15.1 (s, 2C).

**HRMS (ESI+/TOF, *m/z*):** Exact mass calculated for $[C_{56}H_{59}N_3O_8+H]^+$ requires 902.4385; found 902.4380.



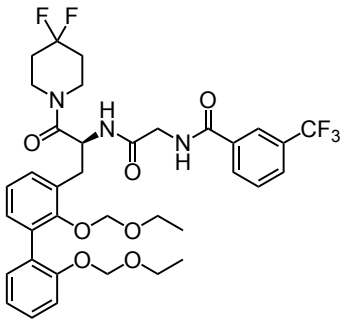

**9o**

**(*S*)-2-(2-((1*S*,3*S*,5*S*,7*S*)-adamantan-2-yl)acetamido)-3-(2,2'-bis(ethoxymethoxy)-[1,1'-biphenyl]-3-yl)-*N*,*N*-dibutylpropanamide (9o)** was synthesized following General Procedure 2 from **8o** using **Amine B.** Crude material purified by normal-phase column chromatography using EtOAc/Hx (0-20%) to give **9o** as a colorless oil (75% yield).

**$^1$H NMR (500 MHz, $CDCl_3$)** δ 7.32 – 7.27 (m, 1H), 7.27 – 7.21 (m, 2H), 7.15 (td, *J* = 7.4, 1.8 Hz, 2H), 7.07 – 7.00 (m, 2H), 6.61 (d, *J* = 8.5 Hz, 1H), 5.26 (td, *J* = 8.8, 6.1 Hz, 1H), 5.17 – 5.10 (m, 2H), 4.59 (q, *J* = 6.3 Hz, 2H), 3.64 – 3.54 (m, 3H), 3.52 – 3.33 (m, 3H), 3.34 – 3.10 (m, 3H), 2.92 (brd, *J* = 14.1, 5.9 Hz, 1H), 2.23 (d, *J* = 8.3 Hz, 2H), 2.11 (d, *J* = 7.8 Hz, 1H), 1.85 – 1.61 (m, 12H), 1.55 – 1.40 (m, 6H), 1.34 (h, *J* = 7.4 Hz, 2H), 1.30 – 1.21 (m, 2H), 1.16 (t, *J* = 7.1 Hz, 3H), 1.08 (t, *J* = 7.0 Hz, 3H), 0.95 (t, *J* = 7.4 Hz, 3H), 0.90 (t, *J* = 7.3 Hz, 3H).

**$^{13}$C NMR (126 MHz, $CDCl_3$)** δ 172.2, 171.9, 154.8, 154.7, 131.9, 131.8, 131.1, 130.5, 130.2, 129.0, 128.9, 123.7, 121.7, 115.6, 98.1, 93.6, 65.6, 64.3, 49.4, 47.7, 46.3, 41.7, 40.3, 39.0, 39.0, 38.4, 34.4, 32.0, 31.8, 31.7, 31.6, 31.5, 29.9, 28.1, 28.0, 20.3, 20.2, 15.2, 15.1, 14.0, 14.0.

**HRMS (ESI+/TOF, *m/z*):** Exact mass calculated for $[C_{41}H_{60}N_2O_6+H]^+$ requires 677.4530; found 677.4536.



**9p**

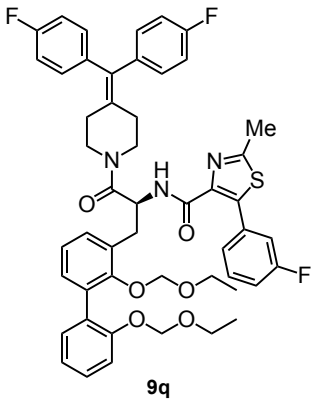
**(*S*)-*N*-(2-((3-(2,2'-bis(ethoxymethoxy)-[1,1'-biphenyl]-3-yl)-1-(4,4-difluoropiperidin-1-yl)-1-oxopropan-2-yl)amino)-2-oxoethyl)-3-(trifluoromethyl)benzamide (9p)** was synthesized following General Procedure 2 from **8p** using **Amine P.** Crude material purified by normal-phase column chromatography using EtOAc/Hx (40-70%) to give **9p** as a yellow foam (70% yield).

**$^{1}$H NMR (500 MHz, $CDCl_3$)** δ 8.08 (s, 1H), 7.97 (d, *J* = 7.8 Hz, 1H), 7.73 (d, *J* = 7.8 Hz, 1H), 7.53 – 7.46 (m, 2H), 7.32 (td, *J* = 7.9, 7.3, 1.7 Hz, 1H), 7.25 – 7.21 (m, 2H), 7.17 (s, 1H), 7.14 (dd, *J* = 7.6, 1.8 Hz, 1H), 7.05 (td, *J* = 7.5, 1.7 Hz, 2H), 5.35 (q, *J* = 7.6 Hz, 1H), 5.14 (s, 2H), 4.61 – 4.53 (m, 2H), 4.17 – 4.05 (m, 2H), 3.70 (qd, *J* = 9.9, 8.4, 3.3 Hz, 3H), 3.60 (qd, *J* = 7.0, 1.5 Hz, 3H), 3.46 (qt, *J* = 7.1, 3.7 Hz, 2H), 3.27 (dd, *J* = 13.2, 7.9 Hz, 1H), 2.98 (dd, *J* = 13.2, 7.0 Hz, 1H), 2.04 – 1.75 (m, 4H), 1.60 – 1.45 (m, 1H), 1.16 (t, *J* = 7.1 Hz, 3H), 1.06 (t, *J* = 7.1 Hz, 3H).

**$^{13}$C NMR (126 MHz, $CDCl_3$)** δ 170.4, 168.4, 166.0, 154.7, 154.5, 134.7, 132.4, 131.8, 131.3 (q, *J* = 33.2 Hz, 1C), 130.5, 129.6, 129.3, 129.3, 128.5, 128.4 (q, *J* = 3.8 Hz, 1C), 124.4 (q, *J* = 3.6 Hz, 1C), 124.0, 123.7 (q, *J* = 274.4 Hz, 1C) 123.4, 122.0, 121.5, 115.6, 98.1, 93.7, 65.8, 64.4, 49.7, 43.2, 42.5, 39.3, 34.3-34.9 (m, 1C), 34.4, 33.4-34.2 (m, 2C), 15.2, 15.1.

**$^{19}$F NMR (471 MHz, $CDCl_3$)** δ -62.75 (s, 3F), -98.19 (s, 2F).

**HRMS (ESI+/TOF, *m/z*):** Exact mass calculated for $[C_{36}H_{40}F_5N_3O_7+H]^+$ requires 722.2865; found 722.2864.



**9q**

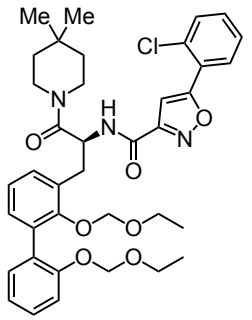
**(*S*)-*N*-(1-(4-(bis(4-fluorophenyl)methylene)piperidin-1-yl)-3-(2,2'-bis(ethoxymethoxy)-[1,1'-biphenyl]-3-yl)-1-oxopropan-2-yl)-5-(3-fluorophenyl)-2-methylthiazole-4-carboxamide (9q)** was synthesized following General Procedure 2 from **8g** using **Amine L.** Crude material purified by normal-phase column chromatography using EtOAc/Hx (10-50%) to give **9q** as a white foam (60% yield).

**$^1$H NMR (500 MHz, $CDCl_3$)** δ 8.22 (d, *J* = 8.9 Hz, 1H), 7.33 – 7.28 (m, 1H), 7.26 – 7.12 (m, 7H), 7.09 – 6.84 (m, 11H), 5.53 (q, *J* = 7.9 Hz, 1H), 5.06 (q, *J* = 7.1 Hz, 2H), 4.64 – 4.53 (m, 2H), 3.68 – 3.41 (m, 6H), 3.41 – 2.96 (m, 4H), 2.69 (s, 3H), 2.36 – 2.12 (m, 3H), 1.98 – 1.82 (m, 1H), 1.12 (t, *J* = 7.1 Hz, 3H), 0.97 (t, *J* = 7.1 Hz, 3H). [1]

**$^3$C NMR (126 MHz, $CDCl_3$)** δ 170.4, 163.7, 162.0 (d, *J* = 246.4 Hz, 1C), 161.8 (d, *J* = 245.6 Hz, 1C), 161.7 (d, *J* = 245.6 Hz, 1C), 160.5, 154.9, 154.5, 141.8, 141.4 (d, *J* = 2,3 Hz, 1C), 137.7 (d, *J* = 2.8 Hz, 1C), 135.6, 134.3, 132.7 (d, *J* = 8.7 Hz, 1C), 132.1, 131.7, 131.3, 131.3 (d, *J* = 7.9 Hz, 2C), 131.2 (d, *J* = 7.9 Hz, 2C), 130.8, 130.4, 129.5 (d, *J* = 8.2 Hz, 1C), 129.0, 128.7, 126.1 (d, *J* = 2.9 Hz, 1C), 123.6, 121.7, 117.5 (d, *J* = 22.8 Hz, 1C), 115.7 (d, *J* = 21.3 Hz, 1C), 115.4, 115.2 (d, *J* = 21.2 Hz, 2C), 115.2 (d, *J* = 21.3 Hz, 2C), 97.7, 93.6, 65.4, 64.3, 48.5, 46.5, 43.5, 35.7, 31.9, 31.1, 19.2, 15.1, 15.1.

**$^{19}$F NMR (471 MHz, $CDCl_3$)** δ -112.99 – -114.21 (m, 1F), -115.10 – -115.85 (m, 2F).

**HRMS (ESI+/TOF, *m/z*):** Exact mass calculated for $[C_{50}H_{48}F_3N_3O_6S+H]^+$ requires 876.3294; found 876.3287.



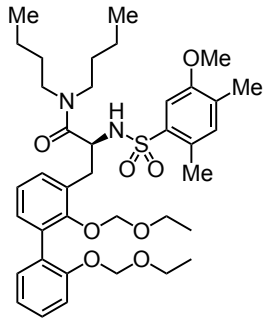

**9r**

**(*S*)-*N*-(3-(2,2'-bis(ethoxymethoxy)-[1,1'-biphenyl]-3-yl)-1-(4,4-dimethylpiperidin-1-yl)-1-oxopropan-2-yl)-5-(2-chlorophenyl)isoxazole-3-carboxamide (9r)** was synthesized following General Procedure 2 from **8r** using **Amine R.** Crude material purified by normal-phase column chromatography using EtOAc/Hx (10-40%) to give **9r** as a white foam (95% yield).

**$^1$H NMR (500 MHz, $CDCl_3$)** δ 7.97 – 7.90 (m, 1H), 7.79 (d, *J* = 8.4 Hz, 1H), 7.54 – 7.47 (m, 1H), 7.43 – 7.34 (m, 2H), 7.34 – 7.27 (m, 3H), 7.26 – 7.22 (m, 1H), 7.22 – 7.15 (m, 2H), 7.05 (q, 2H), 5.55 (q, *J* = 7.7 Hz, 1H), 5.15 (s, 2H), 4.64 (dd, 2H), 3.67 – 3.56 (m, 3H), 3.56 – 3.40 (m, 4H), 3.34 (brm, 2H), 3.14 – 3.07 (m, 1H), 1.37 – 1.21 (m, 3H), 1.17 (t, *J* = 7.1 Hz, 3H), 1.05 (t, *J* = 7.1 Hz, 3H), 0.93 (s, 4H), 0.86 (s, 3H).

**$^{13}$C NMR (126 MHz, $CDCl_3$)** δ 169.4, 167.7, 158.9, 158.2, 154.8, 154.6, 132.1, 132.1, 131.7, 131.5, 131.3, 131.0, 130.7, 129.9, 129.5, 129.0, 128.7, 127.3, 125.9, 123.7, 121.7, 115.3, 104.0, 97.9, 93.5, 65.5, 64.3, 49.0, 42.4, 38.9, 38.8, 38.1, 35.2, 29.1, 28.0, 27.5, 15.2, 15.1.

**HRMS (ESI+/TOF, *m/z*):** Exact mass calculated for $[C_{38}H_{44}ClN_3O_7+H]^+$ requires 690.2946; found 690.2946.



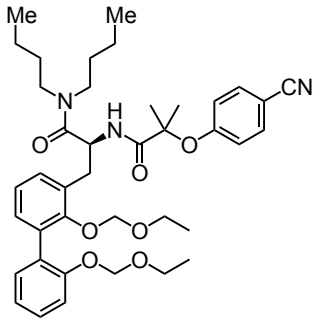

**9s**

**(*S*)-3-(2,2'-bis(ethoxymethoxy)-[1,1'-biphenyl]-3-yl)-*N*,*N*-dibutyl-2-((5-methoxy-2,4-dimethylphenyl)sulfonamido)propenamide (9s)** was synthesized following General Procedure 2 from **8m** using **Amine B.** Crude material purified by normal-phase column chromatography using EtOAc/Hx (0-30%) to give **9s** as a white foam (64% yield).

**$^1$H NMR (500 MHz, $CDCl_3$)** δ 7.35 (s, 1H), 7.29 (ddd, *J* = 8.8, 7.2, 1.8 Hz, 1H), 7.24 (dd, *J* = 8.4, 1.2 Hz, 1H), 7.17 (ddd, *J* = 15.7, 7.5, 1.8 Hz, 2H), 7.08 (dd, *J* = 7.6, 1.8 Hz, 1H), 7.05 – 6.92 (m, 3H), 5.95 (d, *J* = 9.2 Hz, 1H), 5.15 (s, 2H), 4.56 (s, 2H), 4.45 (q, *J* = 8.0 Hz, 1H), 3.81 (s, 3H), 3.61 (q, *J* = 7.0 Hz, 2H), 3.46 – 3.36 (m, 2H), 3.28 – 2.71 (m, 6H), 2.45 (s, 3H), 2.16 (s, 3H), 1.36 – 1.11 (m, 11H), 1.04 (t, *J* = 7.0 Hz, 3H), 0.87 (td, *J* = 7.2, 1.6 Hz, 6H).

**$^{13}$C NMR (126 MHz, $CDCl_3$)** δ 170.8, 155.3, 154.8, 154.2, 136.2, 134.8, 131.8, 131.7, 131.4, 130.7, 129.9, 129.2, 129.0, 128.7, 123.7, 121.6, 115.5, 110.6, 97.8, 93.6, 65.5, 64.3, 55.6, 53.2, 47.3, 46.4, 36.2, 31.0, 29.6, 20.3, 20.1, 19.1, 16.1, 15.2, 15.1, 14.0, 13.7. *Note: tertiary carbon connecting quaternary arm and biphenol not observed*.

**HRMS (ESI+/TOF, *m/z*):** Exact mass calculated for $[C_{38}H_{54}N_2O_8S+H]^+$ requires 699.3679; found 699.3685.



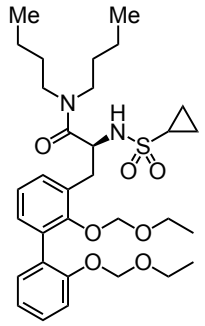

**9t**

**(*S*)-3-(2,2'-bis(ethoxymethoxy)-[1,1'-biphenyl]-3-yl)-*N*,*N*-dibutyl-2-(2-(4-cyanophenoxy)-2-methylpropanamido)propenamide (9t)** was synthesized following General Procedure 2 from **8t** using **Amine B.** Crude material purified by normal-phase column chromatography using EtOAc/Hx (0-30%) to give **9t** as a white foam (78% yield).

**$^1$H NMR (500 MHz, $CDCl_3$)** δ 7.48 – 7.41 (m, 2H), 7.30 (td, *J* = 7.9, 7.2, 1.7 Hz, 2H), 7.26 – 7.14 (m, 3H), 7.07 – 6.94 (m, 3H), 6.86 – 6.80 (m, 2H), 5.23 (td, *J* = 8.7, 5.6 Hz, 1H), 5.14 (q, *J* = 7.0 Hz, 2H), 4.56 (d, *J* = 6.1 Hz, 1H), 4.47 (d, *J* = 6.2 Hz, 1H), 3.60 (q, *J* = 7.0 Hz, 2H), 3.51 – 2.91 (m, 8H), 1.75 – 1.54 (m, 2H), 1.51 (s, 3H), 1.47 – 1.33 (m, 6H), 1.26 (q, *J* = 7.3 Hz, 3H), 1.16 (t, *J* = 7.1 Hz, 3H), 0.99 (dt, *J* = 14.7, 7.2 Hz, 6H), 0.90 (t, *J* = 7.3 Hz, 3H).

**$^{13}$C NMR (126 MHz, $CDCl_3$)** δ 173.2, 171.0, 158.5, 154.7, 154.3, 133.5, 132.0, 131.5, 131.2, 130.1, 129.9, 129.0, 128.4, 123.7, 121.6, 120.2, 118.9, 115.4, 105.5, 97.8, 93.5, 81.7, 65.4, 64.1, 49.7, 47.5, 46.1, 34.1, 31.3, 29.7, 25.0, 25.0, 20.1, 20.1, 15.1, 15.0, 13.9, 13.8.

**HRMS (ESI+/TOF, *m/z*):** Exact mass calculated for $[C_{40}H_{53}N_3O_7+H]^+$ requires 688.3962; found 688.3950.



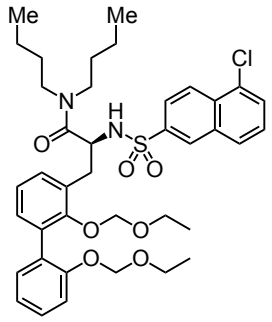

**9u**

**(*S*)-3-(2,2'-bis(ethoxymethoxy)-[1,1'-biphenyl]-3-yl)-*N*,*N*-dibutyl-2-(cyclopropanesulfonamido)propenamide (9u)** was synthesized following General Procedure 2 from **8u** using **Amine B**. Crude material purified by normal-phase column chromatography using EtOAc/Hx (10-40%) to give **9u** as a yellowish oil (41% yield).

**$^1$H NMR** (500 MHz, $CDCl_3$) δ 7.34 – 7.20 (m, 4H), 7.16 (dd, *J* = 7.6, 1.8 Hz, 1H), 7.08 – 7.02 (m, 2H), 5.72 – 5.69 (m, 1H), 5.18 (q, *J* = 7.1 Hz, 2H), 4.68 – 4.54 (m, 3H), 3.68 – 3.53 (m, 2H), 3.38 (dt, *J* = 14.1, 7.1 Hz, 1H), 3.35 – 3.27 (m, 1H), 3.17 – 3.02 (m, 3H), 2.96 (dd, *J* = 13.5, 9.9 Hz, 1H), 1.89 (t, *J* = 4.7 Hz, 1H), 1.70 – 1.44 (m, 4H), 1.38 – 1.27 (m, 4H), 1.16 (t, *J* = 7.1 Hz, 3H), 1.03 (t, *J* = 7.1 Hz, 3H), 0.97 – 0.90 (m, 8H), 0.63 (d, *J* = 8.3 Hz, 2H).

**$^{13}$C NMR** (126 MHz, $CDCl_3$) δ 171.6, 155.1, 154.1, 132.0, 131.4 (brs, 2C), 131.2, 130.6, 129.1, 128.5, 123.8, 121.7, 115.3, 97.7, 93.6, 65.6, 64.2, 54.2, 47.3, 46.2, 36.1, 31.3, 31.1, 29.8, 20.25, 20.18, 15.2, 15.1, 13.9, 13.8, 5.6, 5.5.

**HRMS (ESI+/TOF, *m/z*):** Exact mass calculated for $[C_{32}H_{47}N_2O_7S+H]^+$ requires 605.3260; found 605.3271.



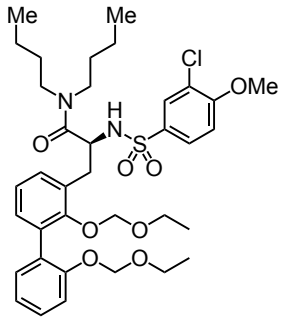

**9v**

**(*S*)-3-(2,2'-bis(ethoxymethoxy)-[1,1'-biphenyl]-3-yl)-*N*,*N*-dibutyl-2-((5-chloronaphthalene)-2-sulfonamido)propanamide (9v)** was synthesized following General Procedure 2 from **8v** using **Amine B**. Crude material purified by normal-phase column chromatography using EtOAc/Hx (10-40%) to give **9v** as a yellowish oil (70% yield).

**$^1$H NMR** (500 MHz, $CDCl_3$) δ 8.26 (s, 1H), 8.21 (d, *J* = 8.9 Hz, 1H), 7.76 (d, *J* = 8.2 Hz, 1H), 7.72 (dd, *J* = 8.9, 1.8 Hz, 1H), 7.67 (d, *J* = 7.4 Hz, 1H), 7.45 (t, *J* = 7.8 Hz, 1H), 7.35 – 7.24 (m, 2H), 7.10 (m, 2H), 7.01 (t, *J* = 7.3 Hz, 1H), 6.97 (dd, *J* = 7.5, 1.7 Hz, 1H), 6.83 (t, *J* = 7.5 Hz, 1H), 6.14 (d, *J* = 9.1 Hz, 1H), 5.19 (s, 2H), 4.55 (brs, 3H), 3.62 (q, *J* = 7.1 Hz, 2H), 3.45 – 3.35 (m, 2H), 3.28 (dt, *J* = 15.5, 7.9 Hz, 1H), 3.22 – 3.16 (m, 1H), 3.05 (brt, *J* = 11.6 Hz, 1H), 3.00 – 2.87 (m, 3H), 1.34 – 1.25 (m, 2H), 1.22 – 1.11 (m, 9H), 1.06 (t, *J* = 7.1 Hz, 3H), 0.83 (dt, *J* = 22.8, 7.1 Hz, 6H).

**$^{13}$C NMR** (126 MHz, $CDCl_3$) δ 170.7, 154.9, 154.2, 138.8, 133.3, 132.14, 132.07, 131.8, 131.5, 131.4, 130.6, 129.8, 129.1, 128.7, 128.6, 128.4, 128.2, 127.2, 125.9, 123.9, 123.7, 121.7, 115.4, 97.8, 93.6, 65.6, 64.3, 53.9, 47.3, 46.3, 35.7, 31.1, 29.6, 20.2, 20.1, 15.2, 15.1, 13.83, 13.78.

**HRMS (ESI+/TOF, *m/z*):** Exact mass calculated for $[C_{39}H_{49}ClN_2O_7S+H]^+$ requires 725.3027; found 725.3034.



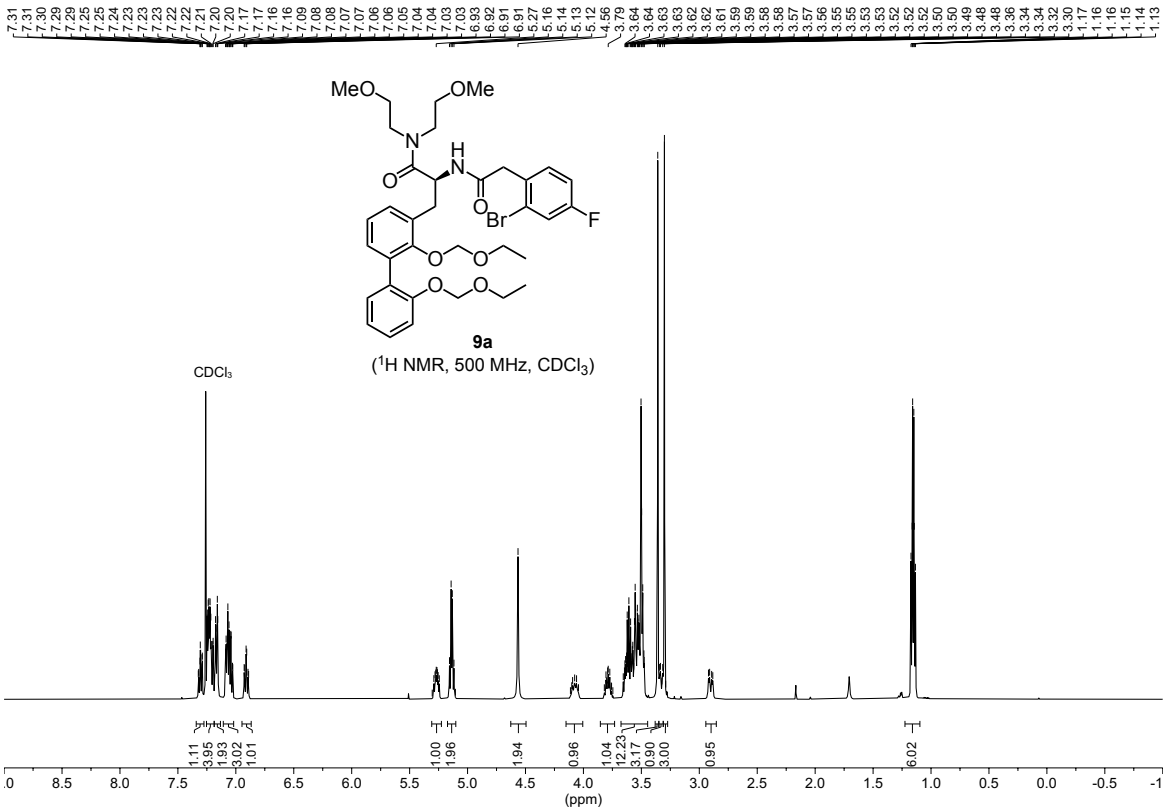

**9w**

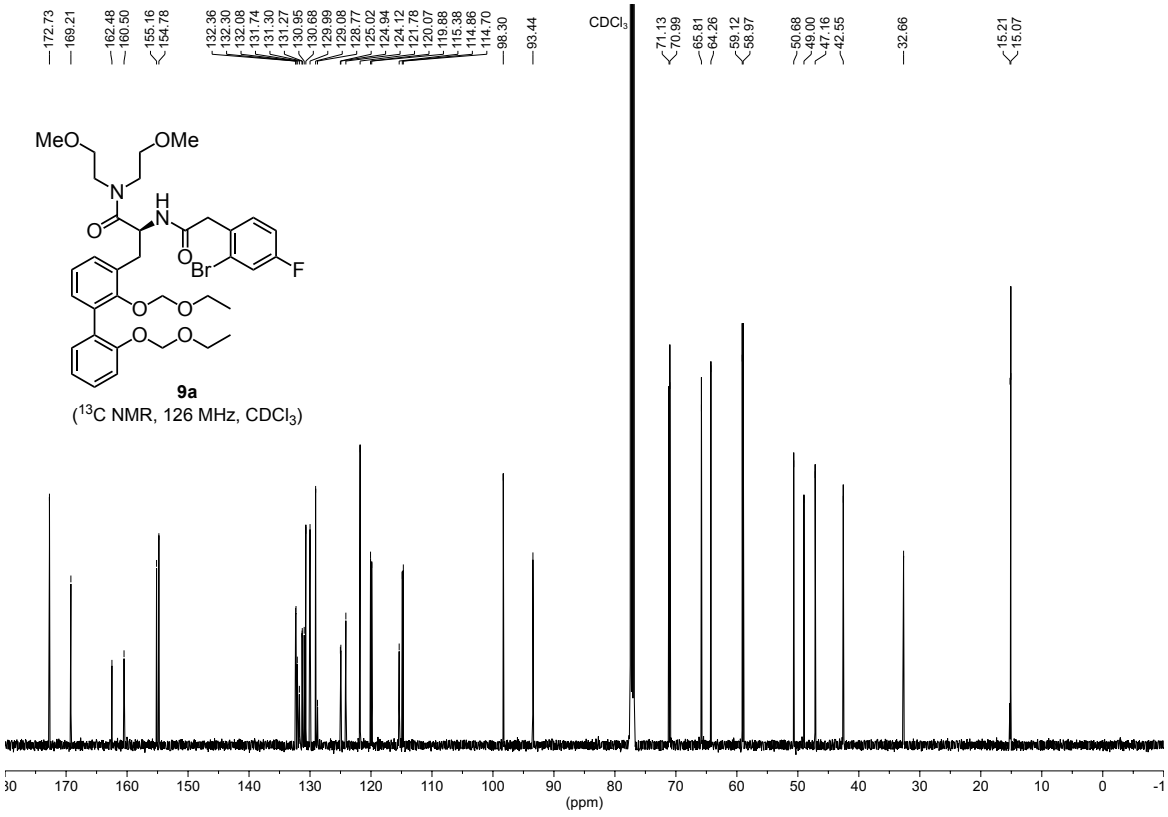
**(*S*)-3-(2,2'-bis(ethoxymethoxy)-[1,1'-biphenyl]-3-yl)-*N*,*N*-dibutyl-2-((3-chloro-4-methoxyphenyl)sulfonamido)propenamide (9w)** was synthesized following General Procedure 2 from **8w** using **Amine B**. Crude material purified by normal-phase column chromatography using EtOAc/Hx (10-40%) to give **9w** as a yellowish oil (53% yield).

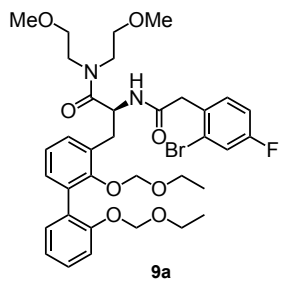
**$^1$H NMR** (500 MHz, $CDCl_3$) δ 7.69 (d, *J* = 2.3 Hz, 1H), 7.56 – 7.51 (m, 1H), 7.31 (td, *J* = 7.8, 7.2, 1.7 Hz, 1H), 7.27 (m, 1H), 7.21 – 7.13 (m, 2H), 7.07 – 7.02 (m, 2H), 6.99 (t, *J* = 7.5 Hz, 1H), 6.82 (d, *J* = 8.7 Hz, 1H), 5.93 (brd, *J* = 9.1 Hz, 1H), 5.18 (s, 2H), 4.56 (s, 2H), 4.44 (brs, 1H), 3.88 (s, 3H), 3.63 (q, *J* = 7.1 Hz, 2H), 3.44 – 3.24 (m, 4H), 3.05 – 2.88 (m, 4H), 1.48 – 1.12 (m, 11H), 1.05 (t, *J* = 7.0 Hz, 3H), 0.92 (dt, *J* = 25.8, 7.2 Hz, 6H). **[1]**

**$^3$C NMR** (126 MHz, $CDCl_3$) δ 170.7, 157.9, 154.9, 154.1, 133.2, 131.8, 131.6, 131.4, 130.7, 129.8, 129.2, 129.0, 128.6, 127.5, 123.7, 122.6, 121.6, 115.4, 111.6, 97.7, 93.6, 65.5, 64.2, 60.4, 56.4, 53.7, 47.3, 46.3, 35.7, 31.1, 29.6, 20.2, 20.1, 15.13, 15.06, 13.9, 13.8.

**HRMS (ESI+/TOF, *m/z*):** Exact mass calculated for $[C_{36}H_{49}ClN_2O_8S+H]^+$ requires 705.2976; found 705.2979.


MeO
OMe
N
H
N
O
O
Br
F
O
O
O
O
9a
(1H NMR, 500 MHz, CDCl3)
CDCl3
1.11
3.95
1.93
3.02
1.01
1.00
1.96
1.94
0.96
1.04
12.23
3.17
0.90
3.00
0.95
6.02
(ppm)

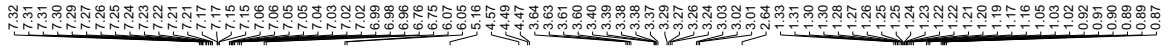

172.73
169.21
162.48
160.50
155.16
154.78
132.36
132.30
132.08
131.74
131.30
131.27
130.95
130.68
129.99
129.08
128.77
125.02
124.94
124.12
121.78
120.07
119.88
115.38
114.86
114.70
98.30
93.44
CDCl3
71.13
70.99
65.81
64.26
59.12
58.97
50.68
49.00
47.16
42.55
32.66
15.21
15.07
MeO
OMe
N
H
N
O
O
Br
F
O
O
O
O
9a
(13C NMR, 126 MHz, CDCl3)
(ppm)

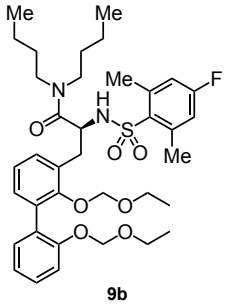


**9a**

($^{19}$F NMR, 471 MHz, $CDCl_3$)

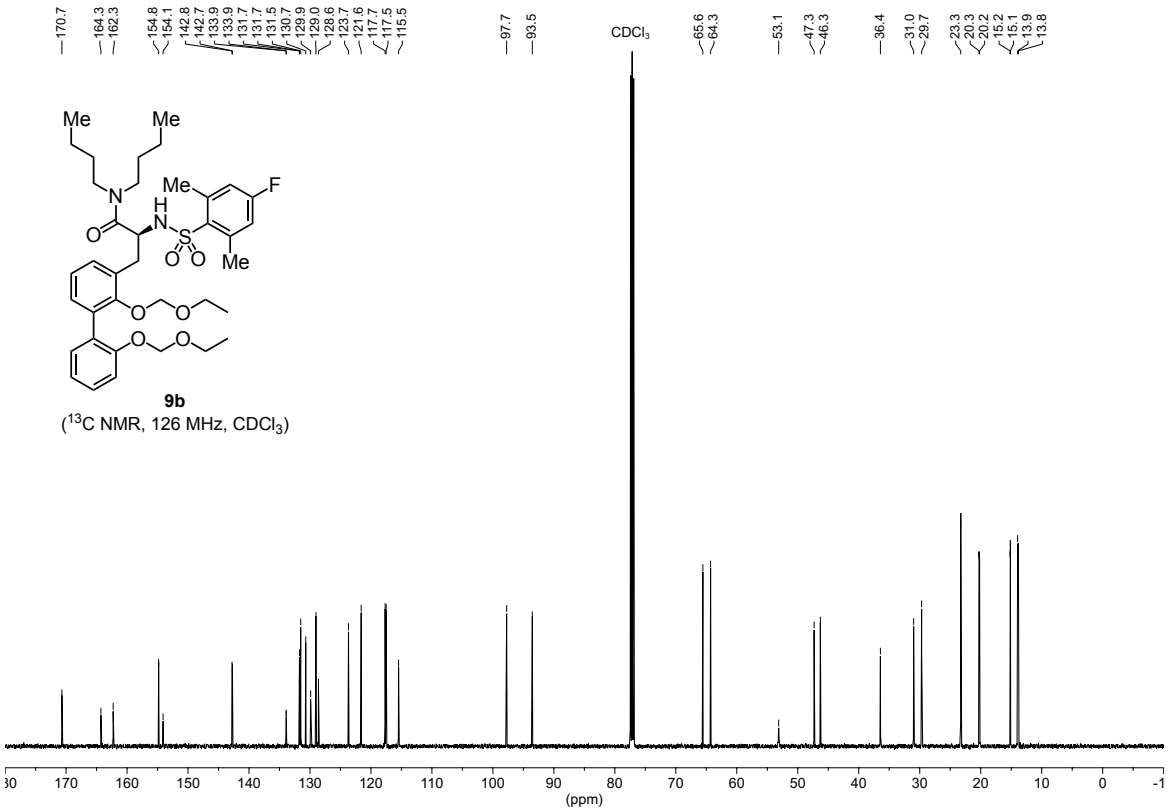




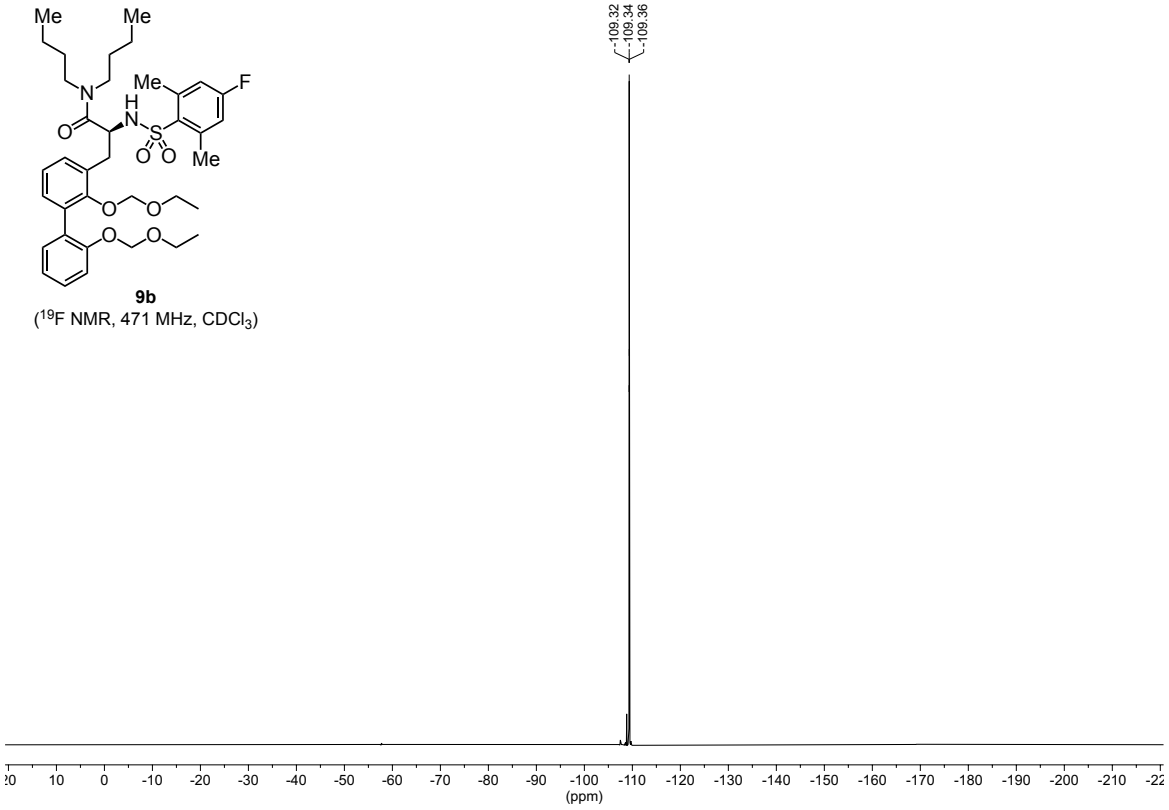
**9b**

($^{1}$H NMR, 500 MHz, $CDCl_3$)



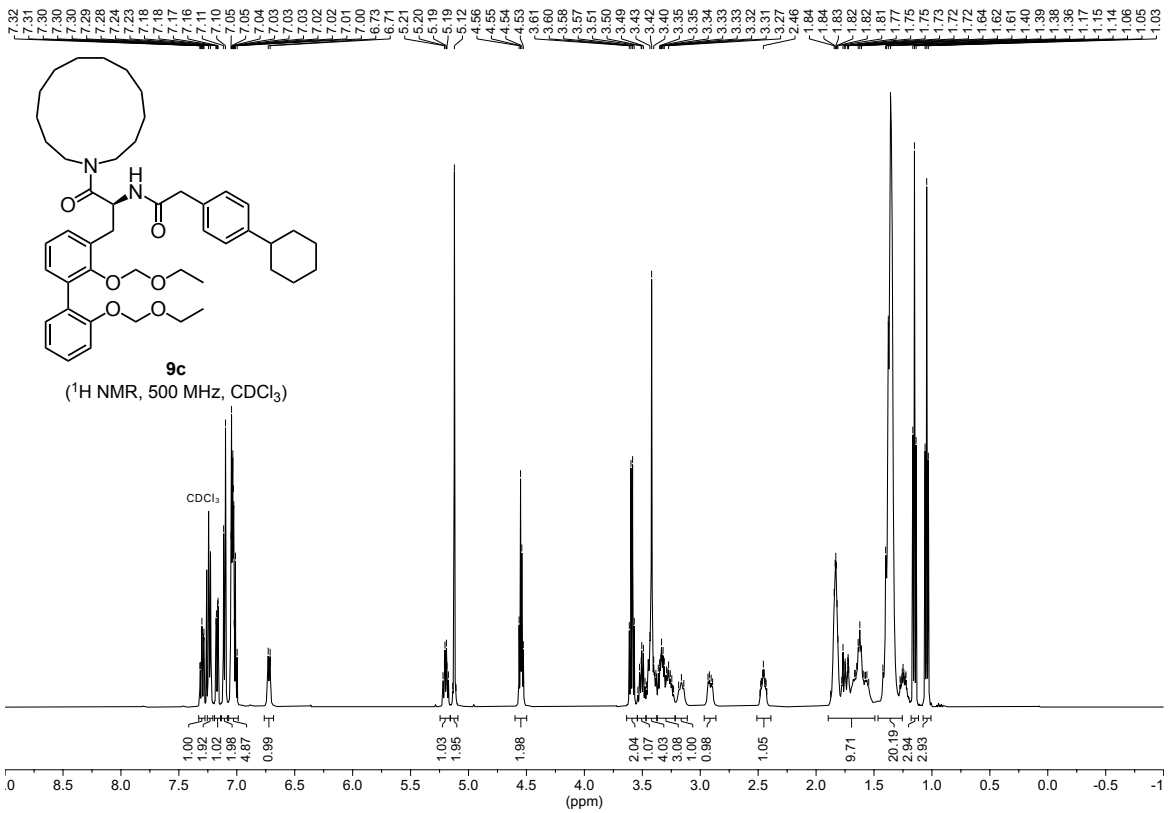

**9b**

($^{13}$C NMR, 126 MHz, $CDCl_3$)



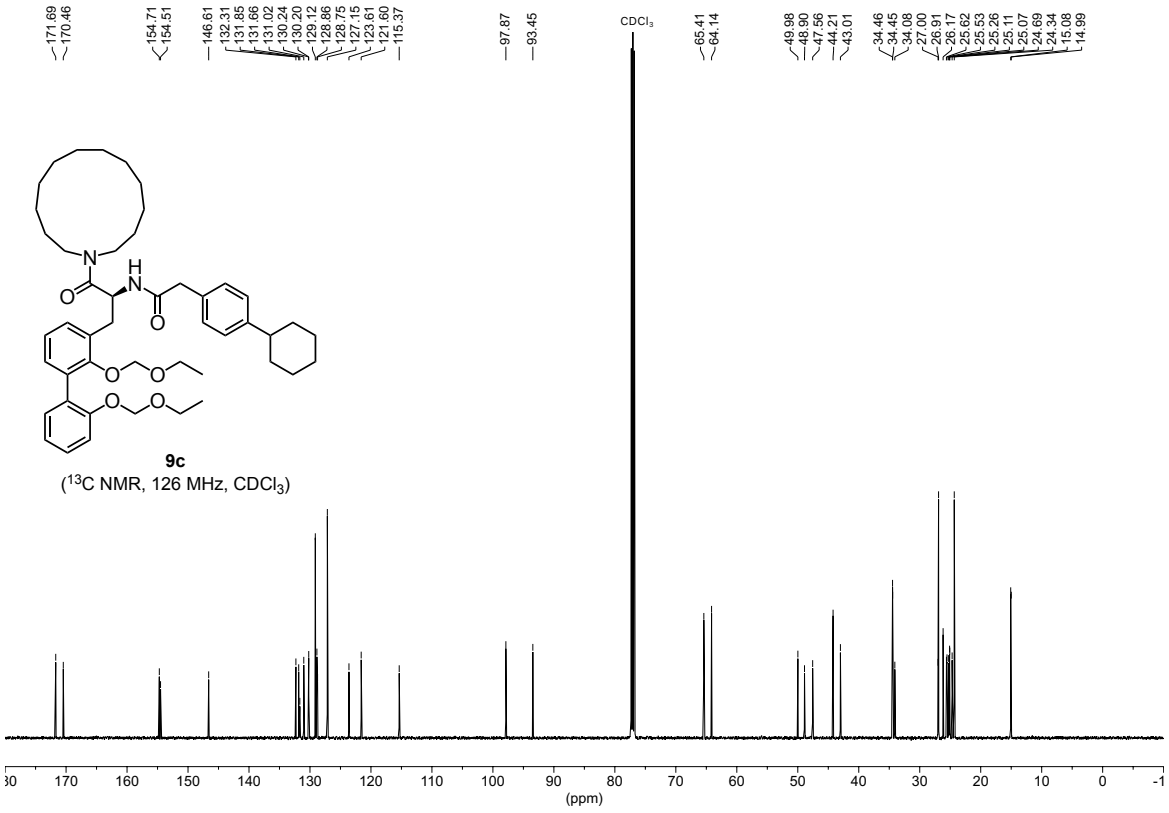

**9b**

($^{19}$F NMR, 471 MHz, $CDCl_3$)



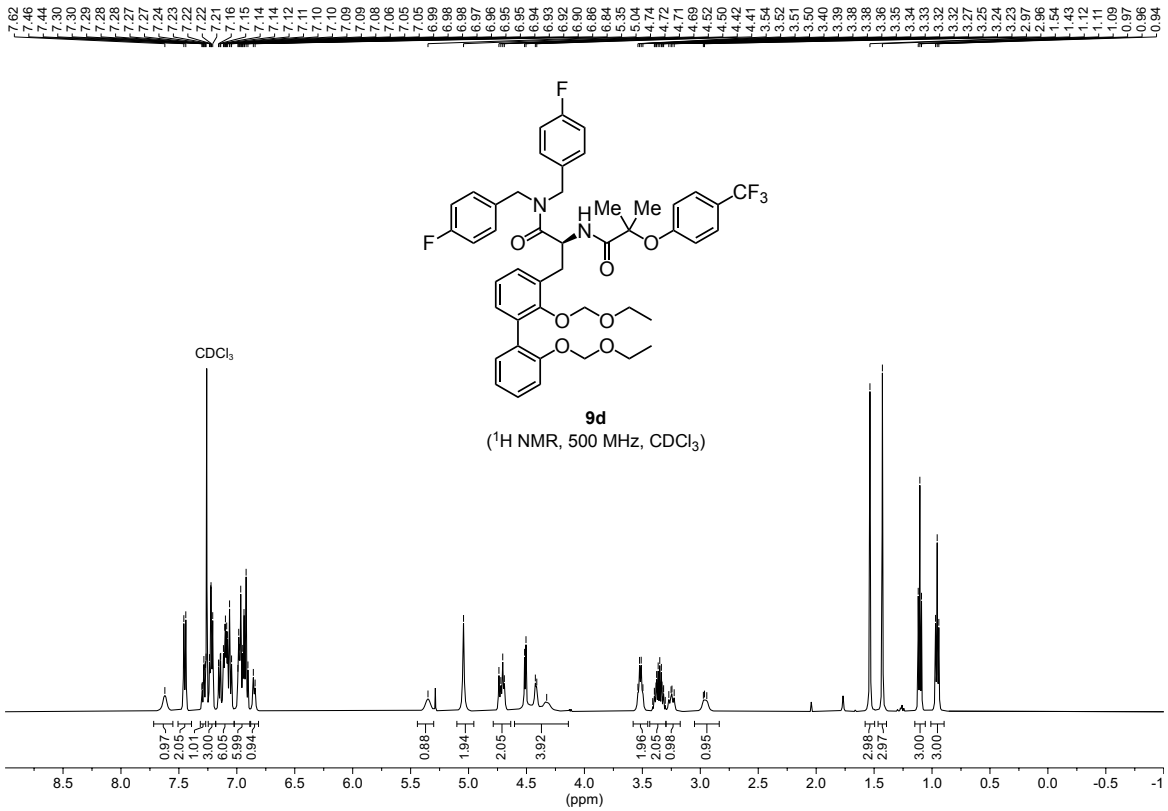

**9c**

($^1$H NMR, 500 MHz, $CDCl_3$)

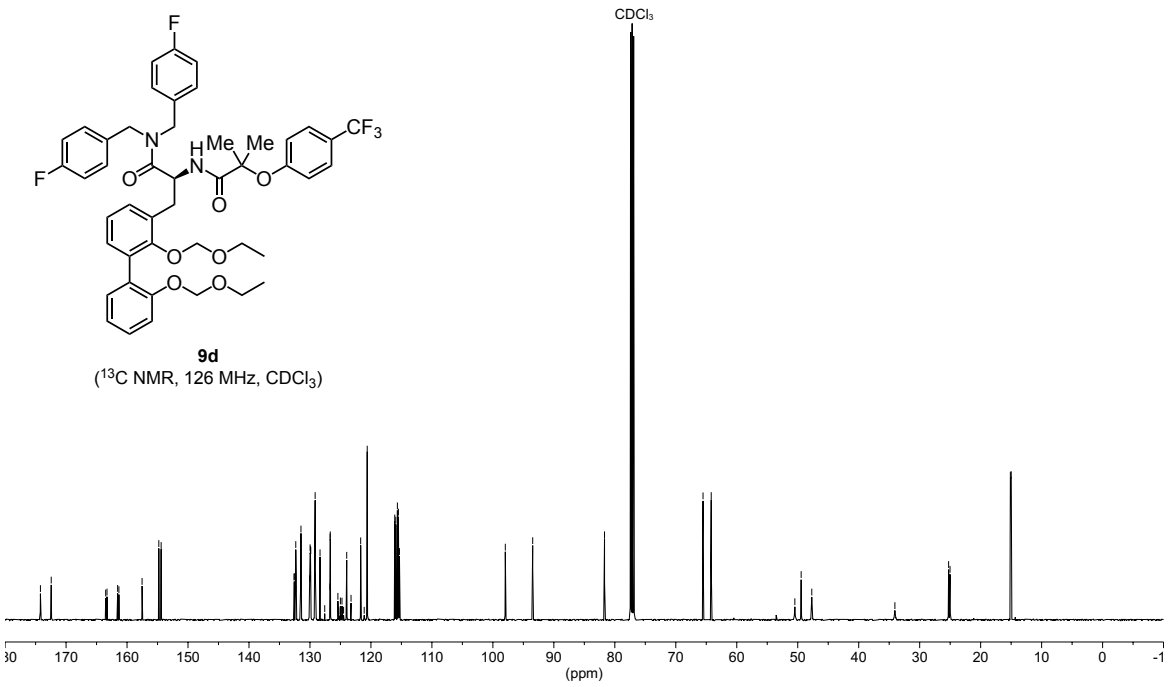



**9c**

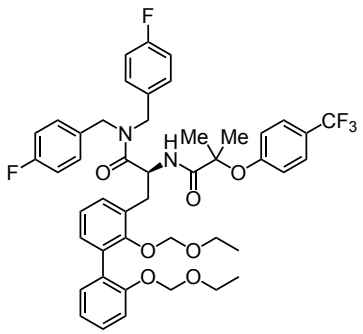
($^{13}$C NMR, 126 MHz, $CDCl_3$)




**9d**
($^{1}$H NMR, 500 MHz, $CDCl_3$)

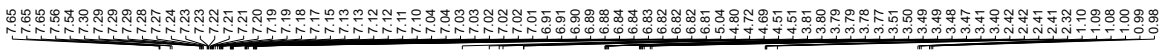


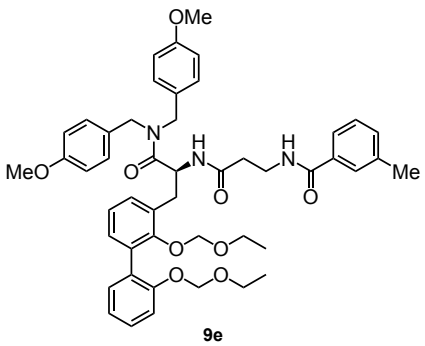

**9d**
($^{13}$C NMR, 126 MHz, $CDCl_3$)



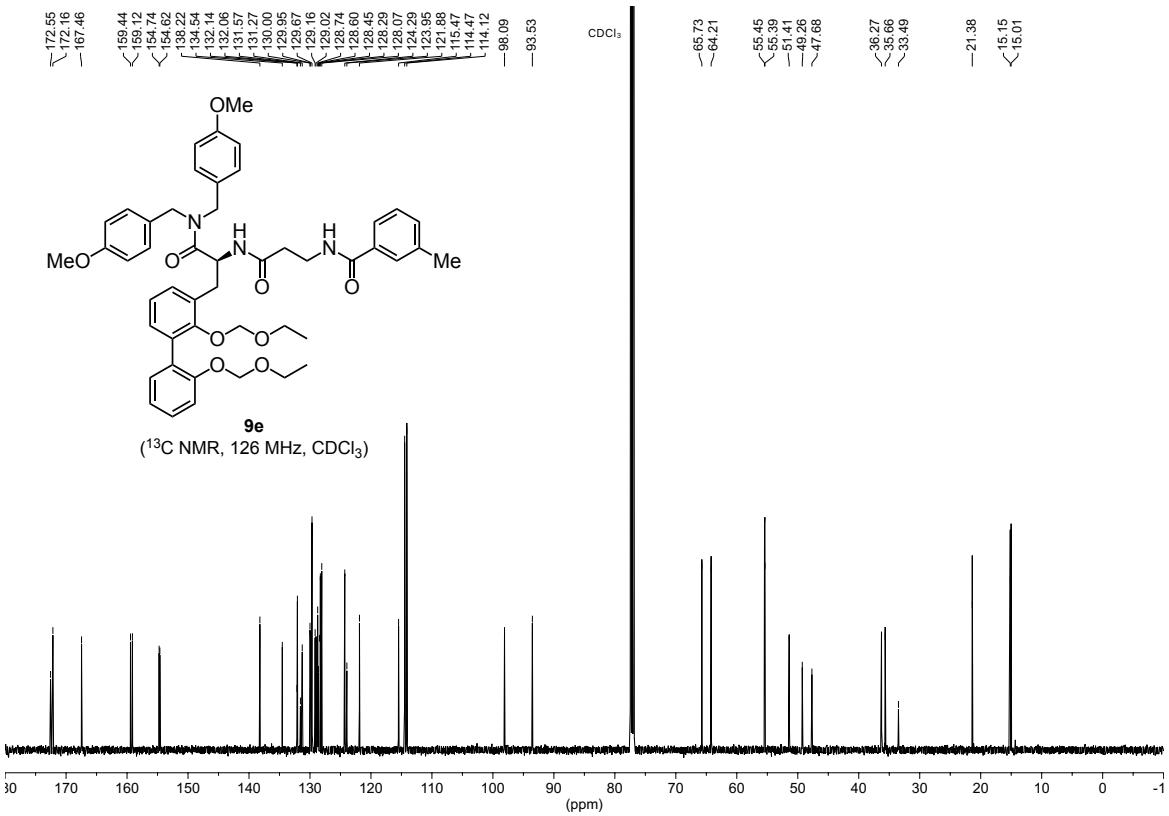
**9d**
($^{19}$F NMR, 471 MHz, $CDCl_3$)





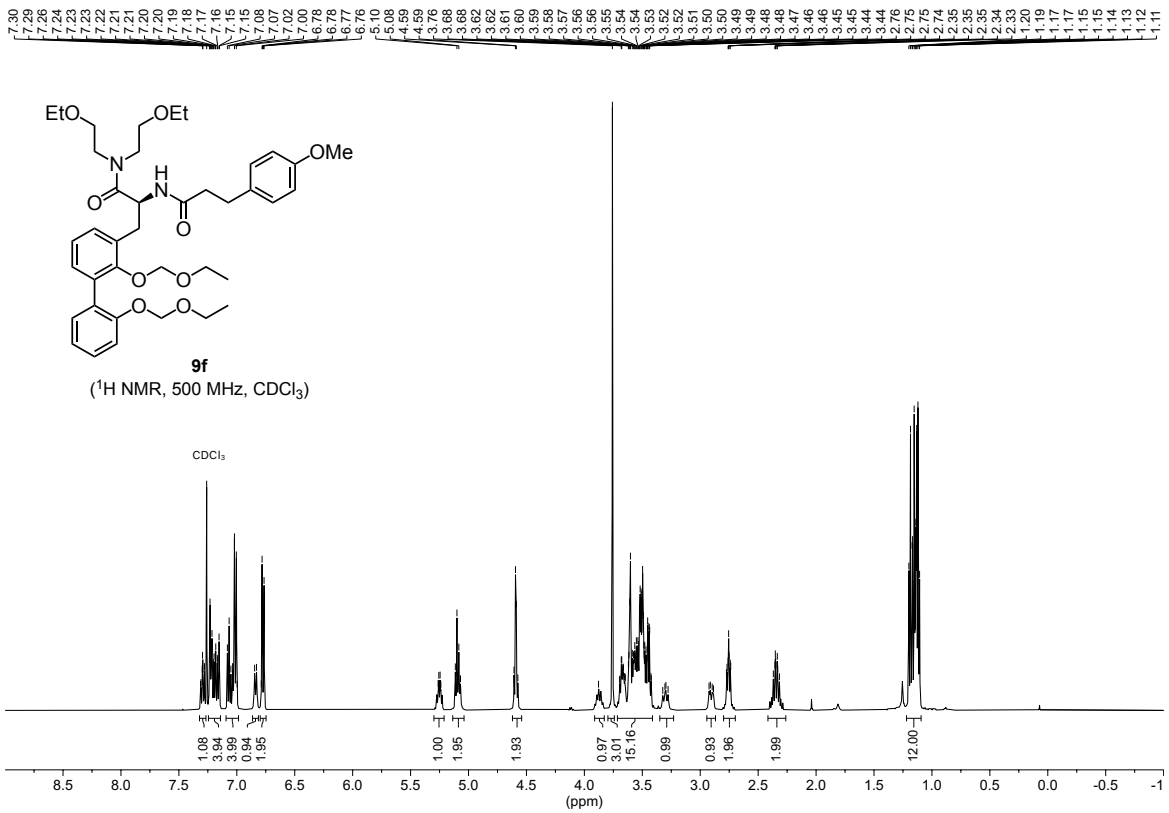


**9e**
($^{1}$H NMR, 500 MHz, $CDCl_3$)



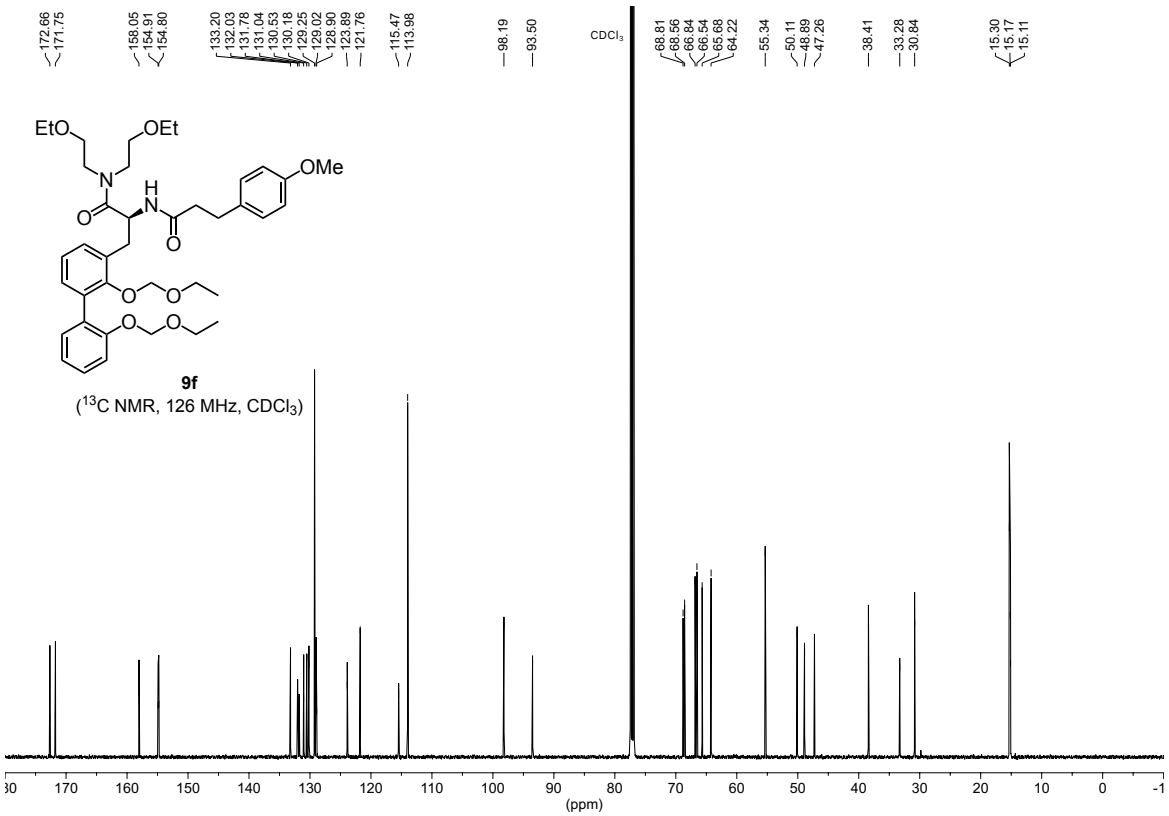

**9e**

($^{13}$C NMR, 126 MHz, $CDCl_3$)




**9f**

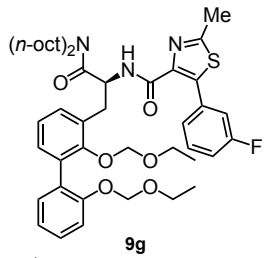
($^{1}$H NMR, 500 MHz, $CDCl_3$)



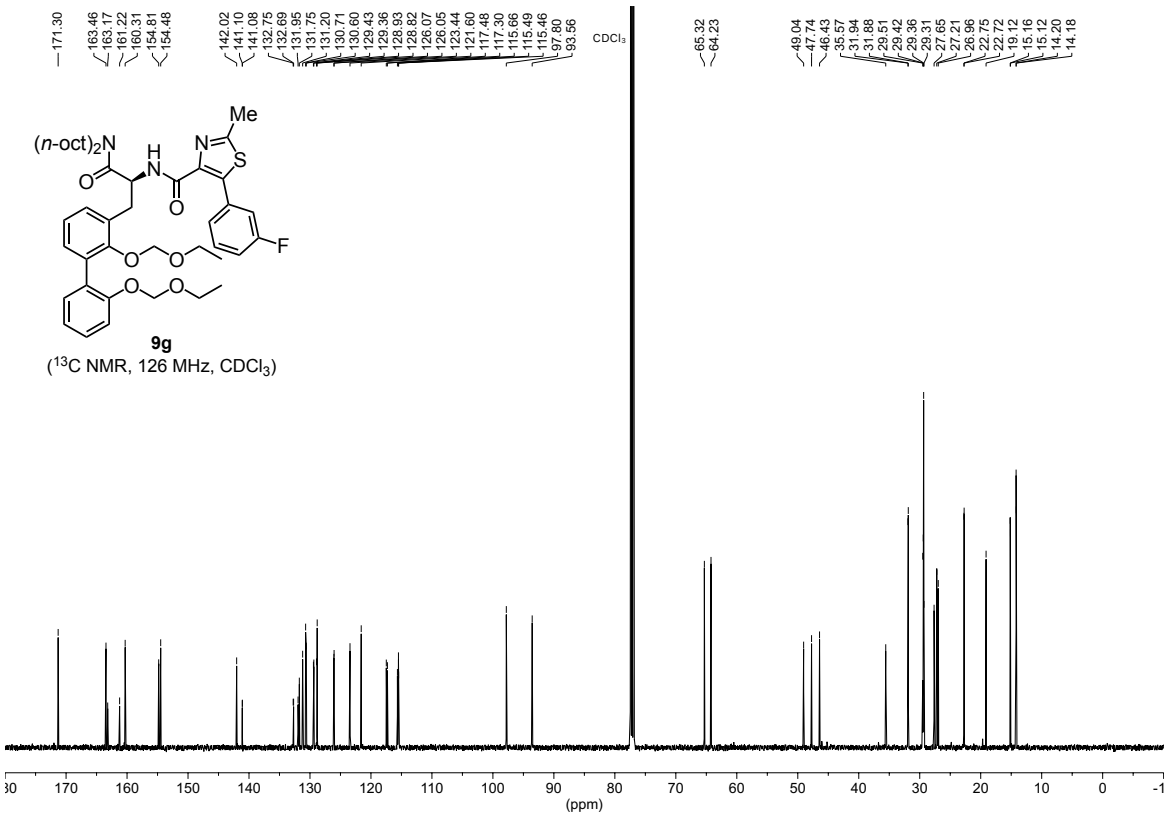

**9f**
($^{13}$C NMR, 126 MHz, $CDCl_3$)





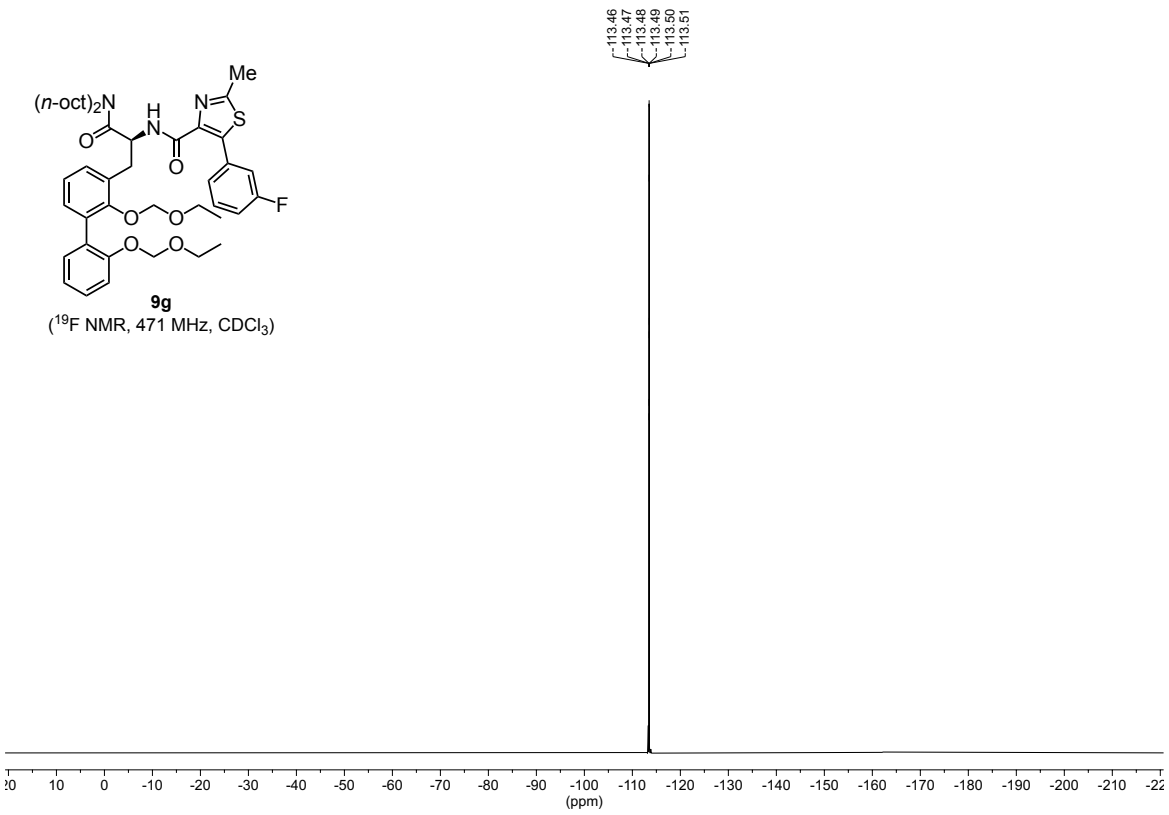




**9g**
($^{1}$H NMR, 500 MHz, $CDCl_3$)



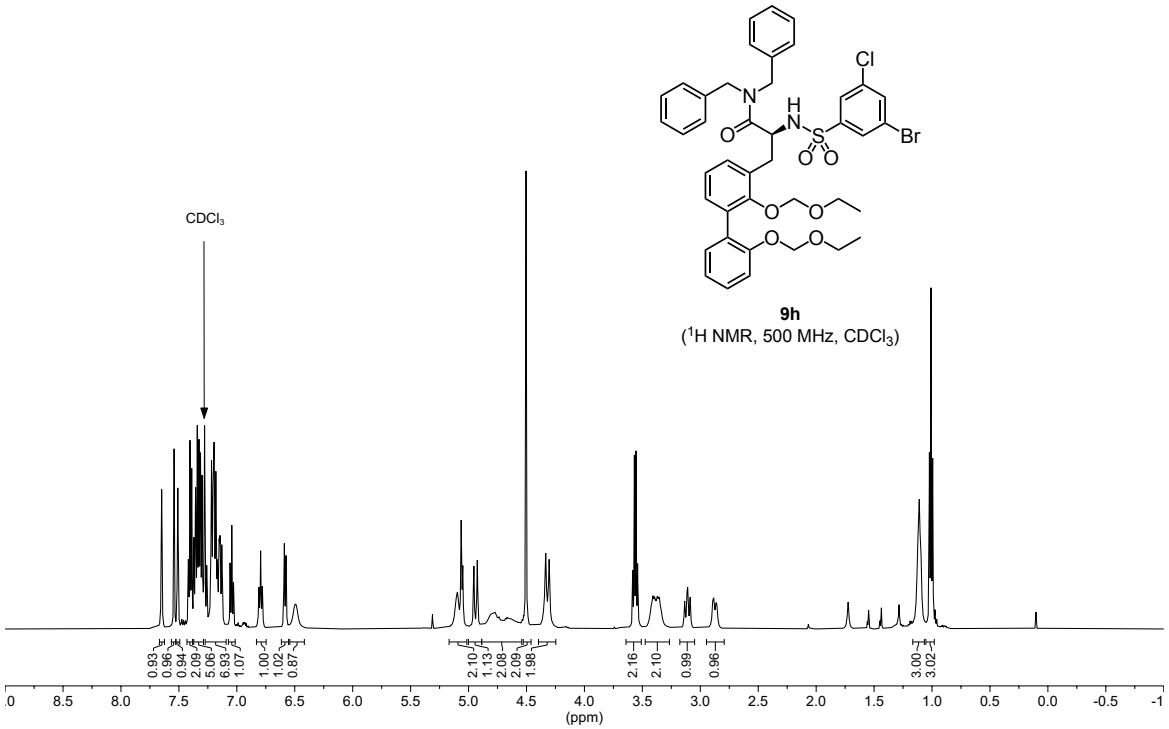

**9g**

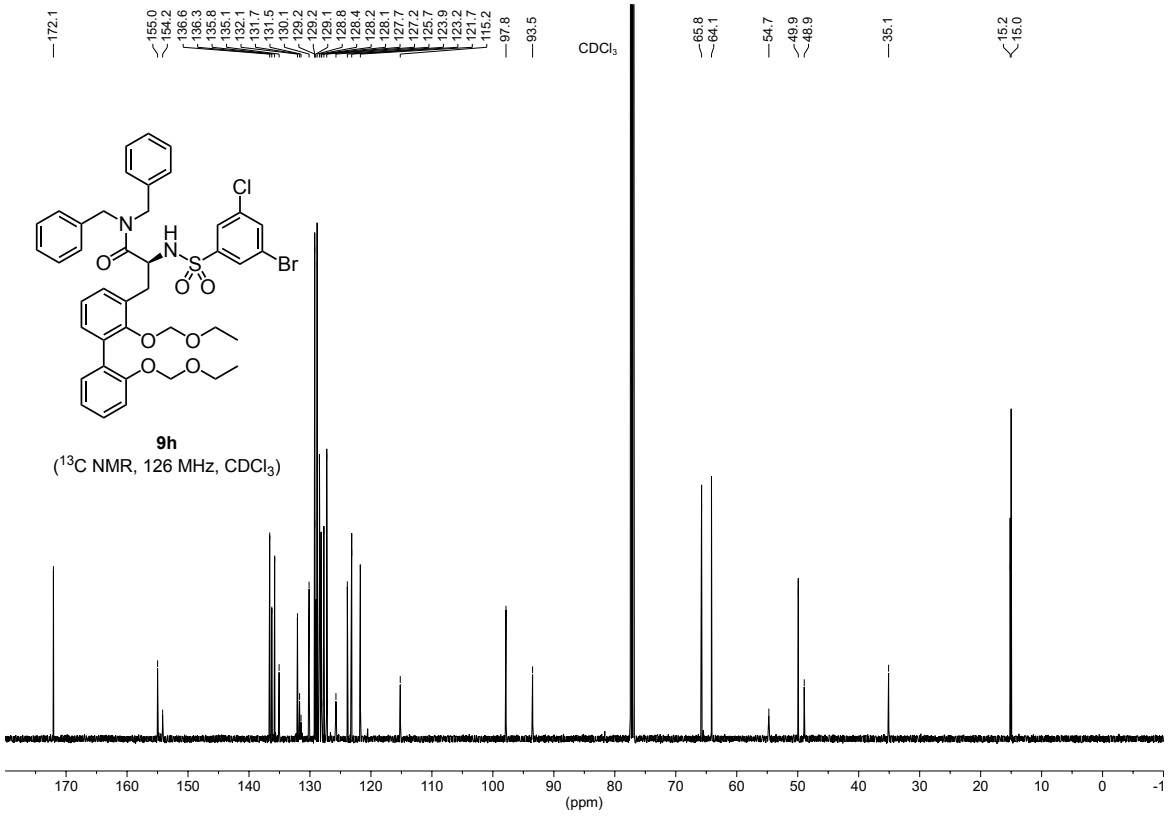
($^{13}$C NMR, 126 MHz, $CDCl_3$)

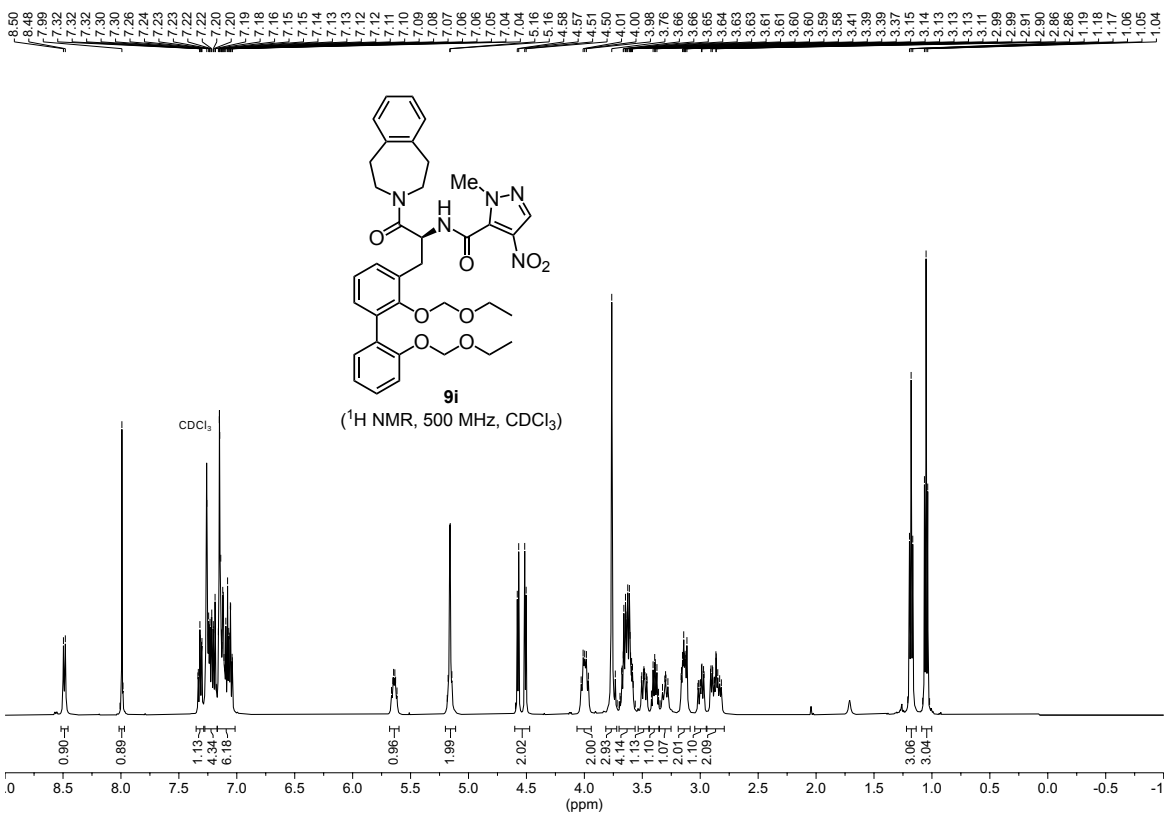



**9g**

($^{19}$F NMR, 471 MHz, $CDCl_3$)

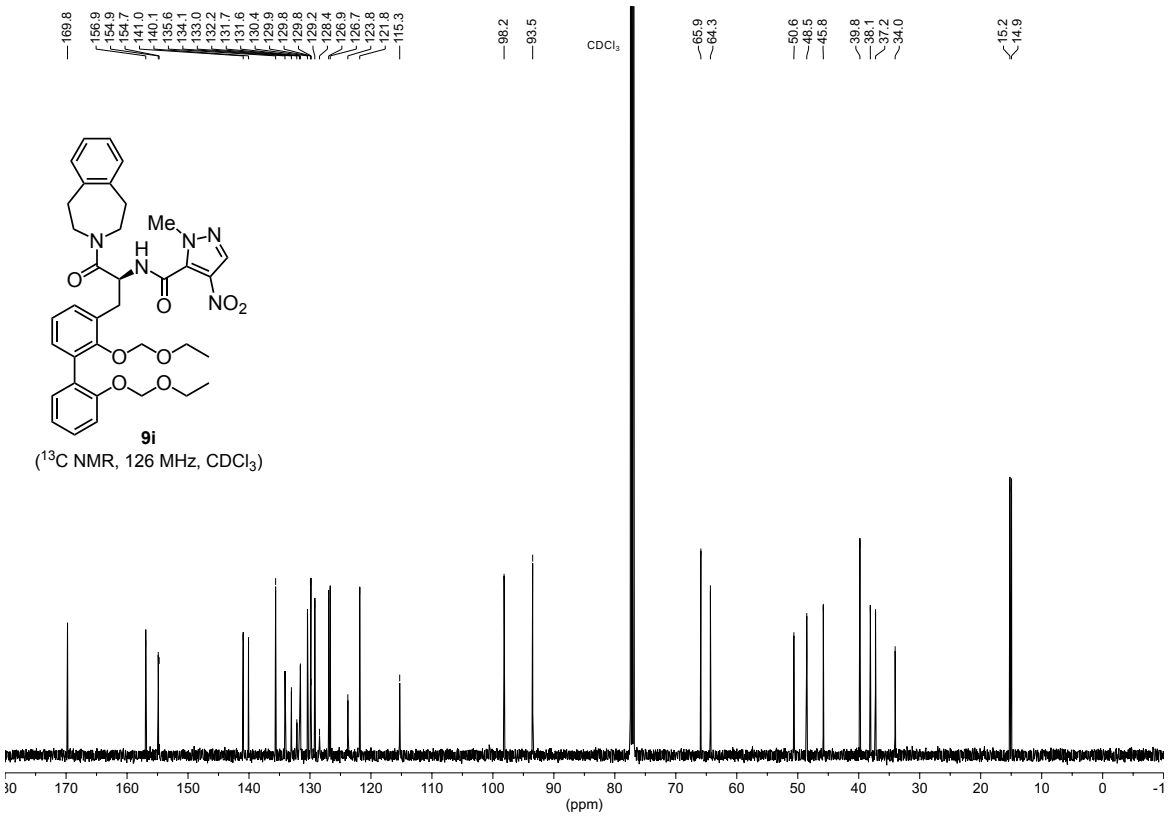

CDCl3
Cl
Br
9h
(1H NMR, 500 MHz, CDCl3)
0.93
0.96
0.94
2.09
5.06
6.93
1.07
1.00
1.02
0.87
2.10
1.13
2.08
2.09
1.98
2.16
2.10
0.99
0.96
3.00
3.02
(ppm)


172.1
155.0
154.2
136.6
136.3
135.8
135.1
132.1
131.7
131.5
130.1
129.2
129.2
129.1
128.8
128.4
128.2
128.1
127.7
127.2
125.7
123.9
123.2
121.7
115.2
97.8
93.5
CDCl3
65.8
64.1
54.7
49.9
48.9
35.1
15.2
15.0
Cl
Br
9h
(13C NMR, 126 MHz, CDCl3)
(ppm)



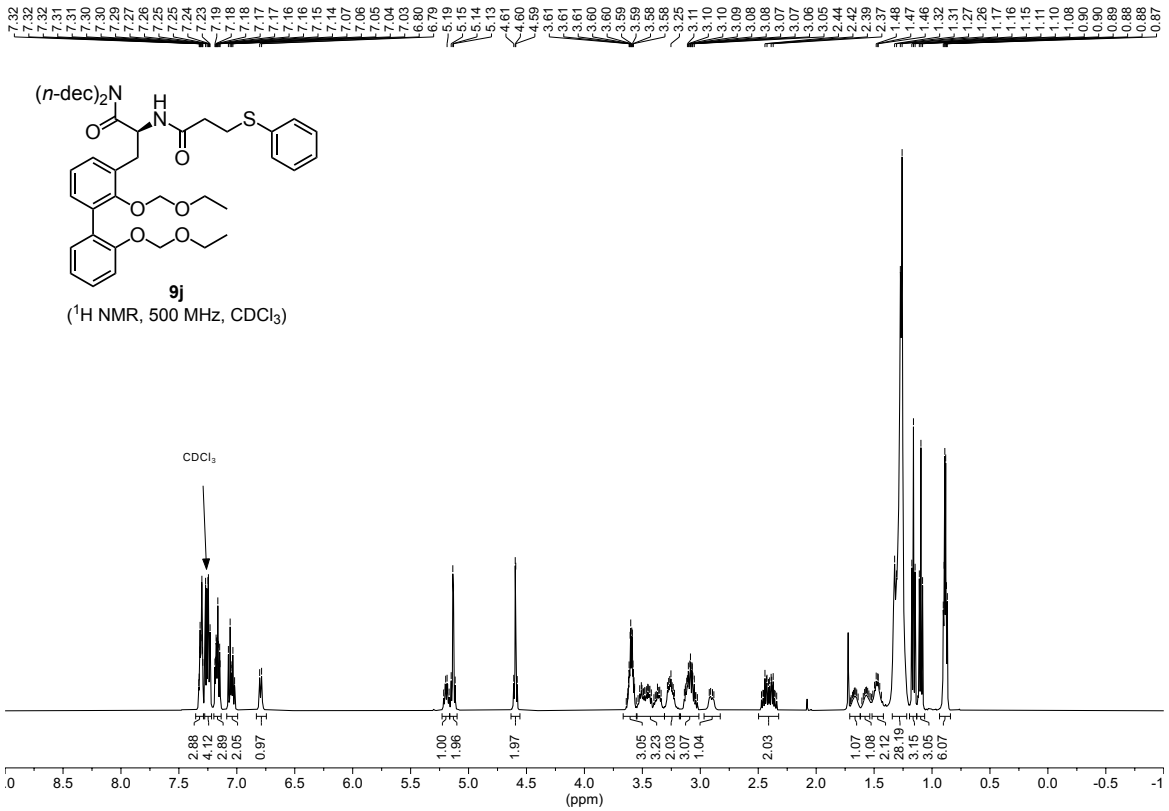

**9i**

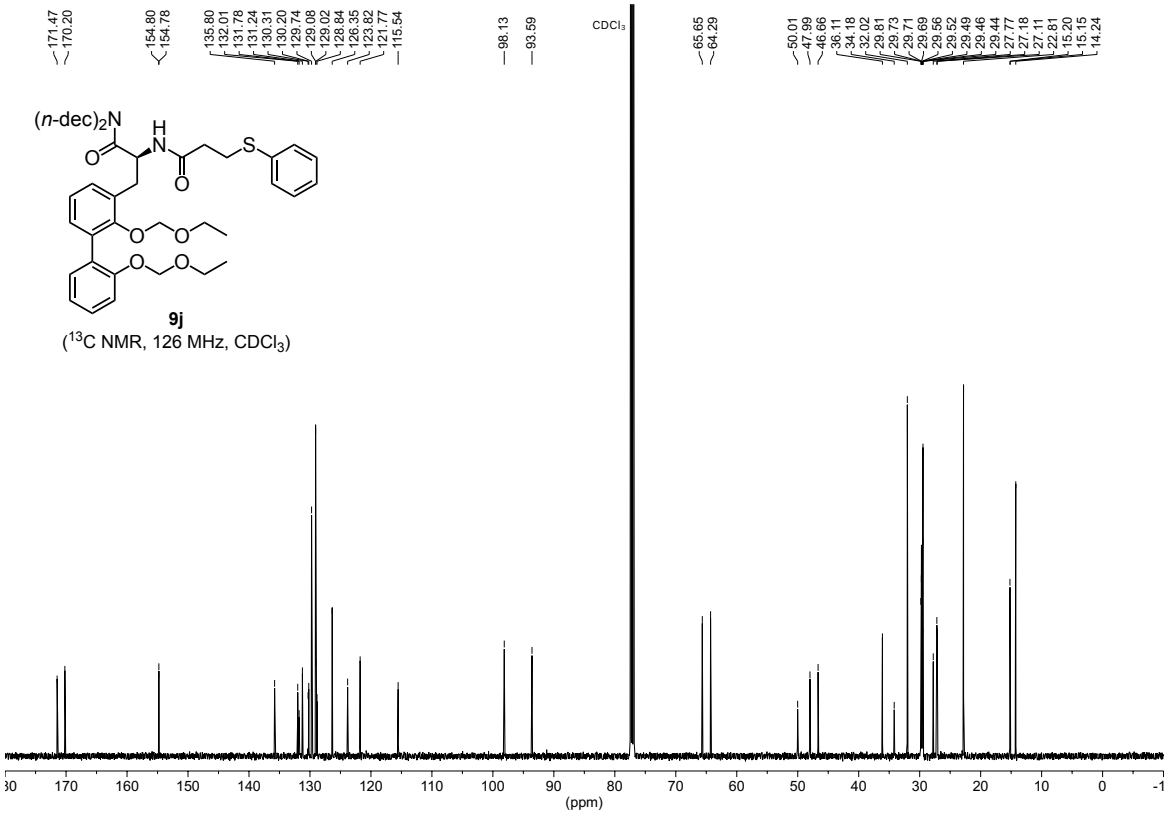
($^1$H NMR, 500 MHz, $CDCl_3$)

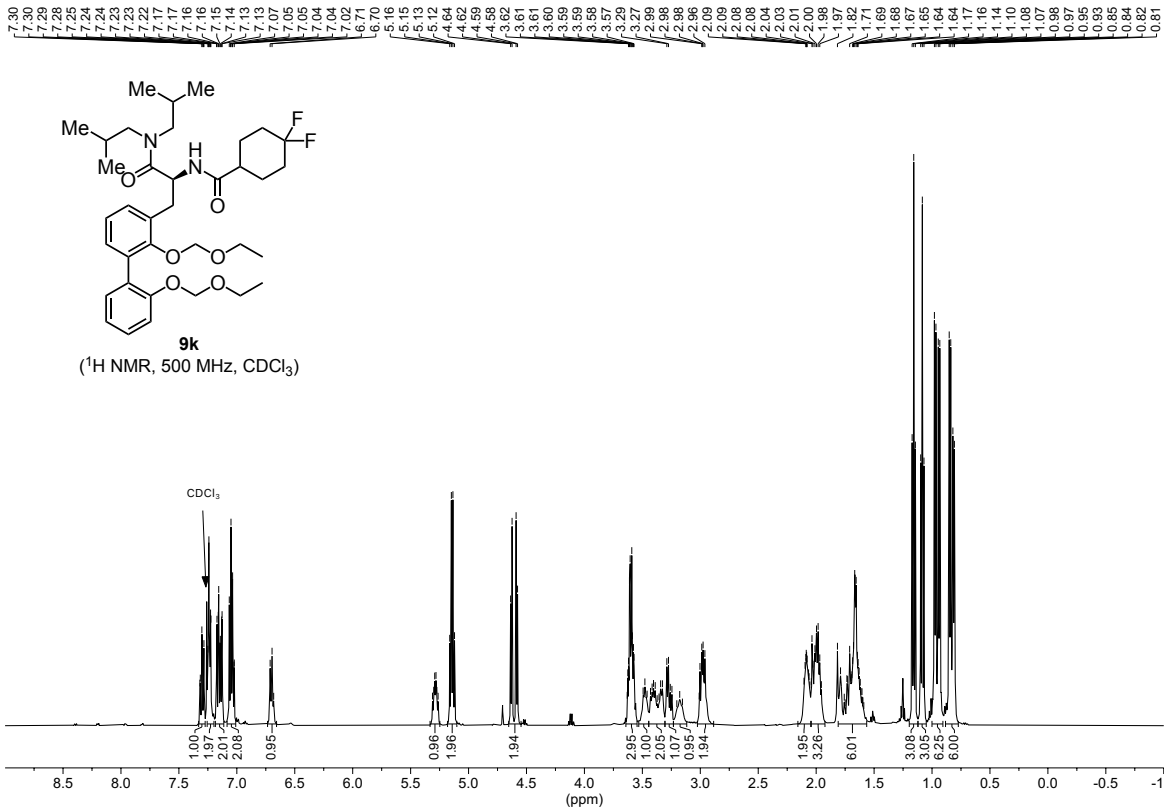



**9i**

($^{13}$C NMR, 126 MHz, $CDCl_3$)

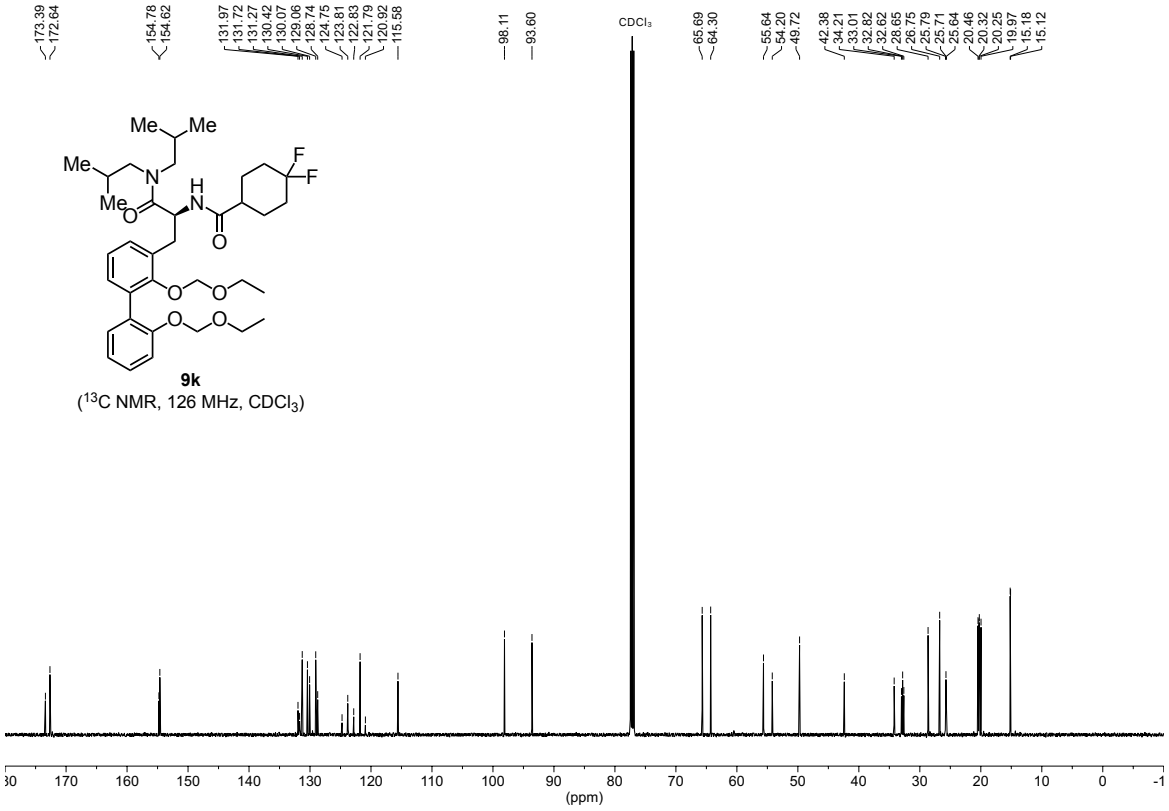

(n-dec)2N
H
N
O
O
S
O
O
O
O
O
9j
(1H NMR, 500 MHz, CDCl3)
CDCl3
2.88
4.12
2.89
2.05
0.97
1.00
1.96
1.97
3.05
3.23
2.03
3.07
1.04
2.03
1.07
1.08
2.12
28.19
3.15
3.05
6.07
(ppm)


171.47
170.20
154.80
154.78
135.80
132.01
131.78
131.24
130.31
130.20
129.74
129.08
129.02
128.84
126.35
123.82
121.77
115.54
98.13
93.59
CDCl3
65.65
64.29
50.01
47.99
46.66
36.11
34.18
32.02
29.81
29.73
29.71
29.69
29.56
29.52
29.49
29.46
29.44
27.77
27.18
27.11
22.81
15.20
15.15
14.24
(n-dec)2N
H
N
O
O
S
O
O
O
O
O
9j
(13C NMR, 126 MHz, CDCl3)
(ppm)



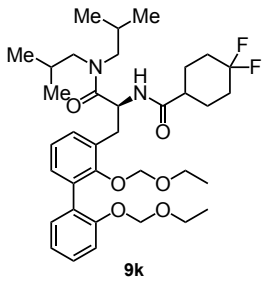

**9k**

($^1$H NMR, 500 MHz, $CDCl_3$)




**9k**

($^{13}$C NMR, 126 MHz, $CDCl_3$)

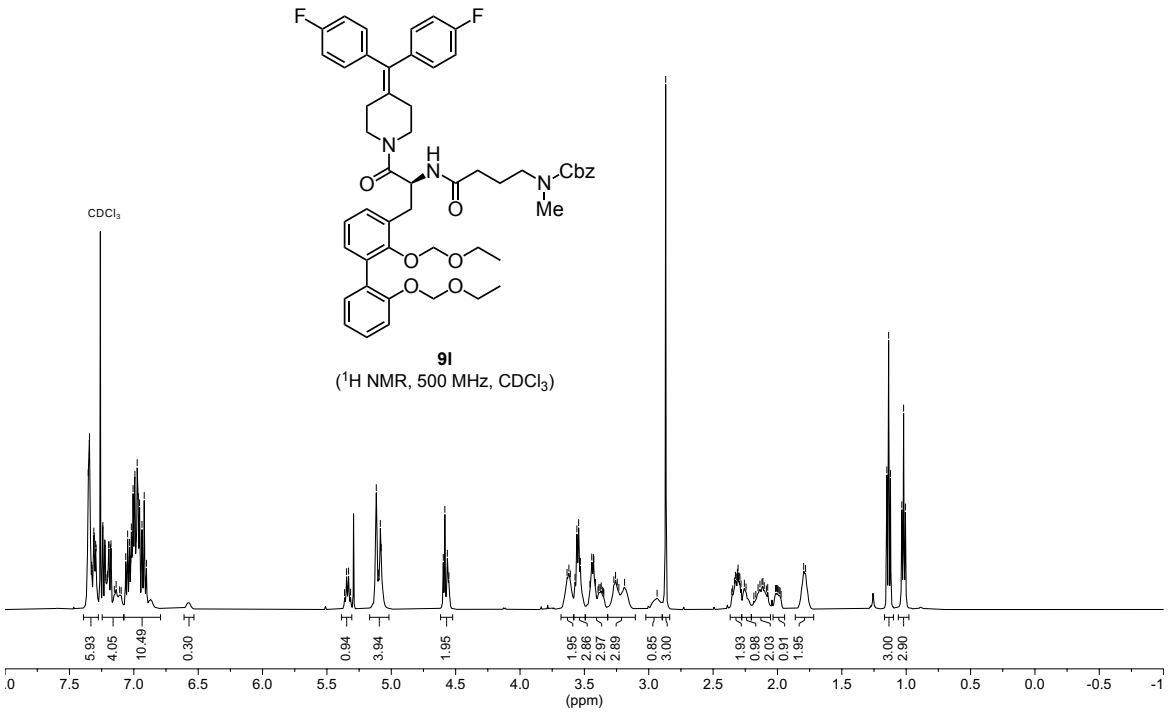


**9k**

($^1$F NMR, 471 MHz, $CDCl_3$)

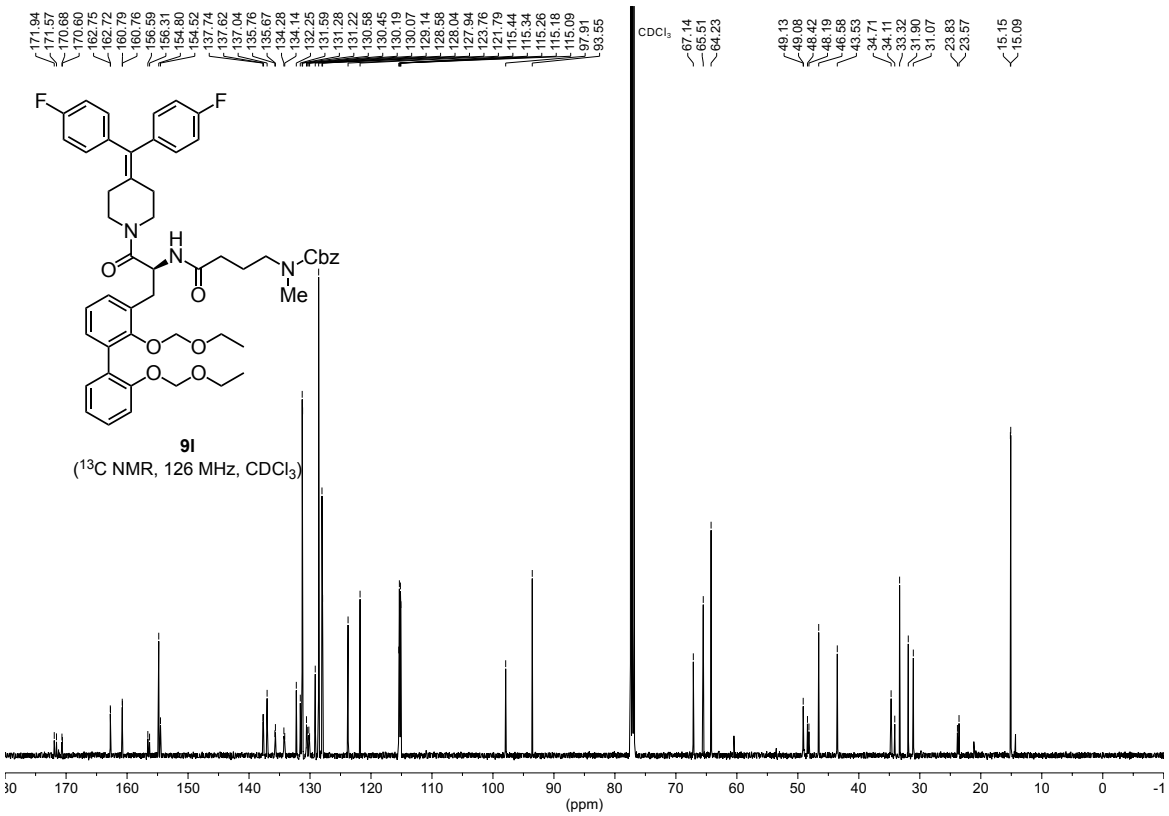




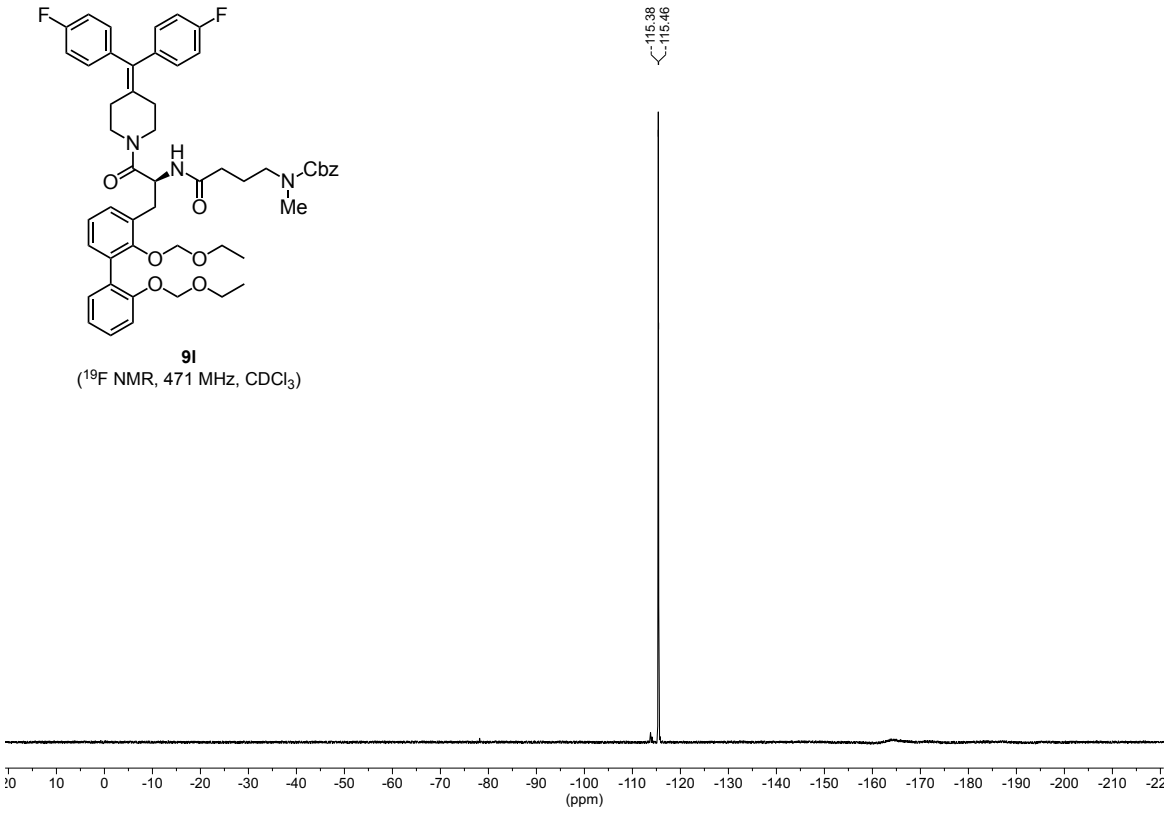

**9l**

($^1$H NMR, 500 MHz, $CDCl_3$)



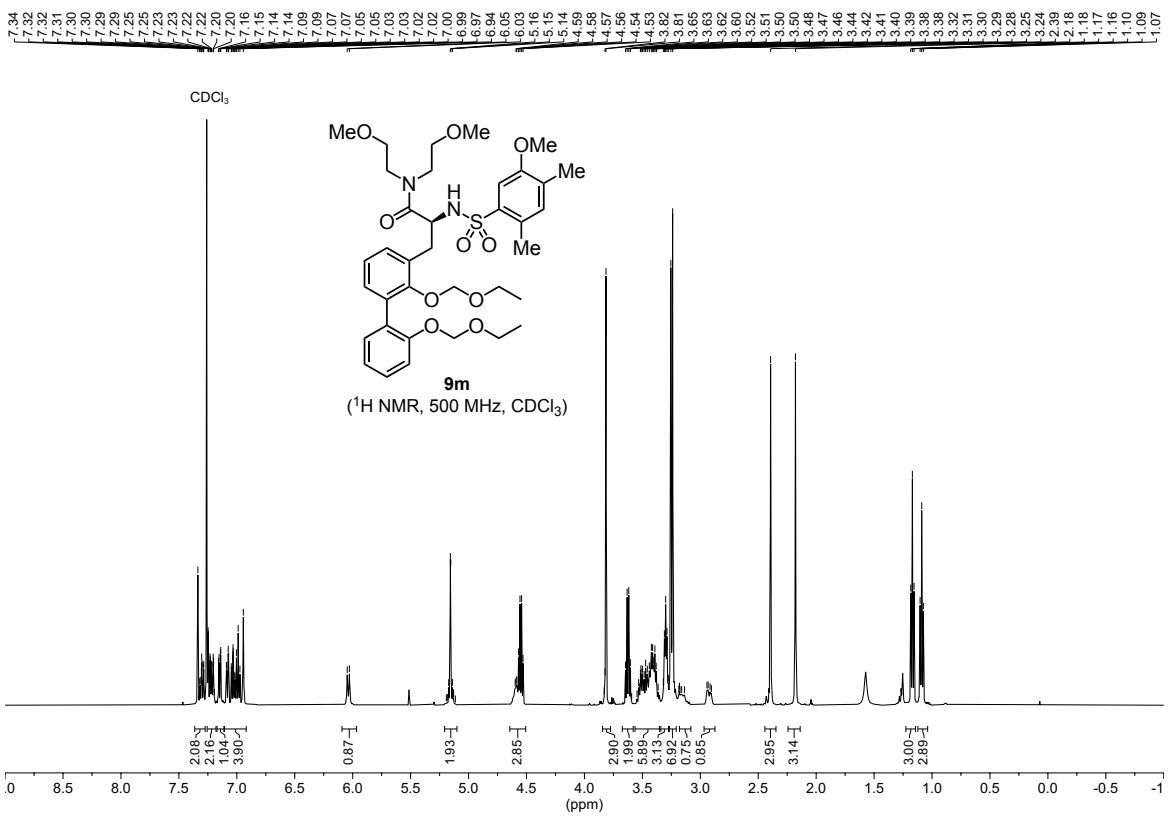

**9l**

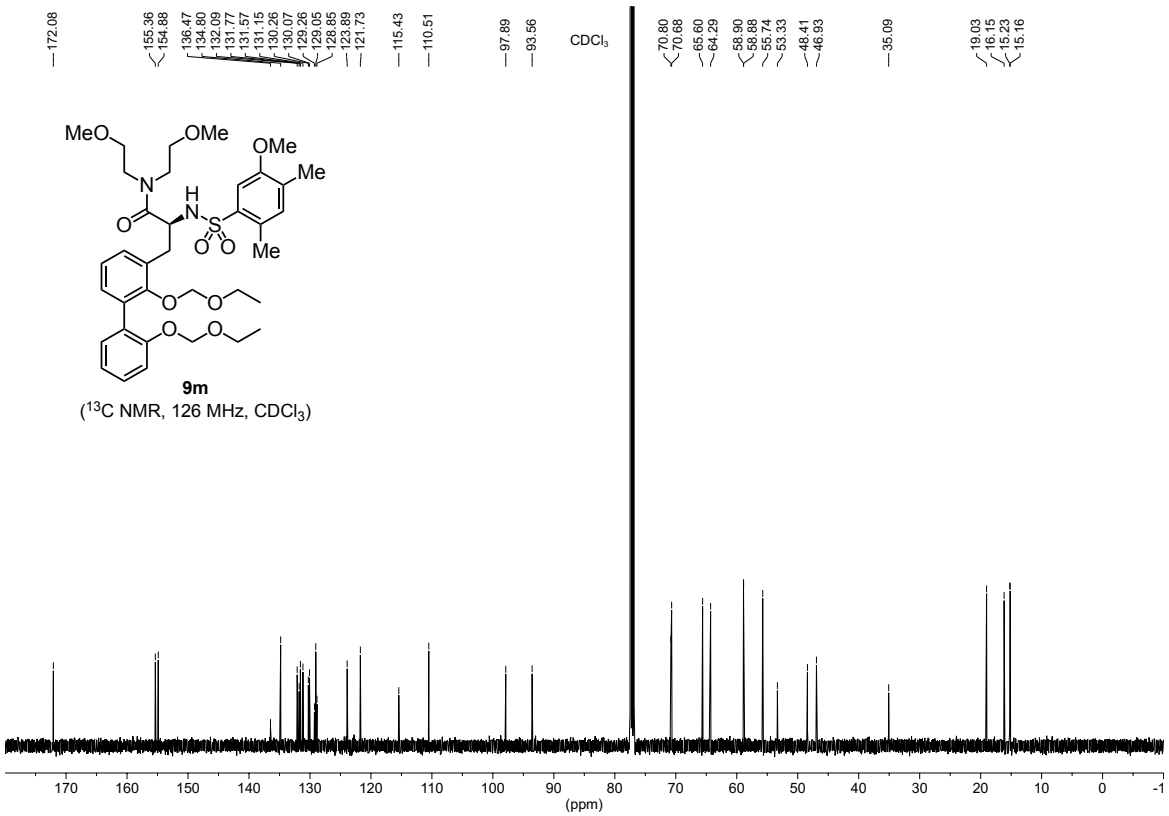
($^{13}$C NMR, 126 MHz, $CDCl_3$)

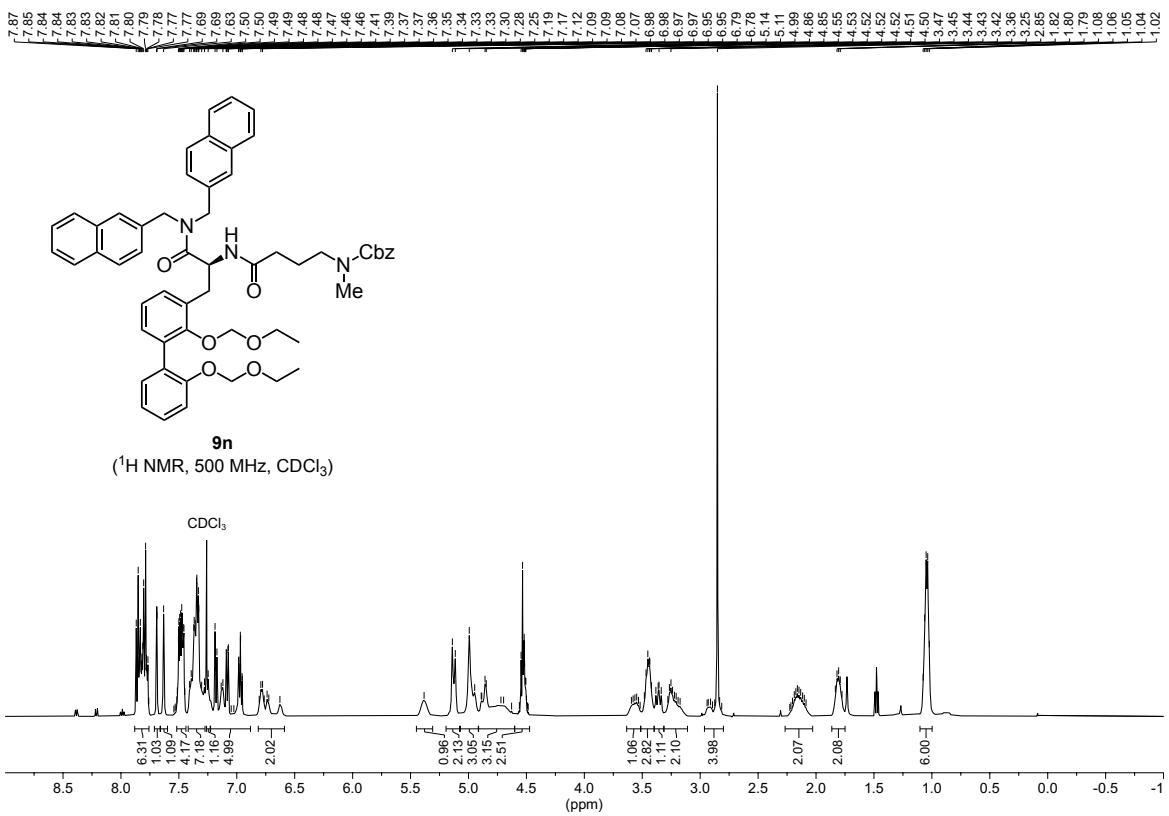



**9l**

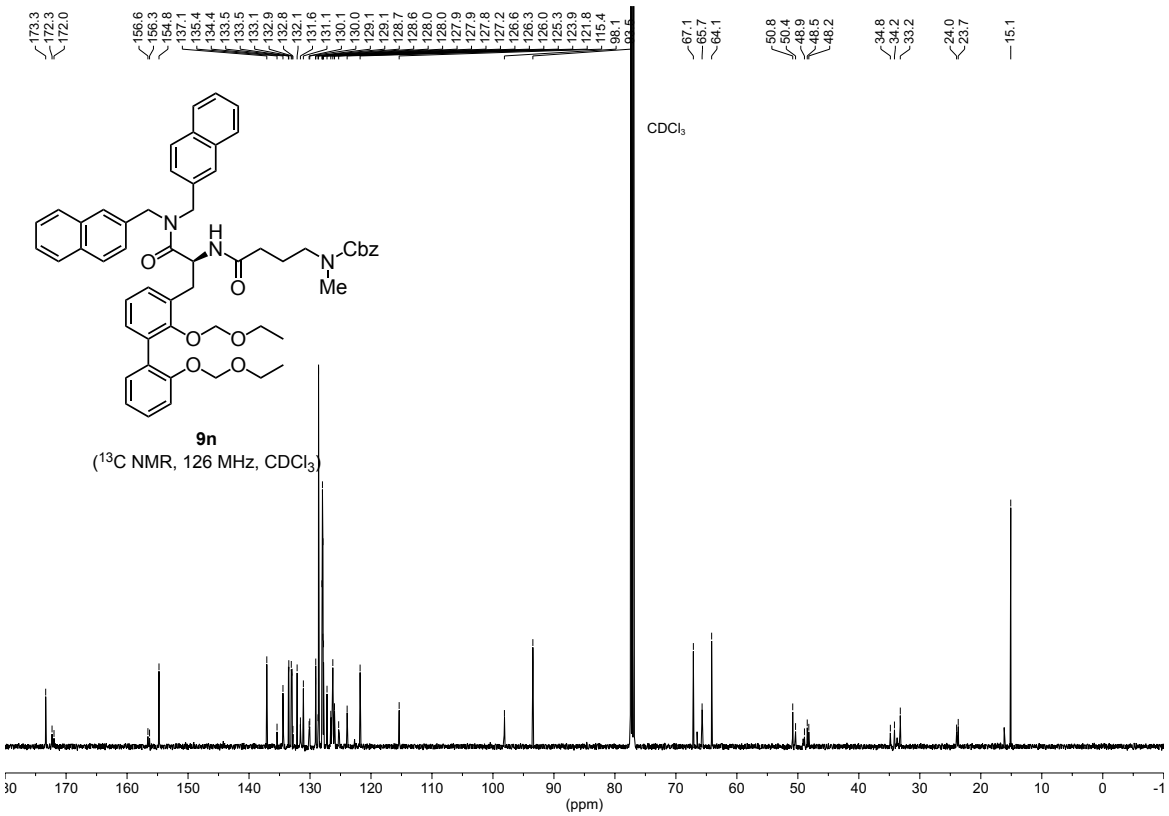
($^{19}$F NMR, 471 MHz, $CDCl_3$)


CDCl3
MeO
OMe
OMe
Me
N
H
N
S
O
O
O
Me
9m
(1H NMR, 500 MHz, CDCl3)
(ppm)

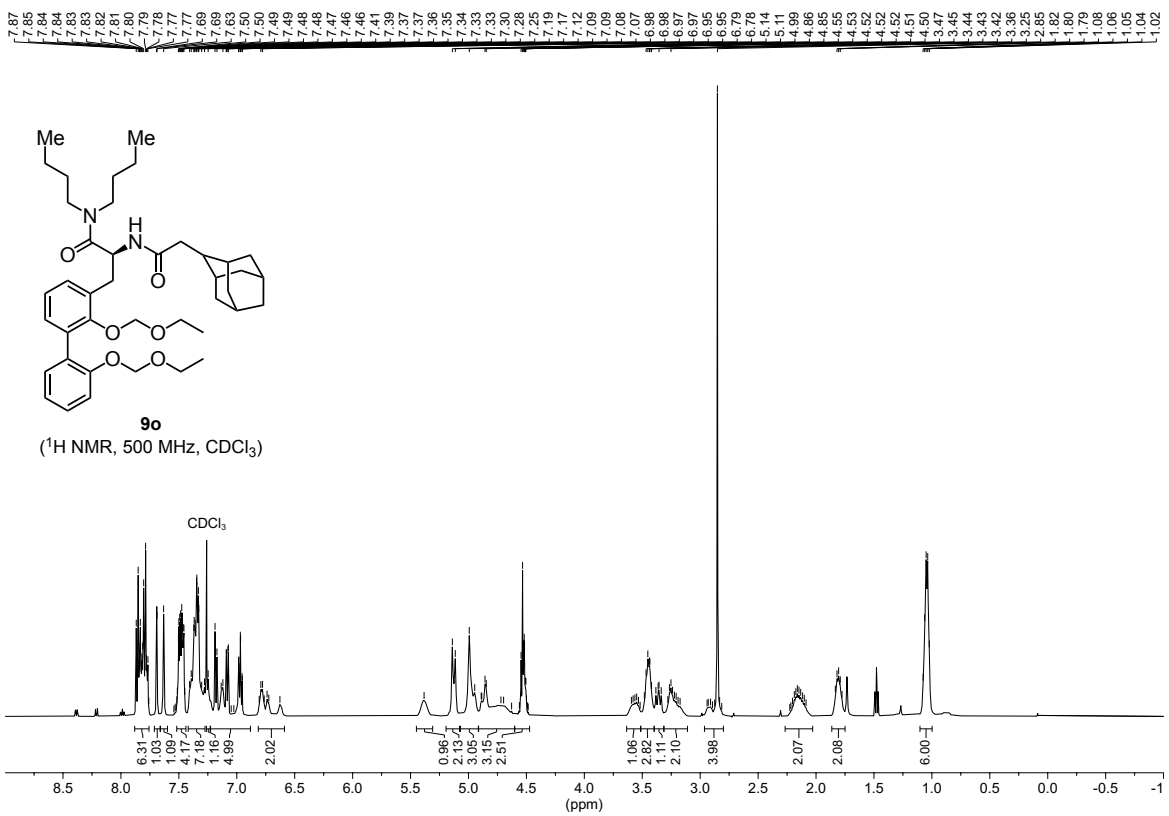

CDCl3
MeO
OMe
OMe
Me
N
H
N
S
O
O
O
Me
9m
(13C NMR, 126 MHz, CDCl3)
(ppm)




**9n**
($^1$H NMR, 500 MHz, $CDCl_3$)

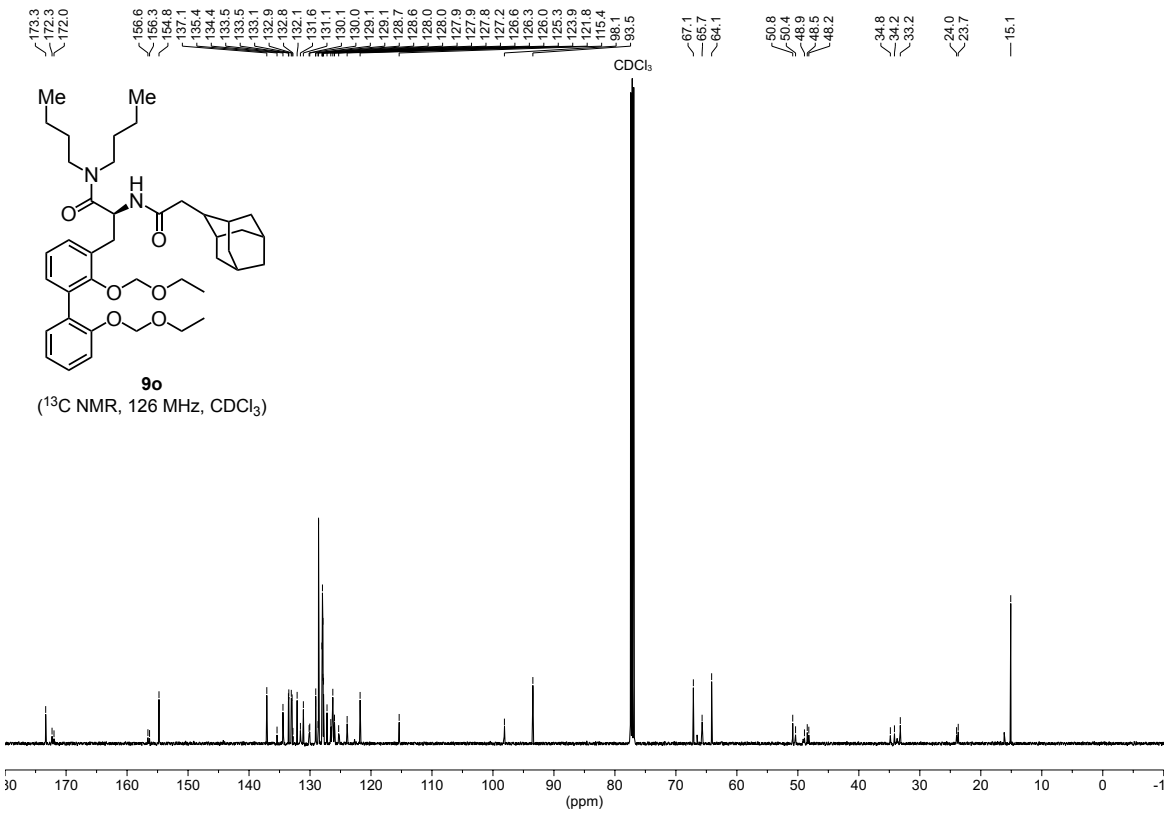



**9n**
($^{13}$C NMR, 126 MHz, $CDCl_3$)



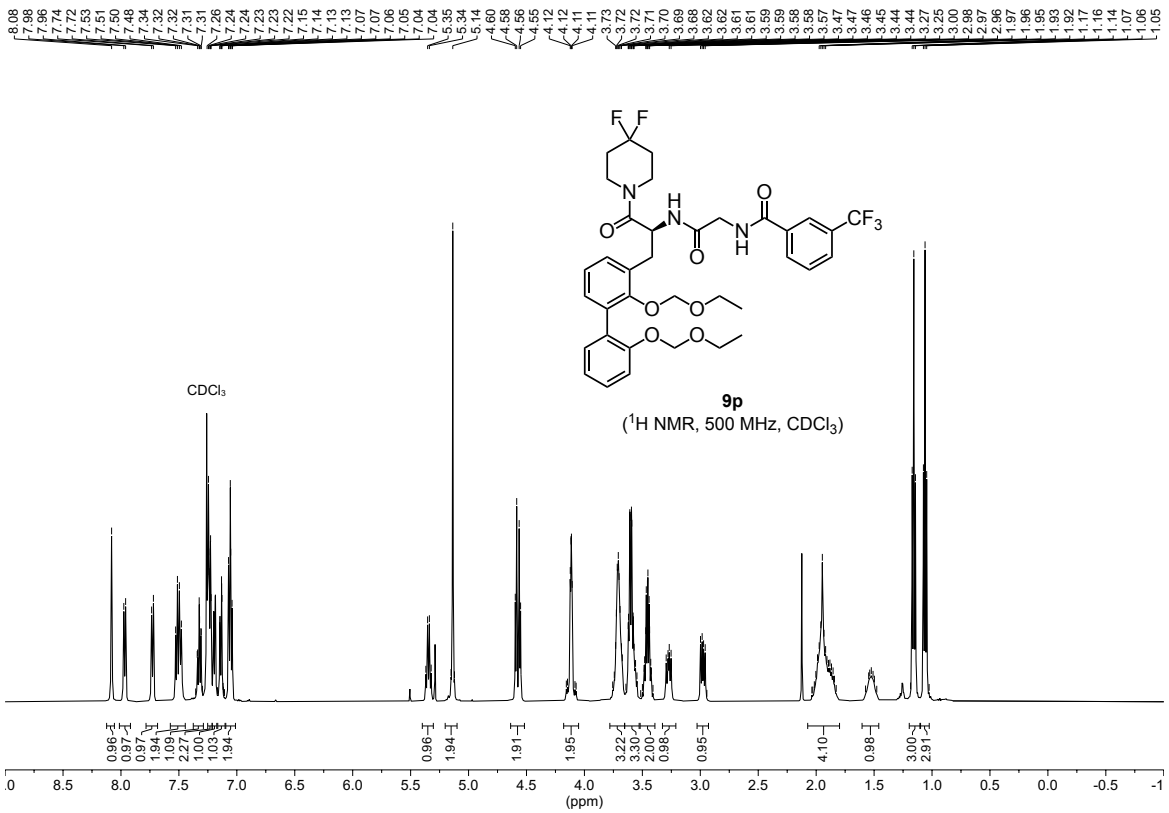

**9o**

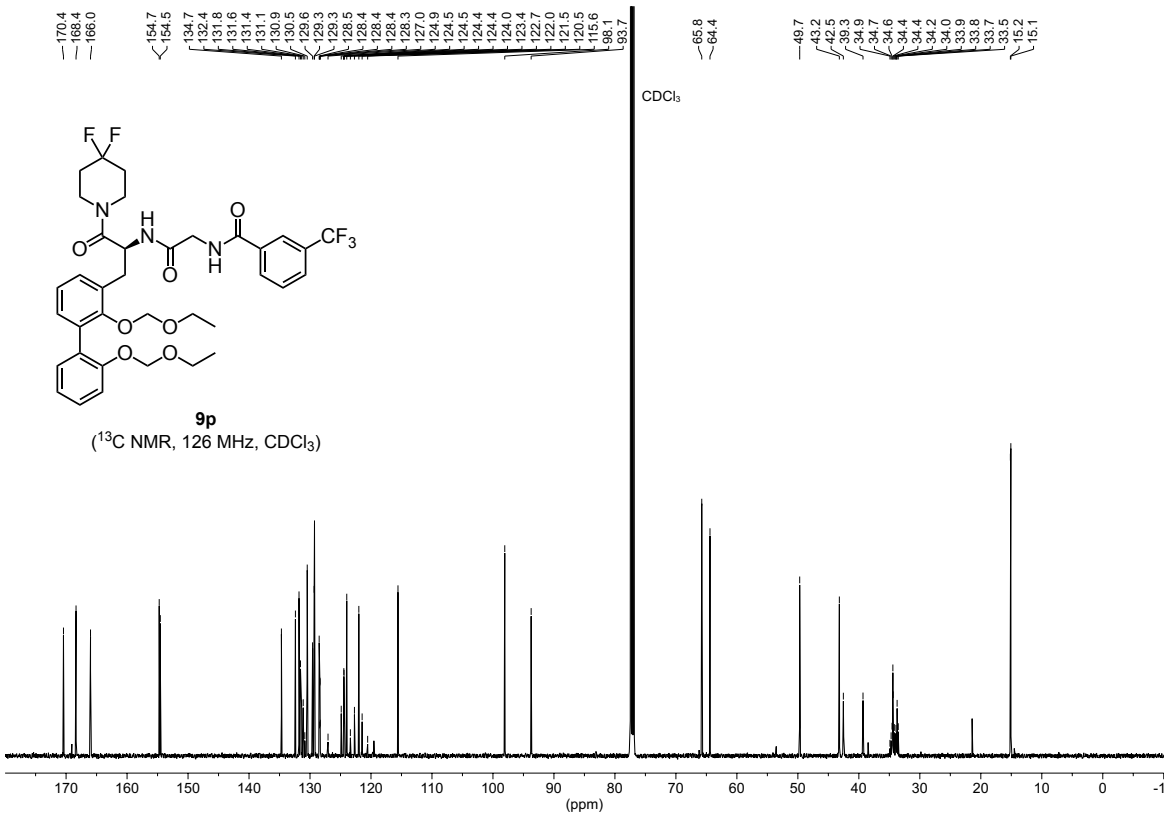
($^{1}$H NMR, 500 MHz, $CDCl_3$)

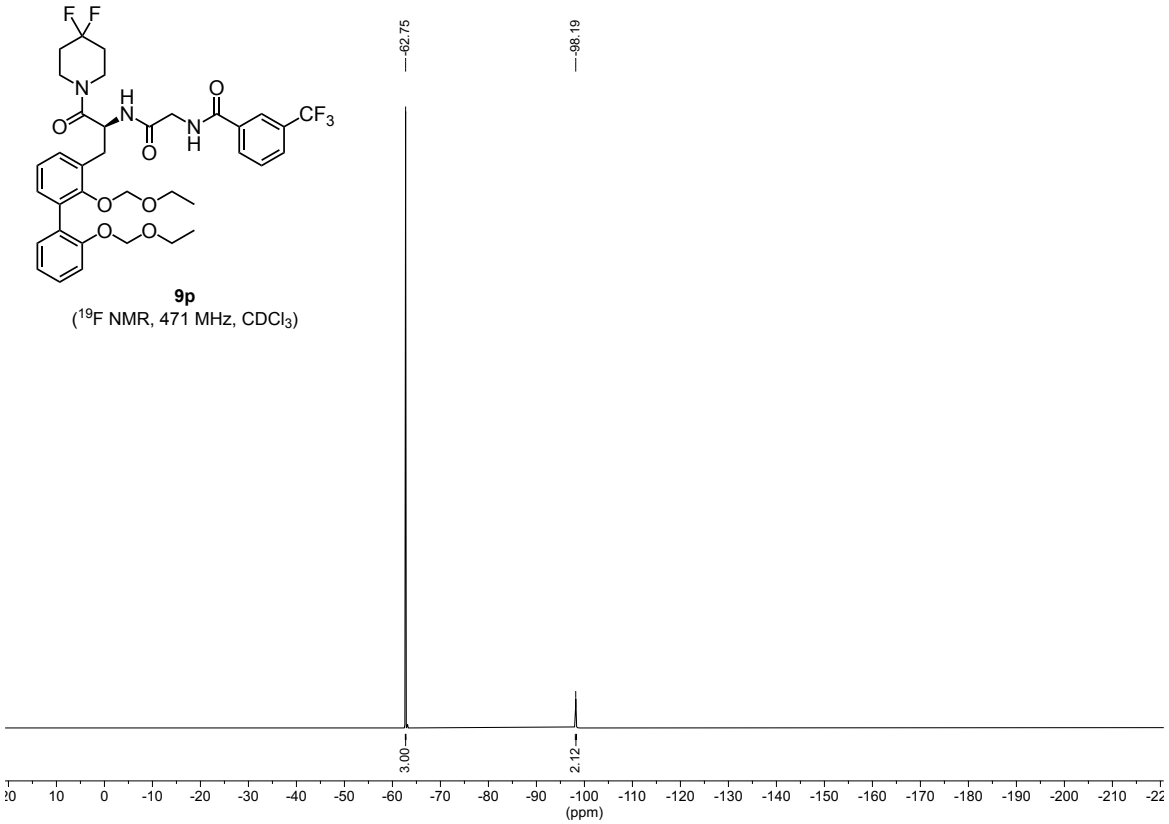



**9o**

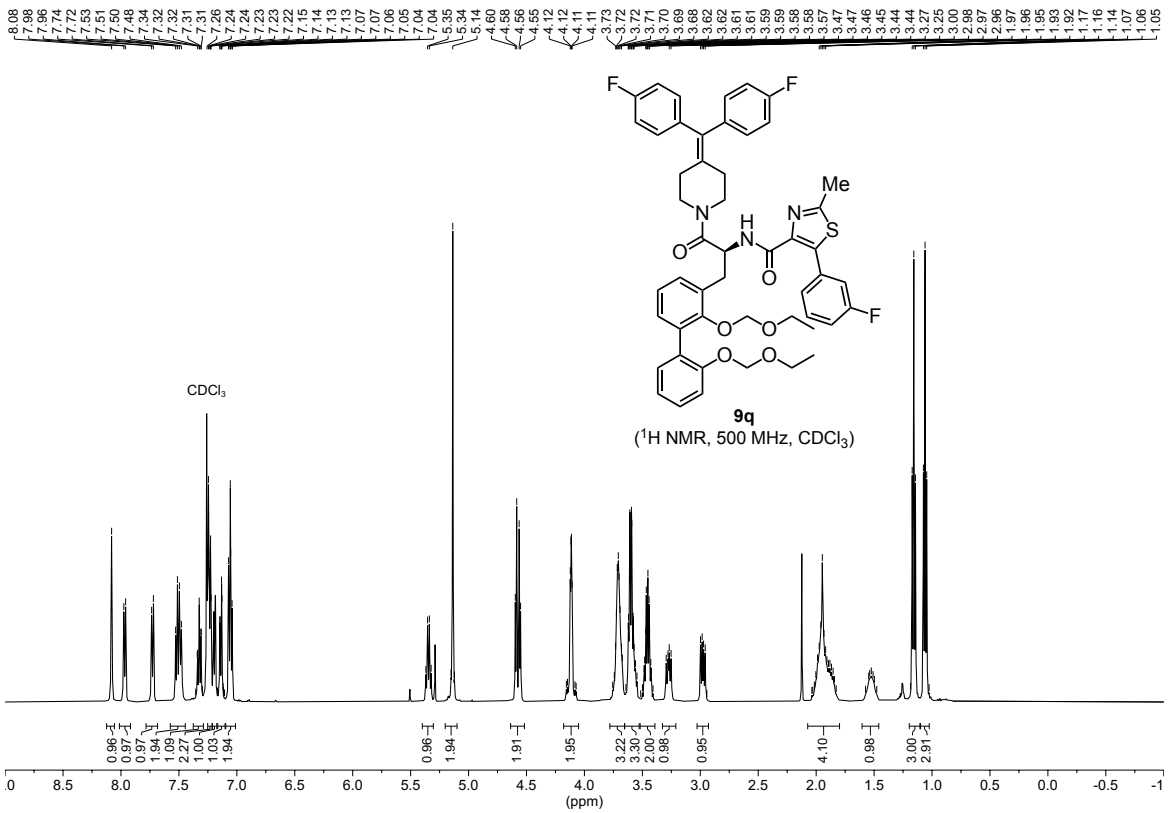
($^{13}$C NMR, 126 MHz, $CDCl_3$)


CDCl3
9p
(1H NMR, 500 MHz, CDCl3)
(ppm)

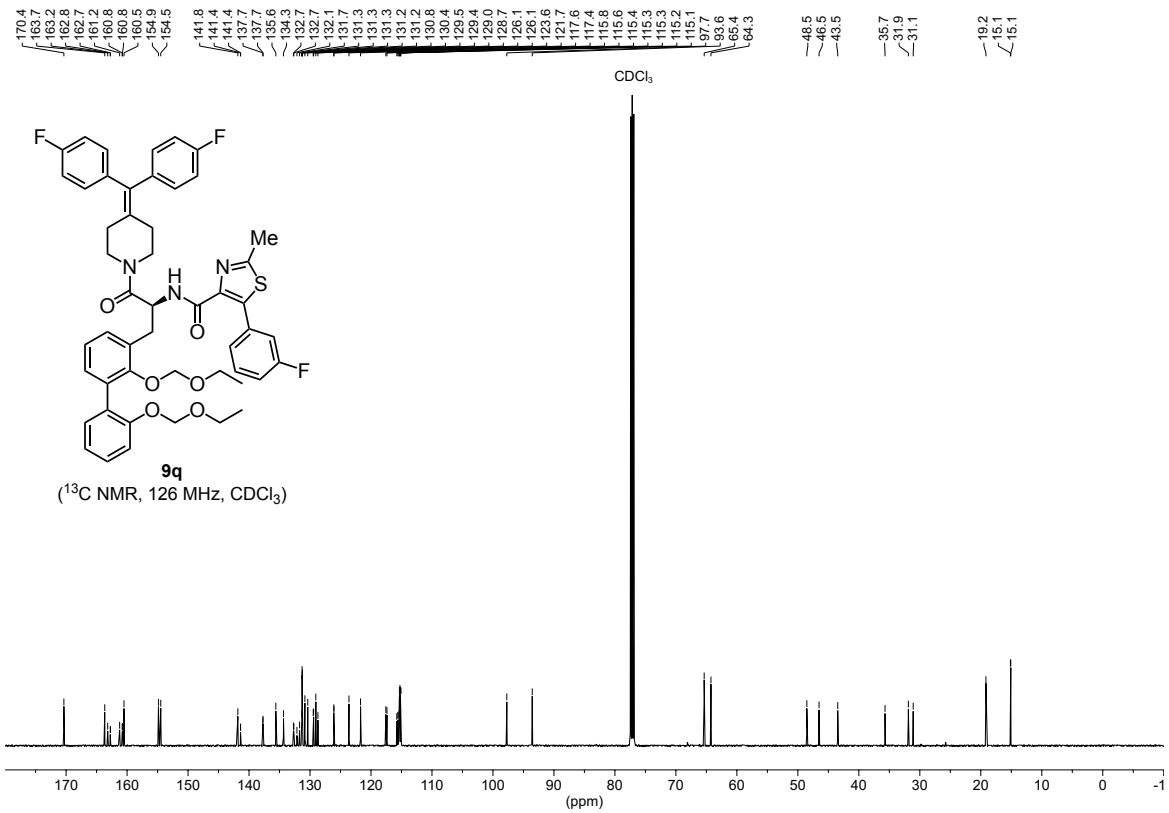

CDCl3
9p
(13C NMR, 126 MHz, CDCl3)
(ppm)




**9p**
($^{19}$F NMR, 471 MHz, $CDCl_3$)

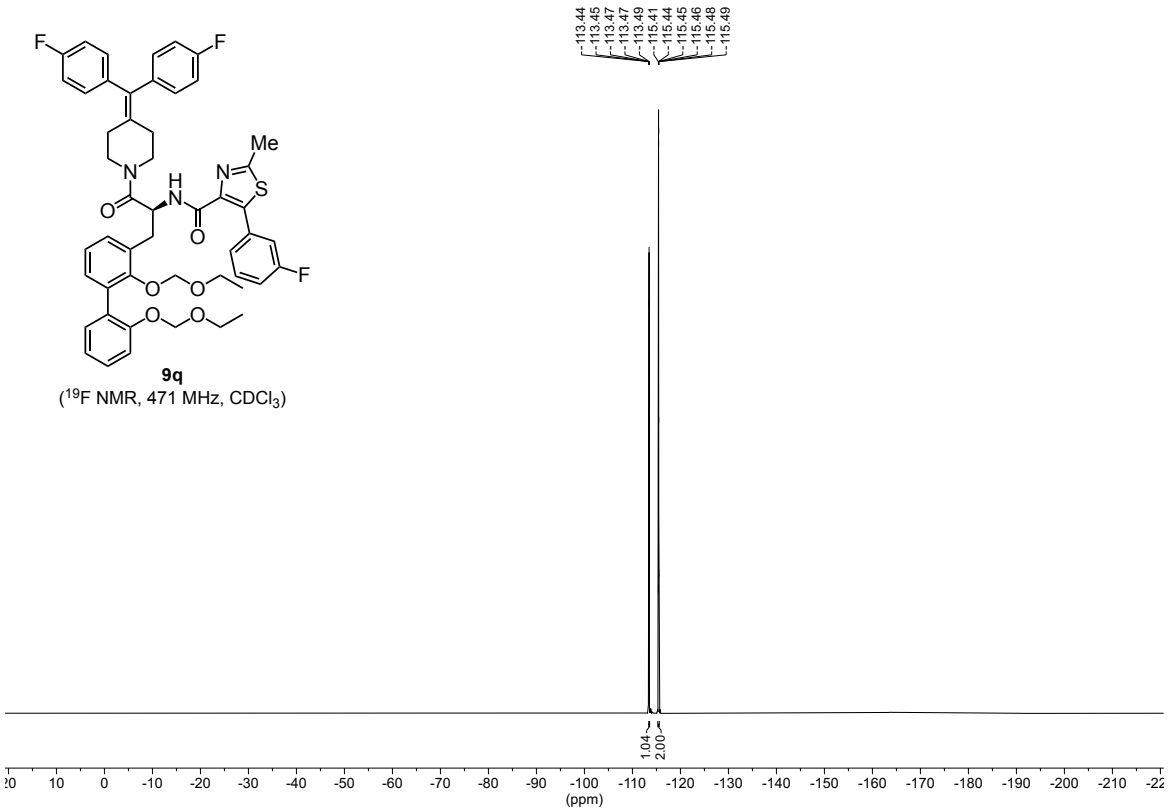



**9q**
($^{1}$H NMR, 500 MHz, $CDCl_3$)



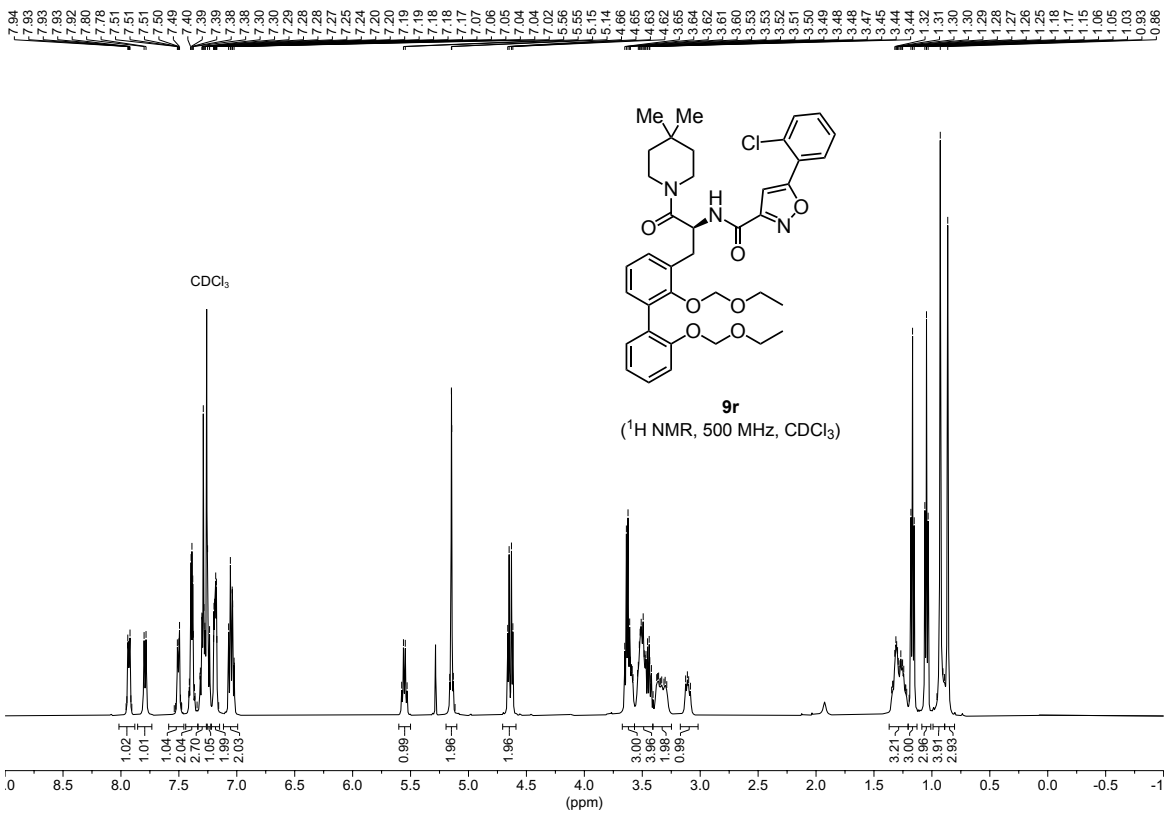

**9q**

($^{13}$C NMR, 126 MHz, $CDCl_3$)



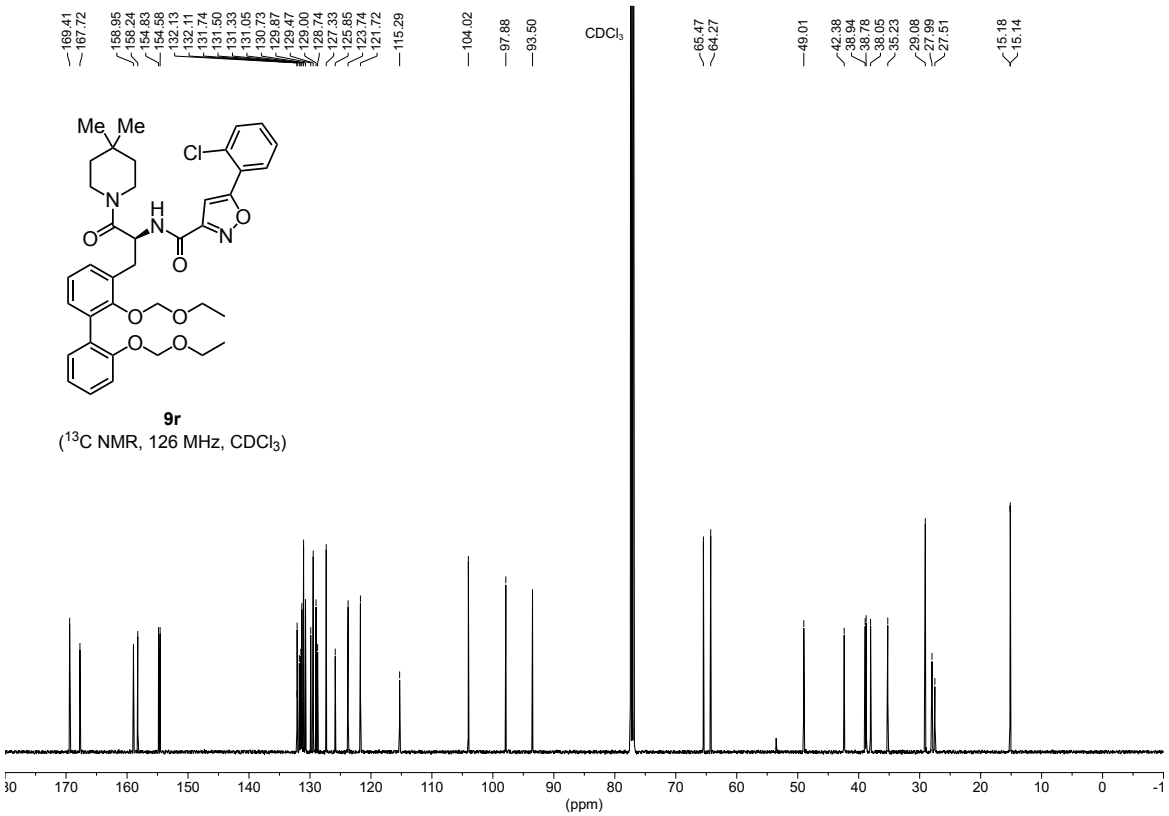

**9q**

($^{19}$F NMR, 471 MHz, $CDCl_3$)



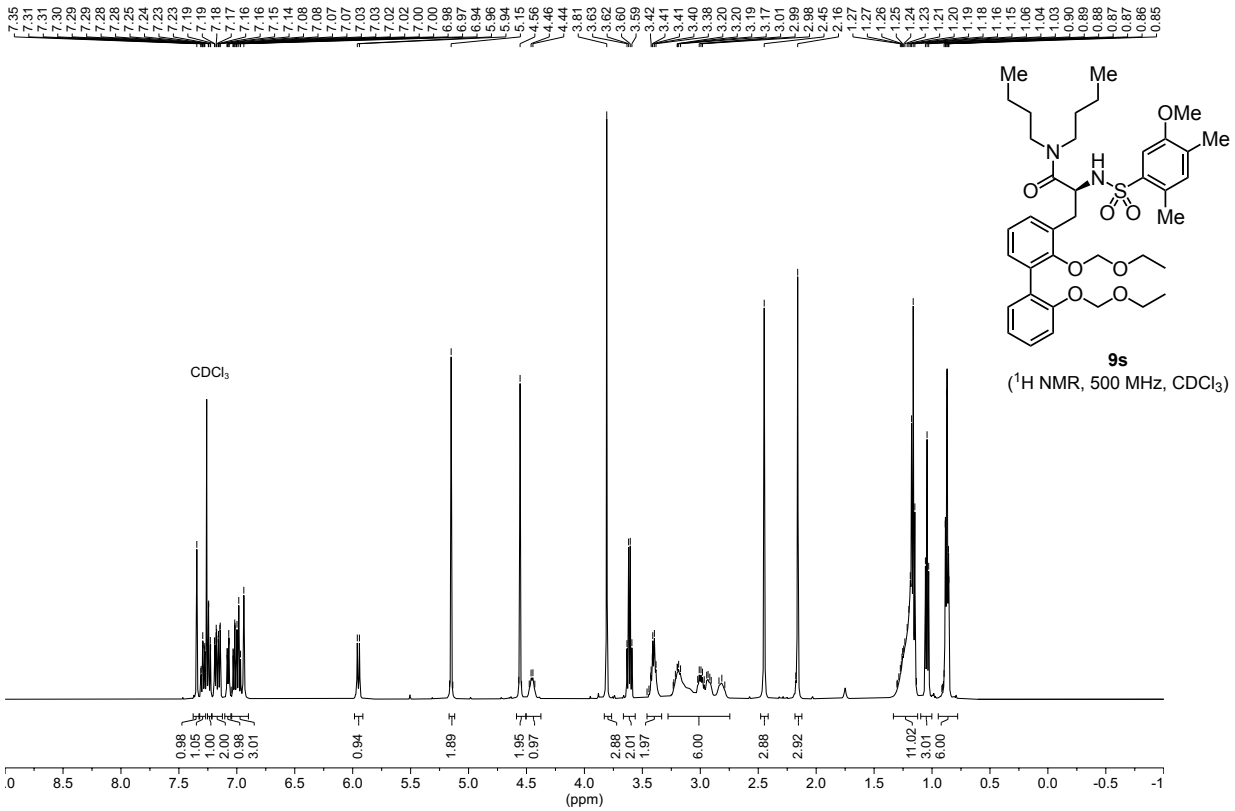

**9r**

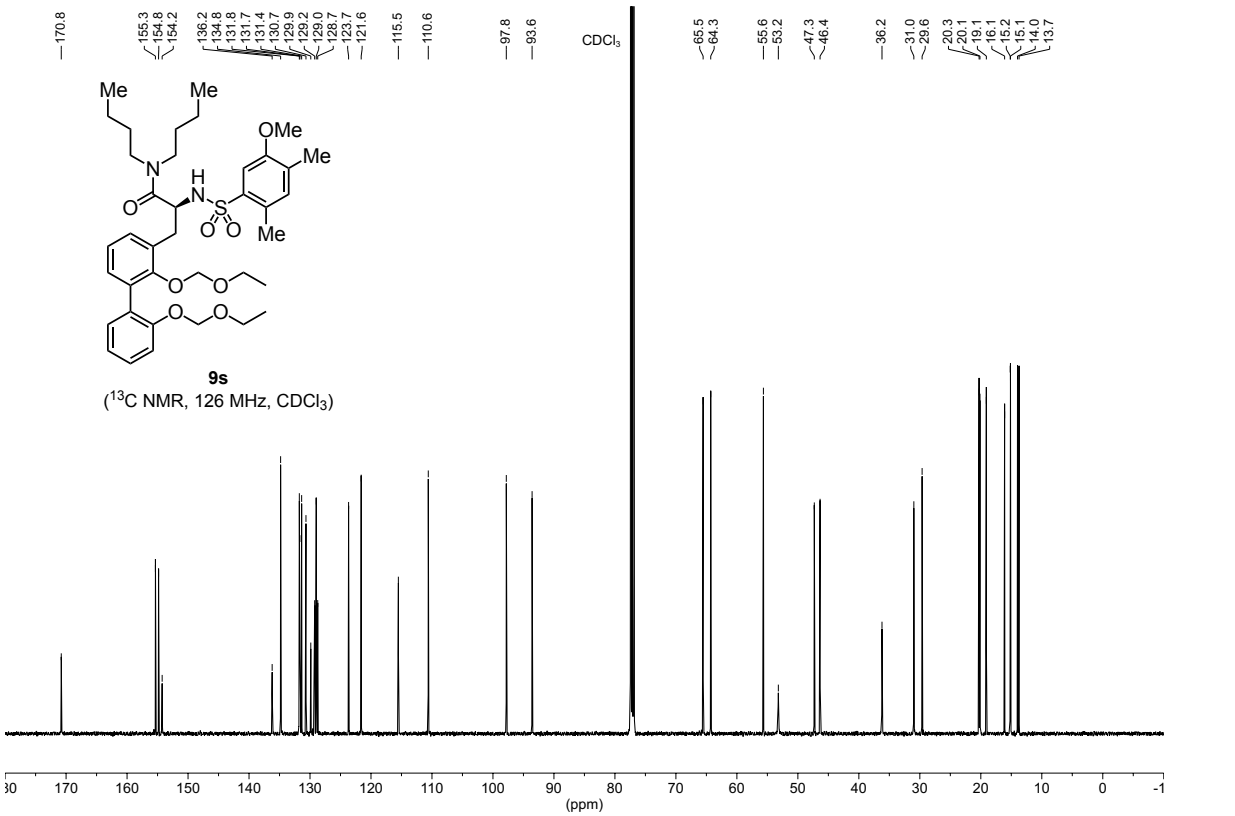
($^1$H NMR, 500 MHz, $CDCl_3$)

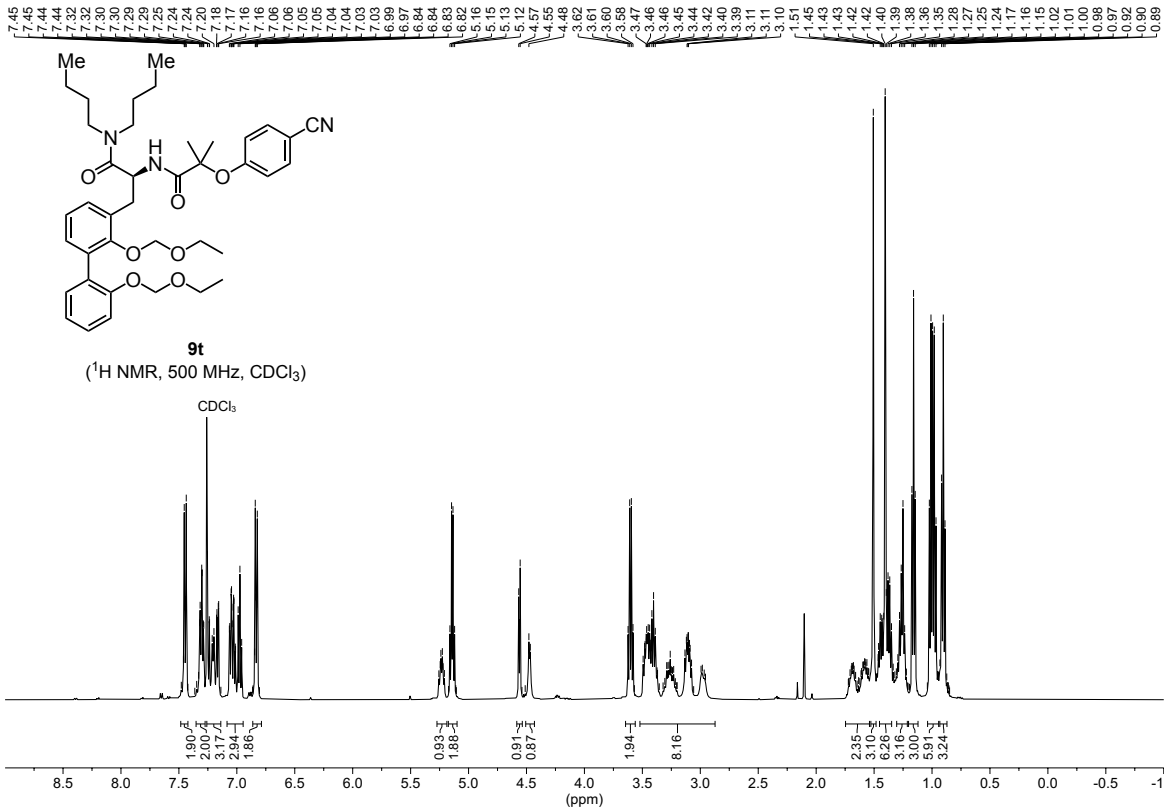



**9r**

($^{13}$C NMR, 126 MHz, $CDCl_3$)


CDCl3
Me
Me
OMe
Me
N
H
N
S
O
O
O
Me
O
O
O
O
9s
(1H NMR, 500 MHz, CDCl3)
(ppm)

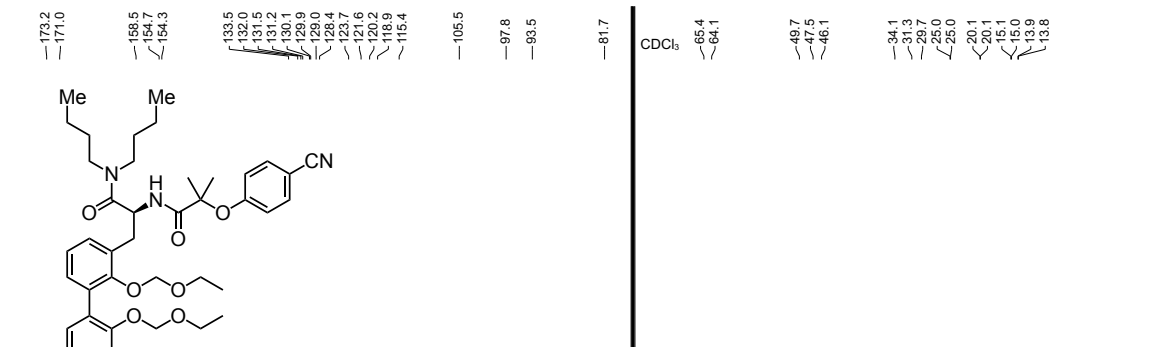

CDCl3
Me
Me
OMe
Me
N
H
N
S
O
O
O
Me
O
O
O
O
9s
(13C NMR, 126 MHz, CDCl3)
(ppm)




**9t**

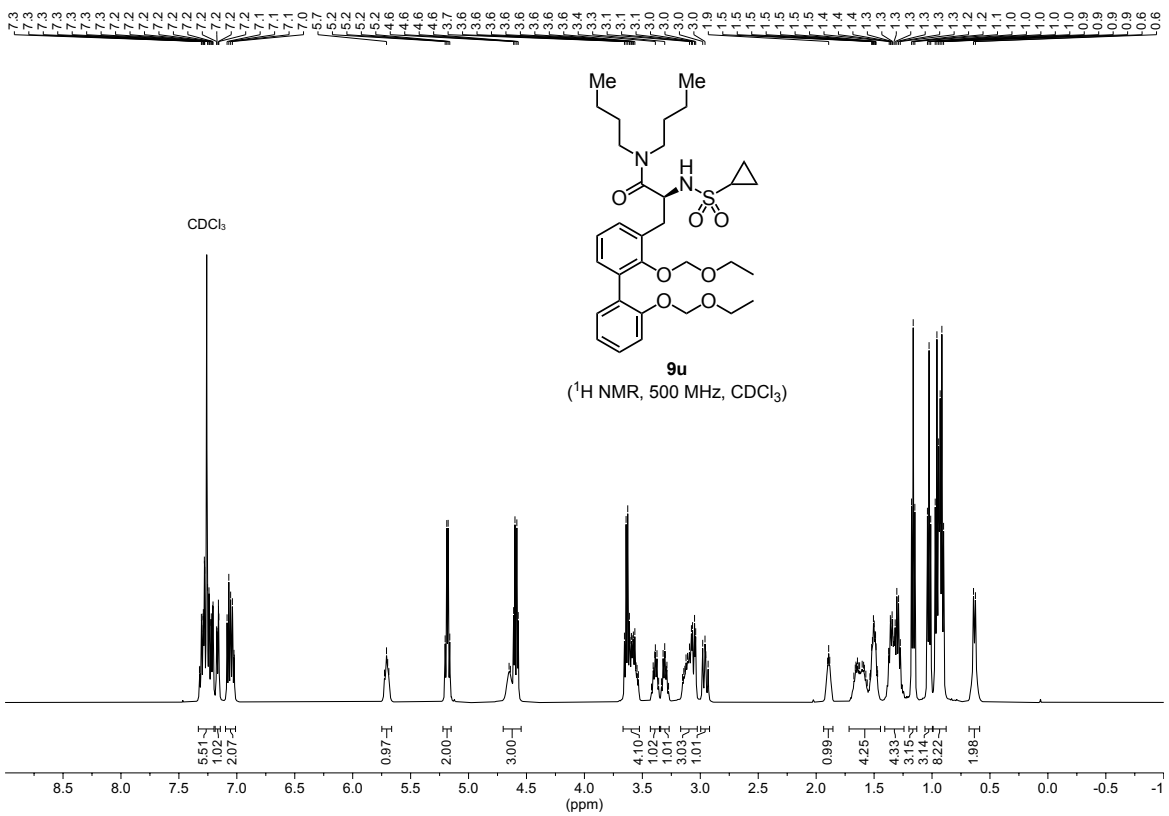
($^{1}$H NMR, 500 MHz, $CDCl_3$)



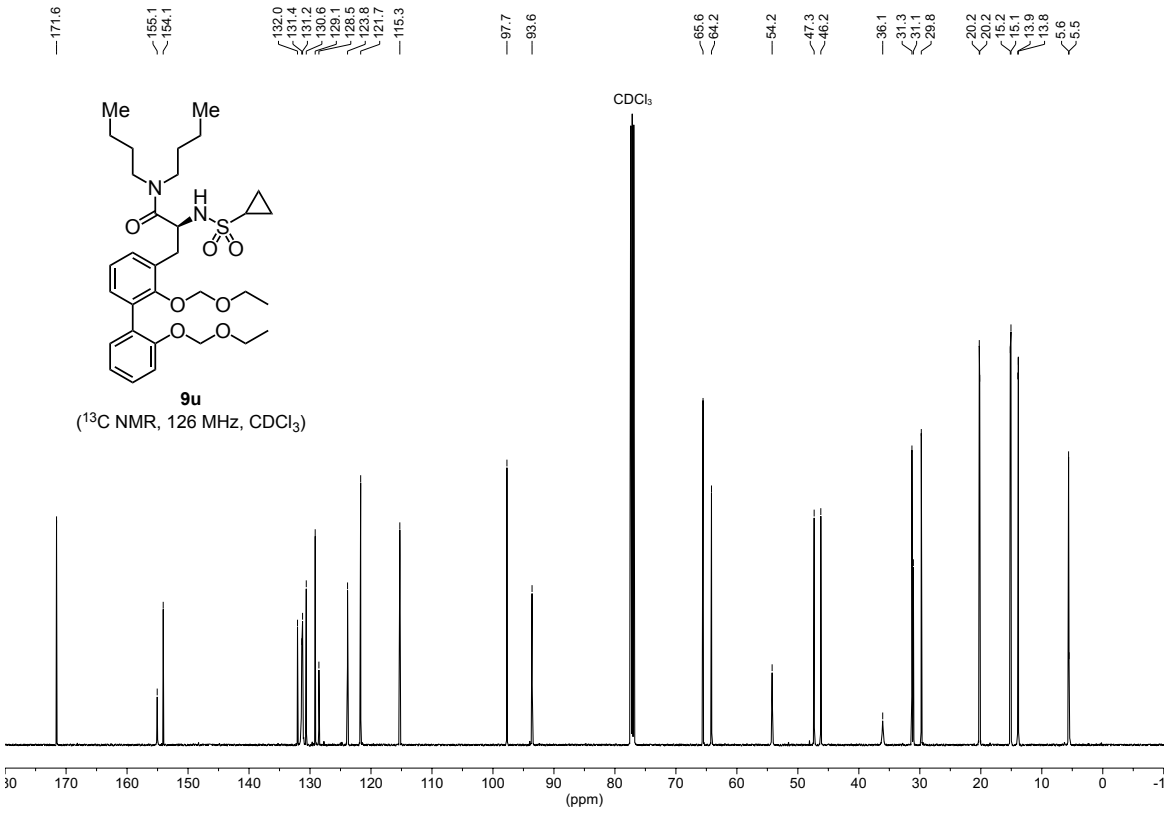

**9t**

($^{13}$C NMR, 126 MHz, $CDCl_3$)



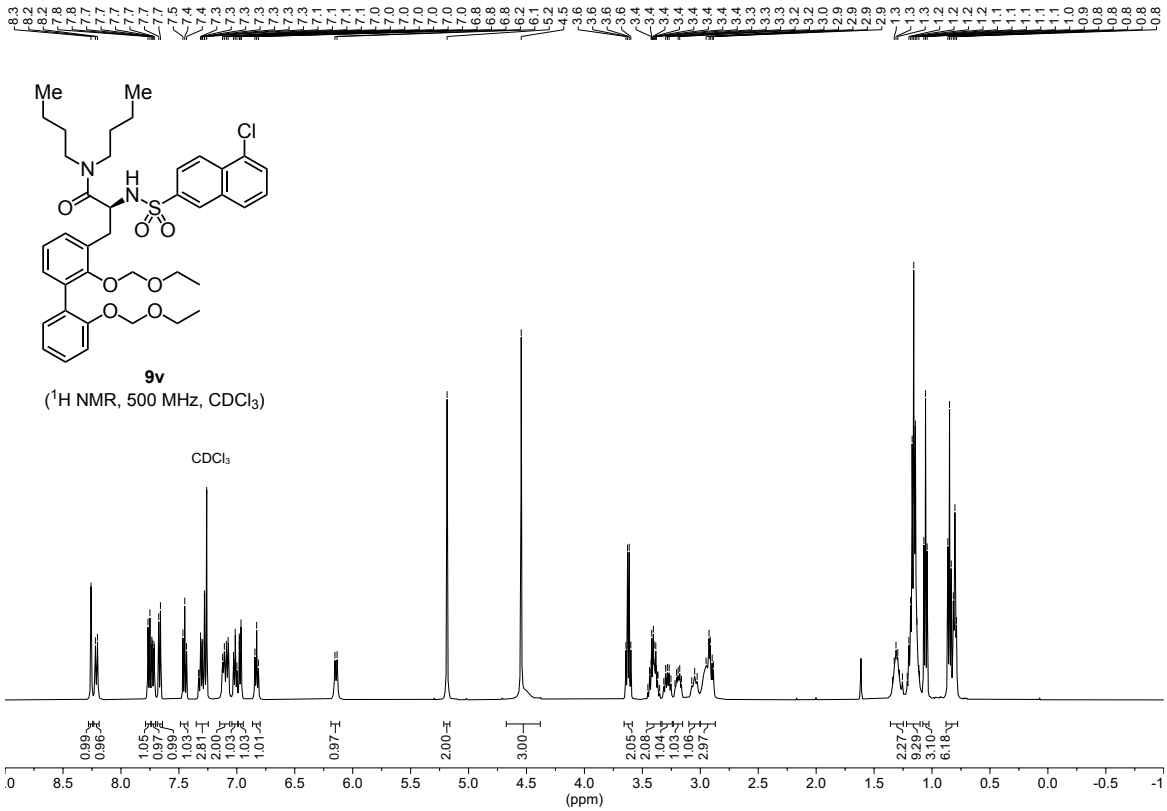

**9u**

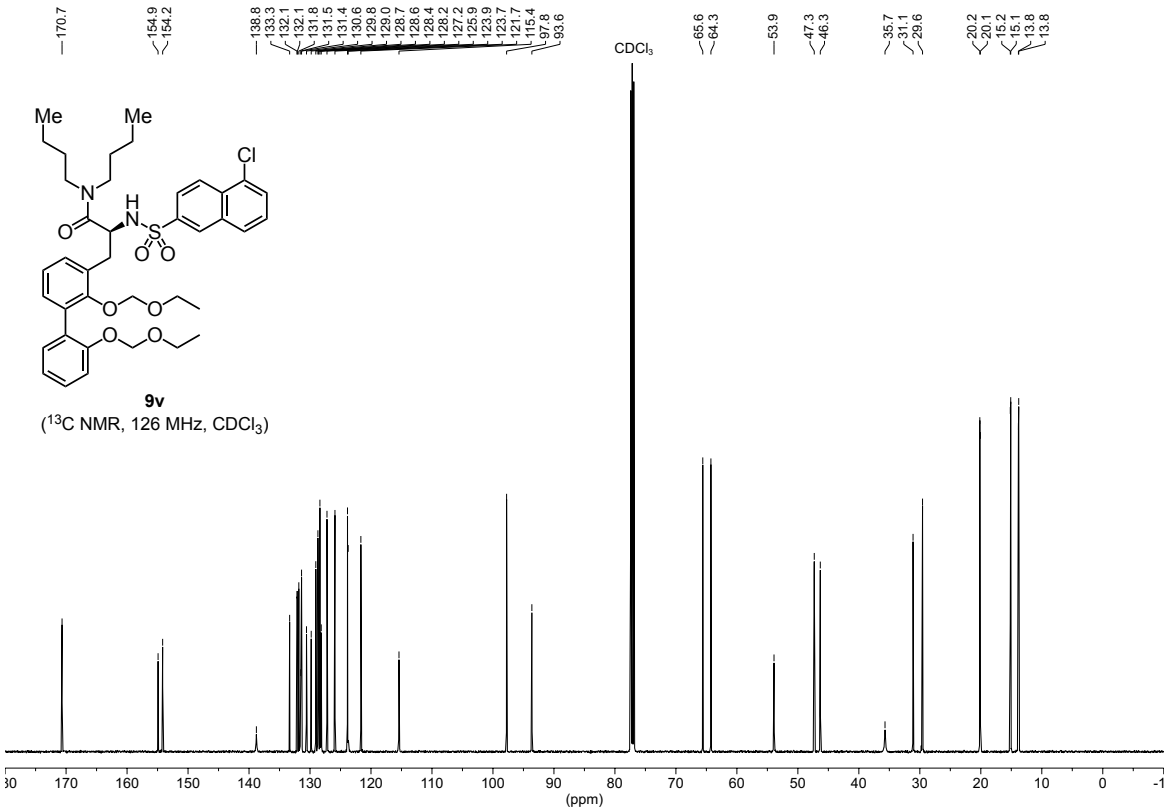
($^{1}$H NMR, 500 MHz, $CDCl_3$)

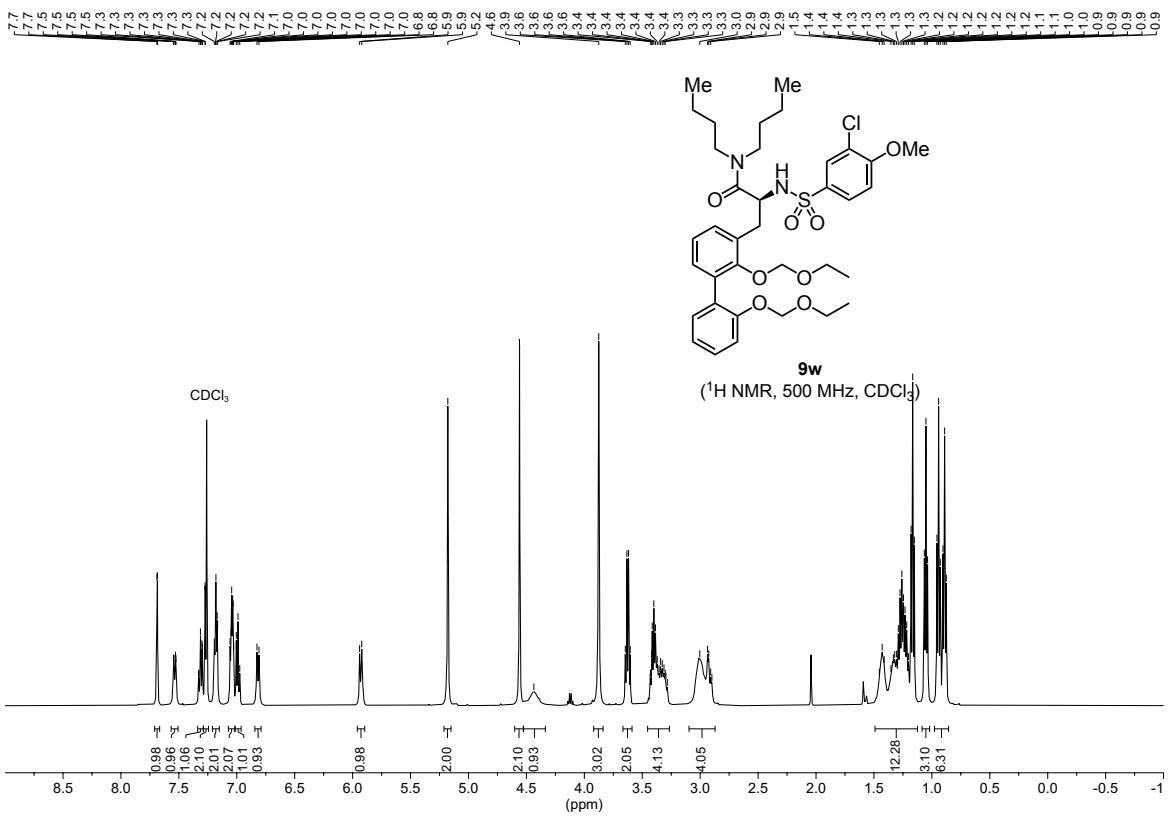



**9u**

($^{13}$C NMR, 126 MHz, $CDCl_3$)

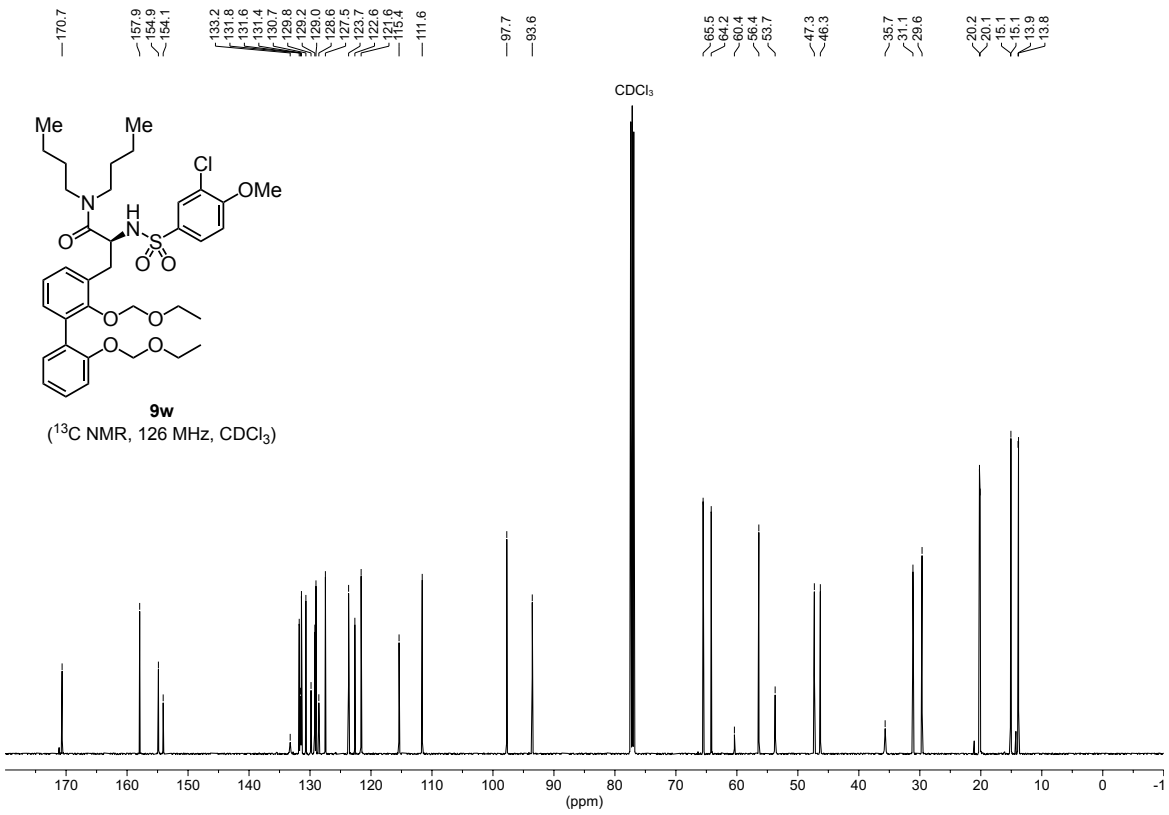

Me
Me
Cl
N
H
N
S
O
O
O
O
O
O
O
9v
(1H NMR, 500 MHz, CDCl3)
CDCl3
(ppm)


Me
Me
Cl
N
H
N
S
O
O
O
O
O
O
O
9v
(13C NMR, 126 MHz, CDCl3)
CDCl3
(ppm)




**9w**

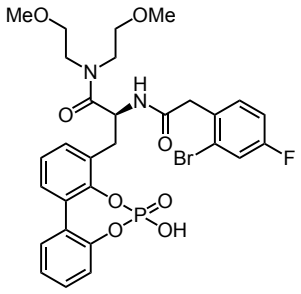
($^{1}$H NMR, 500 MHz, $CDCl_3$)




**9w**

($^{13}$C NMR, 126 MHz, $CDCl_3$)

## 7.2.7. Synthesis and Characterization of Intermediates 9a-w




**P1**

**(*S*)-2-(2-(2-bromo-4-fluorophenyl)acetamido)-3-((*S*)-6-hydroxy-6-oxidodibenzo[*d*,*f*][1,3,2]dioxaphosphepin-4-yl)-*N*,*N*-bis(2-methoxyethyl)propenamide (P1).** Catalyst **P1** was synthesized from **9a** using General Procedures 3B and 4B. Purification was accomplished using reverse phase chromatography using 10-50% acetonitrile in water as eluent (with 1% formic acid). **P1** was obtained as a white solid (6% yield over 3 steps).

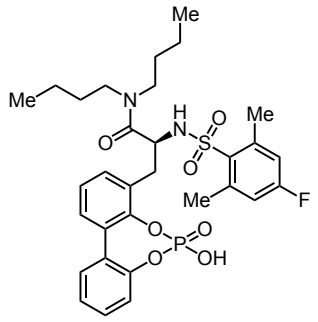
**$^{1}$H NMR (600 MHz, $CDCl_3$) δ:** 7.80 (s, 1H), 7.43 (dd, *J* = 7.6, 1.7 Hz, 1H), 7.34 (dd, *J* = 7.6, 1.7 Hz, 3H), 7.28 – 7.21 (m, 4H), 7.14 (td, *J* = 7.9, 3.2 Hz, 2H), 7.07 (dd, *J* = 8.2, 2.6 Hz, 1H), 6.96 (dd, *J* = 8.6, 6.0 Hz, 1H), 6.73 (td, *J* = 8.2, 2.6 Hz, 1H), 5.42 – 5.15 (m, 1H), 4.09 (d, *J* = 10.4 Hz, 1H), 3.50 – 3.39 (m, 8H), 3.34 – 3.28 (m, 1H), 3.26 (s, 4H), 3.22 (s, 3H), 3.04 (dd, *J* = 14.2, 4.6 Hz, 1H).

**$^{13}$C NMR (151 MHz, $CDCl_3$) δ:** 173.19, 170.67, 161.41 (d, *J* = 250.0 Hz), 147.76 (dd, *J* = 181.8, 8.8 Hz), 132.42 (d, *J* = 8.4 Hz), 130.86, 130.61, 129.90 (d, *J* = 26.9 Hz), 129.31, 129.10, 128.96, 128.77, 125.95 (d, *J* = 17.8 Hz), 124.83 (d, *J* = 9.6 Hz), 121.71 (d, *J* = 3.9 Hz), 119.84 (d, *J* = 24.5 Hz), 114.68 (d, *J* = 21.0 Hz), 70.38 (d, *J* = 13.2 Hz), 58.94 (d, *J* = 18.6 Hz), 50.70, 49.52, 47.43, 41.92, 31.27, 20.50.

**$^{19}$F NMR (565 MHz, $CDCl_3$) δ:** -113.97.

**$^{31}$P NMR (243 MHz, $CDCl_3$) δ:** 2.37.

**HRMS (ESI-/TOF, *m/z*):** Exact mass calculated for $[C_{30}H_{34}BrFN_2O_8P]^-$ requires 663.0913; found 663.0920.




**P2**

**(*S*)-*N*,*N*-dibutyl-2-((4-fluoro-2,6-dimethylphenyl)sulfonamido)-3-((*S*)-6-hydroxy-6-oxidodibenzo[*d*,*f*][1,3,2]dioxaphosphepin-4-yl)propenamide (P2).** Catalyst **P2** was synthesized from **9b** using General Procedures 3A and 4A. Purification was accomplished by reverse phase chromatography using 10–50% acetonitrile in water as eluent. **P2** was obtained as a beige solid (75% yield over 3 steps).

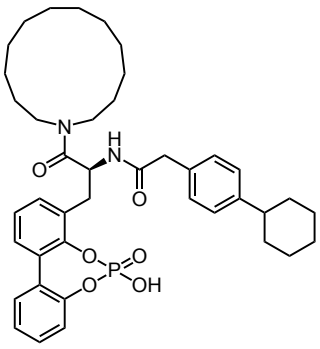
**$^{1}$H NMR (400 MHz, $CDCl_3$) δ:** 11.57 (s, 1H), 7.48 (d, *J* = 7.5 Hz, 1H), 7.41 (t, *J* = 7.4 Hz, 1H), 7.33 (t, *J* = 4.9 Hz, 2H), 7.28 (d, *J* = 8.0 Hz, 1H), 7.03 (d, *J* = 4.7 Hz, 2H), 6.61 (d, *J* = 9.1 Hz, 2H), 4.47 (s, 1H), 3.24 (ddt, *J* = 31.4, 14.4, 7.8 Hz, 5H), 3.05 (dd, *J* = 14.0, 5.4 Hz, 1H), 2.45 (s, 6H), 1.36 (tt, *J* = 13.3, 7.3 Hz, 5H), 1.23 (dh, *J* = 22.4, 7.1 Hz, 5H), 0.85 (dt, *J* = 14.8, 7.3 Hz, 6H).

**$^{13}$C NMR (151 MHz, $CDCl_3$) δ:** 171.91, 164.16, 162.49, 148.73 (d, *J* = 9.0 Hz), 147.28 (d, *J* = 8.3 Hz), 142.91 (d, *J* = 8.9 Hz), 133.94, 130.83, 130.41, 129.96, 129.58, 129.03 (d, *J* = 5.1 Hz), 128.85 (d, *J* = 4.0 Hz), 126.38, 126.12, 122.03 (d, *J* = 4.0 Hz), 117.67 (d, *J* = 21.2 Hz), 53.21, 48.17, 47.16, 33.66, 31.39, 29.70, 23.32, 20.40 (d, *J* = 4.8 Hz), 14.12.

**$^{19}$F NMR (400 MHz; $CDCl_3$) δ:** –108.74.

**$^{31}$P NMR (400 MHz; $CDCl_3$) δ:** 3.26.

**HRMS (ESI-/TOF, *m/z*):** Exact mass calculated for $[C_{31}H_{38}FN_2O_7PS]^-$ requires 631.2049; found 631.205.



**P3**

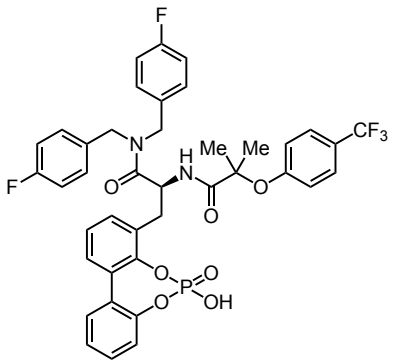
***N*-((*S*)-1-(azacyclotridecan-1-yl)-3-((*S*)-6-hydroxy-6-oxidodibenzo[*d*,*f*][1,3,2]dioxaphosphepin-4-yl)-1-oxopropan-2-yl)-2-(4-cyclohexylphenyl)acetamide (P3)**. Catalyst **P3** was synthesized from **9c** using General Procedures 3A and 4A. Purification was done by normal phase chromatography using 5–15% MeOH/$CH_2Cl_2$ as eluent. **P3** was obtained as a white solid (31% yield over 3 steps).

**$^1$H NMR (600 MHz, $CD_3CN$) δ:** 8.23 (s, 1H), 7.59 (dd, *J* = 7.7, 1.7 Hz, 1H), 7.46 (ddd, *J* = 11.1, 7.7, 1.7 Hz, 2H), 7.36 (tt, *J* = 7.5, 1.2 Hz, 1H), 7.32 – 7.27 (m, 1H), 7.25 (dt, *J* = 8.1, 1.4 Hz, 1H), 7.19 (td, *J* = 7.7, 1.0 Hz, 1H), 6.95 (d, *J* = 8.1 Hz, 2H), 6.87 (d, *J* = 7.9 Hz, 2H), 5.19 (td, *J* = 9.1, 6.2 Hz, 1H), 3.48 (ddd, *J* = 15.1, 9.4, 5.5 Hz, 1H), 3.42 – 3.28 (m, 4H), 3.28 – 3.17 (m, 2H), 2.99 (dd, *J* = 13.7, 6.2 Hz, 1H), 2.39 (tt, *J* = 11.5, 3.4 Hz, 2H), 2.13 – 2.08 (m, 7H, *residual water present*), 2.05 (dt, *J* = 5.0, 2.5 Hz, 2H), 2.02 (q, *J* = 6.8 Hz, 2H), 1.80 – 1.67 (m, 6H), 1.51 – 1.03 (m, 26H).

**$^{13}$C NMR (151 MHz, $CDCl_3$) δ:** 171.60, 170.80, 148.85, 147.45, 144.92, 142.20, 140.18, 138.15, 131.68, 129.15, 128.95, 128.69, 128.45, 128.27, 127.82, 127.23, 125.95, 125.68, 123.84, 123.78, 120.83, 63.38, 49.35, 48.43, 46.98, 44.16, 43.03, 41.16, 33.37, 33.29, 28.66, 28.39, 27.19, 26.08, 25.85, 25.10, 24.44, 24.36, 24.32, 24.12, 24.00, 23.94, 23.53, 23.30, 23.23, 13.08.

**$^{31}$P NMR (243 MHz, $CDCl_3$) δ:** 5.04.

**HRMS (ESI-/TOF, *m/z*):** Exact mass calculated for $[C_{41}H_{53}N_2O_6P]^-$ requires 699.3552; found 699.3557.



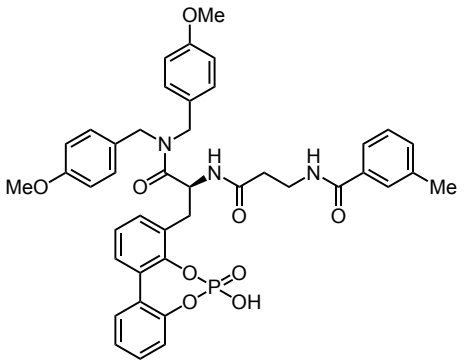
P4

**(*S*)-*N*,*N*-bis(4-fluorobenzyl)-3-((*S*)-6-hydroxy-6-oxidodibenzo[*d*,*f*][1,3,2]dioxaphosphepin-4-yl)-2-(2-methyl-2-(4-(trifluoromethyl)phenoxy)propanamido)propenamide (P4)**. Catalyst **P4** was synthesized from **9d** using General Procedures 3A and 4A. Purification was done by reverse phase chromatography using 10-50% acetonitrile in water as eluent. **P4** was obtained as a white foam (16% yield over 3 steps).

**$^{19}$F NMR (565 MHz, $CDCl_3$) δ:** -61.80 (s, 3F), -113.78 (s, 1F), -114.29 (s, 1F).

**$^{31}$P NMR (243 MHz, $CDCl_3$) δ:** 3.96.

**HRMS (ESI-/TOF, *m/z*):** Exact mass calculated for $[C_{40}H_{34}F_5N_2O_7P]^-$ requires 779.1951; found 779.1951.




**P5**

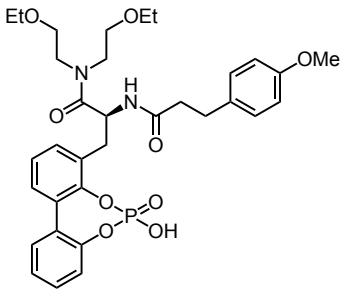
***N*-(3-(((*S*)-1-(bis(4-methoxybenzyl)amino)-3-((*S*)-6-hydroxy-6-oxidodibenzo[*d*,*f*][1,3,2]dioxaphosphepin-4-yl)-1-oxopropan-2-yl)amino)-3-oxopropyl)-3-methylbenzamide (P5)**. Catalyst **P5** was synthesized from **9e** using General Procedures 3A and 4A. Purification was done by reverse phase chromatography using 10–50% acetonitrile in water as eluent. **P5** was obtained as a white solid (18% yield over 3 steps).

**$^{1}$H NMR (600 MHz, $CDCl_3$) δ:** 8.50 (s, 1H), 7.68 (d, *J* = 46.1 Hz, 1H), 7.52 (s, 2H), 7.42 (dd, *J* = 16.3, 7.4 Hz, 4H), 7.36 – 7.21 (m, 4H), 7.21 – 7.08 (m, 3H), 7.02 (d, *J* = 8.0 Hz, 1H), 6.86 (dd, *J* = 16.7, 7.8 Hz, 2H), 6.73 (d, *J* = 8.2 Hz, 2H), 5.30 (s, 1H), 4.60 (d, *J* = 14.5 Hz, 1H), 4.52 (d, *J* = 16.4 Hz, 1H), 4.25 (d, *J* = 15.9 Hz, 1H), 3.74 (s, 3H), 3.70 (s, 3H), 3.58 – 3.45 (m, 2H), 3.44 – 3.33 (m, 1H), 2.92 – 2.61 (m, 1H), 2.25 (s, 3H), 1.27 (t, *J* = 10.7 Hz, 2H).

**$^{13}$C NMR (101 MHz, $CDCl_3$) δ:** 172.99, 172.57, 167.85, 159.22, 158.98, 148.91, 147.53, 138.09, 134.19, 131.99, 130.10, 129.82, 129.54, 129.22, 128.78, 128.54, 128.36, 128.20, 127.91, 125.56, 125.32, 124.14, 121.74, 114.34, 114.03, 55.29, 55.21, 50.74, 49.53, 48.23, 36.38, 34.86, 31.04, 29.73, 21.25.

**$^{31}$P NMR (400 MHz; $CDCl_3$) δ:** 3.86.

**HRMS (ESI-/TOF, *m/z*):** Exact mass calculated for $[C_{42}H_{42}N_3O_9P]^-$ requires 762.2582; found 762.2583.




**P6**

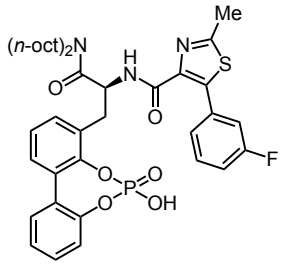
**(*S*)-*N*,*N*-bis(2-ethoxyethyl)-3-((*S*)-6-hydroxy-6-oxidodibenzo[*d*,*f*][1,3,2]dioxaphosphepin-4-yl)-2-(3-(4-methoxyphenyl)propanamido)propenamide (P6).** Catalyst **P6** was synthesized from **9f** using General Procedures 3A and 4A. Purification was done by reverse phase chromatography using 10–50% acetonitrile in water as eluent. **P6** was obtained as a white solid (20% yield over 3 steps).

**$^{1}$H NMR (600 MHz, $CDCl_3$) δ:** 7.85 – 7.69 (brs, 1H), 7.48 (d, *J* = 7.2 Hz, 1H), 7.39 (d, *J* = 6.9 Hz, 2H), 7.33 – 7.23 (m, 4H), 7.20 (d, *J* = 7.3 Hz, 1H), 6.94 (d, *J* = 8.0 Hz, 2H), 6.67 (d, *J* = 8.3 Hz, 2H), 5.41 (s, 1H), 3.96 (s, 1H), 3.75 – 3.60 (m, 4H), 3.54 (t, *J* = 15.0 Hz, 3H), 3.44 (ddd, *J* = 36.1, 13.8, 5.5 Hz, 8H), 3.34 (s, 1H), 3.11 (d, *J* = 9.4 Hz, 1H), 2.60 (d, *J* = 23.6 Hz, 2H), 2.35 (s, 2H), 1.21 – 1.07 (m, 6H).

**$^{13}$C NMR (151 MHz; $CDCl_3$) δ:** 157.85, 129.92, 129.20, 113.77, 68.15, 66.78, 66.48, 55.14, 30.65, 15.15, 15.08.

**$^{31}$P NMR** (600 MHz; $CDCl_3$): δ 2.72.

**HRMS (ESI-/TOF, *m/z*):** Exact mass calculated for $[C_{33}H_{41}N_2O_9P]^-$ requires 639.2477; found 639.2468.




**P7**

***N*-((*S*)- 1-(dioctylamino)-3-((*S*)-6-hydroxy-6-oxidodibenzo[*d*,*f*][1,3,2]dioxaphosphepin-4-yl)-1-oxopropan-2-yl)-5-(3-fluorophenyl)-2-methylthiazole-4-carboxamide (P7).** Catalyst **P7** was synthesized from **9g** using General Procedures 3A and 4A. Purification was done by reverse phase chromatography using 10–50% acetonitrile in water as eluent. **P7** was obtained as a yellow solid (43% yield over 3 steps).

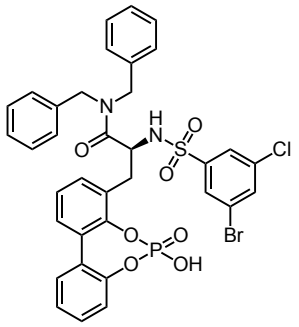
**$^{1}$H NMR (600 MHz, $CDCl_3$) δ** 8.66 (s, 1H), 7.46 (dt, *J* = 15.7, 7.9 Hz, 3H), 7.38 (d, *J* = 7.8 Hz, 1H), 7.36 – 7.28 (m, 1H), 7.22 (d, *J* = 7.5 Hz, 1H), 7.17 (t, *J* = 7.5 Hz, 1H), 7.11 (d, *J* = 7.1 Hz, 1H), 6.93 (s, 2H), 6.81 (s, 1H), 5.51 (d, *J* = 7.1 Hz, 1H), 3.63 (s, 1H), 3.40 (d, *J* = 39.8 Hz, 2H), 3.22 – 2.87 (m, 3H), 2.70 (s, 3H), 1.37 – 1.08 (m, 24H), 0.88 (t, *J* = 6.8 Hz, 3H), 0.81 (t, *J* = 6.9 Hz, 3H).

**$^{13}$C NMR (151 MHz, $CDCl_3$) δ** 169.89, 164.41, 161.67, 147.88, 147.53, 143.46, 139.42, 132.48, 130.17, 129.79, 129.50, 129.37, 128.77, 128.33, 126.11, 125.74, 125.20, 121.83, 116.95 (d, *J* = 23.1 Hz), 115.99 (d, *J* = 21.0 Hz), 49.63, 48.33, 46.54, 34.91, 31.80, 31.74, 29.49, 29.33, 29.23, 29.06, 27.54, 27.01, 26.33, 22.63, 22.57, 19.01, 14.09, 14.05.

**$^{19}$F NMR (600 MHz; $CDCl_3$) δ** –113.38.

**$^{31}$P NMR (600 MHz; $CDCl_3$) δ** 0.36.

**HRMS (ESI-/TOF, *m*/*z*):** Exact mass calculated for $[C_{42}H_{53}FN_3O_6PS]^-$ requires 776.3304; found 776.3305.



**P8**

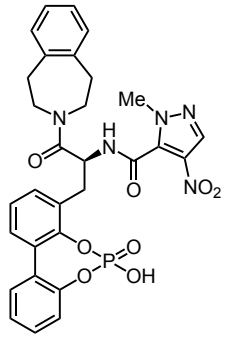
**(*S*)-*N*,*N*-dibenzyl-2-((3-bromo-5-chlorophenyl)sulfonamido)-3-((*S*)-6-hydroxy-6-oxidodibenzo[*d*,*f*][1,3,2]dioxaphosphepin-4-yl)propenamide (P8).** Catalyst **P8** was synthesized from **9h** using General Procedures 3B and 4B. Purification was done by reverse phase chromatography using 10–50% acetonitrile in water as eluent (with 0.1% formic acid). **P9** was obtained as a yellow solid (32% yield over 3 steps).

**$^{1}$H NMR (600 MHz, $CDCl_3$) δ** 7.47 (s, 1H), 7.42 (t, *J* = 7.6 Hz, 3H), 7.36 (dd, *J* = 18.1, 8.1 Hz, 4H), 7.32 – 7.27 (m, 6H), 7.19 (d, *J* = 7.3 Hz, 1H), 6.76 (s, 1H), 6.07 (d, *J* = 4.9 Hz, 1H), 4.88 (d, *J* = 16.4 Hz, 1H), 4.78 (d, *J* = 14.3 Hz, 1H), 4.66 (dd, *J* = 24.7, 16.0 Hz, 2H), 4.37 (d, *J* = 9.8 Hz, 1H), 3.43 (s, 1H), 2.54 (s, 1H).

**$^{13}$C NMR (151 MHz, $CDCl_3$) δ** 173.48, 148.67, 146.78, 143.29, 136.57, 136.08, 135.59, 134.57, 130.01, 129.38, 129.08, 128.88, 128.33, 128.19, 127.80, 127.50, 126.69, 125.85, 125.21, 125.01, 123.00, 121.84, 77.23, 77.01, 76.80, 67.10, 54.68, 50.90, 30.81, 29.71, 1.02.

**$^{31}$P NMR (243 MHz, $CDCl_3$) δ** 3.49.

**HRMS (ESI-/TOF, *m*/*z*):** Exact mass calculated for $[C_{35}H_{28}BrClN_2O_7PS]^-$ requires 765.0227; found 765.0244.



P9

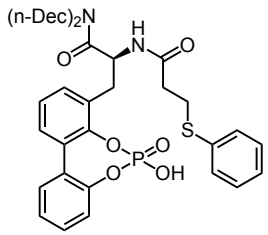
***N*-((*S*)-3-((*S*)-6-hydroxy-6-oxidodibenzo[*d*,*f*][1,3,2]dioxaphosphepin-4-yl)-1-oxo-1-(1,2,4,5-tetrahydro-3*H*-benzo[*d*]azepin-3-yl)propan-2-yl)-1-methyl-4-nitro-1*H*-pyrazole-5-carboxamide (P9).** Catalyst **P9** was synthesized from **9i** using General Procedures 3A and 4A. Purification was done by normal phase chromatography using 10–40% MeOH/$CH_2Cl_2$ as eluent (with 0.5% formic acid). **P9** was obtained as a beige solid (12% yield over 3 steps).

**$^1$H NMR (600 MHz, $CDCl_3$)** δ 9.02 (d, *J* = 7.9 Hz, 1H), 7.87 (d, *J* = 9.5 Hz, 1H), 7.53 – 7.37 (m, 4H), 7.32 (q, *J* = 7.2 Hz, 2H), 7.24 (d, *J* = 8.2 Hz, 1H), 7.18 – 6.90 (m, 7H), 5.70 – 5.48 (m, 1H), 3.92 (dt, *J* = 13.5, 5.4 Hz, 2H), 3.14 (ddd, *J* = 30.2, 14.6, 7.4 Hz, 2H), 2.93 (dd, *J* = 15.6, 8.6 Hz, 1H), 2.79 (td, *J* = 15.8, 7.3 Hz, 2H).

**$^{13}$C NMR (151 MHz, $CDCl_3$) δ** 180.79, 169.92, 157.55, 149.46, 140.60, 139.76, 135.19, 134.95, 134.94, 132.69, 130.17, 130.16, 129.77, 129.39, 128.90, 128.51, 126.75, 126.54, 125.10, 124.93, 121.86, 77.23, 77.01, 76.80, 60.40, 49.98, 48.77, 45.98, 37.88, 36.80, 29.71, 14.20.

**$^{31}$P NMR (243 MHz, $CDCl_3$) δ** 4.70.

**HRMS (ESI-/TOF, *m/z*):** Exact mass calculated for $[C_{30}H_{37}N_2O_{10}PS]^-$ requires 647.1827; found 647.1826.




**P10**

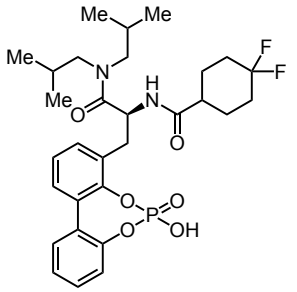
**(*S*)-*N*,*N*-didecyl-3-((*S*)-6-hydroxy-6-oxidodibenzo[*d*,*f*][1,3,2]dioxaphosphepin-4-yl)-2-(3-(phenylthio)propanamido)propenamide (P10).** Catalyst **P10** was synthesized from **9j** using General Procedures 3A and 4B. Purification was done by reverse phase chromatography using 10–20% MeOH/$CH_2Cl_2$ as eluent. **P10** was obtained as a yellow solid (43% yield over 3 steps).

**$^1$H NMR (400 MHz, $CDCl_3$) δ** 8.15 (s, 1H), 7.51 (d, *J* = 7.3 Hz, 1H), 7.47 – 7.38 (m, 2H), 7.34 (dd, *J* = 12.9, 7.5 Hz, 2H), 7.30 – 7.24 (m, 3H), 7.21 (t, *J* = 7.5 Hz, 2H), 7.13 (t, *J* = 7.2 Hz, 1H), 5.30 (q, *J* = 7.7 Hz, 1H), 3.51 – 3.25 (m, 4H), 3.20 (dt, *J* = 13.7, 7.6 Hz, 2H), 3.03 (dp, *J* = 10.4, 5.9 Hz, 2H), 2.52 (t, *J* = 7.5 Hz, 2H), 1.30 (d, *J* = 14.3 Hz, 32H), 0.99 – 0.89 (m, 6H).

**$^{13}$C NMR (151 MHz, $CDCl_3$) δ** 172.11, 171.74, 148.71 (d, *J* = 8.4 Hz), 147.61 (d, *J* = 8.9 Hz), 135.98, 131.13, 130.27, 129.99, 129.79, 129.72 (d, *J* = 3.3 Hz), 129.33, 129.31, 129.26, 129.16, 128.97, 126.36, 126.19, 125.90, 122.09 (d, *J* = 3.9 Hz), 50.30, 48.81, 47.47, 35.85, 32.21, 29.91, 29.89, 29.85, 29.69, 29.67, 29.62, 29.60, 29.56, 29.54, 27.77, 27.35, 27.04, 22.99, 14.43.

**$^{31}$P NMR (400 MHz; $CDCl_3$):** δ 2.08.

**HRMS (ESI-/TOF, *m/z*):** Exact mass calculated for $[C_{44}H_{63}N_2O_6PS]^-$ requires 777.4080; found 777.4082.




**P11**

***N*-((*S*)-1-(diisobutylamino)-3-((*S*)-6-hydroxy-6-oxidodibenzo[*d*,*f*][1,3,2]dioxaphosphepin-4-yl)-1-oxopropan-2-yl)-4,4-difluorocyclohexane-1-carboxamide (P11).** Catalyst **P11** was synthesized from **9k** using General Procedures 3B and 4B. Purification was done by reverse phase chromatography using 10–50% acetonitrile in water as eluent (with 0.1% formic acid). **P11** was obtained as a yellow solid (54% yield over 3 steps and purification).

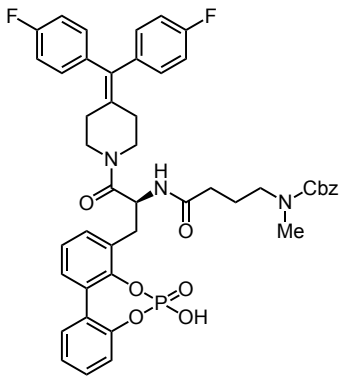
**$^{1}$H NMR (600 MHz, $CDCl_3$) δ** 7.63 (s, 1H), 7.50 (dd, *J* = 7.9, 1.6 Hz, 1H), 7.46 (td, *J* = 5.3, 2.7 Hz, 2H), 7.35 (t, *J* = 7.1 Hz, 2H), 7.26 (td, *J* = 8.8, 4.8 Hz, 2H), 5.39 (q, *J* = 7.8 Hz, 1H), 3.44 (ddd, *J* = 20.6, 13.3, 6.2 Hz, 2H), 3.32 (dd, *J* = 14.5, 8.5 Hz, 1H), 3.20 (s, 2H), 3.06 (dd, *J* = 12.8, 7.7 Hz, 1H), 2.20 (q, *J* = 8.1 Hz, 1H), 2.08 – 1.89 (m, 4H), 1.77 (s, 1H), 1.73 – 1.47 (m, 5H), 1.04 (d, *J* = 6.6 Hz, 3H), 0.98 (d, *J* = 6.6 Hz, 3H), 0.88 (t, *J* = 6.9 Hz, 6H).

**$^{13}$C NMR (151 MHz, $CDCl_3$) δ** 175.50, 172.39, 147.98, 147.23 (d, *J* = 9.3 Hz), 130.19, 129.84, 129.43, 126.20, 125.61, 121.69 (d, *J* = 3.9 Hz), 55.72, 54.16, 49.79, 42.18, 42.08, 32.56 (t, *J* = 24.5 Hz), 28.28, 28.19, 26.51, 25.56 (d, *J* = 9.0 Hz), 25.46 (d, *J* = 8.7 Hz).

**$^{19}$F NMR (565 MHz, $CDCl_3$) δ** -93.10 (d, *J* = 233.0 Hz), -100.79 (d, *J* = 233.0 Hz).

**$^{31}$P NMR (243 MHz, $CDCl_3$) δ** 1.12, 0.75.

**HRMS (ESI-/TOF, *m/z*):** Exact mass calculated for $[C_{30}H_{38}F_2N_2O_6P]^-$ requires 591.2441; found 591.2445.



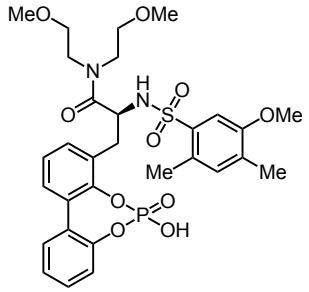

**P12**

**Benzyl (4-(((*S*)-1-(4-(bis(4-fluorophenyl)methylene)piperidin-1-yl)-3-((*S*)-6-hydroxy-6-oxidodibenzo[*d*,*f*][1,3,2]dioxaphosphepin-4-yl)-1-oxopropan-2-yl)amino)-4-oxobutyl)(methyl)carbamate (P12).** Catalyst **P12** was synthesized from **9l** using deprotection General Procedures 3B and 4B. Purification was done by reverse phase chromatography using 10–50% acetonitrile in water as eluent (with 0.1% formic acid). **P12** was obtained as a white solid (9% yield over 3 steps and purification).

**$^{19}$F NMR (565 MHz, $CDCl_3$) δ** -115.28.

**$^{31}$P NMR (243 MHz, $CDCl_3$) δ** 6.32.

**HRMS (ESI-/TOF, *m/z*):** Exact mass calculated for $[C_{46}H_{43}F_2N_3O_8P]^-$ requires 834.2761; found 834.2772.



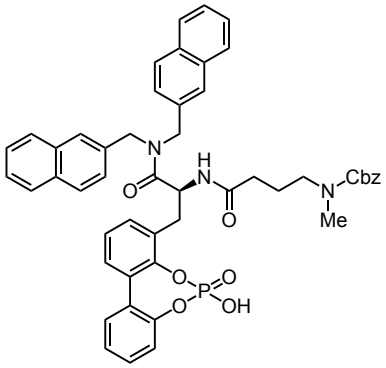

**P13**

***(S)*-3-((*S*)-6-hydroxy-6-oxidodibenzo[*d*,*f*][1,3,2]dioxaphosphepin-4-yl)-2-((5-methoxy-2,4-dimethylphenyl)sulfonamido)-*N*,*N*-bis(2-methoxyethyl)propanamide (P13).** Catalyst **P13** was synthesized from **9m** using deprotection General Procedures 3A and 4B. Purification was done by normal phase chromatography using 10–50% MeOH/$CH_2Cl_2$ as eluent (with 0.5% formic acid). **P13** was obtained as a off-white solid (72% yield over 3 steps).

**$^1$H NMR (600 MHz, $CDCl_3$)** δ 7.49 (dd, *J* = 7.4, 1.8 Hz, 1H), 7.46 – 7.38 (m, 1H), 7.38 – 7.28 (m, 3H), 7.25 (s, 1H), 7.18 – 6.98 (m, 6H), 6.81 (s, 1H), 4.61 (dd, *J* = 9.8, 4.9 Hz, 1H), 3.86 – 3.75 (m, 1H), 3.72 (s, 3H), 3.57 (d, *J* = 4.3 Hz, 1H), 3.50 (t, *J* = 6.5 Hz, 2H), 3.42 (q, *J* = 4.5 Hz, 4H), 3.24 (d, *J* = 5.6 Hz, 6H), 2.19 (s, 3H), 2.15 (s, 3H), 2.10 (s, 1H).

**$^{31}$P NMR (243 MHz, $CDCl_3$)** δ -2.62

**HRMS (ESI-/TOF, *m*/*z*):** Exact mass calculated for $[C_{30}H_{37}N_2O_{10}PS]^-$ requires 647.1827; found 647.1826.




**P14**

**benzyl(4-(((*S*)-1-(bis(naphthalen-2-ylmethyl)amino)-3-((*S*)-6-hydroxy-6-oxidodibenzo[*d*,*f*][1,3,2]dioxaphosphepin-4-yl)-1-oxopropan-2-yl)amino)-4-oxobutyl)(methyl)carbamate (P14).**

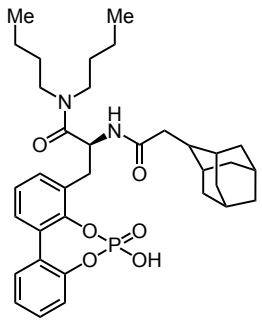
Catalyst **P14** was synthesized from **9n** using General Procedures 3A and 4A. Purification was done by reverse phase chromatography using 5–40% acetonitrile in water as eluent (with 0.5% formic acid). **P14** was obtained as a beige foam (45% yield over 3 steps).

**$^{1}$H NMR (600 MHz, $CD_3CN$) δ** 8.94 (d, *J* = 97.3 Hz, 1H), 7.97 – 7.66 (m, 7H), 7.60 (s, 1H), 7.45 (ddd, *J* = 9.6, 6.5, 3.5 Hz, 5H), 7.39 (d, *J* = 8.5 Hz, 1H), 7.35 – 7.19 (m, 9H), 7.16 (d, *J* = 8.0 Hz, 1H), 6.90 (dd, *J* = 57.1, 30.9 Hz, 2H), 5.37 (s, 1H), 4.91 (d, *J* = 60.5 Hz, 4H), 4.78 – 4.56 (m, 2H), 3.66 – 3.32 (m, 2H), 3.04 – 2.87 (m, 1H), 2.92 – 2.67 (m, 2H), 2.58 (s, 2H), 2.51 (s, 2H), 1.60 – 1.38 (m, 3H), 1.27 (s, 3H).

**$^{13}$C NMR (151 MHz, $CD_3CN$) δ** 174.62, 173.18, 156.74, 150.62, 149.20, 137.78, 135.51, 135.25, 133.93, 133.89, 133.37, 133.23, 130.45, 129.99, 129.11, 128.95, 128.75, 128.30, 128.24, 128.17, 128.10, 127.07, 126.98, 126.75, 126.71, 126.64, 126.56, 126.40, 125.98, 122.38, 117.89, 67.21, 66.72, 51.36, 49.88, 48.49, 34.37, 33.79, 32.71, 32.23, 30.81, 29.95, 24.14, 23.36, 22.98, 13.97.

**$^{31}$P NMR (243 MHz, $CD_3CN$) δ** 5.25.

**HRMS (ESI-/TOF, *m/z*):** Exact mass calculated for $[C_{50}H_{46}N_3O_8P]^-$ requires 846.2963; found 846.2961.




**P15**

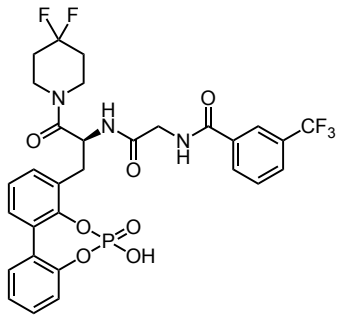
**(*S*)-2-(2-((1*S*,3*S*,5*S*,7*S*)-adamantan-2-yl)acetamido)-*N*,*N*-dibutyl-3-((*S*)-6-hydroxy-6-oxidodibenzo[*d*,*f*][1,3,2]dioxaphosphepin-4-yl)propenamide (P15).**
Catalyst **P15** was synthesized from **9o** using deprotection General Procedures 3A and 4A. Purification was done by reverse phase chromatography using 10–70% acetonitrile in water as eluent. **P15** was obtained as a white solid (22% yield over 3 steps).

**$^{1}$H NMR (400 MHz, $CDCl_3$) δ** 7.61 – 7.40 (m, 4H), 7.33 (dd, *J* = 19.9, 7.9 Hz, 3H), 7.21 (d, *J* = 6.3 Hz, 2H), 5.38 (s, 1H), 3.53 (s, 1H), 3.35 (s, 2H), 3.19 (s, 3H), 2.26 (s, 2H), 1.99 (s, 1H), 1.68 (d, *J* = 34.3 Hz, 8H), 1.58 – 1.12 (m, 16H), 1.06 – 0.71 (m, 8H).

*Note: $^{13}$C NMR spectrum could not be obtained; poor solubility in all available deuterated solvents.*

**$^{31}$P NMR (400 MHz; $CDCl_3$): δ** 1.15.

**HRMS (ESI-/TOF, *m/z*):** Exact mass calculated for $[C_{35}H_{47}N_2O_6P]^-$ requires 621.3099; found 621.3098.



**P16**

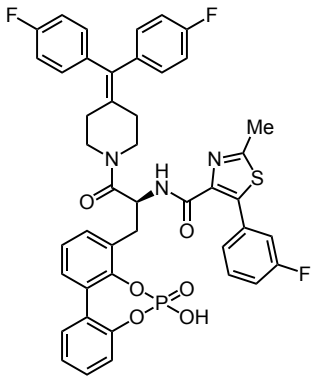
***N*-(2-(((*S*)-1-(4,4-difluoropiperidin-1-yl)-3-((*S*)-6-hydroxy-6-oxidodibenzo[*d*,*f*][1,3,2]dioxaphosphepin-4-yl)-1-oxopropan-2-yl)amino)-2-oxoethyl)-3-(trifluoromethyl)benzamide (P16)**. Catalyst **P16** was synthesized from **9p** using General Procedures 3A and 4B. Purification was done by normal phase chromatography using 5–55% MeOH/$CH_2Cl_2$ as eluent. **P16** was obtained as a yellow solid (23% yield over 3 steps).

**$^{13}$C NMR (151 MHz, $CDCl_3$)** δ 206.01, 169.53, 168.67, 167.07, 165.45, 164.90, 147.77, 146.63, 133.01, 132.37, 129.68, 129.53, 129.42, 128.93, 128.83, 128.63, 128.32, 128.22, 128.04, 127.91, 127.60, 127.32, 127.07, 124.67, 124.49, 123.52, 123.47, 121.72, 120.57, 120.05, 52.40, 48.63, 42.23, 41.53, 40.19, 38.26, 35.69, 32.38, 30.90, 29.90, 28.68, 28.34, 27.21, 27.00, 21.67, 13.09.

**$^{19}$F NMR (376 MHz, $CDCl_3$)** δ -60.83 – -64.53 (m, 3F), -98.24 (brs, 2F).

**$^{31}$P NMR (243 MHz, $CDCl_3$) δ** 3.57.

**HRMS (ESI-/TOF, *m/z*):** Exact mass calculated for $[C_{30}H_{27}F_5N_3O_7P]^-$ requires 666.1431; found 666.1429.



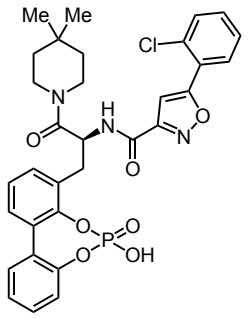
P17

***N*-((*S*)-1-(4-(bis(4-fluorophenyl)methylene)piperidin-1-yl)-3-((*S*)-6-hydroxy-6-oxidodibenzo[*d*,*f*][1,3,2]dioxaphosphepin-4-yl)-1-oxopropan-2-yl)-5-(3-fluorophenyl)-2-methylthiazole-4-carboxamide (P17)**. Catalyst **P17** was synthesized from **9q** using General Procedures 3B and 4B. Purification was done by reverse phase chromatography using 10–50% acetonitrile in water as eluent (with 1% formic acid). **P17** was obtained as a white solid (17% yield over 3 steps).

**$^{19}$F NMR (565 MHz, $CDCl_3$) δ** -113.03, -115.50, -115.62.

**$^{31}$P NMR (243 MHz, $CDCl_3$) δ** 4.41.

**HRMS (ESI-/TOF, *m/z*):** Exact mass calculated for $[C_{44}H_{35}F_3N_3O_6PS]^-$ requires 820.1864; found 820.1859.




**P18**

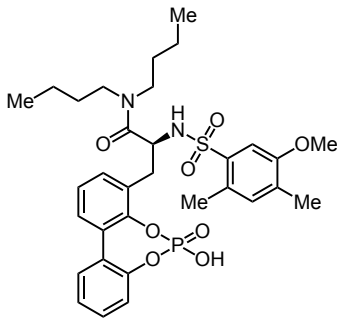
**5-(2-chlorophenyl)-*N*-((*S*)-1-(4,4-dimethylpiperidin-1-yl)-3-((*S*)-6-hydroxy-6-oxidodibenzo[*d*,*f*][1,3,2]dioxaphosphepin-4-yl)-1-oxopropan-2-yl)isoxazole-3-carboxamide (P18)**. Catalyst **P18** was synthesized from **9r** using General Procedures 3A and 4B. Purification was done by reverse phase chromatography using 20–50% acetonitrile in water as eluent. **P18** was obtained as a yellow foam (64% yield over 3 steps).

**$^{1}$H NMR (600 MHz, $CDCl_3$) δ** 8.17 (s, 1H), 7.73 (s, 1H), 7.54 – 7.05 (m, 14H, solvent), 5.79 (s, 1H), 3.92 – 2.96 (m, 6H), 1.47 – 0.93 (m, 6H), 0.80 (s, 3H), 0.74 (s, 3H).

**$^{13}$C NMR (151 MHz, $CDCl_3$) δ** 169.17, 167.76, 158.75, 158.62, 148.71 (d, $J$ = 8.0 Hz), 147.49 (d, $J$ = 7.7 Hz), 132.00, 131.79, 130.86, 129.90, 129.75, 129.52, 129.42, 128.97, 128.73, 127.15, 125.80, 125.61, 121.79, 103.97, 48.87, 42.53, 39.08, 38.23, 37.95, 34.05, 29.77, 28.85, 28.29, 26.81.

**$^{31}$P NMR (600 MHz; $CDCl_3$):** δ 3.04.

**HRMS (ESI-/TOF, *m/z*):** Exact mass calculated for $[C_{32}H_{31}ClN_3O_7P]^-$ requires 634.1511; found 634.1510.



P19

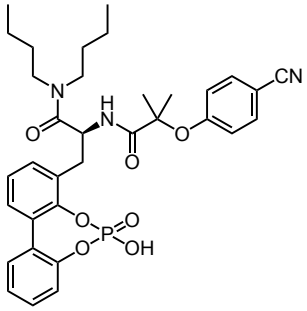
**(*S*)-*N*,*N*-dibutyl-3-((*S*)-6-hydroxy-6-oxidodibenzo[*d*,*f*][1,3,2]dioxaphosphepin-4-yl)-2-((5-methoxy-2,4-dimethylphenyl)sulfonamido)propenamide (P19)**. Catalyst **P19** was synthesized from **9s** using General Procedures 3B and 4B. Purification was done by reverse phase chromatography using 10–50% acetonitrile in water as eluent (with 0.1% formic acid). **P19** was obtained as a white solid (22% yield over 3 steps).

**$^{1}$H NMR (600 MHz, $CDCl_3$) δ** 8.47 (d, *J* = 38.2 Hz, 1H), 7.39 (d, *J* = 6.8 Hz, 2H), 7.27 (d, *J* = 10.0 Hz, 2H), 7.15 (t, *J* = 7.0 Hz, 1H), 6.83 (t, *J* = 6.8 Hz, 1H), 6.72 (d, *J* = 15.4 Hz, 2H), 4.27 (s, 1H), 3.68 (s, 3H), 3.55 (s, 1H), 3.06 (s, 2H), 3.01 – 2.71 (m, 4H), 2.65 (s, 1H), 2.11 (s, 3H), 2.05 (s, 3H), 1.20 (d, *J* = 24.1 Hz, 4H), 1.11 – 0.94 (m, 2H), 0.94 – 0.75 (m, 3H), 0.73 (t, *J* = 6.6 Hz, 3H).

**$^{13}$C NMR (151 MHz, $CDCl_3$) δ** 172.08, 155.10, 150.34 (d, *J* = 8.9 Hz), 148.83 (d, *J* = 8.5 Hz), 136.13, 134.76, 130.92, 130.62, 129.88, 129.66, 129.02, 128.96, 128.68, 127.95, 124.62, 124.44, 122.55, 110.63, 55.77, 53.21, 47.67, 46.82, 31.19, 29.41, 20.18, 18.64, 16.06, 13.95, 13.85.

**$^{31}$P NMR (243 MHz, $CDCl_3$) δ** 5.92.

**HRMS (ESI-/TOF, *m/z*):** Exact mass calculated for $[C_{32}H_{40}N_2O_6PS]^-$ requires 643.2249; found 643.2252.



**P20**

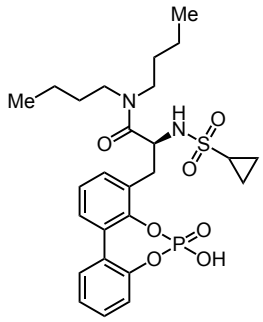
**(*S*)-*N*,*N*-dibutyl-2-(2-(4-cyanophenoxy)-2-methylpropanamido)-3-((*S*)-6-hydroxy-6-oxidodibenzo[*d*,*f*][1,3,2]dioxaphosphepin-4-yl)propenamide (P20)**.
Catalyst **P20** was synthesized from **9t** using deprotection General Procedures 3A and 4A. Purification was done by reverse phase chromatography using 10–50% acetonitrile in water as eluent (with 0.1% formic acid). **P20** was obtained as a yellow solid (28% yield over 3 steps).

**$^{1}$H NMR (600 MHz, $CDCl_3$) δ** 7.43 (d, *J* = 7.6 Hz, 1H), 7.31 (d, *J* = 7.5 Hz, 3H), 7.24 (d, *J* = 7.6 Hz, 1H), 7.20 – 7.03 (m, 4H), 6.69 – 6.48 (m, 2H), 5.13 (s, 1H), 3.70 (d, *J* = 16.1 Hz, 1H), 3.16 – 2.77 (m, 2H), 1.34 (s, 3H), 1.30 – 0.95 (m, 14H), 0.95 – 0.80 (m, 4H), 0.76 (d, *J* = 7.4 Hz, 3H).

**$^{13}$C NMR (151 MHz, $CDCl_3$) δ** 173.58, 171.63, 158.64, 149.93, 148.41, 133.10, 130.10, 129.61, 129.52, 129.08, 128.95, 128.11, 124.91, 124.74, 121.97, 119.10, 118.77, 104.03, 80.84, 49.28, 47.64, 46.47, 31.22, 29.71, 29.28, 25.19, 24.05, 19.97, 19.85, 13.85, 13.66, 1.02.

**$^{31}$P NMR (243 MHz, $CDCl_3$) δ** 7.45.

**HRMS (ESI-/TOF, *m*/*z*):** Exact mass calculated for $[C_{34}H_{39}N_3O_7P]^-$ requires 632.2531; found 632.2534.




**V1**

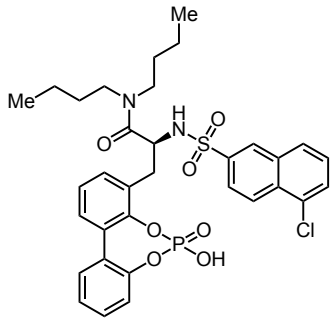
**(*S*)-*N*,*N*-dibutyl-2-(cyclopropanesulfonamido)-3-((*S*)-6-hydroxy-6-oxidodibenzo[*d*,*f*][1,3,2]dioxaphosphepin-4-yl)propenamide (V1).**
Catalyst **V1** was synthesized from **9u** using General Procedures 3B and 4B. Purification was performed using reverse phase chromatography with 10–50% acetonitrile in water as eluent (with 0.1% formic acid). **V1** was obtained as an off-white foam (70% yield over 3 steps).

**$^{1}$H NMR (500 MHz, $CDCl_3$) δ** 7.49 (d, *J* = 7.7 Hz, 1H), 7.46 – 7.39 (m, 2H), 7.37 – 7.27 (m, 4H), 4.72 (t, *J* = 7.4 Hz, 1H), 3.45 – 3.23 (m, 4H), 3.20 – 3.13 (m, 2H), 2.02 (brs, 1H), 1.58 (dp, *J* = 15.2, 7.6 Hz, 1H), 1.49 – 1.13 (m, 8H), 0.98 (d, *J* = 5.0 Hz, 2H), 0.86 (dt, *J* = 28.0, 7.4 Hz, 6H), 0.77 – 0.63 (m, 2H).

**$^{13}$C NMR (126 MHz, $CDCl_3$)** δ 172.0, 148.4 (d, *J* = 8.7 Hz), 147.3 (d, *J* = 8.6 Hz), 131.2, 130.1, 129.7, 129.4, 129.0 (s, 2C), 128.7, 126.1, 125.9, 121.8, 53.4, 48.0, 47.1, 33.4, 31.1, 31.0, 29.7, 29.3, 20.1, 20.0, 13.8, 5.7, 5.4.

**$^{31}$P NMR (203 MHz, $CDCl_3$) δ** 2.69.

**HRMS (ESI+/TOF, *m*/*z*):** Exact mass calculated for $[C_{26}H_{35}N_2O_7PS+H]^+$ requires 551.1981; found 551.1985.




**V2**

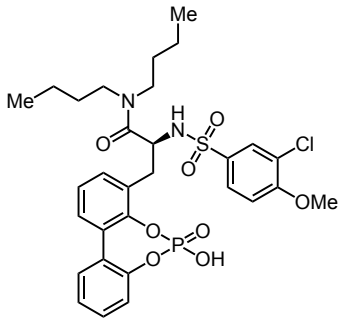
**(*S*)-*N*,*N*-dibutyl-2-((5-chloronaphthalene)-2-sulfonamido)-3-((*S*)-6-hydroxy-6-oxidodibenzo[*d*,*f*][1,3,2]dioxaphosphepin-4-yl)propenamide (V2)**.
Catalyst **V2** was synthesized from **9v** using General Procedures 3B and 4B. Purification was done by reverse phase chromatography using 10–50% acetonitrile in water as eluent (with 0.1% formic acid). **V2** was obtained as a white foam (47% yield over 3 steps).

**$^{1}$H NMR (500 MHz, DMSO) δ** 8.79 (d, *J* = 8.8 Hz, 1H), 8.26 (s 1H), 8.06 (d, *J* = 8.9 Hz, 1H), 7.99 (d, *J* = 8.2 Hz, 1H), 7.83 (d, *J* = 7.4 Hz, 1H), 7.72 (dd, *J* = 9.0, 1.8 Hz, 1H), 7.57 (t, *J* = 7.9 Hz, 1H), 7.47 – 7.39 (m, 2H), 7.31 (t, *J* = 7.5 Hz, 1H), 7.23 – 7.15 (m, 3H), 6.91 (t, *J* = 7.6 Hz, 1H), 4.43 (td, *J* = 8.8, 5.8 Hz, 1H), 3.24 – 3.11 (m, 2H), 3.01 – 2.87 (m, 4H), 1.38 – 1.28 (m, 1H), 1.23 – 1.07 (m, 3H), 1.03 – 0.87 (m, 4H), 0.71 (dt, *J* = 40.2, 7.3 Hz, 6H).

**$^{13}$C NMR (126 MHz, DMSO) δ** 169.8, 148.9 (d, *J* = 9.1 Hz), 147.5 (d, *J* = 8.8 Hz), 139.4, 133.0, 131.4, 130.9, 130.6, 129.6, 129.4, 129.2, 128.9 (d, *J* = 3.5 Hz), 128.8, 128.6, 128.1, 127.5, 127.2, 125.2, 124.8, 124.5, 123.9, 121.6, 121.5, 52.7, 46.8, 45.4, 33.0, 30.8, 29.0, 19.5, 19.3, 13.7, 13.6.

**$^{31}$P NMR (203 MHz, $CDCl_3$)** δ 3.84.

**HRMS (ESI+/TOF, *m*/*z*):** Exact mass calculated for $[C_{33}H_{36}ClN_2O_7PS+H]^+$ requires 671.1748; observed 671.1750.




**V3**

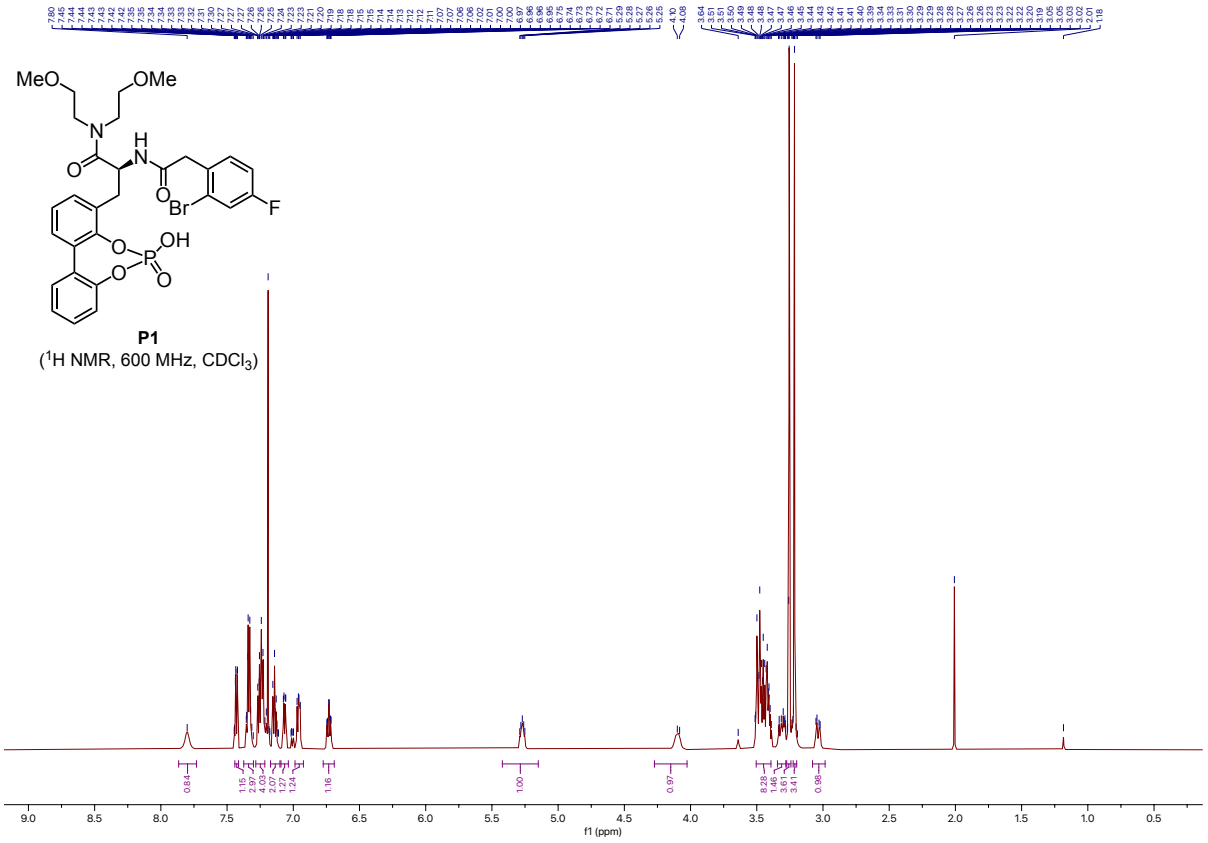
**(*S*)-*N*,*N*-dibutyl-2-((3-chloro-4-methoxyphenyl)sulfonamido)-3-((*S*)-6-hydroxy-6-oxidodibenzo[*d*,*f*][1,3,2]dioxaphosphepin-4-yl)propenamide (V3).**
Catalyst **V3** was synthesized from **9w** using General Procedures 3B and 4B. Purification was done by reverse phase chromatography using 10–50% acetonitrile in water as eluent (with 0.1% formic acid). **V3** was obtained as a white foam (51% yield over 3 steps).

**$^{1}$H NMR (500 MHz, $CDCl_3$)** δ 7.61 (d, *J* = 8.8 Hz, 1H), 7.57 (d, *J* = 2.3 Hz, 1H), 7.47 (d, *J* = 7.6, 1H), 7.40 (t, *J* = 7.4 Hz, 1H), 7.34 – 7.28 (m, 3H), 7.10 – 7.08 (m, 2H), 6.72 (d, *J* = 8.7 Hz, 1H), 4.58 – 4.52 (m, 1H), 3.78 (s, 3H), 3.39 (dd, *J* = 14.0, 9.5 Hz, 1H), 3.26 – 3.07 (m, 4H), 2.98 (brdd, *J* = 14.1, 6.1 Hz, 1H), 1.53 – 1.40 (m, 1H), 1.38 – 1.23 (m, 5H), 1.17 (h, *J* = 7.3 Hz, 2H), 0.85 (dt, *J* = 37.5, 7.3 Hz, 6H).

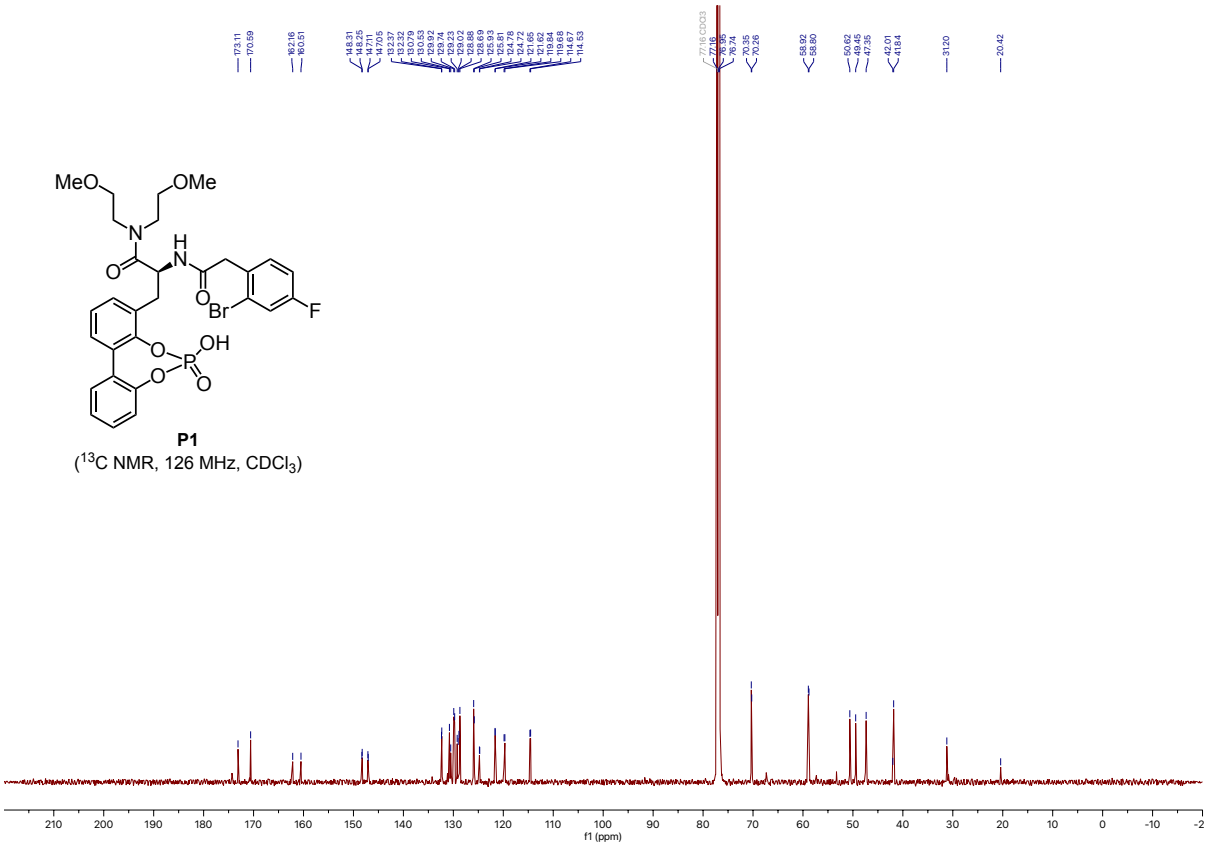
**$^{13}$C NMR (126 MHz, $CDCl_3$)** δ 171.2, 157.8, 148.5 (d, *J* = 8.9 Hz), 147.0 (d, *J* = 8.5 Hz), 132.9, 131.0, 130.0, 129.6, 129.1, 128.9, 128.8, 128.6, 128.4 (d, *J* = 4.1 Hz), 127.5, 125.9, 125.5, 122.6, 121.7 (d, *J* = 4.1 Hz), 111.5, 56.3, 53.2, 47.9, 46.9, 33.3, 31.0, 29.3, 20.1, 19.9, 13.81, 13.75.

**$^{31}$P NMR (203 MHz, $CDCl_3$)** δ 3.57.

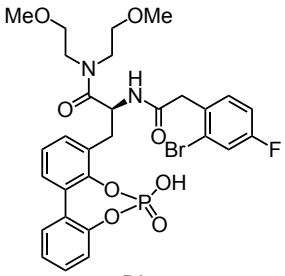
**HRMS (ESI+/TOF, *m*/*z*):** Exact mass calculated for $[C_{30}H_{36}ClN_2O_8PS+H]^+$ requires 651.1697; observed 651.1705.




**P1**
($^1$H NMR, 600 MHz, $CDCl_3$)



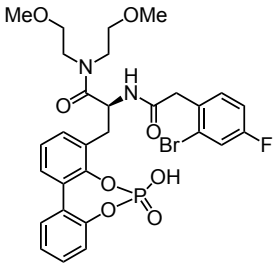

**P1**
($^{13}$C NMR, 126 MHz, $CDCl_3$)




**P1**

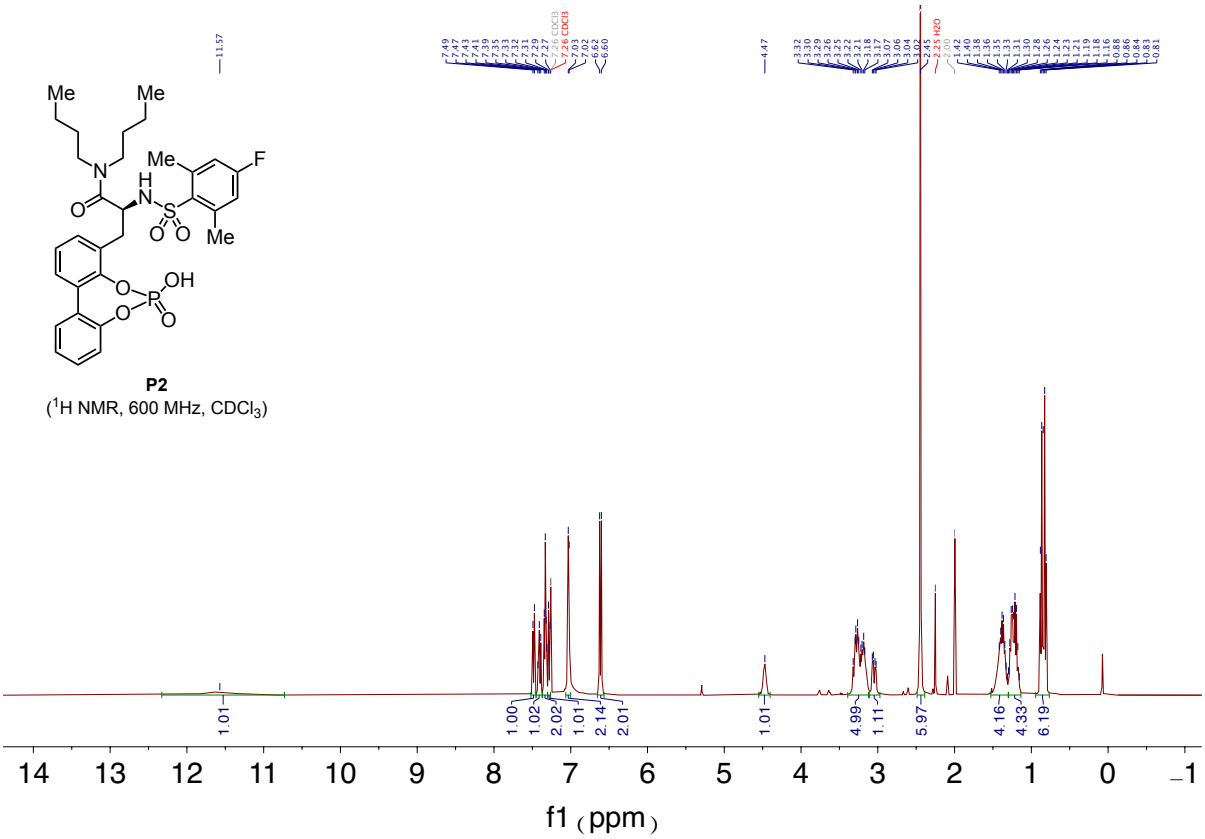
($^{19}$F NMR, 471 MHz, $CDCl_3$)



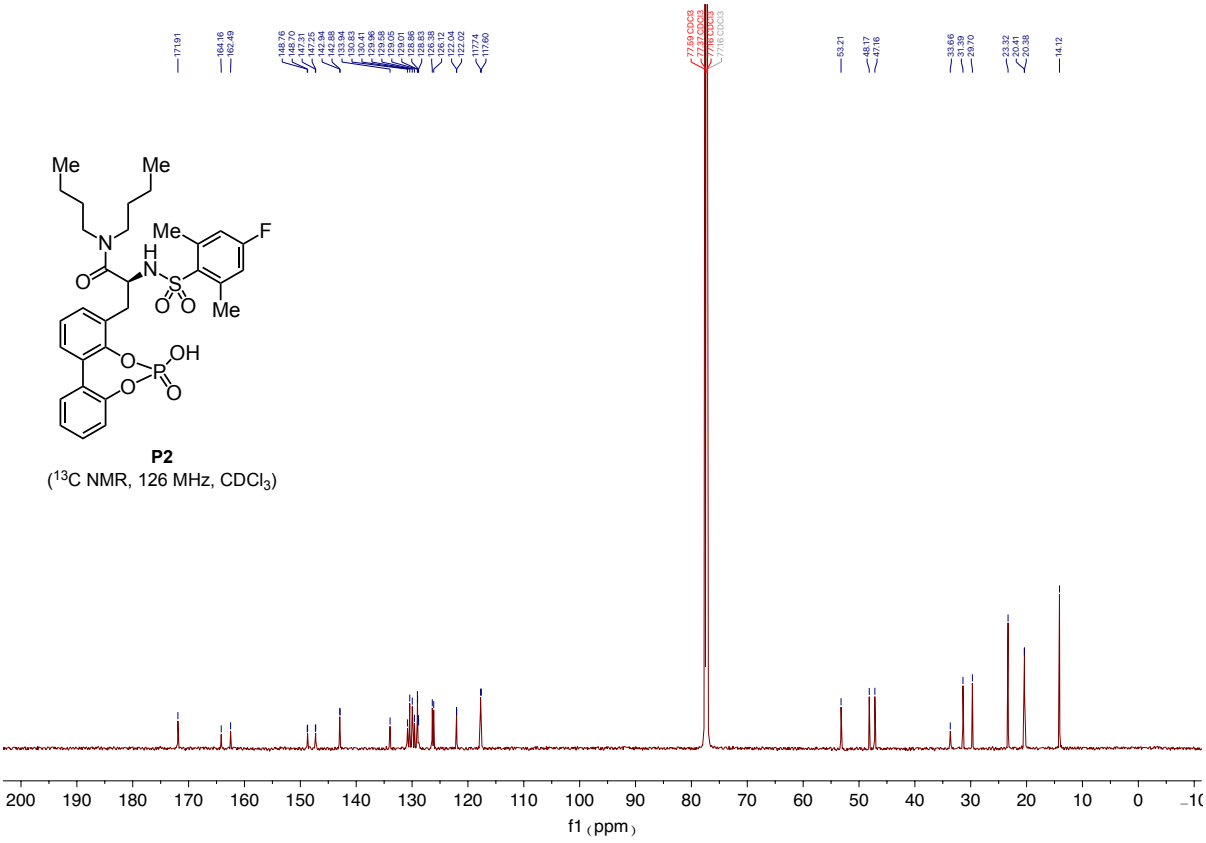




**P1**

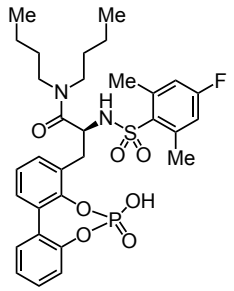
($^{31}$P NMR, 243 MHz, $CDCl_3$)




**P2**
($^1$H NMR, 600 MHz, $CDCl_3$)

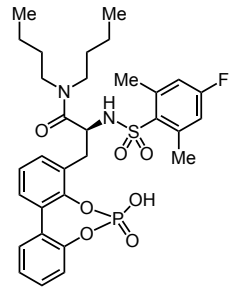



**P2**
($^{13}$C NMR, 126 MHz, $CDCl_3$)

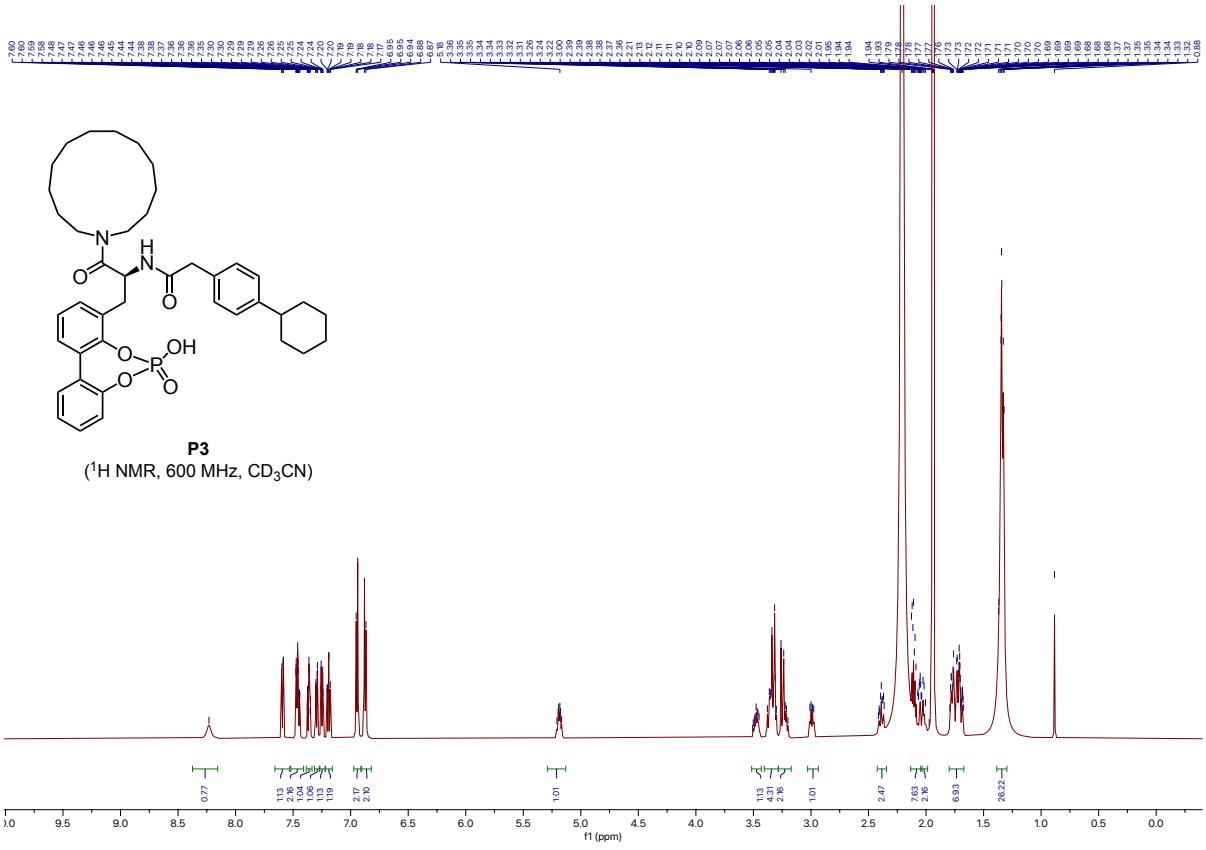


**P2**
($^{19}$F NMR, 471 MHz, $CDCl_3$)

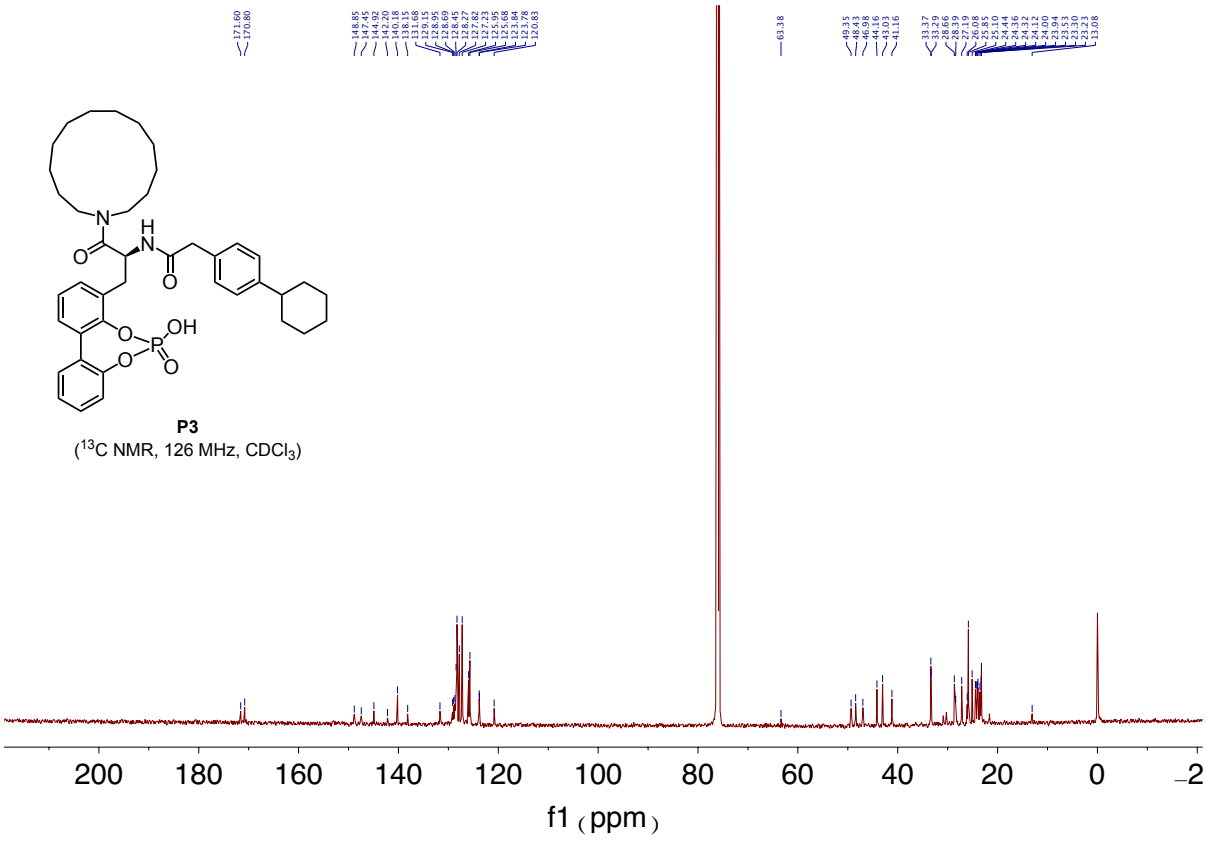


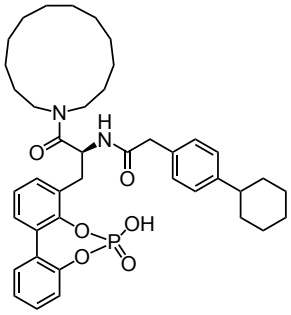
**P2**
($^{31}$P NMR, 243 MHz, $CDCl_3$)



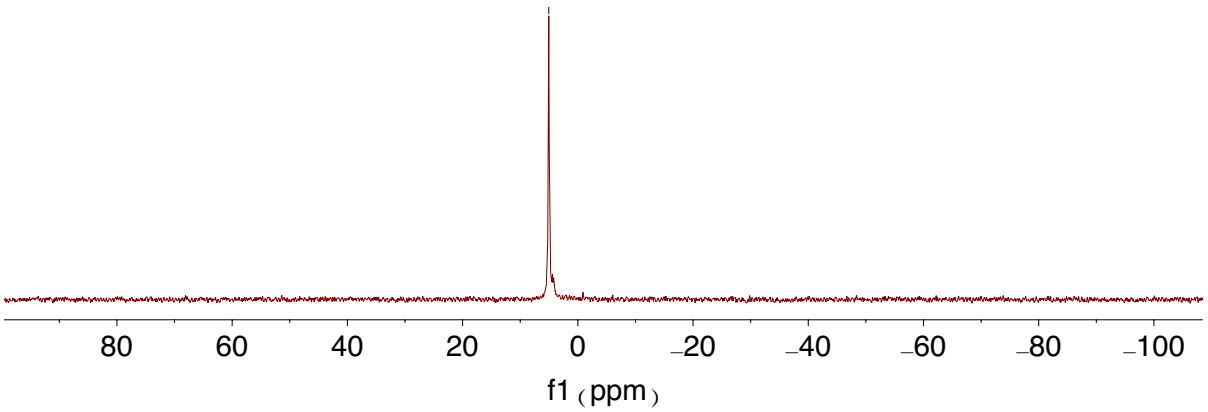
**P3**
($^{1}$H NMR, 600 MHz, $CD_3CN$)

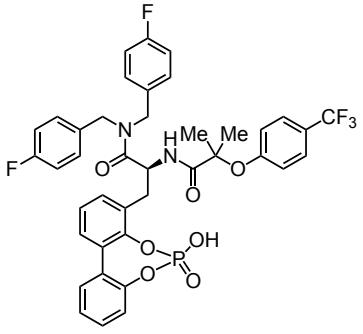


**P3**
($^{13}$C NMR, 126 MHz, $CDCl_3$)

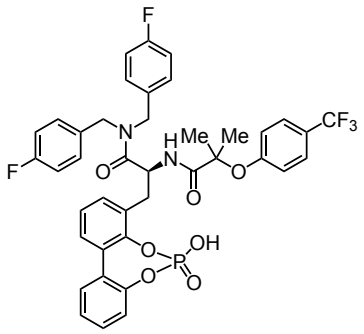


**P3**
($^{31}$P NMR, 243 MHz, $CDCl_3$)



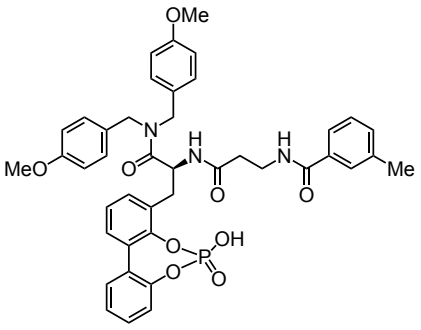



**P4**
($^{19}$F NMR, 471 MHz, $CDCl_3$)

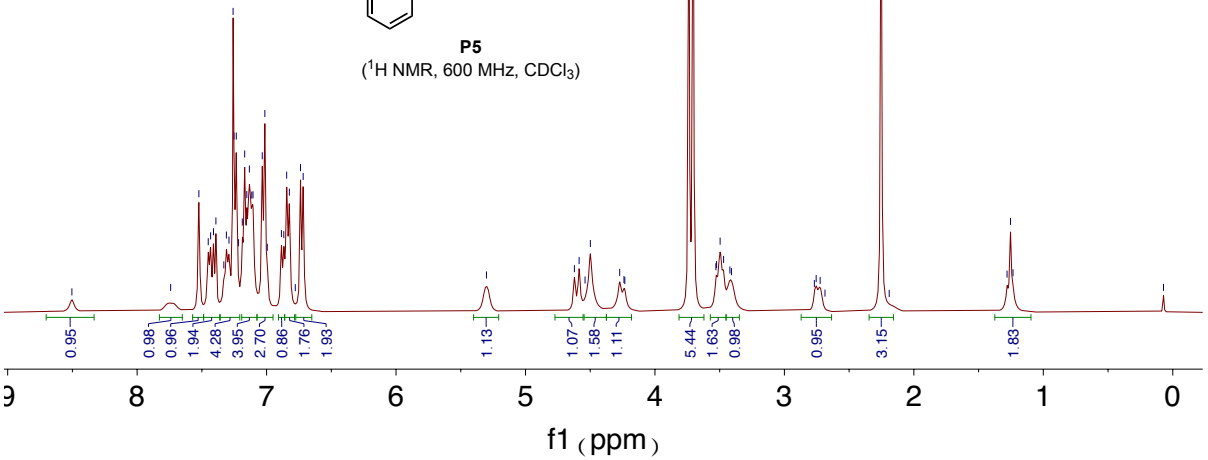


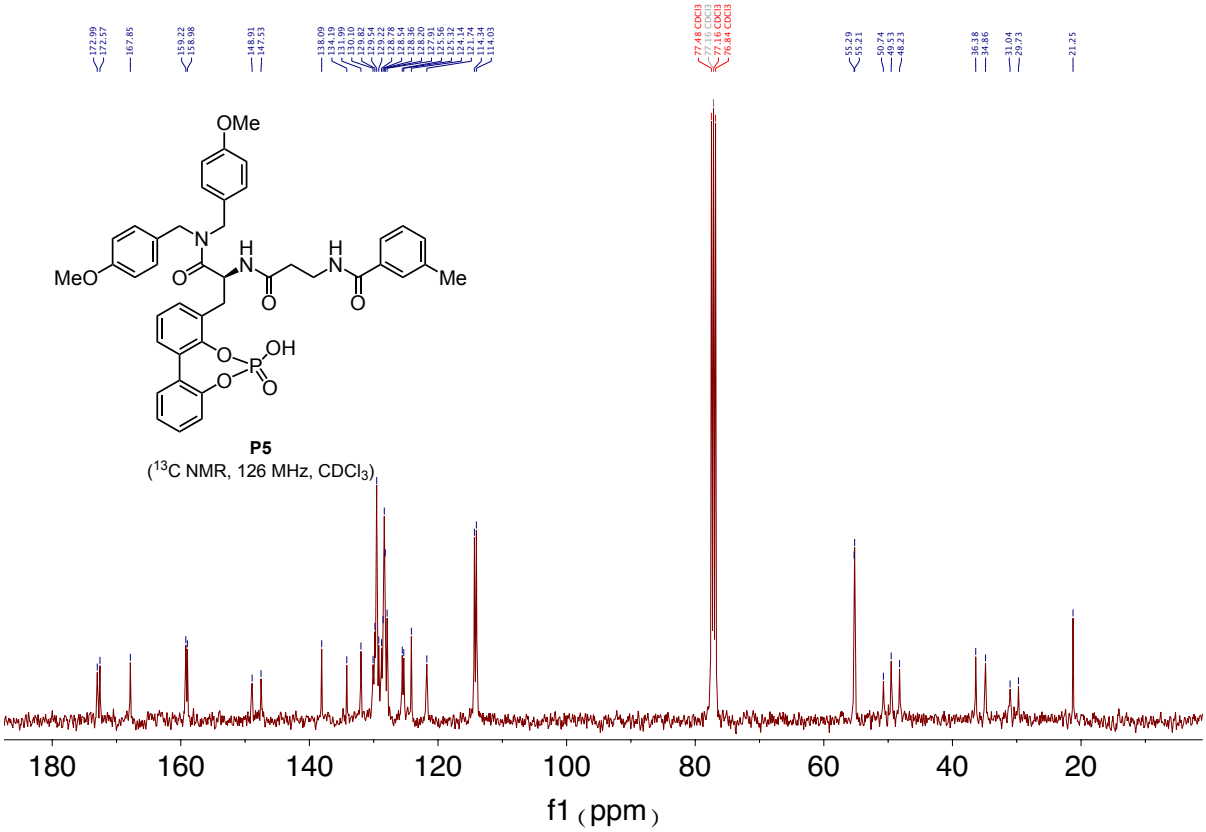
**P4**
($^{31}$P NMR, 243 MHz, $CDCl_3$)

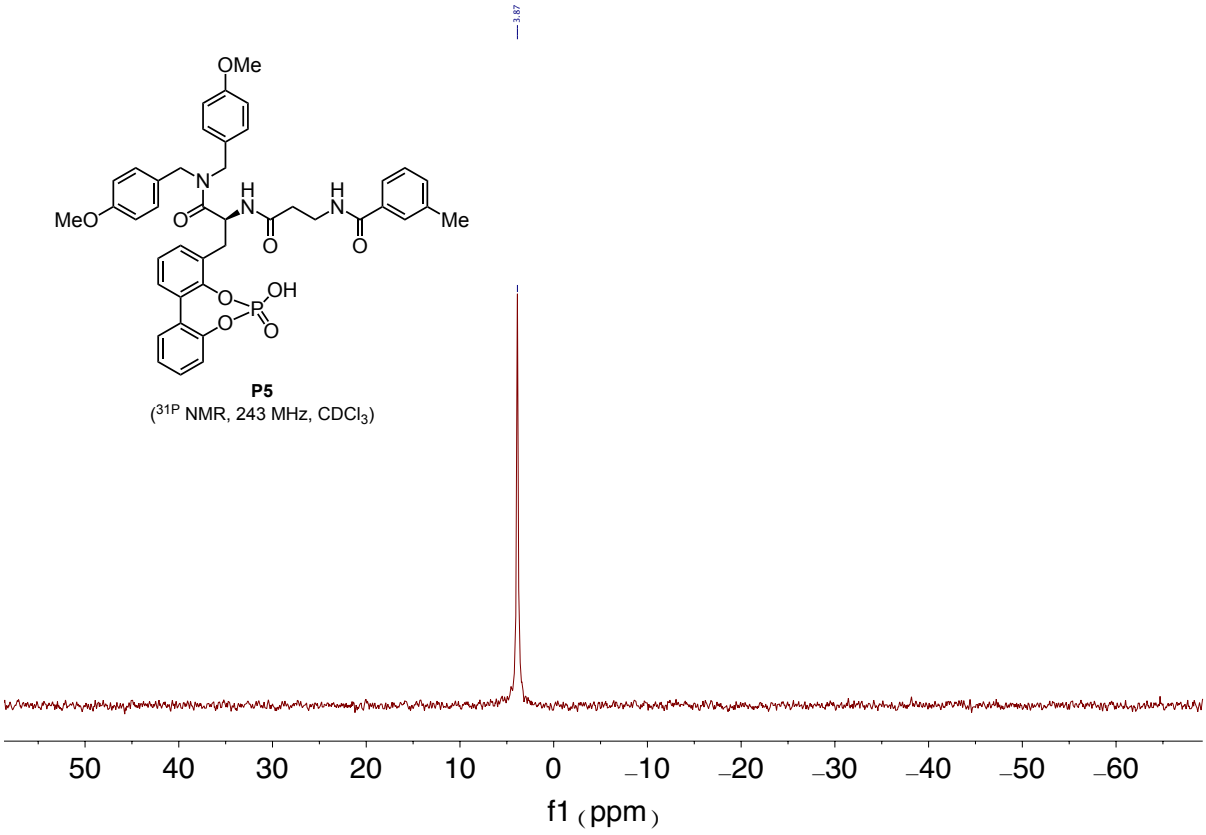


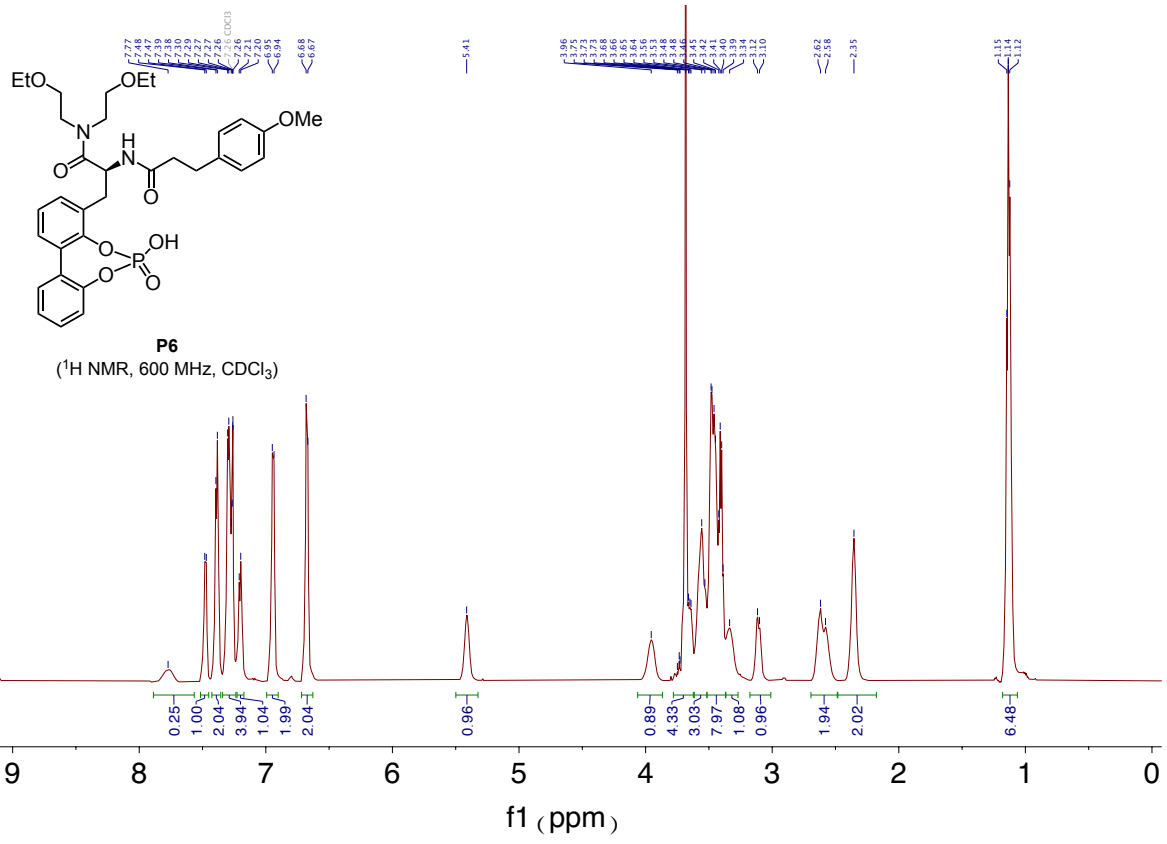


**P5**
($^{1}$H NMR, 600 MHz, $CDCl_3$)




OMe
MeO
Me
OH
P5
(13C NMR, 126 MHz, CDCl3)
180
160
140
120
100
80
60
40
20
f1 ( ppm )

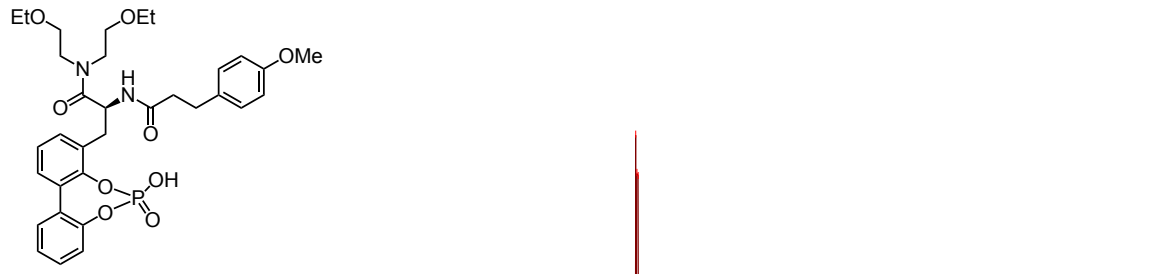

OMe
MeO
Me
OH
P5
(31P NMR, 243 MHz, CDCl3)
50
40
30
20
10
0
−10
−20
−30
−40
−50
−60
f1 ( ppm )




**P6**

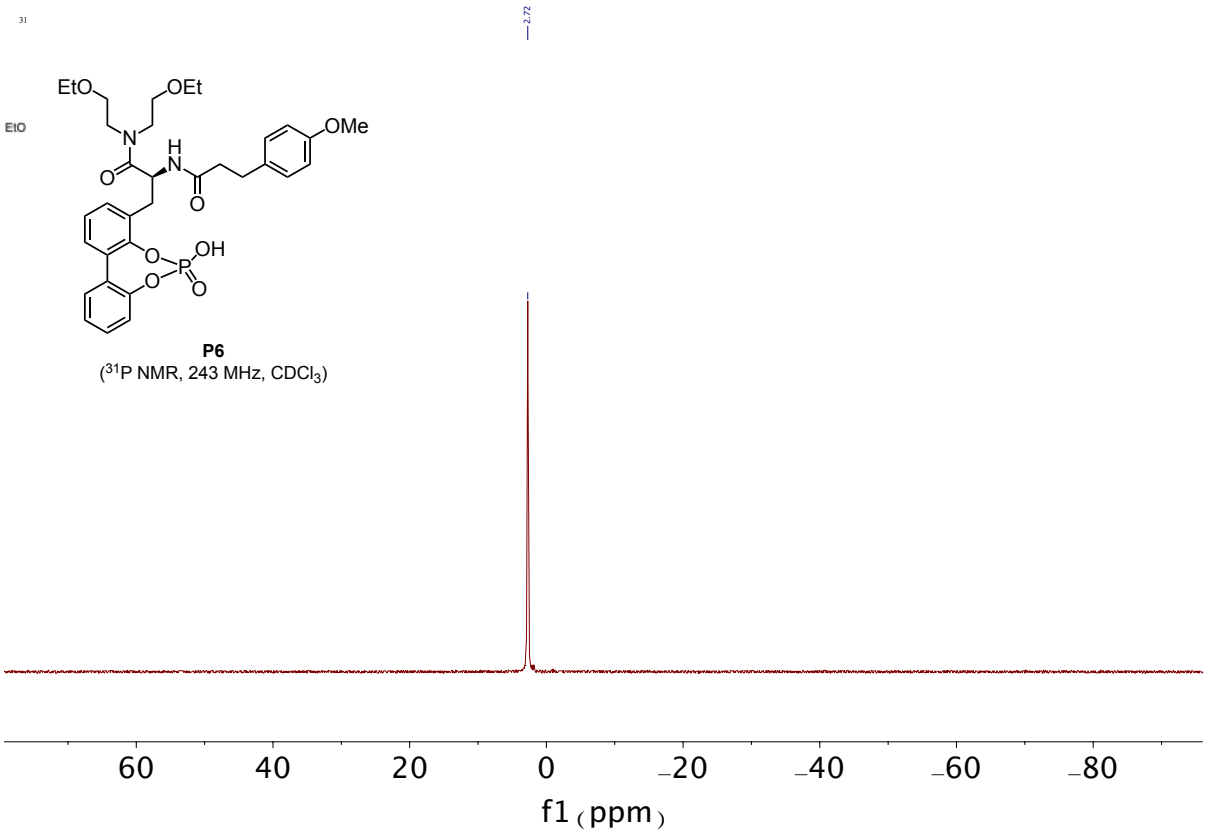
($^1$H NMR, 600 MHz, $CDCl_3$)



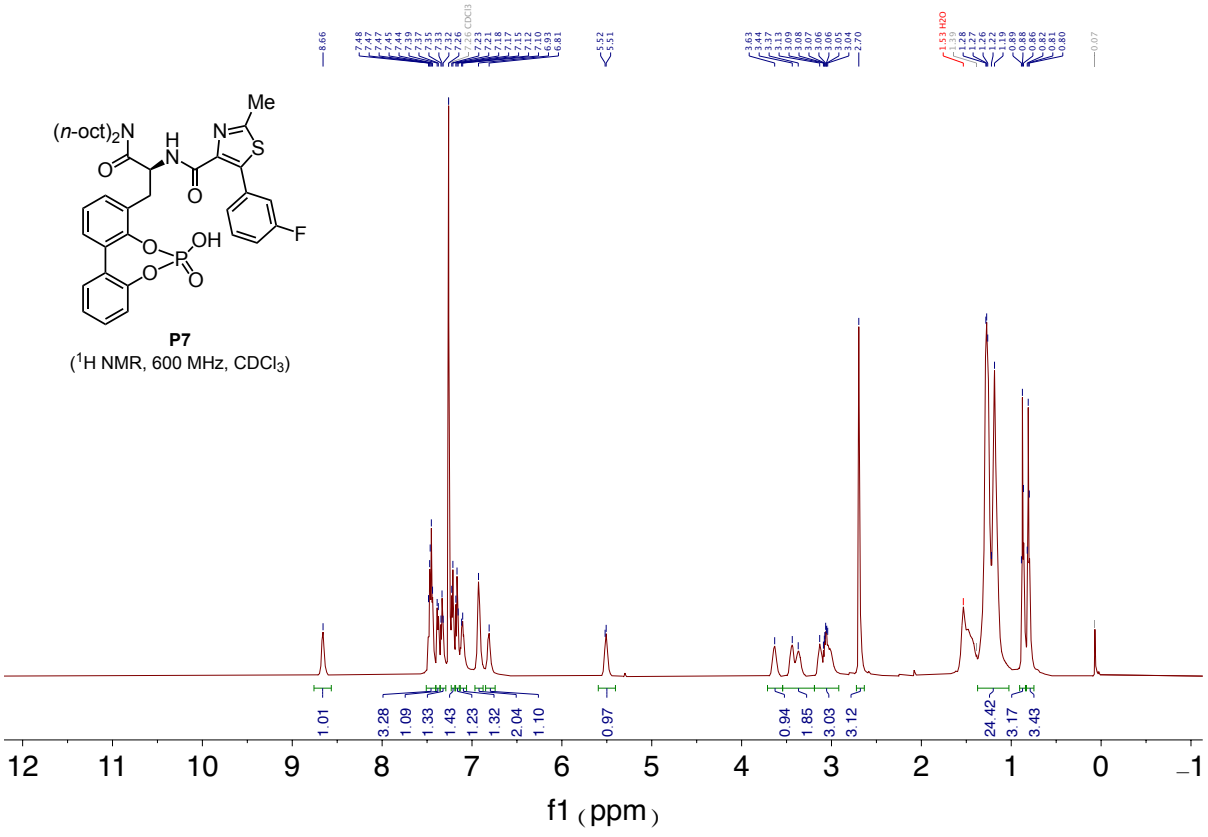




**P6**

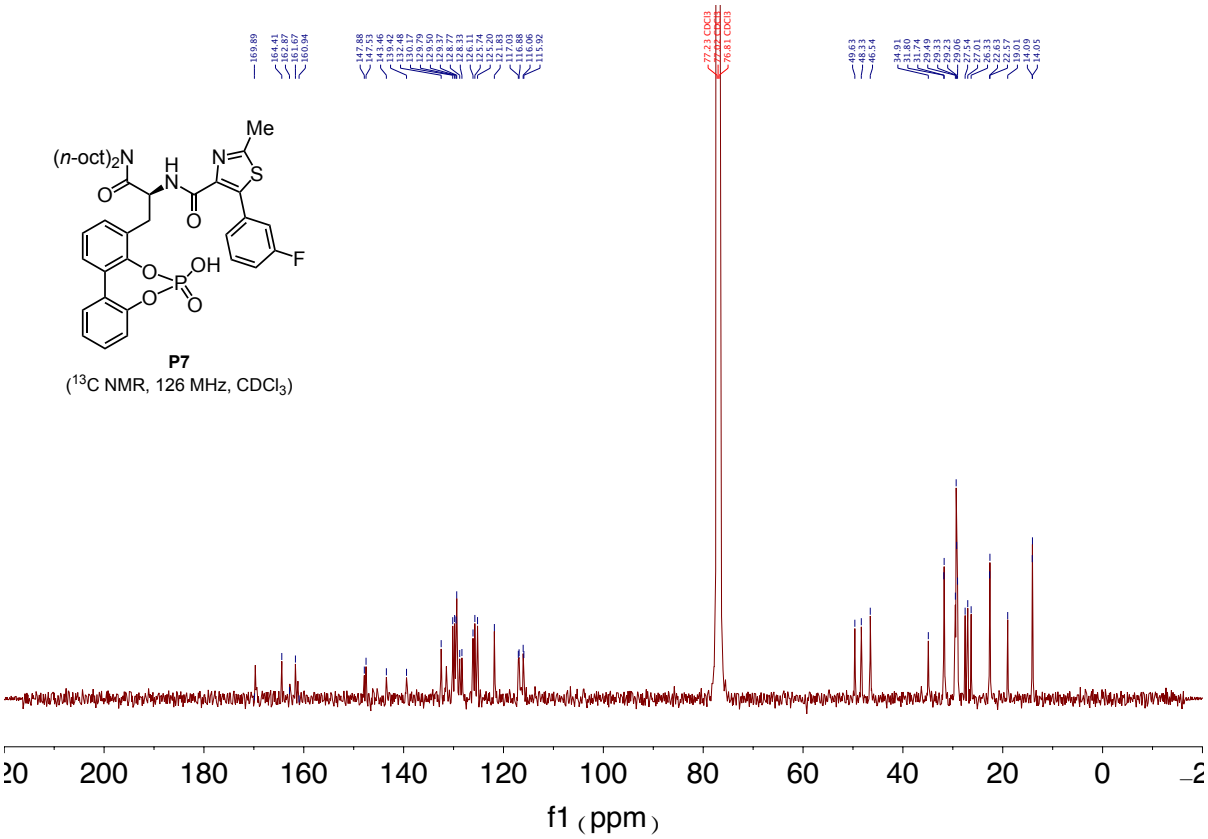
($^{13}$C NMR, 126 MHz, $CDCl_3$)

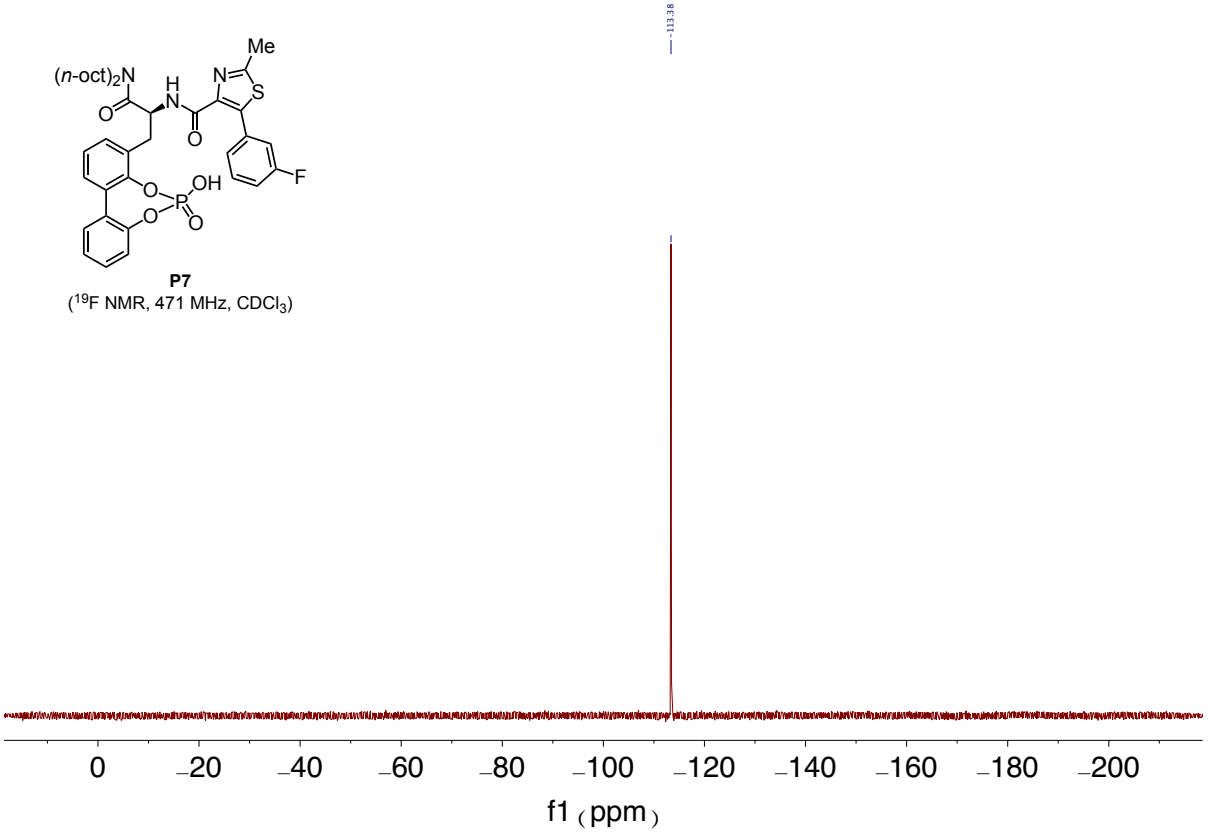


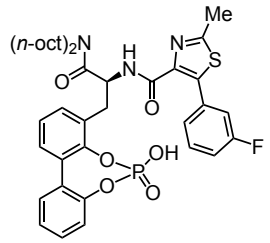

**P6**
($^{31}$P NMR, 243 MHz, $CDCl_3$)




**P7**
($^{1}$H NMR, 600 MHz, $CDCl_3$)

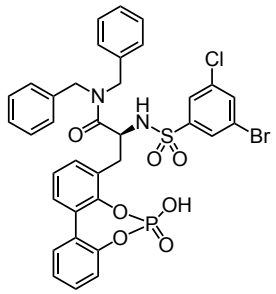

(n-oct)2N
Me
F
OH
P7
(13C NMR, 126 MHz, CDCl3)
f1 ( ppm )


(n-oct)2N
Me
F
OH
P7
(19F NMR, 471 MHz, CDCl3)
f1 ( ppm )

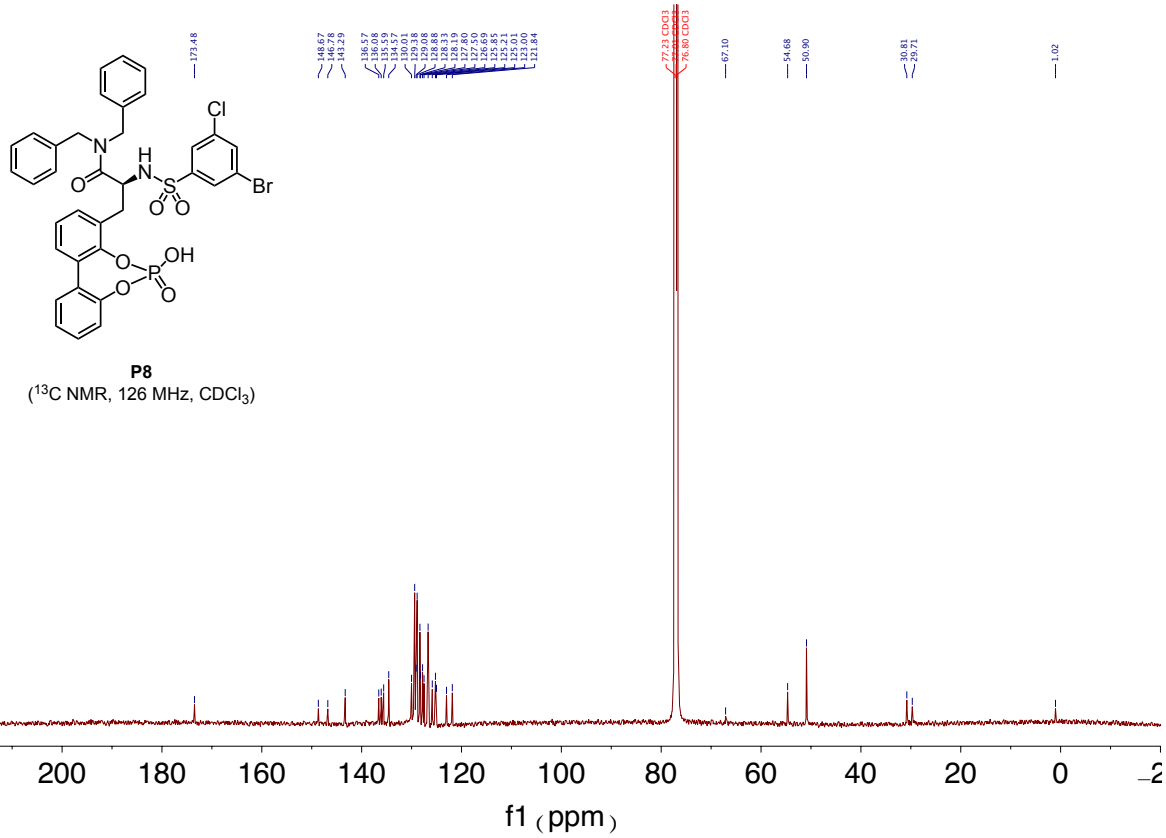



**P7**
($^{31}$P NMR, 243 MHz, $CDCl_3$)

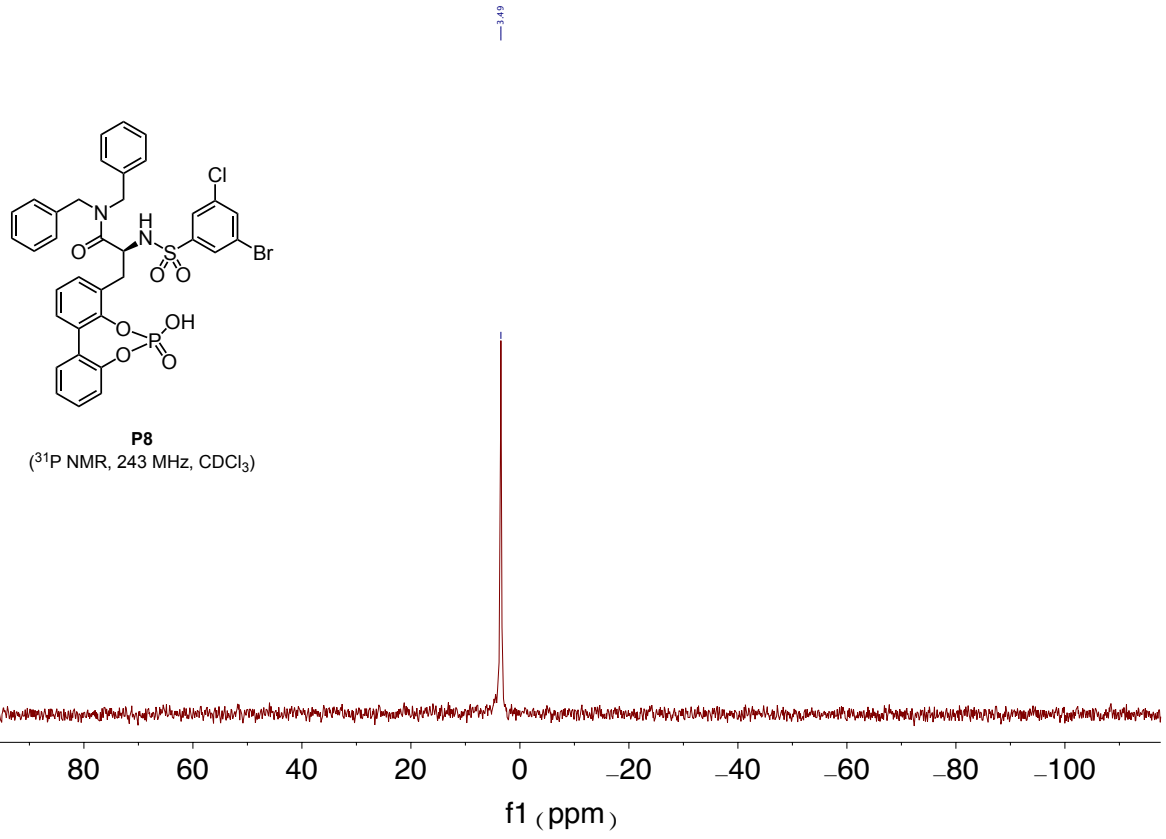


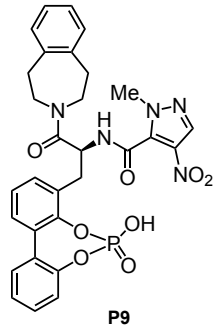

**P8**
($^{1}$H NMR, 600 MHz, $CDCl_3$)




**P8**
($^{13}$C NMR, 126 MHz, $CDCl_3$)



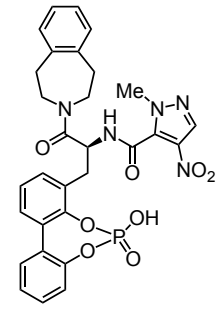

**P8**
($^{31}$P NMR, 243 MHz, $CDCl_3$)



**P9**

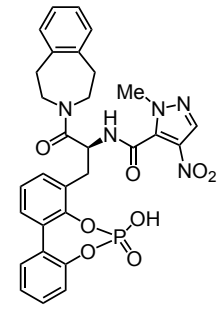
($^1$H NMR, 500 MHz, $CDCl_3$)



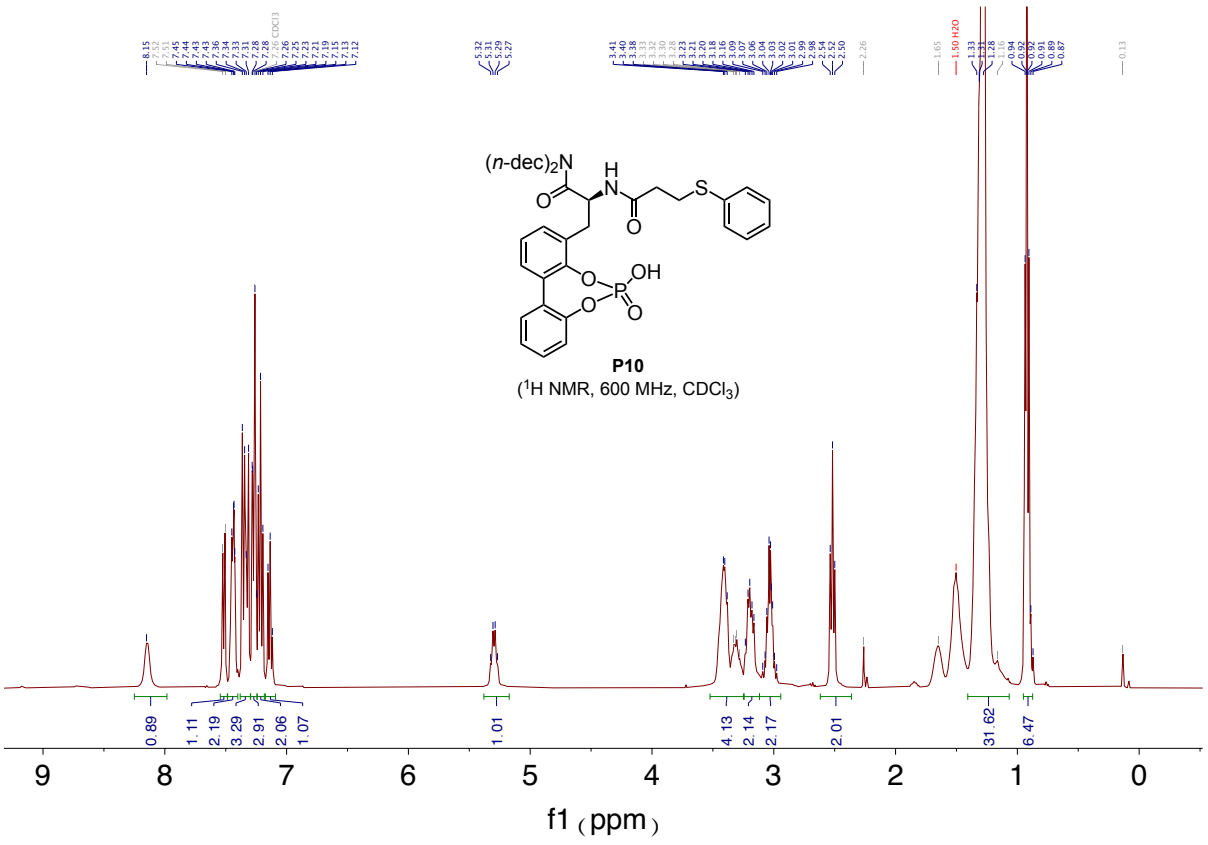
**P9**

($^{13}$C NMR, 126 MHz, $CDCl_3$)

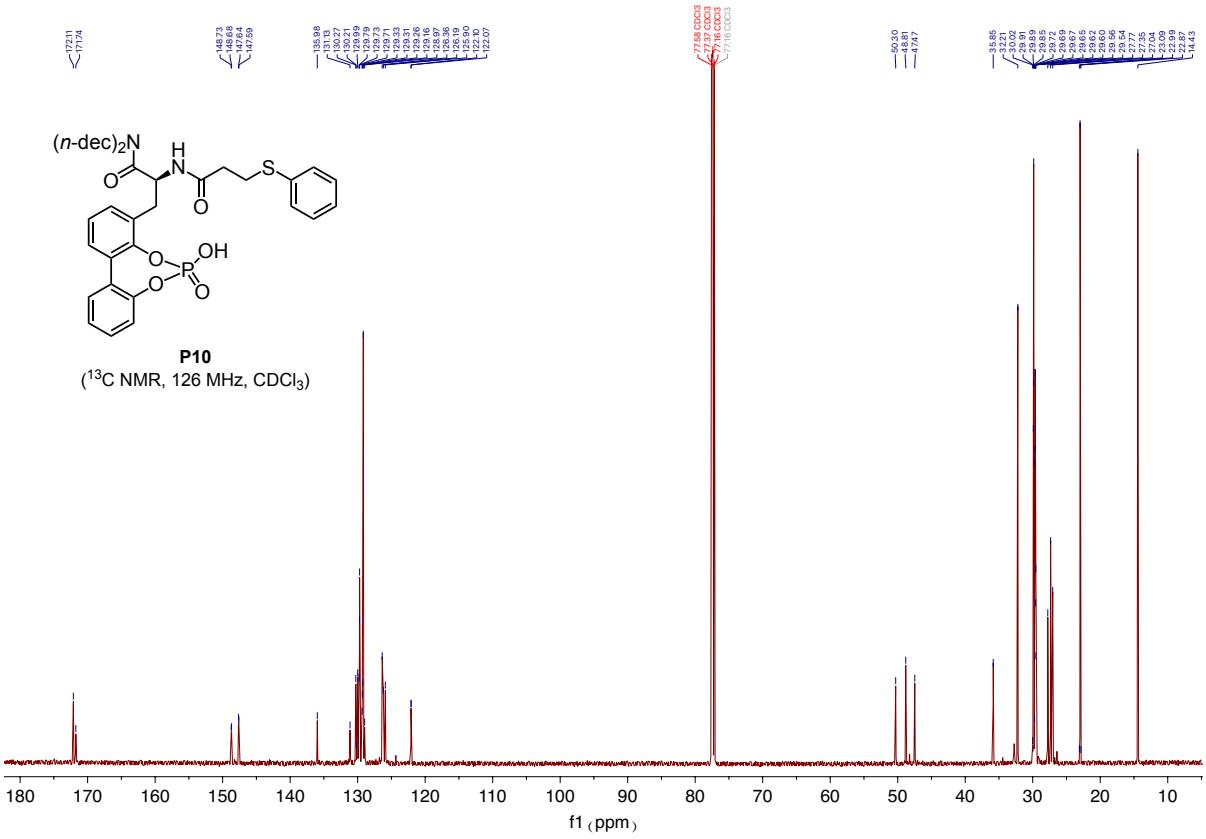


**P9**
($^{31}$P NMR, 243 MHz, $CDCl_3$)

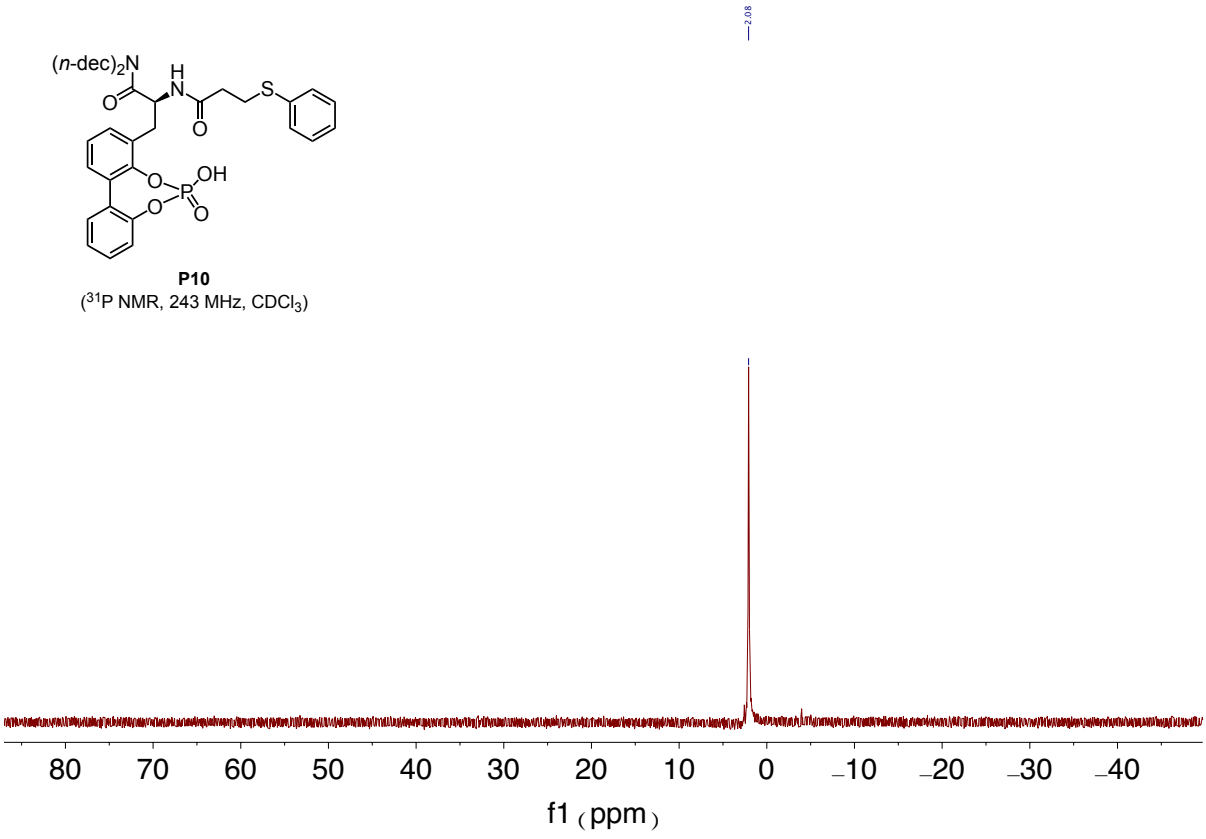


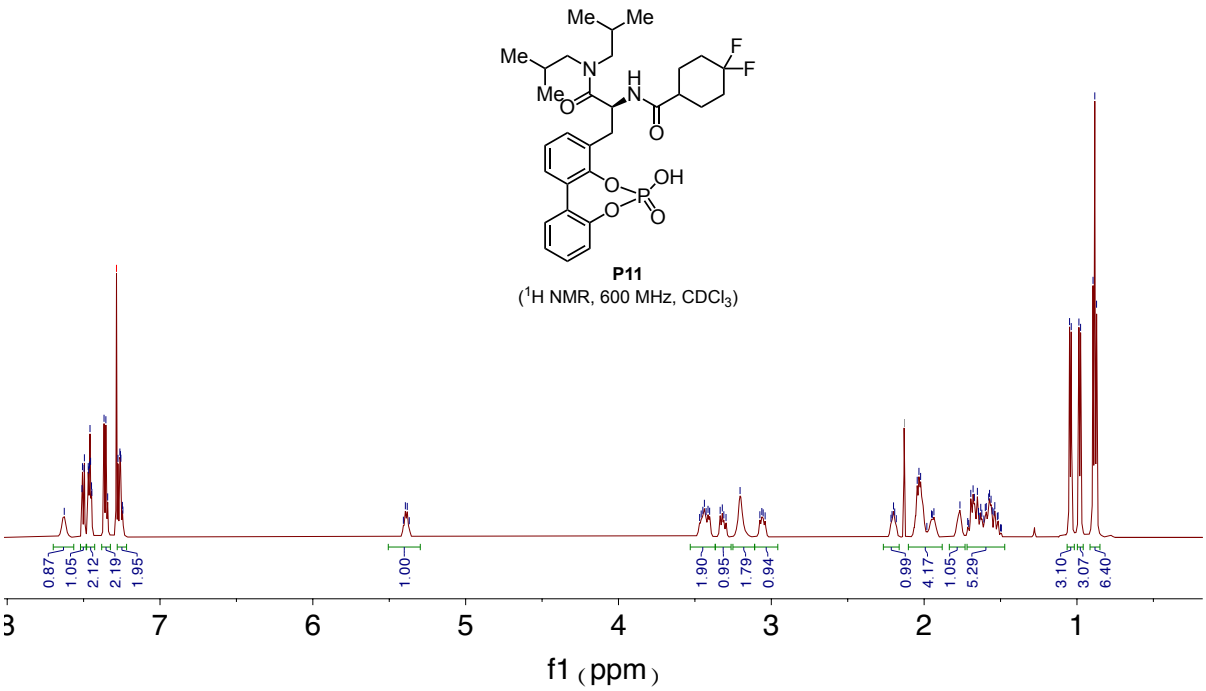

**P10**
($^{1}$H NMR, 600 MHz, $CDCl_3$)

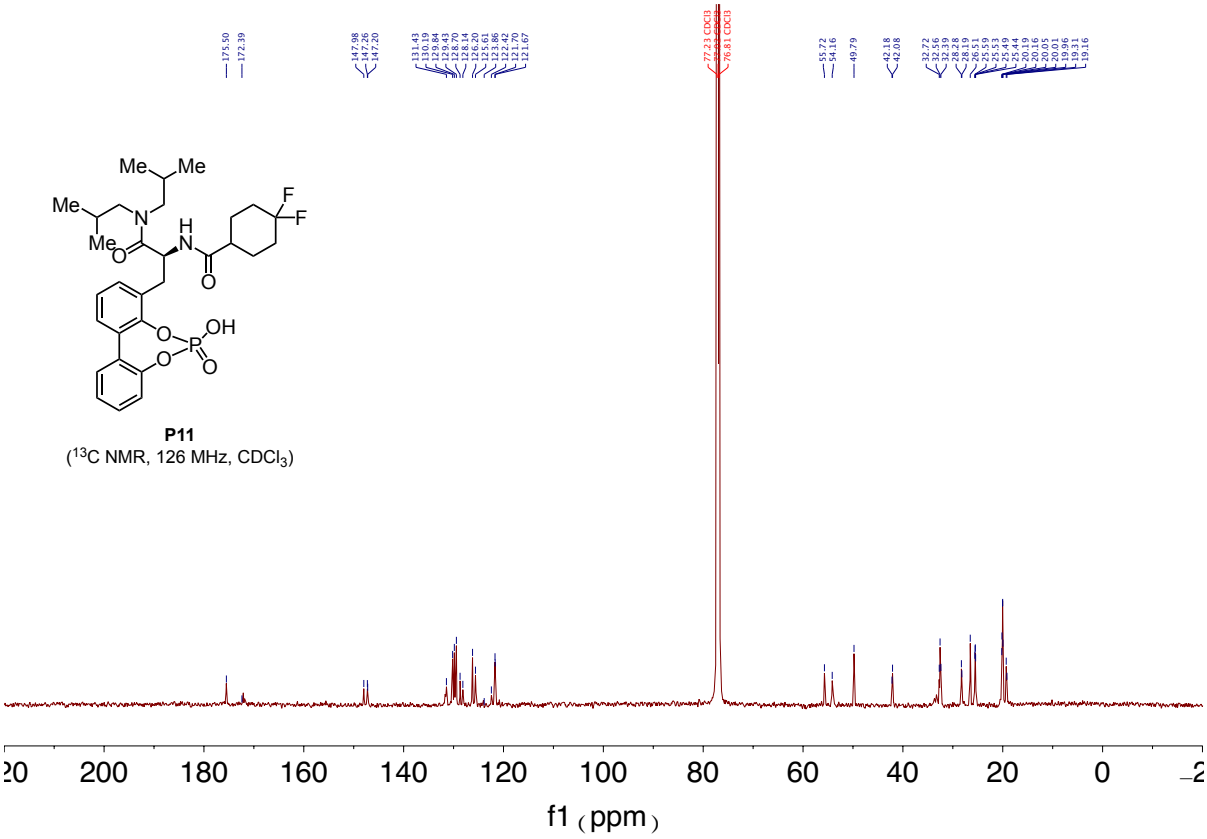


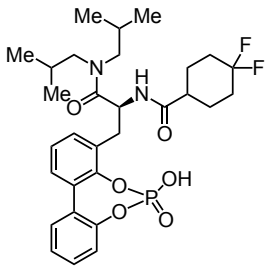

**P10**
($^{13}$C NMR, 126 MHz, $CDCl_3$)



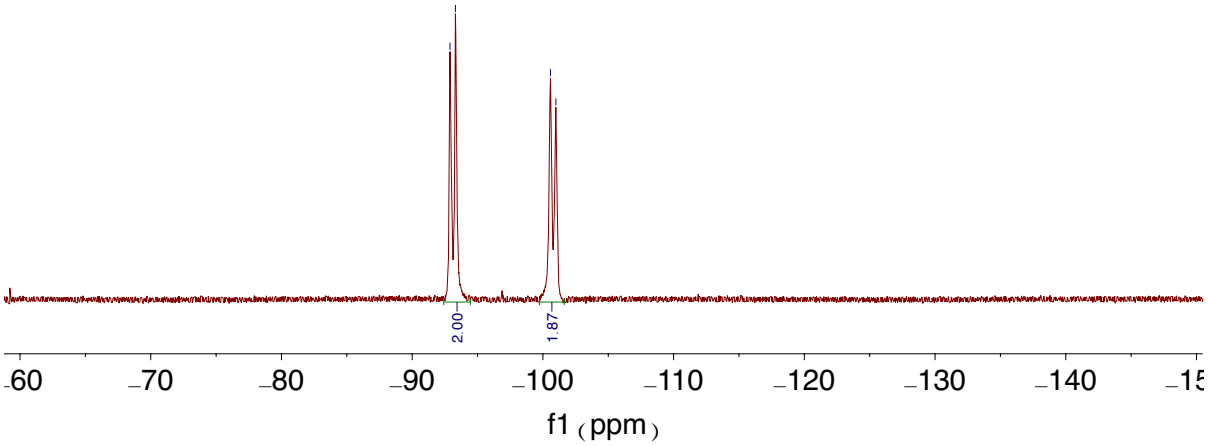

**P10**
($^{31}$P NMR, 243 MHz, $CDCl_3$)

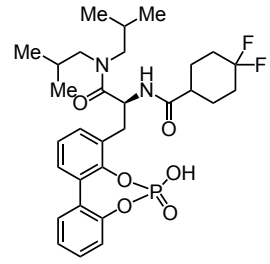

Me
Me
Me
N
Me
O
H
N
F
F
O
O
O
P
OH
O
P11
(1H NMR, 600 MHz, CDCl3)
0.87
1.05
2.12
2.19
1.95
1.00
1.90
0.95
1.79
0.94
0.99
4.17
1.05
5.29
3.10
3.07
6.40
f1 ( ppm )


Me
Me
Me
N
Me
O
H
N
F
F
O
O
O
P
OH
O
P11
(13C NMR, 126 MHz, CDCl3)
f1 ( ppm )

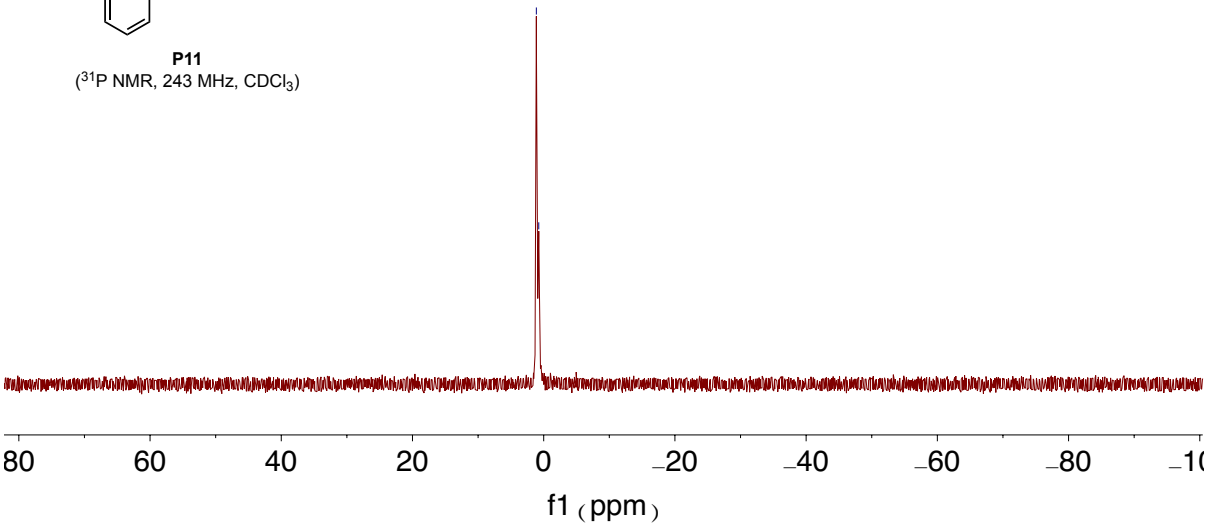


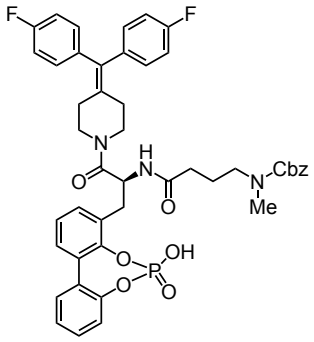
**P11**
($^{1}$F NMR, 471 MHz, $CDCl_3$)



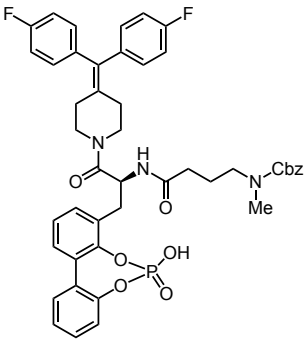
**P11**
($^{31}$P NMR, 243 MHz, $CDCl_3$)



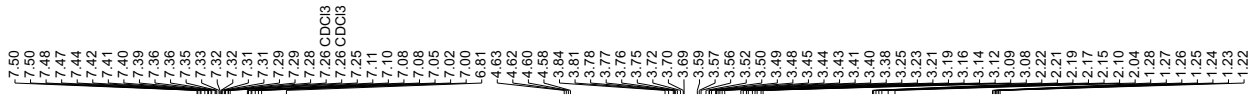


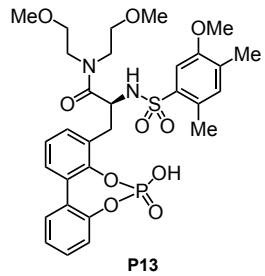
**P12**
($^{19}$F NMR, 471 MHz, $CDCl_3$)



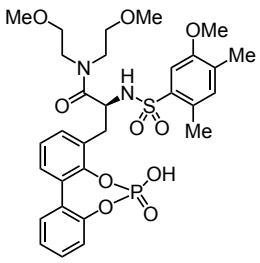
**P12**
($^{31}$P NMR, 243 MHz, $CDCl_3$)



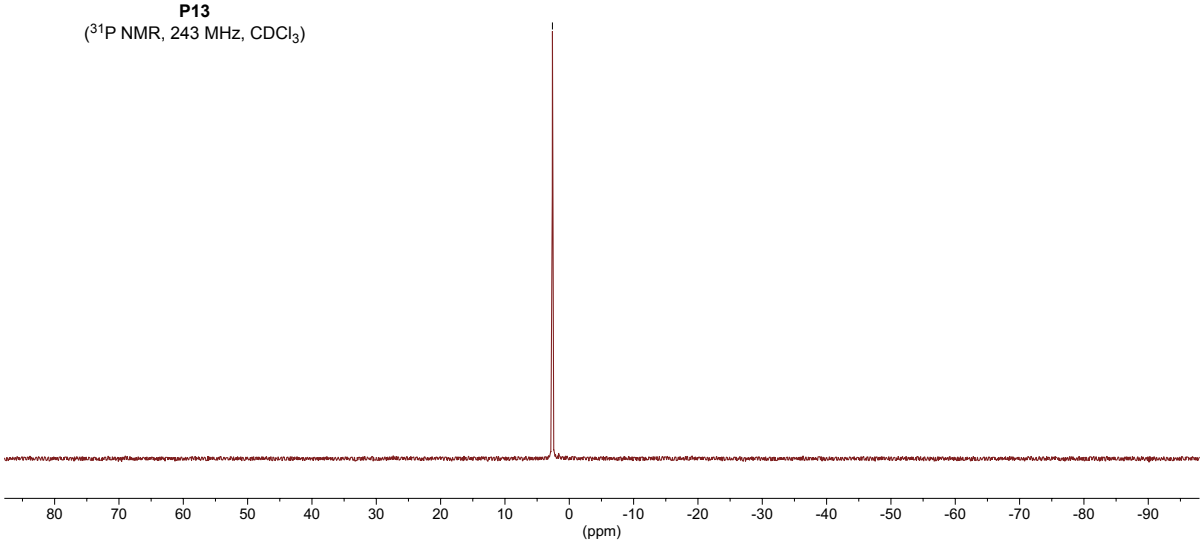


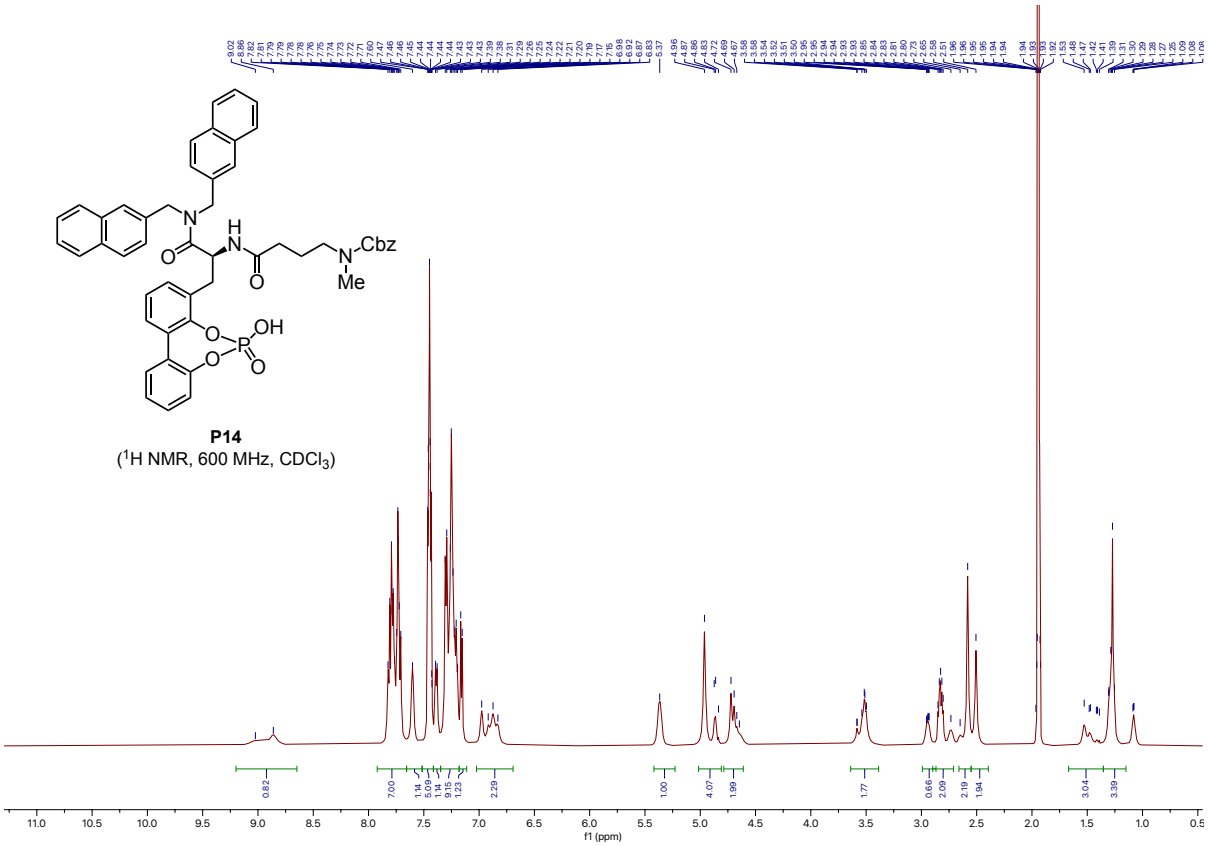
**P13**
($^{1}$H NMR, 500 MHz, $CDCl_3$)



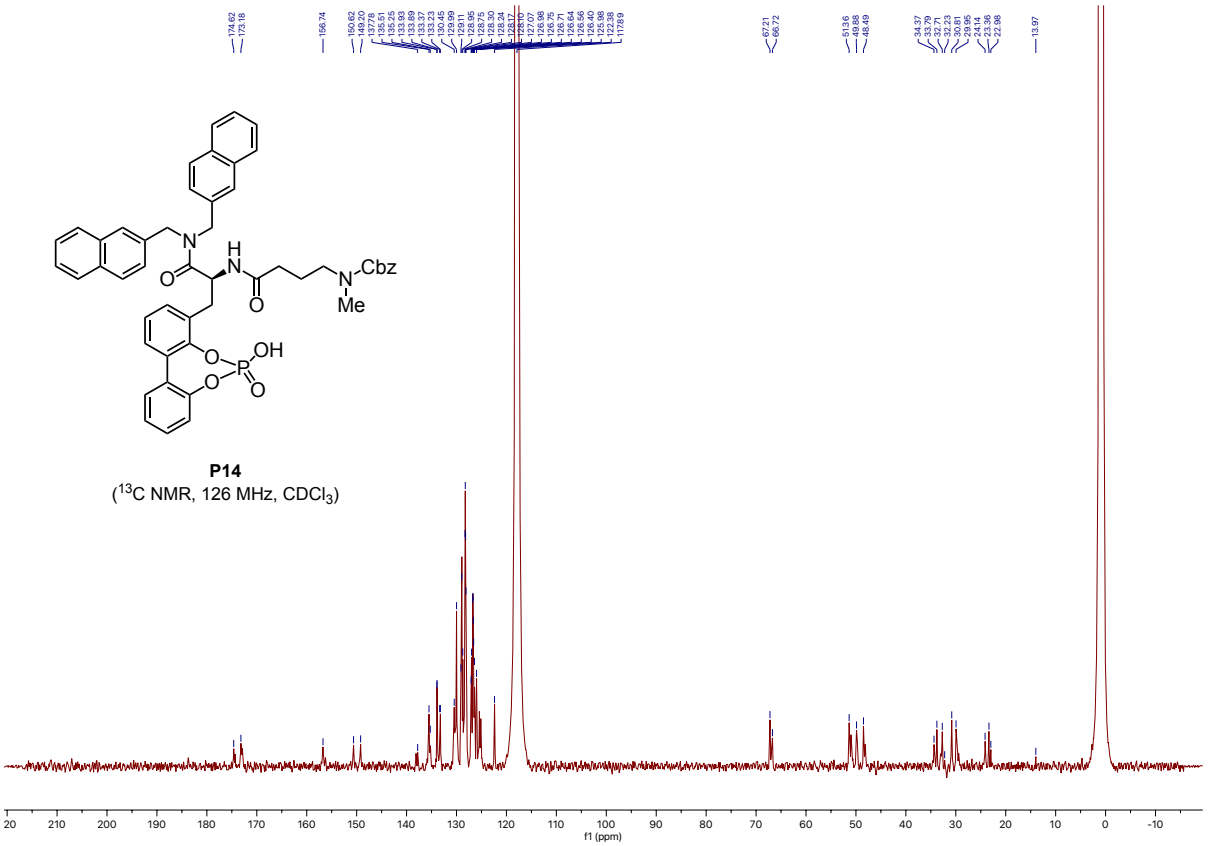


**P13**
($^{31}$P NMR, 243 MHz, $CDCl_3$)

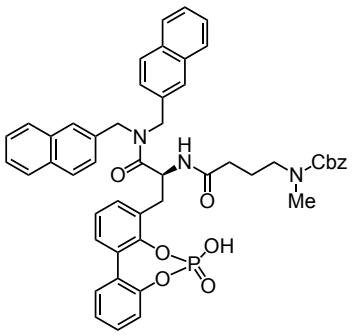





**P14**
($^{1}$H NMR, 600 MHz, $CDCl_3$)

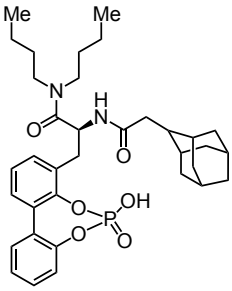



**P14**
($^{13}$C NMR, 126 MHz, $CDCl_3$)

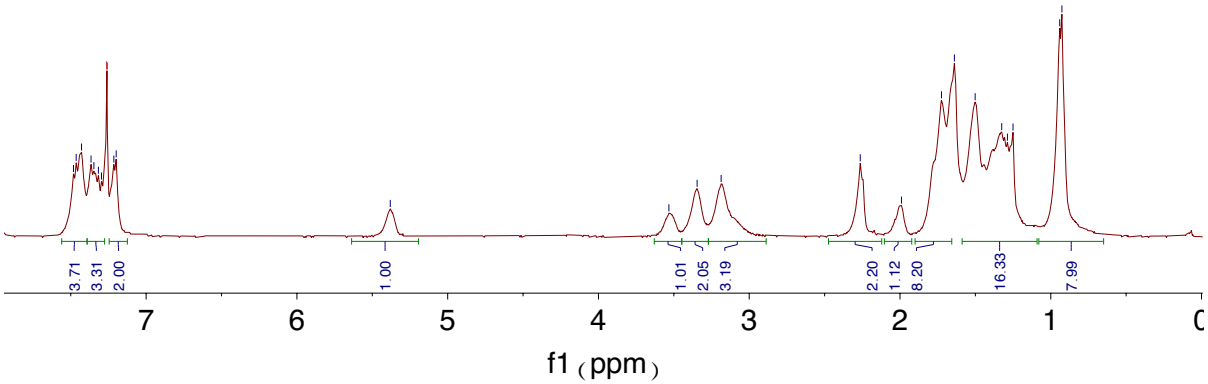


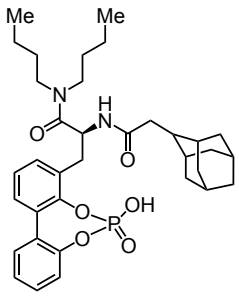
**P14**
($^{31}$P NMR, 243 MHz, $CDCl_3$)



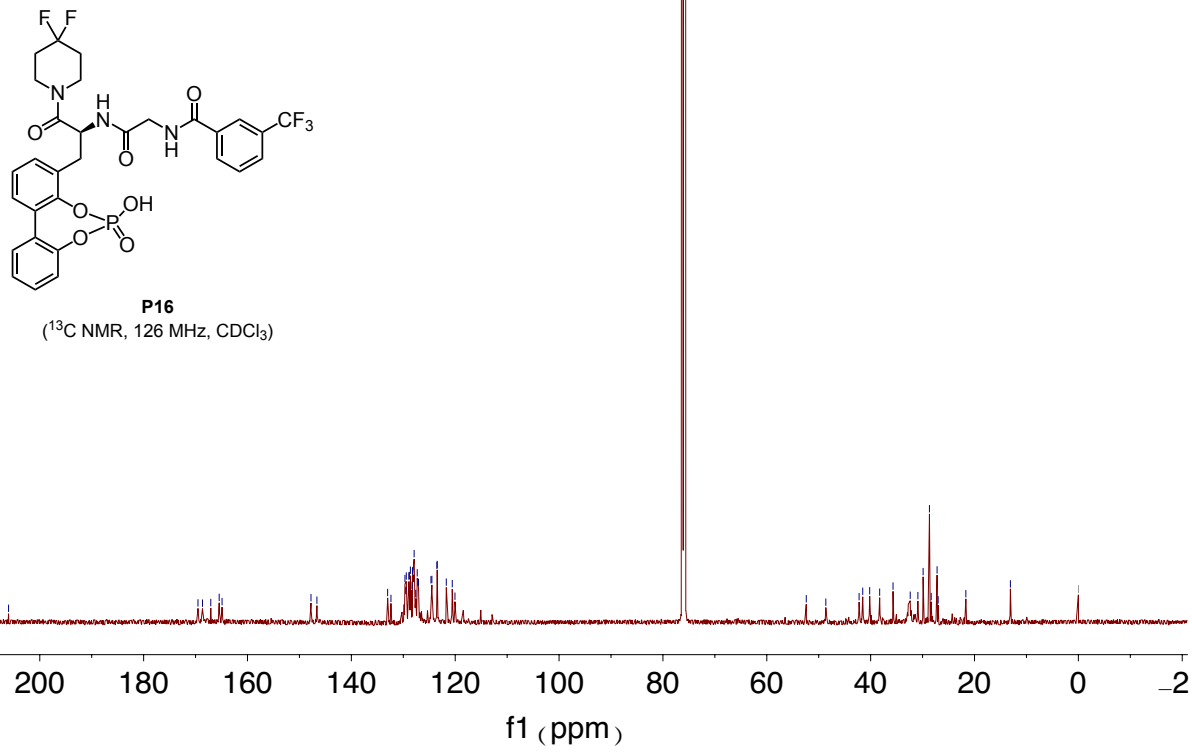
**P15**
($^{1}$H NMR, 600 MHz, $CDCl_3$)



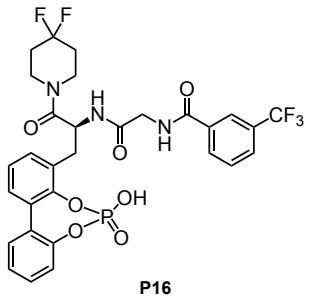



**P15**
($^{31}$P NMR, 243 MHz, $CDCl_3$)



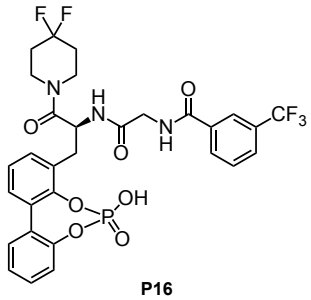




**P16**
($^{13}$C NMR, 126 MHz, $CDCl_3$)

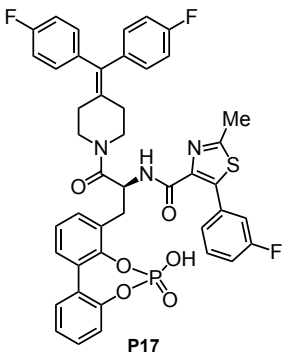


**P16**
($^{19}$F NMR, 471 MHz, $CDCl_3$)



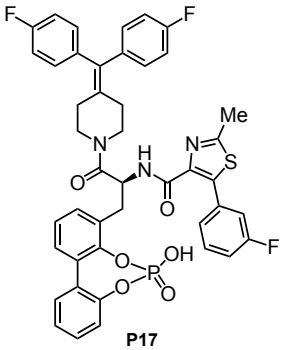
**P16**
($^{31}$P NMR, 243 MHz, $CDCl_3$)



**P17**

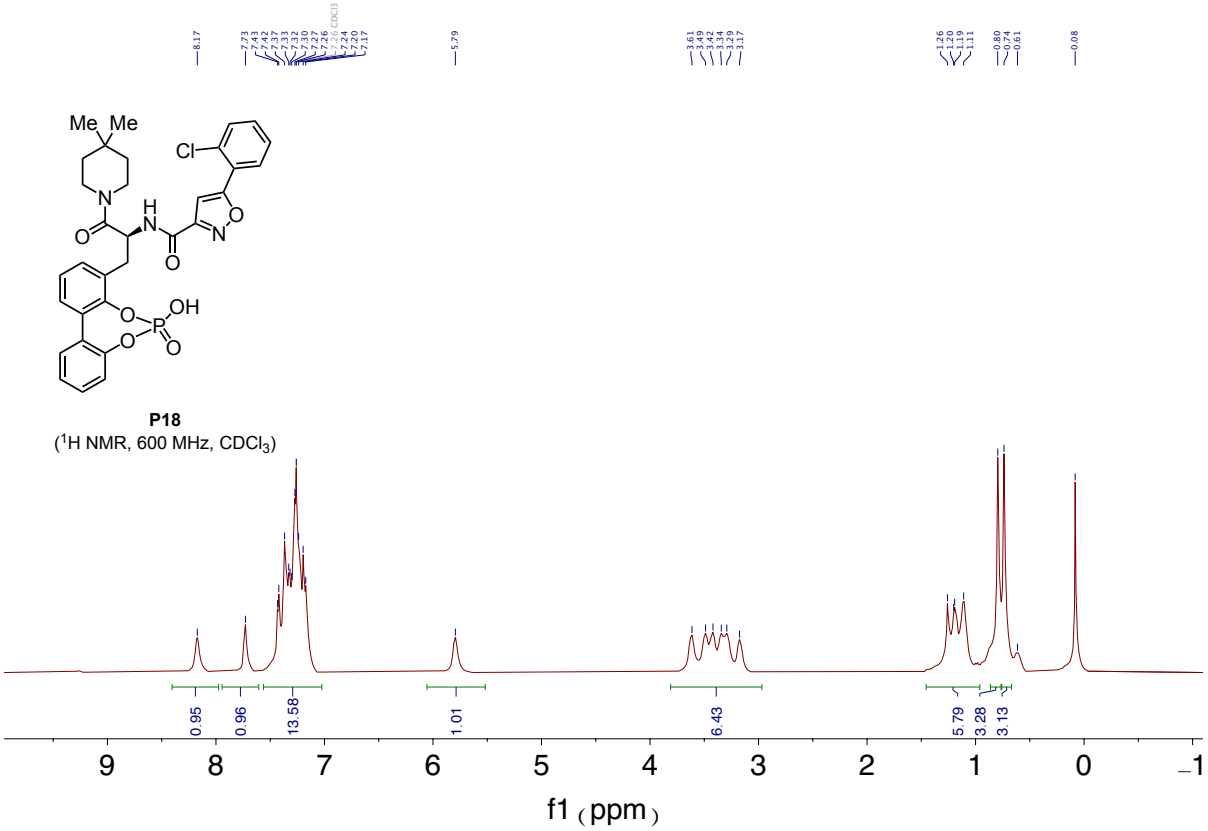
($^{19}$F NMR, 471 MHz, $CDCl_3$)

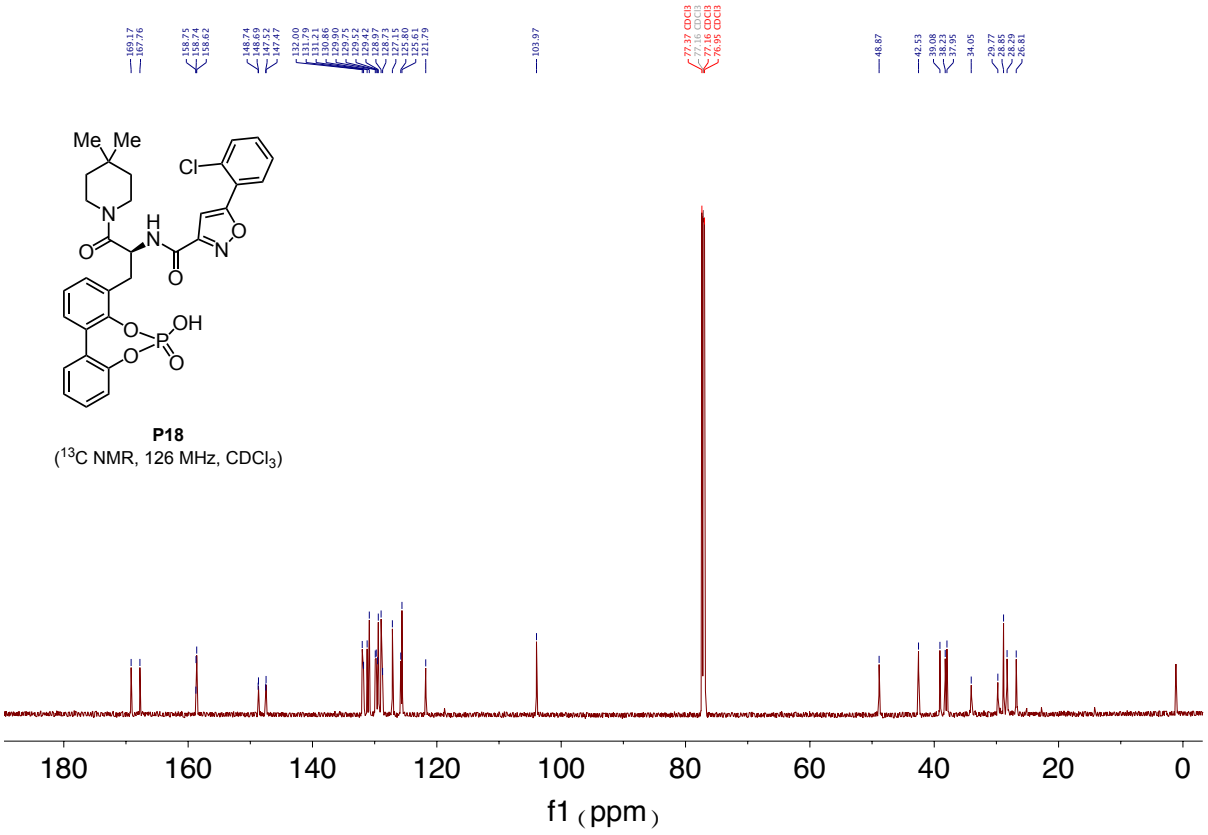


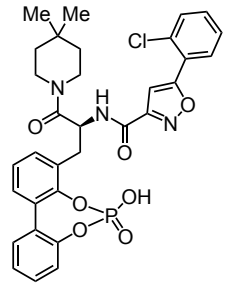



**P17**

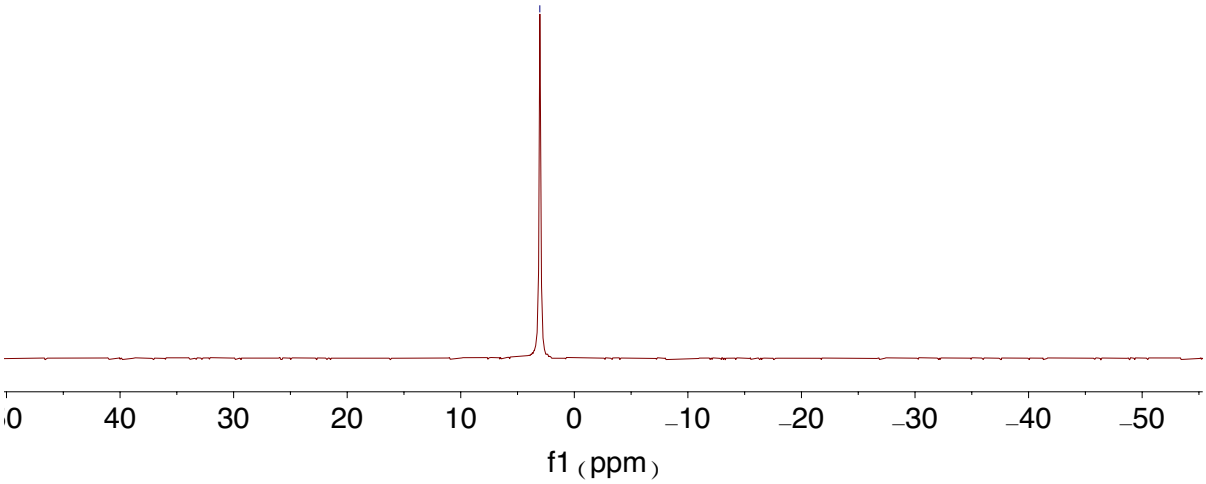
($^{31}$P NMR, 243 MHz, $CDCl_3$)

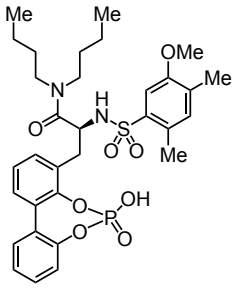

Me Me
Cl
N
H
N
O
O
O
O
O
P
OH
O
P18
(1H NMR, 600 MHz, CDCl3)
0.95
0.96
13.58
1.01
6.43
5.79
3.28
3.13
9
8
7
6
5
4
3
2
1
0
–1
f1 ( ppm )


Me Me
Cl
N
H
N
O
O
O
O
O
P
OH
O
P18
(13C NMR, 126 MHz, CDCl3)
180
160
140
120
100
80
60
40
20
0
f1 ( ppm )

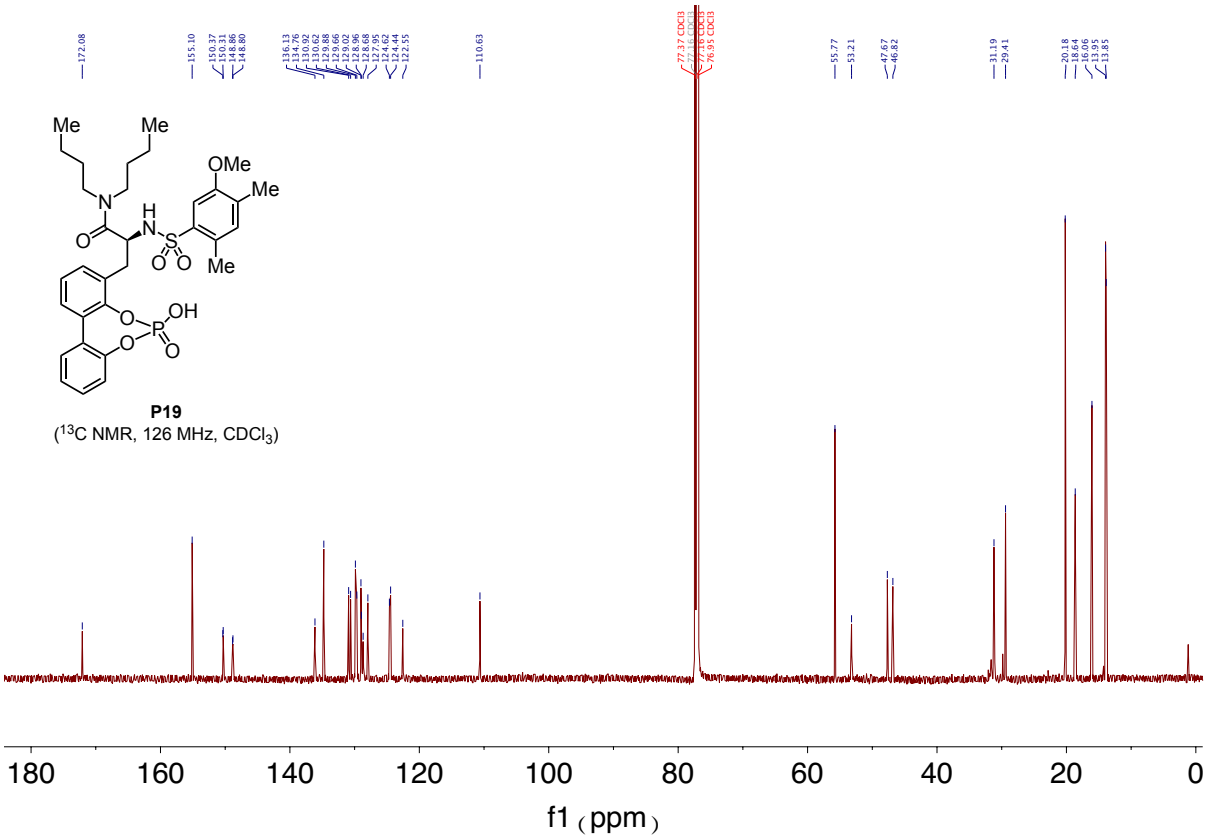


**P18**
($^{31}$P NMR, 243 MHz, $CDCl_3$)

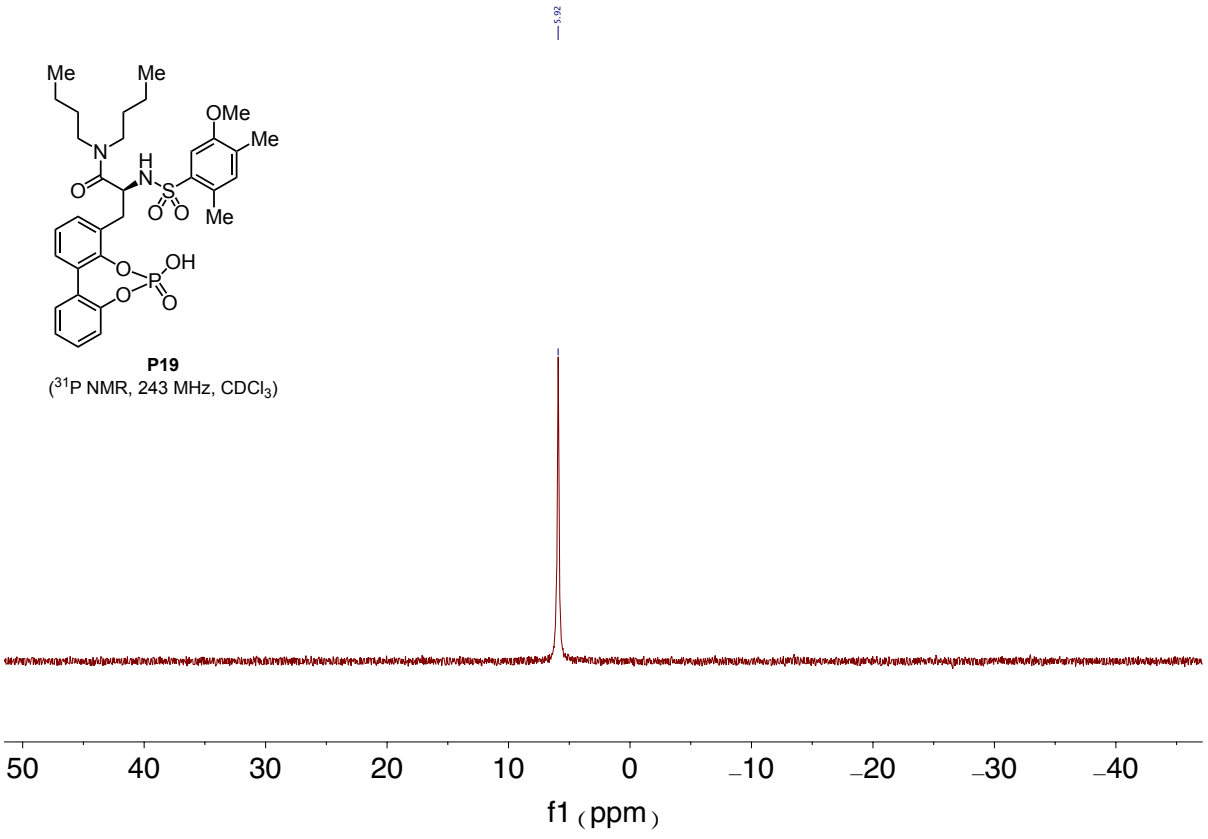


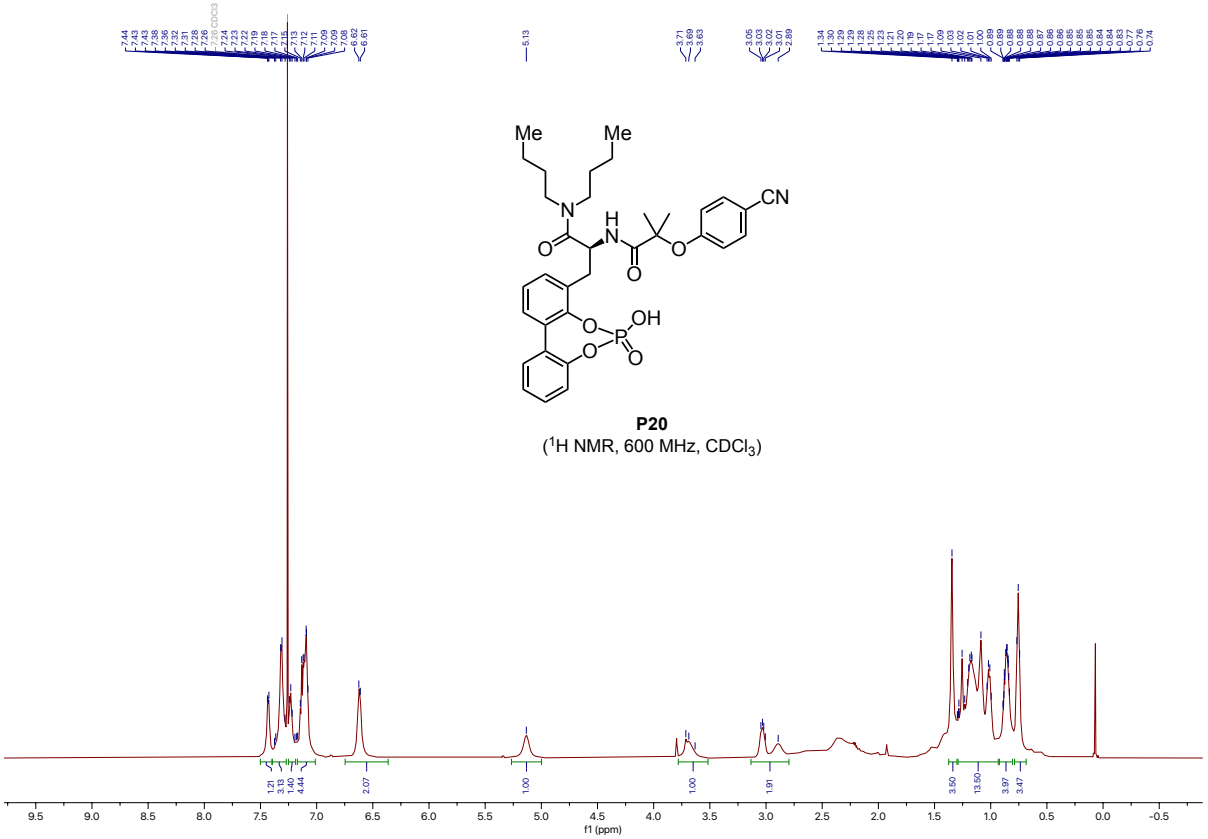
**P19**
($^{1}$H NMR, 600 MHz, $CDCl_3$)




**P19**
($^{13}$C NMR, 126 MHz, $CDCl_3$)

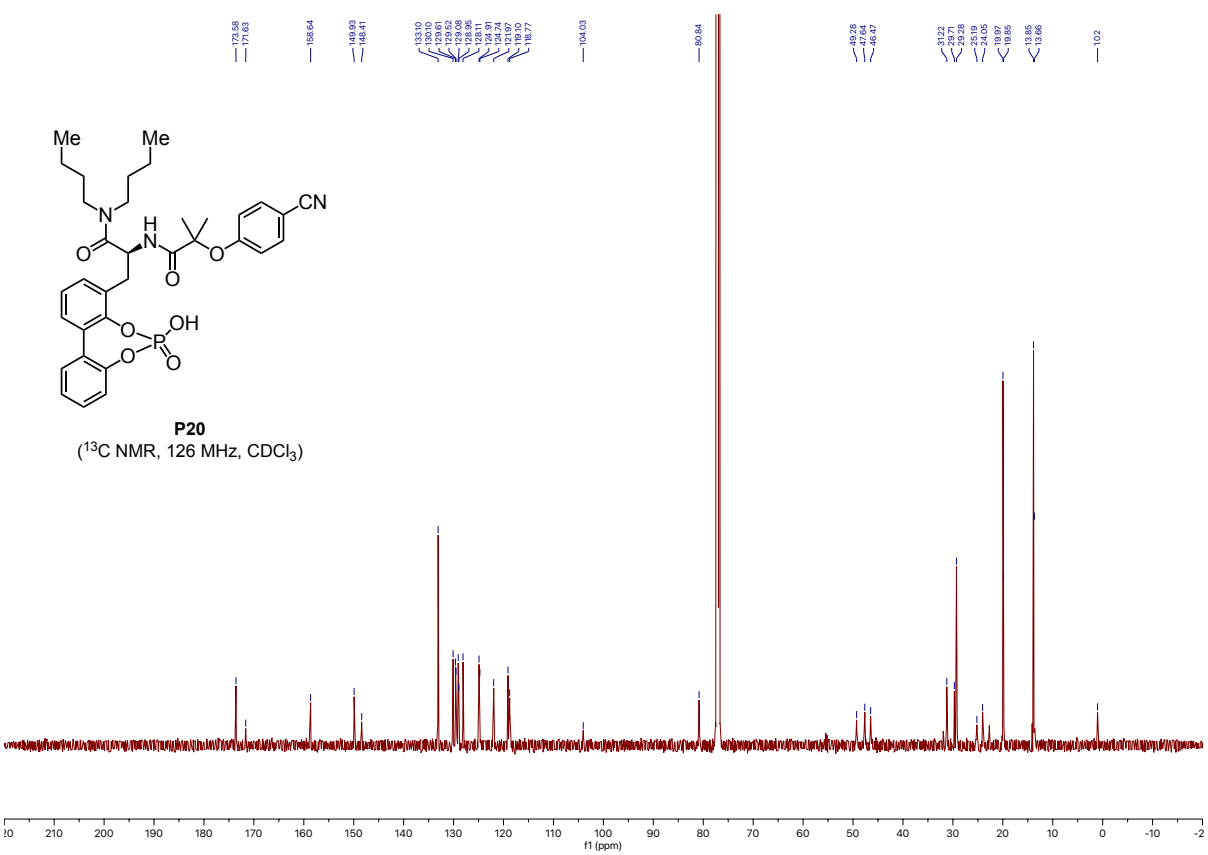



**P19**
($^{31}$P NMR, 243 MHz, $CDCl_3$)



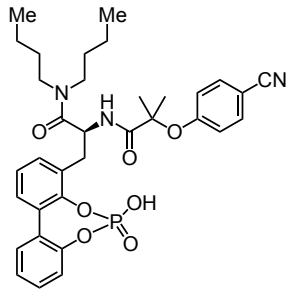

**P20**

($^{1}$H NMR, 600 MHz, $CDCl_3$)




**P20**

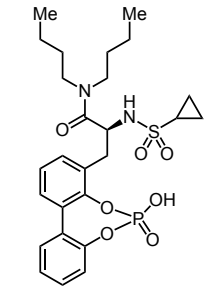
($^{13}$C NMR, 126 MHz, $CDCl_3$)




**P20**

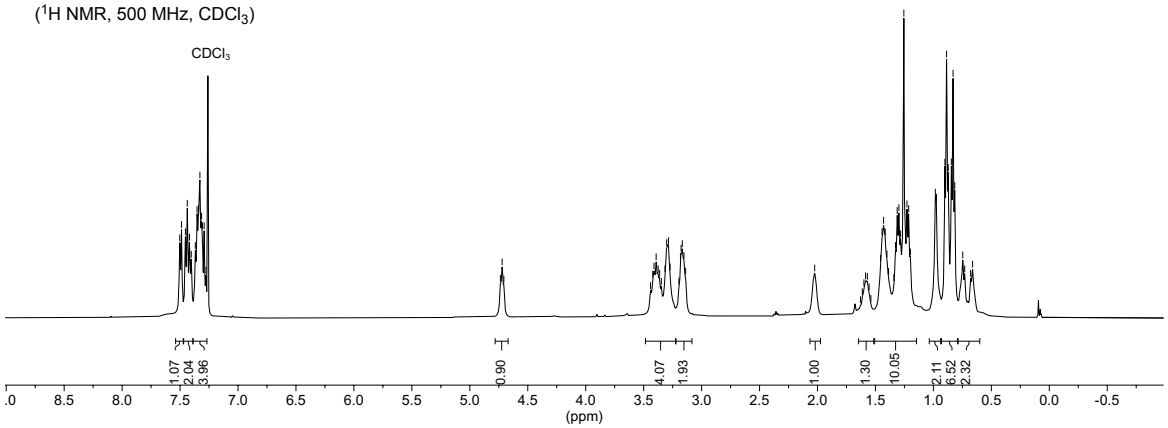
($^{31}$P NMR, 243 MHz, $CDCl_3$)

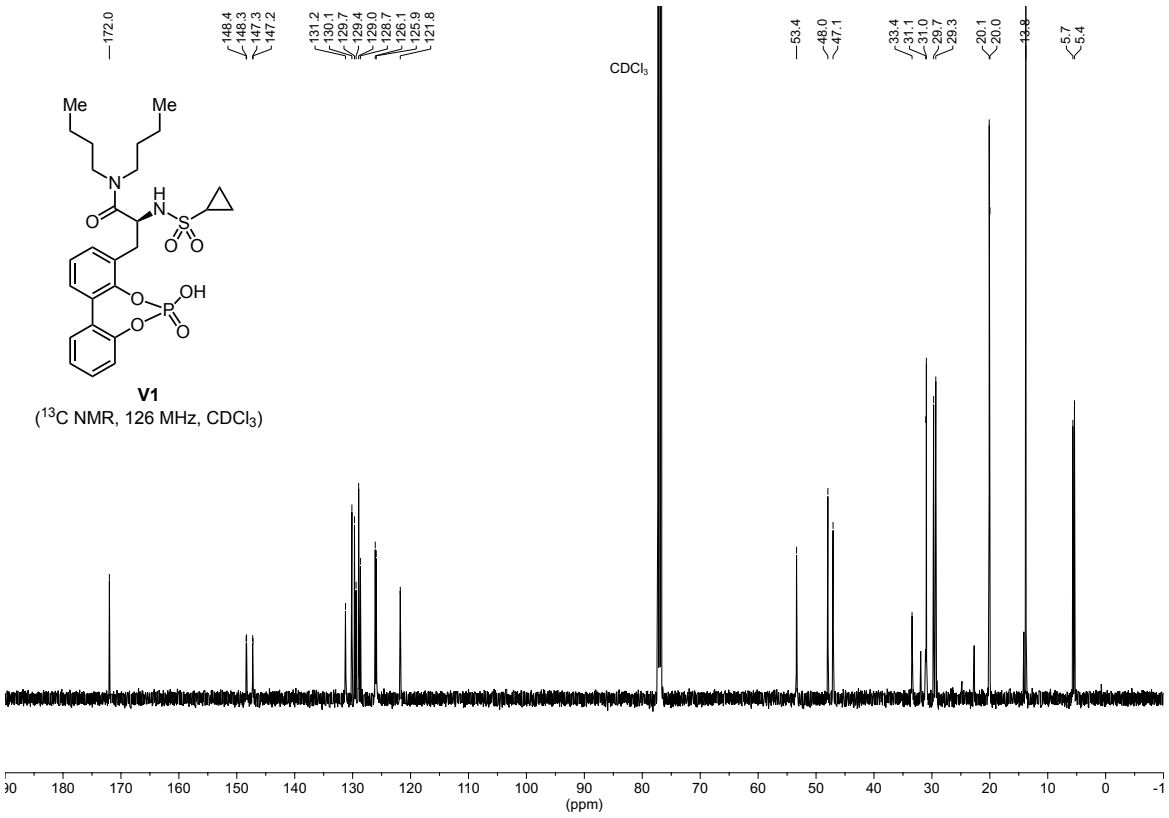



**V1**

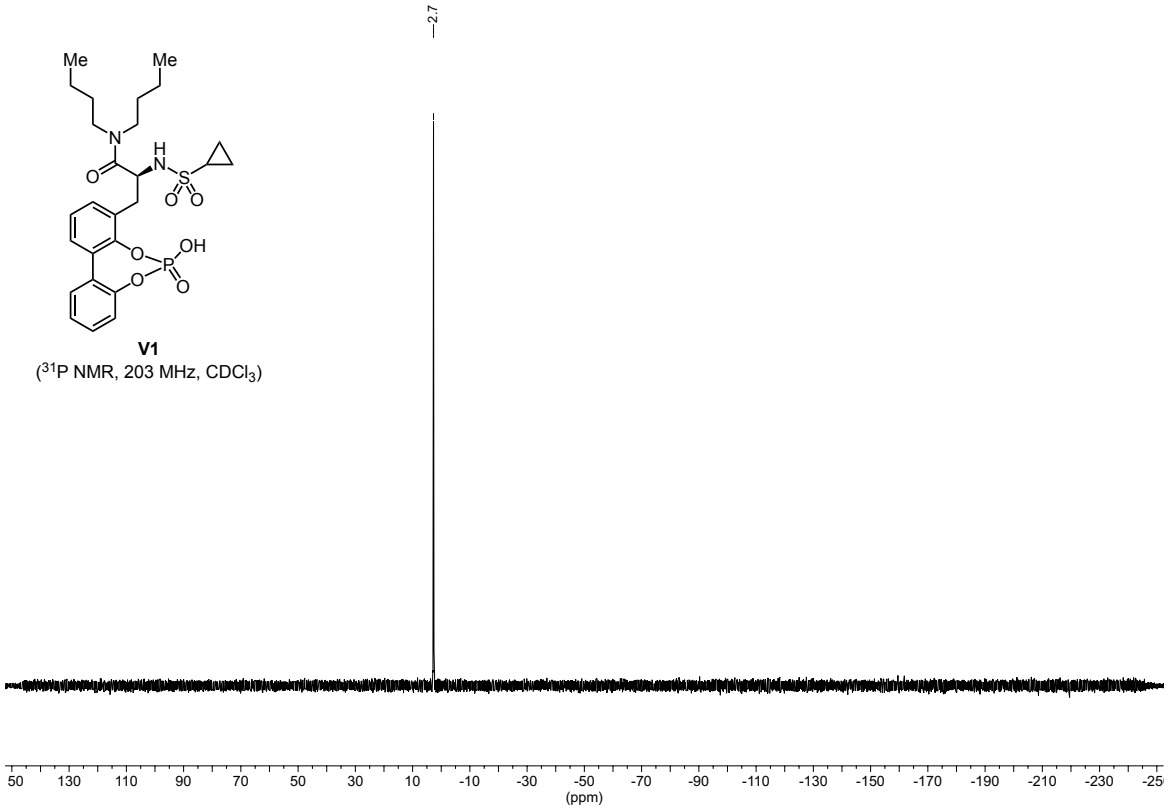
($^{1}$H NMR, 500 MHz, $CDCl_3$)





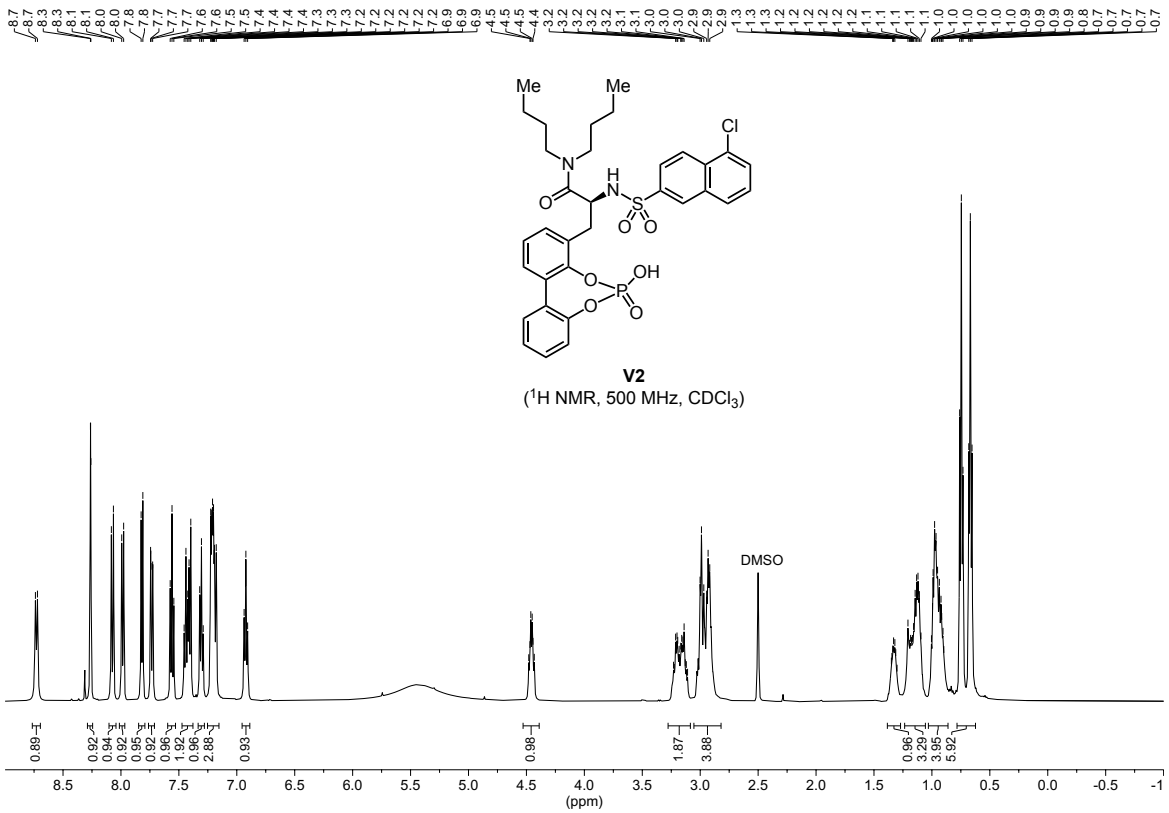

**V1**

($^{13}$C NMR, 126 MHz, $CDCl_3$)

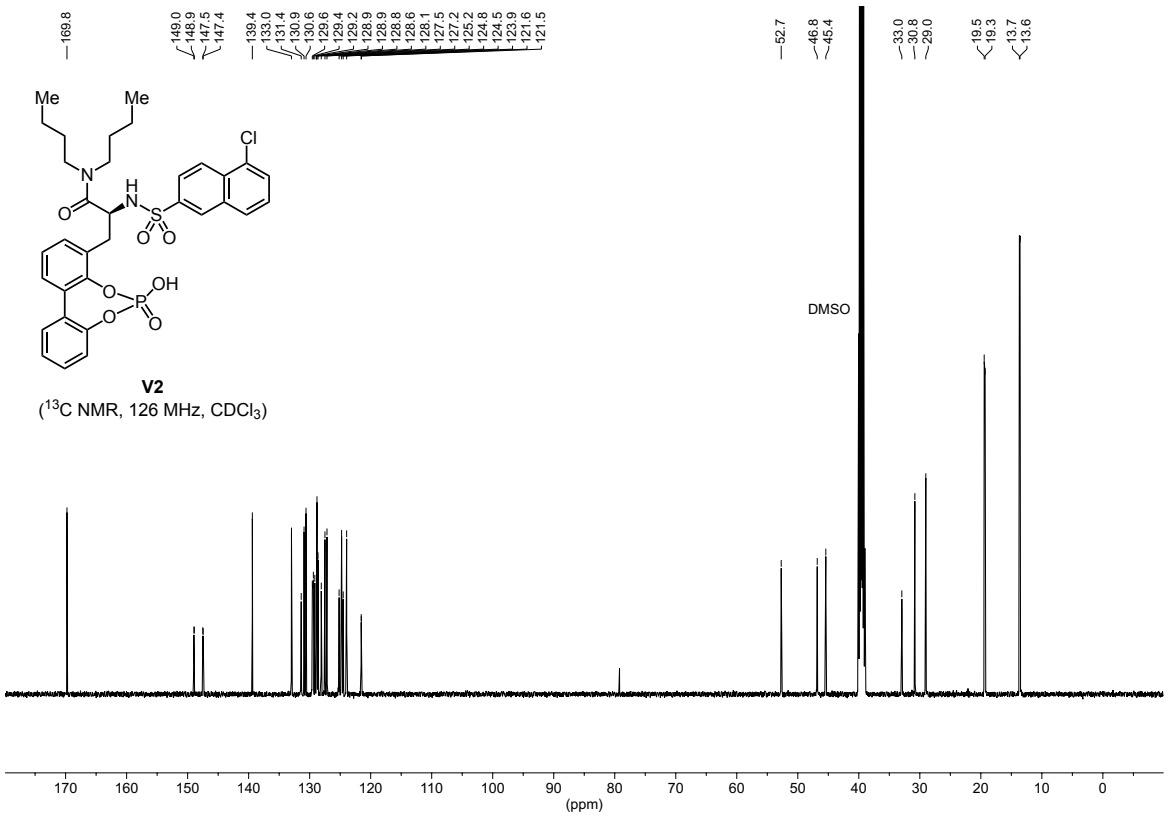



**V1**

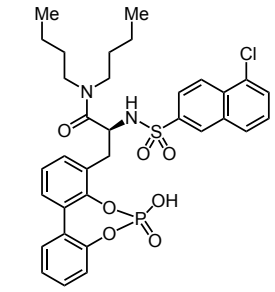
($^{31}$P NMR, 203 MHz, $CDCl_3$)




**V2**
($^{1}$H NMR, 500 MHz, $CDCl_3$)




**V2**
($^{13}$C NMR, 126 MHz, $CDCl_3$)



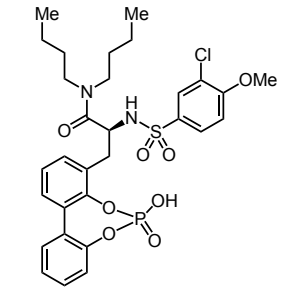

**V2**

($^{31}$P NMR, 203 MHz, $CDCl_3$)



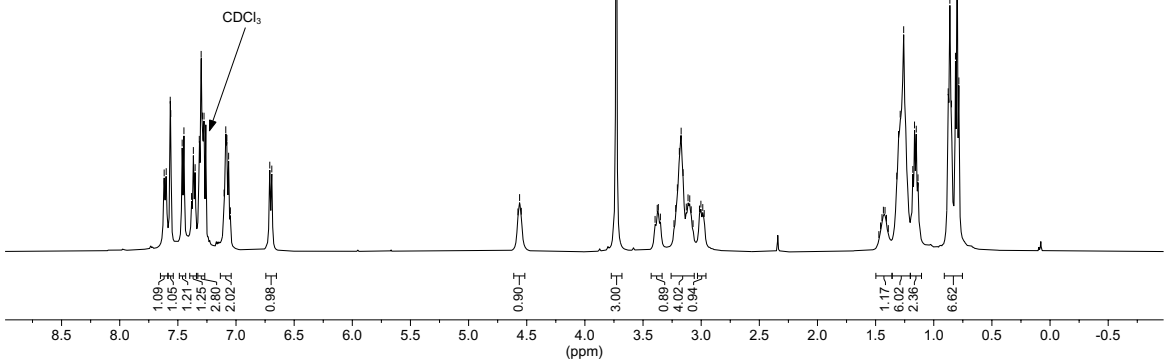


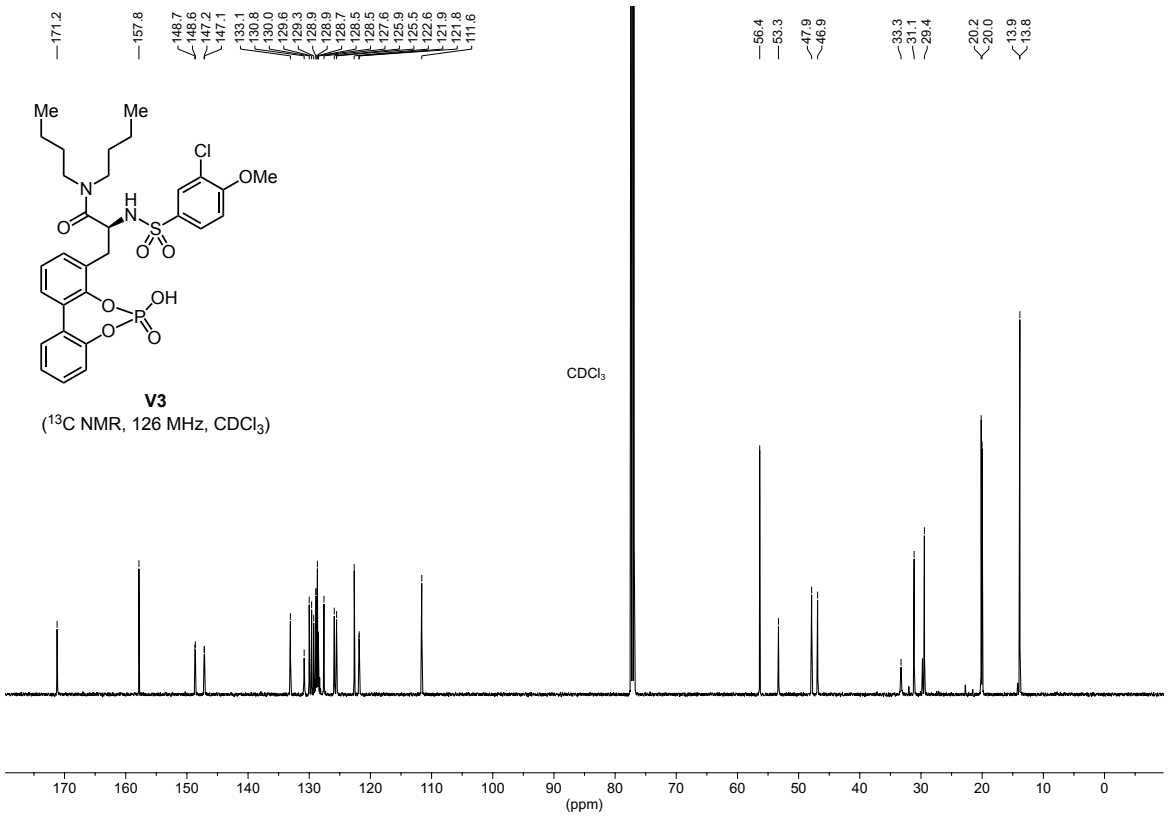





**V3**

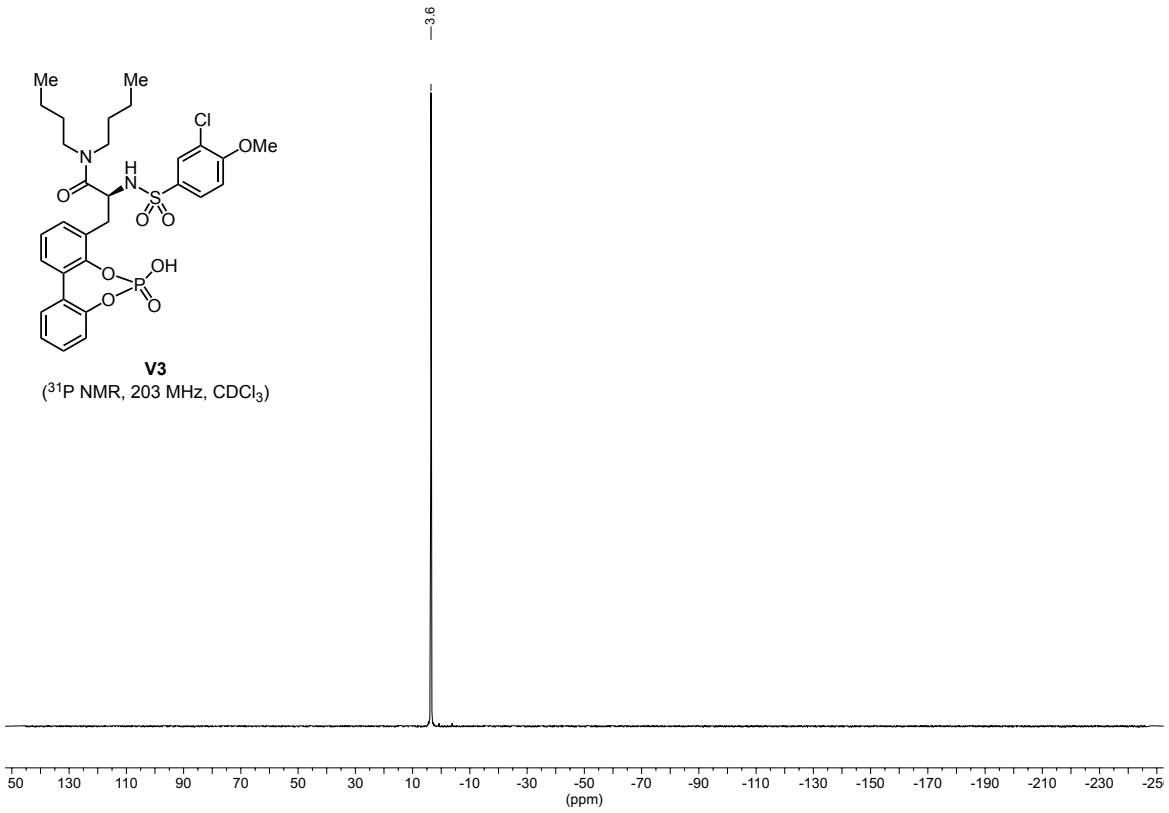
($^{1}$H NMR, 500 MHz, $CDCl_3$)






**V3**

($^{13}$C NMR, 126 MHz, $CDCl_3$)




**V3**

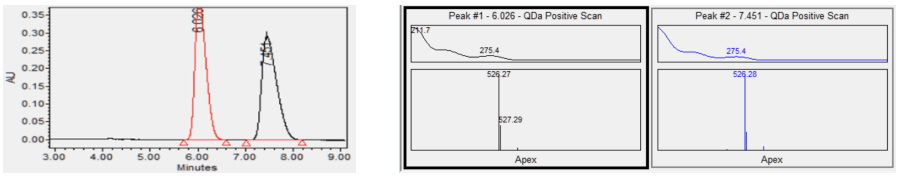
($^{31}$P NMR, 203 MHz, $CDCl_3$)

### 7.2.8. Enantiopurity Considerations

The initial route design was validated to show no racemization during the Negishi coupling or the installation of the amide groups. Additionally, the free amine backbone was re-protected abd analyzed to show that no racemization occurred during storage.

**A) <u>Negishi Coupling and Backbone</u>**

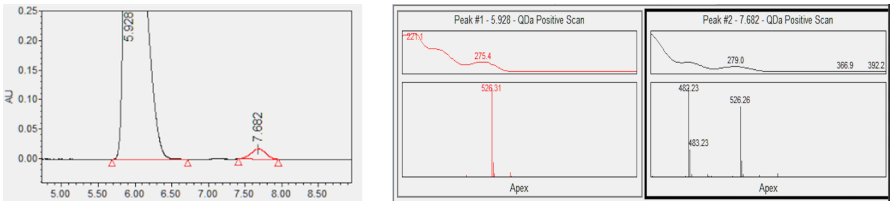
| Retention | %Area |
|---|---|
| 6.026 | 50.03 |
| 7.451 | 49.97 |




**(rac)-7**

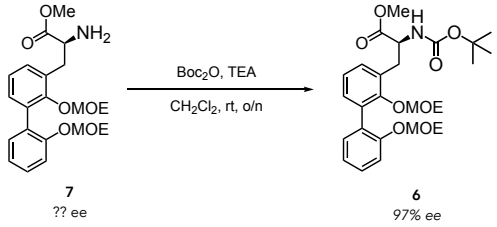
*CEL-2 MeOH Gradient 0-5% over 20 min.*

| Retention | %Area |
|---|---|
| 5.928 | 98.05 |
| 7.682 | 1.95 |




**7**

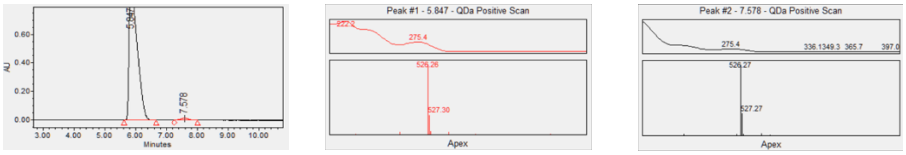
*CEL-2 MeOH Gradient 0-5% over 20 min.*




**7**
?? ee

**6**
97% ee

| Retention | %Area |
|---|---|
| 5.847 | 98.46 |
| 7.578 | 1.54 |

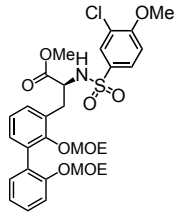



**7-after storage**

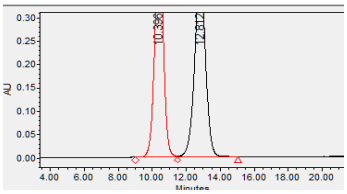
*CEL-2 MeOH Gradient 0-5% over 20 min.*

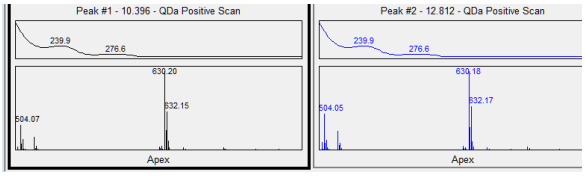
## B) Sulfonamide Coupling

| Retention | %Area |
|---|---|
| 10.396 | 49.42 |
| 12.812 | 50.58 |



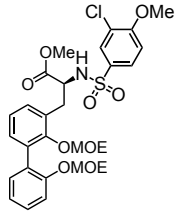

8w



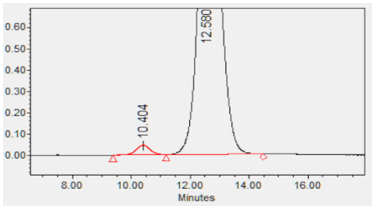



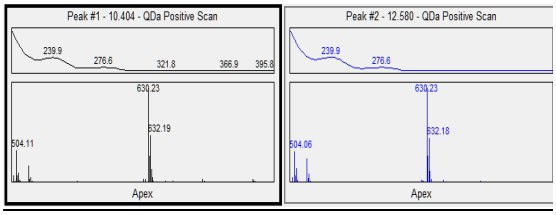

**(rac)-8w**

| Retention | %Area |
|---|---|
| 10.404 | 1.74 |
| 12.580 | 98.26 |



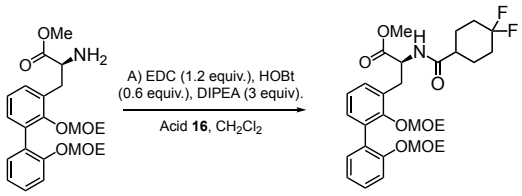

8w




**8w**

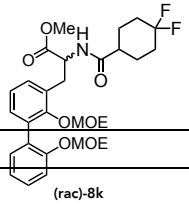
## C) EDC-HOBt Coupling



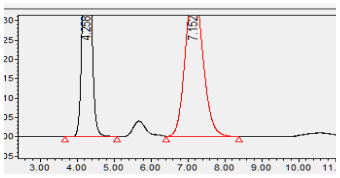

7
Starting ee: 97%

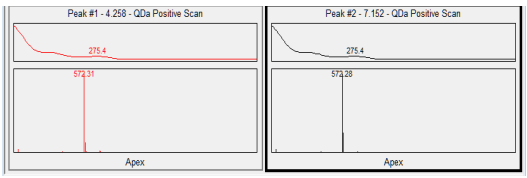
8k

| Retention | %Area |
|---|---|
| 4.258 | 50.40 |
| 7.152 | 49.60 |



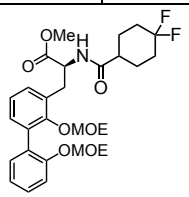

(rac)-8k



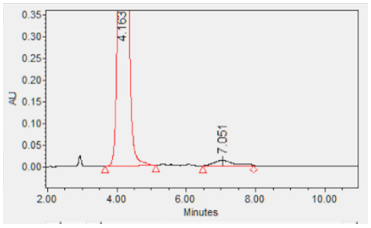




**(rac)-8k**

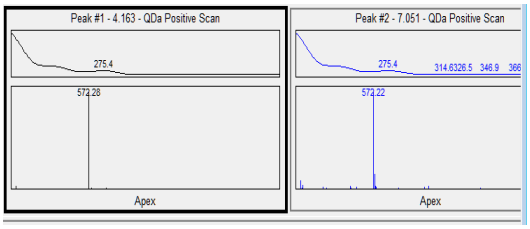
| Retention | %Area |
|---|---|
| 4.163 | 97.90 |
| 7.051 | 2.10 |



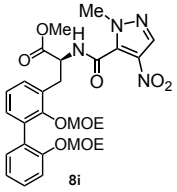

8k



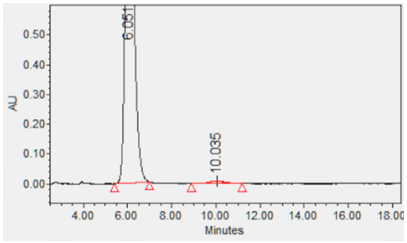

**8k**

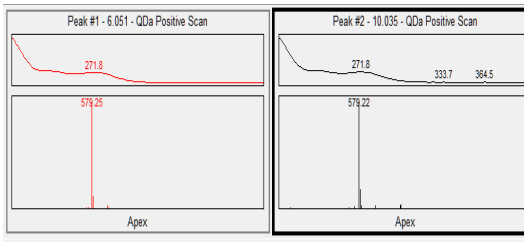



| Retention | %Area |
|---|---|
| 6.051 | 98.59 |
| 10.035 | 1.41 |




8i

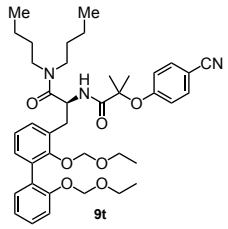


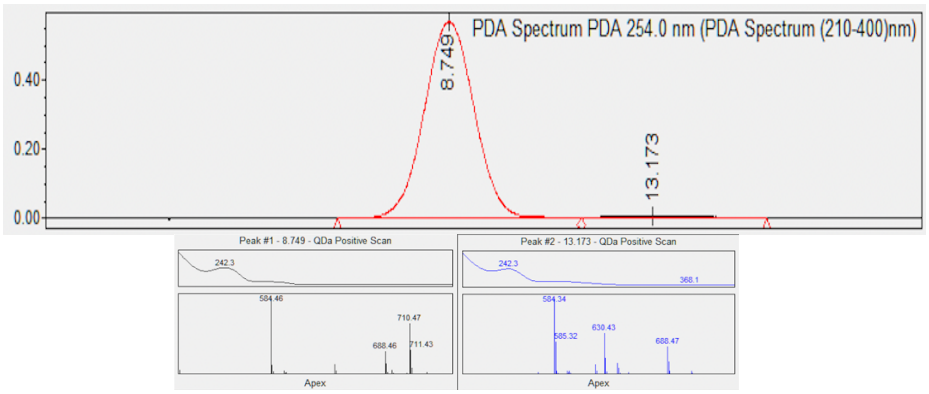




**8i**

## D) Saponification and DEPBT Coupling

| Retention | %Area |
|---|---|
| 8.748 | 49.82 |
| 13.173 | 50.18 |

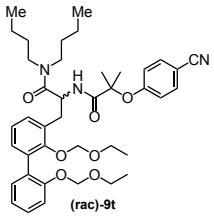


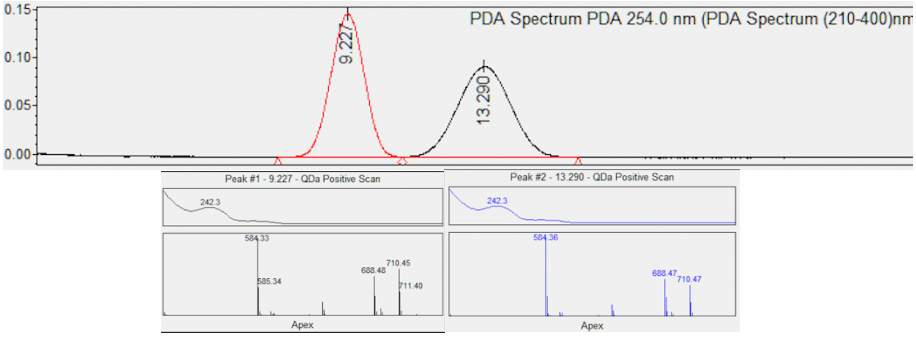




**9t**

*SFC conditions: ADH, 8% MeOH (isocratic)*

| Retention | % Area |
|---|---|
| 9.227 | 49.82 |
| 13.290 | 50.18 |

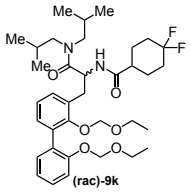


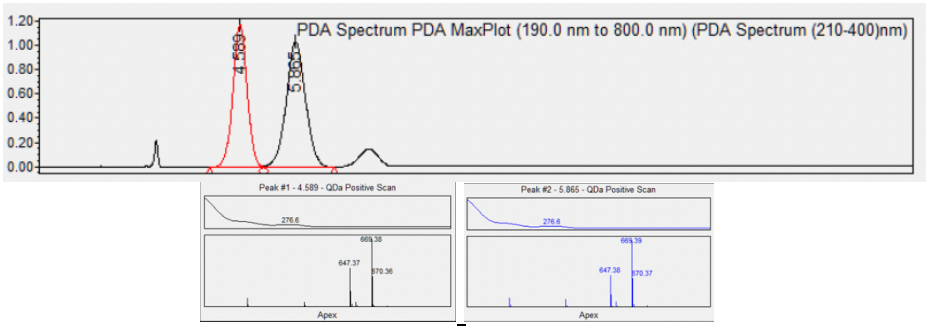




**(rac)-9t**

*SFC conditions: ADH, 8% MeOH (isocratic)*

| Retention | %Area |
|---|---|
| 4.589 | 45.63 |
| 5.865 | 54.37 |

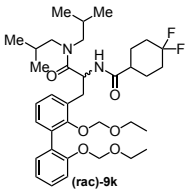


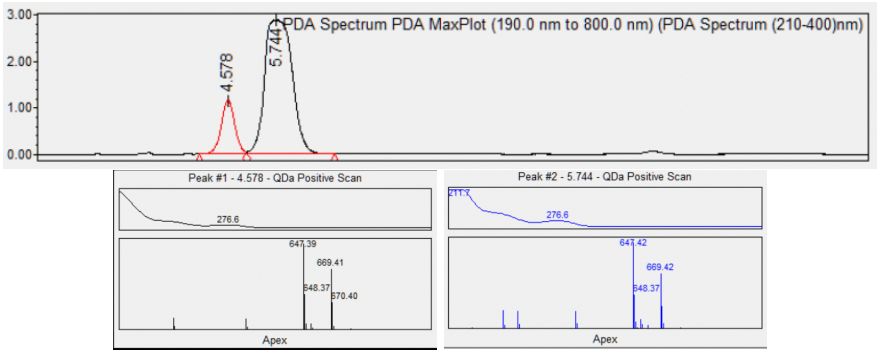




**(rac)-9k**

*OZ-H, 7% MeOH (iso)*

| Retention | %Area |
|---|---|
| 4.587 | 16.49 |
| 5.744 | 83.51 |



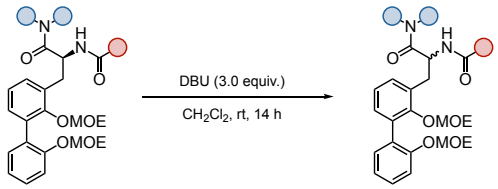

**9k**

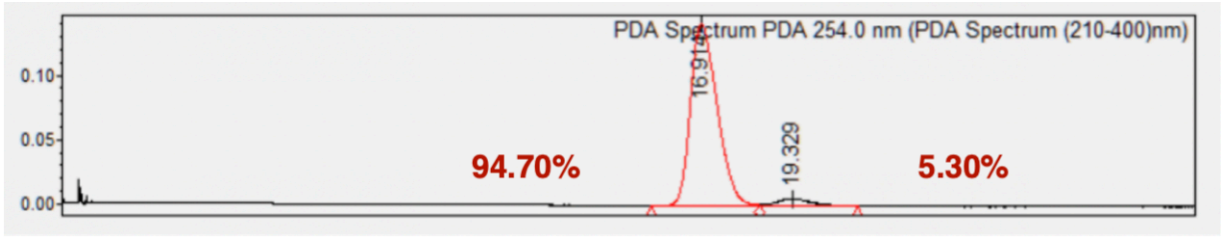
*OZ-H, 7% MeOH (iso)*

## F) Experiments to assess the risks of enantio-erosion during phosphorylation

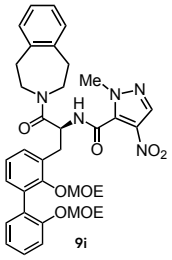
We hoped to attain racemic or scalemic samples of intermediates 9 for HPLC analysis by using a strong base (DBU, pKa(DBU-$H^+$)= 12 vs Pyridinium pKa= 5.2). We were pleased to find that even under forcing conditions and a large excess of base, the intermediates tested did not suffer much or any racemization. The same lack of erosion of the enantiopurity was observed when precursors 9 or deprotected biphenol intermediates **S2** were stirred in neat pyridine at elevated temperature.

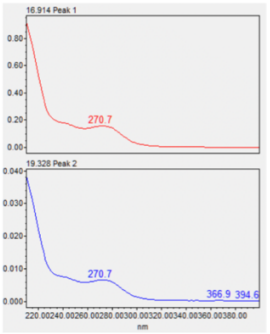
i. Attempt to racemize precursors 9 with 3 equiv. DBU, room temperature, 14 hours

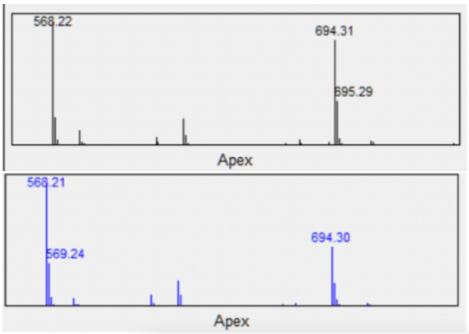



| Retention | % Area |
|---|---|
| 16.914 | 94.70 |
| 19.329 | 5.30 |

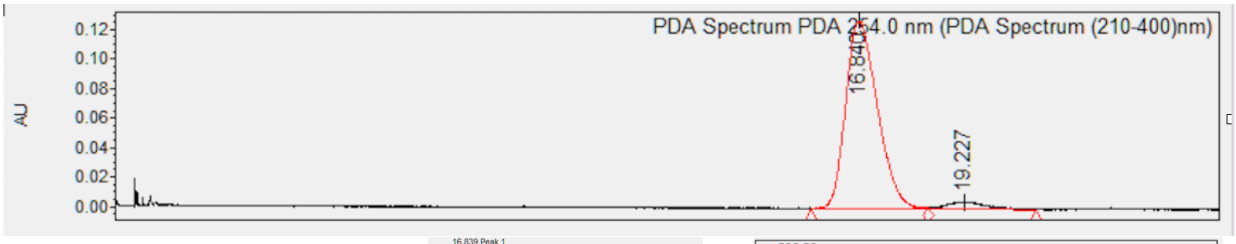


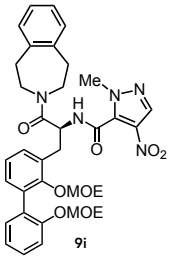



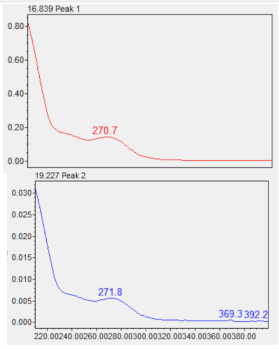

**9i- no base**

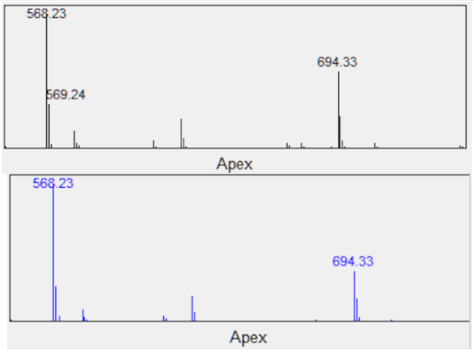
*CEL-I, MeOH grad 5-10% over 20 min*




| Retention | % Area |
|---|---|
| 16.840 | 95.00 |
| 19.227 | 5.00 |



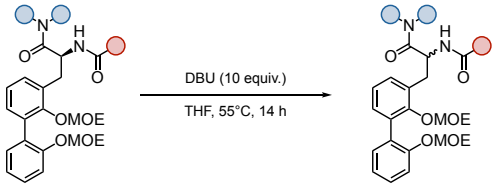



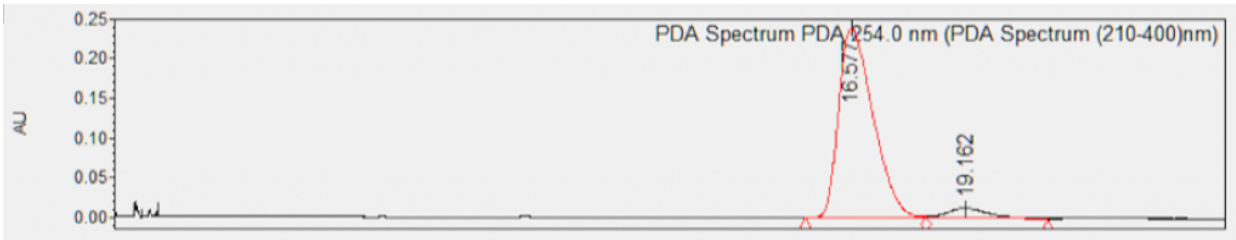




**9i- DBU (3 equiv.)**

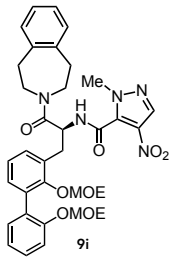
*CEL-I, MeOH grad 5-10% over 20 min*

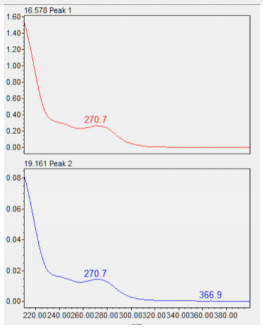
ii. Attempt to racemize precursors 9 with 10 equiv. DBU, 55 °C, 16 hours

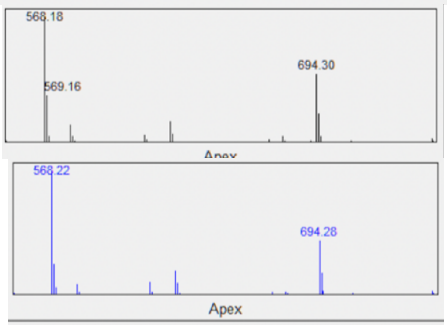



| Retention | % Area |
|---|---|
| 16.577 | 93.99 |
| 19.162 | 6.01 |



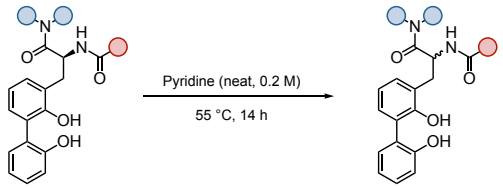



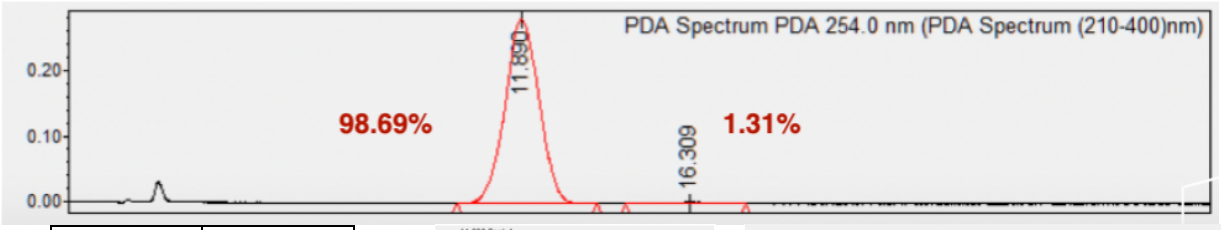




**9i- DBU (10 equiv.)**

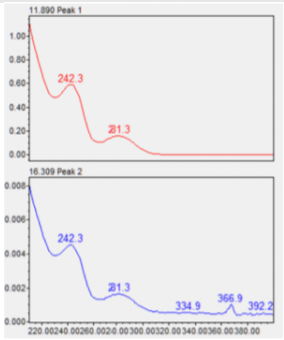
*CEL-I, MeOH grad 5-10% over 20 min*

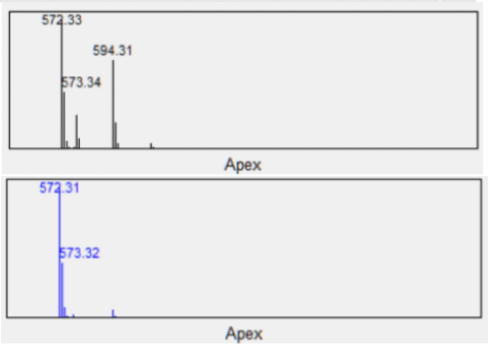
iii. Precursors **S2** in pyridine, 55 °C, 14 hours

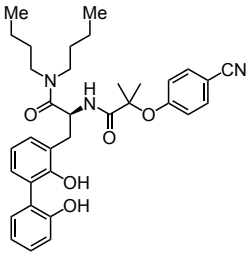



| Retention | % Area |
|---|---|
| 11.890 | 98.69 |
| 16.309 | 1.31 |



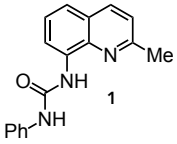

**S2-t – Pyridine (neat)**

*AD-H, MeOH gradient 5-10% (hold at 10)*

## 7.3. Reaction Screening

### 7.3.3. Transfer Hydrogenation of 8-Aminoquinoline 1

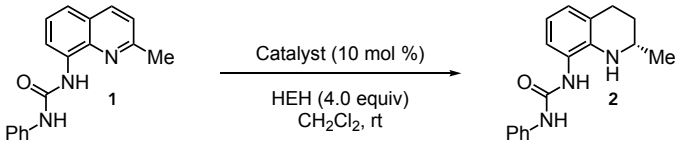
*i. Substrate Synthesis and Characterization*



**1-(2-methylquinolin-8-yl)-3-phenylurea (1)** was synthesized according to Shugrue et al. on 6.32 mmol scale.[20] The product was obtained in 73% yield (1.29 g, 4.67 mmol) as a white solid.

**$^1$H NMR** (500 MHz, $CDCl_3$) **δ** 9.46 (s, 1H), 8.56 (d, J = 7.7, 1.3 Hz, 1H), 8.02 (d, J = 8.4 Hz, 1H), 7.51 – 7.43 (m, 3H), 7.39 (t, J = 8.0, 1.4 Hz, 3H), 7.33 – 7.24 (m, 2H), 7.17 (t, J = 7.4, 1.3 Hz, 1H), 6.78 (brs, 1H), 2.67 (d, J = 1.2 Hz, 3H).
**$^{13}$C NMR** (126 MHz, $CDCl_3$) **δ** 157.0, 152.9, 138.3, 136.7, 134.7, 129.5, 126.7, 126.2, 124.4, 122.4, 121.6, 120.1, 115.3, 25.2. Experimental data correspond with literature description of the compound.[20]

*ii. Screening Procedure*



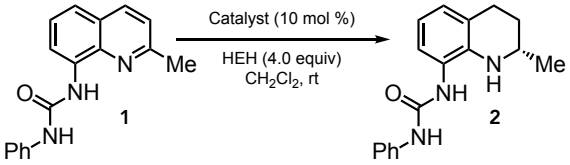

To a flame-dried half dram vial charged with a magnetic stir bar was added **(1)**(1 equiv., 0.025 mmol) and Catalyst (0.1 equiv., 0.0025 mmol). The mixture was dissolved in dry $CH_2Cl_2$ (0.2 mL, 0.125 M), proceeded by the addition Hantzsch Ester-Hydride (HEH, 4 equiv., 0.1 mmol). The vial was sealed with a Teflon-cap and further secured with electrical tape. The reaction mixture was stirred vigorously for 16 h and quenched with the addition of ammonium chloride (2 mL) and diluted with $CH_2Cl_2$ (5 mL). The organics were separated, and the aqueous layer was extracted once more with $CH_2Cl_2$ (10 mL). The combined organics were dried over sodium sulfate, filtered, and concentrated to yield crude product **10** as an off-white solid. The resulting crude mixture was used to determine conversion using $^1$H NMR. The sample was then purified via preparative TLC before determining enantiomeric ratio via SFC (CEL 1 column, 10% IPA; retention times: 9.4 min (minor), 11.2 min (major)). Racemic sample prepared using diphenylphosphate as a control catalyst and obtained in 96% as an off-white solid.

**$^1$H NMR (500 MHz, $CDCl_3$) δ** 7.37 – 7.29 (m, 2H), 7.31 – 7.22 (m, 2H), 7.07 – 6.98 (m, 2H), 6.94 (d, *J* = 7.9 Hz, 2H), 6.63 (t, *J* = 7.6 Hz, 1H), 6.52 (brs, 1H), 4.12 (brs, *J* = 7.2 Hz, 1H), 3.45 – 3.35 (m, 1H), 2.91 – 2.73 (m, 2H), 1.99 – 1.90 (m, 1H), 1.62 – 1.50 (m, 1H), 1.21 (d, *J* = 6.4, 1.4 Hz, 3H).

**$^{13}$C NMR (126 MHz, $CDCl_3$) δ** 155.0, 140.7, 138.3, 128.9, 128.4, 125.4, 123.4, 123.2, 119.9, 117.0, 47.3, 29.6, 26.6, 22.5, 14.2. Experimental data correspond with literature description of the compound.[20]

*iii. Screening Results*

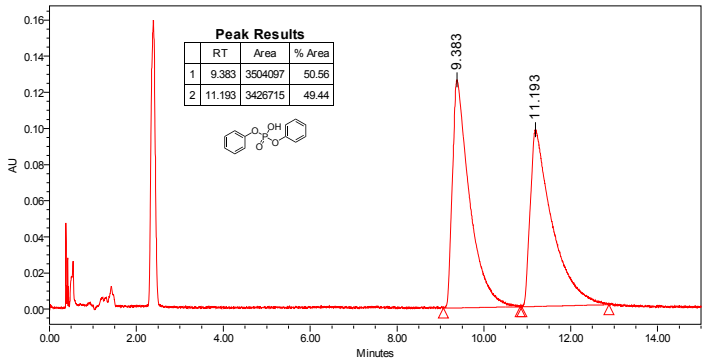
**Table S 3:** Full Training Set Screening Data for Transfer Hydrogenation.

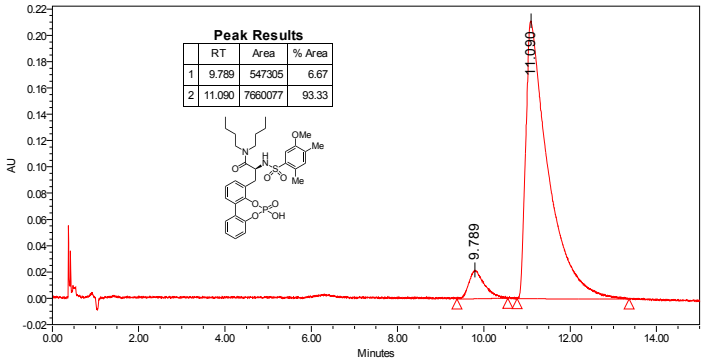



| Transfer Hydrogenation[a] | | |
|---|---|---|
| Catalyst | % yield[b] | er[b] |
| P1 | 39 | 50.5:49.5 |
| P2 | 71 | 91.5:8.5 |
| P3 | 73 | 50.5:49.5 |
| P4[c] | 89 | 77.5:22.5 |
| P5 | 76 | 49.5:50.5 |
| P6 | 74 | 50.5:49.5 |
| P7 | 81 | 57:43 |
| P8 | 71 | 87.5:12.5 |
| P9 | 48 | 77:23 |
| P10 | 71 | 50:50 |
| P11 | 71 | 50:50 |
| P12 | 58 | 52:48 |
| P13[c] | 69 | 85:15 |
| P14[c] | 63 | 50:50 |
| P15 | 77 | 49.5:50.5 |
| P16 | 77 | 59.5:40.5 |
| P17[c] | 65 | 77:23 |
| P18 | 54 | 52.5:47.5 |
| P19 | 83 | 93.5:6.5 |
| P20 | 75 | 68:32 |
| Validation Set | | |
| V1 | 97 | 90:10 |
| V2 | 98 | 92.5:7.5 |
| **V3** | **97** | **95:5** |

[a]Conditions: **1** (0.025 mmol), Hantzsch Ester Hydride (HEH, 0.1 mmol), catalyst (10 mol%), $CH_2Cl_2$ (0.25 mL) for 18 h in a sealed half dram vial. Representative selection of catalysts from training set. [b]Yields determined using NMR. Selectivity analyzed using chiral SFC. [c]Selectivities for catalysts with < 5% yield not obtained.

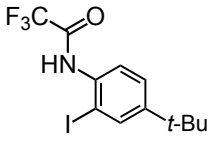
*iv. Representative SFC Traces*



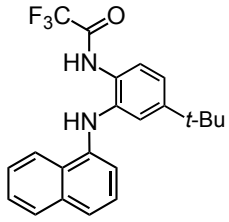



### i.3.2. Atroposelective Cyclodehydration

*i. Substrate Synthesis and Characterization*

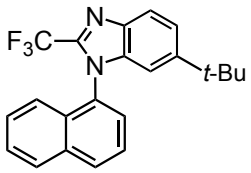


**N-(4-(tert-butyl)-2-iodophenyl)-2,2,2-trifluoroacetamide (S3).** A 100 mL round-bottom flask equipped with a magnetic stir bar was charged with $CH_2Cl_2$ (40 mL, 0.1 M), and 4-(*tert*-butyl)-2-iodoaniline (1.86 g, 6.76 mmol, 1.0 equiv.) and cooled to 0 °C. To this stirring solution were subsequently added $Et_3N$ (1.02 g, 1.41 mL, 10.1 mmol, 1.5 equiv.) and TFA2O (1.70 g, 1.13 mL, 8.11 mmol, 1.2 equiv.). The reaction mixture was allowed to warm to room temperature and stirred for 12 hours. Upon completion of the reaction as monitored by TLC, the crude mixture was diluted with $CH_2Cl_2$ and quenched with aq. Sat. NH4Cl. The aqueous layer was extracted with $CH_2Cl_2$ (3 x 20 mL). The collected organic fractions were dried over $Na_2SO_4$ and concentrated in vacuo. The crude product was purified by flash column chromatography using 30% $CH_2Cl_2$/Hexanes as mobile phase to afford the title compound as an orange solid (4.8 g, 90 % yield). **$^1$H NMR** (400 MHz, Chloroform-*d*) δ 8.21 (s, 1H), 8.08 (d, *J* = 8.6 Hz, 1H), 7.81 (d, *J* = 2.1 Hz, 1H), 7.43 (dd, *J* = 8.6, 2.1 Hz, 1H), 1.31 (s, 9H). **$^{13}$C NMR** (151 MHz, Chloroform-*d*) δ 154.73 (q, *J* = 37.5 Hz), 151.51, 136.10, 133.11, 126.69, 121.87, 115.68 (q, *J* = 288.7 Hz), 90.67, 34.53, 31.08. **$^{19}$F NMR** (565 MHz, Chloroform-*d*) δ -75.77. Experimental data correspond with literature description of the compound.[21]



**N-(4-(tert-butyl)-2-(napthalen-1-ylamino)-phenyl)-2,2,2-trifluoroacetamide (10)**. An oven-dried, three-necked 250 mL flask was charged with 1-naphthylamine (2.0 g, 16 mmol, 2.0 equiv.) in MeCN/DMF (2:1, 30 mL, 0.2 M), and placed under inert atmosphere by freeze-pump-thaw (three times). Under a positive atmosphere of nitrogen, CuI (152 mg, 0.8 mmol, 10 mol%), 2,2'-bisphenol (150 mg, 0.8 mmol, 10 mol%), $K_3PO_4$ (4.0 g, 20 mmol, 2.2 equiv.), and *N*-(4-*tert*-butyl)-2-iodophenyl)-2,2,2-trifluoroacetamide (**S3**) (3.0 g, 8.0 mmol, 1.0 equiv.) were added. The flask was left under nitrogen and heated to 60 °C for 14 hours. The crude mixture was allowed to cool to room temperature, diluted with EtOAc and quenched with sat. aq. $NaHCO_3$. The aqueous layer was extracted three times with EtOAc. The combined layers were dried over $Na_2SO_4$ and concentrated in vacuo. The crude product was purified by flash column chromatography on normal phase silica gel using 10% EtOAc/Hexanes as mobile phase to afford the title compound as a pink powder (800 mg, 26 %). **$^1$H NMR** (400 MHz; $CDCl_3$): δ 8.32 (s, 1H), 8.03 (dd, *J* = 6.9, 3.3 Hz, 2H), 7.92 – 7.85 (m, 1H), 7.60 – 7.52 (m, 2H), 7.48 (d, *J* = 8.1 Hz, 1H), 7.34 – 7.25 (m, 2H), 7.24 (d, *J* = 2.2 Hz, 1H), 6.60 (dd, *J* = 7.6, 1.1 Hz, 1H), 5.87 (s, 1H), 1.39 – 1.30 (m, 1H), 1.26 – 1.19 (m, 1H). **$^{13}$C NMR** (151 MHz; $CDCl_3$): δ 155.1, 154.9, 150.9, 140.0, 134.6, 133.5, 128.9, 127.3, 126.3, 126.3, 126.1, 125.9, 125.1, 124.6, 122.7, 122.2, 123.0, 121.8, 120.5, 120.3, 110.9, 34.7, 31.4, 31.3, 31.2, 31.1, 30.9. **$^{19}$F NMR** (400 MHz; $CDCl_3$): δ –74.8 (3F). Experimental data correspond with literature description of the compound.[21]

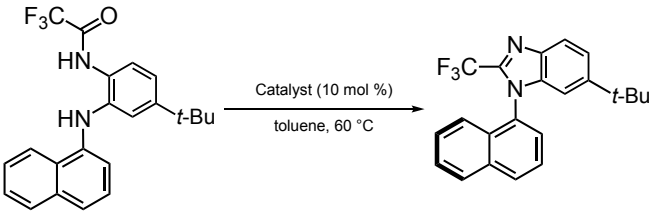
*ii. Racemic Sample Preparation*



(**rac)-6-(*tert*-Butyl)-1-(naphthalen-1-yl)-2-(trifluoromethycl)-1*H*-benzo[*d*]imidazole** (**11**). An oven-dried 8 mL vial equipped with a magnetic stir bar was charged with *N*-(4-(*tert*-Butyl)-2-(naphthalen-1-ylamino)phenyl)-2,2,2-trifluoroacetamide (8 mg, 0.02 mmol, 1.0 equiv.) and 100 μL of anhydrous toluene. A stock solution of phosphoric acid was prepared by diluting $H_3PO_4$ (0.4 g, 20 μL, 0.4 mmol) in anhydrous toluene (10 mL). 100 μL of the prepared phosphoric acid solution were syringed in the reaction vial (final concentration of phosphoric acid 0.4 mg, 4 μmol, 20 mol%; final concentration of the substrate in toluene 0.1 M). The vial was sealed with parafilm and heated to 60 °C for 8 hours. The crude product mixture was passed through a plug of silica in a Pasteur pipette and flushed with toluene, and concentrated to obtain the desired product in 98 % yield. **$^1$H NMR** (600 MHz, $CDCl_3$) δ 8.11 (d, *J* = 8.3 Hz, 1H), 8.02 (d, *J* = 8.4 Hz, 1H), 7.93 (d, *J* = 8.7 Hz, 1H), 7.70 – 7.55 (m, 4H), 7.52 (dd, *J* = 8.8, 1.8 Hz, 1H), 7.48 – 7.41 (m, 1H), 7.12 (d, *J* = 8.5 Hz, 1H), 6.81 (d, *J* = 1.5 Hz, 1H), 1.23 (s, 7H). **$^{13}$C NMR** (151 MHz, $CDCl_3$) δ 150.00, 141.52, 138.70, 138.00, 137.67, 134.26, 130.80, 130.71, 130.28, 128.45, 127.78, 127.11, 126.58, 125.32, 122.61, 122.21, 120.77, 119.90, 116.08, 107.23, 35.18, 31.53. **$^{19}$F NMR** (565 MHz, $CDCl_3$) δ -61.48. Experimental data correspond with literature description of the compound.[22]

Enantiomeric excess of the product was determined by chiral HPLC analysis: DAICEL CHIRALCEL® AD-H, φ 0.46 x 25 cm, hexane:$^i$PrOH = 96:04, 0.5 mL/min, 254 nm, $t_R$ (1) = 6.52 min, $t_R$ (2) = 7.92 min. An example HPLC trace below shows the ratio of the enantiomers of the products.

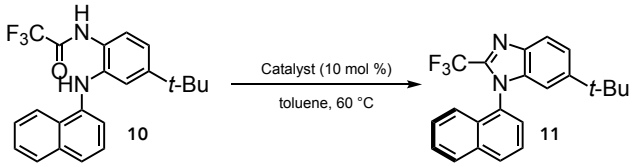
*iii. Screening Procedure*




An oven-dried 8 mL vial equipped with a magnetic stir bar was charged with the substrate N-(4-(tert-butyl)-2-(napthalen-1-ylamino)-phenyl)-2,2,2-trifluoroacetamide (8 mg, 0.020 mmol, 1.0 equiv) and flexible chiral phosphoric acid catalyst (0.0020 mmol, 0.10 equiv). The reagents were subsequently dissolved in toluene (0.20 mL, 0.10 M). The vial was sealed with parafilm and electrical tape and heated to 60 ºC for 24 h. The crude reaction mixtures were cooled down to room temperature and concentrated. Analysis by $^{19}$F NMR was obtained after addition of α,α,α-trifluorotoluene (1.0 equiv) as a stock solution in $CDCl_3$ for internal standard. The samples were then purified by preparatory TLC in 100 % toluene to isolate the desired product. The latter was dissolved in 10% isopropanol/hexanes for HPLC analysis. A sample HPLC trace below shows the separation of the two enantiomers when **P2** was used.

*iv. Screening Results*

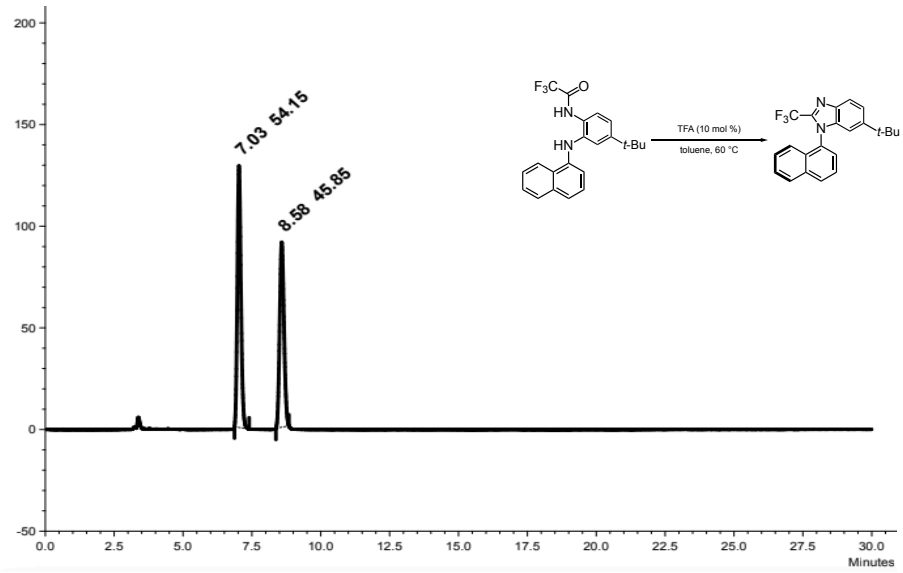
**Table S 4:** Selectivity Data for Atroposelective Cyclodehydration.

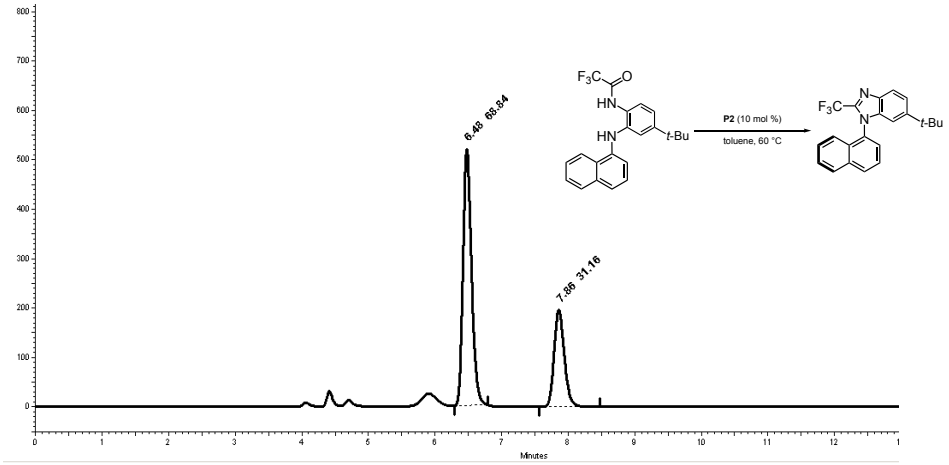



| Atroposelective Cyclodehydration[a] | | |
|---|---|---|
| Catalyst | % yield[b] | er[b] |
| P1 | 78 | 48:52 |
| P2 | 83 | 67:33 |
| P3 | 35 | 48.5:51.5 |
| P4 | 51 | 87.5:12.5[d] |
| P5 | 30 | 48.5:51.5 |
| P6 | 65 | 48.5:51.5 |
| P7 | 95 | 62.5:37.5 |
| P8 | 79 | 67:33 |
| P9 | 83 | 62:38 |
| P10 | 80 | 48:52 |
| P11 | 80 | 48.5:51.5 |
| P12 | 66 | 50:50 |
| P13 | 5 | 57:43 |
| P14 | 8 | 50:50 |
| P15 | 50 | 48:52 |
| P16 | 27 | 54:46 |
| P17 | 6 | 64:36 |
| P18 | 77 | 51.5:48.5 |
| P19 | 82 | 71:29 |
| P20 | 95 | 70:30 |

[a]Conditions: substrate (0.025 mmol), catalyst (10 mol%), in toluene at 60 °C for 14 h in a sealed 4 mL vial. Representative selection of catalysts from training set. [b]Yields determined using $^{19}$F NMR. Selectivity analyzed using chiral HPLC. [c]Selectivities for catalysts with < 5% yield not obtained. [d] Removed from modeling.

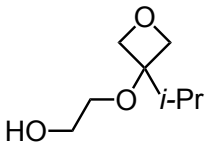
*i. Representative HPLC Traces*



### 7.3.3. Oxetane Desymmetrization

*i. Substrate Synthesis and Characterization*

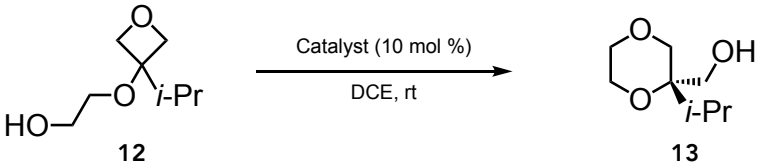


**2-((3-isopropyloxetan-3-yl)oxy)ethan-1-ol (12)** was synthesized from ethyl 2-((3-isopropyloxetan-3-yl)oxy)acetate on 2.3 mmol scale according to Yang *et al*, yielding a colorless oil (81% yield, 300 mg, 1.87 mmol).[23]

**$^1$H NMR** (500 MHz, CDCl3) δ 4.66 (d, J = 7.1 Hz, 2H), 4.50 (d, J = 7.1 Hz, 2H), 3.78 – 3.73 (m, 2H), 3.61 (t, J = 4.3 Hz, 2H), 2.21 – 1.93 (m, 2H), 0.97 (dd, J = 6.8, 1.4 Hz, 6H).

**$^{13}$C NMR** (126 MHz, CDCl3) δ 82.1, 77.7, 64.3, 62.2, 31.7, 16.2. Experimental data correspond with literature description of the compound.[23]

*ii. Screening Procedure*




**12** **13**

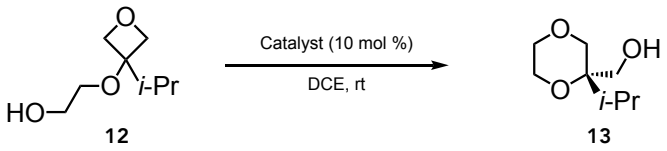
To a flame-dried half dram vial charged with a magnetic stir bar was added Catalyst (0.1 equiv., .0025 mmol). Oxetane (**12**) (1.0 equiv., 0.025 mmol) dissolved in dichloroethane (DCE, 0.25 mL, 0.1 M) was then added to the vial via syringe. The vial was sealed with a Teflon-cap and further secured with electrical tape. The reaction mixture was stirred for 16 hour at room temperature and concentrated to afford crude **13**. This mixture was dissolved in diethyl ether ($Et_2O$) and passed through a silica plug to remove catalyst and afford crude **13** as a colorless oil. The crude mixture was dissolved in $CDCl_3$ to determine conversion using $^1$H NMR. The sample was then derivatized using TEA (1 equiv., 0.025 mmol) and 4-nitrobenzoyl chloride (2 equiv, 0.05 mmol) to provide a UV-active sample for determination of enantiomeric ratio. The resulting derivatized dioxane was purified via preparative TLC (25% EtOAc/Hexanes) before determining enantiomeric ratio via SFC (CEL 2 column 3% IPA, 2.0 mL/min; retention times: 2.3 min (major), 2.5 (minor). Racemic sample prepared using diphenylphosphate as a catalyst and obtained in 95% yield as a colorless oil.

**$^1$H NMR** (500 MHz, $CDCl_3$) δ 3.80 – 3.72 (m, 2H), 3.72 – 3.58 (m, 6H), 2.35 (hept, $J$ = 7.0 Hz, 1H), 1.89 (t, $J$ = 5.9 Hz, 1H), 0.92 (dd, $J$ = 12.0, 7.1 Hz, 6H).

**$^{13}$C NMR** (126 MHz, $CDCl_3$) δ 75.5, 67.7, 66.6, 60.7, 60.2, 28.6, 16.9, 16.2. Experimental data correspond with literature description of the compound.[23]

*i. Screening Results*

**Table S 5:** Selectivity Data for Oxetane Desymmetrization.

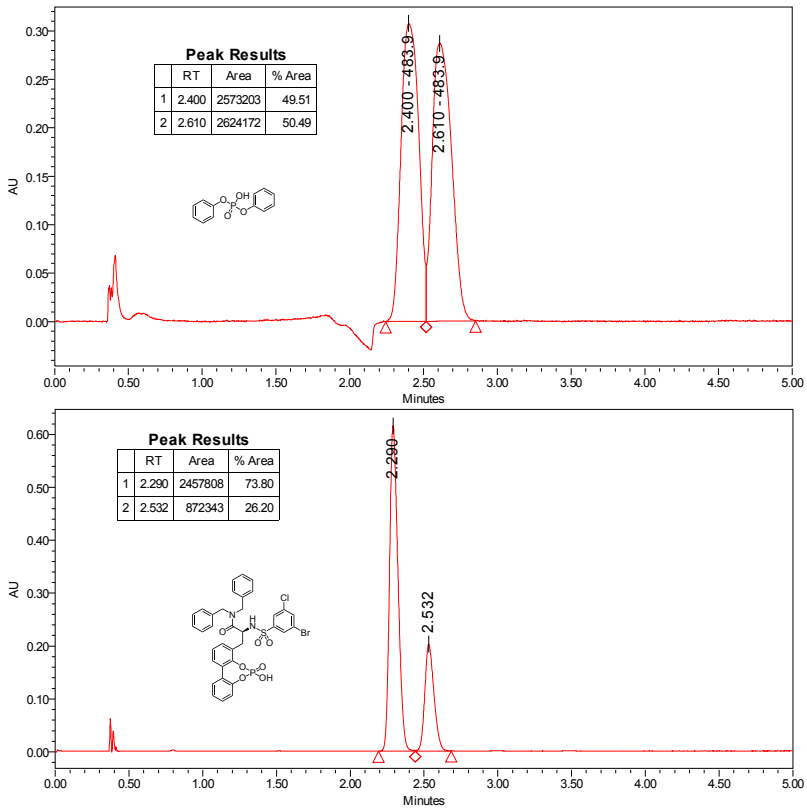



**12** **13**

| Oxetane Desymmetrization[a] | | |
|---|---|---|
| Catalyst | % yield[b] | er[b] |
| P1 | 98 | 50:50 |
| P2 | 96 | 71:28 |
| P3 | 20 | 51:49 |
| P4 | 4[c] | - |
| P5 | 24 | 50.5:49.5 |
| P6 | 27 | 50.5:49.5 |
| P7 | 23 | 49.5:50.5 |
| P8 | 100 | 74:26 |
| P9 | 100 | 57.5:42.5 |
| P10 | 80 | 50:50 |
| P11 | 86 | 50:50 |
| P12 | 69 | 51:49 |
| P13 | 0[c] | - |
| P14 | 0[c] | - |
| P15 | 12 | 50:50 |
| P16 | 18 | 53.5:46.5 |
| P17 | 0[c] | - |
| P18 | 33 | 50.5:49.5 |
| P19 | 100 | 73:27 |
| P20 | 34 | 67:33 |

[a]Conditions: substrate (0.025 mmol), catalyst (10 mol%), DCE (0.25 mL) for 18 h in a sealed 4 mL vial. Representative selection of catalysts from training set. [b]Yields determined using $^1$H NMR. Selectivity analyzed using chiral SFC. [c]Selectivities for catalysts with < 5% yield not obtained.

*iii. Representative SFC Traces*



## 7.4. Computational Details

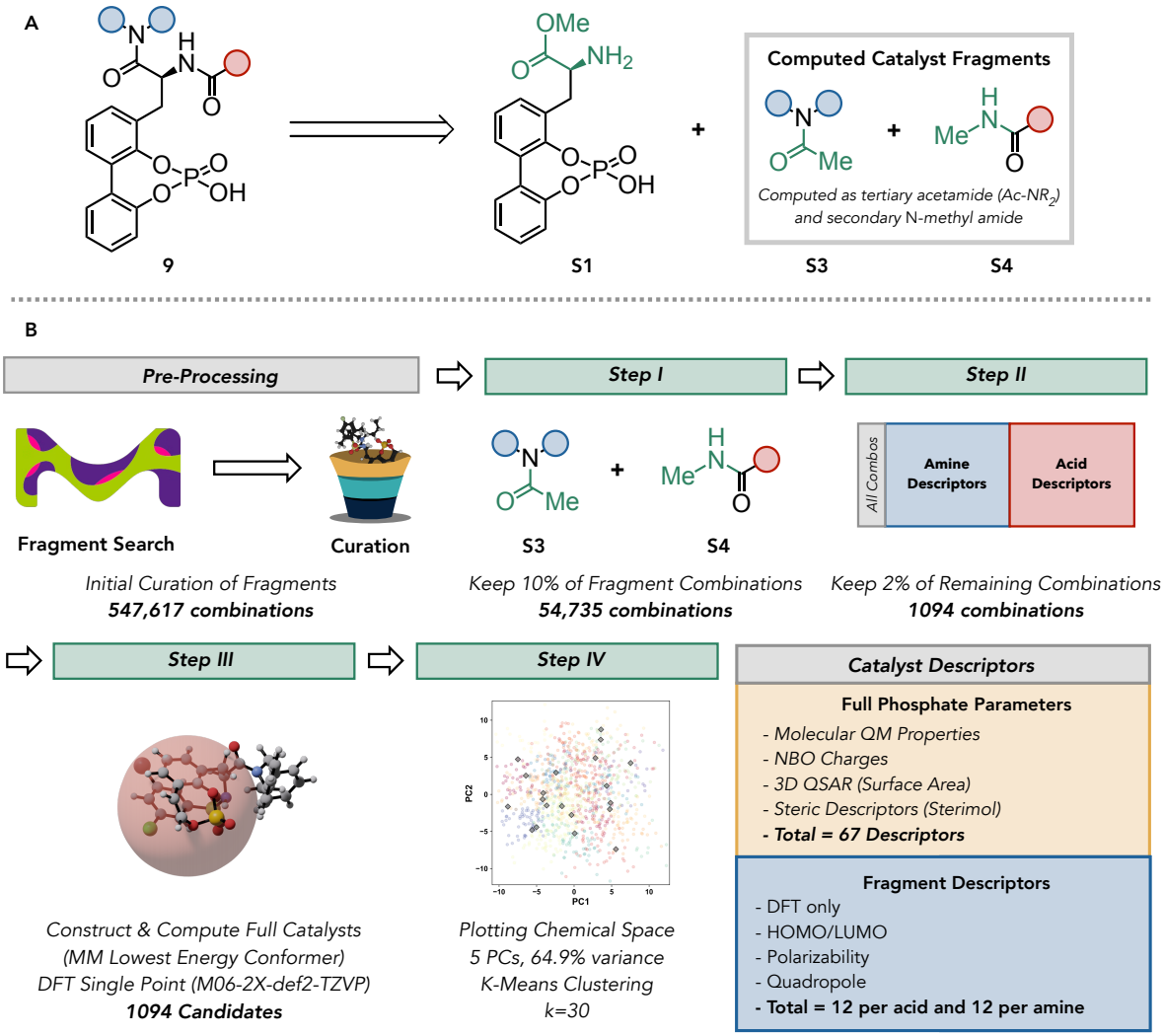
### 7.4.1. General Computational Methods

Conformational ensembles were gathered through conformational searching using Macromodel (part of the Schrödinger Suite) and the OPLS3e (v. 11.8)[24] or OPLS4 (release 2022-1)[25] force field (10,000 steps, 5 kcal/mol energy window).[26,27] Conformational clustering was employed using the minimum Kelley Penalty score to select the optimal number of conformers per catalyst as implemented in Macromodel.[28] Next, each conformer was optimized in the gas-phase with PW6B95D3(BJ)/6-31+(d,p) using Gaussian 16 (Revision C.01). Single point calculations were run with PW6B95D3/cc-pVTZ. Optimized geometries were verified by frequency computations as minima (zero imaginary frequencies) and parameters were acquired from these ground state structures. NBO charges were calculated using NBO 3.1 at the PW6B95D3(BJ)/cc-pVTZ level.[28] ChelpG and Hirshfield charges were computed as implemented in Gaussian 16 at the PW6B95D3/cc-pVTZ level.[29] NMR computations were calculated at the PW6B95D3(BJ)/cc-pVTZ level using the GIAO method.[30] Triple-zeta energy corrections were computed using Paton GoodVibes (v3.0.0).[31] Buried volumes and Sterimol values were calculated using Paton's DBSTEP package.[32] All synthesized catalysts were built in-silico as the corresponding truncated catalyst phosphate (note: backbone dihedral not fixed during conformational searching or optimization to allow for interconversion of the tropaxis).[33] Classification of selective vs. non-selective catalysts was accomplished using a previously disclosed in-house univariate classification algorithm..[34] Statistical modeling was performed using an in-house python modeling script using the forward-stepwise regression algorithm as implemented in the scikit-learn package.

### 7.4.2. Computational Training Set Design Workflow

Our initial goal was to develop a diverse library of catalyst candidates that could serve as a representative selection from the chemical space accessible to the adaptive catalyst scaffold. Incorporating data science from the outset of training set design, it was hypothesized diversity of catalyst structure would provide diversity of reaction output.[35] Since the scaffold was designed with two positions of modularity, different acid and amine fragments could be combined and incorporated into the scaffold via successive amide couplings.

This proved ideal for a combinatorial training set design strategy, and a systematic workflow for training set design was implemented. Exploration of chemical space for the adaptive scaffold began by identifying all commercially available carboxylic acids, sulfonyl chlorides, and secondary amines (pre-processing). The search was limited to compounds available through MilliporeSigma as identified using Reaxys. Fragments bearing chiral centers or functional groups incompatible with the synthetic route (including primary amines, fragments containing multiple secondary amines, carboxylic acids, thiols, azides, boronic acids/esters, etc.) were removed using substructure matching implemented within RDKit.[36] Lastly, the molecular weight of any individual fragment was restricted to 300 g/mol. Note: In preliminary catalyst testing, using unsymmetrical secondary amines as the second coupling partner resulted in unresolved tertiary amide rotamers observed via NMR. Thus, only symmetrical amines were considered when developing accessible chemical space.




## Combinatorial Training Set Design

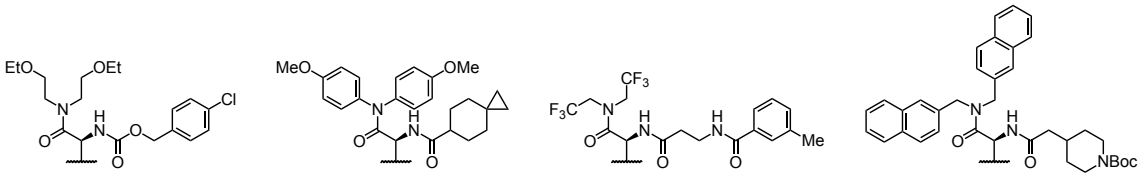
A) Retrosynthetic analysis of the adaptive scaffold shows potential for combinatorial design strategy.

B) Pre-processing) Fragment search performed using Reaxys; library was filtered by route compatibility. Step I) After curation, 2D and 3D QSAR parameters were calculated for each fragment. Clustering (k-means) was employed to reduce acid library to 615 potential fragments. Step II) Catalyst candidates were represented as combinations of fragment parameters. Step III) Each remaining fragment combination was used to build the final candidate library in-silico, providing a selection of 1094 catalysts. Each catalyst was optimized using molecular mechanics and computed at the DFT level (M06-2X/def2-TZVP). Step IV) Full catalyst descriptors were combined with fragment descriptors and subjected to principal component analysis (PCA). A final round of clustering (k=30) was employed to select the final training set.

Ultimately, this pre-processing step resulted in 6,153 fragment possibilities for the acid substituent, and 89 possible symmetrical secondary amines for the tertiary amide position (547,617 possible combinations). At this stage, 2D and 3D QSAR descriptors (Mordred) were calculated for both fragment libraries.[37] However, to mitigate computational cost and avoid a combinatorial explosion, the acid fragment database was curated using k-means clustering.[38] The number of clusters (k) was selected such that 10% of the total possible acid candidates would be retained, resulting in 615 potential fragments (Step I, 54,735 possible combinations). From this truncated

fragment library, further curation was still necessary to enable acquisition of DFT descriptors from the full catalyst scaffold. Representing each candidate as a combination of acid and amine descriptors, two percent of the remaining combinations were selected for further evaluation through k-means clustering, resulting in 1094 structures (Step II). Each candidate was optimized using molecular mechanics and single point energy calculations at the DFT level (M06-2X/def2-TZVP) were performed to enable descriptor acquisition (Step III).[39,40] To define PC space for the final clustering of these candidate structures, 91 descriptors were used (67 from the entire catalyst scaffold, along with 18 and 12 each from acid and amine fragments, respectively).

From this set of 1094 catalysts, a training set of thirty catalysts was selected through cluster analysis. We reasoned k=30 to be an acceptable tradeoff between computational cost and synthetic workload while providing enough data to employ statistical modeling techniques to guide further scaffold optimization. To ensure that synthetically challenging, chemically unstable, or costly catalysts were avoided, one catalyst from each cluster was selected based on chemical intuition. However, several of the clusters were deemed 'synthetically inaccessible' due to route compatibility issues, cost, or synthetic accessibility. Thus, the final synthesized training set was reduced to 20 catalysts (one from 20/30 clusters).



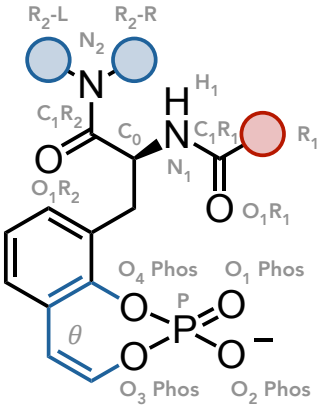

**Representative Inaccessible Cluster Selections**

Several clusters contained catalysts with synthetically inaccessible fragment combinations. Diarylamines and highly electron deficient amines were incompatible as tertiary amide coupling partners (Cluster 04, Cluster 11). Several additional functional groups were manually filtered (e.g. Boc-protecting groups, labile ethers) due to incompatibilities with the MOE deprotection step.

### 7.4.3. Catalyst Parameters

All catalyst parameters calculated are reported in the accompanying spreadsheets. The descriptor set used to develop the initial chemical space of 1094 candidates is also disclosed. Catalyst descriptors were collected using the catalyst model below as a guide. Global catalyst properties calculated include dipole, frontier molecular orbitals (HOMO/LUMO), polarizability, and quadrupole. Partial charges (Hirshfield, CM5, ChelpG), natural atomic orbitals (NBOs), and NMR shifts were calculated for various atoms on each catalyst conformer, with an emphasis on the phosphate and the two positions of modularity. NMR values and NBO charges are known to be useful parameters for describing electronic and steric features.[41] ChelpG partial charges have been demonstrated to be robust and useful descriptors in numerous contexts, including transition state analysis, heterogenous catalysis, and organocatalysis, and are among the most robust partial charge measurements.[42-44] The dihedral of the scaffold is defined below (blue bonds, absolute value

used). Sterimol and buried volumes were computed at various points on the catalyst with an emphasis on the two modular arms and phosphate. DFT conformer energies were used to compute Boltzmann weighted descriptors for each catalyst conformational ensemble. Maximum, minimum, and lowest energy DFT conformer properties were also acquired.




| Parameters Discussed in Manuscript | | |
|---|---|---|
| **ChelpG $O_1R_1$**<br>Boltzmann Average | **Hirshfield Charge $N_1$**<br>Lowest Energy Conformer | **ChelpG $O_2$ Phos**<br>Minimum Value |
| **Backbone Dihedral**<br>Maximum Value | **Buried Volume (5 Å)**<br>Maximum Value | **Hirshfield Charge $H_1$**<br>Lowest Energy Conformer |
| **NBO $O_3$**<br>Boltzmann Average | **NMR $N_2$**<br>Maximum Value | **Reaction Classification**<br>TH = 0, ATR = 1, OX = 2 |

### 7.4.4. Model Development

Experimental $\Delta\Delta G^{\ddagger}$ values were calculated using **Equation S1** where R is the gas constant (in kcal/mol), T is temperature (in Kelvin), and er is the enantiomeric ratio. Statistical modeling was performed using an in-house python script using the forward-stepwise regression algorithm as implemented in the scikit-learn package to obtain predicted $\Delta\Delta G^{\ddagger}$ values. Forward stepwise linear regression was employed for model development and selection; collinear parameters were removed, defined by 0.4 collinear criteria.[45] Normalized parameters were employed using the StandardScaler implemented in scikit-learn such that the coefficients reflect the relative importance of each descriptor.

$$\Delta\Delta G^{\ddagger} = -RT\ln(er) \qquad \textbf{(Equation S1)}$$

### 7.4.5. Model Validation: Transfer Hydrogenation of 8-aminoquinoline 1

The transfer hydrogenation model was validated using external validation techniques. Due to the small dataset of selective catalysts (11), all catalysts were used to train the initial model. Thus, external validation was necessary and provided an opportunity to extrapolate to a better performing catalyst. Three sulfonamide catalysts were selected as validation catalysts by revisiting the initial chemical space of 1094 candidates. Predicted $\Delta\Delta G^{\ddagger}$ values were computed for each validation catalyst revealing two interpolations and a predicted extrapolation. After screening the validation catalysts in the transfer hydrogenation, three metrics were used to evaluate the statistical model: mean average error (MAE) of the validation set predictions, Test $R^2$, and the relative orderings of each prediction. Analyzing these metrics, the Test $R^2 = 0.98$ (close to 1.00) which indicates a good fit with the initial regression line. The test MAE was found to be 0.08 kcal/mol, and all predictions were within 0.15 kcal/mol of the experimental selectivity values. Finally, the relative order of each prediction was accurate. Taken together, these evaluation metrics provide evidence that the initial model is robust and not overfit to the initial training data.

### 7.4.6. Model Validation: Global Three-Reaction Statistical Model

The three-reaction statistical model including the transfer hydrogenation, atroposelective cyclodehydration, and oxetane desymmetrization was generated using the same forward-stepwise modeling approach. After global classification, 11 catalysts were predicted to be active for each transformation (33 total data points). Opting to cross-validate this model, the data set was partitioned into a training set (TS) and validation set (VS) with a 70:30 split (TS:VS) using the random function implemented in scikit-learn. After using a simple classifier term to differentiate reactions (0,1,2), a three-parameter model with good statistics was revealed (Test $R^2 = 0.83$, Train MAE = 0.16 kcal/mol, Train k-fold = 0.74). To evaluate this model, we then analyzed the validation set metrics. Satisfactorily, the validation set was predicted with a high degree of accuracy (Test $R^2 = 0.87$, Test MAE = 0.14 kcal/mol). This analysis demonstrates the global model is indeed competent at predictions across all three reactions

## 7.5. Supplemental Figures

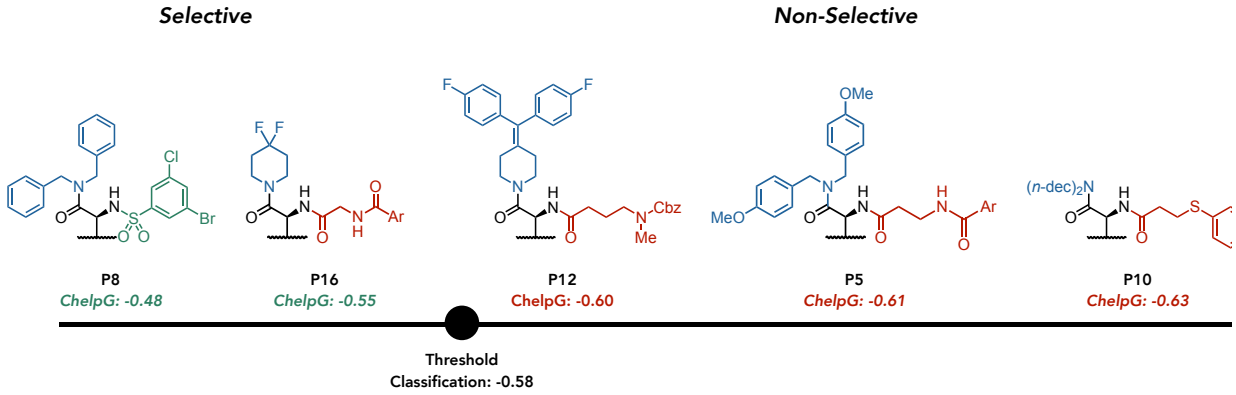



Figure S 2 : Trends for classification of selective vs non-selective catalysts

Univariate classification of training set performance in the transfer hydrogenation reaction produced no misclassifications (ChelpG $O_{R1}$). Sulfonamide catalysts calculated as an average partial charge across both oxygens. Alkyl-bearing fragments at the secondary amide position led to non-selective catalysts (**P10**). Analysis of charges for distal H-bonding catalysts also led to correct classification (**P12**, **P5**). Interestingly, **P16** bears a distal H-bonding site but is correctly classified as selective. Due to distal H-bonding with the phosphate, **P5** and **P12** do not display conformations that adopt the observed N—H/P=O hydrogen bonding network present in other amide catalysts.

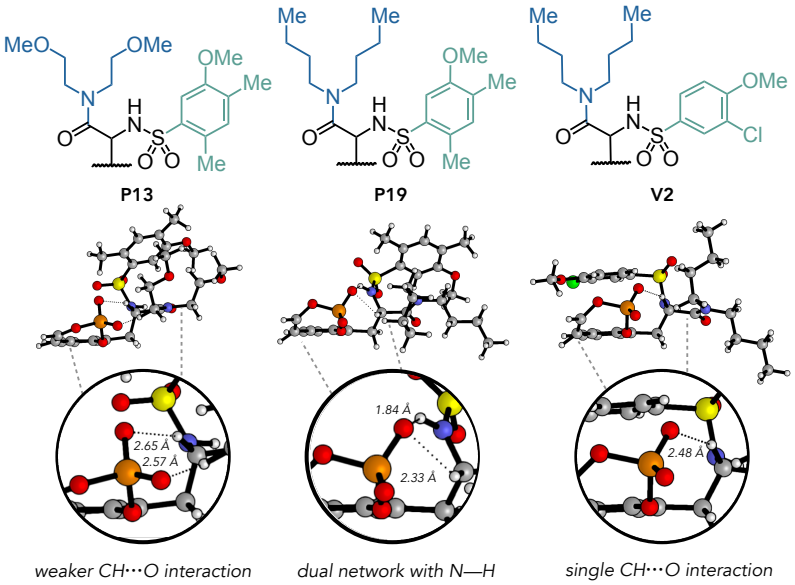



Figure S 3 : Title Hydrogen bonding network observed in sulfonamide catalysts P13, P19, and V2.

Visualization of the three observed H-bonding networks within the sulfonamide subclass of catalysts. Catalysts **P13** and **V2** discussed in text. Catalyst **P19** bears unique dual H-bonding network both (CH—O and NH—O), resulting in a lower overall CH—O interaction length. All three networks provide an opportunity for the relay of chiral information to the phosphate and, in turn, substrate. All seven sulfonamide catalysts tested preferentially adopt conformations bearing one of the three H-bonding networks classified above.

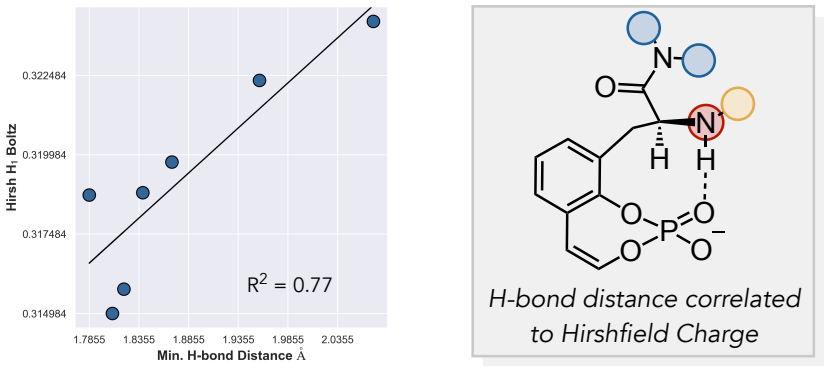



Figure S 4 : Title of Univariate N—H bond length vs selectivity for amide catalysts

Correlation between Hirshfield charge ($N_1$) and H-bond distance (Å) across the seven tested selective amide catalysts (post-classification). Strong univariate trend provides evidence the Hirshfield charge on $N_1$ impacts the nature of the intramolecular H-bonding network between the N—H and P=O (and strength of the H-bonding interaction). This trend suggests amide catalysts bearing a shorter H-bond between the N—H and P=O are more selective. The more positive the Hirsh $N_1$ becomes, the less selective the catalyst. This correlation could provide an avenue for tuning the amide catalysts through changing the nature of the substitution at the secondary amide position to achieve more effective chirality transfer to substrate through lowering the Hirsh $N_1$ charge and reinforcing the H-bonding network.

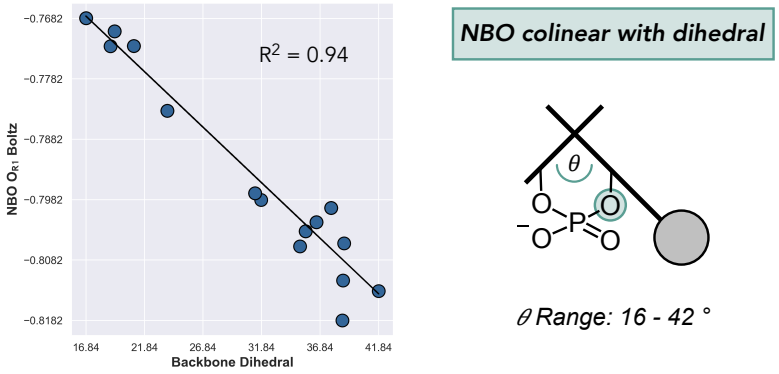



Figure S 5 : Univariate NBO O(P3) vs dihedral angle of the chiral pocket

Correlation between the NBO $O_3$ (global MLR model) and the catalyst backbone dihedral (width of the chiral pocket). Classification of non-selective catalysts using ChelpG $O_1$ performed prior to producing correlation. NBO charge at the $O_3$ position is heavily influenced by the dihedral angle of the chiral pocket. As the dihedral angle of the pocket increases, more torsion is placed on the upper internal oxygen, resulting in a more negative NBO charge. Due to the high coefficient weighting of the NBO $O_3$ term in the global MLR model, this suggests catalysts with wider chiral pockets provide more selective catalysts.

## 8. References


1. Armarego, W.L.F., and Perrin, D.D. (1997). Purification of laboratory chemicals, Fourth Edition (Butterworth-Heinemann).
2. Pangborn, A.B., Giardello, M.A., Grubbs, R.H., Rosen, R.K., and Timmers, F.J. (1996). Safe and Convenient Procedure for Solvent Purification. Organometallics *15*, 1518–1520.
3. Still, W.C., Kahn, M., and Mitra, A. (1978). Rapid chromatographic technique for preparative separations with moderate resolution. Journal of Organic Chemistry *43*, 2923–2925.
4. Li, J., Grosslight, S., Miller, S.J., Sigman, M.S., and Toste, F.D. (2019). Site-Selective Acylation of Natural Products with BINOL-Derived Phosphoric Acids. ACS Catal. *9*, 9794–9799. 10.1021/acscatal.9b03535.
5. Han, J.H., Kwon, Y.E., Sohn, J.-H., and Ryu, D.H. (2010). A facile method for the rapid and selective deprotection of methoxymethyl (MOM) ethers. Tetrahedron *66*, 1673–1677.
6. Oberboersch, S., Schunk, S., Reich, M., Hees, S., Ruth, J., Engels, M., Kless, A., Christoph, T., Schiene, K., Germann, T., and Bijsterveld, E. (2008) Substituted Sulfonamide Derivatives.
7. Basu, S., Barawkar, D.A., Thorat, S., Shejul, Y.D., Patel, M., Naykodi, M., Jain, V., Salve, Y., Prasad, V., Chaudhary, S., et al. (2017). Design, Synthesis of Novel, Potent, Selective, Orally Bioavailable Adenosine A2A Receptor Antagonists and Their Biological Evaluation. J Med Chem *60*, 681-694. 10.1021/acs.jmedchem.6b01584.
8. Liu, Y., Sun, G., David, A., and Sayre, L.M. (2004). Model Studies on the Metal-Catalyzed Protein Oxidation: Structure of a Possible His-Lys Cross-Link. Chem. Res. Toxicol. *17*, 110–118. 10.1021/acs.jmedchem.6b01584.
9. Aissaoui, H., Boss, C., Koberstein, R., Sifferlen, T., and Trachsel, D. (2009) 2-aza-bicyclo[2.2.1]heptane derivatives.
10. Ochiai, K., Kuppusamy, S., Yasui, Y., Okano, T., Matsumoto, Y., Gupta, N.R., Takahashi, Y., Kubota, T., Kobayashi, J., and Hayashi, Y. (2016). Total Synthesis of the 7,10-Epimer of the Proposed Structure of Amphidinolide N, Part I: Synthesis of the C1–C13 Subunit. Chem. Eur. J. *22*, 3282–3286. 10.1002/chem.201504674.
11. Gopalan, B., Ponpandian, T., Kachhadia, V., Bharathimohan, K., Vignesh, R., Sivasudar, V., Narayanan, S., Mandar, B., Praveen, R., Saranya, N., et al. (2013). Discovery of adamantane based highly potent HDAC inhibitors. Bioorg. Med. Chem. Lett. *23*, 2532–2537. 10.1016/j.bmcl.2013.03.002.
12. Zhang, X., Hufnagel, H.R., Hou, C., Johnson, D.L., Sui, Z., Fegely, B., and Breslin, D. (2010) 4-Azetidinyl-1-heteroaryl-cyclohexanol antagonist of CCR2. United States.
13. Thorarensen, A., Ruble, C., Fischer, J.F., Romero, D.L., Beauchamp, T.J., and Northuis, J.M. (2004) Antibacterial benzoic acid derivatives.
14. Kumar, R., Gleißner, E.H., Tiu, E.G.V., and Yamakoshi, Y. (2016). C70 as a Photocatalyst for Oxidation of Secondary Benzylamines to Imines. Org. Lett. *18*, 184–187. 10.1021/acs.orglett.5b03194.
15. Bell, C., Benz, J., Gobbi, L., Grether, U., Groebke Zbinden, K., Hansen, D.J., Hornsperger, B., Kocer, B., Kroll, C., Kuhn, B., et al. (2019) Oxazine monocylglycerol lipase (MAGL) inhibitors.
16. Wang, X., and List, B. (2008). Asymmetric Counteranion-Directed Catalysis for the Epoxidation of Enals. Angew Chem Int Ed Engl *47*, 1119–1122. 10.1002/anie.200704185.

17. Aissaoui, H., Boss, C., Gude, M., Koberstein, R., and Sifferlein, T. (2007) Azetidine compounds as orexin receptor antagonists. United States patent application 12/377.349, 9/2/10.
18. Choudhury, R., and Ramamurthy, V. (2017). Understanding the complexation of aliphatic and aromatic acids guests with octa acid. J. Phys. Org. Chem. *31*. 10.1002/poc.3795.
19. Li, F., Ma, C., DeGrado, W.F., and Wang, J. (2016). Discovery of Highly Potent Inhibitors Targeting the Predominant Drug-Resistant S31N Mutant of the Influenza A Virus M2 Proton Channel. J. Med. Chem. *59*, 1207–1216. 10.1021/acs.jmedchem.5b01910.
20. Shugrue, C.R., and Miller, S.J. (2015). Phosphothreonine as a Catalytic Residue in Peptide-Mediated Asymmetric Transfer Hydrogenations of 8-Aminoquinolines. Angew Chem Int Ed Engl *54*, 11173–11176. 10.1002/anie.201505898.
21. Kwon, A., Chinn, A.J., Byoungmoo, K., and Miller, S.J. (2018). Divergent Control of Point and Axial Stereogenicity: Catalytic Enantioselective C−N Bond-Forming Cross-Coupling and Catalyst-Controlled Atroposelective Cyclodehydration. Angew Chem Int Ed Engl *57*, 6251–6255. 10.1002/anie.201802963.
22. Kwon, A., Li, J., Reid, J.P., Crawford, J.M., Jacob, R., Sigman, M.S., Toste, F.D., and Miller, S.J. (2019). Disparate Catalytic Scaffolds for Atroposelective Cyclodehydration. Journal of the American Chemical Society *141*, 6698–6705. 10.1021/jacs.9b01911.
23. Yang, W., and Sun, J. (2015). Organocatalytic Enantioselective Synthesis of 1,4-Dioxanes and Other Oxa-Heterocycles by Oxetane Desymmetrization. Angew Chem Int Ed Engl *55*, 1868–1871. 10.1002/anie.201509888.
24. Roos, K., Wu, C., Damm, W., Reboul, M., Stevenson, J.M., Lu, C., Dahlgren, M.K., Mondal, S., Chen, W., Wang, L., and al, e. (2019). OPLS3e: Extending Force Field Coverage for Drug-Like Small Molecules. J. Chem. Theory Comput. *15*, 1863–1874. 10.1021/acs.jctc.8b01026.
25. MacroModel (2022). (Schrödinger, LLC).
26. Schrödiner Release 2022-1. MacroModel, Schrödinger, LLC, New York, NY, 2022.
27. Kelley, L.A., Gardner, S.P., and Sutcliffe, M.J. (1996). An automated approach for clustering an ensemble of NMR-derived protein structures into conformationally related subfamilies. Protein Eng. *9*, 1063–1065.
28. 11. Gaussian 16, Revision C.01, Frisch, M. J.; Trucks, G. W.; Schlegel, H. B.; Scuseria, G. E.; Robb, M. A.; Cheeseman, J. R.; Scalmani, G.; Barone, V.; Petersson, G. A.; Nakatsuji, H.; Li, X.; Caricato, M.; Marenich, A. V.; Bloino, J.; Janesko, B. G.; Gomperts, R.; Mennucci, B.; Hratchian, H. P.; Ortiz, J. V.; Izmaylov, A. F.; Sonnenberg, J. L.; Williams-Young, D.; Ding, F.; Lipparini, F.; Egidi, F.; Goings, J.; Peng, B.; Petrone, A.; Henderson, T.; Ranasinghe, D.; Zakrzewski, V. G.; Gao, J.; Rega, N.; Zheng, G.; Liang, W.; Hada, M.; Ehara, M.; Toyota, K.; Fukuda, R.; Hasegawa, J.; Ishida, M.; Nakajima, T.; Honda, Y.; Kitao, O.; Nakai, H.; Vreven, T.; Throssell, K.; Montgomery, J. A., Jr.; Peralta, J. E.; Ogliaro, F.; Bearpark, M. J.; Heyd, J. J.; Brothers, E. N.; Kudin, K. N.; Staroverov, V. N.; Keith, T. A.; Kobayashi, R.; Normand, J.; Raghavachari, K.; Rendell, A. P.; Burant, J. C.; Iyengar, S. S.; Tomasi, J.; Cossi, M.; Millam, J. M.; Klene, M.; Adamo, C.; Cammi, R.; Ochterski, J. W.; Martin, R. L.; Morokuma, K.; Farkas, O.; Foresman, J. B.; Fox, D. J. Gaussian, Inc., Wallingford CT, 2016.

29. Goerigk, L., Hansen, A., Bauer, C., Ehrlich, S., Najibi, A., and Grimme, S. (2017). A look at the density functional theory zoo with the advanced GMTKN55 database for general main group thermochemistry, kinetics and noncovalent interactions. Phys. Chem. Chem. Phys. *19*, 32184–32215. 10.1039/c7cp04913g.
30. Glendening, E.D., Reed, A.E., Carpenter, J.E., and Weinhold, F. (2003). NBO Version 3.1. (Gaussian Inc.).
31. Breneman, C.M., and Wiberg, K.B. (1990). Determining Atom-Centered Monopoles from Molecular Electrostatic Potentials. The Need for High Sampling Density in Formamide Conformational Analysis. J. Comput. Chem. *11*, 361–373. 10.1002/jcc.540110311.
32. Cheeseman, J.R., Trucks, G.W., Keith, T.A., and Frisch, M.J. (1996). A comparison of models for calculating nuclear magnetic resonance shielding tensors. J. Chem. Phys. *104*, 5497–5509. 10.1063/1.471789.
33. Luchini, G., Alegre-Requena, J.V., Funes-Ardoiz, I., and Paton, R.S. (2020). GoodVibes: automated thermochemistry for heterogeneous computational chemistry data. F1000Research. 10.12688/f1000research.22758.1.
34. Luchini, G., Patterson, T., and Paton, R.S. (2022). DBSTEP: DFT Based Steric Parameters. 10.5281/zondu.4702097.
35. Nakamura, T., Sakaue, S., Fujii, K., Harabuchi, Y., Maeda, S., and Iwata, S. (2022). Selecting molecules with diverse structures and properties by maximizing submodular functions of descriptors learned with graph neural networks. . Sci. Rep. *12*, 1124. 10.1038/s41598-022-04967-9.
36. RDKit: Open-source cheminformatics (https://www.rdkit.org).
37. Moriwaki, H., Tian, Y.S., Kawashita, N., and Takagi, T. (2018). Mordred: a molecular descriptor calculator. J. Cheminform *10*, 4. 10.1186/s13321-018-0258-y.
38. Lloyd, S.P. (1982). Least Squares Quantization in PCM. IEEE Trans. Inf. Theory *28*, 129–137. 10.1109/TIT.1982.1056489.
39. Zhao, Y., and Truhlar, D.G. (2007). The M06 suite of density functionals for main group thermochemistry, thermochemical kinetics, noncovalent interactions, excited states, and transition elements: two new functionals and systematic testing of four M06-class functionals and 12 other functionals. Theor. Chem. Acc. *120*, 215–241. 10.1007/s00214-007-0310-x.
40. Weigend, F., and Ahlrichs, R. (2005). Balanced basis sets of split valence, triple zeta valence and quadruple zeta valence quality for H to Rn: Design and assessment of accuracy. Phys. Chem. Chem. Phys. *7*, 3297–3305. 10.1039/b508541a.
41. Yamamoto, E., Hilton, M.J., Orlandi, M., Saini, V., Toste, F.D., and Sigman, M.S. (2016). Development and Analysis of a Pd(0)-Catalyzed Enantioselective 1,1-Diarylation of Acrylates Enabled by Chiral Anion Phase Transfer. J. Am. Chem. Soc. *138*, 15877–15880. 10.1021/jacs.6b11367.
42. Newman-Stonebraker, S.H., Smith, S.R., Borowski, J.E., Peters, E., Gensch, T., Johnson, H.C., Sigman, M.S., and Doyle, A.G. (2021). Univariate classification of phoshine ligation state and reactivity in cross-coupling catalysis. Science *374*, 301–308.
43. Santiago, C.B., Guo, J.Y., and Sigman, M.S. (2018). Predictive and mechanistic multivariate linear regression models for reaction development. Chem. Sci. *9*, 2398–2412. 10.1039/c7sc04679k.

44. Bahmanyar, S., and Houk, K.N. (2001). The origin of stereoselectivity in proline-catalyzed intramolecular aldol reactions. J. Am. Chem. Soc. *123*, 12911–12912.
45. Meng, Q., Huang, Y., Deng, D., Yang, Y., Sha, H., Zou, X., Faller, R., Yuan, Y., and Zhu, G. (2020). Porous Aromatic Framework Nanosheets Anchored with Lewis Pairs for Efficient and Recyclable Heterogeneous Catalysis. Adv. Sci. *7*, 2000067. 10.1002/advs.202000067.

# Chapter 3

## Aiming for regioselectivity in the synthesis of N-Methyl Pyrazoles

The work presented hereafter was performed collaboratively between the Toste group at UC Berkeley and the Process Chemistry group at Genentech, Inc.

**UC Berkeley** – René Rahimoff, Vlad Roytman, F. Dean Toste.

**Genentech, Inc** – Derek Dalton, [rest of Genentech team here]

# I. Introduction

## 1.1. The importance of N-containing heterocycles

Nitrogen-containing heterocyclic compounds are abundant in nature and biological systems, and have been critical structures in medicinal chemistry due to their bioactivity. As of 2020, it was estimated that over 75% of FDA-approved drug compounds contained one or more nitrogen-containing heterocyclic motif.[1] The particular interest in medicinal chemistry for these moieties is well-founded, as a vast number of compounds have proved potent in a wide range of pharmacological applications ranging from anti-cancer drugs, anti-malarial and anti-microbial treatments, and diabetes drugs.[2,3]

The electron-rich character of nitrogen often gives these moieties the ability to act as bases and partake in a variety of non-covalent interactions such as hydrogen bonding with desired biological targets, thereby improving compounds' solubility, bioavailability, and binding with the target.[4] Five-membered heterocycles in particular are well-known bioactive motifs, but can often represent a synthetic challenge, thereby limiting their incorporation in drug candidates. Within the nomenclature of five-membered, nitrogen-containing heterocycles (Figure 1), pyrazoles have shown much promise as medicinal chemistry fragments[5-8] as well as for applications in the agrochemical industry[9] and novel materials.[10-12] However, significant challenges in the selective synthesis of substituted pyrazole, both at nitrogen and carbon, are still prohibitive for their widespread inclusion in candidate screenings.

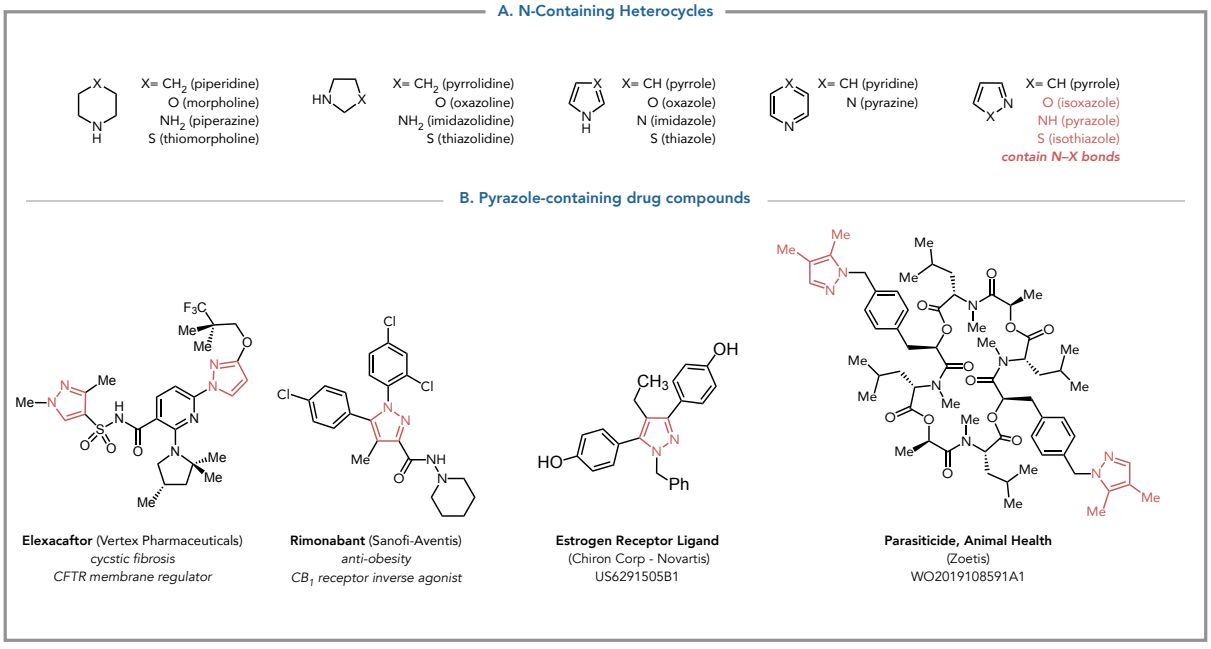



Figure 1: A) Types of N-containing heterocycles. B) Examples of pyrazole-based drug compounds.

## 1.2. Pyrazoles: an important yet synthetically challenging motif

The first synthesis of substituted pyrazoles was reported by Knorr in 1883, wherein he described the cyclocondensation of primary hydrazines and 1,3-dicarnonyl compounds under acidic conditions (Figure 2).[13] The Knorr mechanism is proposed to begin with the protonation of dicarbonyl compound **1** followed by the nucleophilic addition of the substituted hydrazine **2**. Dehydration and collapse of the tetrahedral intermediate (**7**) provides an intermediate hydrazone (**8**). The latter undergoes a second, intramolecular nucleophilic addition-dehydration sequence to yield cyclic intermediate (**11**), which is rapidly deprotonated, providing aromatized pyrazole products (**3, 4**).[14] Although this approach is the best-established route and starts with readily available starting materials, in the case of asymmetric 1,3-dicarbonyl substrates, regioselectivity challenges arise from the determination of which of the two carbonyl carbons will be added into first. Additional complications can occur when the two nitrogens on the substituted hydrazine partner have similar nucleophilicities.[15,16]

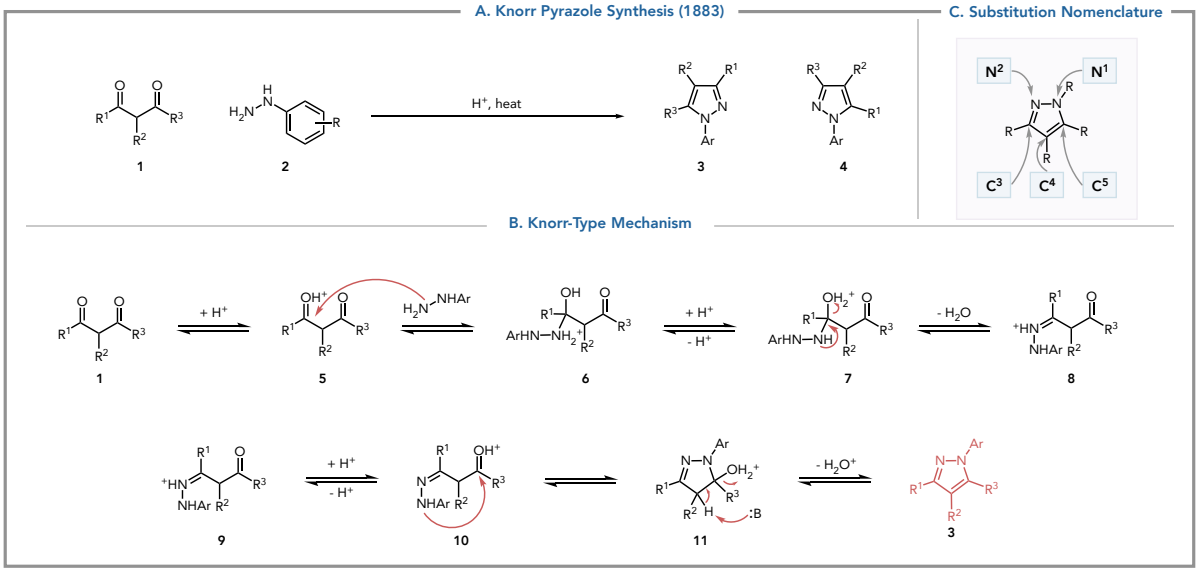



Figure 2: A) Knorr synthesis of pyrazole (1883). B) Proposed Knorr-type mechanism. C) Nomenclature of pyrazole substitution.

A multitude of variations on the original Knorr synthesis have been developed in an effort to achieve more efficient and selective syntheses of substituted pyrazoles.[15,17,18] Most of these methods still rely on condensation reactions with primary hydrazines, but the selection of possible partner starting materials has been expanded considerably to include various α,β-unsaturated carbonyl compounds,[19-22] acetylenic ketones,[23,24], and aldehydes (Figure 3).[25]

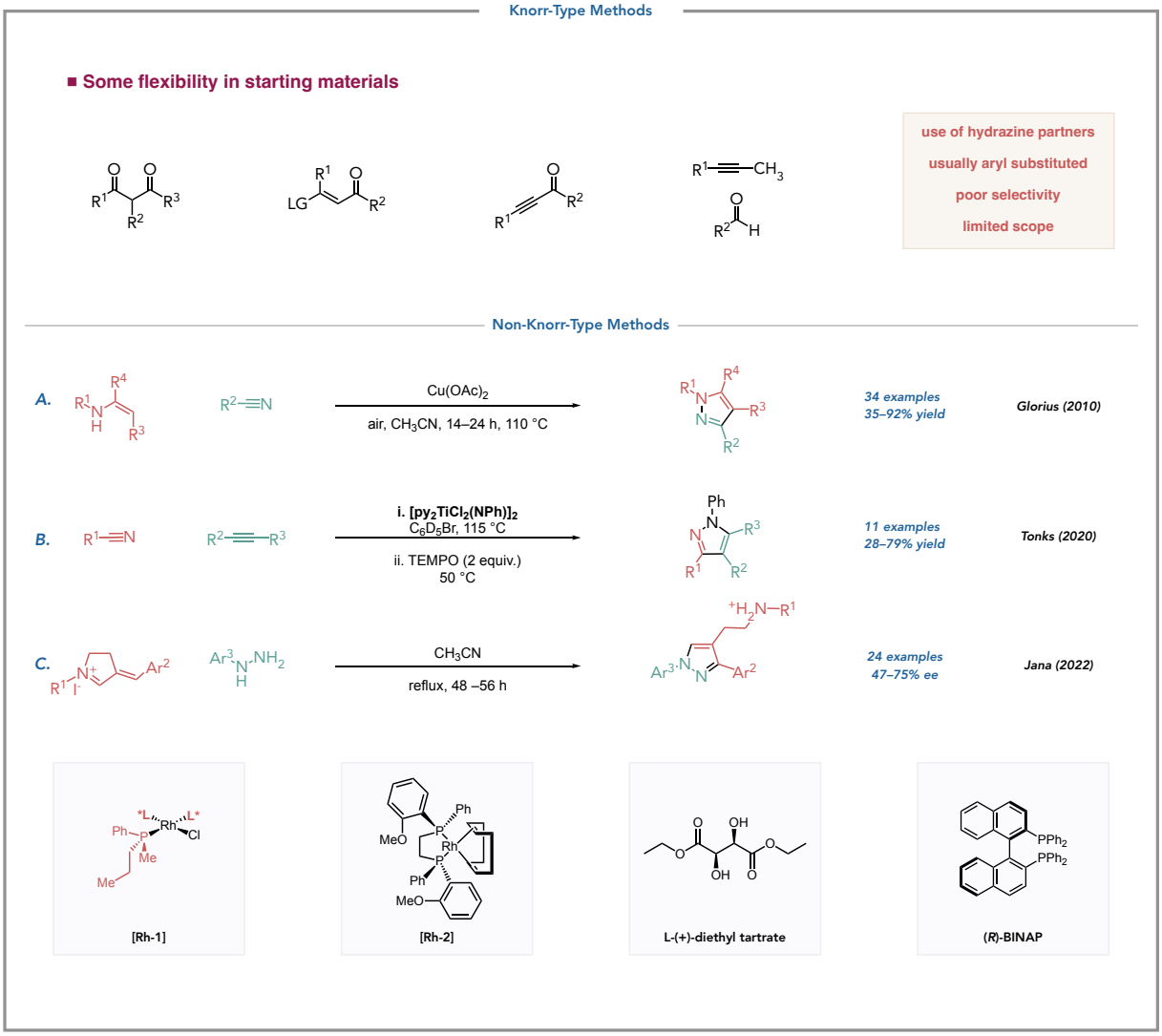



Figure 3: Examples of recent synthetic methods for substituted pyrazoles.

Despite the risks associated with the use of hydrazine reagents, few synthetic methods have been established to synthesize pyrazoles from direct N–N bond formation due to the unfavorable thermodynamics of such reactions stemming from the low N–N bond dissociation energy (estimated around 24 kcal/mol).[26] Some elegant examples using transition metals have emerged in recent years using copper,[27-30] nickel[31] or titanium complexes,[32] with the caveat that these reactions usually require stoichiometric transition metal or oxidant to proceed. Creative methods have emerged to enable the synthesis of selected substituted pyrazole compounds with good selectivity, but often lack generality or suffer from long protection/deprotection sequences or the poor availability of the designed starting materials that they rely on (Figure 3).[33]

Small alkyl nitrogen substituents represent a particular challenge in that regard, and selectivity remains elusive in the synthesis of these important biologically relevant motifs. Optimization of synthetic routes, especially during the process development of pharmaceutical compounds, can rapidly become a costly endeavor, both with regards to chemical resources and time invested by the researchers.

## II. Project Design

The research project described herein was initiated out of previous studies using Brønsted acid catalysts to induce selectivity in a variety of organic transformations. Recognizing the challenges presented by the synthesis of N-methyl pyrazoles, we sought to determine whether non-covalent interactions available to Brønsted acid catalysts might enable the regioselective cyclization of these biologically relevant moieties. In particular, the minimal steric and lack of significant electronic factors on a cyclization partner such as methylhydrazine raised the question of how to design a catalyst that might efficiently direct the cyclization without reliance on substrate-specific interactions. In the context of improving the efficiency of synthetic processes, understanding the selectivity patterns would, hopefully, provide the insight necessary to establish sets of conditions to effortlessly switch the selectivity for one or the other isomer at will from the same substrates.

These objectives presented an opportunity for the application of statistical methods such as Bayesian optimization. Indeed, the subtlety and cooperativity of the interactions at play in these transformations could convolute the analysis and present a challenge for traditional, experimental-only optimization methods to highlight the most important selectivity-determining factors. Relying on computational methods to guide the optimization process could provide an opportunity to optimize both selective transformations at once to provide tailored conditions for each desired isomeric product.

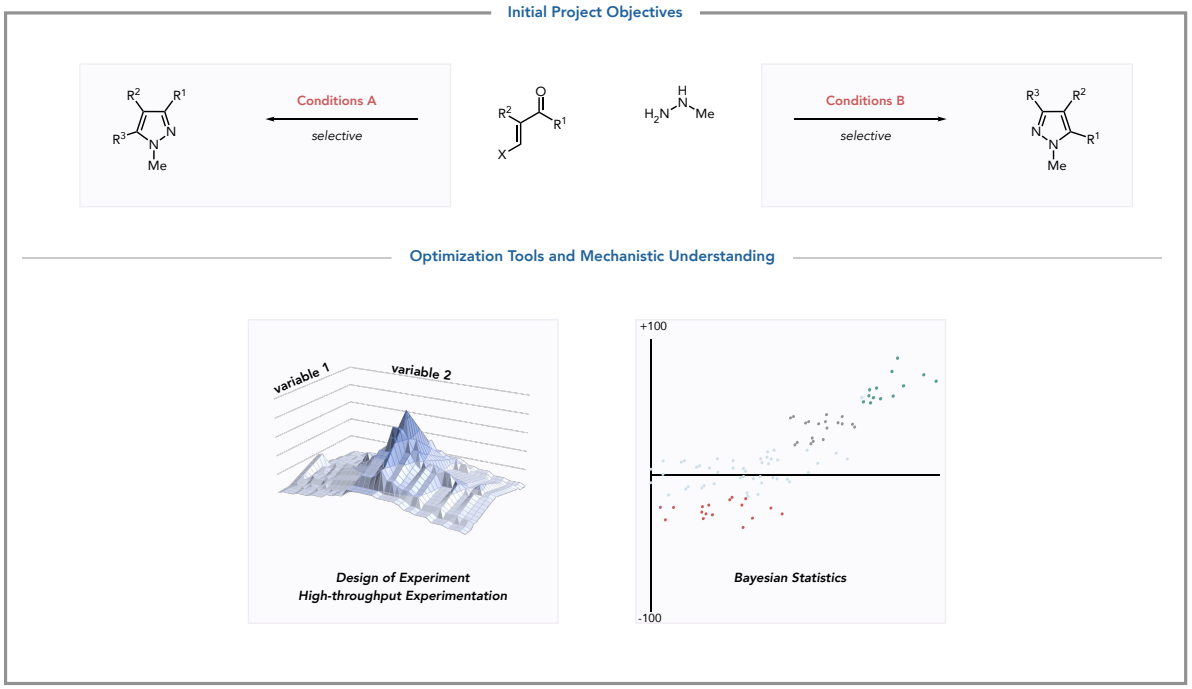
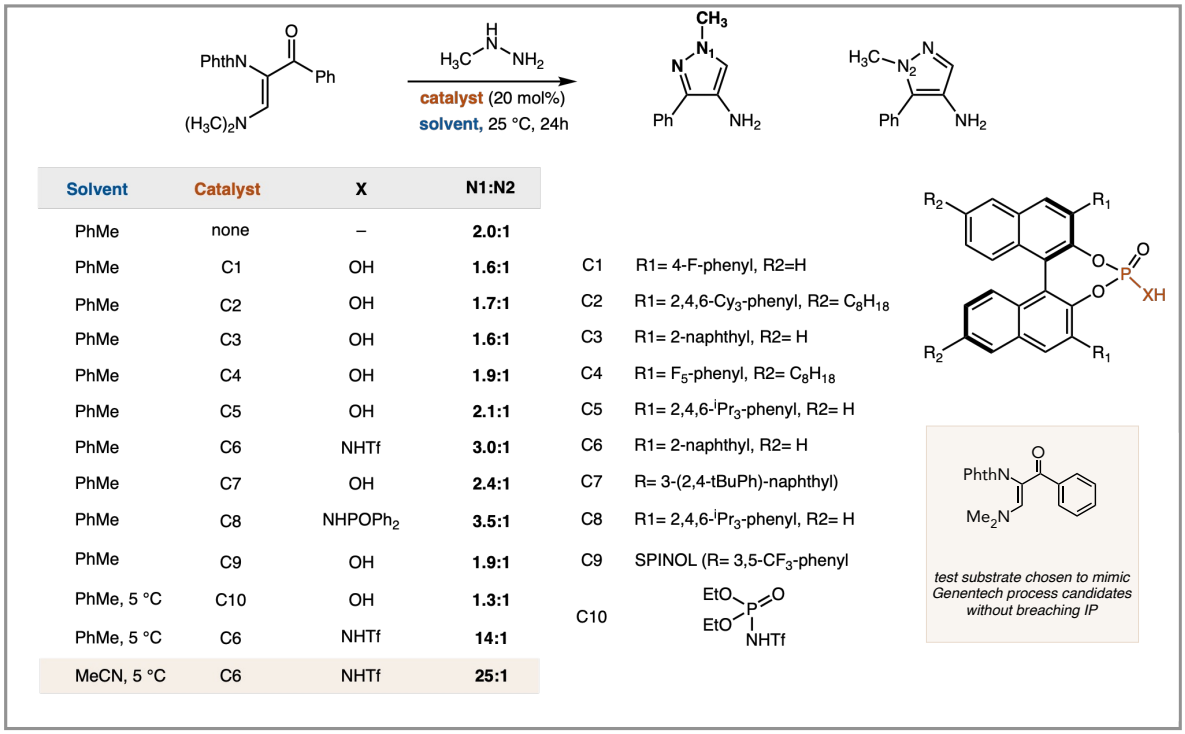



Figure 4: Initial objectives for the project.

## III. Results and Discussion

### 3.1. Initial Screening of Brønsted Acid Catalysts




| Solvent | Catalyst | X | N1:N2 |
|---|---|---|---|
| PhMe | none | – | **2.0:1** |
| PhMe | C1 | OH | **1.6:1** |
| PhMe | C2 | OH | **1.7:1** |
| PhMe | C3 | OH | **1.6:1** |
| PhMe | C4 | OH | **1.9:1** |
| PhMe | C5 | OH | **2.1:1** |
| PhMe | C6 | NHTf | **3.0:1** |
| PhMe | C7 | OH | **2.4:1** |
| PhMe | C8 | $NHPOPh_2$ | **3.5:1** |
| PhMe | C9 | OH | **1.9:1** |
| PhMe, 5 °C | C10 | OH | **1.3:1** |
| PhMe, 5 °C | C6 | NHTf | **14:1** |
| MeCN, 5 °C | C6 | NHTf | **25:1** |

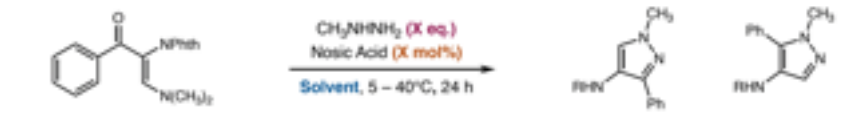
| | |
|---|---|
| C1 | R1= 4-F-phenyl, R2=H |
| C2 | R1= 2,4,6-$Cy_3$-phenyl, R2= $C_8H_{18}$ |
| C3 | R1= 2-naphthyl, R2= H |
| C4 | R1= $F_5$-phenyl, R2= $C_8H_{18}$ |
| C5 | R1= 2,4,6-$^iPr_3$-phenyl, R2= H |
| C6 | R1= 2-naphthyl, R2= H |
| C7 | R= 3-(2,4-tBuPh)-naphthyl) |
| C8 | R1= 2,4,6-$^iPr_3$-phenyl, R2= H |
| C9 | SPINOL (R= 3,5-$CF_3$-phenyl |
| C10 | EtO, EtO, P, O, NHTf |

Figure 5: Initial set of Brønsted acid catalysts.

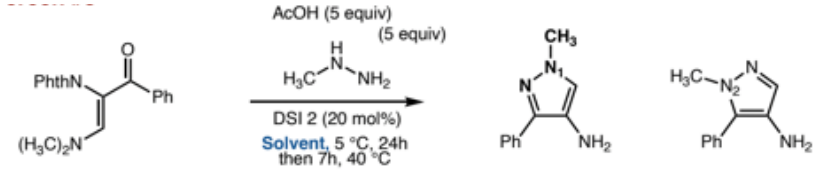
Our initial search for regioselective conditions begun with screening a set of Brønsted acid catalysts in the hope that these privileged structures would provide a starting point for optimization. The initial substrate, (*Z*)-2-(1-(dimethylamino)-3-oxo-3-phenylprop-1-en-2-yl)isoindoline-1,3-dione, was chosen to bear similar features as current candidates in the Genentech process pipeline candidates without significantly overlapping with proprietary structures. The choice of nitrogen protecting group was guided by the ease of synthesizing these starting materials relative to the boc- or tosyl analogues, which had previously been reported in the literature.

The first screening attempts (Figure 5) provided mitigated results but revealed some key information regarding the transformation and potential analytical challenges. Traditional phosphoric acid catalysts failed to provide adequate selectivity for either isomer. Although good selectivities were observed with N-triflyl phosphoramides (NTP) and di-sulfonamide catalysts**,** none of the catalysts provided good conversion to the desired products. Further analysis of the NTP revealed that they suffered considerable hydrolysis to the corresponding phosphoric acids, which could explain their stifled performance. Additionally, the analysis was further complicated by the partial deprotection of the phthaloyl nitrogen under the reaction, which provided a mixture of protected and unprotected cyclization products for which the ratios was independent of observed selectivity. The possibility that the cyclized products might not be deprotected at the

same rates, along with the potential for each intermediate to be deprotected prior to the cyclization and aromatization steps made the analysis of regioselectivity ambiguous.



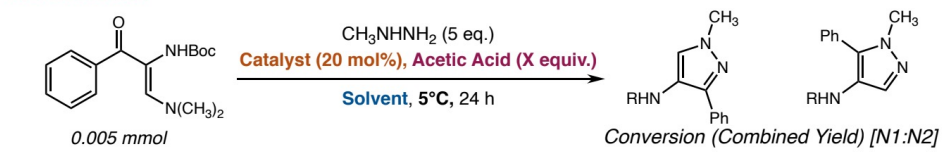

| Nosic Acid | Solvent | $MeNHNH_2$ | RSM (3ppm) | 4.03ppm | 3.93ppm | 3.84ppm | 3.65ppm |
|---|---|---|---|---|---|---|---|
| 20 mol% | MeCN | 1 eq | 84% | 14% | 1% | 2% | 2% |
| 20 mol% | MeCN | 2 eq | 70% | 22% | 2% | 1% | 7% |
| 1 eq. | MeCN | 1 eq | 61% | 0% | 19% | 3% | 15% |
| 1 eq. | MeCN | 2 eq | 70% | 15% | trace | 10% | 3% |
| 20 mol% | Toluene | 1 eq | 93% | 3% | trace | trace | 2% |
| 20 mol% | Toluene | 2 eq | 79% | 14% | trace | 3% | 7% |
| 1 eq. | Toluene | 1 eq | 96% | 1% | trace | trace | trace |
| 1 eq. | Toluene | 2 eq | 85% | 5% | trace | 4% | 5% |
| 20 mol% | MeCN | 5 eq | 60% | 18% | 2% | 2% | 10% |
| 20 mol% | MeCN | 5 eq, 5 eq AcOH | 58% | 16% | 1% | 11% | 10% |
| None | MeCN | 5 eqn 5 eq AcOH | 57% | 13% | trace | 5% | 7% |

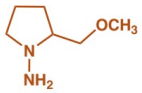



| Solvent | SM | 3.84ppm | 3.65ppm | 3.84/3.65 | 7.05/8.4 |
|---|---|---|---|---|---|
| Benzene | 15% | 26% | 36% | 1:1.4 | 1:1.4 |
| DME | 0% | 31% | 51% | 1:1.63 | 1:1.4 |
| ACN | 7% | 27% | 58% | 1:2.15 | 1:1.6 |
| DMF | 34% | 24% | 62% | 1:2.55 | 1:2.7 |
| THF | 2% | 39% | 65% | 1:1.68 | 1:1.3 |
| Tol | 0% | 33% | 52% | 1.58 | 1:1.44 |
| Dioxane | 0% | 32% | 64% | 1:1.97 | 1:1.50 |
| Et2O | 0% | 28% | 59% | 1:2.14 | 1:1.7 |
| DCE | 27% | 15% | 30% | 1:2.0 | 1:2.0 |
| DCM | 0% | 28% | 40% | 1:1.4 | 1:1.3 |

Figure 6: Some representative screening data from extensive experimentation for the cyclization of the phthalimide-protected model substrate.

Converting the protecting group to tosyl was unsuccessful, providing only low conversions and mediocre selectivity. More satisfying conversions were obtained using the boc-protected analogues (up to 94% yield of cyclized products), although the range of selectivity observed was still poor (up to 4.6:1). However, these mitigated results were still contradictory with the initial goal of finding a straightforward and rapid model system to probe the selectivity trends for the cyclization reaction.

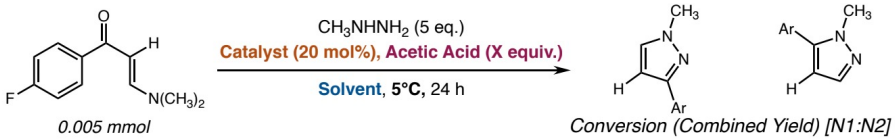


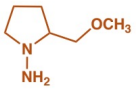

| | No catalyst |  | DSI2 | Acetic Acid equivalents |
|---|---|---|---|---|
| $CH_2Cl_2$ | 2% (trace) [ND] | 33% (2%) [ND] | 66% (36%) [1 : 1.6] | 0 |
| | 84% (82%) [1 : 1.5] | 92% (89%) [1 : 1.5] | 87% (62%) [1 : 2] | 2.5 |
| | 97% (95%) [1 : 2] | 99% (98%) [1 : 1.8] | 62% (53%) [1 : 2] | 5 |
| THF | 34% (8%) (2 : 1] | 30% (3%) [ND] | 60% (9%) [1.1 :2] | 0 |
| | 30% (29%) [1.3 : 1] | 62% (52%) [1 : 1.2] | 80% (79%) [1 : 1.5] | 2.5 |
| | 78% (73%) [1 : 1.9] | 85% (72%) [1 : 1.3] | 83% (86%) [1 : 1.7] | 5 |
| MeCN | 50% (11%) [2 : 1] | 47% (10%) [2 : 1] | 63% (23%) [1.1 : 1] | 0 |
| | 81% (77%) [1: 1.3] | 93% (83%) [1 : 1.3] | 78% (87%) [1 : 1.4] | 2.5 |
| | 97% (87%) [1 : 1.6] | 97% (94%) [1 : 1.4] | 82% (49%) [1 : 1.1] | 5 |

*Same screening was done on the Ts-protected substrate: poor conversions/yield and mediocre selectivity

*$^1$H NMR vs Mesitylene*

Figure 7: Representative screening results for the *N*-Boc protected model substrate.




| | No catalyst |  | DSI2 | Acetic Acid equivalents |
|---|---|---|---|---|
| $CH_2Cl_2$ | 2% (0%) [ND] | 0% (0%) [ND] | 66% (28%) [1 : 6] | 0 |
| | 100% (87%) [1 : 1] | 100% (72%) [1 : 1.25] | 100% (93%) [1 : 1.05] | 2.5 |
| | 100% (96%) [1 : 1.3] | 100% (98%) [1 : 1.2] | 100% (90%) [1 : 1.4] | 5 |
| THF | 1% (0%) [ND] | 1% (trace) [ND] | 24% (18%) [1:8] | 0 |
| | 18% (14%) [1 : 1.8] | 40% (30%) [2 : 1] | 99% (97%) [1 : 2] | 2.5 |
| | 90% (79%) [1 : 1.3] | 82% (71%) [1.3 : 1] | 95% (70%) [1 : 1.3] | 5 |
| MeCN | 29% (18%) [1 : 2] | 21% (8%) [1.6 : 1] | 43% (20%) [1 : 2.33] | 0 |
| | 100% (94%) [1.4 : 1] | 100% (97%) [1.5: 1] | 100% (93%) [1 : 1.4] | 2.5 |
| | 100% (99%) [1.05 : 1] | 99% (78%) [1.05 : 1] | 100% (94%) [1 : 1.5] | 5 |

*The same screen was done at 25 °C and 40 °C — Most reactions led to decomposition into 6–7 different F-containing species with very little desired products observed.*

Figure 8: Representative screening results for the simplified model substrate.

Hoping to drastically simplify the substrate and the analysis, a switch to 3-(dimethylamino)-1-(4-fluorophenyl)prop-2-en-1-one was made, thereby eliminating any convoluting interactions from the alpha substituent, and providing a fluorine handle for $^{19}F$ NMR analysis. Gratifyingly, we found that this substrate provided good conversions to products (up to quantitative) and better selectivity (up to 1:6) than previously observed.

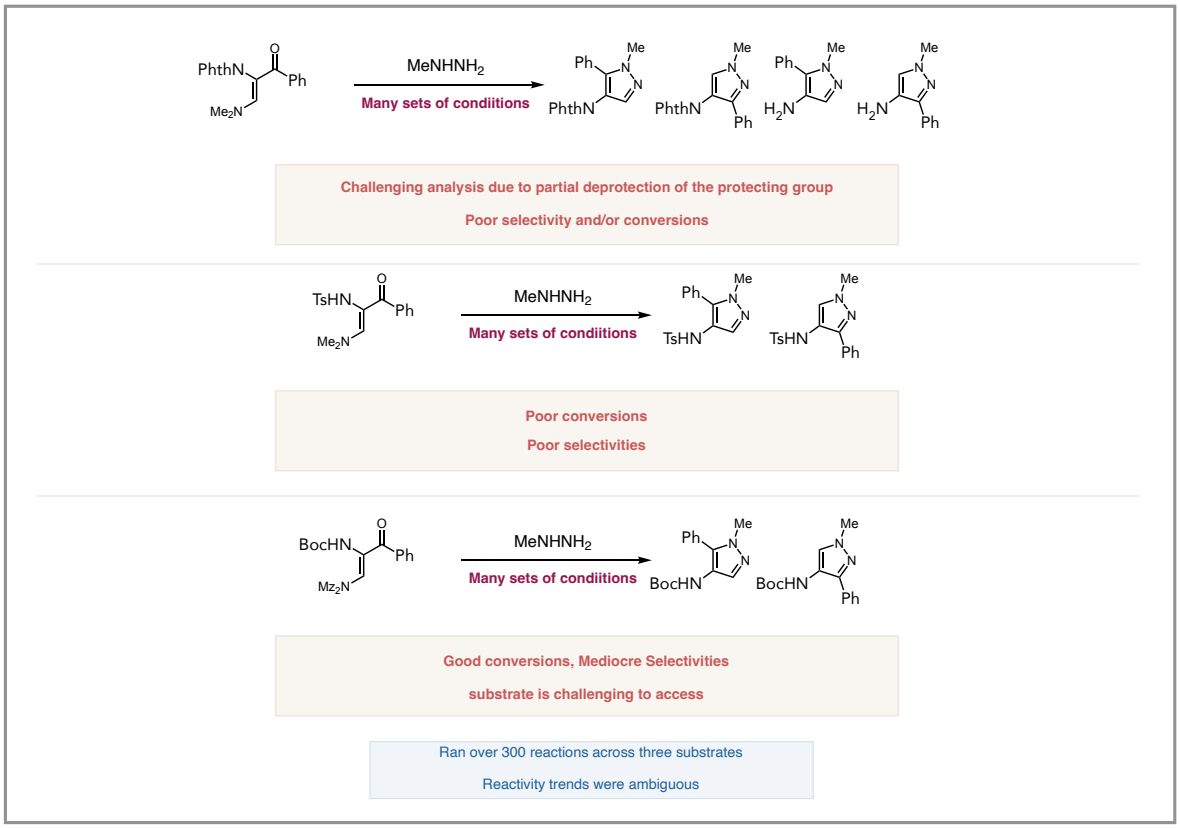



Figure 9: Challenges encountered in reaction optimization.

Although our initial optimization efforts did not provide the desired conditions to obtain selectivity for either isomer, they revealed some important features on the variability of the results. Indeed, we noticed a large solvent dependence, with and without catalyst, on the selectivity of the reaction. Further exploration into additives and phase transfer catalysts also provided mitigated results (Figure 10).

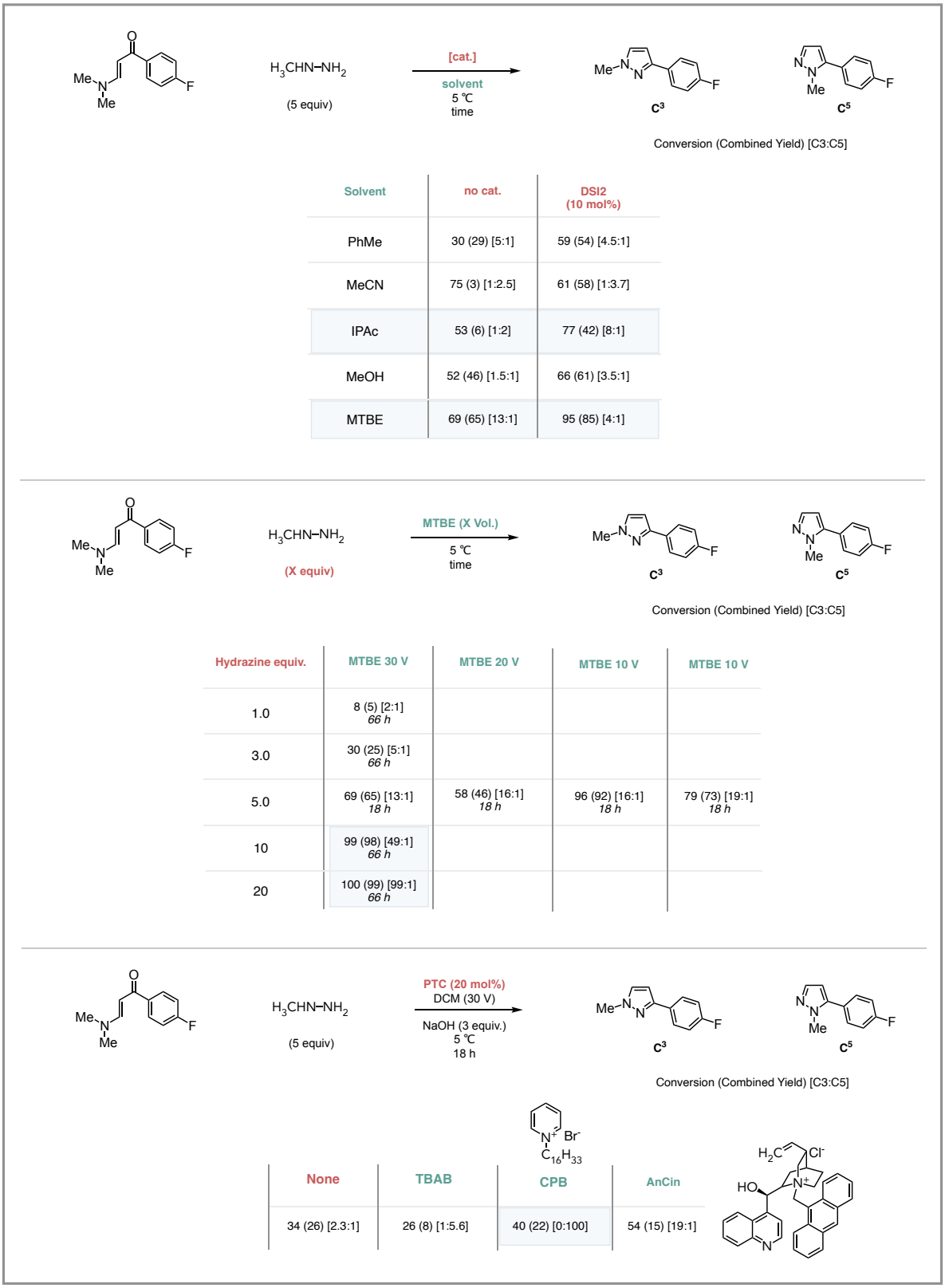



**Figure 10:** Additional exploration into solvent effects, additives, and phase transfer catalysis.

## 3.2. Bayesian Optimization and Regioselectivity Results

High-throughput experimentation (HTE) has increasingly been used in academia and industry to address the needs for more efficient reaction discovery and optimization. A particular feature of HTE is the large amount of data generated at once with amplified consistency across experiments, especially when robotics are used to bypass potential human experimental error. In a large number of settings, a binary analysis of HTE results can often be sufficient to achieve desired results. Rather than seeking trends in the data, ligands, catalysts, or solvents can be selected or disregarded based on a predetermined efficiency or selectivity threshold.

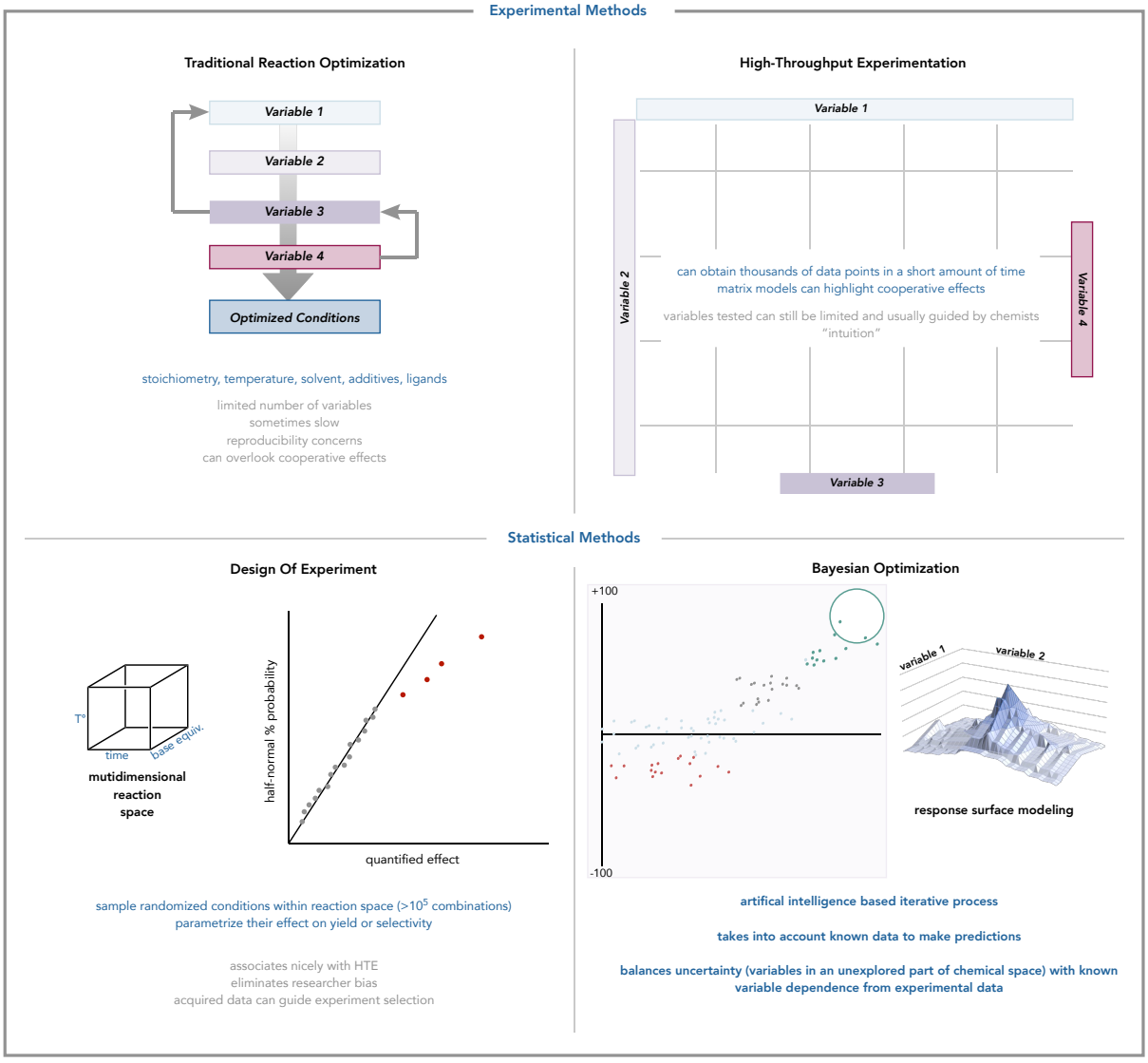



Figure 11: Reaction optimization methods and tools

This approach is particularly attractive in the context of time and resource-economy. Indeed, the large amount of data generated by HTE can represent an analytical challenge to find the most appropriate and helpful ways to present and reveal important reactivity trends and features in the hope of guiding additional optimization efforts. Researcher bias can further bias this analysis, and exclude some areas of chemical space which might otherwise provide improved results. Statistical models and artificial intelligence tools such as Design of Experiment and Bayesian Statistics can guide the design of experiments to generate more meaningful data by removing bias and graphically deconvoluting reactivity trends.[34-36]

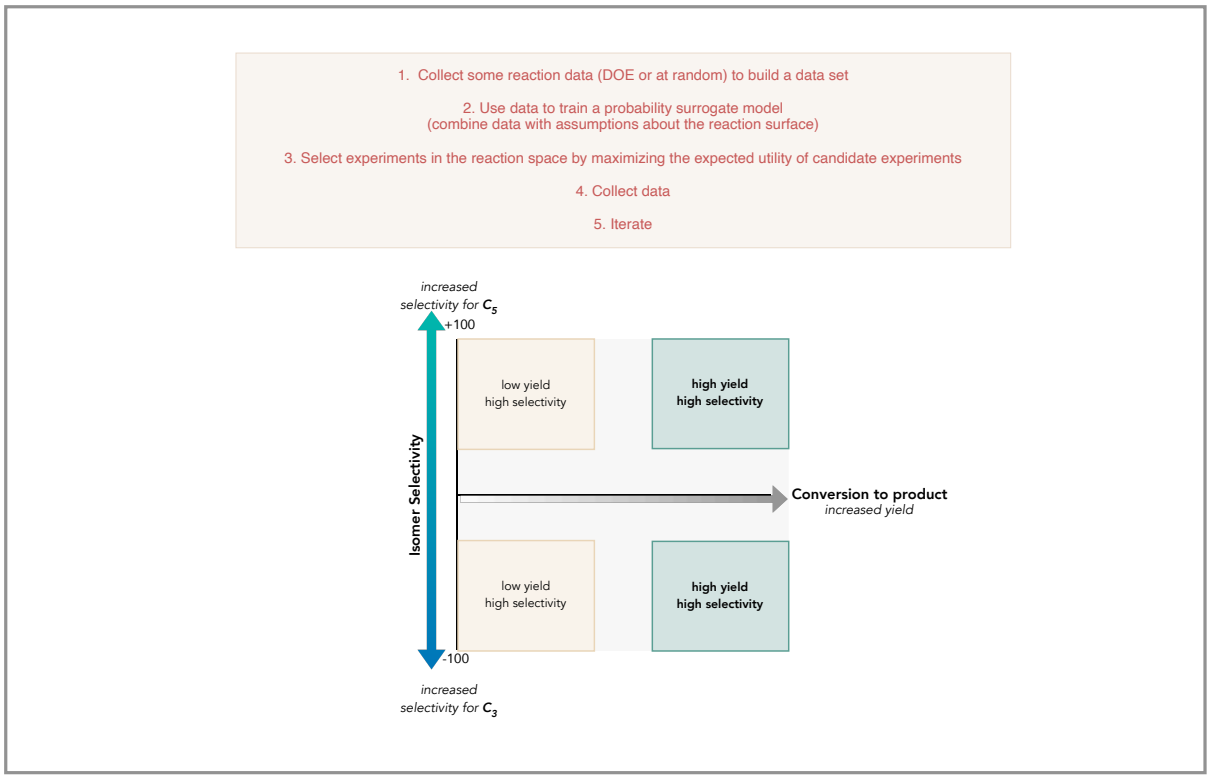



Figure 12: Graphical summary of Bayesian Optimization methods.

The large set of experimental data collected during our initial attempts to discern trends in the reactivity and selectivity of this transformation was first compiled into a training set for the Bayesian Optimization (Figure 12). As expected, the iterative processing of the data generated possible reaction conditions which were then tested to obtain corresponding experimental data. The latter was further utilized to train the algorithm and improve the accuracy of the predictions (Figure 13).

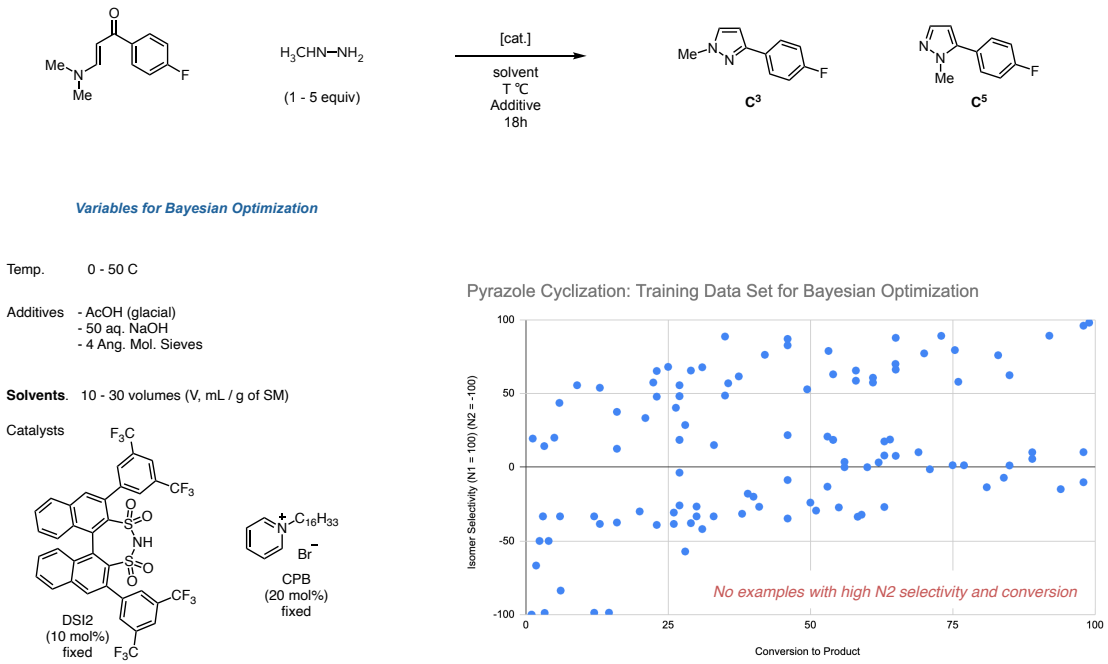



Figure 13: Initial Bayesian Optimization Training Set

We were pleased to observe that four iterations of optimization enabled the discovery of highly selective conditions for the $C^5$ isomer of the cyclized product in great conversions. Although high selectivity could be achieved for the $C^3$ isomer, low conversions remain a challenge, and we note that the predictions were generally more accurate for the $C^5$ cyclization than for the $C^3$ cyclization. This could suggest a difference in mechanism or a difference in the variables that most affect the rates of conversions to either product, and will necessitate further iterations to deconvolute.

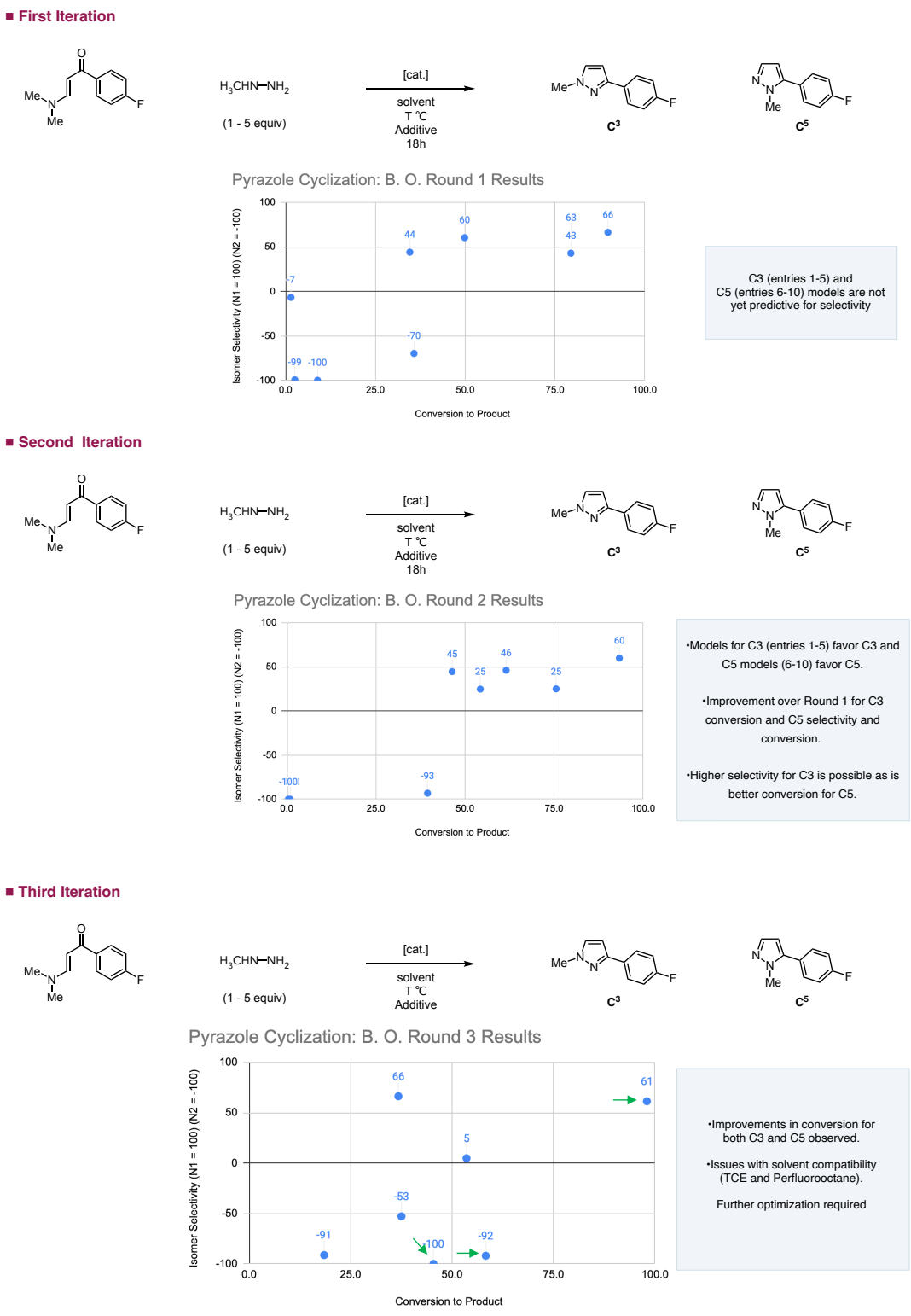



**Figure 14:** Three consecutive iterations of Bayesian Optimization were performed.

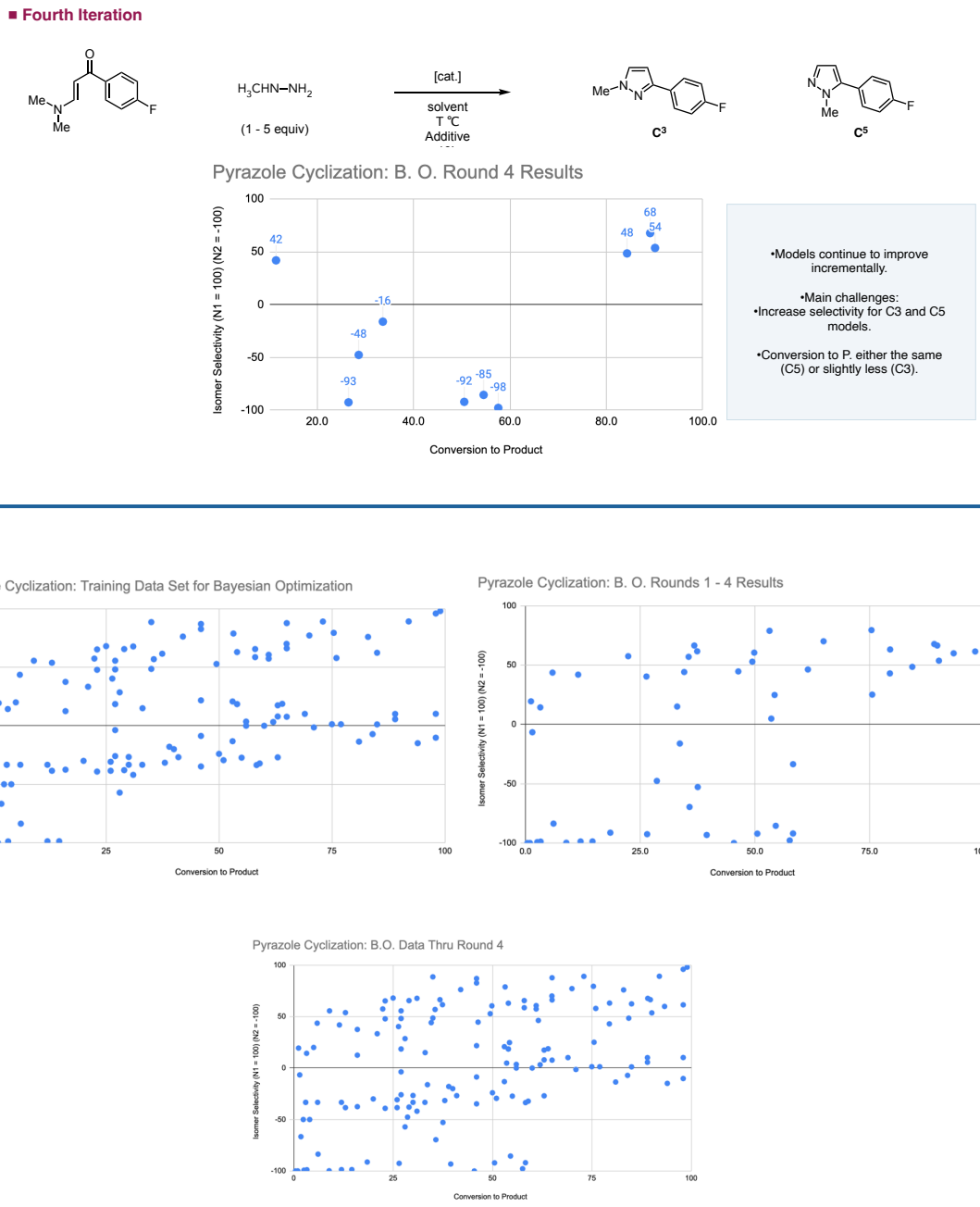



Figure 15: Final iteration and combined results

## IV. Conclusions and Outlook

The work presented herein describes the optimization process for the regioselective cyclization of N-methyl pyrazoles. Hoping to move away from substrate-driven selectivity, the small size of the hydrazine partner, lack of significant electronic induction from either starting materials, as well as the high variability of selectivity on multiple reaction parameters presented a challenge for traditional optimization methods. We describe the iterative use of Bayesian statistics to obtain catalyst-free yet selective reaction conditions for the synthesis of 3-(4-fluorophenyl)-1-methyl-1*H*-pyrazole, as well as the progress made towards the selective synthesis of isomer 5-(4-fluorophenyl)-1-methyl-1*H*-pyrazole.

The opportunities for future work offered by this study are manifold. Although optimized conditions have been obtained, the initial goal of developing selective cyclization conditions was not limited to one specific substrate. Considering the high variability on substrate structure observed early in the optimization studies, assessment of the robustness of the conditions found via the Bayesian optimization is necessary.

With optimized conditions in hands, questions regarding the origins of the selectivity remain. Particularly in a catalyst-free environment, the driving forces at play between substrates, additives and solvent might be more subtle than a traditional steric-based catalytic system. Insight into these interactions could be obtained from the parametrization of the data obtained throughout the Bayesian optimization and could inform future decisions in the optimization of similar transformations. Rate analysis along with KIE studies could also provide information on the mechanistic pathway and any variations thereof based on substrate structures.

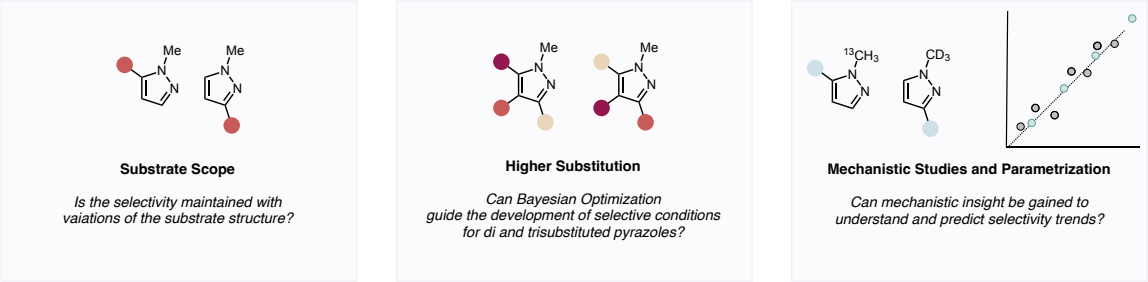



Figure 16: Opportunities for future work

## V. Supplemental Information

Commercial reagents were purified prior to use according to the procedures outlined by Perrin and Armarego unless otherwise indicated.[37] Dry organic solvents (Tetrahydrofuran, Toluene, Acetonitrile, and Dichloromethane) were purified according to the method of Grubbs et al. and used directly after withdrawal from dry Argon solvent stills after passing through activated alumina.[38] Solutions in organic solvents were concentrated *in vacuo* using a Büchi rotary evaporator equipped with a temperature-controlled water bath and an isopropyl alcohol-dry ice bath to trap volatile compounds, and further dried on Schlenck high-vacuum lines. Chromatographic purification of products was accomplished using flash chromatography on silica gel (Sigma Aldrich, 60 Å pore size, 230-400 mesh particle size, 40-63 μm particle size) according to the method of Still[32], or by reversed-phase flash chromatography using a CombiFlash-*Rf* ® (Teledyne ISCO) and Teledyne-ISCO RediSep-*Rf* $C_{18}$ Silica columns (60 Å pore size, 230-400 mesh particle size, 40-63 μm particle size, 86g). Analytical thin-layer chromatography (TLC) was performed on TLC plates from Silicycle Siliaplate™ glass backed TLC plates (250 μm thickness, 60 Å porosity, F-254 indicator). Visualization of the developed plates was accomplished by fluorescence quenching or staining with a $KMnO_4$ solution.

$^{1}H$ NMR, $^{13}C$ NMR, $^{19}F$ NMR, and $^{31}P$ NMR spectra were taken with Bruker spectrometers operating at 300, 400, 500, or 600 MHz for $^{1}H$ at the UC Berkeley NMR Facility in the college of Chemistry, or on a 900 MHz spectrometer administered by the California Institute for Quantitative Biosciences (QB3) Facility. The spectra were internally referenced to residual protic DMSO-$d_6$ signals (2.54 ppm, Cambridge Isotope Laboratories Inc.), $CHCl_3$ (7.26 ppm, Cambridge Isotope Laboratories Inc.), or $CD_2Cl_2$ (5.32 ppm, Cambridge Isotope Laboratories Inc.) signals. $^{1}H$ NMR data reported in this work follow the format: chemical shift (δ ppm), multiplicity (s = singlet, d = doublet, t = triplet, q = quartet, m = multiplet, dd = doublet of doublets, dt = doublet of triplets, br = broad), coupling constant (Hz), integration.

Brønsted acid catalysts were used directly from the collaborative Toste group catalyst library, or provided by the Genentech process group. (2E)-3-(dimethylamino)-1-(4-fluorophenyl)prop-2-en-1-one was purchased from Combi-Blocks and used directly as received. 3-(dimethylamino)-1-phenyl-2-phthalimido-2-propen-1-one was prepared according to the literature procedure reported by Franchini *et al.*[39] (E)-*t*Butyl-(1-(dimethylamino)-3-oxo-3-phenylpro-1-en-2-yl)carbamate was synthesized according to the procedure reported by Merck&Co, Inc.[40]

**Reaction Optimization Screening at UC Berkeley**

The reactions were performed in 4 mL vials equipped with stir bars, in a cold room maintained at a temperature between 4 °C and 5 °C. Solid reagents were first added to the reaction vials as adequately calculated for the specific screen. When glacial acetic acid was used as an additive, it was prepared as a stock solution, cooled to 0°C in an ice bath, in the appropriate solvent and added to the reaction vial using a Hamilton micro-syringe. Finally, a stock solution of methylhydrazine was also cooled to 0 °C and added by syringe to the reaction mixture. The vials

were capped and stirred between 4 °C and 5 °C for 12–24 hours. The crude mixtures were analyzed by $^{1}H$ or $^{19}F$ NMR in $CDCl_3$.

**Bayesian Optimization Screening at Genentech, Inc.**

The following reaction screens were conducted in which each vial with magnetic stir bar was added in the amount specified in the materials section of the experimental electronic notebook as specified in the table below. Each line of the table will be represented alphabetically beginning with A and progressing in order to Z.

| Rxn ID | AcOH (equiv) | NaOH (equiv) | Methyl Hydrazine (equiv) | DSI2 Catalyzed (1 - yes, 0 - no) | PTC Catalyzed (1/0) | 4 Ang MS (1/0) | Temp C | Solvent Vol (ml/g SM) | Solvent Name | SM A% | N1 A% | N2 A% | N1' | N2' | Conv to Prod | SM Consumption | N1'-N2' |
|---|---|---|---|---|---|---|---|---|---|---|---|---|---|---|---|---|---|
| 27A1_GPR_ei_01_n1 | 0 | 1 | 1 | 1 | 1 | 1 | 0 | 10 | MTBE | 100.0 | 0.0 | 0.0 | 0 | 0 | 0 | 0 | 0 |
| 27B1_GPR_ucb_2_n1 | 1 | 0 | 1 | 1 | 1 | 1 | 0 | 10 | MTBE | 36.0 | 40.0 | 9.9 | 80 | 20 | 50 | 64 | 60 |
| 27C1_RFR_ei_01_n1 | 0 | 5 | 2 | 0 | 1 | 0 | 50 | 10 | ethyl acetate | 22.4 | 24.9 | 9.7 | 72 | 28 | 35 | 78 | 44 |
| 27D1_RFR_ucb_2_n1 | 0 | 5 | 1 | 0 | 1 | 0 | 25 | 10 | DMF | 34.3 | 0.7 | 0.8 | 47 | 53 | 2 | 66 | -7 |
| 27E1_MLP_ei_01_n1 | 5 | 0 | 5 | 0 | 1 | 0 | 50 | 10 | tributylamine | 0.2 | 64.8 | 14.7 | 82 | 18 | 79 | 100 | 63 |
| 27F1_GPR_ei_01_n2 | 3 | 0 | 3 | 1 | 1 | 1 | 25 | 10 | DPMU | 0.8 | 56.8 | 22.7 | 71 | 29 | 79 | 99 | 43 |
| 27G1_GPR_ucb_2_n2 | 5 | 0 | 5 | 1 | 1 | 1 | 50 | 30 | p-Cymene | 0.0 | 74.7 | 15.1 | 83 | 17 | 90 | 100 | 66 |
| 27H1_RFR_ucb_2_n2 | 0 | 5 | 2 | 1 | 0 | 1 | 50 | 30 | 2-MeTHF | 26.7 | 5.4 | 30.3 | 15 | 85 | 36 | 73 | -70 |
| 27I1_MLP_ei_01_n2 | 0 | 5 | 1 | 0 | 0 | 1 | 50 | 30 | tributylamine | 51.8 | 0.0 | 2.6 | 0 | 100 | 3 | 48 | -99 |
| 27J1_MLP_ucb_2_n2 | 0 | 5 | 1 | 0 | 0 | 1 | 25 | 10 | tributylamine | 72.0 | 0.0 | 8.9 | 0 | 100 | 9 | 28 | -100 |

| Rxn ID | AcOH (equiv) | NaOH (equiv) | Methyl Hydrazine (equiv) | DSI2 Catalyzed (1 - yes, 0 - no) | PTC Catalyzed (1/0) | 4 Ang MS (1/0) | Temp C | Solvent Vol (ml/g SM) | Solvent Name | SM A% | N1 A% | N2 A% | N1' | N2' | Conv to Prod | SM Consumption | N1'-N2' |
|---|---|---|---|---|---|---|---|---|---|---|---|---|---|---|---|---|---|
| GPR_ei_05_n1 | 2 | 0 | 5 | 1 | 0 | 0 | 0 | 10 | triethylamine | 51.4 | 33.5 | 12.8 | 72 | 28 | 46 | 49 | 45 |
| RFR_ei_05_n1 | 2 | 0 | 5 | 1 | 0 | 0 | 25 | 20 | 1,1,2,2-tetrachlor | 0.3 | 33.9 | 20.4 | 62 | 38 | 54 | 100 | 25 |
| RFR_ucb_2_n1 | 5 | 0 | 5 | 1 | 0 | 0 | 50 | 30 | 1,1,2,2-tetrachlor | 0.0 | 45.0 | 16.6 | 73 | 27 | 62 | 100 | 46 |
| MLP_ei_05_n1 | 3 | 0 | 5 | 1 | 1 | 1 | 50 | 10 | MeCN | 0.0 | 74.6 | 18.7 | 80 | 20 | 93 | 100 | 60 |
| MLP_ucb_2_n1 | 5 | 0 | 1 | 1 | 0 | 0 | 50 | 30 | formamide | 8.9 | 47.2 | 28.3 | 63 | 37 | 76 | 91 | 25 |
| GPR_ei_05_n2 | 0 | 4 | 1 | 0 | 0 | 1 | 0 | 10 | triethylamine | 95.7 | 0.0 | 0.0 | 0 | 0 | 0 | 4 | 0 |
| GPR_ucb_2_n2 | 0 | 4 | 1 | 0 | 1 | 1 | 0 | 10 | triethylamine | 97.0 | 0.0 | 0.0 | 0 | 0 | 0 | 3 | 0 |
| RFR_ucb_2_n2 | 0 | 5 | 5 | 0 | 0 | 1 | 25 | 10 | diethylamine | 25.9 | 1.3 | 38.2 | 3 | 97 | 39 | 74 | -93 |
| MLP_ei_05_n2 | 0 | 5 | 5 | 0 | 1 | 1 | 0 | 10 | formamide | 75.2 | 0.0 | 1.0 | 0 | 100 | 1 | 25 | -100 |
| MLP_ucb_2_n2 | 0 | 5 | 1 | 0 | 0 | 0 | 0 | 10 | carbon tetrachlor | 87.2 | 0.0 | 0.4 | 0 | 100 | 0 | 13 | -100 |

| Rxn ID | AcOH (equiv) | NaOH (equiv) | Methyl Hydrazine (equiv) | DSI2 Catalyzed (1 - yes, 0 - no) | PTC Catalyzed (1/0) | 4 Ang MS (1/0) | Temp C | Solvent Vol (ml/g SM) | Solvent Name | SM A% | N1 A% | N2 A% | N1' | N2' | Conv to Prod | SM Consumption | N1'-N2' |
|---|---|---|---|---|---|---|---|---|---|---|---|---|---|---|---|---|---|
| GPR_ei_05_n1 | 0 | 0.56 | 5 | 1 | 1 | 1 | 0 | 10 | alpha-Terpineol | 47.6 | 30.6 | 6.2 | 83 | 17 | 37 | 52 | 66 |
| GPR_ucb_2_n1 | 0 | 0.56 | 5 | 1 | 1 | 1 | 50 | 10 | 1-decanol | 29.5 | 11.4 | 33.7 | 25 | 75 | 45 | 71 | -49 |
| RFR_ei_05_n1 | 0 | 2.78 | 5 | 0 | 1 | 0 | 25 | 10 | MTBE | 39.4 | 2.3 | 56.0 | 4 | 96 | 58 | 61 | -92 |
| MLP_ei_05_n1 | 5 | 0.00 | 1 | 1 | 0 | 1 | 50 | 30 | Dimethyl sulfoxid | 39.4 | 28.1 | 29.0 | 49 | 51 | 57 | 61 | -1 |
| MLP_ucb_2_n1 | 5 | 0.00 | 5 | 0 | 0 | 0 | 0 | 10 | Isoamyl alcohol | 0.0 | 79.1 | 18.9 | 81 | 19 | 98 | 100 | 61 |
| GPR_ei_05_n2 | 0 | 3.89 | 5 | 1 | 1 | 0 | 50 | 10 | tetrachloroethyle | 11.0 | 0.0 | 0.0 | 0 | 0 | 0 | 89 | 0 |
| GPR_ucb_2_n2 | 0 | 3.89 | 5 | 1 | 0 | 0 | 50 | 10 | tetrachloroethyle | 16.3 | 0.0 | 0.0 | 0 | 0 | 0 | 84 | 0 |
| RFR_ei_05_n2 | 0 | 2.78 | 5 | 0 | 0 | 0 | 37.5 | 10 | Perfluorooctane | 100.0 | 0.0 | 0.0 | 0 | 0 | 0 | 0 | 0 |
| RFR_ucb_2_n2 | 0 | 5 | 5 | 0 | 0 | 1 | 37.5 | 10 | di-n-butyl ether | 21.8 | 1.6 | 32.9 | 5 | 95 | 34 | 78 | -91 |
| MLP_ei_05_n2 | 0 | 5 | 5 | 1 | 1 | 1 | 12.5 | 23.3 | 1-decanol | 27.2 | 0.0 | 45.4 | 0 | 100 | 45 | 73 | -100 |

| Rxn ID | AcOH (equiv) | NaOH (equiv) | Methyl Hydrazine (equiv) | DSI2 Catalyzed (1 - yes, 0 - no) | PTC Catalyzed (1/0) | 4 Ang MS (1/0) | Temp C | Solvent Vol (ml/g SM) | Solvent Name | SM A% | N1 A% | N2 A% | N1' | N2' | Conv to Prod | SM Consumption | N1'-N2' |
|---|---|---|---|---|---|---|---|---|---|---|---|---|---|---|---|---|---|
| GPR_ei_05_n1 | 5 | 0 | 3 | 0 | 1 | 0 | 25 | 10 | cyclohexane | 0.2 | 74.7 | 14.4 | 84 | 16 | 89 | 100 | 68 |
| GPR_ucb_2_n1 | 5 | 0 | 1 | 0 | 1 | 1 | 25 | 10 | cyclopentane | 2.0 | 62.6 | 21.7 | 74 | 26 | 84 | 98 | 48 |
| RFR_ucb_2_n1 | 0 | 1.67 | 5 | 0 | 0 | 0 | 12.5 | 10 | MTBE | 32.1 | 4.0 | 50.6 | 7 | 93 | 55 | 68 | -85 |
| MLP_ei_05_n1 | 5 | 0 | 5 | 1 | 1 | 1 | 0 | 30 | tributylamine | 76.5 | 8.1 | 3.3 | 71 | 29 | 11 | 23 | 42 |
| MLP_ucb_2_n1 | 5 | 0 | 5 | 0 | 1 | 0 | 50 | 10 | nitroethane | 0.0 | 69.2 | 20.9 | 77 | 23 | 90 | 100 | 54 |
| GPR_ei_05_n2 | 0 | 2.78 | 5 | 1 | 1 | 0 | 37.5 | 10 | triethylamine | 34.3 | 1.0 | 25.5 | 4 | 96 | 27 | 66 | -93 |
| RFR_ei_05_n2 | 0 | 3.89 | 5 | 1 | 0 | 1 | 12.5 | 10 | tributylamine | 22.6 | 2.0 | 48.5 | 4 | 96 | 51 | 77 | -92 |
| RFR_ucb_2_n2 | 0 | 2.78 | 5 | 0 | 1 | 0 | 12.5 | 10 | tributylamine | 30.7 | 0.6 | 57.0 | 1 | 99 | 58 | 69 | -98 |
| MLP_ei_05_n2 | 0 | 3.89 | 1 | 1 | 1 | 0 | 37.5 | 30 | m-cresol | 12.2 | 14.1 | 19.5 | 42 | 58 | 34 | 88 | -16 |
| MLP_ucb_2_n2 | 0 | 5 | 1 | 0 | 0 | 0 | 50 | 10.0 | Glycerol | 14.3 | 7.5 | 21.1 | 26 | 74 | 29 | 86 | -48 |

*General Procedure*

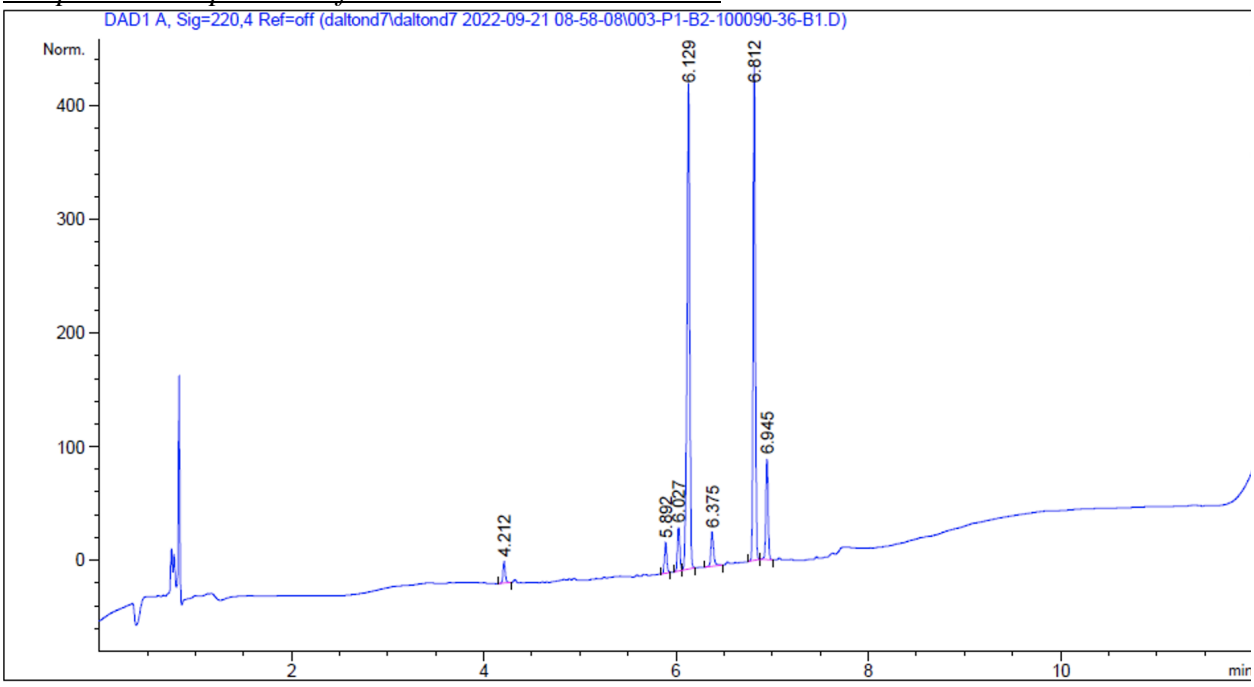
(2E)-3-(dimethylamino)-1-(4-fluorophenyl)prop-2-en-1-one (G, 0.010 g, 0.050 mmol, 97 mass%),(11bS)-2,6-Bis[3,5-bis(trifluoromethyl)phenyl]dinaphtho[2,1-d:1',2'-f][1,3,2]dithiazepine 3,3,5,5-tetraoxide (0.1 equiv., 0.0050 mmol, 95 mass%), cetylpyridinium bromide (0.2 equiv., 0.010 mmol, 98 mass%) catalyst (s) as indicated), 10 mg 4 Angstrom powdered Mol. Sieves (activated) were added to the reaction vials. Solvent was then added via syringe and the vials placed in an aluminum block at the specified temperature. After 1-2 min,

liquid reagents were added directly to the reaction mixture (not to the side of the vial wall) via calibrated syringe in the following order (if indicated): glacial AcOH, aq. 50% NaOH, Methylhydrazine. Samples were analyzed for conversion by reverse phase HPLC (6 µL reaction sample in 500 µL diluent: 8:2 MeCN/Water).

*HPLC Method*

Column: XBridge BEH C10, 3x100mm, 2.5 um. Rate: 0.7mL/min, 30 C, 220 nm UV detection. Mobile Phase A: 0.05% TFA in Water, Mobile Phase B: 0.05% TFA in ACN. Ellution: 0-0.5' 2%B; 4' 35%B; 7-10' 90%B, 10.1-12' 2% B.

*Sample HPLC Spectrum of the crude reaction mixtures:*




N1 isomer observed at 6.812 min
N2 Isomer observed at 6.945 min.
Starting material observed at 6.129 min.
N2 intermediate 6.027 min.
N1 intermediate 6.375 min.

**Computational Supplementary Information: Bayesian Optimization**

Bayesian optimization was carried out using previously published algorithms implemented in python using the Scikit-Learn library.[41,42] For this work, each round consisted of ten experiments conducted in parallel. These were split into five targeting C3 selectivity and five targeting C5 selectivity. In order to recommend ten sets of conditions, three models were trained: Gaussian process, random forest, and Bayesian neural network. Each one was used to predict both yield and selectivity, and their predictions and uncertainties were used in conjunction with two acquisition functions: expected improvement and upper confidence bound (see Brochu *et al*). Solvents were parameterized using the COSMO-RS parameters as reported by Moity et al.[43] Use of molecular sieves or use of catalyst were modeled as Boolean variables. Numeric variables such as

temperature or solvent volume were scaled using a standard scaler prior to fitting. Equivalents of acetic acid and NaOH were combined into one numeric variable, with positive values equal to equivalents of acetic acid and negative values equal to the negative of NaOH equivalents. Categorical variables were modeled in the Gaussian process kernel using a transformed kernel as described by Garrido-Merchán et al.[44] Data from all experiments were pooled for predicting subsequent rounds.

## VI. References


1. Kerru, N., Gummidi, L., Maddila, S., Gangu, K.K., and Jonnalagadda, S.B. (2020). A Review on Recent Advances in Nitrogen-Containing Molecules and Their Biological Applications. Molecules *25*. 10.3390/molecules25081909.
2. Smith, B.R., Eastman, C.M., and Njardarson, J.T. (2014). Beyond C, H, O, and N analysis of the elemental composition of U.S. FDA approved drug architectures. J. Med. Chem. *57*, 9764–9773.
3. Vitaku, E., Smith, D.T., and Njardarson, J.T. (2014). Analysis of the structural diversity, substitution patterns, and frequency of nitrogen heterocycles among U.S. FDA approved Pharmaceuticals. J. Med. Chem. *57*, 10257–10274.
4. Akhtar, J., Khan, A.A., Ali, Z., Haider, R., and Yar, M.S. (2017). Structure-activity relationship (SAR) study and design strategies of nitrogen-containing heterocyclic moieties for their anticancer activities. Eur. J. Med. Chem. *125*, 143–189.
5. Baumann, M., Baxendale, I.R., Ley, S.V., and Nikbin, N. (2011). An overview of the key routes to the bestselling 5-membered ring heterocyclic pharmaceuticals. Beilstein J. Org. Chem. *7*, 442–495.
6. Karrouchi, K., Radi, S., Ramli, Y., Taoufik, J., Mabkhot, Y.N., Al-Aizari, F.A., and Ansar, M. (2018). Synthesis and pharmacological activities of pyrazole derivatives: A Review. Molecules *23*, 134.
7. Silva, V.L.M., Elguero, J., and Silva, A.M.S. (2018). Current progress on antioxidants incorporating the pyrazole core. Eur. J. Med. Chem. *156*, 394–429.
8. Ansari, A., Ali, A., and Asif, M. (2017). Review: Biologically active pyrazole derivatives. New J. Chem. *41*, 16–41.
9. Wu, J., Song, B.-A., Hu, D.-Y., Yue, M., and Yang, S. (2011). Design, synthesis and insecticidal activities of novel pyrazole amides containing hydrazone substructures. Pest Management Science *68*, 801–810.
10. Bhattacharya, S., Goswami, A., Gole, B., Ganguly, S., Bala, S., Sengupta, S., Khanra, S., and Mondal, R. (2014). Construction of Bis-pyrazole Based Co(II) Metal–Organic Frameworks and Exploration of Their Chirality and Magnetic Properties. Cryst. Growth Des. *14*, 2853–2865.
11. Pettinari, C., Tăbăcaru, A., and Gallic, S. (2016). Coordination polymers and metal–organic frameworks based on poly(pyrazole)-containing ligands. Coord. Chem. Rev. *1–31*.
12. Jin, J.-K., Wu, K., Liu, X.-Y., Huang, G.-Q., Huang, Y.-L., Luo, D., Xie, M., Zhao, Y., Lu, W., Zhou, X.-P., et al. (2021). Building a Pyrazole–Benzothiadiazole–Pyrazole Photosensitizer into Metal–Organic Frameworks for Photocatalytic Aerobic Oxidation. J. Am. Chem. Soc. *143*, 21340–21349.

13. Knorr, L. (1883). Einwirkung von acetessigester auf phenylhydrazin. Eur. J. Inorg. Chem. *16*, 2597–2599.
14. Singh, S.R., Kumar, D., Batra, H., Naithani, R., Rozas, I., and Elguero, J. (2000). The reaction between hydrazines and β-dicarbonyl compounds: Proposal for a mechanism. Can. J. Chem. *78*, 1109–1120.
15. Fustero, S., Sánchez-Roselló, M., Barrio, P., and Simon-Fuentes, A. (2011). From 2000 to Mid-2010: A Fruitful Decade for the Synthesis of Pyrazoles. Chem. Rev. *111*, 6984–7034.
16. Lévai, A., Silva, A.M.S., Cavaleiro, J.A.S., Alkorta, I., Elguero, J., and József, J. (2006). Synthesis of Pyrazoles by Treatment of 3-Benzylchromones, 3-Benzylflavones and Their 4-Thio Analogues with Hydrazine. Eur. J. Org. Chem. *2006*, 2825–2832.
17. Ramadan, M., Aly, A.A., El-Haleem, L.E.A., Alshammari, M.B., and Bräse, S. (2021). Substituted Pyrazoles and Their Heteroannulated Analogs—Recent Syntheses and Biological Activities. Molecules *26*, 4995.
18. Heller, S.T., and Natarajan, S.R. (2006). 1,3-Diketones from Acid Chlorides and Ketones: A Rapid and General One-Pot Synthesis of Pyrazoles. Org. Lett. *8*, 2675−2678.
19. Alberola, A., González-Ortega, A., Sádaba, M.L., and Sañudo, M.C. (1998). β-Aminoenones in the regioselective synthesis of 1,3,5- trialkylpyrazoles. The influence of the substituents in the mechanism and the regioselectivity of the reaction. J. Chem. Soc. Perkin Trans. *1*, 4061–4066
20. Ponnala, S., and Sahu, D.P. (2007). Iodine-Mediated Synthesis of 2-Arylbenzoxazoles, 2-Arylbenzimidazoles, and 1,3,5-Trisubstituted Pyrazoles. Synth. Commun. *36*, 2189–2194.
21. Rao, V.K., Tiwari, R., Chhikara, B.S., Shirazi, A.N., Parang, K., and Kumar, A. (2013). Copper triflate-mediated synthesis of 1,3,5-triarylpyrazoles in [bmim][PF6] ionic liquid and evaluation of their anticancer activities. RSC Adv. *3*, 15396–15403.
22. Huang, Y.R., and Katzenellenbogen, J.A. (2000). Regioselective synthesis of 1,3,5-triaryl-4-alkylpyrazoles: Novel ligands for the estrogen receptor. Org. Lett. *2*, 2833–2836.
23. Moureu, C., and Delange, R. (1901). Bull. Soc. Chim. Fr. *25*, 302–313.
24. Baldwin, J.E., Pritchard, G.J., and Rathmell, R.E. (2001). The reactions of diacetylenic ketones with nitrogen nucleophiles; facile preparation of alkynyl substituted pyrimidines and pyrazoles. J. Chem. Soc. Perkin Trans. *1*, 2906–2908.
25. Deng, X., and Mani, S.N. (2006). Reaction of N-Monosubstituted Hydrazones with Nitroolefins: A Novel Regioselective Pyrazole Synthesis. Org. Lett. *8*, 3505–3508.
26. Cyranński, M.K. (2005). Energetic Aspects of Cyclic Pi-Electron Delocalization: Evaluation of the Methods of Estimating Aromatic Stabilization Energies. Chem. Rev. *105*, 3773−3811.
27. Neumann, J.J., Suri, M., and Glorius, F. (2010). Efficient Synthesis of Pyrazoles: Oxidative C-C/N-N Bond-Formation Cascade. Angew. Chem. Int. Ed. Engl. *49*, 7790−7794.
28. Suri, M., Jousseaume, T., Neumann, J.J., and Glorius, F. (2012). An Efficient Copper-Catalyzed Formation of Highly Substituted Pyrazoles Using Molecular Oxygen as the Oxidant. Green Chem. *14*, 2193.

29. Tang, X., Huang, L., Yang, J., Xu, Y., Wu, W., and Jiang, H. (2014). Practical Synthesis of Pyrazoles via a Copper-Catalyzed Relay Oxidation Strategy. Chem. Commun. *50*, 14793−14796.
30. Chen, B., Zhu, C., Tang, Y., and Ma, S. (2014). Copper-Mediated Pyrazole Synthesis from 2,3-Allenoates or 2-Alkynoates, Amines and Nitriles. Chem. Commun. *50*, 7677.
31. Diccianni, J.B., Hu, C., and Diao, T. (2016). N-N Bond Forming Reductive Elimination via a Mixed-Valent Nickel(II)-Nickel(III) Intermediate. Angew. Chem. Int. Ed. Engl. *55*, 7534−7538.
32. Pearce, A.J., Harkins, R.P., Reiner, B.R., Wotal, A.C., Dunscomb, R.J., and Tonks, I.A. (2020). Multicomponent Pyrazole Synthesis from Alkynes, Nitriles, and Titanium Imido Complexes via Oxidatively Induced N−N Bond Coupling. J. Am. Chem. Soc. *142*, 4390−4399.
33. Hughes, D.L. (2019). Patent Review of Synthetic Routes and Crystalline Forms of the CFTR-Modulator Drugs Ivacaftor, Lumacaftor, Tezacaftor, and Elexacaftor. Org. Process Res. Dev. *23*, 2302–2322.
34. Shields, B.J., Stevens, J., Li, J., Parasram, M., Damani, F., Alvarado, J.I.M., Janey, J.M., Adams, R.P., and Doyle, A.G. (2021). Bayesian reaction optimization as a tool for chemical synthesis. Nature *590*, 89-96. 10.1038/s41586-021-03213-y.
35. Weissman, S.A. (2015). Application of Design of Experiments to Process Development. Org. Process Res. Dev. *19*, 1604.
36. Weissman, S.A., and Anderson, N.G. (2015). Design of Experiments (DoE) and Process Optimization. A Review of Recent Publications. Org. Process Res. Dev. *19*, 1605–1633.
37. Armarego, W.L.F., and Perrin, D.D. (1997). Purification of laboratory chemicals, Fourth Edition (Butterworth-Heinemann).
38. Pangborn, A.B., Giardello, M.A., Grubbs, R.H., Rosen, R.K., and Timmers, F.J. (1996). Safe and Convenient Procedure for Solvent Purification. Organometallics *15*, 1518–1520.
39. Franchini, C.M., Bonini, B.F., Camaggi, C.M., Gentili, D., Pession, A., Rani, M., and Srocchi, E. (2010). Design and synthesis of novel 3,4-disubstituted pyrazoles for nanomedicine applications against malignant gliomas. Eur. J. Med. Chem. *45*, 2024–2033.
40. TRKA Kinase Inhibitors, Compositions and Methods Thereof. (2015).
41. Brochu, E., Cora, V.M., and De Freitas, N. (2010). A tutorial on Bayesian optimization of expensive cost functions, with application to active user modeling and hierarchical reinforcement learning. arXiv preprint 1012.2599.
42. Pedregosa, F., Varoquaux, G., Gramfort, A., Michel, V., Thirion, B., Grisel, O., Blondel, M., Prettenhofer, P., Weiss, R., Dubourg, V., et al. (2011). Scikit-learn: Machine Learning in Python. J. M. L. R. *12*, 2825–2830.
43. Moity, L., Durand, M., Benazzouz, A., Pierlot, C., Molinier, V., and Aubry, J.M. (2012). Panorama of sustainable solvents using the COSMO-RS approach. Green chemistry *14*, 1132–1145.
44. Garrido-Merchán, E.C., and Hernández-Lobato, D. (2020). Dealing with categorical and integer-valued variables in bayesian optimization with gaussian processes. Neurocomputing *380*, 20–35.